Journal of *Fungi*

Special Issue Reprint

Fungal Communities in Various Environments

Edited by
Ke Dong and Nan Li

mdpi.com/journal/jof

MDPI

Fungal Communities in Various Environments

Fungal Communities in Various Environments

Guest Editors

Ke Dong
Nan Li

MDPI

Basel • Beijing • Wuhan • Barcelona • Belgrade • Novi Sad • Cluj • Manchester

Guest Editors

Ke Dong
Department of Life Science
Kyonggi University
Suwon
Republic of Korea

Nan Li
College of Ocean and
Meteorology
Guangdong Ocean University
Zhanjiang
China

Editorial Office
MDPI AG
Grosspeteranlage 5
4052 Basel, Switzerland

This is a reprint of the Special Issue, published open access by the journal *Journal of Fungi* (ISSN 2309-608X), freely accessible at: https://www.mdpi.com/journal/jof/special_issues/78EPK80F29.

For citation purposes, cite each article independently as indicated on the article page online and as indicated below:

Lastname, A.A.; Lastname, B.B. Article Title. *Journal Name* **Year**, *Volume Number*, Page Range.

ISBN 978-3-7258-6900-8 (Hbk)
ISBN 978-3-7258-6901-5 (PDF)
https://doi.org/10.3390/books978-3-7258-6901-5

© 2026 by the authors. Articles in this reprint are Open Access and distributed under the Creative Commons Attribution (CC BY) license. The reprint as a whole is distributed by MDPI under the terms and conditions of the Creative Commons Attribution-NonCommercial-NoDerivs (CC BY-NC-ND) license (https://creativecommons.org/licenses/by-nc-nd/4.0/).

Contents

Nan Li and Ke Dong
Fungal Communities in Various Environments
Reprinted from: *J. Fungi* **2025**, *11*, 560, https://doi.org/10.3390/jof11080560 . . . . . **1**

Yao Jiang, Xiao-Yong Mo, Li-Ting Liu, Guo-Zhen Lai and Guo-Wei Qiu
Changes in the Arbuscular Mycorrhizal Fungal Community in the Roots of *Eucalyptus grandis* Plantations at Different Ages in Southern Jiangxi, China
Reprinted from: *J. Fungi* **2024**, *10*, 404, https://doi.org/10.3390/jof10060404 . . . . . **8**

Beiping Liu, Chunhuan Li, Xiuhai Zhao, Chunyu Zhang, Xinyi He, Laiye Qu and Naili Zhang
Contrasting Patterns of Fungal and Bacterial Endophytes Inhabiting Temperate Tree Leaves in Response to Thinning
Reprinted from: *J. Fungi* **2024**, *10*, 470, https://doi.org/10.3390/jof10070470 . . . . . **22**

Lei Chen, Zhi Yu, Mengchen Zhao, Dorsaf Kerfahi, Nan Li, Lingling Shi, et al.
Elevational Variation in and Environmental Determinants of Fungal Diversity in Forest Ecosystems of Korean Peninsula
Reprinted from: *J. Fungi* **2024**, *10*, 556, https://doi.org/10.3390/jof10080556 . . . . . **40**

Wenjing Meng, Lin Chang, Zhaolei Qu, Bing Liu, Kang Liu, Yuemei Zhang, et al.
Dominant Tree Species and Litter Quality Govern Fungal Community Dynamics during Litter Decomposition
Reprinted from: *J. Fungi* **2024**, *10*, 690, https://doi.org/10.3390/jof10100690 . . . . . **54**

Ross A. Joseph, Abolfazl Masoudi, Mateo J. Valdiviezo and Nemat O. Keyhani
Discovery of *Gibellula floridensis* from Infected Spiders and Analysis of the Surrounding Fungal Entomopathogen Community
Reprinted from: *J. Fungi* **2024**, *10*, 694, https://doi.org/10.3390/jof10100694 . . . . . **76**

Glen Dierickx, Lowie Tondeleir, Pieter Asselman, Kris Vandekerkhove and Annemieke Verbeken
What Quality Suffices for Nanopore Metabarcoding? Reconsidering Methodology and Ectomycorrhizae in Decaying *Fagus sylvatica* Bark as Case Study
Reprinted from: *J. Fungi* **2024**, *10*, 708, https://doi.org/10.3390/jof10100708 . . . . . **98**

Jieying Mao, Qiong Wang, Yaying Yang, Feng Pan, Ziwei Zou, Xiaona Su, et al.
A Treasure Trove of Urban Microbial Diversity: Community and Diversity Characteristics of Urban Ancient *Ginkgo biloba* Rhizosphere Microorganisms in Shanghai
Reprinted from: *J. Fungi* **2024**, *10*, 720, https://doi.org/10.3390/jof10100720 . . . . . **121**

Jinping Wang, Jihong Yuan, Qiong Ren, Liyin Zhou, Huanhuan Zeng, Lujun Miao, et al.
The Fungal Community Structure Regulates Elevational Variations in Soil Organic Carbon Fractions in a Wugong Mountain Meadow
Reprinted from: *J. Fungi* **2024**, *10*, 772, https://doi.org/10.3390/jof10110772 . . . . . **140**

Zhaojuan Zhang, Liang He, Yuqing Sun, Zhuang Li, Yingkun Yang, Chao Zhai, et al.
New Species and Records Expand the Checklist of Cellular Slime Molds (Dictyostelids) in Jilin Province, China
Reprinted from: *J. Fungi* **2024**, *10*, 834, https://doi.org/10.3390/jof10120834 . . . . . **158**

Sebastian N. Fajardo, Tyler B. Bourret, Susan J. Frankel and David M. Rizzo
Phytophthora Species and Their Associations with Chaparral and Oak Woodland Vegetation in Southern California
Reprinted from: *J. Fungi* **2025**, *11*, 33, https://doi.org/10.3390/jof11010033 . . . . . **179**

Xiaofang Shi, Shengyao Zhou, Lanzi Xu, Rajapakshalage Thashikala Nethmini, Yu Zhang, Liangliang Huang, et al.
Shifts in Soil Fungal Community and Trophic Modes During Mangrove Ecosystem Restoration
Reprinted from: *J. Fungi* **2025**, *11*, 146, https://doi.org/10.3390/jof11020146 . . . . . **201**

Jie Fang, Mihal Blaschkauer, Assaf Distelfeld, Zihao Liu, Bin Song, Shimon Rachmilevitch and Jonathan M. Adams
Comparison of Rhizosphere Microbiomes Between Domesticated and Wild Wheat in a Typical Agricultural Field: Insights into Microbial Community Structure and Functional Shifts
Reprinted from: *J. Fungi* **2025**, *11*, 168, https://doi.org/10.3390/jof11030168 . . . . . **217**

Kang Fang, Guoce Xu, Xin Chen, Jing Li, Yuting Cheng and Yifan Cheng
Distribution Pattern and Assembly Process of Fungal Communities Along Altitude Gradient in Sediments of the Yellow River Basin
Reprinted from: *J. Fungi* **2025**, *11*, 214, https://doi.org/10.3390/jof11030214 . . . . . **235**

Yueling Li, Guangyu Luo, Shijie Wu, Dang Yang, Pengpeng Lv, Zexin Jin and Junmin Li
Variation of Arbuscular Mycorrhizal Fungi Communities Between Root and Rhizosphere Soil of Endangered Plant *Heptacodium miconioides* Along Elevation Gradient
Reprinted from: *J. Fungi* **2025**, *11*, 222, https://doi.org/10.3390/jof11030222 . . . . . **254**

Valentino Bergamaschi, Maria Teresa Valente and Rosario Muleo
Pomegranate Woody Mycobiota Associated with Wood Decay
Reprinted from: *J. Fungi* **2025**, *11*, 254, https://doi.org/10.3390/jof11040254 . . . . . **272**

Shengyao Zhou, Xiaojie Deng, Rajapakshalage Thashikala Nethmini, Huaxian Zhao, Qing He, Gonglingxia Jiang, et al.
Fungal Community Complexity and Stability in Clay Loam and Sandy Soils in Mangrove Ecosystems
Reprinted from: *J. Fungi* **2025**, *11*, 262, https://doi.org/10.3390/jof11040262 . . . . . **291**

Vitória Pinto Farias, Maria do Perpétuo Socorro Progene Vilhena, Antonio Walison Gondim-Vieira, Richard Bruno Mendes-Freire, Renan Domingues Pacheco, Braian Saimon Frota da Silva and Adriene Mayra da Silva Soares
Distribution Patterns of Wood-Decay Macrofungi (Agaricomycetes) in Floodplain Forest Islands of the Eastern Amazon
Reprinted from: *J. Fungi* **2025**, *11*, 288, https://doi.org/10.3390/jof11040288 . . . . . **306**

Yiwen Fu, Muxin Fan, Haiyan Qin, Zeyu Zhang, Shijun Liu, Shuwen Wu, et al.
Interactions Between Morel Cultivation, Soil Microbes, and Mineral Nutrients: Impacts and Mechanisms
Reprinted from: *J. Fungi* **2025**, *11*, 405, https://doi.org/10.3390/jof11060405 . . . . . **324**

Journal of *Fungi*

MDPI

Editorial

Fungal Communities in Various Environments

Nan Li [1,*] and Ke Dong [2,*]

[1] Key Laboratory of Climate, Resources and Environment in Continental Shelf Sea and Deep Sea of Department of Education of Guangdong Province, Department of Oceanography, Key Laboratory for Coastal Ocean Variation and Disaster Prediction, College of Ocean and Meteorology, Guangdong Ocean University, Zhanjiang 524088, China

[2] Major in Life Science, College of Convergence Science, Kyonggi University, 154-42, Gwanggyosan-ro, Yeongtong-gu, Suwon-si 16227, Gyeonggi-do, Republic of Korea

* Correspondence: nli0417@163.com (N.L.); dongke@kgu.ac.kr (K.D.)

1. Introduction

Fungi are fundamental components of ecosystems that play indispensable roles in biomass decomposition and nutrient cycling. Through complex symbiotic and antagonistic interactions with flora, fauna, and diverse microbial communities, fungi contribute to the regulation of ecosystem balance and the maintenance of biodiversity [1–3]. Fungal communities display significant variability in both their taxonomic composition and functional potential across diverse environmental contexts and spatiotemporal scales. These variations underscore the adaptive strategies employed by fungi in response to specific environmental perturbations and offer valuable insights into how environmental changes affect ecosystem functioning, resilience, and stability [4–7].

This Special Issue comprises 18 original research articles that collectively advance our understanding of the fungal diversity, ecological functions, and mechanisms governing community assembly across a range of ecosystems. The contributions specifically examine fungal community responses to environmental gradients, including variations in soil type, nutrient availability, elevation, and vegetation composition. Furthermore, the studies elucidate the complex interactions between the biotic and abiotic factors that govern fungal diversity, co-occurrence networks, and functional traits. Spanning ecosystems from mangrove forests to temperate woodlands, and from rhizosphere microbiomes to high-elevation sediments, the studies encompass molecular to ecosystem-level analyses, providing a comprehensive exploration of fungal community dynamics. In addition to synthesizing the core findings of these contributions, this editorial aims to contextualize them within a broader ecological framework, thereby bridging established knowledge with emerging research. Notable examples include the application of long-read sequencing technologies and the investigation of the ecological significance of particular fungal lineages in ecosystem processes. Moving beyond a mere summary, this editorial seeks to provide an integrative perspective that is firmly grounded in prior research while highlighting future directions for advancing fungal ecological studies.

2. Overview of Published Articles

A group of studies in this Special Issue illuminated the responses of fungal communities to environmental variability across diverse ecosystems, offering insights from multiple ecological perspectives. For instance, Contribution 1 investigated fungal co-occurrence

networks in clay versus sandy soils and found that networks in clayey soils exhibited significantly greater complexity and stability in mangrove ecosystems. Ammonium nitrogen (NH_4^+-N) and total nitrogen were identified as key drivers of the network structure. In clay soils, both fungal α-diversity and soil physicochemical properties jointly influenced the complexity and stability of communities, whereas in sandy soils, β-diversity played a more dominant role. Similarly, Contribution 2 examined the fungal community shifts during mangrove restoration and found that the dominant taxa and trophic modes differed significantly across successional stages. Although α-diversity remained relatively stable, β-diversity varied markedly. Total nitrogen and inorganic phosphorus strongly influenced α-diversity, while temperature and pH were key determinants of β-diversity. Trophic mode diversity was further driven by the total carbon, total nitrogen, and phosphorus fractions. Collectively, these findings highlight the central role of nutrient availability in shaping the structure and function of the fungal community. In forest ecosystems, Contribution 3 explored fungal functional dynamics during litter decomposition in a mixed plantation of Liquidambar formosana and Pinus thunbergii. The study reported that fungal functional guilds in mixed forests differ significantly from those in monoculture systems. The decomposition stage and litter type (leaf vs. twig) influenced enzymatic activity and nutrient-cycling gene abundance, with ectomycorrhizal fungi being more abundant in the mixed stands. In agricultural soils, Contribution 4 revealed that different *Morchella* species can distinctly restructure soil fungal communities and mineral nutrient availability through species-specific microbial and nutrient interactions. Functional shifts between the early and late stages of decomposition underscored the integrated effects of dominant tree species, litter quality, and decomposition time on fungal community composition and associated processes. Furthermore, Contribution 5 documented the contrasting responses of foliar endophytic fungi and bacteria to thinning intensity within temperate forest phyllosphere ecosystems. Fungal diversity and the complexity of co-occurrence networks increased in response to thinning; however, shifts in microbial communities were predominantly driven by indirect effects. Specifically, thinning altered the diversity of neighboring trees, which subsequently modified leaf traits, such as the specific leaf area and dry matter content, ultimately reshaping endophyte fungal assemblages.

Elevation gradients have emerged as consistent determinants of fungal community dynamics. For example, Contribution 6 reported divergent elevational trends in fungal diversity across three mountain ranges on the Korean Peninsula, each situated within a different climatic zone, underscoring the pronounced sensitivity of fungal communities to environmental gradients. Contribution 7 showed that in both the rhizosphere and root endosphere of the endangered Heptacodium miconioides, arbuscular mycorrhizal fungal (AMF) colonization rates and spore densities increased with elevation, whereas internal AMF diversity concomitantly declined. Contribution 8 further demonstrated that elevation-induced changes in the fungal community structure affected microbial residual carbon and soil organic carbon (SOC) stabilization, suggesting that the SOC retention capacity may decline in high-elevation environments due to shifts in fungal assemblages. Contribution 9 examined the elevational responses of fungal communities along the Yellow River in sedimentary ecosystems. They observed a decline with regard to the diversity with increasing altitude, whereas the co-occurrence networks became more complex and positively interactive at higher elevations. Community assembly processes are dominated by deterministic forces, particularly homogeneous selection, at higher elevations.

Rhizosphere microbiomes, as critical mediators of plant–soil interactions, are shaped by plant identity, developmental stage, and edaphic variables. Contribution 7 identified soil pH, available phosphorus, and total nitrogen as the main drivers of rhizosphere AMF

composition, whereas internal AMF communities were more responsive to nitrate, available potassium, and acid phosphatase activity. Contribution 10 compared the rhizosphere microbiota of cultivated wheat and its wild progenitor (Triticum dicoccoides) in agricultural systems and revealed largely conserved community structures, although cultivated wheat harbored more fungal pathogens, greater functional redundancy, and the enhanced enrichment of carbon and nitrogen cycling genes. In an urban context, Contribution 11 investigated ancient versus mature Ginkgo biloba trees in Shanghai and showed that ancient trees supported richer rhizosphere AMF communities dominated by Paraglomus and Glomus, with a higher abundance of viable AMF propagules. These findings emphasize the influence of pH and phosphorus on community assembly. Similarly, Contribution 12 studied eucalyptus plantations of varying stand ages in southern Jiangxi, noting shifts in AMF community composition across successional stages, driven by phosphorus, nitrogen, and soil bulk density.

Several studies have investigated the diversity and the ecological roles of specific fungal taxa in distinct ecosystems. For instance, Contribution 13 documented 88 species of Agaricomycetes wood-decaying fungi across the Amazonian floodplain forest islands, revealing pronounced community differentiation among the islands and underscoring the region's exceptional fungal diversity and conservation significance.

Moreover, Contribution 14 identified multiple previously unrecorded Myxomycetes species in Jilin Province, underscoring their importance in regional biodiversity surveys, while the pathogenic fungi associated with plants and arthropods also represented a significant area of focus. Contribution 15 identified Neofusicoccum parvum and Diaporthe spp. as key agents in complex pomegranate wood canker diseases, indicating multifactorial interactions between fungi and abiotic stressors. In the Angeles National Forest, Contribution 16 recorded 14 Phytophthora species, including the first report of P. taxon oakpath (subclade 8e), in both symptomatic and asymptomatic plants, especially near water sources—raising concerns about cryptic Phytophthora diversity and the risk of disease in drought-stressed Californian ecosystems. Contribution 17 describes *Gibellula floridensis*, a novel spider-pathogenic species identified in the subtropical habitats of north–central Florida. Their findings revealed broad yet habitat-dependent distributions of entomopathogenic fungi, prompting further inquiries into their occurrence, prevalence, and potential ecological functions beyond their interactions with arthropod hosts.

Finally, the rapid advancement of high-throughput sequencing technologies has substantially improved the resolution and scalability of fungal community analysis. Contribution 18 assessed the applicability of nanopore sequencing to fungal metabarcoding using ectomycorrhizal fungi in decayed *Fagus sylvatica* bark. The study proposed an "eNano" workflow and compared two taxonomic assignment strategies: reference matching based on the UNITE Species Hypotheses (SH) framework and de novo OTU clustering at 98% similarity. Both approaches effectively processed Nanopore data, with SH offering higher cross-study comparability, and OTU-based clustering performing better under $Q \geq 25$ thresholds. Ecological analysis revealed that the degree of wood decay significantly shaped the ectomycorrhizal community structure, with Laccaria amethystina and Tomentella sublilacina dominating the root tips of decayed logs. This study not only confirmed the feasibility of nanopore sequencing in fungal ecology but also demonstrated the role of decay-driven niche partitioning in forest ecosystems.

3. Outlook and Prospects

As the research on fungal communities across diverse ecosystems continues to advance, our understanding of their diversity patterns, environmental response mechanisms,

and ecological functions has grown substantially. However, several conceptual and methodological bottlenecks remain and new frontiers are rapidly emerging. First, both spatial and temporal scales of fungal ecological research require substantial expansion. Most current studies offer only a narrow view that constrains our understanding of broad-scale biogeographic patterns and long-term temporal dynamics [8]. Future research should prioritize long-term ecological monitoring and large-scale multisite comparisons to integrate macroecological processes with microbial-scale responses, thereby uncovering the spatiotemporal dynamics of fungal community assemblies and their contributions to ecosystem functionality. Second, greater emphasis must be placed on community-level functional attributes, because the transition from taxonomic diversity to functional trait-based approaches has emerged as a central theme in modern ecology. However, the fundamental aspects of fungal community function, such as functional redundancy, niche partitioning, and mechanistic coupling with carbon, nitrogen, and phosphorus cycling, remain insufficiently characterized [9–12]. Systematic experimental validation and theoretical modeling are essential for developing a coherent framework that links fungal community traits to biogeochemical processes [13,14]. Parallel efforts must focus on improving the annotation and empirical verification of putative functional genes in order to reduce dependence on computational predictions lacking experimental substantiation. Third, technological innovations continue to open new avenues for fungal ecological studies. Long-read sequencing platforms (e.g., Nanopore and PacBio) and single-cell omics provide enhanced taxonomic resolution and enable the detection of rare or cryptic taxa in complex environments [15,16]. Coupled with metabolomics, stable isotope tracing, and ecological stoichiometry, these approaches support a critical transition from merely identifying community composition ("who is there") to elucidating functional roles and activities ("what they are doing"). Such integration approaches are essential to develop a mechanistic understanding of the roles of fungi in ecosystems. Moreover, fungal ecology must be situated within a broader interdisciplinary framework because interactions between fungi and other organisms, including plants, animals, bacteria, and viruses, are fundamental for maintaining ecosystem resilience and network stability. Incorporating fungi into "multihabitat, multikingdom" interaction networks is crucial for achieving a systems-level perspective on ecological equilibrium. This integration is particularly urgent in the context of global environmental change because extreme climatic events, land-use transformations, and biological invasions may drive nonlinear or threshold responses in fungal communities, with cascading effects on ecosystem functions [17–21]. Balancing fungal bioprospecting with ecological conservation warrants further investigation. Numerous studies have highlighted the rich and often unique fungal diversity in sensitive environments such as tropical rainforests, mangroves, and sedimentary habitats. These taxa have untapped potential for applications in medicine, agriculture, and environmental remediation [22–25]. However, any exploitation of these resources must be preceded by rigorous assessments of their ecological vulnerability and sustainability, ideally embedded within risk-controlled conservation frameworks.

We anticipate that future fungal ecology will be increasingly defined through cross-scale, cross-system, and cross-disciplinary integration. Such approaches are essential for transitioning the field from foundational biodiversity assessments to deeper mechanistic explanations of ecosystem processes, ultimately supporting sustainable management and policy development in a changing world.

Funding: Nan Li is supported by the Guangdong Ocean University Innovative Team (Early-warning of marine disasters) (Grant number 2023KCXTD015); Guangxi Key Research and Development Program (Grant number AB24010109); and the Scientific Research Start Funds of Guangdong Ocean

University. Ke Dong is supported by the National Research Foundation of Korea (NRF) grant funded by the Korean government (MSIT) (Grant No. RS-2022-NR073058).

Conflicts of Interest: The authors declare no conflicts of interest.

List of Contributions:

1. Zhou, S.; Deng, X.; Nethmini, R.; Zhao, H.; He, Q.; Jiang, G.; Hou, Q.; Chen, Q.; Li, X.; Dong, K.; Li, N. Fungal Community Complexity and Stability in Clay Loam and Sandy Soils in Mangrove Ecosystems. *J. Fungi* **2025**, *11*, 262. https://doi.org/10.3390/jof11040262.
2. Shi, X.; Zhou, S.; Xu, L.; Nethmini, R.; Zhang, Y.; Huang, L.; Dong, K.; Zhao, H.; Pan, L. Shifts in Soil Fungal Community and Trophic Modes During Mangrove Ecosystem Restoration. *J. Fungi* **2025**, *11*, 146. https://doi.org/10.3390/jof11020146.
3. Meng, W.; Chang, L.; Qu, Z.; Liu, B.; Liu, K.; Zhang, Y.; Huang, L.; Sun, H. Dominant Tree Species and Litter Quality Govern Fungal Community Dynamics during Litter Decomposition. *J. Fungi* **2024**, *10*, 690. https://doi.org/10.3390/jof10100690.
4. Fu, Y.; Fan, M.; Qin, H.; Zhang, Z.; Liu, S.; Wu, S.; Wang, Y.; Yuan, X. Interactions Between Morel Cultivation, Soil Microbes, and Mineral Nutrients: Impacts and Mechanisms. *J. Fungi* **2025**, *11*, 405. https://doi.org/10.3390/jof11060405.
5. Liu, B.; Li, C.; Zhao, X.; Zhang, C.; He, X.; Qu, L.; Zhang, N. Contrasting Patterns of Fungal and Bacterial Endophytes Inhabiting Temperate Tree Leaves in Response to Thinning. *J. Fungi* **2024**, *10*, 470. https://doi.org/10.3390/jof10070470.
6. Chen, L.; Yu, Z.; Zhao, M.; Kerfahi, D.; Li, N.; Shi, L.; Qi, X.; Lee, C.; Dong, K.; Lee, H.; Lee, S. Elevational Variation in and Environmental Determinants of Fungal Diversity in Forest Ecosystems of Korean Peninsula. *J. Fungi* **2024**, *10*, 556. https://doi.org/10.3390/jof10080556.
7. Li, Y.; Luo, G.; Wu, S.; Yang, D.; Lv, P.; Jin, Z.; Li, J. Variation of Arbuscular Mycorrhizal Fungi Communities Between Root and Rhizosphere Soil of Endangered Plant Heptacodium miconioides Along Elevation Gradient. *J. Fungi* **2025**, *11*, 222. https://doi.org/10.3390/jof11030222.
8. Wang, J.; Yuan, J.; Ren, Q.; Zhou, L.; Zeng, H.; Miao, L.; Sun, Z.; Wan, F.; Yan, Y. The Fungal Community Structure Regulates Elevational Variations in Soil Organic Carbon Fractions in a Wugong Mountain Meadow. *J. Fungi* **2024**, *10*, 772. https://doi.org/10.3390/jof10110772.
9. Fang, K.; Xu, G.; Chen, X.; Li, J.; Cheng, Y.; Cheng, Y. Distribution Pattern and Assembly Process of Fungal Communities Along Altitude Gradient in Sediments of the Yellow River Basin. *J. Fungi* **2025**, *11*, 214. https://doi.org/10.3390/jof11030214.
10. Fang, J.; Blaschkauer, M.; Distelfeld, A.; Liu, Z.; Song, B.; Rachmilevitch, S.; Adams, J. Comparison of Rhizosphere Microbiomes Between Domesticated and Wild Wheat in a Typical Agricultural Field: Insights into Microbial Community Structure and Functional Shifts. *J. Fungi* **2025**, *11*, 168. https://doi.org/10.3390/jof11030168.
11. Mao, J.; Wang, Q.; Yang, Y.; Pan, F.; Zou, Z.; Su, X.; Wang, Y.; Liu, W.; Tang, Y. A Treasure Trove of Urban Microbial Diversity: Community and Diversity Characteristics of Urban Ancient Ginkgo biloba Rhizosphere Microorganisms in Shanghai. *J. Fungi* **2024**, *10*, 720. https://doi.org/10.3390/jof10100720.
12. Jiang, Y.; Mo, X.; Liu, L.; Lai, G.; Qiu, G. Changes in the Arbuscular Mycorrhizal Fungal Community in the Roots of Eucalyptus grandis Plantations at Different Ages in Southern Jiangxi, China. *J. Fungi* **2024**, *10*, 404. https://doi.org/10.3390/jof10060404.
13. Farias, V.; Vilhena, M.; Gondim-Vieira, A.; Mendes-Freire, R.; Pacheco, R.; da Silva, B.; Soares, A. Distribution Patterns of Wood-Decay Macrofungi (Agaricomycetes) in Floodplain Forest Islands of the Eastern Amazon. *J. Fungi* **2025**, *11*, 288. https://doi.org/10.3390/jof11040288.
14. Zhang, Z.; He, L.; Sun, Y.; Li, Z.; Yang, Y.; Zhai, C.; Stephenson, S.; Xie, X.; Li, Y.; Liu, P. New Species and Records Expand the Checklist of Cellular Slime Molds (Dictyostelids) in Jilin Province, China. *J. Fungi* **2024**, *10*, 834. https://doi.org/10.3390/jof10120834.
15. Bergamaschi, V.; Valente, M.; Muleo, R. Pomegranate Woody Mycobiota Associated with Wood Decay. *J. Fungi* **2025**, *11*, 254. https://doi.org/10.3390/jof11040254.

16. Fajardo, S.; Bourret, T.; Frankel, S.; Rizzo, D. Phytophthora Species and Their Associations with Chaparral and Oak Woodland Vegetation in Southern California. *J. Fungi* **2025**, *11*, 33. https://doi.org/10.3390/jof11010033.
17. Joseph, R.; Masoudi, A.; Valdiviezo, M.; Keyhani, N. Discovery of Gibellula floridensis from Infected Spiders and Analysis of the Surrounding Fungal Entomopathogen Community. *J. Fungi* **2024**, *10*, 694. https://doi.org/10.3390/jof10100694.
18. Dierickx, G.; Tondeleir, L.; Asselman, P.; Vandekerkhove, K.; Verbeken, A. What Quality Suffices for Nanopore Metabarcoding? Reconsidering Methodology and Ectomycorrhizae in Decaying Fagus sylvatica Bark as Case Study. *J. Fungi* **2024**, *10*, 708. https://doi.org/10.3390/jof10100708.

References

1. Gautam, A.K.; Verma, R.K.; Avasthi, S.; Sushma; Bohra, Y.; Devadatha, B.; Niranjan, M.; Suwannarach, N. Current insight into traditional and modern methods in fungal diversity estimates. *J. Fungi* **2022**, *8*, 226. [CrossRef] [PubMed]
2. Dai, Z.; Xiong, X.; Zhu, H.; Xu, H.; Leng, P.; Li, J.; Tang, C.; Xu, J. Association of biochar properties with changes in soil bacterial, fungal and fauna communities and nutrient cycling processes. *Biochar* **2021**, *3*, 239–254. [CrossRef]
3. Pawlowska, T.E. Symbioses between fungi and bacteria: From mechanisms to impacts on biodiversity. *Curr. Opin. Microbiol.* **2024**, *80*, 102496. [CrossRef] [PubMed]
4. Runnel, K.; Tedersoo, L.; Krah, F.S.; Piepenbring, M.; Scheepens, J.F.; Hollert, H.; Johann, S.; Meyer, N.; Bassler, C. Toward harnessing biodiversity–ecosystem function relationships in fungi. *Trends Ecol. Evol.* **2024**, *40*, 180–190. [CrossRef]
5. Brown, A.J.P. Fungal resilience and host–pathogen interactions: Future perspectives and opportunities. *Parasite Immunol.* **2023**, *45*, e12946. [CrossRef]
6. Philippot, L.; Griffiths, B.S.; Langenheder, S. Microbial community resilience across ecosystems and multiple disturbances. *Microbiol. Mol. Biol. Rev.* **2021**, *85*, e00026-20. [CrossRef]
7. Gupta, S.; Kumar, D. Challenges, Resilience, and Adaptation. In *Rhizosphere Revolution*; CRC Press: Boca Raton, FL, USA, 2024; pp. 325–344.
8. Patterson, C.W.; Drury, J.P. Interspecific behavioural interference and range dynamics: Current insights and future directions. *Biol. Rev.* **2023**, *98*, 2012–2027. [CrossRef]
9. Zhu, L.; Luan, L.; Chen, Y.; Wang, X.; Zhou, S.; Zou, W.; Han, X.; Duan, Y.; Zhu, B.; Li, Y.; et al. Community assembly of organisms regulates soil microbial functional potential through dual mechanisms. *Glob. Change Biol.* **2024**, *30*, e17160. [CrossRef]
10. Yang, D.; He, Z.; Lin, Y.; He, X.; Kong, X. Priority Colonization of Endophytic Fungal Strains Drives Litter Decomposition and Saprotroph Assembly via Functional Trait Selection in Karst Oak Forests. *Microorganisms* **2025**, *13*, 1066. [CrossRef]
11. Ogola, H.J.O.; Ijoma, G.N.; Edokpayi, J.N. Hydrological regime and niche partitioning drive fungal community structure and function in arid wetlands sediments of South Africa. *Environ. Sci. Pollut. Res.* **2025**, *32*, 15217–15231. [CrossRef]
12. Yang, N.; Zhang, Y.; Li, J.; Li, X.; Ruan, H.; Bhople, P.; Keiblinger, K.; Mao, L.; Liu, D. Interaction among soil nutrients, plant diversity and hypogeal fungal trophic guild modifies root-associated fungal diversity in coniferous forests of Chinese Southern Himalayas. *Plant Soil* **2022**, *481*, 395–408. [CrossRef]
13. Wan, J.; Crowther, T.W. Uniting the scales of microbial biogeochemistry with trait-based modelling. *Funct. Ecol.* **2022**, *36*, 1457–1472. [CrossRef]
14. Wasner, D. *Mechanisms That Link Climate, Soil Properties and Microbes to Macroscale Soil Organic Carbon Dynamics: Insights from a Geoclimatic Gradient*; ETH: Zurich, Switzerland, 2024.
15. Tedersoo, L.; Albertsen, M.; Anslan, S.; Callahan, B. Perspectives and benefits of high-throughput long-read sequencing in microbial ecology. *Appl. Environ. Microbiol.* **2021**, *87*, e00626-21. [CrossRef]
16. Ermini, L.; Driguez, P. The application of long-read sequencing to cancer. *Cancers* **2024**, *16*, 1275. [CrossRef]
17. Stern, N.; Stiglitz, J.; Taylor, C. The economics of immense risk, urgent action and radical change: Towards new approaches to the economics of climate change. *J. Econ. Methodol.* **2022**, *29*, 181–216. [CrossRef]
18. Mortimer, P.; Wanasinghe, D.N.; Mortimer, P.E. The impact of land use change on the diversity and emergence of fungal pathogens. *Authorea* **2023**, preprints. [CrossRef]
19. Bahlai, C.A.; Hart, C.; Kavanaugh, M.T.; White, J.D.; Ruess, R.W.; Brinkman, T.J.; Ducklow, H.W.; Foster, D.R.; Fraser, W.R.; Genet, H.; et al. Cascading effects: Insights from the US long term ecological research network. *Ecosphere* **2021**, *12*, e03430. [CrossRef]
20. Lázaro-Lobo, A.; Ervin, G.N. Wetland invasion: A multi-faceted challenge during a time of rapid global change. *Wetlands* **2021**, *41*, 64. [CrossRef]
21. Schmeller, D.S.; Urbach, D.; Bates, K.; Catalan, J.; Cogălniceanu, D.; Fisher, M.C.; Friesen, J.; Füreder, L.; Gaube, V.; Haver, M. Scientists' warning of threats to mountains. *Sci. Total Environ.* **2022**, *853*, 158611. [CrossRef]

22. Mohammad, I.; Ansari, M.R.; Bari, M.D.; Khan, M.S.; Kamal, M.A.; Anwar, M. Enhancing Food Safety: Adapting to Microbial Responses Under Diverse Environmental Stressors. *Trends Ecol. Indoor Environ. Eng.* **2025**, *3*, 12–26. [CrossRef]
23. Wadhwa, K.; Kapoor, N.; Kaur, H.; Abu-Seer, E.A.; Tariq, M.; Siddiqui, S.; Yadav, V.K.; Niazi, P.; Kumar, P.; Alghamdi, S. A Comprehensive Review of the Diversity of Fungal Secondary Metabolites and Their Emerging Applications in Healthcare and Environment. *Mycobiology* **2024**, *52*, 335–387. [CrossRef] [PubMed]
24. Singh, M.; Singh, D.; Rai, P.K.; Suyal, D.C.; Saurabh, S.; Soni, R.; Giri, K.; Yadav, A.N. Fungi in remediation of hazardous wastes: Current status and future outlook. In *Recent Trends in Mycological Research: Volume 2: Environmental and Industrial Perspective*; Springer: Cham, Switzerland, 2021; pp. 195–224.
25. Abd-Elsalam, K.A.; Almoammar, H.; Hashem, A.H.; AbuQamar, S.F. Endophytic Fungi: Exploring Biodiversity and Bioactive Potential. In *Fungal Endophytes Volume I: Biodiversity and Bioactive Materials*; Springer: Cham, Switzerland, 2025; pp. 1–42.

Disclaimer/Publisher's Note: The statements, opinions and data contained in all publications are solely those of the individual author(s) and contributor(s) and not of MDPI and/or the editor(s). MDPI and/or the editor(s) disclaim responsibility for any injury to people or property resulting from any ideas, methods, instructions or products referred to in the content.

Journal of *Fungi*

MDPI

Article

Changes in the Arbuscular Mycorrhizal Fungal Community in the Roots of *Eucalyptus grandis* Plantations at Different Ages in Southern Jiangxi, China

Yao Jiang [1], Xiao-Yong Mo [1], Li-Ting Liu [2,*], Guo-Zhen Lai [2] and Guo-Wei Qiu [3]

[1] College of Forestry and Landscape Architecture, South China Agricultural University, Guangzhou 510642, China; jiangyy@scbg.ac.cn (Y.J.); motree@163.com (X.-Y.M.)
[2] Jiangxi Academy of Forestry, Nanchang 330000, China; laiguozhen@jxlky.cn
[3] Jinpenshan Forest Farm, Xinfeng 341600, China; xfjpslc@163.com
* Correspondence: more_trees@163.com

Abstract: Eucalyptus roots form symbiotic relationships with arbuscular mycorrhizal (AM) fungi in soil to enhance adaptation in challenging environments. However, the evolution of the AM fungal community along a chronosequence of eucalypt plantations and its relationship with soil properties remain unclear. In this study, we evaluated the tree growth, soil properties, and root AM fungal colonization of *Eucalyptus grandis* W. Hill ex Maiden plantations at different ages, identified the AM fungal community composition by high-throughput sequencing, and developed a structural equation model among trees, soil, and AM fungi. Key findings include the following: (1) The total phosphorus (P) and total potassium (K) in the soil underwent an initial reduction followed by a rise with different stand ages. (2) The rate of AM colonization decreased first and then increased. (3) The composition of the AM fungal community changed significantly with different stand ages, but there was no significant change in diversity. (4) *Paraglomus* and *Glomus* were the dominant genera, accounting for 70.1% and 21.8% of the relative abundance, respectively. (5) The dominant genera were mainly influenced by soil P, the N content, and bulk density, but the main factors were different with stand ages. The results can provide a reference for fertilizer management and microbial formulation manufacture for eucalyptus plantations.

Keywords: stand ages; soil properties; *Paraglomus*; *Glomus*

1. Introduction

Arbuscular mycorrhizal (AM) fungi, forming symbiotic relationships with the roots of approximately 80% of vascular plants globally, act as conduits for material transport between plants and soil [1]. While deriving organic nutrients from plants and soil, AM fungi enhance the absorption of water and mineral elements by plants in the soil [2,3], aiding in stress alleviation [4,5]. The significant application potential of AM fungi in enhancing forest quality, mitigating adverse afforestation effects, and contributing to ecological restoration has garnered increasing attention [6–8].

The establishment of mycorrhiza in eucalyptus has been demonstrated in many studies [9–11], and this symbiotic relationship plays an important role in promoting plant growth and boosting productivity [12]. The influence of AM fungi on plant growth is contingent on their community composition [13,14]. Finding functional symbiotic AM strains and further manufacturing microbial formulations are key steps toward commercial application. However, the reliability of the traditional morphological identification method is low [15,16]. At present, the understanding of the AM fungal community composition of eucalyptus species roots in the natural environment is incomplete. High-throughput sequencing technology based on DNA extraction can effectively improve the accuracy of

fungal identification [17], providing a way to supplement and improve the AM fungal classification system of eucalyptus roots.

Some studies have found that the community structure of AM fungi in artificial forests tends to change regularly as stand ages increase [18,19]. This is partly due to the changes in the physiological characteristics and growth states of plants at different stand ages, which affect the ability of AM fungi to colonize roots [20] and the allocation of carbon from plants to AM fungi [21], thereby altering the AM fungal community structure. Additionally, as plantations mature, the availability of soil resources for AM fungi also changes continuously. Research has shown that factors such as the soil pH value [22] and nutrient content [23,24] significantly influence the composition of AM fungal communities. Despite these findings, the relationships among the AM fungal community, tree growth, and soil properties remain unclear.

The hilly region of southern Jiangxi, China constitutes a vital segment of the red soil belt in southern China, where severe soil erosion prevails due to overexploitation and recurrent heavy rainfall [25,26]. *Eucalyptus grandis* W. Hill ex Maiden is a prominent afforestation tree with robust adaptability, rapid growth rates, and high productivity, which can create huge economic and ecological benefits for the local area [27,28]. Understanding the changes in the AM fungal community composition of the *E. grandis* root and its influencing factors can provide a reference for the management of plantations in the hilly areas of southern Jiangxi. Consequently, this study focused on six monoculture *E. grandis* plantations of different ages (2, 3, 5, 6, 7, and 9 years old) in the hilly region of southern Jiangxi Province. We investigated tree growth, analyzed soil physicochemical properties, determined root AM fungal colonization, and identified the composition of the AM fungal community by high-throughput sequencing. Subsequently, we analyzed the correlations among tree growth status, soil properties, and AM fungal communities in *E. grandis* plantations of different ages, and we established a structural equation model to reveal the causality of the soil–tree–mycorrhiza system. Our objective was to address the following specific questions: Is there a difference in AM fungal community structure in *E. grandis* roots of different ages? If so, are changes in the AM fungal community structure with age related to changes in soil properties?

2. Materials and Methods

2.1. Experimental Site and Sampling

This study was conducted at plantations in southern Jiangxi Province, China (114°32′–115°59′ E, 24°42′–26°33′ N; elevation between 220 and 360 m). This study area lies on the southern edge of Central Asia and is characterized by a subtropical humid monsoon climate, with an annual average temperature of 18.9 °C and a frost-free period of 287 d. The mean annual precipitation is 1605 mm, mostly between April and June (China Meteorological Data Service Center). The soil at the study site has a loamy texture and is colonized by native grasses and forbs (such as *Miscanthus floridulus* (Labill.) Warburg ex K. Schumann, *Dicranopteris dichotoma* (Thunb.) Bernh., and *Rubus innominatus* S. Moore). *E. grandis* plantations are widely planted in the study area, and the stand spacing is usually 1.67 m × 4 m.

All planted areas with relatively consistent slopes (25–35°) and uniform management modes were selected. Besides adding base fertilizer in the year of planting, these plantations received a topdressing for three consecutive years. The ratio of N, P, and K in these fertilizers is 15:15:15. These woodlands are effectively protected by cutting prohibitions and fire prevention. The chronosequence of *E. grandis* plantations includes six ages (2, 3, 5, 6, 7, and 9 years old). Two to three stands were selected for each stand age, and 20 m × 20 m plots were set for each stand, constituting 17 plots in total. The average tree height and diameter at breast height (DBH) were measured in each plot.

Three sampling points with a distance of more than 10 m between them were randomly selected for each sample plot, and soil samples with a depth of more than 0–20 cm were drilled with a ring knife for bulk density measurement. At the same time, 500 g soil

samples were taken from each sampling point for other physical and chemical properties' measurements. All samples were stored in a foam box with an ice pack and transported to the laboratory. Five trees were randomly selected from each plot, the fine roots were carefully collected along the taproots of the trees, and then the fine roots collected in the plot were mixed into one sample. The fine roots were cleaned with running water in the laboratory, passed through a 0.2 mm sieve, and dried with a towel. The soil properties of *Eucalyptus grandis* plantations with different stand ages are shown in Table 1.

Table 1. The soil properties of *Eucalyptus grandis* plantations with different stand ages.

Stand Age (Years)	pH Value	Soil Moisture (%)	Bulk Density	Sand Content % (2–0.05 mm)	Powder Content % (0.05–0.002 mm)	Clay Content % (<0.002 mm)
2a	4.74 ± 0.22	0.20 ± 0.02	1.38 ± 0.03	46.33 ± 3.79	35.00 ± 5.20	18.67 ± 1.53
3a	4.22 ± 0.00	0.24 ± 0.04	1.36 ± 0.09	32.50 ± 4.95	42.00 ± 2.83	25.50 ± 2.12
5a	4.52 ± 0.03	0.22 ± 0.02	1.37 ± 0.08	31.33 ± 2.08	45.67 ± 4.16	23.00 ± 3.61
6a	4.65 ± 0.07	0.23 ± 0.03	1.30 ± 0.06	46.67 ± 17.24	31.00 ± 7.94	22.33 ± 9.50
7a	4.71 ± 0.33	0.22 ± 0.07	1.42 ± 0.11	44.67 ± 9.02	34.33 ± 3.21	21.00 ± 6.24
9a	4.55 ± 0.07	0.23 ± 0.03	1.32 ± 0.11	45.00 ± 5.57	33.67 ± 8.02	21.33 ± 2.89

Note: Data expressed as mean ± standard deviation.

2.2. Soil Properties

The soil water content was measured using the AOAC [29] method, and the bulk density was calculated. Soil pH was measured using the glass electrode method. Total nitrogen (N), total phosphorus (P), and total potassium (K) contents were quantified using Kelvin-distillation titration, sodium hydroxide fusion–Mo-Sb colorimetric, and sodium hydroxide fusion–flame atomic absorption spectrometry, respectively [30]. The available N, P, and K contents were quantified by the alkali diffusion method, hydrochloric acid–ammonium fluoride extraction–Mo-Sb colorimetric, and ammonium acetate extraction–flame atomic absorption spectrometry. In addition to the common soil elements mentioned above, boron (B) is widely believed to be involved in the growth of eucalyptus trees, especially in root nutrition [31,32]. The available B content was measured using the curcumin colorimetry method [33].

2.3. AM Fungi Colonization

According to the method of Phillips and Hayman [34], partial root samples were alkalified in 10% KOH solution for 3 h (water bath at 90 °C), then bleached with 3% H_2O_2 for 20 min, acidified with 2% HCl for 30 min, and finally dyed with 0.1% acid fuchsia at 60 °C for 1 h. The stained root samples were made into slides, and AM fungi colonization was measured [35]. One hundred views for each slide were randomly observed using a compound microscope at 200× magnification. The presence of hyphae or arbuscules was recorded with each view, and the results were calculated using the following formulas: hyphal colonization rate = the number of views with a hyphal structure/total number of views; arbuscular colonization rate = the number of views with arbuscular structure/total number of views.

2.4. Sequencing and Data Analysis

2.4.1. Sequencing

DNA was extracted from eucalyptus roots using an EZNA Gel Extraction Kit (Omega, Irving, TX, USA). DNA integrity and purity were monitored on 1% agarose gels. DNA concentration and purity were measured using the NanoDrop One at the same time. 18SrRNA genes of distinct regions (V4/V5) were amplified using a specific primer (528F and 706R) with a 12 bp barcode [36,37]. PCR reactions, containing 25 μL 2x Premix Taq, 1 μL each primer (10 mM), and 3 μL DNA (20 ng/μL) template in a volume of 50 μL, were

amplified by thermocycling: 5 min at 94 °C for initialization; 30 cycles of 30 s denaturation at 94 °C, 30 s annealing at 52 °C, and 30 s extension at 72 °C; followed by 10 min final elongation at 72 °C. Three replicates per sample and each PCR product of the same sample were mixed, with the PCR instrument BioRad S1000. The length and concentration of the PCR product were detected by 1% agarose gel electrophoresis. Samples with bright main strips could be used for further experiments. PCR products were mixed in equidense ratios according to the GeneTools Analysis Software (Version 4.03.05.0, SynGene). Then, the mixture of PCR products was purified with an EZNA Gel Extraction Kit. Sequencing libraries were generated using a NEBNext® Ultra™ DNA Library Prep Kit for Illumina® (New England Biolabs, Ipswich, MA, USA) and index codes were added. The library quality was assessed on a Qubit@ 2.0 Fluorometer and Agilent Bioanalyzer 2100 system. At last, the library was sequenced on an IlluminaHiseq2500 platform, and 250 bp paired-end reads were generated.

2.4.2. Sequencing Data Processing

Quality filtering on the paired-end raw reads was performed under specific filtering conditions to obtain high-quality clean reads according to the Trimmomatic (V0.33, http://www.usadellab.org/cms/?page=trimmomatic, accessed on 23 April 2024) quality-controlled process. Paired-end clean reads were merged using FLASH (V1.2.11, https://ccb.jhu.edu/software/FLASH/, accessed on 23 April 2024) according to the relationship of the overlap between the paired-end reads; when at least 10 of the reads overlapped the read generated from the opposite end of the same DNA fragment, the maximum allowable error ratio of the overlap region was 0.1, and the spliced sequences were called Raw Tags. Sequences were assigned to each sample based on their unique barcode and primer using Mothur software (V1.35.1, http://www.mothur.org, accessed on 23 April 2024), after which the barcodes and primers were removed and the effective Clean Tags were obtained.

2.4.3. OTU Cluster and Species Annotation

Sequence analyses were performed by Usearch software (V8.0.1517, http://www.drive5.com/usearch/, accessed on 23 April 2024). Sequences with ≥97% similarity were assigned to the same operational taxonomic units (OTUs). The most frequently occurring sequence was extracted as representative for each OTU and screened for further annotation. During clustering, a Usearch can remove the chimera sequence and singleton OTU at the same time. For each representative sequence, the Silva database (https://www.arb-silva.de/, accessed on 23 April 2024) was used to annotate taxonomic information (setting the confidence threshold to default to ≥0.5). We removed the polluted OTUs and obtained the number of effective tags and an OTU taxonomy synthesis information table for the final analysis. OTU abundance information was normalized using a standard sequence number corresponding to the sample with the fewest sequences. Subsequent analyses were performed based on these outputted normalized data. Alpha diversity was applied in analyzing the complexity of species diversity for a sample through 5 indices: observed species (I_{obs}, the number of OTUs measured in the sample), Chao1 (I_{chao1}, see Equation (1)), dominance (I_{dom}, see Equation (2)), Shannon index (I_{shn}, see Equation (3)), and Simpson index (I_{sim}, see Equation (4)). All these indices in our samples were calculated with QIIME (V1.9.1) and displayed with R software [38].

$$I_{chao1} = I_{obs} + \frac{n_1(n_1 - 1)}{2(n_2 + 1)} \quad (1)$$

where n_1 is the number of OTUs containing only one sequence; and n_2 is the number of OTUs containing only two sequences.

$$I_{dom} = \sum p_i^2 \quad (2)$$

where p_i represents the proportion of the *i*-th OTU in the total OTUs.

$$I_{shn} = -\sum_{i=1}^{I_{obs}} \frac{n_i}{N} \ln \frac{n_i}{N} \quad (3)$$

$$I_{sim} = 1 - \frac{\sum_{i=1}^{I_{obs}} n_i(n_i - 1)}{N(N-1)} \quad (4)$$

where n_i is the number of OTUs containing *i*-th sequences. N is the number of all sequences.

2.5. Statistical Analysis

One-way ANOVA and multiple comparisons were used to detect the differences in tree height and DBH of trees at different ages. The changes in soil properties and mycorrhizal colonization rates with age were analyzed using regression analysis. To test the significance of the variation in AM fungal community composition with different stand ages, an analysis of similarities was conducted using the function "ANOSIM" in the R package VEGAN [39]. The relative abundance data for AM fungi were visualized using non-metric multidimensional scaling (implemented using the R package VEGAN) to elucidate the dissimilarities in AM fungal community composition across sites along the chronosequence [39]. Pearson's correlation analysis evaluated the relationship between age-affected soil properties and AM fungal attributes. Structural equation modeling was used to show a causal relationship between these variables, and the significance of the standardized regression weights was determined [40,41]. Structural equation modeling was performed using the LAVAAN package in R [42]. In addition, we used the Chi-square/df, *p*-value, and CFI index to examine the overall model fit. The model fit the data well when the Chi-square/df was less than 2, the *p*-value was more than 0.05, or the CFI index was more than 0.9.

3. Results

3.1. Growth Statuses of Eucalypts with Different Stand Ages

The one-way ANOVA showed that there were significant differences in tree height ($p < 0.01$) and DBH ($p < 0.01$) among different age groups. The results of multiple comparisons using the LSD method (Figure 1) showed that the mean tree height and DBH first increased rapidly and then slowly with an increase in stand age. There were significant differences in tree height between 2 and 3 years old and between 3 and 5 years old and in DBH between 3 and 5 years old.

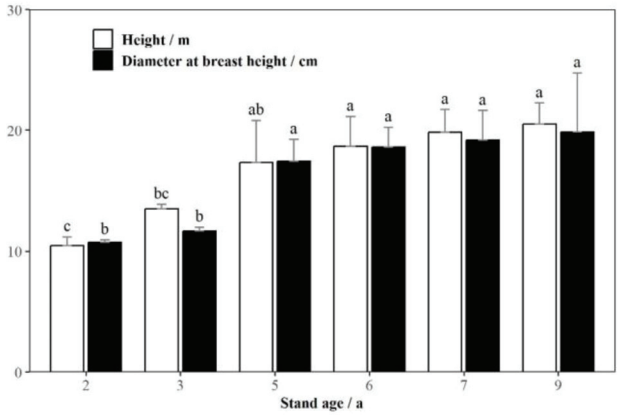


Figure 1. Heights and diameters at breast height of *Eucalyptus grandis* with different stand ages. Note: Different letters show significant differences at the $p < 0.05$ level according to the LSD test.

3.2. Soil Properties of Eucalypt Plantations with Different Stand Ages

The regression analysis showed that with the increase in stand age, the contents of total P ($R^2 = 0.37$, $p < 0.05$) and total K ($R^2 = 0.42$, $p < 0.05$) in the soil decreased first and then increased. The contents of these two elements were the lowest at 5 and 6 years old, respectively. Soil pH, bulk density, and the contents of available B, total N, N, P, and K did not change significantly (Figure 2).

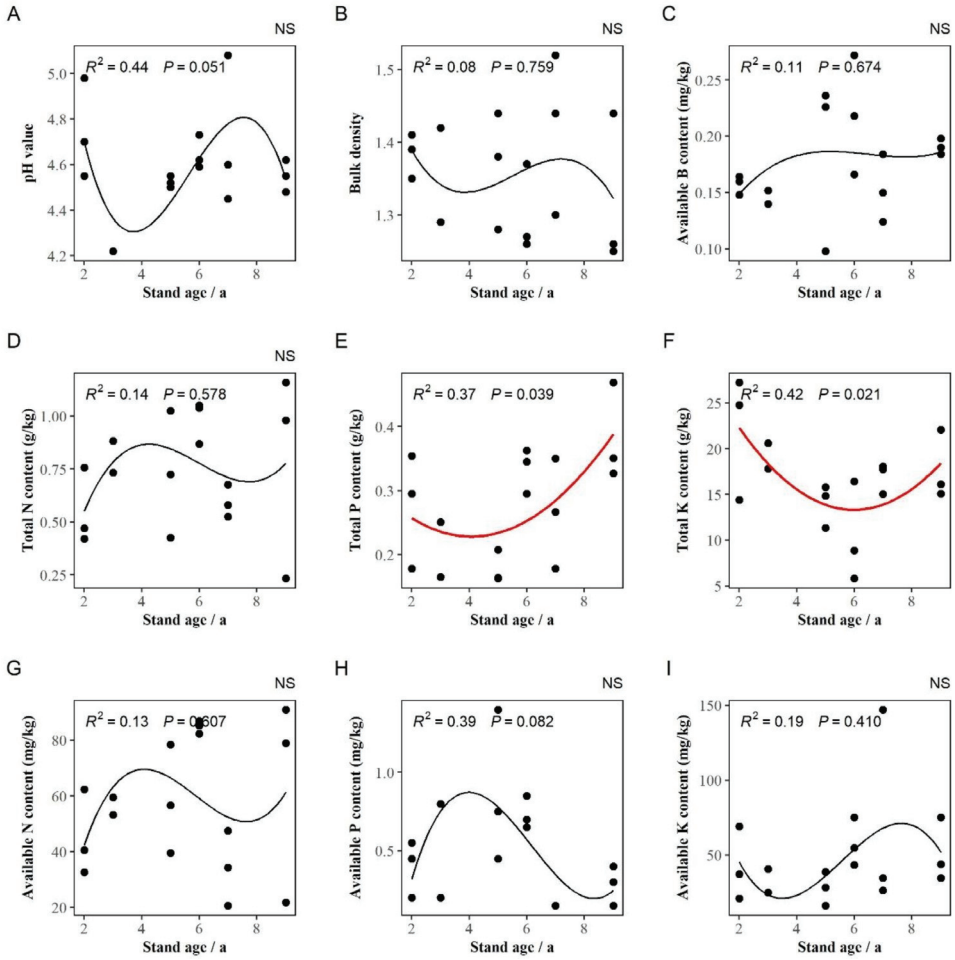


Figure 2. Changes in soil properties in *Eucalyptus grandis* plantations with different stand ages. (**A**–**I**) represent the change in soil pH value, bulk density, available boron content, total nitrogen content, total phosphorus content, total potassium content, available nitrogen content, available phosphorus content, and available potassium content, respectively. Note: The R^2 and *p*-values at the top of the images represent the correlations and significance levels of the regression analysis, respectively. NS represents non-significant regressions with different stand ages ($p \geq 0.05$). The red curves represent significant regression results.

3.3. AM Fungal Colonization Rates in the Roots of Eucalypts with Different Stand Ages

The regression analysis showed that the hyphal ($R^2 = 0.40$, $p < 0.05$) and arbuscular ($R^2 = 0.45$, $p < 0.05$) colonization rates in roots of eucalypts decreased first and then increased with the increase in stand age and that the arbuscular colonization rate decreased slightly at 9-year-old stands (Figure 3). The highest hyphal and arbuscular colonization rates were found in 2-year-old stands, reaching 0.81 and 0.58, respectively. The lowest hyphal and arbuscular colonization rates were 0.62 and 0.35, respectively, at 5 years old.

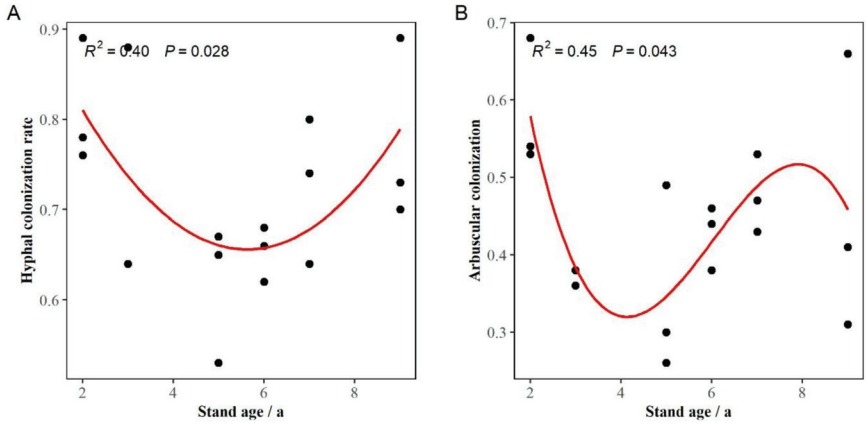


Figure 3. Changes in AM fungal colonization rate in the roots of *Eucalyptus grandis* with different stand ages. (**A**,**B**) represent the change in hyphal and arbuscular colonization rates, respectively. Note: The R^2 and *p*-values at the top of the images represent the correlations and significance levels of the regression analysis, respectively. The red curves represent significant regression results.

3.4. AM Fungal Identification and Community Composition with Different Stand Ages

Through high-throughput sequencing, more than 50,000 eligible 18S sequences were obtained. Of these sequences, 2103 OTUs were annotated after being classified according to the 97% similarity criterion. Among these, 1750 OTUs were identified at the genus level. Through the identification of the AM fungal community in roots, a total of one phylum, one class, four orders, seven families, and nine genera were found (Figure 4). The AM fungal communities were composed predominantly of members of the genus *Paraglomus* (70.1%), followed by *Glomus* (21.8%). Along the chronosequence, the relative abundance of *Paraglomus* in AM fungal communities showed a significant difference ($F = 4.76$, $p < 0.05$), and that of *Glomus* showed a highly significant difference ($F = 8.58$, $p < 0.01$). The 6-year-old stands were significantly different from other ages, with the lowest *Paraglomus* abundance (43%) and the highest *Glomus* abundance (52%). ANOSIM showed that the AM fungal community composition was significantly affected by stand age ($R^2 = 0.52$, $p < 0.01$). Non-metric multidimensional scaling analysis showed clear clustering of the AM fungal communities in the roots of *E. grandis* at different stand ages (Figure 5). However, the diversity of the AM fungal community was not affected by stand age in this study.

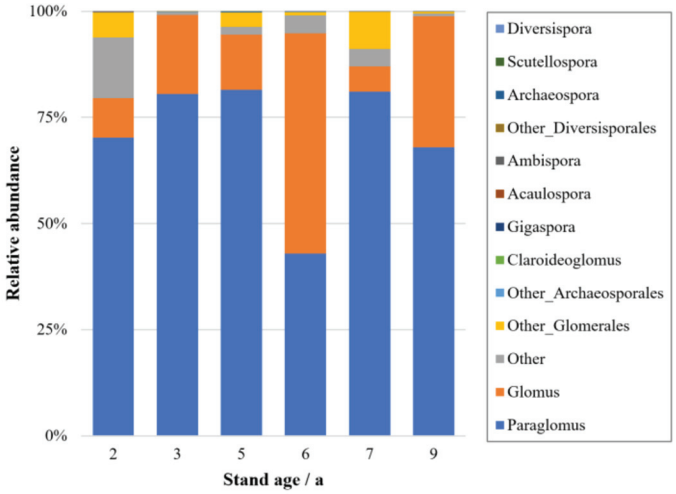


Figure 4. Proportions of AM fungal genera in roots of *Eucalyptus grandis* with different stand ages based on the relative abundance of genera. Note: Some genera with very low relative abundance are labeled only with their orders, and "Other_" is added as the prefix.

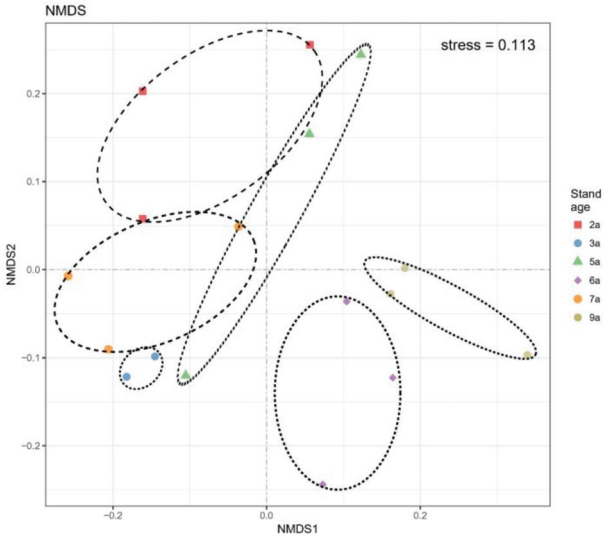


Figure 5. Non-metric multidimensional scaling plots of the variation in the AM fungal community, based on the profiles of the relative abundance of OTUs.

3.5. Relationships among Plant Growth, Soil Properties, and AM Fungal Attributes

The correlational relationships between the age-affected soil properties and AM fungal attributes are shown in Figure 6. The relative abundances of *Glomus* and *Paraglomus* were significantly negatively correlated. The relative abundance of *Paraglomus* was significantly negatively correlated with soil total P and available N content and significantly positively correlated with soil bulk density. The relative abundance of *Glomus* was positively correlated with soil total P and the available N content but negatively correlated with total K and the bulk density. Both the hyphal and arbuscular colonization rates were positively correlated with the soil total K. In addition, the arbuscular colonization rate was positively correlated with soil pH and negatively correlated with total N and the available N content. Both the Shannon index and Chao1 index were positively correlated with soil available B.

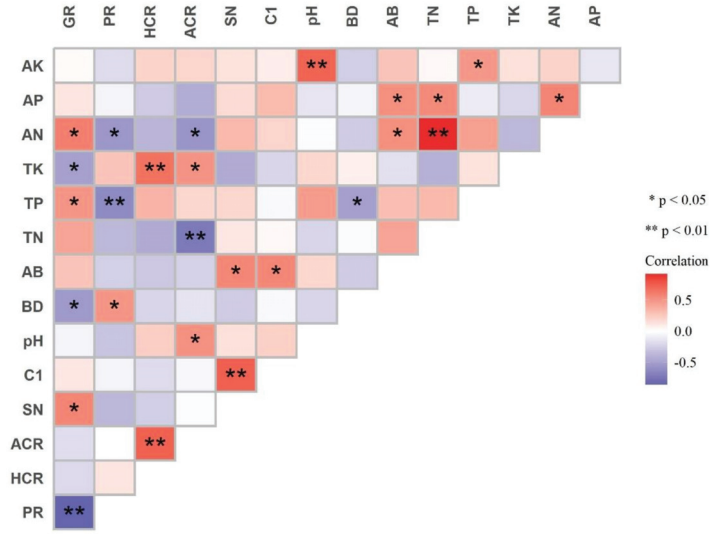


Figure 6. Pearson correlations between age-affected soil properties and AM fungal attributes in *Eucalyptus grandis* plantations. Note: *: significant at $p < 0.05$; **: significant at $p < 0.01$; PR: *Paraglomus* abundance; GR: *Glomus* abundance; HCR: hyphal colonization rate; ACR: arbuscular colonization rate; SN: Shannon index; C1: Chao1 index; pH: pH value; BD: bulk density; AB: available B; TN: total N; TP: total P; TK: total K; AN: available N; AP: available P; AK: available K.

A structural equation model was used to analyze the relationship between the dominant genera, tree growth, and soil properties. The model analysis results indicated the following (Figure 7): (1) In 2–6 years of eucalypt plantations, the soil total P, total N, and available N contents were continuously consumed with the increase in tree height. The decrease in total P and available N increased the abundance of *Paraglomus* but decreased the abundance of *Glomus*. (2) The soil total P content at 7–9 years of eucalypt plantations gradually accumulated with the increase in DBH, resulting in decreased *Paraglomus* abundance and *Glomus* abundance. The growth of DBH also directly reduced *Paraglomus* abundance, while the decrease in soil bulk density increased *Paraglomus* abundance.

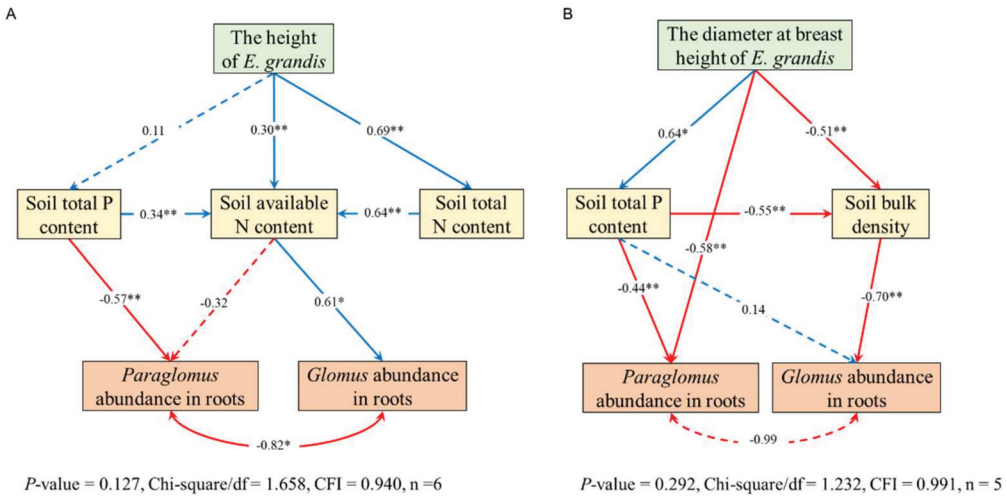


Figure 7. Structural equation model of relationships among age-affected growth statuses, soil properties, and AM fungal attributes in *Eucalyptus grandis* plantations. (**A**,**B**) show the model in 2–6 years plantations and 7–9 years plantations, respectively. Note: The lines among these parameters are the standardized regression weights (*: significant at $p < 0.05$; **: significant at $p < 0.01$). Red solid lines: the standardized regression weights are negative; blue solid lines: the standardized regression weights are positive; dotted lines: the standardized regression weights are insignificant ($p > 0.05$).

4. Discussion

Our analysis of the growth statuses of eucalypt plantations of different ages showed that the growth of eucalypts underwent rapid development and a slow-down stage. In the rapid development stage (2–6 years old), the main change in soil properties was that the total P and total K contents gradually decreased with the increase in stand age, and the lowest values appeared in the 5- or 6-year-old stands. This may have been due to the high metabolism of the trees during this period and the high consumption of nutrients [43]. At the same time, the contents of available N and P in the soil gradually increased. With the increase in stand age, the increase in soil microorganisms and root exudates in the understory promoted the conversion of nutrients from insoluble to soluble [44]. The reason for the decrease in the available K content is that during rapid development, the maintenance of leaf photosynthetic capacity [45] and the improvement of water use efficiency [46] make the consumption of K much higher than that of other elements. Regarding AM fungal properties, hyphal and arbuscular colonization rates decreased gradually with the increase in stand age and dropped to the lowest for 5-year-old stands. This was because the survival of AM fungi depends on the carbon source provided by plants [47]. In the period of vigorous growth, the nutrient allocation of trees is more inclined to go to the aboveground parts, while the carbon allocation of the underground parts is gradually reduced [48]. During the growth-slowing stage (7–9 years old), the total P and K contents in the soil gradually increased with the stand age. Soil microorganisms and root exudates decomposed the increasing understory litter and returned to the soil as nutrients [49]. At the same time, hyphal and arbuscular colonization rates increased gradually because the increased numbers of lateral and fibrous roots provided more sites for AM fungi to colo-

nize [50]. Currently, most eucalypt plantations in the study area have a five-year rotation period, meaning that the stand is cut down before nutrients are returned to the soil as litter. Incomplete nutrient cycling reduces the net nutrient supply and the amount of mycelium required for the next growth in the soil, increasing the dependence on fertilizer [51,52]. Therefore, proper crop rotation expansion is an important measure for the sustainable management of eucalypt plantations.

Through high-throughput sequencing of AM fungi in roots of *E. grandis*, one phylum, one class, four orders, seven families, and nine genera were identified. Among these, the major genera, such as *Acaulospora*, *Archaeospora*, *Gigaspora*, *Glomus*, *Paraglomus*, and *Scutellospora*, have been shown to form symbiotic structures with eucalypts [53,54]. *Ambispora*, *Claroideoglomus*, and *Diversispora* are also found in eucalypt plantations [55,56]. Most have studies confirmed the dominant position of *Glomus* in the AM fungal community in eucalyptus roots [57,58]. However, in this study, the relative abundance of *Paraglomus* (70.1%) was higher than that of *Glomus* (21.8%) in the AM fungal community in the roots of *E. grandis* in southern Jiangxi, China. One reason could be that the spores of *Paraglomus* are very similar to those of some *Glomus*, meaning the presence of *Paraglomus* species may go unrecognized by traditional spore-based AM fungal identification techniques [59]. Other studies have suggested that Paraglomerales is usually distributed in patches, which may explain the large differences in fungal abundance detected at different locations [60]. The relative abundance of *Paraglomus* was significantly superior in almost all stand ages of *E. grandis* plantations, which may also be related to the host tree's preference for AM fungi [61]. The relative abundance of *Glomus* was greater than that of *Paraglomus* only at 6 years old, possibly because *Glomus* is more competitive than other genera when stand growth slows and the carbon allocation to underground parts decreases [62]. This kind of genus is characterized by rapid colonization and various colonization routes [63]. Other studies have also shown that plants can adapt to new environments by increasing symbiotic structures with more competitive dominant species [64,65]. Our study revealed significant differences in the compositions of the AM fungal community in the roots of eucalypts with different stand ages, which was consistent with the findings of other scholars [11,66,67]. In this study, the diversity of AM fungal communities did not change significantly over time, which is related to maintaining the diversity of aboveground plant communities [68]. In addition to AM fungi, *E. grandis* roots also form symbiotic structures with ectomycorrhizal fungi [69]. Further studies should consider the contribution of different mycorrhizal types and their community composition to ecosystem functioning.

The correlation analysis between soil properties and AM fungal attributes under the influence of age indicated that the mycorrhizal colonization rate was affected by soil pH, total K, total N, and the available N content. In other studies, the rhizosphere environment has also been found to affect the mycorrhizal colonization process [70], but the specific mechanism is still unclear. Both the Shannon index and Chao1 index were positively correlated with available soil B, indicating that the diversity of AM fungi may be mainly affected by soil trace elements. Correlation analysis revealed the basic relationship between soil properties and AM fungal attribute variables. On this basis, the structural equation model further demonstrated the relationship between tree growth, soil properties, and dominant genera at different stages. The total P content in the soil was always the main factor limiting the relative abundance of *Paraglomus*. The relative abundance of *Glomus* was mainly affected by the available soil N content at the rapid growth stage (2a–6a) and was significantly negatively correlated with soil bulk density at the growth slow-down stage (7a–9a). This is consistent with the view of most studies that AM fungi generally have a high affinity for P and N elements [71,72]. Numerous studies have shown that P is the main limiting factor in plantations in southern China [73,74]. AM fungi can absorb P from the soil through the mycelium network, which helps trees grow in a poor P environment [75]. Studies have shown that the mycelia of *Glomus* tend to be very thin and that these heavily extended and dispersed epiphytic mycelia can stabilize soil aggregates under a low soil bulk density [76] and improve soil water relations. Our structural equation

model revealed the effects of soil properties on the AM fungal community at different growth stages. The findings are particularly important for optimizing fertilization strategies and introducing AM fungal inoculants at specific growth stages. In conclusion, changes in the AM fungal community composition in tree roots can be attributed to changes in soil properties caused by tree growth. Ideally, future research should focus on building a specific understanding of the functional properties of AM fungal species, to enable the precise use of AM fungal agents.

5. Conclusions

This study delved into the growth dynamics and soil properties of monospecific *E. grandis* at varying ages, employing high-throughput sequencing technology to unravel the composition of the root AM fungal community. Through comprehensive statistical analyses, we scrutinized the interplay between growth statuses, soil properties, and the successional patterns of the root AM fungal community in eucalypt plantations of diverse ages. The findings revealed that with the increase in stand age, the soil total phosphorus (P) and total potassium (K) decreased first and then increased; the rate of AM colonization decreased first, reached the lowest in 5a stands, and then increased; there was no significant change in the community diversity of root AM fungi, but a significant change in community composition, especially in the relative abundance of two dominant genera, *Glomus* and *Paraglomus*. It could be seen from the structural equation model that the soil total P content limited the abundance of *Paraglomus*. The abundance of *Glomus* was mainly affected by the soil-available nitrogen (N) content in the rapid-growing period (2–6 years old) and the soil bulk density in the slow-growing period (7–9 years old). In conclusion, prolonged cultivation of monospecific *E. grandis* significantly influenced the accumulation of soil K and N, thereby inducing shifts in the structure of the AM fungal community, which was primarily evident in the relative abundance alterations of *Glomus* and *Paraglomus*. The results of this study are of great significance for optimizing fertilization measures at different growth stages and improving tree productivity in nutrient-poor environments of eucalyptus plantations. Subsequent research endeavors should prioritize exploring the functional disparities among different AM fungal species to unlock the full potential of AM fungi in driving vegetation restoration and enhancing forest quality.

Author Contributions: Conceptualization, Y.J. and X.-Y.M.; methodology, Y.J. and L.-T.L.; software, Y.J.; validation, Y.J., G.-Z.L. and G.-W.Q.; formal analysis, Y.J.; investigation, Y.J., G.-Z.L. and G.-W.Q.; resources, G.-Z.L. and G.-W.Q.; data curation, Y.J., G.-Z.L. and G.-W.Q.; writing—original draft preparation, Y.J.; writing—review and editing, Y.J. and L.-T.L.; visualization, Y.J.; supervision, X.-Y.M. and L.-T.L.; project administration, X.-Y.M. and L.-T.L.; funding acquisition, X.-Y.M. and L.-T.L. All authors have read and agreed to the published version of the manuscript.

Funding: This research was funded by the National Key R&D Program of China "Technology for efficient and sustainable management of Eucalypts" (grant number 2016YFD0600505) and the Major Project of Jiangxi Academy of Forestry "Key technology for quality improvement of low-efficiency broad-leaved forests" (grant number 2017511201).

Institutional Review Board Statement: Not applicable.

Informed Consent Statement: Not applicable.

Data Availability Statement: The datasets used to produce the main results are available upon reasonable request to the corresponding author.

Acknowledgments: We thank Xiaodong Xv, Ying Song, and Jiaqi Yang for their help with our investigation and experiment. We gratefully acknowledge the Ganzhou Huajin Paper Products Co., Ltd. staff and the State-owned Jinpenshan Forest Farm for contributing to our study.

Conflicts of Interest: The authors declare no conflicts of interest.

References

1. Smith, S.E.; Read, D.J. Mycorrhizal symbiosis. *Q. Rev. Biol.* **2008**, *3*, 273–281.
2. Gianinazzi, S.; Gollotte, A.; Binet, M.N.; Tuinen, D.V.; Redecker, D.; Wipf, D. Agroecology: The key role of arbuscular mycorrhizas in ecosystem services. *Mycorrhiza* **2010**, *20*, 519–530. [CrossRef]
3. Lima, F.d.S.; Sousa, C.d.S. Growth and nutrition of eucalyptus clones seedlings inoculated with mycorrhizal fungi. *Pesqui. Agropecu. Trop.* **2014**, *44*, 110–118. [CrossRef]
4. Augé, R.M. Arbuscular mycorrhizae and soil/plant water relations. *Can. J. Soil Sci.* **2004**, *84*, 373–381. [CrossRef]
5. Wheeler, J.A.; Frey, S.D.; Stinson, K.A. Tree seedling responses to multiple environmental stresses: Interactive effects of soil warming, nitrogen fertilization, and plant invasion. *For. Ecol. Manag.* **2017**, *403*, 44–51. [CrossRef]
6. Vasconcellos, R.L.; Bonfim, J.A.; Baretta, D.; Cardoso, E.J. Arbuscular mycorrhizal fungi and glomalin-related soil protein as potential indicators of soil quality in a recuperation gradient of the Atlantic forest in Brazil. *Land Degrad. Dev.* **2016**, *27*, 325–334. [CrossRef]
7. Gao, X.; Guo, H.; Zhang, Q.; Guo, H.; Zhang, L.; Zhang, C.; Gou, Z.; Liu, Y.; Wei, J.; Chen, A. Arbuscular mycorrhizal fungi (AMF) enhanced the growth, yield, fiber quality and phosphorus regulation in upland cotton (*Gossypium hirsutum* L.). *Sci. Rep.* **2020**, *10*, 2084. [CrossRef]
8. Bagyaraj, D.J.; Sridhar, K.R.; Revanna, A. Arbuscular mycorrhizal fungi influence crop productivity, plant diversity, and ecosystem services. In *Fungal Diversity, Ecology and Control Management*; Springer: Singapore, 2022; pp. 345–362.
9. Adams, F.; Reddell, P.; Webb, M.J.; Shipton, W.A. Arbuscular mycorrhizas and ectomycorrhizas on *Eucalyptus grandis* (Myrtaceae) trees and seedlings in native forests of tropical north-eastern Australia. *Aust. J. Bot.* **2006**, *54*, 271–281. [CrossRef]
10. Murugan, R.; Beggi, F.; Kumar, S. Belowground carbon allocation by trees, understory vegetation and soil type alter microbial community composition and nutrient cycling in tropical Eucalyptus plantations. *Soil Biol. Biochem.* **2014**, *76*, 257–267. [CrossRef]
11. Liu, S.; Lu, X.; Yang, G.; He, C.; Shi, Y.; Li, C.; Liu, S.; Wang, Y.; Wang, Z.; Chen, L. Variation of arbuscular mycorrhizal fungi communities in the rhizosphere soil of Eucalyptus plantations based on different stand ages and its effect on phosphorus fractionation. *Appl. Soil Ecol.* **2023**, *189*, 104908. [CrossRef]
12. Mitra, D.; Djebaili, R.; Pellegrini, M.; Mahakur, B.; Sarker, A.; Chaudhary, P.; Khoshru, B.; Gallo, M.D.; Kitouni, M.; Barik, D.P. Arbuscular mycorrhizal symbiosis: Plant growth improvement and induction of resistance under stressful conditions. *J. Plant Nutr.* **2021**, *44*, 1993–2028. [CrossRef]
13. Öpik, M.; Metsis, M.; Daniell, T.J.; Zobel, M.; Moora, M.J.N.P. Large-scale parallel 454 sequencing reveals host ecological group specificity of arbuscular mycorrhizal fungi in a boreonemoral forest. *New Phytol.* **2009**, *184*, 424–437. [CrossRef]
14. Lin, G.; McCormack, M.L.; Guo, D. Arbuscular mycorrhizal fungal effects on plant competition and community structure. *J. Ecol.* **2015**, *103*, 1224–1232. [CrossRef]
15. Cavagnaro, T.; Gao, L.; Smith, F.A.; Smith, S.E. Morphology of arbuscular mycorrhizas is influenced by fungal identity. *New Phytol.* **2001**, *151*, 469–475. [CrossRef]
16. Vierheilig, H.; Schweiger, P.; Brundrett, M. An overview of methods for the detection and observation of arbuscular mycorrhizal fungi in roots. *Physiol. Plant.* **2005**, *125*, 393–404. [CrossRef]
17. Egan, C.P.; Rummel, A.; Kokkoris, V.; Klironomos, J.; Lekberg, Y.; Hart, M. Using mock communities of arbuscular mycorrhizal fungi to evaluate fidelity associated with Illumina sequencing. *Fungal Ecol.* **2018**, *33*, 52–64. [CrossRef]
18. Moebius-Clune, D.J.; Anderson, Z.U.; Pawlowska, T.E. Arbuscular mycorrhizal fungi associated with a single agronomic plant host across the landscape: The structure of an assemblage. *Soil Biol. Biochem.* **2013**, *64*, 181–190. [CrossRef]
19. Xu, J.; Liu, S.; Song, S.; Guo, H.; Tang, J.; Yong, J.W.H.; Ma, Y.; Chen, X. Arbuscular mycorrhizal fungi influence decomposition and the associated soil microbial community under different soil phosphorus availability. *Soil Biol. Biochem.* **2018**, *120*, 181–190. [CrossRef]
20. Hishi, T.; Tateno, R.; Fukushima, K.; Fujimaki, R.; Itoh, M.; Tokuchi, N. Changes in the anatomy, morphology and mycorrhizal infection of fine root systems of *Cryptomeria japonica* in relation to stand ageing. *Tree Physiol.* **2016**, *37*, 61–70.
21. Nakano-Hylander, A.; Olsson, P.A. Carbon allocation in mycelia of arbuscular mycorrhizal fungi during colonisation of plant seedlings. *Soil Biol. Biochem.* **2007**, *39*, 1450–1458. [CrossRef]
22. Dumbrell, A.J.; Nelson, M.; Helgason, T.; Dytham, C.; Fitter, A.H. Relative roles of niche and neutral processes in structuring a soil microbial community. *ISME J.* **2010**, *4*, 337–345. [CrossRef]
23. Jerbi, M.; Labidi, S.; Bahri, B.A.; Laruelle, F.; Tisserant, B.; Jeddi, F.B.; Sahraoui, A.L.-H. Soil properties and climate affect arbuscular mycorrhizal fungi and soil microbial communities in Mediterranean rainfed cereal cropping systems. *Pedobiologia* **2021**, *87*, 150748. [CrossRef]
24. Carrenho, R.; Trufem, S.F.B.; Bononi, V.L.R.; Silva, E.S. The effect of different soil properties on arbuscular mycorrhizal colonization of peanuts, sorghum and maize. *Acta Bot. Bras.* **2007**, *21*, 723–730. [CrossRef]
25. Xu, R.K.; Zhao, A.Z.; Li, Q.M.; Kong, X.L.; Ji, G.L. Acidity regime of the Red Soils in a subtropical region of southern China under field conditions. *Geoderma* **2003**, *115*, 75–84. [CrossRef]
26. Wang, L.; Yan, H.; Wang, X.; Wang, Z.; Yu, S.; Wang, T.; Shi, Z. The potential for soil erosion control associated with socio-economic development in the hilly red soil region, southern China. *Catena* **2020**, *194*, 104678. [CrossRef]
27. Turnbull, J.W. Eucalypt plantations. *New For.* **1999**, *17*, 37–52. [CrossRef]

28. Cuong, T.; Chinh, T.T.Q.; Zhang, Y.; Xie, Y. Economic performance of forest plantations in Vietnam: Eucalyptus, Acacia mangium, and Manglietia conifera. *Forests* **2020**, *11*, 284. [CrossRef]
29. AOAC. *Official Methods of Analysis of AOAC International*, 16th ed.; AOAC: Rockville, MA, USA, 1995; Volume 1.
30. Jorhem, L. Determination of Metals in Foods by Atomic Absorption Spectrometry after Dry Ashing: NMKL1 Collaborative Study. *J. AOAC Int.* **2000**, *83*, 1204–1211. [CrossRef]
31. Grattan, S.; Shannon, M.; Grieve, C.; Poss, J.; Suarez, D.; Leland, F. Interactive effects of salinity and boron on the performance and water use of eucalyptus. In *II International Symposium on Irrigation of Horticultural Crops 449*; ISHS: Leuven, Belgium, 1996; pp. 607–614.
32. Hodecker, B.E.R.; De Barros, N.F.; Da Silva, I.R.; Diola, V.; Sarkis, J.E.S.; Loureiro, M.E. Boron delays dehydration and stimulates root growth in *Eucalyptus urophylla* (Blake, ST) under osmotic stress. *Plant Soil* **2014**, *384*, 185–199. [CrossRef]
33. Page, A.L. *Methods of Soil Analysis. Part 2. Chemical and Microbiological Properties*; American Society of Agronomy, Soil Science Society of America: Madison, WI, USA, 1982.
34. Phillips, J.M.; Hayman, D.S. Improved procedures for cleaning and staining parasitic and vesicular arbuscular mycorrhizal fungi for rapid assessment of infection. *Trans. Br. Mycol. Soc.* **1970**, *55*, 158. [CrossRef]
35. Koske, R.E.; Gemma, J.N. A modified procedure for staining roots to detect VA mycorrhizas. *Mycol. Res.* **1989**, *92*, 486–488. [CrossRef]
36. Zimmermann, J.; Jahn, R.; Gemeinholzer, B. Barcoding diatoms: Evaluation of the V4 subregion on the 18S rRNA gene, including new primers and protocols. *Org. Divers. Evol.* **2011**, *11*, 173–192. [CrossRef]
37. Yan, L.; Mu, X.; Han, B.; Zhang, S.; Qiu, C.; Ohore, O.E. Ammonium loading disturbed the microbial food webs in biofilms attached to submersed macrophyte *Vallisneria natans*. *Sci. Total Environ.* **2019**, *659*, 691–698. [CrossRef]
38. Caporaso, J.G.; Kuczynski, J.; Stombaugh, J.; Bittinger, K.; Bushman, F.D.; Costello, E.K.; Fierer, N.; Pena, A.G.; Goodrich, J.K.; Gordon, J.I.; et al. QIIME allows analysis of high-throughput community sequencing data. *Nat. Methods* **2010**, *7*, 335–336. [CrossRef]
39. Dixon, P. VEGAN, a package of R functions for community ecology. *J. Veg. Sci.* **2003**, *14*, 927–930. [CrossRef]
40. Taniguchi, T.; Kanzaki, N.; Tamai, S.; Yamanaka, N.; Futai, K.J.N.P. Does ectomycorrhizal fungal community structure vary along a Japanese black pine (*Pinus thunbergii*) to black locust (*Robinia pseudoacacia*) gradient? *New Phytol.* **2007**, *173*, 322–334. [CrossRef]
41. Zheng, Y.; Chen, L.; Luo, C.-Y.; Zhang, Z.-H.; Wang, S.-P.; Guo, L.-D. Plant Identity Exerts Stronger Effect than Fertilization on Soil Arbuscular Mycorrhizal Fungi in a Sown Pasture. *Microb. Ecol.* **2016**, *72*, 647–658. [CrossRef]
42. Rosseel, Y. Lavaan: An R package for structural equation modeling. *J. Stat. Softw.* **2012**, *48*, 1–36. [CrossRef]
43. Wu, H.; Xiang, W.; Ouyang, S.; Xiao, W.; Li, S.; Chen, L.; Lei, P.; Deng, X.; Zeng, Y.; Zeng, L. Tree growth rate and soil nutrient status determine the shift in nutrient-use strategy of Chinese fir plantations along a chronosequence. *For. Ecol. Manag.* **2020**, *460*, 117896. [CrossRef]
44. Richardson, A.E. Prospects for using soil microorganisms to improve the acquisition of phosphorus by plants. *Aust. J. Plant Physiol.* **2001**, *28*, 897–906. [CrossRef]
45. Laclau, J.P.; Almeida, J.C.; Gonçalves, J.L.; Saint-André, L.; Ventura, M.; Ranger, J.; Moreira, R.M.; Nouvellon, Y. Influence of nitrogen and potassium fertilization on leaf lifespan and allocation of above-ground growth in Eucalyptus plantations. *Tree Physiol.* **2009**, *29*, 111. [CrossRef]
46. de Moraes Goncalves, J.L.; Stape, J.L.; Laclau, J.P.; Smethurst, P.; Gava, J.L. Silvicultural effects on the productivity and wood quality of eucalypt plantations. *For. Ecol. Manag.* **2004**, *193*, 45–61. [CrossRef]
47. Parihar, M.; Rakshit, A.; Meena, V.S.; Gupta, V.K.; Rana, K.; Choudhary, M.; Tiwari, G.; Mishra, P.K.; Pattanayak, A.; Bisht, J.K. The potential of arbuscular mycorrhizal fungi in C cycling: A review. *Arch. Microbiol.* **2020**, *202*, 1581–1596. [CrossRef]
48. Hasselquist, N.J.; Metcalfe, D.B.; Inselsbacher, E.; Stangl, Z.; Oren, R.; Näsholm, T.; Högberg, P. Greater carbon allocation to mycorrhizal fungi reduces tree nitrogen uptake in a boreal forest. *Ecology* **2016**, *97*, 1012–1022. [CrossRef]
49. Wang, B.; Liu, G.; Xue, S. Effect of black locust (*Robinia pseudoacacia*) on soil chemical and microbiological properties in the eroded hilly area of China's Loess Plateau. *Environ. Earth Sci.* **2012**, *65*, 597–607. [CrossRef]
50. Yang, H.; Zhang, Q.; Dai, Y.; Liu, Q.; Tang, J.; Bian, X.; Chen, X. Effects of arbuscular mycorrhizal fungi on plant growth depend on root system: A meta-analysis. *Plant Soil* **2015**, *389*, 361–374. [CrossRef]
51. Gonçalves, J.D.M.; Barros, N.F.; Nambiar, E.K.S.; Novais, R.F. Management of soil, nutrients and water in tropical plantation forests. In *Soil and Stand Management for Short-Rotation Plantations*; Australian Centre for International Agricultural Research (ACIAR): Canberra, Australia, 1997.
52. Laclau, J.P.; Ranger, J.; Deleporte, P.; Nouvellon, Y.; Saint-André, L.; Marlet, S.; Bouillet, J.-P. Nutrient cycling in a clonal stand of Eucalyptus and an adjacent savanna ecosystem in Congo: 3. Input–output budgets and consequences for the sustainability of the plantations. *For. Ecol. Manag.* **2003**, *210*, 375–391. [CrossRef]
53. Carrenho, R.; Barbosa, F.F.; Araújo, C.V.; Alves, L.J.; Santos, O.M. Mycorrhizal associations in *Eucalyptus* spp.: Status and needs. *Tree For. Sci. Biotechnol.* **2008**, *2*, 57–67.
54. Khaekhum, S.; Lumyong, S.; Kuyper, T.W.; Boonlue, S. Species richness and composition of arbuscular mycorrhizal fungi occurring on eucalypt trees (*Eucalyptus camaldulensis* Dehnh.) in rainy and dry season. *Curr. Res. Environ. Appl. Mycol.* **2017**, *7*, 282–292. [CrossRef]

55. Lu, N.; Zhang, P.; Wang, P.; Wang, X.; Ji, B.; Mu, J. Environmental factors affect the arbuscular mycorrhizal fungal community through the status of host plants in three patterns of Chinese fir in southern China. *Glob. Ecol. Conserv.* **2022**, *36*, e02121. [CrossRef]
56. Weber, O.B.; da Silva, M.C.B.; da Silva, C.F.; Correia, D.; dos Santos Garruti, D.; Pagano, M.C. Diversity of mycorrhizal fungi and soil indicative species in coastal plantations of northeast Brazil. *J. For. Res.* **2021**, *32*, 1203–1211. [CrossRef]
57. Schwarzott, D.; Walker, C.; Schüßler, A. Glomus, the largest genus of the arbuscular mycorrhizal fungi (Glomales), is nonmonophyletic. *Mol. Phylogenet. Evol.* **2001**, *21*, 190–197. [CrossRef]
58. Rodrigues, K.; Rodrigues, B. *Glomus (Chapter 27)*; Academic Press: Cambridge, MA, USA, 2020.
59. Błaszkowski, J.; Kovács, G.M.; Gáspár, B.K.; Balázs, T.K.; Buscot, F.; Ryszka, P. The arbuscular mycorrhizal *Paraglomus majewskii* sp. nov. represents a distinct basal lineage in Glomeromycota. *Mycologia* **2012**, *104*, 148–156. [CrossRef]
60. Gosling, P.; Proctor, M.; Jones, J.; Bending, G.D. Distribution and diversity of *Paraglomus* spp. in tilled agricultural soils. *Mycorrhiza* **2014**, *24*, 1–11. [CrossRef]
61. Freitas, R.D.; Buscardo, E.; Nagy, L.; Maciel, A.B.D.; Carrenho, R.; Luizao, R.C.C. Arbuscular mycorrhizal fungal communities along a pedo-hydrological gradient in a Central Amazonian terra firme forest. *Mycorrhiza* **2014**, *24*, 21–32. [CrossRef]
62. Herrmann, L.; Lesueur, D.; Bräu, L.; Davison, J.; Jairus, T.; Robain, H.; Öpik, M. Diversity of root-associated arbuscular mycorrhizal fungal communities in a rubber tree plantation chronosequence in Northeast Thailand. *Mycorrhiza* **2016**, *26*, 863–877. [CrossRef]
63. Klironomos, J.N.; Hart, M.M. Colonization of roots by arbuscular mycorrhizal fungi using different sources of inoculum. *Mycorrhiza* **2002**, *12*, 181–184. [CrossRef]
64. Fu, W.; Chen, B.; Rillig, M.C.; Jansa, J.; Ma, W.; Xu, C.; Luo, W.; Wu, H.; Hao, Z.; Wu, H. Community response of arbuscular mycorrhizal fungi to extreme drought in a cold-temperate grassland. *New Phytol.* **2022**, *234*, 2003–2017. [CrossRef]
65. Bennett, A.E.; Classen, A.T. Climate change influences mycorrhizal fungal–plant interactions, but conclusions are limited by geographical study bias. *Ecology* **2020**, *101*, e02978. [CrossRef]
66. Qin, H.; Chen, J.H.; Wu, Q.F.; Niu, L.M.; Li, Y.C.; Liang, C.F.; Shen, Y.; Xu, Q.F. Intensive management decreases soil aggregation and changes the abundance and community compositions of arbuscular mycorrhizal fungi in Moso bamboo (*Phyllostachys pubescens*) forests. *For. Ecol. Manage.* **2017**, *400*, 246–255. [CrossRef]
67. Gao, S.; He, Q.; Huang, D.; Wang, Z.; Mao, J.; Xie, X.; Su, Y.; Qiu, Q.; Li, J.; Chen, Z. Responses of fungal community structure and functional composition to short-term fertilization and dry season irrigation in *Eucalyptus urophylla* × *Eucalyptus grandis* plantation soils. *Forests* **2022**, *13*, 854. [CrossRef]
68. Garcia de Leon, D.; Moora, M.; Opik, M.; Neuenkamp, L.; Gerz, M.; Jairus, T.; Vasar, M.; Bueno, C.G.; Davison, J.; Zobel, M. Symbiont dynamics during ecosystem succession: Co-occurring plant and arbuscular mycorrhizal fungal communities. *FEMS Microbiol. Ecol.* **2016**, *92*, fiw097. [CrossRef]
69. Pagano, M.C.; Scotti, M.R. Arbuscular and ectomycorrhizal colonization of two Eucalyptus species in semiarid Brazil. *Mycoscience* **2008**, *49*, 379–384. [CrossRef]
70. Frater, P.N.; Borer, E.T.; Fay, P.A.; Jin, V.; Knaeble, B.; Seabloom, E.; Sullivan, L.; Wedin, D.A.; Harpole, W.S. Nutrients and environment influence arbuscular mycorrhizal colonization both independently and interactively in *Schizachyrium scoparium*. *Plant Soil* **2018**, *425*, 493–506. [CrossRef]
71. Ezawa, T.; Smith, S.E.; Smith, F.A. P metabolism and transport in AM fungi. *Plant Soil* **2002**, *244*, 221–230. [CrossRef]
72. Bücking, H.; Kafle, A. Role of arbuscular mycorrhizal fungi in the nitrogen uptake of plants: Current knowledge and research gaps. *Agronomy* **2015**, *5*, 587–612. [CrossRef]
73. Yan, T.; Lü, X.-T.; Zhu, J.-J.; Yang, K.; Yu, L.-Z.; Gao, T. Changes in nitrogen and phosphorus cycling suggest a transition to phosphorus limitation with the stand development of larch plantations. *Plant Soil* **2018**, *422*, 385–396. [CrossRef]
74. Li, L.; Liu, L.; Yu, Z.; Peñuelas, J.; Sardans, J.; Chen, Q.; Xu, J.; Zhou, G. Carbon, nitrogen and phosphorus stoichiometry in natural and plantation forests in China. *Forests* **2022**, *13*, 755. [CrossRef]
75. Etesami, H.; Jeong, B.R.; Glick, B.R. Contribution of arbuscular mycorrhizal fungi, phosphate–solubilizing bacteria, and silicon to P uptake by plant. *Front. Plant Sci.* **2021**, *12*, 699618. [CrossRef]
76. Rillig, M.C. Arbuscular mycorrhizae, glomalin, and soil aggregation. *Can. J. Soil Sci.* **2004**, *84*, 355–363. [CrossRef]

Disclaimer/Publisher's Note: The statements, opinions and data contained in all publications are solely those of the individual author(s) and contributor(s) and not of MDPI and/or the editor(s). MDPI and/or the editor(s) disclaim responsibility for any injury to people or property resulting from any ideas, methods, instructions or products referred to in the content.

Journal of *Fungi*

MDPI

Article

Contrasting Patterns of Fungal and Bacterial Endophytes Inhabiting Temperate Tree Leaves in Response to Thinning

Beiping Liu [1,2,†], Chunhuan Li [1,2,†], Xiuhai Zhao [3], Chunyu Zhang [3], Xinyi He [1,2], Laiye Qu [4] and Naili Zhang [1,2,5,*]

[1] State Key Laboratory of Efficient Production of Forest Resources, College of Forestry, Beijing Forestry University, Beijing 100083, China; liubeiping22@163.com (B.L.); lichunhuan318@163.com (C.L.); hexinyi0611@bjfu.edu.cn (X.H.)
[2] The Key Laboratory for Silviculture and Conservation of Ministry of Education, College of Forestry, Beijing Forestry University, Beijing 100083, China
[3] Research Center of Forest Management Engineering of State Forestry and Grassland Administration, Beijing Forestry University, Beijing 100083, China; zhaoxh@bjfu.edu.cn (X.Z.); zcy_0520@163.com (C.Z.)
[4] Research Center for Eco-Environmental Sciences, Chinese Academy of Sciences, Beijing 100085, China; lyqu@rcees.ac.cn
[5] Ecological Observation and Research Station of Heilongjiang Sanjiang Plain Wetlands, National Forestry and Grassland Administration, Shuangyashan 518000, China
* Correspondence: zhangnaili@bjfu.edu.cn
† These authors contributed equally to this work.

Abstract: The phyllosphere is an important but underestimated habitat for a variety of microorganisms, with limited knowledge about leaf endophytes as a crucial component of the phyllosphere microbiome. In this study, we investigated the mechanisms of communities and co-occurrence networks of leaf endophytes in response to forest thinning in a temperate forest. As we expected, contrasting responses of fungal and bacterial endophytes were observed. Specifically, the diversity of leaf endophytic fungi and the complexity of their co-occurrence networks increased significantly with thinning intensity, whereas the complexity of endophytic bacterial co-occurrence networks decreased. In particular, microbiota inhabiting damaged leaves seem to be more intensively interacting, showing an evident fungi–bacteria trade-off under forest thinning. In damaged leaves, besides the direct effects of thinning, thinning-induced changes in neighbor tree diversity indirectly altered the diversity of leaf fungal and bacterial endophytes via modifying leaf functional traits such as leaf dry matter content and specific leaf area. These findings provide new experimental evidence for the trade-offs between leaf endophytic fungi and bacteria under the different magnitudes of deforestation, highlighting their dependence on the presence or absence of leaf damage.

Keywords: leaf damage; leaf endophytes; neighbor tree diversity; temperate forest; thinning intensity

1. Introduction

Leaf microbial endophytes constitute a group of microorganisms inhabiting the leaves of plants, forming a harmonious symbiotic association with host trees after experiencing a long-term evolutionary history [1]. Intrinsic factors such as genotype, age, plant species, and developmental stage influence their diversity and composition [1,2], as well as external factors such as soil characteristics [3], the hydrothermal environment [4], neighboring plants [5], phytophagous insects [6], and plant pathogens [7]. The intricate environmental diversity enables leaf endophytic microbiota to demonstrate greater adaptability to environmental changes compared to inter-root microbes [8]. Despite the undeniable influence of leaf endophytic microbiota on plants [9], our understanding of the underlying mechanisms, particularly under varying thinning intensities, significantly lags behind the knowledge available for inter-root microbiota [10,11].

Thinning, the common anthropogenic disturbance being conducted prevalently in temperate forests, influences the structure and function of forest ecosystems by directly

changing tree density and indirectly altering tree growth, functional traits, and composition through the modulation of sunlight penetration and precipitation [12–15]. The penetration of sunlight is closely associated with the traits and functions of leaves since they are photosynthetic organs [16]. The effects of thinning generally depend on the thinning intensity. Large-scale thinning usually leads to the excessive exploitation of forest resources, resulting in tree species loss, substantial variations in functional traits, and threats to ecosystem functions [17]. However, when managed appropriately, it has the potential to foster tree growth, promote leaf traits and their associations with microbial endophytes, alleviate competitive pressures among tree species [18], and improve the stability of forest communities [19,20].

The thinning-induced variations in tree spatial distribution play a crucial role in shaping ecological processes such as recruitment, growth, dispersal, and competition [21]. According to the "moderate disturbance hypothesis" proposed by Connell [22], when disturbance intensity is too high, it becomes challenging for the majority of species to survive, leading to the dominance of a small number of reproductively strong or expansive colonizers. Conversely, if disturbance intensity is too low, dominant competitors may become excessively strong and outcompete disadvantaged species, resulting in reduced species diversity [23,24]. Moderate thinning is deemed to stimulate the growth of specific leaf endophytic microbiota by increasing light availability, creating additional space resources, and enhancing the water use efficiency of leaves [25]. However, excessive thinning can decrease community-level and neighbor tree diversity, resulting in a significant change in the diversity and abundance of leaf endophytic microbiota inhabiting focal tree species [26,27]. Moreover, thinning-induced changes in neighbor tree richness may modulate herbivorous insects, conferring a cascading effect on leaf endophytic microbiota, a phenomenon often referred to as neighborhood effects [28]. The neighborhood effects can trigger changes in the herbivorous insect density and their feeding activity [29,30]. The extent of leaf damage by these insect herbivores has been predicted to modulate endophytic microbiota owing to the dispersal and colonization of some external microbes via the edges of damaged leaf tissues [27,29]. This raises an intriguing question: what are the differences in the environmental adaptation of endophytic microbiota residing in damaged leaves compared to those in healthy leaves?

In this study, we aim to investigate the responses of leaf endophytic fungal and bacterial assemblages to neighbor tree species richness and herbivorous insect-caused leaf damage in temperate forests under different thinning intensities. We established three plots with different thinning intensities (i.e., control check (CK), light, and moderate thinning) in a broad-leaved *Pinus koraiensis* forest in Northeast China. Five dominant tree species (i.e., *Pinus koraiensis*, *Ulmus davidiana* var. *japonica*, *Tilia amurensis*, *Fraxinus mandshurica*, and *Acer pictum* subsp. *mono*) were selected for the study. First, we hypothesized that thinning intensities can significantly change the diversity and composition of endophytic microflora in leaves, with a trade-off between leaf endophytic fungi and bacteria. Specifically, endophytic bacterial diversity may decrease as an enhancement of fungal diversity. Second, the intensities of thinning can significantly alter the network structure of leaf endophytes. Third, we predicted that leaf endophytes would be simultaneously regulated via the abundance of neighboring trees around the focal tree individual, via leaf functional characteristics, and via leaf damage caused by herbivorous insect feeding.

2. Materials and Methods

2.1. Study Site and Experimental Design

The study was carried out in a broad-leaved *Pinus koraiensis* forest at an altitude of 575~784 m, situated in the Jiaohe Forestry Experimental Area Administration of Jilin Province, China (127°45.287′–127°45.790′ E, 43°57.524′–43°58.042′ N). The average temperature from June to August here reaches 3.8 °C, and the average annual precipitation is 696 mm [31]. The soil type is mountain dark brown forest soil, with a depth range of 20 to 80 cm. The vegetation belongs to Changbai Mountain flora, with common tree species such

as *Juglans mandshurica*, *Carpinus cordata*, *Quercus mongolica*, and so on. The undergrowth consists of *Syringa reticulata* subsp. *amurensis*, *Corylus mandshurica*, *Eleutherococcus senticosus*, etc. [32].

In December 2011, three 1ha plots were established in the broad-leaved *P. koraiensis* forest and were logged with different thinning intensities after obtaining the approval of the Jilin Provincial Forestry Department. The thinning intensities were as follows: 0% (control check, CK), 15% (light thinning, LT), and 30% (moderate thinning, MT) [33]. Five dominant species were selected, including *P. koraiensis* (PK), *Ulmus davidiana* var. *japonica* (UD), *Tilia amurensis* (TA), *Fraxinus mandshurica* (FM), and *Acer pictum* subsp. *mono* (AP). Four individual plants were randomly selected from each focal species in each plot for leaf sampling. To ensure consistency in sampling and minimize the effects of other environmental factors, we selected sample plots in forests with flat terrain and a slope of less than 5 degrees [34]. Additionally, the forest gaps around the target tree species were essentially uniform, thereby mitigating the potential influence of light and wind speed.

2.2. Sample Collection and Measurement

From late July to early August 2022, we collected leaves of the target tree species. Prior to this, the diameter at breast height (DBH) of each focal tree species was measured, and the neighboring trees surrounding each focal tree within a 5 m radius were recorded. Mature leaves were randomly selected from the mid-canopy layers, and their status was recorded as healthy or damaged. Leaves eaten by phytophagous insects were classified as damaged, while leaves without insect feeding were classified as healthy. The leaves were then put into sterile sealed bags and carried down the hill in a portable refrigerator. Vernier calipers were used to measure leaf thickness. The leaf thickness (LT) of each individual tree was obtained by averaging the thickness of five leaves, and all the leaves were scanned for further analysis. Image Pro Plus was used to determine the area (LA), length (LL), and width (LW) of the blade.

In the meantime, three leaves were chosen at random for each sample, and their fresh weight was determined. The leaves were then degreened at 105 °C for 15 min and dried at 65 °C to a constant weight for dry weight determination. The leaf dry matter weight (LDMC) was determined as the ratio of leaf dry weight to leaf fresh weight, and the specific leaf area (SLA) was calculated as the ratio of leaf area to leaf dry matter weight. The measurements of leaf trait variables per individual tree were taken three times, and the mean values were recorded. After grinding the leaves for 150 s with a 55 Hz grinding instrument, the nutrient content of the leaves was measured after passing through a 150-mesh screen. An elemental analyzer was used to measure the total nitrogen (N) and total carbon (C) content of the leaves (Vario EL Cube, Elementar, Germany) and to obtain the C/N ratio of the leaves. An inductively coupled plasma mass spectrometer was used to determine the content of P, K, Ca, Cu, Mg, and Zn in leaves (ICP-MS, NexION 300X, Perkin Elmre, Shelton, CT, USA), and the leaves were dissolved via the $HNO_3/HClO_4$ method.

Five soil cores beneath the canopy of each target tree were collected and thoroughly mixed into a composite sample, which was then placed in sterile sealed bags and transported to a lab for analysis. After removing impurities with a 2 mm sieve, the remaining soil was measured for soil moisture and pH value. Ten grams of fresh soil was weighed and dried at 105 °C to a constant mass. The dried soil was then reweighed to determine its moisture content (SWC). Soil pH was measured using a pH meter (PB-10, Sartorius AG 21992271, Göttingen, Germany) with a water-to-soil volume ratio of 1:2.5.

2.3. DNA Extraction, PCR Amplification, and Sequencing of Leaf Endophytic Bacterial and Fungal Communities

The subsamples of leaves were washed with running water, soaked in 75% alcohol for 1 min, soaked in pure water for another 1 min, and, finally, washed with 75% alcohol again for surface sterilization. After allowing all the alcohol to evaporate, the leaves were

placed in aseptic bags and stored at −80 °C to measure endophytic fungi and bacteria in the leaves.

DNA extraction was carried out following the instructions of the TruSeqTM DNA Sample Prep Kit. NanoDrop 2000 and 1% agarose gel electrophoresis were utilized to analyze the concentration, purity, and quality of DNA extracted from the leaves. The extracted leaf DNA served as the template for polymerase chain reaction (PCR) amplification. The primers, 799F-AACMGGATTAGATACCCKG and 1193R-ACGTCATCCCCACCTTCC, were used to amplify endophytic bacterial variable region V3–V4 [35]. The PCR amplification process consisted of 3 min of predenaturation at 95 °C and 27 cycles (denatured at 95 °C for 30 s, annealed at 55 °C for 30 s, and extended at 72 °C for 30 s). Finally, the reaction time was extended for 10 min at 72 °C and then stored at 4 °C. The primers, fITS7F-GTGARTCATCGAATCTTTG and ITS4R-TCCTCCGCTTATTGATATGC, were used to amplify the endophytic fungal ITS2 region [36]. The process of PCR amplification consisted of predenaturation at 95 °C for 5 min, in 30 cycles (denaturated at 94 °C for 60 s, annealed at 58 °C for 50 s, and extended at 68 °C for 60 s), and finally an extension at 68 °C for 10 min and preservation at 10 °C. The PCR amplification system consisted of a 20 μL mixture containing 4 μL of 5 × Fast Pfu buffer, 2 μL 2.5 mM dNTPs, 0.8 μL of each primer (5 μM), 0.8 μL of Fast Pfu polymerase, 10 ng of the DNA template, and ddH2O. The AxyPrep DNA gel extraction kit (Axygen Biosciences, Union City, CA, USA) was utilized for purifying PCR products and detecting them with 2% agarose gel electrophoresis. The Illumina MiSeq platform (Illumina, San Diego, CA, USA) was used to sequence the purified PCR products following the established protocol of Megi Biopharmaceutical Co., LTD. (Shanghai, China). The original sequencing data were stored in FASTQ format.

2.4. Bioinformatics Analysis

We selected Quantitative Insights into Microbial Ecology 2 (QIIME2) (v 2022.08) [37], an advanced microbiome analysis platform, for the detailed processing of all raw FASTQ data. First, the data import process was completed manually by executing the "qiime tools import" command in QIIME2. During the data cleaning and preprocessing phase, we used the "qiime dada2 denoise paired" plug-in [38], which incorporates advanced functions including quality pruning, noise reduction, sequence merging, and chimera detection. The approach efficiently grouped non-singleton amplified sequence variants (ASVs).

After quality filtering, the ASV abundance table was normalized to achieve the consistency of sampling depth using the "Interactive Sample Detail" feature within the "table.qzv" file. The "qiime feature-classifier classify-sklearn" plugin in QIIME2 was then employed to classify fungal and bacterial ASVs. The ASVs were merged and taxonomically classified by a trained Naive classifier based on the Greengenes database, clustering species with 99% similarity. Two authoritative reference databases, SILVA (www.arb-silva.de/act (accessed on 24 May 2024)) and UNITE (https://unite.ut.ee/ (accessed on 24 May 2024)), were used for the taxonomic assignment of endophytic fungi and bacteria, respectively. The resulting endophytic fungi amplicon sequences were validated via comparison with the NCBI database.

2.5. Statistical Analysis

All statistical analyses and data visualizations in this study were performed using R statistical software (v.4.2.3). We conducted tests to evaluate the effects of different thinning intensities, tree species, damage, and their interactions on the assembly of endophytic bacteria and fungi. The lmer function from the lme4 package was employed to fit a mixed linear model, with the thinning intensity, tree species, and damage treated as fixed effects, and the DBH of target tree species and the composition of surrounding tree species treated as random effects. The significance of the fixed effects was assessed using the Anova function from the Car package. To examine the diversity and composition of endophytic fungi and bacteria, leaf traits, soil variables, and diversity of neighboring trees under different thinning intensities, we performed the Kruskal–Wallis nonparametric test.

Differences between different thinning intensities were further analyzed using the Wilcoxon test (Wilcox.test function).

To identify the bacterial genera exhibiting significant differences in relative abundance across various thinning intensities, an LEfSe analysis was employed, with a threshold LDA > 2 and $p < 0.05$, and the bacterial genera with relative abundance greater than 0.05% were screened. A correlation network analysis was performed using the igraph package, with species selected based on Spearman correlation $|r| > 0.6$, $p < 0.05$. The ggclust package [39] was utilized to analyze core species within the network, categorizing node attributes into four types based on their topological characteristics. The fungal community function was predicted using the FUNGuild method [40], while the bacterial community function was predicted using the FAPROTAX method [41]. The structural equation modeling (SEM) posits a causal pathway where thinning intensity affects the richness of endophytic bacteria and fungi in leaves through altering neighbor tree diversity, soil variables, and leaf traits, as conceptualized (Figure S1a); this pathway was constructed using the piecewiseSEM package [42]. The path coefficient expresses the direction and intensities of the direct influence between the two variables. Graphs were generated using the ggplot2 package.

3. Results

3.1. Alpha Diversity of Leaf Endophytic Fungi and Bacteria

The mixed-effect model analysis revealed that the alpha diversity (i.e., richness and Shannon index) of the leaf endophytic bacteria was significantly influenced by tree species, the degree of damage, and their interaction. However, thinning intensity and tree species identity had significant effects on the alpha diversity of endophytic fungi (Table 1). Thinning intensity notably increased the alpha diversity of endophytic fungi. It decreased that of the endophytic bacterial community, compared to the CK plots (Figure 1). The richness and Shannon index of the leaf endophytic bacterial community were lowest in LT plots, whereas those of leaf endophytic fungi were highest in LT plots.

In *F. mandshurica*, the endophytic bacterial richness and Shannon index were significantly lower in MT plots than in CK plots (Figure S2). In *U. davidiana*, the richness of endophytic bacteria was significantly lower in MT plots than in CK plots, while the richness of endophytic fungi showed the opposite trend (Figure S2). Except for *T. amurensis* species, the diversity of leaf endophytic bacteria, indicated by both richness and the Shannon index, was lower in thinning plots compared to CK plots, with diversity generally higher in damaged leaves than in healthy leaves (Figure S3). Conversely, the diversity of leaf endophytic fungal, except for in *T. amurensis*, increased due to forest thinning, with diversity generally lower in damaged leaves than in healthy leaves (Figure S3).

Table 1. Effects of different thinning intensity, tree species, damage degree, and their interactions on alpha diversity of endophytic fungi and endophytic bacteria in leaves.

Factor	Bacteria				Fungi			
	Richness		Shannon Index		Richness		Shannon Index	
	Chisq	*p*	Chisq	*p*	Chisq	*p*	Chisq	*p*
Thinning intensity (T)	4.40	0.111	3.11	0.21	14.8	<0.001	10.2	0.006
Species (S)	80.2	<0.001	26.3	<0.001	14.7	0.005	14.3	0.006
Damaged (D)	19.1	<0.001	21.5	<0.001	1.05	0.305	1.14	0.286
T × S	6.49	0.592	3.28	0.915	13.0	0.112	13.6	0.092.
T × D	0.21	0.899	0.32	0.852	0.69	0.71	0.27	0.875
S × D	20.8	<0.001	13.9	<0.001	5.13	0.274	3.80	0.434
T × S × D	4.96	0.762	6.26	0.617	2.75	0.949	7.89	0.444

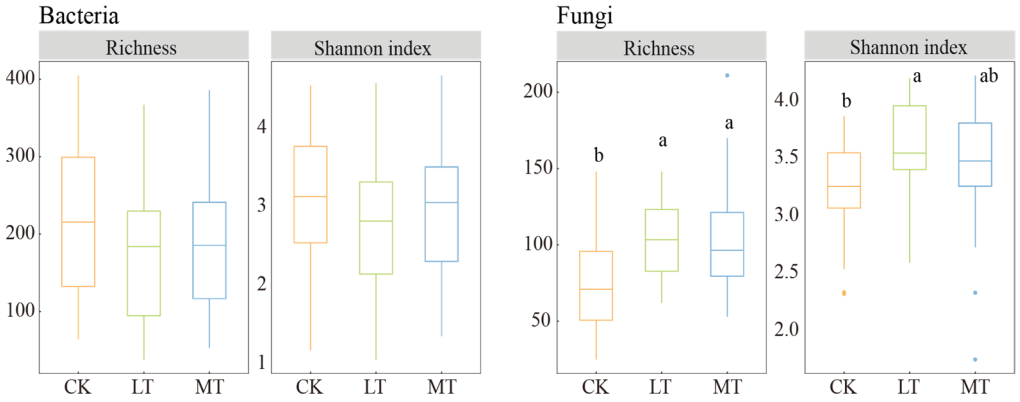


Figure 1. Alpha diversity index of endophytic fungi and bacteria under different thinning intensities. CK: control check; LT: light thinning; MT: moderate thinning. Different letters indicate significant differences ($p < 0.05$). Asterisks are outliers.

3.2. Composition of Leaf Endophytic Fungi and Bacteria

We analyzed 120 leaf samples to identify fungal and bacterial endophytes, resulting in the identification of 4672 bacterial ASVs and 6390 fungal ASVs. The top 10 genera with the highest relative abundance of endophytic bacteria at the genus level included *Achromobacter*, *Pseudomonas*, *Sphingomonas*, *Rhodococcus*, *Delftia*, *Methylobacterium*, *Agrobacterium*, *Friedmanniella*, *Variovorax*, and *Curtobacterium* (Figure 2). The relative abundance of the remaining genera and unknown species accounted for more than 25% across all plots. Regarding fungal endophytes, the top 10 genera with the highest relative abundance were *Tripospermum*, *Vishniacozyma*, *Sphaerulina*, *Dioszegia*, *Trichomerium*, *Pucciniastrum*, *Buckleyzyma*, *Cyphellophora*, *Papiliotrema*, and *Taphrina* (Figure 2). More than 50% of the remaining genera and unknown species across all plots were also identified.

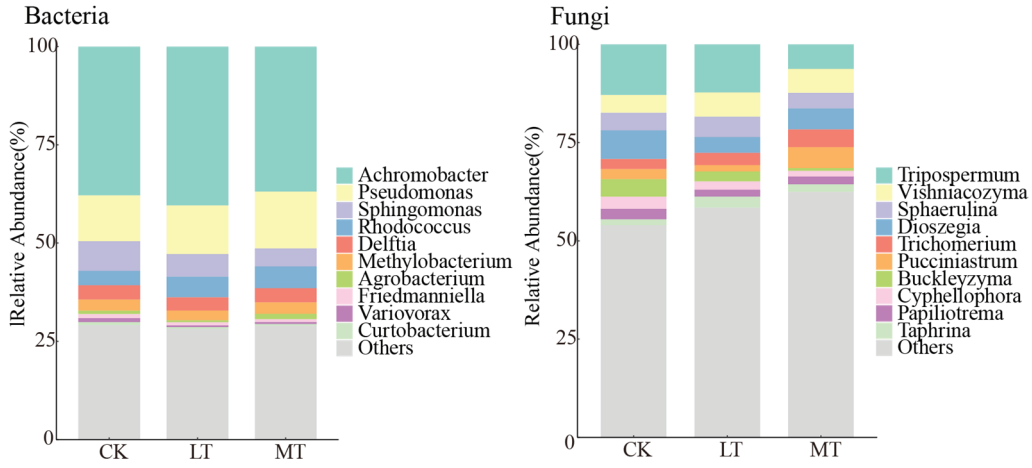


Figure 2. Composition of endophytic fungal and bacterial communities at different thinning intensities. CK: control check; LT: light thinning; MT: moderate thinning.

We observed that thinning intensity influenced the relative abundance of endophyte taxa at genus levels (Figure 3). Among the endophytic bacteria, genera such as *Sphingomonas*, *Variovorax*, and *Devosia* exhibited the highest relative abundance in CK plots (Figure 3). Conversely, the relative abundance of *Pseudomonas* and *Rhodococcus* increased with the thinning intensity. For endophytic fungi, genera such as *Tripospermum*, *Buckleyzyma*, *Cyphellophora*, *Apiotrichum*, and *Neoacrodontiella* decreased in relative abundance with increasing thinning intensity (Figure 3). Notably, among endophytic fungi, *Camptophora*, *Tricladiella*, and *Genolevuria* had the highest relative abundance in LT plots.

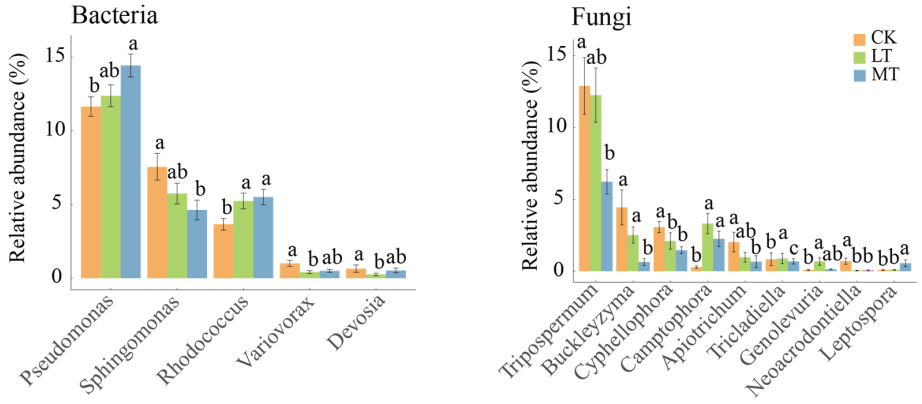


Figure 3. Relative abundance of endophytic bacterial and fungal communities at different thinning intensities. CK: control check; LT: light thinning; MT: moderate thinning. Values are means ± SE for panels (n = 40). Different letters represent significant differences ($p < 0.05$).

F. mandshurica, the relative abundance of endophytic bacteria, including *Pseudomonas*, *Sphingomonas*, *Variovorax*, and *Devosia*, significantly changed with thinning intensity (Figure S4). In *U. davidiana*, the relative abundance of *Sphingomonas* and *Variovorax* significantly decreased with thinning intensity (Figure S4). Regarding endophytic fungi, in *T. amurensis*, the relative abundance of endophytic fungi such as *Buckleyzyma*, *Cyphellophora*, and *Neoacrodontiella* decreased with thinning intensity, which was also true for *Tripospermum*, *Cyphellophora* in *P. Koraiensis*, and for *Buckleyzyma* in *U. davidiana* (Figure S4).

In the damaged leaves, only three genera of endophytic bacteria, namely *Sphingomonas*, *Rhodococcus*, and *Variovorax*, were significantly impacted by thinning intensity (Figure S5). In *U. davidiana*, the relative abundance of the endophytic fungi, particularly *Neoacrodontiella*, significantly responded to thinning intensity in both healthy and damaged leaves, with the highest abundance observed in CK plots (Figure S5). Discrepancies in the abundance of certain fungi between healthy and damaged leaves in response to thinning intensity were also observed in *A. pictum*, *P. Koraiensis*, and *T. amurensis* (Figure S5).

3.3. Co-Occurrence Networks of Leaf Endophytic Fungi and Bacteria

A co-occurrence network was performed using the Spearman correlation coefficient. Node attributes were compared in Table 2, including the number of nodes, edges, edge density, average degree, and relative modularity. For the endophytic bacterial community, the CK plot exhibited a higher number of nodes, edges, edge density, average degree, and relative modularity compared to LT and MT plots. The network structure of the bacterial community appeared more complex in the CK plot, which was reduced with the thinning intensity. For the endophytic fungal community, however, the MT plot showed a higher number of nodes, edges, edge density, average degree, and relative modularity compared to CK and LT plots. Increased thinning intensity resulted in greater complexity in the structure of the endophytic fungal community network.

The network nodes were categorized by genus, with *Sphingomonas* showing the highest proportion among endophytic bacteria and *Dioszegia* among endophytic fungi (Figure 4a). The key taxa were classified at the genus level via the core node discrimination method of the Zi-Pi network (Figure 4b). The topological characteristics of nodes divide node attributes into four types: module hubs (nodes with high connectivity within modules), connectors (nodes with high connectivity between two modules), network hubs (nodes that have high connectivity throughout the network), and peripherals (nodes that do not have high connectivity within or between modules). The remaining three types of nodes, excluding peripherals, are generally classified as key species. After the modularization of the endophytic bacterial network, the intra-module connectivity (Zi) and inter-module connectivity (Pi) of the different nodes were calculated, showing 14 key species in the CK plots, 7 key species in the LT plots, and 12 key species in the MT plots (Figure 4b). These

key species act as modular hubs and connectors, for instance, ASV_3211 appeared in both CK and MT plots, but only the Cystobacterace family has been identified in ASV_3211. In addition, CK and MT samples shared the presence of the *Methylbacterium* genus. In endophytic fungi, the Zi-Pi values indicated 8 key species in CK plots, 5 key species in LT plots, and 13 key species in MT plots, with these key species functioning as modular hubs. Both CK and LT plots contained ASV_2271, identified as a Chaetothyriales order, and the CK and LT plots shared a common genus of *Erythrobasidiomycetes* (Figure 4b). We also observed that the leaves of *T. amurensis*, *A. pictum*, *U. davidiana*, and *P. Koraiensis* harbored key species belonging to the genera *Methylobacterium* and *Sphingomonas* within their endophytic bacterial communities. Similarly, the endophytic fungi in the leaves of *T. amurensis*, *A. pictum*, and *P. Koraiensis* featured key species belonging to the *Erythrobasidium* genus (Table S1).

Table 2. Topological information of endophytic fungi and bacteria networks across different thinning intensities.

	Thinning Intensity	Edges	Nodes	Edge Density	Average Degree	Relative Modularity
Bacteria	CK	3286	470	0.030	13.983	1.761
	LT	1439	388	0.019	7.418	1.232
	MT	2574	448	0.026	11.491	1.48
Fungi	CK	17,922	1134	0.028	31.609	6.761
	LT	21,922	1264	0.027	34.687	7.198
	MT	23,597	1271	0.029	37.131	7.823

Note: relative modularity refers to the extent measures to which a network is compartmentalized into different modules. CK: control check; LT: light thinning; MT: moderate thinning.

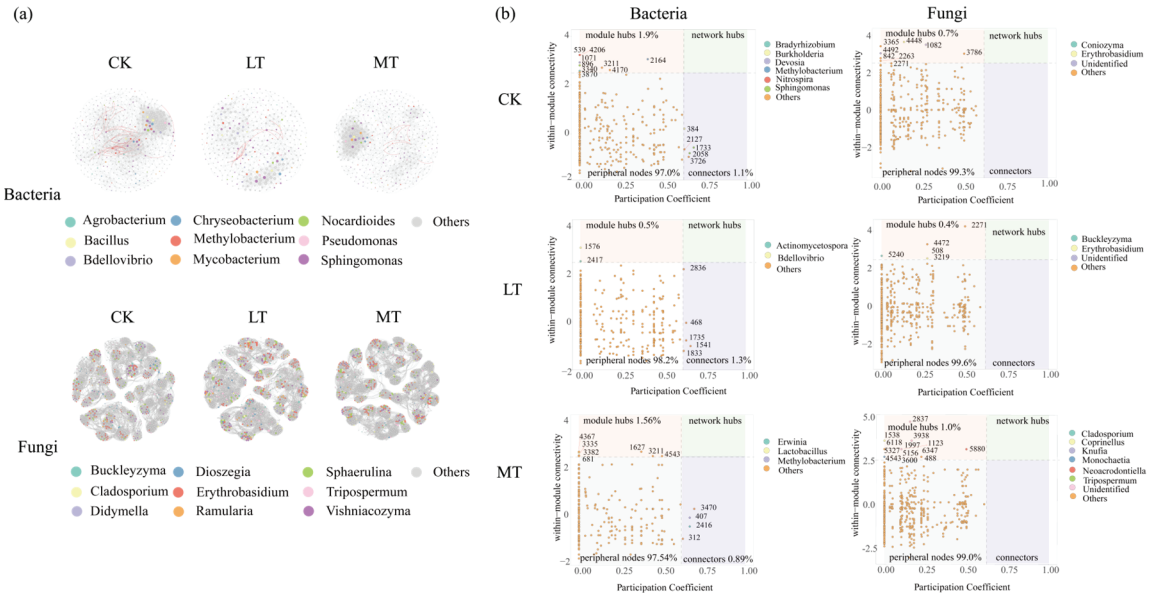


Figure 4. Network structure of endophytic fungal and bacterial communities across different thinning intensities. (**a**) Co-occurrence networks of endophytic bacterial and fungal communities. Gray lines indicate positive correlations and red lines indicate negative correlations. The nodes are colored based on the genus-level taxonomic classification of microbes. The node size corresponds to the degree level. (**b**) Zi-Pi diagram of the ecological network of endophytic bacterial and fungal communities. According to corresponding criteria, we identified module hubs ($Zi \geq 2.5$, $Pi < 0.62$), connectors ($Zi < 2.5$, $Pi \geq 0.62$), and network hubs ($Zi \geq 2.5$, $Pi \geq 0.62$), which are referred to as keystone nodes. All other nodes were categorized as peripherals. CK: control check; LT: light thinning; MT: moderate thinning.

3.4. Functional Prediction of Leaf Endophytic Fungi and Bacteria

Using the FAPROTAX functional annotation method, the ecological categories of endophytic bacteria were classified into three types, i.e., those involved in the carbon cycle, nitrogen cycle, and energy source. The dominant communities were Chemoheterotrophy, Aerobic Chemoheterotrophy, and Anaerobic Chemoheterotrophy, collectively accounting for over 50% (Figure 5a). As thinning intensity increased, functional groups involved in nitrogen respiration and nitrate reduction significantly increased. Concurrently, the functional groups of Aerobic Chemoheterotrophy and Chemoheterotrophy significantly decreased (Figure 5b).

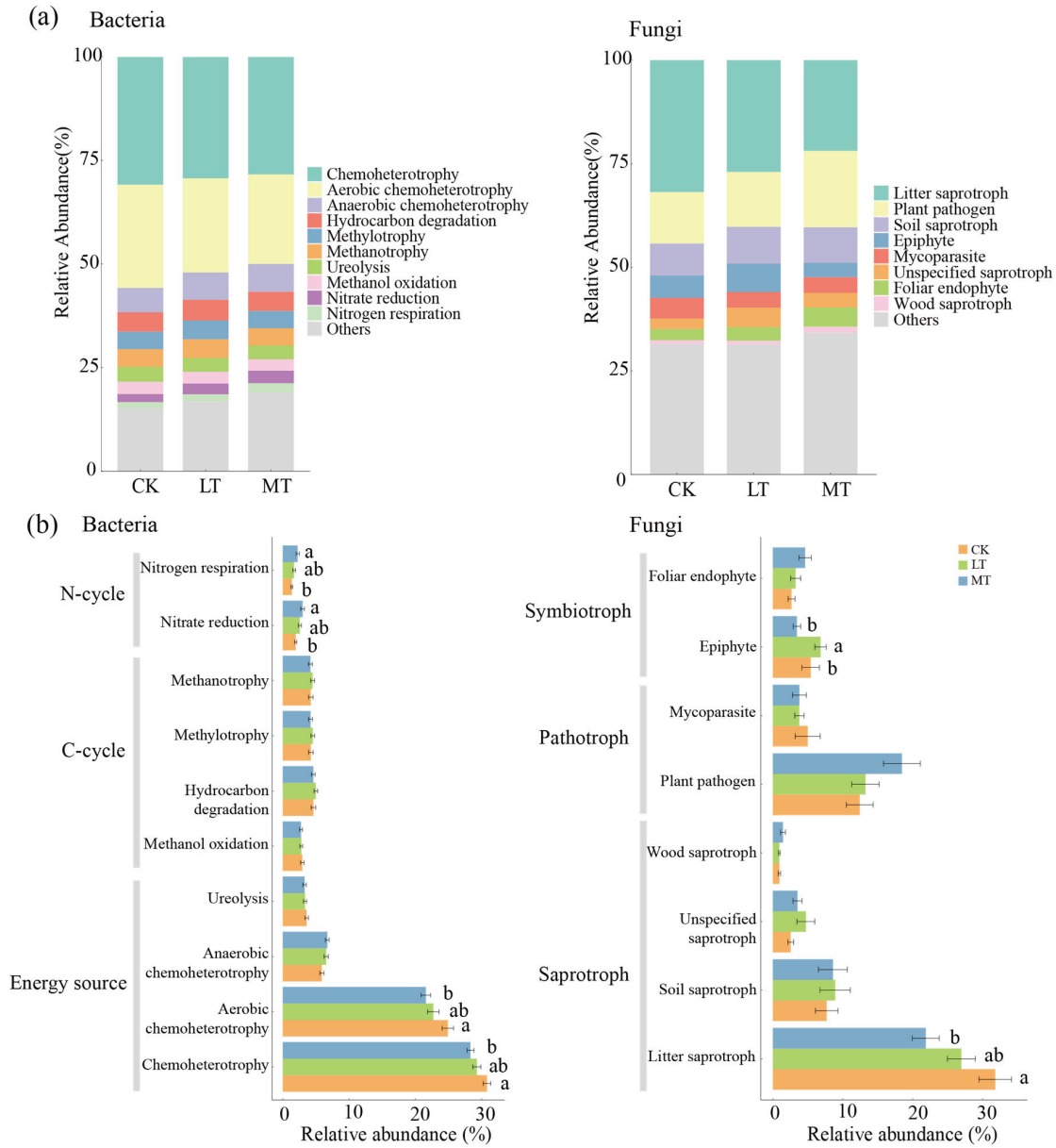


Figure 5. Functional prediction of endophytic fungal and bacterial communities across different thinning intensities. (**a**) Functional composition of endophytic bacterial and fungal communities. (**b**) Differences in functional composition of endophytic bacterial and fungal communities. CK: control check; LT: light thinning; MT: moderate thinning. Values are means ± SE for panels (n = 40). Different letters represent significant differences ($p < 0.05$).

The ecological classification of endophytic fungi is based on FUNGuild functional prediction, divided primarily into three types, i.e., saprotroph, pathotroph, and sym-

biotroph. The dominant communities include litter saprotrophs, plant pathogens, and soil saprotrophs, collectively accounting for more than 50% of the communities (Figure 5a). Litter saprotrophs declined significantly with the increase in thinning intensity, whereas plant pathogens increased significantly under the same condition. However, there was no significant difference in soil saprotrophs (Figure 5b).

Except for *U. davidiana* species, the endophytic bacteria involved in Aerobic Chemoheterotrophy and Chemoheterotrophy decreased with thinning intensity. In *F. mandshurica*, the endophytic bacteria involved in nitrogen respiration and nitrate reduction increased with thinning intensity (Figure S6). Similarly, the plant fungal pathogen also increased with thinning intensity (Figure S6, lower panels). In *P. Koraiensis*, the litter saprotroph of endophytic fungi decreased with thinning intensity.

There were no significant differences in endophytic bacteria in both healthy and damaged leaves (Figure S7). In *F. mandshurica*, among the endophytic fungi of damaged leaves, the plant pathogen was the highest in the LT plot. In contrast, in healthy leaves, the endophytic fungi increased with the rise in thinning intensity, peaking in the MT plot (Figure S7, lower panels). In *P. Koraiensis*, litter saprotrophs of endophytic fungi decreased with the increasing thinning intensity, observed in both healthy and damaged leaves.

3.5. Drivers Triggering Variations in the Assemblages of Leaf Endophytic Fungi and Bacteria

Thinning intensity had significant effects on SLA, LDMC, Zn, and P (Table 3). Using stepwise forward regression, we selected leaf traits that significantly explained the richness of leaf bacterial and fungal endophytes (Figure S1b). A preliminary model was constructed based on previous studies (Figure S1a). During the adjustment process of the structural equation model, SLA and LDMC were further identified as key leaf trait factors regulating the relationship between thinning intensity and leaf endophytic bacterial communities. Therefore, in the structural equation model, the composite variables of leaf traits comprised SLA and LDMC, and pH and soil moisture content were categorized as soil variables (Figure 6).

Table 3. Response of leaf traits, soil variables, and neighbor tree diversity to thinning intensity.

Factor	Thinning Intensity		
	CK	**LT**	**MT**
Ca (g/kg)	2.33 ± 0.19 a	2.14 ± 0.18 a	2.26 ± 0.19 a
Cu (mg/kg)	6.49 ± 0.32 a	6.39 ± 0.42 a	6.06 ± 0.39 a
K (g/kg)	9.84 ± 0.63 a	9.69 ± 0.55 a	9.03 ± 0.54 a
Mg (g/kg)	2.31 ± 0.15 a	2.21 ± 0.12 a	2.31 ± 0.14 a
Zn (mg/kg)	37.30 ± 2.43 **a**	33.07 ± 3.12 **ab**	24.84 ± 2.35 **b**
P (g/kg)	2.3 ± 0.08 **a**	2.06 ± 0.06 **b**	2.09 ± 0.07 **ab**
C (g/kg)	461.13 ± 2.99 a	461 ± 4.78 a	462.07 ± 5.17 a
N (g/kg)	24.90 ± 1.11 a	22.14 ± 0.8 a	22.56 ± 0.88 a
C/N	20.48 ± 1.21 a	22.41 ± 1.19 a	22.28 ± 1.24 a
SLA (cm^2/g)	204.27 ± 16.88 **a**	155.06 ± 13.64 **b**	160.02 ± 11.88 **ab**
LA (cm^2)	27.54 ± 2.53 a	23.17 ± 2.03 a	25.49 ± 2.04 a
LDMC (g/g)	0.32 ± 0.02 **ab**	0.31 ± 0.01 **b**	0.35 ± 0.01 **a**
LL (cm)	10.11 ± 0.37 a	9.67 ± 0.29 a	9.76 ± 0.33 a
LW (cm)	4.80 ± 0.41 a	4.44 ± 0.39 a	4.74 ± 0.41 a
LT (mm)	0.17 ± 0.01 a	0.17 ± 0.01 a	0.16 ± 0.01 a
Neighbor_diversity	0.99 ± 0.08 **a**	0.65 ± 0.06 **b**	0.35 ± 0.08 **c**
pH	4.40 ± 0.07 **a**	4.29 ± 0.08 **a**	3.99 ± 0.08 **b**
SWC (%)	47.05 ± 0.88 a	45.22 ± 1.25 a	45.57 ± 1.62 a

Note: Ca: total leaf calcium; Cu: total leaf copper; K: total leaf potassium; Mg: total leaf magnesium; Zn: total leaf zinc; P: total leaf phosphorus; C: total leaf carbon; N: total leaf nitrogen; C/N: carbon/nitrogen ratio; SLA: specific leaf area; LA: leaf area; LDMC: leaf dry matter content; LL: leaf length; LW: leaf width; LT: leaf thickness; Neighbor_diversity: neighbor tree richness; pH: soil pH; SWC: soil moisture content. CK: control check; LT: light thinning; MT: moderate thinning. Values are means ± SE for panels (n = 40). Different letters represent significant differences ($p < 0.05$). Bold the indicators with significant differences under different thinning intensities and bold the letters.

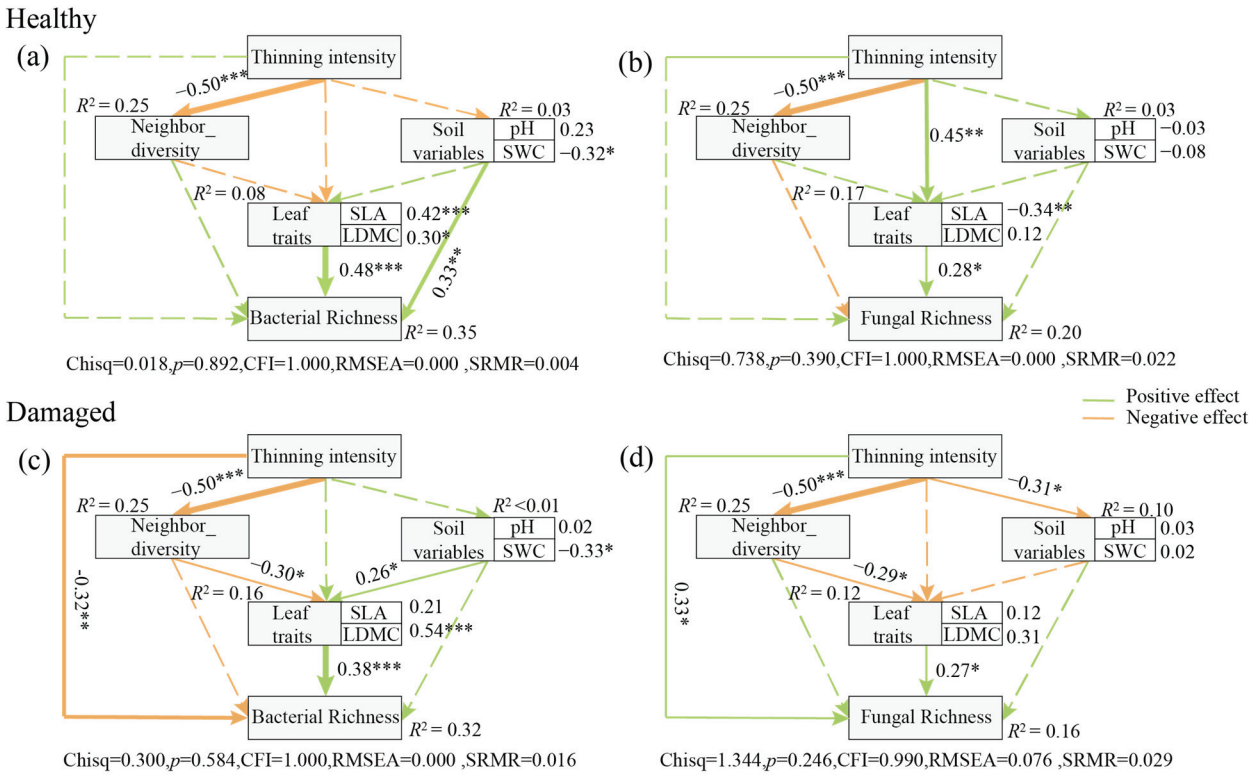


Figure 6. Structural equation models for evaluating factors closely associated with the richness of endophytic bacterial and fungal communities in leaves under different thinning intensities. (**a**) Endophytic bacteria in healthy leaves. (**b**) Endophytic fungi in healthy leaves. (**c**) Endophytic bacteria in damaged leaves. (**d**) Endophytic fungi in damaged leaves. Neighbor_diversity: neighbor tree richness; SLA: specific leaf area; LDMC: leaf dry matter content; pH: soil pH; SWC: soil moisture content. The green arrows indicate a positive correlation, and the orange arrows indicate a negative correlation. The solid lines indicate a significant relationship ($p < 0.05$), and the dashed arrows indicate an insignificant relationship ($p > 0.05$). The asterisks showed the p-value significance level—* $p < 0.05$, ** $p < 0.01$, *** $p < 0.001$.

In healthy leaves, thinning intensity positively influenced the richness of endophytic fungi and bacteria, although the effect was not statistically significant (Figure 6). Moreover, thinning intensity indirectly affected the richness of the leaf endophytic fungi through modulating leaf traits (Figure 6b). Additionally, the richness of endophytic bacteria was significantly affected by leaf traits, as well as soil variables (Figure 6a). However, soil variables such as soil pH and water content did not affect endophytic fungal richness.

In damaged leaves, thinning intensity significantly negatively affected the richness of endophytic bacteria, while it significantly positively influenced the richness of endophytic fungi (Figure 6c,d). Furthermore, thinning intensity conferred indirect effects on the richness of both endophytic bacteria and fungi by modulating the neighbor tree diversity, which consequently changed the leaf traits of focal tree species and their associated bacterial and fungal richness (Figure 6c,d). Additionally, in damaged leaves, soil variables were found to positively affect leaf traits (Figure 6c).

4. Discussion

4.1. The Contrasting Responses of the Diversity of Leaf Endophytic Fungi and Bacteria to Thinning Intensity

The susceptibility of soil bacteria to abiotic stresses is higher compared to fungi [43,44]. However, there is limited literature regarding leaf endophytes in this context. Our findings indicate that under light thinning intensity, leaf endophytic fungal diversity significantly surpassed that of the control group, while leaf endophytic bacterial diversity was slightly

lower in the thinning treatment compared to the control, although not significantly different (Figure 1). This suggests that leaf endophytic fungi exhibit greater sensitivity to thinning, whereas leaf endophytic bacteria demonstrate greater stability in response to thinning. Therefore, temperate forest thinning may intensify antagonistic interactions between leaf endophytic fungi and bacteria. In general, soil bacteria and fungi compete for resources, resulting in antagonism between these microbial groups [45], which may provide a plausible explanation for the contrasting trends observed in the diversity of fungal and bacterial communities. Furthermore, we observed that the most significant increase under the thinning gradient was in pathogenic fungi, while the dominant decrease in bacterial community diversity was observed in chemo-energy heterotrophs (Figure 5), supporting the notion that changes in bacterial diversity were driven by competition. Additionally, we found that host plant identity had a more significant impact on the structure of leaf endophytic bacterial communities compared to thinning intensity (Figure S2, Table 1). This finding aligns with previous studies, indicating that the host plant primarily regulates leaf endophytes and is less influenced by inter-host dispersal [26], which helps explain the lack of significant changes in leaf endophytic bacterial diversity with thinned intensity.

In terms of community composition, the temperate forest thinning significantly increased the relative abundance of *Rhodococcus* spp. in the endophytic bacterial community (Figures 2 and 3) and concurrently reduced the relative abundance of *Cyphellophora* spp. in the endophytic fungal community. Conversely, thinning led to a significant increase in the relative abundance of *Camptophora* spp. in the endophytic fungal community (Figures 2 and 3). Thinning is generally predicted to alter the community structure of host trees, accelerating nutrient availability and modifying organic matter content [46]. Moreover, thinning can cause significant changes in habitat conditions, such as increased exposure to direct sunlight and soil disturbance [47]. The changes can greatly influence the makeup of microbial communities, resulting in the emergence of communities adapted to the new habitat conditions and resource utilization strategies. Consequently, leaf endophytes with adaptive advantages to the altered habitat conditions and resource utilization strategies, such as the fungal and bacterial species mentioned above, become more prevalent, while non-adapted communities may be outcompeted and eliminated through competition.

4.2. The Contrasting Trends of the Complexity of Leaf Endophytic Fungal and Bacterial Co-Occurrence Networks

Thinning can exert significant effects on plant leaves by altering canopy density [48], water content [49], and the diversity of neighboring species [50]. We observed a progressive reduction in the complexity of the co-occurrence network of leaf bacterial endophytes with increasing thinning intensity, resulting in a simpler network topology, which is consistent with changes in diversity (Figure 4). This indicates that thinning leads to a decrease in interactions among leaf endophytic bacteria. Conversely, the topological features of the network of leaf endophytic fungi became progressively more complex with increasing thinning intensity (Figure 4). These characteristics reflect the level of connectivity and interactions among microorganisms [51]. One explanation for this topological variation is the differentiation of ecological niches within leaf tissues due to changes in the diversity of leaf endophyte communities triggered by thinning intensity [52]. The increased diversity of leaf endophytic fungi associated with higher thinning intensity led to a more homogeneous distribution of ecotopes for leaf endophytic fungi. Weak ecotope differentiation may enhance interactions between microorganisms [53]. Conversely, the decrease in the diversity of leaf endophytic bacteria may have resulted in significant ecotope differentiation, reducing competition, and allowing microorganisms to coexist within the community for extended periods. Additionally, this ecological niche differentiation may have inhibited interactions between different species of endophytic bacteria [54]. Similarly, bacteria and fungi were predominantly positively correlated in microbial networks under thinning. Positive and negative correlations in microbial networks represent mutually beneficial symbiotic or

competitive relationships among interrelated species [55]. This pattern may arise from resource abundance and reduced competition among bacterial species, resulting in higher synergism between bacterial communities [56].

Node attributes in microbial networks can be categorized into four types based on the node's topological characteristics: module hubs, connectors, network hubs, and peripherals. Typically, network hubs denote nodes that have a high degree of connectivity throughout the network (Zi > 2.5 and Pi > 0.62), i.e., nodes that play an important role both within modules and between different modules [57]. From an ecological perspective, peripherals are considered specialists, while network hubs are super-generalists. Due to environmental determinism, specialists constitute a major part of most systems, whereas super-generalists are very few [51,58]. In this study, network hubs were present neither in bacterial nor fungal networks. However, module hubs and connectors, which are closer to generalists, were found to varying degrees. These module hubs and connectors play an important role, highlighting their significance in bacterial and fungal endophytic network structures in temperate forests.

Given the intricate nature of leaf microbial communities, the concepts of microbial persistence (core taxa) and their significance in the microbial network (pivotal taxa) have been utilized to identify microbes playing key roles in leaf communities [59,60]. Furthermore, as the thinning intensity changed, different ASVs were assigned to different modules, indicating that thinning intensity altered the key taxa within the network of the leaf endophyte community. Most of the key taxa showed strong specificity for leaf endophytes. Notably, the CK plots and MT plots shared a genus, *Methylobacterium*. It has been well documented that the enrichment of plant biomes with the genus *Methylobacterium* can promote plant growth and productivity, as well as plant drought tolerance [61,62]. For leaf endophytic fungi, the CK and LT plots share a genus, *Erythrobasidium*, whose members have not been well studied, with only eight species found in nature so far [63,64], and whose functions are even less understood. It should be noted, however, that these key taxa are not the same across time and environments, that is, key species may play a critical role only under certain conditions [58,65]. Our results support that this environmental deterministic influence applies equally well in leaf endophyte communities.

For different tree species, we found that there was a high variability of bacterial and fungal key taxa among the different tree species, suggesting that the key taxa of the endophytic bacteria in leaves are highly plant species-specific. Interestingly, when extending the bacterial key taxa to the genus level, we found the genus *Sphingomonas* existed in four of the tree species. Bacteria of the genus *Sphingomonas* are widespread in nature due to their low nutrient concentration requirements and have been shown to have resistance to bacterial pathogens. Additionally, they can spread vertically between plant generations through seeds [66]. Overall, when investigating the network complexity of leaf endophytes, the key taxa should be well considered.

4.3. Leaf Trait-Mediated Thinning Effects on Leaf Fungal and Bacterial Endophytes

Leaf surfaces present hostile environments where inhabiting microorganisms are exposed to various physicochemical stresses, including intense light and ultraviolet (UV) radiation, fluctuating temperature and humidity, and limited nutrient availability [27]. Our findings indicate that both endophytic bacterial and fungal community richness were significantly positively influenced by leaf functional traits (Figure 6). Previous studies demonstrate that changes in endophytic microbial colonization and diversity are regulated by leaf economic profiles, which encompass trade-off strategies for leaf nutrient utilization [67]. It is because most leaf endophytes are horizontally transmitted via airborne spores, that endophyte spores and mycelium inevitably interact with leaf traits. Upon reaching the leaf surface, endophytes typically colonize the tissue through wounding and stomatal infiltration [15]. Consequently, traits related to leaf defense performance, such as specific leaf area and leaf dry matter mass, become particularly important for leaf endophytic bacterial communities. Furthermore, we found that leaf endophyte communities

were less influenced by neighbors (Figure 6). This further corroborates our previous conclusion that endophytes may be primarily regulated by the host and less influenced by inter-host dispersal.

Unlike inter-root and soil microbial communities, leaf microbes are inevitably influenced by pollinating insects and herbivorous visitors, which introduce and redistribute microbiota [30]. Our findings reveal that in healthy leaves, soil properties can positively influence leaf endophytic bacterial abundance, whereas this relationship was not significant among damaged leaves. Previous studies indicate that the bacterial composition in leaves exhibits greater similarity to taxa present in soil than to bacteria in flowers and fruits [68]. This suggests that bacterial members in the interleaf microflora in the healthy statues are primarily soil-derived, emphasizing the essential role of soil properties in shaping the bacterial community. Furthermore, we found that neighbor diversity, in the presence of leaf damage, indirectly affects leaf endophyte communities by influencing leaf functional traits (Figure 6). Functional traits, serving as the foundation of leaf economic profiles, effectively express the ecological strategies of plants in resource acquisition and the optimal allocation of limited available resources [69,70]. The intensification of thinning is expected to decrease the neighborhood diversity of the target tree species and further increase ecological niches in the community, leading to an adjustment of the ecological strategy of the target tree species from a defensive to an aggressive development strategy. Finally, our results further elucidate that the effects of thinning on leaf endophytes may be primarily mediated by leaf damage, indicating that airborne microbial transmission and secretions from insect feeding possibly contribute to the reconstitution of the leaf microbial community.

Unlike those inhabiting healthy leaves, thinning had significant negative and positive effects on leaf endophytic bacteria and endophytic fungi in damaged leaves, respectively (Figure 6). Compared to the plant surface, the inner layers of leaves may provide a richer nutrient environment that protects microorganisms from external atmospheric fluctuations, including UV radiation and moisture [27]. However, this proximity to the plant's immune surveillance mechanisms and defense compounds may inhibit the colonization potential of endophytes, and leaf damage provides a pathway for changes in the microbial community. Damaged leaves expose the living environment for endophytes, triggering the growth of endophytic pathogenic fungi, consistent with previous observations [71,72] that many pathogens causing forest leaf diseases require wounds or scrapes to penetrate host tissues, typically caused by mechanical damage from herbivores or other physical factors such as wind or water [73]. In contrast, endophytic bacteria may be inhibited by fungal growth during competition, leading to a decrease under thinning gradients, representing a trade-off between different thinning intensities on leaf endophyte communities. The competition of both bacteria and fungi for resources among limited ecological niches inevitably results in a tendency for them to outcompete each other [54]. This further explains that the changes in leaf endophyte communities' diversity and co-occurrence network construction under different thinning intensities may be mediated by leaf damage.

5. Conclusions

Leaf endophytic fungi and bacteria exhibited contrasting responses to thinning intensity in temperate forest ecosystems. Specifically, endophytic fungal diversity increased significantly with thinning intensity, accompanied by an increase in the complexity of the co-occurrence network. Conversely, bacterial diversity did not show significant differences, but the complexity of the symbiotic network decreased as the thinning intensity increased. Moreover, the contrasting effects of thinning intensity on leaf fungal and bacterial endophytes were particularly noticeable in damaged leaves, compared to in healthy leaves, suggesting that the condition of the leaves—whether damaged or healthy—may be critical for constructing the trade-offs between leaf fungal and bacterial endophytes under forest thinning. Additionally, leaf endophytes were more strongly modulated by their host tree, with leaf functional traits having a significant positive effect on them, and the neighbor tree diversity also conferred an indirect effect on leaf endophytes via altering the leaf traits

of host trees. Overall, our findings provide insight into the trade-offs between fungal and bacterial endophytes in response to forest thinning, particularly in damaged leaves.

Supplementary Materials: The following supporting information can be downloaded at https://www.mdpi.com/article/10.3390/jof10070470/s1: Figure S1: A prior structural equation model (SEM) and regression analysis of the richness of endophytic bacteria and fungi in leaves. (a) The prior structural equation model (SEM) assumes a causal pathway by which thinning intensity affects the richness of endophytic bacteria and fungi in leaves by altering neighbor tree diversity, soil variables, and leaf traits. (b) Regression analysis of leaf traits on the richness of endophytic bacteria and fungi in leaves. Ca: total leaf calcium; Cu: total leaf cuprum; Mg: total leaf magnesium; Zn: total leaf zinc; C: total leaf carbon; N: total leaf nitrogen; SLA: specific leaf area; LDMC: leaf dry matter content; LL: leaf length; LW: leaf width; LT: leaf thickness. The asterisks showed the *p*-value significance level, * $p < 0.05$ *** $p < 0.001$. Figure S2: Alpha diversity index of endophytic bacterial and fungal communities in leaves of different tree species under different thinning intensities. CK: control check; LT: light thinning; MT: moderate thinning. AP: *Acer pictum* subsp. *mono*; FM: *Fraxinus mandshurica*; PK: *Pinus koraiensis*; TA: *Tilia amurensis*; UD: *Ulmus davidiana* var. *japonica*. Different letters indicate significant differences ($p < 0.05$). Figure S3: Alpha diversity index of endophytic bacterial and fungal communities in healthy and damaged leaves of different tree species under different thinning intensities. CK: control check; LT: light thinning; MT: moderate thinning. AP: *Acer pictum* subsp. *mono*; FM: *Fraxinus mandshurica*; PK: *Pinus koraiensis*; TA: *Tilia amurensis*; UD: *Ulmus davidiana* var. *japonica*. Figure S4: Differences in relative abundance of endophytic bacterial and fungal communities in leaves of different tree species under different thinning intensities. CK: control check; LT: light thinning; MT: moderate thinning. AP: *Acer pictum* subsp. *mono*; FM: *Fraxinus mandshurica*; PK: *Pinus koraiensis*; TA: *Tilia amurensis*; UD: *Ulmus davidiana* var. *japonica*. Values are means ± SE for panels ($n = 8$). Different letters indicate significant differences ($p < 0.05$). Figure S5: Differences in relative abundance of endophytic bacterial and fungal communities in healthy and damaged leaves of different tree species under different thinning intensities. CK: control check; LT: light thinning; MT: moderate thinning. AP: *Acer pictum* subsp. *mono*; FM: *Fraxinus mandshurica*; PK: *Pinus koraiensis*; TA: *Tilia amurensis*; UD: *Ulmus davidiana* var. *japonica*. Values are means ± SE for panels ($n = 4$). The asterisks showed the *p*-value significance level, * $p < 0.05$. Figure S6: Differences in functional composition of endophytic bacterial and fungal communities in leaves of different tree species under different thinning intensities. CK: control check; LT: light thinning; MT: moderate thinning. AP: *Acer pictum* subsp. *mono*; FM: *Fraxinus mandshurica*; PK: *Pinus koraiensis*; TA: *Tilia amurensis*; UD: *Ulmus davidiana* var. *japonica*. Values are means ± SE for panels ($n = 8$). Different letters indicate significant differences ($p < 0.05$). Figure S7: Differences in functional composition of endophytic bacterial and fungal communities in healthy and damaged leaves of different tree species under different thinning intensities. CK: control check; LT: light thinning; MT: moderate thinning. AP: *Acer pictum* subsp. *mono*; FM: *Fraxinus mandshurica*; PK: *Pinus koraiensis*; TA: *Tilia amurensis*; UD: *Ulmus davidiana* var. *japonica*. Values are means ± SE for panels ($n = 4$). The asterisks showed the *p*-value significance level, * $p < 0.05$. Table S1: Keystone of endophytic bacteria and fungi Zi-Pi network in leaves of different tree species.

Author Contributions: Conceptualization, C.L. and N.Z.; methodology, B.L.; formal analysis, B.L.; investigation, X.Z., C.Z., X.H. and L.Q.; data curation, B.L.; writing—original draft preparation, B.L. and C.L.; writing—review and editing, N.Z.; visualization, B.L.; supervision, N.Z. All authors have read and agreed to the published version of the manuscript.

Funding: The study is supported by the National Key Research and Development Program of China (2023YFF1304003-02 and 2022YFF1303201) and the Beijing Natural Science Foundation Project (5222016).

Institutional Review Board Statement: Not applicable.

Informed Consent Statement: Not applicable.

Data Availability Statement: The microbial raw DNA sequences have been deposited into the NCBI database, with the accession numbers SRR29007114-SRR29007233 and SRR29019700-SRR29019819.

Conflicts of Interest: The authors declare no conflicts of interest.

References

1. Zhan, C.; Matsumoto, H.; Liu, Y.; Wang, M. Pathways to Engineering the Phyllosphere Microbiome for Sustainable Crop Production. *Nat. Food* **2022**, *3*, 997–1004. [CrossRef] [PubMed]
2. Wagner, M.R.; Lundberg, D.S.; del Rio, T.G.; Tringe, S.G.; Dangl, J.L.; Mitchell-Olds, T. Host Genotype and Age Shape the Leaf and Root Microbiomes of a Wild Perennial Plant. *Nat. Commun.* **2016**, *7*, 12151. [CrossRef] [PubMed]
3. Eschen, R.; Hunt, S.; Mykura, C.; Gange, A.C.; Sutton, B.C. The Foliar Endophytic Fungal Community Composition in Cirsium Arvense Is Affected by Mycorrhizal Colonization and Soil Nutrient Content. *Fungal Biol.* **2010**, *114*, 991–998. [CrossRef] [PubMed]
4. Aydogan, E.L.; Moser, G.; Müller, C.; Kämpfer, P.; Glaeser, S.P. Long-Term Warming Shifts the Composition of Bacterial Communities in the Phyllosphere of Galium Album in a Permanent Grassland Field-Experiment. *Front. Microbiol.* **2018**, *9*, 144. [CrossRef] [PubMed]
5. Meyer, K.M.; Porch, R.; Muscettola, I.E.; Vasconcelos, A.L.S.; Sherman, J.K.; Metcalf, C.J.E.; Lindow, S.E.; Koskella, B. Plant Neighborhood Shapes Diversity and Reduces Interspecific Variation of the Phyllosphere Microbiome. *ISME J.* **2022**, *16*, 1376–1387. [CrossRef] [PubMed]
6. Humphrey, P.T.; Whiteman, N.K. Insect Herbivory Reshapes a Native Leaf Microbiome. *Nat. Ecol. Evol.* **2020**, *4*, 221–229. [CrossRef]
7. Arnold, A.E.; Mejía, L.C.; Kyllo, D.; Rojas, E.I.; Maynard, Z.; Robbins, N.; Herre, E.A. Fungal Endophytes Limit Pathogen Damage in a Tropical Tree. *Proc. Natl. Acad. Sci. USA* **2003**, *100*, 15649–15654. [CrossRef] [PubMed]
8. Liu, H.; Brettell, L.E.; Singh, B. Linking the Phyllosphere Microbiome to Plant Health. *Trends Plant Sci.* **2020**, *25*, 841–844. [CrossRef]
9. Xu, P.; Fan, X.; Mao, Y.; Cheng, H.; Xu, A.; Lai, W.; Lv, T.; Hu, Y.; Nie, Y.; Zheng, X.; et al. Temporal Metabolite Responsiveness of Microbiota in the Tea Plant Phyllosphere Promotes Continuous Suppression of Fungal Pathogens. *J. Adv. Res.* **2022**, *39*, 49–60. [CrossRef]
10. Liu, H.; Brettell, L.E.; Qiu, Z.; Singh, B.K. Microbiome-Mediated Stress Resistance in Plants. *Trends Plant Sci.* **2020**, *25*, 733–743. [CrossRef]
11. Tian, J.; He, N.; Kong, W.; Deng, Y.; Feng, K.; Green, S.M.; Wang, X.; Zhou, J.; Kuzyakov, Y.; Yu, G. Deforestation Decreases Spatial Turnover and Alters the Network Interactions in Soil Bacterial Communities. *Soil Biol. Biochem.* **2018**, *123*, 80–86. [CrossRef]
12. Carreño-Rocabado, G.; Peña-Claros, M.; Bongers, F.; Alarcón, A.; Licona, J.-C.; Poorter, L. Effects of Disturbance Intensity on Species and Functional Diversity in a Tropical Forest. *J. Ecol.* **2012**, *100*, 1453–1463. [CrossRef]
13. Both, S.; Riutta, T.; Paine, C.E.T.; Elias, D.M.O.; Cruz, R.S.; Jain, A.; Johnson, D.; Kritzler, U.H.; Kuntz, M.; Majalap-Lee, N.; et al. Logging and Soil Nutrients Independently Explain Plant Trait Expression in Tropical Forests. *New Phytol.* **2019**, *221*, 1853–1865. [CrossRef]
14. Xu, R.; Wang, L.; Zhang, J.; Zhou, J.; Cheng, S.; Tigabu, M.; Ma, X.; Wu, P.; Li, M. Growth Rate and Leaf Functional Traits of Four Broad-Leaved Species Underplanted in Chinese Fir Plantations with Different Tree Density Levels. *Forests* **2022**, *13*, 308. [CrossRef]
15. Huang, Y.-L.; Zimmerman, N.; Arnold, A. Observations on the Early Establishment of Foliar Endophytic Fungi in Leaf Discs and Living Leaves of a Model Woody Angiosperm, Populus Trichocarpa (Salicaceae). *J. Fungi* **2018**, *4*, 58. [CrossRef]
16. Murakami, K.; Matsuda, R. Optical and Physiological Properties of a Leaf. In *LED Lighting for Urban Agriculture*; Kozai, T., Fujiwara, K., Runkle, E.S., Eds.; Springer: Singapore, 2016; pp. 113–123, ISBN 978-981-10-1846-6.
17. Le Provost, G.; Badenhausser, I.; Le Bagousse-Pinguet, Y.; Clough, Y.; Henckel, L.; Violle, C.; Bretagnolle, V.; Roncoroni, M.; Manning, P.; Gross, N. Land-Use History Impacts Functional Diversity across Multiple Trophic Groups. *Proc. Natl. Acad. Sci. USA* **2020**, *117*, 1573–1579. [CrossRef]
18. Zhang, X.; Guan, D.; Li, W.; Sun, D.; Jin, C.; Yuan, F.; Wang, A.; Wu, J. The Effects of Forest Thinning on Soil Carbon Stocks and Dynamics: A Meta-Analysis. *For. Ecol. Manag.* **2018**, *429*, 36–43. [CrossRef]
19. Baraloto, C.; Hérault, B.; Paine, C.E.T.; Massot, H.; Blanc, L.; Bonal, D.; Molino, J.-F.; Nicolini, E.A.; Sabatier, D. Contrasting Taxonomic and Functional Responses of a Tropical Tree Community to Selective Logging. *J. Appl. Ecol.* **2012**, *49*, 861–870. [CrossRef]
20. Addo-Fordjour, P.; Ofosu-Bamfo, B.; Kwofie, F.; Akyea-Bobi, N.; Rahman, F.A.; Amoah, E. Changes in Liana Community Structure and Functional Traits along a Chronosequence of Selective Logging in a Moist Semi-Deciduous Forest in Ghana. *Plant Ecol. Divers.* **2020**, *13*, 75–84. [CrossRef]
21. Liu, P.; Wang, W.; Bai, Z.; Guo, Z.; Ren, W.; Huang, J.; Xu, Y.; Yao, J.; Ding, Y.; Zang, R. Competition and Facilitation Co-Regulate the Spatial Patterns of Boreal Tree Species in Kanas of Xinjiang, Northwest China. *For. Ecol. Manag.* **2020**, *467*, 118167. [CrossRef]
22. Connell, J.H. Diversity in Tropical Rain Forests and Coral Reefs: High Diversity of Trees and Corals Is Maintained Only in a Nonequilibrium State. *Science* **1978**, *199*, 1302–1310. [CrossRef] [PubMed]
23. Bongers, F.; Poorter, L.; Hawthorne, W.D.; Sheil, D. The Intermediate Disturbance Hypothesis Applies to Tropical Forests, but Disturbance Contributes Little to Tree Diversity. *Ecol. Lett.* **2009**, *12*, 798–805. [CrossRef]
24. Dos Santos, F.A.S.; Johst, K.; Grimm, V. Neutral Communities May Lead to Decreasing Diversity-Disturbance Relationships: Insights from a Generic Simulation Model: Diversity-Disturbance Curve of Neutral Theory. *Ecol. Lett.* **2011**, *14*, 653–660. [CrossRef]

25. Christian, N.; Sedio, B.E.; Florez-Buitrago, X.; Ramírez-Camejo, L.A.; Rojas, E.I.; Mejía, L.C.; Palmedo, S.; Rose, A.; Schroeder, J.W.; Herre, E.A. Host Affinity of Endophytic Fungi and the Potential for Reciprocal Interactions Involving Host Secondary Chemistry. *Am. J. Bot.* **2020**, *107*, 219–228. [CrossRef]
26. Yang, X.; Wang, P.; Xiao, B.; Xu, Q.; Guo, Q.; Li, S.; Guo, L.; Deng, M.; Lu, J.; Liu, L.; et al. Different Assembly Mechanisms of Leaf Epiphytic and Endophytic Bacterial Communities Underlie Their Higher Diversity in More Diverse Forests. *J. Ecol.* **2023**, *111*, 970–981. [CrossRef]
27. Sohrabi, R.; Paasch, B.C.; Liber, J.A.; He, S.Y. Phyllosphere Microbiome. *Annu. Rev. Plant Biol.* **2023**, *74*, 539–568. [CrossRef]
28. Underwood, N.; Inouye, B.D.; Hambäck, P.A. A Conceptual Framework for Associational Effects: When Do Neighbors Matter and How Would We Know? *Q. Rev. Biol.* **2014**, *89*, 1–19. [CrossRef] [PubMed]
29. Rowe, H.I.; Holland, J.D. High Plant Richness in Prairie Reconstructions Support Diverse Leafhopper Communities. *Restor. Ecol.* **2013**, *21*, 174–180. [CrossRef]
30. Atkinson, B.; Bailey, S.; Vaughan, I.P.; Memmott, J. A Comparison of Clearfelling and Gradual Thinning of Plantations for the Restoration of Insect Herbivores and Woodland Plants. *J. Appl. Ecol.* **2015**, *52*, 1538–1546. [CrossRef]
31. Tan, L.-Z.; Fan, C.-Y.; Fan, X.-H. Relationships between Species Diversity or Community Structure and Productivity of Woody-Plants in a Broad-Leaved Korean Pine Forest in Jiaohe, Jilin, China. *Chin. J. Plant Ecol.* **2017**, *11*, 1149–1156. [CrossRef]
32. Yan, Y.; Xin-Na, Z.; Jie, Y.; Chun-Yu, Z.; Xiu-Hai, Z. Composition and Temporal Dynamics of Tree Seedlings at Different Successional Stages of Conifer and Broad-Leaved Mixed Forests in Jiaohe, Jilin Province, China. *Chin. J. Plant Ecol.* **2016**, *40*, 127–139. [CrossRef]
33. Li, M.; Wu, Z.; Qiu, H.; Zhang, C.; Zhao, X. Short-Term Effects of Tending Felling on Ecological Services of Mixed broadleavedKorean Pine Forests at Jiaohe in Jilin Province, Northeastern China. *J. Beijing For. Univ.* **2019**, *41*, 40–49. [CrossRef]
34. Chen, Q. *Comparative Study on Photosynthetic Physiological Characteristics of Pinus Koraiensis Seedlings with Different Regeneration Methods in Jiaohe, Jilin, China*; Beijing Forestry University: Beijing, China, 2021.
35. Zhang, Y.; Cao, B.; Pan, Y.; Tao, S.; Zhang, N. Metabolite-Mediated Responses of Phyllosphere Microbiota to Rust Infection in Two Malus Species. *Microbiol. Spectr.* **2023**, *11*, e03831-22. [CrossRef]
36. Li, S.; Deng, Y.; Wang, Z.; Zhang, Z.; Kong, X.; Zhou, W.; Yi, Y.; Qu, Y. Exploring the Accuracy of Amplicon-based Internal Transcribed Spacer Markers for a Fungal Community. *Mol. Ecol. Resour.* **2020**, *20*, 170–184. [CrossRef]
37. Bolyen, E.; Rideout, J.R.; Dillon, M.R.; Bokulich, N.A.; Abnet, C.C.; Al-Ghalith, G.A.; Alexander, H.; Alm, E.J.; Arumugam, M.; Asnicar, F.; et al. Reproducible, Interactive, Scalable and Extensible Microbiome Data Science Using QIIME 2. *Nat. Biotechnol.* **2019**, *37*, 852–857. [CrossRef]
38. Callahan, B.J.; McMurdie, P.J.; Rosen, M.J.; Han, A.W.; Johnson, A.J.A.; Holmes, S.P. DADA2: High-Resolution Sample Inference from Illumina Amplicon Data. *Nat. Methods* **2016**, *13*, 581–583. [CrossRef] [PubMed]
39. Wen, T.; Xie, P.; Yang, S.; Niu, G.; Liu, X.; Ding, Z.; Xue, C.; Liu, Y.; Shen, Q.; Yuan, J. ggClusterNet: An R Package for Microbiome Network Analysis and Modularity-based Multiple Network Layouts. *iMeta* **2022**, *1*, e32. [CrossRef] [PubMed]
40. Põlme, S.; Abarenkov, K.; Henrik Nilsson, R.; Lindahl, B.D.; Clemmensen, K.E.; Kauserud, H.; Nguyen, N.; Kjøller, R.; Bates, S.T.; Baldrian, P.; et al. FungalTraits: A User-Friendly Traits Database of Fungi and Fungus-like Stramenopiles. *Fungal Divers.* **2020**, *105*, 1–16. [CrossRef]
41. Louca, S.; Parfrey, L.W.; Doebeli, M. Decoupling Function and Taxonomy in the Global Ocean Microbiome. *Science* **2016**, *353*, 1272–1277. [CrossRef]
42. Lefcheck, J.S. piecewiseSEM: Piecewise Structural Equation Modelling in r for Ecology, Evolution, and Systematics. *Methods Ecol. Evol.* **2016**, *7*, 573–579. [CrossRef]
43. Bahram, M.; Hildebrand, F.; Forslund, S.K.; Anderson, J.L.; Soudzilovskaia, N.A.; Bodegom, P.M.; Bengtsson-Palme, J.; Anslan, S.; Coelho, L.P.; Harend, H.; et al. Structure and Function of the Global Topsoil Microbiome. *Nature* **2018**, *560*, 233–237. [CrossRef] [PubMed]
44. De Vries, F.T.; Griffiths, R.I.; Bailey, M.; Craig, H.; Girlanda, M.; Gweon, H.S.; Hallin, S.; Kaisermann, A.; Keith, A.M.; Kretzschmar, M.; et al. Soil Bacterial Networks Are Less Stable under Drought than Fungal Networks. *Nat. Commun.* **2018**, *9*, 3033. [CrossRef] [PubMed]
45. Mille-Lindblom, C.; Fischer, H.J.; Tranvik, L. Antagonism between Bacteria and Fungi: Substrate Competition and a Possible Tradeoff between Fungal Growth and Tolerance towards Bacteria. *Oikos* **2006**, *113*, 233–242. [CrossRef]
46. Kreutzweiser, D.P.; Hazlett, P.W.; Gunn, J.M. Logging Impacts on the Biogeochemistry of Boreal Forest Soils and Nutrient Export to Aquatic Systems: A Review. *Environ. Rev.* **2008**, *16*, 157–179. [CrossRef]
47. Wang, Z.; Li, Y.; Wang, G.; Zhang, Z.; Chen, Y.; Liu, X.; Peng, R. Drivers of Spatial Structure in Thinned Forests. *For. Ecosyst.* **2024**, *11*, 100182. [CrossRef]
48. Waters, C.M.; Gonsalves, L.; Law, B.; Melville, G.; Toole, I.; Brassil, T.; Tap, P. The Effect of Thinning on Structural Attributes of a Low Rainfall Forest in Eastern Australia. *For. Ecol. Manag.* **2018**, *409*, 571–583. [CrossRef]
49. Simmons, L.A.; Anderson, S.H. Effects of Logging Activities on Selected Soil Physical and Hydraulic Properties for a Claypan Landscape. *Geoderma* **2016**, *269*, 145–152. [CrossRef]
50. Yang, H.; Ciais, P.; Frappart, F.; Li, X.; Brandt, M.; Fensholt, R.; Fan, L.; Saatchi, S.; Besnard, S.; Deng, Z.; et al. Global Increase in Biomass Carbon Stock Dominated by Growth of Northern Young Forests over Past Decade. *Nat. Geosci.* **2023**, *16*, 886–892. [CrossRef]

51. Deng, Y.; Jiang, Y.-H.; Yang, Y.; He, Z.; Luo, F.; Zhou, J. Molecular Ecological Network Analyses. *BMC Bioinform.* **2012**, *13*, 113. [CrossRef]
52. Li, J.; Li, C.; Kou, Y.; Yao, M.; He, Z.; Li, X. Distinct Mechanisms Shape Soil Bacterial and Fungal Co-Occurrence Networks in a Mountain Ecosystem. *FEMS Microbiol. Ecol.* **2020**, *96*, fiaa030. [CrossRef]
53. Faust, K.; Raes, J. Microbial Interactions: From Networks to Models. *Nat. Rev. Microbiol.* **2012**, *10*, 538–550. [CrossRef]
54. Ma, B.; Wang, H.; Dsouza, M.; Lou, J.; He, Y.; Dai, Z.; Brookes, P.C.; Xu, J.; Gilbert, J.A. Geographic Patterns of Co-Occurrence Network Topological Features for Soil Microbiota at Continental Scale in Eastern China. *ISME J.* **2016**, *10*, 1891–1901. [CrossRef]
55. Montoya, J.M.; Pimm, S.L.; Solé, R.V. Ecological Networks and Their Fragility. *Nature* **2006**, *442*, 259–264. [CrossRef] [PubMed]
56. Coyle, J.R.; Halliday, F.W.; Lopez, B.E.; Palmquist, K.A.; Wilfahrt, P.A.; Hurlbert, A.H. Using Trait and Phylogenetic Diversity to Evaluate the Generality of the Stress-dominance Hypothesis in Eastern North American Tree Communities. *Ecography* **2014**, *37*, 814–826. [CrossRef]
57. Olesen, J.M.; Bascompte, J.; Dupont, Y.L.; Jordano, P. The Modularity of Pollination Networks. *Proc. Natl. Acad. Sci. USA* **2007**, *104*, 19891–19896. [CrossRef] [PubMed]
58. Shi, S.; Nuccio, E.E.; Shi, Z.J.; He, Z.; Zhou, J.; Firestone, M.K. The Interconnected Rhizosphere: High Network Complexity Dominates Rhizosphere Assemblages. *Ecol. Lett.* **2016**, *19*, 926–936. [CrossRef]
59. Agler, M.T.; Ruhe, J.; Kroll, S.; Morhenn, C.; Kim, S.-T.; Weigel, D.; Kemen, E.M. Microbial Hub Taxa Link Host and Abiotic Factors to Plant Microbiome Variation. *PLoS Biol.* **2016**, *14*, e1002352. [CrossRef]
60. Carlström, C.I.; Field, C.M.; Bortfeld-Miller, M.; Müller, B.; Sunagawa, S.; Vorholt, J.A. Synthetic Microbiota Reveal Priority Effects and Keystone Strains in the Arabidopsis Phyllosphere. *Nat. Ecol. Evol.* **2019**, *3*, 1445–1454. [CrossRef] [PubMed]
61. Jorge, G.L.; Kisiala, A.; Morrison, E.; Aoki, M.; Nogueira, A.P.O.; Emery, R.J.N. Endosymbiotic *Methylobacterium oryzae* Mitigates the Impact of Limited Water Availability in Lentil (*Lens culinaris* Medik.) by Increasing Plant Cytokinin Levels. *Environ. Exp. Bot.* **2019**, *162*, 525–540. [CrossRef]
62. Palberg, D.; Kisiała, A.; Jorge, G.L.; Emery, R.J.N. A Survey of Methylobacterium Species and Strains Reveals Widespread Production and Varying Profiles of Cytokinin Phytohormones. *BMC Microbiol.* **2022**, *22*, 49. [CrossRef]
63. Lu, Y.-F.; Chai, C.-Y.; Hui, F.-L. Two New Erythrobasidium Species Inhabiting the Phyllosphere Discovered in the Baotianman Nature Reserve in China. *Front. Microbiol.* **2024**, *15*, 1287984. [CrossRef] [PubMed]
64. Li, A.-H.; Yuan, F.-X.; Groenewald, M.; Bensch, K.; Yurkov, A.M.; Li, K.; Han, P.-J.; Guo, L.-D.; Aime, M.C.; Sampaio, J.P.; et al. Diversity and Phylogeny of Basidiomycetous Yeasts from Plant Leaves and Soil: Proposal of Two New Orders, Three New Families, Eight New Genera and One Hundred and Seven New Species. *Stud. Mycol.* **2020**, *96*, 17–140. [CrossRef] [PubMed]
65. Lu, L.; Yin, S.; Liu, X.; Zhang, W.; Gu, T.; Shen, Q.; Qiu, H. Fungal Networks in Yield-Invigorating and -Debilitating Soils Induced by Prolonged Potato Monoculture. *Soil Biol. Biochem.* **2013**, *65*, 186–194. [CrossRef]
66. Matsumoto, H.; Fan, X.; Wang, Y.; Kusstatscher, P.; Duan, J.; Wu, S.; Chen, S.; Qiao, K.; Wang, Y.; Ma, B.; et al. Bacterial Seed Endophyte Shapes Disease Resistance in Rice. *Nat. Plants* **2021**, *7*, 60–72. [CrossRef] [PubMed]
67. González-Teuber, M.; Palma-Onetto, V.; Aguilera-Sammaritano, J.; Mithöfer, A. Roles of Leaf Functional Traits in Fungal Endophyte Colonization: Potential Implications for Host–Pathogen Interactions. *J. Ecol.* **2021**, *109*, 3972–3987. [CrossRef]
68. Zarraonaindia, I.; Owens, S.M.; Weisenhorn, P.; West, K.; Hampton-Marcell, J.; Lax, S.; Bokulich, N.A.; Mills, D.A.; Martin, G.; Taghavi, S.; et al. The Soil Microbiome Influences Grapevine-Associated Microbiota. *mBio* **2015**, *6*, e02527-14. [CrossRef] [PubMed]
69. Wright, I.J.; Reich, P.B.; Westoby, M.; Ackerly, D.D.; Baruch, Z.; Bongers, F.; Cavender-Bares, J.; Chapin, T.; Cornelissen, J.H.C.; Diemer, M.; et al. The Worldwide Leaf Economics Spectrum. *Nature* **2004**, *428*, 821–827. [CrossRef]
70. Reich, P.B. The World-wide 'Fast–Slow' Plant Economics Spectrum: A Traits Manifesto. *J. Ecol.* **2014**, *102*, 275–301. [CrossRef]
71. Biere, A.; Bennett, A.E. Three-way Interactions between Plants, Microbes and Insects. *Funct. Ecol.* **2013**, *27*, 567–573. [CrossRef]
72. Schuldt, A.; Hönig, L.; Li, Y.; Fichtner, A.; Härdtle, W.; Von Oheimb, G.; Welk, E.; Bruelheide, H. Herbivore and Pathogen Effects on Tree Growth Are Additive, but Mediated by Tree Diversity and Plant Traits. *Ecol. Evol.* **2017**, *7*, 7462–7474. [CrossRef]
73. García-Guzmán, G.; Dirzo, R. Patterns of Leaf-pathogen Infection in the Understory of a Mexican Rain Forest: Incidence, Spatiotemporal Variation, and Mechanisms of Infection. *Am. J. Bot.* **2001**, *88*, 634–645. [CrossRef] [PubMed]

Disclaimer/Publisher's Note: The statements, opinions and data contained in all publications are solely those of the individual author(s) and contributor(s) and not of MDPI and/or the editor(s). MDPI and/or the editor(s) disclaim responsibility for any injury to people or property resulting from any ideas, methods, instructions or products referred to in the content.

Journal of *Fungi*

MDPI

Article

Elevational Variation in and Environmental Determinants of Fungal Diversity in Forest Ecosystems of Korean Peninsula

Lei Chen [1], Zhi Yu [2], Mengchen Zhao [1], Dorsaf Kerfahi [3], Nan Li [4], Lingling Shi [5], Xiwu Qi [6], Chang-Bae Lee [7,8], Ke Dong [9,*], Hae-In Lee [7,*] and Sang-Seob Lee [1,*]

[1] Department of Integrative Biotechnology, Sungkyunkwan University, Suwon 16419, Republic of Korea
[2] Department of Environmental Health Sciences, Graduate School of Public Health, Seoul National University, Seoul 08826, Republic of Korea
[3] Department of Biological Sciences, School of Natural Sciences, Keimyung University, Daegu 42601, Republic of Korea
[4] Key Laboratory of Climate, Resources and Environment in Continental Shelf Sea and Deep Sea of Department of Education of Guangdong Province, Department of Oceanography, Key Laboratory for Coastal Ocean Variation and Disaster Prediction, College of Ocean and Meteorology, Guangdong Ocean University, Zhanjiang 524091, China
[5] Department of Geosciences, Geo-Biosphere Interactions, Faculty of Sciences, University of Tuebingen, 72074 Tuebingen, Germany
[6] Jiangsu Key Laboratory for the Research and Utilization of Plant Resources, Institute of Botany, Jiangsu Province and Chinese Academy of Sciences, Nanjing 210014, China
[7] Biodiversity and Ecosystem Functioning Major, Department of Climate Technology Convergence, Forest Carbon Graduate School, Kookmin University, Seoul 02707, Republic of Korea
[8] Department of Forestry, Environment and Systems, College of Science and Technology, Kookmin University, Seoul 02707, Republic of Korea
[9] Department of Biological Sciences, Kyonggi University, Suwon 16227, Republic of Korea
* Correspondence: dongke@kyonggi.ac.kr (K.D.); haein@kookmin.ac.kr (H.-I.L.); syhwh@skku.edu (S.-S.L.)

Abstract: Exploring species diversity along elevational gradients is important for understanding the underlying mechanisms. Our study focused on analyzing the species diversity of fungal communities and their subcommunities at different trophic and taxonomic levels across three high mountains of the Korean Peninsula, each situated in a different climatic zone. Using high-throughput sequencing, we aimed to assess fungal diversity patterns and investigate the primary environmental factors influencing fungal diversity. Our results indicate that soil fungal diversity exhibits different elevational distribution patterns on different mountains, highlighting the combined effects of climate, soil properties, and geographic topology. Notably, the total and available phosphorus contents in the soil emerged as key determinants in explaining the differences in diversity attributed to soil properties. Despite the varied responses of fungal diversity to elevational gradients among different trophic guilds and taxonomic levels, their primary environmental determinants remained remarkably consistent. In particular, total and available phosphorus contents showed significant correlations with the diversity of the majority of the trophic guilds and taxonomic levels. Our study reveals the absence of a uniform diversity pattern along elevational gradients, underscoring the general sensitivity of fungi to soil conditions. By enriching our understanding of fungal diversity dynamics, this research enhances our comprehension of the formation and maintenance of elevational fungal diversity and the response of microbial communities in mountain ecosystems to climate change. This study provides valuable insights for future ecological studies of similar biotic communities.

Keywords: fungi; diversity patterns; elevation; environmental determinants

1. Introduction

Ecologists have long endeavored to decipher biodiversity patterns, with variations along elevational gradients being pivotal in shaping the discourse on biodiversity patterns.

The study of elevational diversity gradients represents a compelling facet of ecological research that reflects the complex interplay between abiotic and biotic factors that influence species distribution and abundance [1,2]. Numerous studies have documented the influence of elevation on a diverse array of fauna and flora [3,4], and the biodiversity of these organisms typically adheres to one of three general elevational patterns: a hump-shaped pattern with peak diversity at mid-elevations [5,6], monotonically decreasing diversity with increasing elevation [7,8], or monotonically increasing diversity with increasing elevation [9–11]. These patterns have been extensively studied in macroorganisms, providing substantial insights into their biogeographical distribution. However, the patterns exhibited by microorganisms along elevation gradients are more challenging to observe and measure compared to larger organisms in terrestrial ecosystems [12–14]. Therefore, exploring the distribution of microorganisms is essential to fully understand the nuances of biodiversity patterns along elevational gradients.

Fungi are crucial components of soil microbial communities and drive numerous vital ecological processes, including litter decomposition, nutrient cycling, and the regulation of plant growth [15]. Their presence and activity are pivotal for maintaining the health and stability of ecosystems, thereby influencing both aboveground and belowground biodiversity [16–18]. Emerging research has revealed diverse fungal distribution patterns in terrestrial ecosystems [19–22]. Fungal communities are often classified into various taxonomic groups and functional guilds [23]. For example, mycorrhizal fungi enhance plant nutrient uptake, whereas saprotrophic fungi play a key role in organic matter decomposition [24,25]. The diversity of these fungal subcategories tends to change along elevational gradients. For example, studies have shown that the diversity of arbuscular mycorrhizal fungi is negatively correlated with elevation [26]. Nevertheless, when studying the entire fungal community, or its different taxonomic groups and functional guilds, these fungi consistently demonstrate rapid responses to environmental changes.

The diversity of soil fungal communities along elevational gradients is influenced by the complex interplay between various environmental factors. Many studies have emphasized the substantial impact of climatic conditions, such as mean annual temperature (MAT) and mean annual precipitation (MAP), on fungal diversity [21,27]. Soil properties, such as the soil pH and C:N ratio, are also recognized as factors that affect the diversity of fungal communities [28–30]. Additionally, geographical factors play a crucial role in shaping fungal diversity [31]. These findings illustrate the complex interactions among the environmental factors that regulate soil fungal diversity. However, despite extensive research on this topic, a lack of consensus remains regarding the response of fungal diversity to changes in environmental factors. By understanding how fungal community diversity responds to changes in climatic factors, soil properties, and geographical factors, we can predict how ecosystems will change under varying climatic conditions. This knowledge is essential for developing strategies to adapt to and mitigate the impacts of environmental change.

To gain a deeper understanding of the patterns of soil fungal diversity along elevational gradients, as well as the environmental factors influencing this diversity, we collected soil samples at six different elevations on three mountains in the Korean Peninsula. By sequencing the internal transcribed spacer (ITS) region, we investigated the fungal communities on these mountains with the objectives of clarifying (1) the patterns of fungal diversity along the elevational gradients on these three mountains, (2) the relationship between fungal diversity and environmental factors, and (3) the associations between elevational and environmental gradients and fungal diversity at different taxonomic or functional levels. This study provides a comprehensive examination of how fungal communities respond to elevational and environmental gradients, thereby contributing valuable insights into the biogeographic patterns of fungal diversity.

2. Materials and Methods

2.1. Sampling Site

Sampling was conducted in August and September of 2019 and 2020 and focused on three prominent mountains in the East Asian temperate zone: Mt. Halla, Mt. Jiri, and Mt. Seorak (Figure 1). These mountains were selected for their distinct climatic and ecological features that are representative of the region's biodiversity.

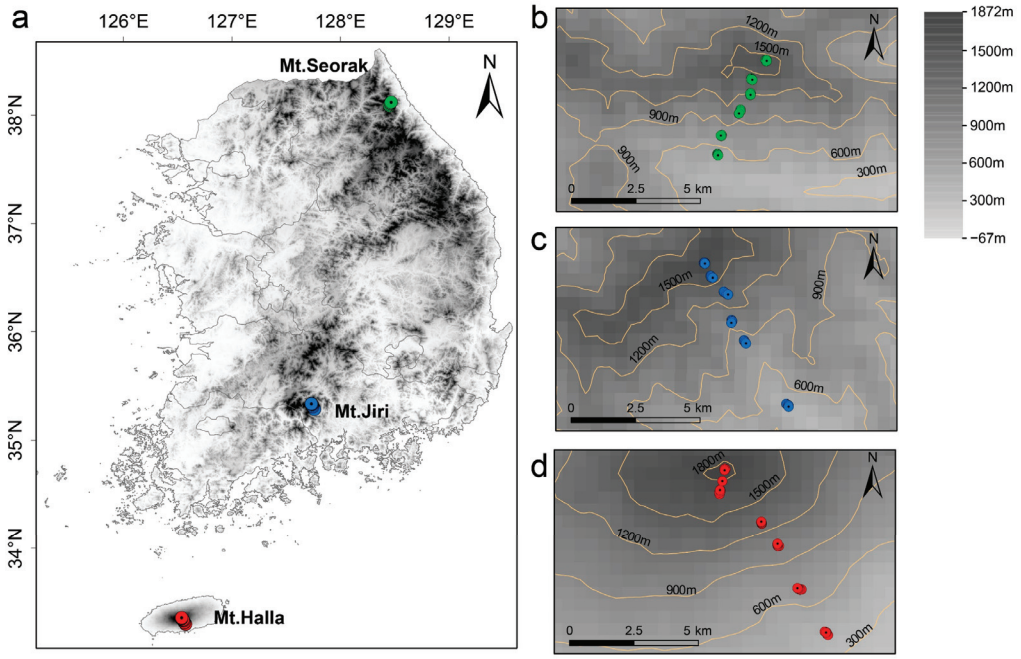


Figure 1. Sampling site (**a**) and schematic diagram of sampling points: Mt. Seorak (**b**), Mt. Jiri (**c**), and Mt. Halla (**d**). The green, blue, and red dots represent Mt. Halla, Mt. Jiri, and Mt. Seorak, respectively.

Mt. Halla (33.3° N, 126.5° E), located on Jeju Island, is the highest shield volcano in South Korea, with an elevation of 1950 m. Jeju Island has a warm temperate climate with an MAT of 15.3 °C and MAP of 1424 mm. The MAT at the summit of Mt. Halla is considerably lower, reaching only 3.7 °C. The native vegetation on the lower slopes of Mt. Halla mainly consists of evergreen broadleaf forests dominated by communities of *Castanopsis cuspidata* var. *sieboldii*, *Quercus salicina*, and *Quercus glauca*. As the elevation increases, the predominant vegetation transitions from deciduous *Quercus serrata* forests (600–1400 m) with *Abies koreana* (1400 m) to shrub belts that include *Juniperus chinensis*, *Empetrum nigrum*, and *Ilex crenata* [12,32].

Mt. Jiri (35.3° N, 127.7° E), standing at 1915 m, is the second highest peak in South Korea. It has a MAT of 13 °C and MAP of approximately 1400 mm [33]. Low-elevation areas are dominated by *Quercus variabilis* and *Pinus densiflora*, while mid-elevation zones feature a mix of *Carpinus laxiflora*, *Quercus serrata*, *Acer mono*, *Larix leptolepis*, and *Pinus koraiensis* (Choi and An, 2013). Higher elevations are characterized by *Quercus mongolica*, *Agrostis clavata*, *Rhododendron mucronulatum*, and *Abies koreana* [34].

Mt. Seorak (38.08° N, 128.3° E), located in Eastern South Korea, has an elevation of 1708 m. It has the lowest MAT among the three mountains, averaging 3.05 °C along its elevation gradient, and a MAP of 1537 mm [35]. The diverse vegetation includes low-elevation species, such as *Pinus densiflora* and *Abies holophylla* in the lowlands and *Betula ermanii*, *Pinus koraiensis*, *Quercus mongolica*, and *Abies nephrolepis* in the highlands. The summit and highlands are home to dwarf species, such as *Pinus pumila*, *Taxus caespitosa*, and *Thuja koraiensis*, as well as arctic–alpine plants, such as *Arctous ruber*, *Crataegus komarovii*, and *Vaccinium uliginosum* [36].

The sampling methods were consistent across the three mountains. Soil samples were collected from six different elevations along an elevational transect, with five sampling points at each elevation band, and approximately 300 m of elevation difference between each elevation band. To account for natural heterogeneity within each elevation band, five separate sampling points were established at 20 m intervals at each elevation to capture the variation within the elevation range. This is a common practice in ecological studies to ensure robust and representative data [37–41]. To validate the consistency of samples within the same elevation, we conducted analyses with Bray–Curtis non-metric multidimensional scaling and clustering, both of which confirmed the consistency of samples within each elevation band (Supplementary Figure S1). During the sampling process, all sampling points were located at least three meters away from the nearest tree. For each individual sample, five soil cores (0–10 cm depth, just below the litter layer) were collected from the corners and center of a 1 m × 1 m quadrat and then combined to form a composite sample. Visible roots and litter were removed from each fresh soil sample, which was then sieved through a 2 mm mesh. Each composite soil sample was subsequently divided into two subsamples: one stored at 4 °C for subsequent measurement of soil physical and chemical properties, and the other stored at −20 °C for soil environmental DNA extraction. In total, 90 soil samples were collected, with 30 samples from each mountain (6 elevation gradients × 5 replicates = 30 samples per mountain).

2.2. Environmental Data Sources and Measurement

Sixteen environmental attributes were measured at each sampling point (Supplementary Table S1). Climatic variables, including MAT and MAP, were obtained from the National Digital Climate Map compiled by the National Meteorological Center of the Korea Meteorological Administration [42]. Soil characteristics were measured at the National Instrumentation Center for Environmental Management, Seoul National University, following the standard protocols of the Soil Science Society of America. The measured soil properties included total organic carbon (TOC), total nitrogen (TN), NH_4^+, NO_3^-, total phosphorus (TP), available phosphorus (P_2O_5), pH value, moisture content, and texture, which were determined based on the proportions of sand, silt, and clay (Supplementary Table S1).

2.3. High-Throughput Sequencing and Amplicon Data Analysis

Environmental DNA was extracted from 0.25 g of soil, using a PowerSoil DNA extraction kit (Mo Bio Laboratories, Carlsbad, CA, USA), following the manufacturer's instructions. High-throughput sequencing of the fungal ITS2 region was performed on the Illumina MiSeq platform (Illumina, Inc., San Diego, CA, USA) at the Centre for Comparative Genomics and Evolutionary Bioinformatics at Dalhousie University. The primer combination used was ITS86F (5′-GTGAATCATCGAATCTTTGAA-3′) and ITS4(R) (5′-TCC TCCGCTTATTGATATGC-3′) [43]. The polymerase chain-reaction conditions included an initial denaturation at 95 °C for 10 min, followed by 30 cycles at 95 °C for 30 s, 55 °C for 30 s, and 72 °C for 30 s, with a final extension at 72 °C for 7 min.

Raw ITS reads were obtained in the fastq format. Sequence data were processed using mothur (version 1.48.0, http://www.mothur.org; accessed on 27 October 2023), following the MiSeq SOP [44]. Forward and reverse reads were combined using the "make.contigs" command. Sequences shorter than 200 bp, chimeric sequences, and rare sequences were excluded from downstream analysis. High-quality sequences were assigned to operational taxonomic units (OTUs) at ≥97% similarity. This threshold has been widely used in the literature and provides a practical compromise for capturing fungal diversity without over-splitting OTUs [45–47]. Meanwhile, singletons and doubletons were removed to prevent the inclusion of potentially erroneous reads generated by sequencing errors. A smaller subset of 2764 high-quality sequences from the original set was randomly selected using the "sub.sample" command to ensure consistent sequencing depth across samples. The classification of each OTU was performed using the "classify.seqs" command with

1000 iterations against the UNITE [48] database, with a naive Bayesian bootstrap cutoff of 80% (Supplementary Table S2).

2.4. Statistical Analysis

Fungal functional guilds were assigned using FUNGuild (https://github.com/brendanf/FUNGuildR; accessed on 15 November 2023), which taxonomically parses fungal OTUs by analyzing the ecological guilds of sequencing databases [49]. Three broad trophic modes—pathotrophs, symbiotrophs, and saprotrophs—were defined based on the primary feeding habits of the fungi. Only "highly likely" guild assignments were considered. Otherwise, OTUs remained unclassified and categorized as "Others" (Supplementary Figure S3). To avoid confusion arising from the terminology used in the FUNGuild database and to better convey the ecological significance of our results, we adopt the terms "mycorrhizal" and "parasitic" instead of "symbiotic" and "pathogenic", respectively, except when directly referring to FUNGuild outputs.

Diversity indices, including the Shannon index, Chao index, Simpson index (1-D), and OTU richness, were estimated at different taxonomic levels and in different functional guilds. These indices were calculated using the diversity function of the "vegan" package in R (version 4.1.3) [50]. The Shannon index was used for linear regression analysis of diversity in response to environmental factors (Supplementary Table S3). The diversity of the fungal subcommunities was calculated using the same methods after rarefaction. To examine the influence of elevation on diversity, linear, quadratic, and cubic models were selected based on the Akaike information criterion (AIC). Spearman's rank correlation was used to examine the relationships between diversity and environmental variables [51].

Variation partitioning analysis (VPA) was conducted using the "vegan" package in R to illustrate the independent or combined effects of three grouped environmental factors (climate, geography, and soil properties) on the variance in fungal alpha diversity (Shannon index) [52]. Environmental variables were categorized into three groups: climatic factors (MAT and MAP), geographical factors (elevation, longitude, and latitude), and soil factors (pH, TOC, TN, NH_4^+, NO_3^-, P_2O_5, moisture content, TP, sand, clay, and silt). To assess the relative importance of environmental variables in driving fungal diversity, analysis was performed using the "randomForest" package in R (version 4.7.1). Regression was performed using the "randomForest" function, and variable importance was determined based on the mean squared error increase (Inc MSE, %) value computed using the "importance" function.

3. Results

3.1. Alpha Diversity Patterns along Elevational Gradients

The biodiversity of the fungal community exhibited different patterns along the elevational gradients of the three mountains. On Mt. Halla, no significant patterns in alpha diversity were observed along the elevational gradient. This lack of significant variation extended across major fungal phyla and classes, as well as the three dominant functional guilds (Figure 2a; Supplementary Figure S2; Supplementary Tables S4 and S5). On Mt. Jiri, the fungal alpha diversity displayed a U-shaped distribution along the elevational gradient ($R^2 = 0.4556$, $p < 0.001$). Specifically, Tremellomycetes and pathotrophs displayed this U-shaped pattern, reflecting the overall diversity trend. In contrast, Ascomycota and Dothideomycetes demonstrated a more complex pattern, with alpha diversity initially decreasing, then increasing, and finally decreasing (Figure 2b; Supplementary Tables S1 and S2). On Mt. Seorak, the fungal alpha diversity showed a complex pattern characterized by an initial increase, followed by a decrease and then an increase along the elevational gradient ($R^2 = 0.2758$, $p < 0.05$). Specifically, Ascomycota showed a linear decreasing trend in alpha diversity ($p < 0.05$), whereas the Zygomycota_class_Incertae_sedis diversity mirrored the overall trend with an initial increase, subsequent decrease, and final increase. However, no significant elevational gradient patterns were observed for the three most dominant functional guilds (Figure 2c; Supplementary Figure S3; Supplementary Tables S4 and S5).

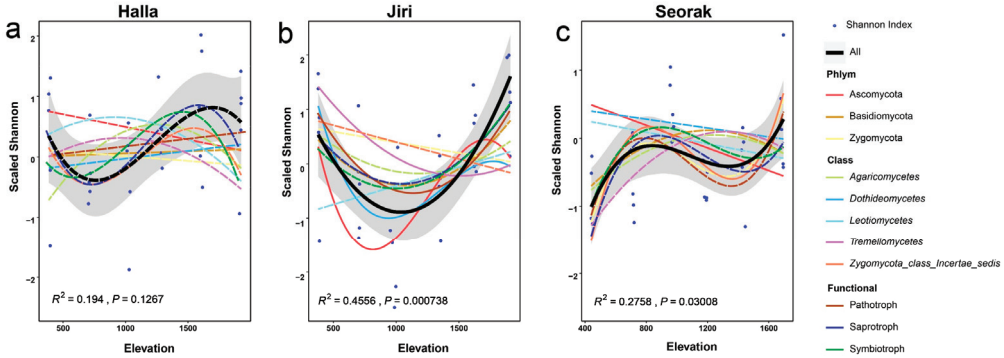


Figure 2. Elevational patterns of fungal community diversity, including overall and specific phylum, class, and functional diversity, indicated by blue dots, black fitted curves, and gray confidence intervals, respectively. Panels (**a**–**c**) represent alpha diversity (Shannon index transformed by z-score) for Mt. Halla, Mt. Jiri, and Mt. Seorak. The quadratic model was selected based on the AIC (refer to Supplementary Table S1). Blue dots represent the values of the Shannon index transformed by z-score at each sampled sites for each mountain. Solid lines indicate significant trends, while dashed lines represent non-significant trends.

3.2. Impact of Environmental Factors on Elevational Patterns of Fungal Diversity

The VPA results revealed that geographical factors, climatic factors, and soil properties collectively explained a substantial proportion of the variation in fungal community diversity. On Mt. Seorak, these factors accounted for the highest variance, explaining 67.1% of the variation in fungal community diversity. On Mt. Jiri and Mt. Halla, these factors explained 52.7% and 38% of the variation in diversity, respectively (Figure 3). Climatic factors were the primary explanatory variables for the variation in fungal community diversity on Mt. Jiri, with a variance explanation rate of 49.0%. Notably, 28.3% of the explanatory power was solely attributed to climatic factors, whereas the remaining portion (20.7%) was due to overlap between climatic factors, geographical factors, and soil properties. In contrast, the influence of climatic factors on fungal community diversity variation was lower on Mt. Halla (4.3%) and higher on Mt. Seorak (28.9%). Soil properties exhibited the highest explanatory power for fungal community diversity variation on Mt. Seorak, explaining 64.9% of the variance. Notably, 44.8% of the explanatory power was shared by geographical and climatic factors. Soil properties contributed to 31.1% and 17.1% of the variation in fungal community diversity on Mt. Halla and Mt. Jiri, respectively. In comparison to climatic and soil properties, geographical factors showed the lowest explanatory power for fungal community diversity variation on Mt. Jiri and Mt. Seorak, accounting for 24.4% and 20.3%, respectively. On Mt. Halla, geographical factors explained 11.8% of the variation.

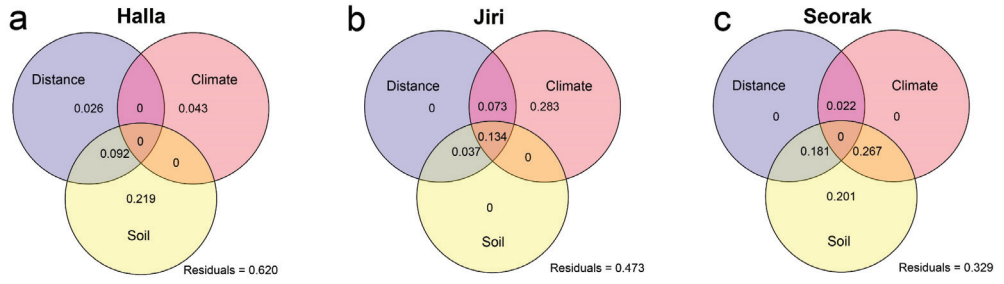


Figure 3. Variance partitioning analysis (VPA) demonstrates the combined influence of geographical, climatic, and soil properties on the fungal community alpha diversity indices across the three mountains. Panels (**a**–**c**) represent Mt. Halla, Mt. Jiri, and Mt. Seorak, respectively. Geographical factors include longitude and latitude; climatic factors include mean annual temperature (MAT) and mean annual precipitation (MAP); and soil properties include pH, total organic carbon (TOC), total nitrogen (TN), NH_4^+, NO_3^-, available phosphorus (P_2O_5), moisture content, total phosphorus (TP), and soil texture (sand, silt, and clay).

Correlation and Random Forest variable importance analyses indicated that no common soil properties exhibited a strong correlation with fungal alpha diversity (represented by the Shannon index) on the three mountains (Figure 4a; Supplementary Table S6). However, soil TP emerged as the primary environmental variable that simultaneously influenced the Shannon index on Mt. Jiri ($R = 0.59$, $p < 0.001$) and Mt. Seorak ($R = 0.55$, $p < 0.01$), and P_2O_5 also had similar positive correlations on both mountains (Mt. Jiri: $R = 0.59$, $p < 0.001$; Mt. Seorak: $R = 0.55$, $p < 0.01$). Moreover, pH ($R = 0.46$, $p < 0.05$) and TOC ($R = -0.56$, $p < 0.01$) exhibited significant correlations with the Shannon index only on Mt. Seorak, while TN showed a significant positive correlation only on Mt. Jiri ($R = 0.52$, $p < 0.01$). Regarding climatic factors, there was no evidence of a correlation between MAP and the Shannon index, whereas MAT had a negative correlation with the Shannon index only on Mt. Jiri ($R = -0.37$, $p < 0.05$). Geographical factors had low explanatory power for fungal community diversity on all three mountains (Figure 4a). The correlations between environmental variables and fungal diversity that were expressed by OTU richness and the Chao index were consistent with those expressed by the Shannon index (Figure 4a).

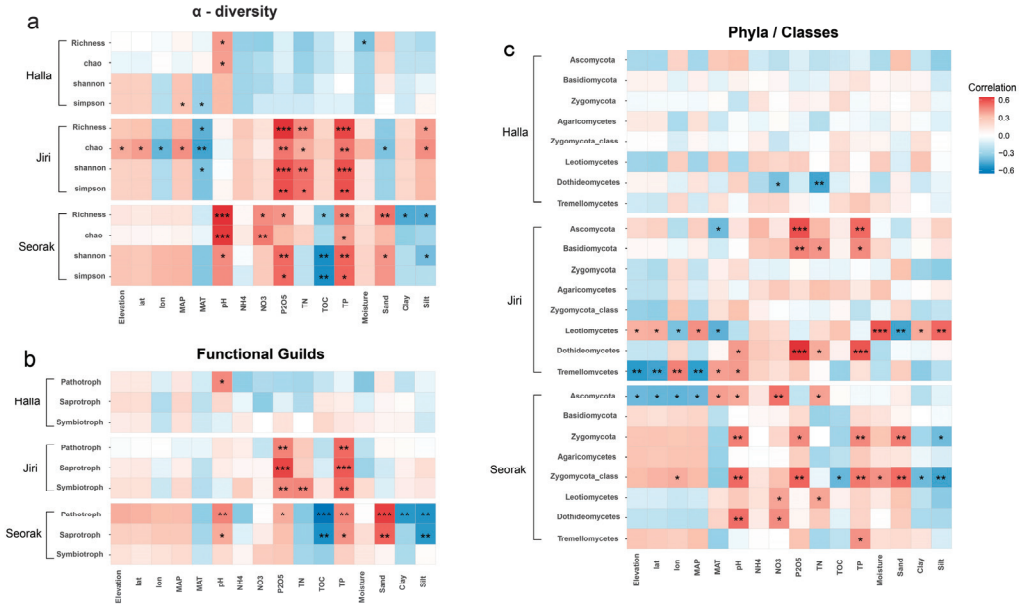


Figure 4. The correlation between fungal alpha diversity (**a**), including richness and Chao, Shannon, and Simpson indices), fungal functions (**b**), and the alpha diversity of dominant fungal phyla and genera (**c**) with environmental factors across the three mountains. * $p < 0.05$, ** $p < 0.01$, and *** $p < 0.001$.

3.3. Environmental Drivers of Dominant Taxa and Functional Group Diversity along Elevational Gradients

Pathotrophs, saprotrophs, and symbiotrophs were the three main functional guilds identified in this study (Figure 4b; Supplementary Table S6). The alpha diversity of the pathotrophs exhibited significant positive correlations with TP and P_2O_5 on both Mt. Jiri and Mt. Seorak ($p < 0.01$). Additionally, soil pH showed significant positive correlations with the pathotroph Shannon index on Mt. Halla and Mt. Seroka ($p < 0.05$). On Mt. Seorak, pathotroph diversity was also strongly correlated with elevation ($R = 0.37$, $p < 0.05$), latitude ($R = 0.36$, $p < 0.05$), TOC ($R = -0.64$, $p < 0.001$), and soil texture (sand: $R = 0.62$, $p < 0.001$; clay: $R = -0.52$, $p < 0.01$; silt: $R = -0.54$, $p < 0.01$). The environmental factors influencing the saprotroph groups were similar to those affecting pathotrophs. Additionally, TP had a positive correlation with saprotroph diversity on both Mt. Jiri and Mt. Seorak ($p < 0.05$), whereas P_2O_5 showed a positive correlation with saprotroph diversity only on Mt. Jiri ($R = 0.62$, $p < 0.001$). On Mt. Seorak, pH ($R = 0.38$, $p < 0.05$), TOC ($R = -0.55$, $p < 0.01$), and soil texture (sand: $R = 0.55$, $p < 0.01$; silt: $R = -0.52$, $p < 0.01$) were significantly correlated with saprotroph diversity. Notably, TP and AP exhibited significant positive

correlations with the diversity of all three functional groups on Mt. Jiri ($p < 0.01$). Unlike soil properties, climatic and geographic factors were not significantly correlated with fungal functional diversity.

We investigated the influence of environmental factors on the major fungal taxonomic groups (Figure 4c; Supplementary Table S6). On Mt. Jiri, the alpha diversity of Ascomycota, Basidiomycota, and Dothideomycetes was positively correlated with TP, P_2O_5, and TN ($p < 0.05$). Meanwhile, Leotiomycetes and Tremellomycetes showed significant correlations with climatic (MAT and MAP) and geographic variables (elevation, latitude, and longitude) ($p < 0.01$), but variables that positively influenced Leotiomycetes negatively affected Tremellomycetes and vice versa. On Mt. Seorak, the alpha diversity of Zygomycota and Zygomycota_class_Incertae_sedis was positively correlated with TP, P_2O_5, and pH ($p < 0.05$), whereas that of Ascomycota was significantly positively correlated with climatic and geographic variables ($p < 0.01$). Additionally, the alpha diversity of Zygomycota, Leotiomycetes, and Dothideomycetes was positively correlated with NO_3^- ($p < 0.05$).

4. Discussion

Species diversity varies along elevational gradients, with fungal communities often exhibiting particularly complex patterns. This complexity stems primarily from the high sensitivity of fungi to changes in the soil microenvironment [21]. Fungal communities quickly respond to subtle changes in microclimatic conditions, soil chemistry, and biotic interactions, resulting in complex and variable diversity patterns along elevational gradients [53]. Our study, focusing on three mountains reaching approximately 2000 m above sea level at different latitudes on the Korean Peninsula, provides insights into the diverse patterns of fungal community diversity along elevational gradients. The three mountains exhibited distinctly different diversity trends with increasing elevation. As elevation increased, Mt. Seorak's fungal alpha diversity first increased and then decreased, showing the highest species diversity at mid-elevation zones. Conversely, Mt. Jiri displayed a U-shaped distribution, with the lowest diversity at mid-elevation zones, while Mt. Halla showed no significant change in fungal alpha diversity with changing elevation. Classic ecological theories have posited that diversity generally decreases with elevation, suggesting that a similar trend would exist for fungi, with fungal abundance decreasing along mountain elevational gradients [21]. This phenomenon is typically associated with the increasing harshness of the environment at higher elevations [54]. For example, studies have observed a monotonic decline in soil fungal diversity along elevations ranging from 700 to 2600 m on Changbai Mountain [20]. However, as ecological research has advanced, more studies have found that peak diversity occurs at mid-elevation zones. For example, ectomycorrhizal fungi on Mt. Fuji in Japan exhibit a hump-shaped distribution along the elevational gradient [55,56]. Several theories have been proposed to explain the peak fungal diversity at mid-elevation zones. The "community overlap" hypothesis suggests that mid-elevation zones function as transitional areas between the distinct environments of the mountain top and base, resulting in higher species diversity due to the inclusive nature of transitional habitats. Another widely recognized explanation is the "mid-domain effect", which posits that if species ranges are randomly distributed between the mountain top and base boundaries, the mid-elevation zone will exhibit the highest species overlap [57]. While these theories emphasize the importance of deterministic processes, such as climatic and geographical factors, in influencing soil fungal diversity, Wang et al. [13] suggested that stochastic processes can also substantially affect mountain fungal community diversity under certain conditions. Although a U-shaped pattern (with the lowest diversity at mid-elevation zones) is uncommon, studies on fungal diversity in Korean pine forests on Changbai Mountain have found the lowest community diversity at mid-elevation zones [58], which is consistent with our findings on Mt. Jiri. Additionally, the primary vegetation from low- to mid-elevation zones on Mt. Jiri is *Pinus densiflora* [34], indicating that soil properties influenced by Korean pines may negatively affect fungal diversity, warranting further research. Birch trees (*Betula* spp.) play a significant role in shaping soil

properties and influencing fungal diversity. Birch trees can alter soil pH, organic matter content, and nutrient availability, thereby affecting fungal biomass and communities [59,60]. This impact is particularly important at mid to high elevations, where birch trees are more prevalent. On Mt. Halla, the fungal community alpha diversity did not show significant changes with elevation, differing from previously observed distribution patterns. However, a study in Southeastern Tibet reported a similar lack of a gradient pattern in fungal diversity, generally attributed to the variation in habitats along the elevational gradient [61].

Elevational gradients are associated with changes in various environmental factors. As elevation increases, many environmental variables, such as temperature, humidity, soil pH, and soil trace-element content, also change accordingly [62]. For example, although lower temperatures and higher humidity at high elevations can support specific fungal communities, reduced soil nutrient levels (such as TN and TOC) and extreme climatic conditions limit the survival of many fungal species [63]. Understanding the distribution and diversity of fungi at different elevations provides crucial insights into how mountain ecosystems respond to environmental changes [64]. Our findings confirmed the important role of climatic, soil, and geographical factors in shaping the elevational gradient of fungal community alpha diversity.

Climate is a crucial factor controlling fungal community diversity [65–67], and it indirectly controls the relative abundance of fungal community diversity through its strong influence on ecosystem types, vegetation, and soil properties [68]. In our study, fungal community alpha diversity showed a significant correlation with not only MAP but also MAT. Specifically, on Mt. Jiri, fungal community alpha diversity was negatively correlated with MAT, consistent with previous studies indicating that temperature directly affects fungal communities through physical tolerance and enzymatic processes and indirectly affects them through its impact on vegetation turnover [69–72]. Compared to climatic factors, soil properties have a more significant impact on soil fungal diversity. Soil nutrient availability has been shown to significantly influence fungal community composition [73–75]. In particular, P is an important energy source for microorganisms, significantly influencing the elevational distribution patterns of soil microbes by determining their metabolism [76–78]. Our study showed that TP and P_2O_5 positively affected the alpha diversity of fungal communities and different taxonomic groups across the three mountains, possibly due to the preference of certain fungi for specific elements [66]. Many studies have found that soil nutrients such as TP [79] and available N [80] affect fungal growth [73,81,82] and may limit the maximum potential fungal diversity in the soil [80]. Additionally, phosphates are crucial for fungal proliferation, stress response, cell wall synthesis, and carbon metabolism, serving as key mediators in interactions with other organisms. The availability of phosphates influences fungal adaptation to environmental stress and host interactions, directly impacting the structure and diversity of soil fungal communities. Furthermore, phosphates act as signaling molecules within fungal cells, regulating nutrient acquisition, stress responses, and metabolic processes, enabling fungi to adjust their diversity and distribution in various soil environments [83]. In our study, TN and TOC also influenced the alpha diversity of fungal communities on different mountains. In contrast, soil pH did not significantly affect fungal biodiversity, likely because of fungi's broad optimal pH range for growth [84]. The influence of geographical factors on soil microbial communities depends on the spatial scale [85–87]. Our study focused on the elevational gradients of individual mountains in a local-scale investigation. Therefore, the geographical factors in this study were insufficient to affect the fungal community diversity more than the environmental factors. This finding aligns with previous research indicating that, at regional scales, geographical factors explain some variations in soil fungal diversity [88], whereas at local scales, fungal diversity changes are primarily regulated by environmental factors [89].

It is well understood that underground microbial communities are largely determined by the diversity and composition of the aboveground plant species [88,90]. For example, Tedersoo et al. [88] found that, as the proportion of *Pinus sylvestris* increases in forests, tree diversity has a negative effect on fungal diversity, with species-identity effects dominating

aboveground–belowground relationships beyond plant diversity. Therefore, the influence of vegetation on fungal communities cannot be ignored. In our study, we sampled the bulk soil rather than rhizosphere soil on the three mountains to minimize the influence from vegetation on fungi communities, making it possible to explore the effects of a more diverse series of environmental factors. Indeed, the relative low abundance of functional groups of arbuscular mycorrhizal fungi and Ectomycorrhizal fungi confirmed the success of our sampling plan.

Although the three main functional groups (i.e., pathotrophs, saprotrophs, and symbiotrophs) exhibited varied responses to environmental constraints, the saprotrophs responded to environmental factors in a manner similar to that of pathotrophs on all the three mountains. Future studies should be conducted to comprehensively understand their effects on fungal diversity. The diversity of parasitic fungi on Mt. Jiri exhibited a U-shaped distribution, consistent with the findings of previous research. TP was significantly positively correlated with the diversity of parasitic fungi. This may be because P, as an essential nutrient, promotes microbial growth and reproduction. Parasitic fungi obtain nutrients by damaging host cells; thus, they thrive and reproduce easily in high-P environments [83]. On Mt. Seorak, the diversity of parasitic fungi was also found to be influenced by pH, TOC, and soil texture (sand, clay, and silt). This may be because parasitic fungi tend to thrive in nutrient-rich environments, where these soil properties provide favorable conditions for their growth [49,91]. Notably, the diversity patterns of the three functional groups on Mt. Jiri and Mt. Seorak were consistent with the overall trend and were significantly correlated with TP, indicating the important role of fungal functional groups in determining the overall diversity. Interestingly, our study reveals that, within each mountain, the environmental factors influencing the diversity patterns of different fungal functional groups are generally consistent. However, significant differences exist in the environmental factors affecting the diversity of these fungal functional groups across the three mountains. This variability may be attributed to the distinct fungal community diversity patterns observed in each mountain.

5. Conclusions

This study investigated the patterns of soil fungal community diversity along elevational gradients on three major mountains in the Korean Peninsula: Mt. Halla, Mt. Jiri, and Mt. Seorak. By employing high-throughput sequencing to analyze fungal communities, we elucidated the diversity patterns at different elevations and identified the key environmental factors influencing these patterns. The results revealed distinct elevational diversity patterns of fungal communities on each mountain. Geographic distance, climatic factors, and soil properties collectively explained a significant portion of the variation in fungal community diversity. Among these factors, soil properties, particularly total phosphorus and available phosphorus, emerged as critical determinants of fungal diversity, highlighting the importance of soil nutrients in shaping fungal communities. These findings offer new insights into the biogeographical distribution of fungi and the ecological processes driving fungal diversity in temperate forest ecosystems. Overall, our study enhances the understanding of fungal diversity dynamics along elevational gradients and underscores the necessity of considering multiple environmental factors when assessing microbial biodiversity. The results provide valuable references for future ecological research and conservation efforts of similar biotic communities, especially in the context of changing environmental conditions.

Supplementary Materials: The following supporting information can be downloaded at: https://www.mdpi.com/article/10.3390/jof10080556/s1.

Author Contributions: Conceptualization, L.C. and K.D.; methodology, K.D. and M.Z.; software, C.-B.L.; validation, D.K., N.L. and L.S.; formal analysis, L.C.; investigation, H.-I.L.; resources, X.Q.; data curation, Z.Y.; writing—original draft preparation, L.C. and K.D.; writing—review and editing,

L.C.; visualization, L.S.; supervision, K.D.; project administration, K.D.; funding acquisition, S.-S.L. All authors have read and agreed to the published version of the manuscript.

Funding: This work was supported by the National Research Foundation of Korea (NRF) grant funded by the Korea Government (MSIP) (Grant No. NRF-2022R1F1A1066643), and the Korea Dementia Research Project through the Korea Dementia Research Center (KDRC), funded by the Ministry of Health & Welfare and Ministry of Science and ICT, Republic of Korea (Grant No. RS-2023-00211632). Several researchers of this work were also supported by a grant from the Guangxi Natural Science Foundation (Grant No. 2018GXNSFDA281006); the National Natural Science Foundation of China (Grant No. 41966005); and the 'One Hundred Talents' Project of Guangxi (Grant No. 6020303891251).

Institutional Review Board Statement: Not applicable.

Informed Consent Statement: Not applicable.

Data Availability Statement: The original contributions presented in the study are included in the article/Supplementary Materials, further inquiries can be directed to the corresponding authors.

Conflicts of Interest: The authors declare no conflicts of interest.

References

1. Rahbek, C. The elevational gradient of species richness: A uniform pattern? *Ecography* **2006**, *18*, 200–205. [CrossRef]
2. Whittaker, R.J.; Willis, K.J.; Field, R. Scale and species richness: Towards a general, hierarchical theory of species diversity. *J. Biogeogr.* **2001**, *28*, 453–470. [CrossRef]
3. Costa, F.V.d.; Viana-Júnior, A.B.; Aguilar, R.; Silveira, F.A.O.; Cornelissen, T.G. Biodiversity and elevation gradients: Insights on sampling biases across worldwide mountains. *J. Biogeogr.* **2023**, *50*, 1879–1889. [CrossRef]
4. Dong, K.; Moroenyane, I.; Tripathi, B.; Kerfahi, D.; Takahashi, K.; Yamamoto, N.; An, C.; Cho, H.; Adams, J. Soil nematodes show a mid-elevation diversity maximum and elevational zonation on Mt. Norikura, Japan. *Sci. Rep.* **2017**, *7*, 3028. [CrossRef] [PubMed]
5. Guo, Q.; Kelt, D.A.; Sun, Z.; Liu, H.; Hu, L.; Ren, H.; Wen, J. Global variation in elevational diversity patterns. *Sci. Rep.* **2013**, *3*, 3007. [CrossRef]
6. Werenkraut, V.; Ruggiero, A. Quality of basic data and method to identify shape affect richness-altitude relationships in meta-analysis. *Ecology* **2011**, *92*, 253–260. [CrossRef]
7. Castro, F.S.d.; Da Silva, P.G.; Solar, R.; Fernandes, G.W.; Neves, F.d.S. Environmental drivers of taxonomic and functional diversity of ant communities in a tropical mountain. *Insect Conserv. Divers.* **2020**, *13*, 393–403. [CrossRef]
8. Rahbek, C. The role of spatial scale and the perception of large-scale species-richness patterns. *Ecol. Lett.* **2004**, *8*, 224–239. [CrossRef]
9. Kessler, M.; Kluge, J.; Hemp, A.; Ohlemüller, R. A global comparative analysis of elevational species richness patterns of ferns. *Glob. Ecol. Biogeogr.* **2011**, *20*, 868–880. [CrossRef]
10. McCain, C.M. Elevational Gradients in Diversity of Small Mammals. *Ecology* **2005**, *86*, 366–372. [CrossRef]
11. Sanders, N.J.; Moss, J.; Wagner, D. Patterns of ant species richness along elevational gradients in an arid ecosystem. *Glob. Ecol. Biogeogr.* **2003**, *12*, 93–102. [CrossRef]
12. Singh, D.; Lee-Cruz, L.; Kim, W.-S.; Kerfahi, D.; Chun, J.-H.; Adams, J.M. Strong elevational trends in soil bacterial community composition on Mt. Halla, South Korea. *Soil Biol. Biochem.* **2014**, *68*, 140–149. [CrossRef]
13. Wang, J.; Hu, A.; Meng, F.; Zhao, W.; Yang, Y.; Soininen, J.; Shen, J.; Zhou, J. Embracing mountain microbiome and ecosystem functions under global change. *New Phytol.* **2022**, *234*, 1987–2002. [CrossRef] [PubMed]
14. Nottingham, A.T.; Fierer, N.; Turner, B.L.; Whitaker, J.; Ostle, N.J.; McNamara, N.P.; Bardgett, R.D.; Leff, J.W.; Salinas, N.; Silman, M.R.; et al. Microbes follow Humboldt: Temperature drives plant and soil microbial diversity patterns from the Amazon to the Andes. *Ecology* **2018**, *99*, 2455–2466. [CrossRef] [PubMed]
15. Chen, Y.L.; Deng, Y.; Ding, J.Z.; Hu, H.W.; Xu, T.L.; Li, F.; Yang, G.B.; Yang, Y.H. Distinct microbial communities in the active and permafrost layers on the Tibetan Plateau. *Mol. Ecol.* **2017**, *26*, 6608–6620. [CrossRef] [PubMed]
16. Ni, Y.; Tong, Z.; Rong, D.; Zhou, Z.; Xu, X. Accurate thermal buckling analysis of functionally graded orthotropic cylindrical shells under the symplectic framework. *Thin-Walled Struct.* **2018**, *129*, 1–9. [CrossRef]
17. Yang, W.; Li, S.; Wang, X.; Liu, F.; Li, X.; Zhu, X. Soil properties and geography shape arbuscular mycorrhizal fungal communities in black land of China. *Appl. Soil Ecol.* **2021**, *167*, 104109. [CrossRef]
18. Zhou, Y.; Jia, X.; Han, L.; Liu, Z.; Kang, S.; Zhao, Y. Fungal community diversity in soils along an elevation gradient in a Quercus aliena var. acuteserrata forest in Qinling Mountains, China. *Appl. Soil Ecol.* **2021**, *167*, 104104. [CrossRef]
19. Ogwu, M.C.; Takahashi, K.; Dong, K.; Song, H.K.; Moroenyane, I.; Waldman, B.; Adams, J.M. Fungal Elevational Rapoport pattern from a High Mountain in Japan. *Sci. Rep.* **2019**, *9*, 6570. [CrossRef]
20. Yang, T.; Adams, J.M.; Shi, Y.; He, J.S.; Jing, X.; Chen, L.; Tedersoo, L.; Chu, H. Soil fungal diversity in natural grasslands of the Tibetan Plateau: Associations with plant diversity and productivity. *New Phytol.* **2017**, *215*, 756–765. [CrossRef]

21. Shen, C.; Gunina, A.; Luo, Y.; Wang, J.; He, J.Z.; Kuzyakov, Y.; Hemp, A.; Classen, A.T.; Ge, Y. Contrasting patterns and drivers of soil bacterial and fungal diversity across a mountain gradient. *Environ. Microbiol.* **2020**, *22*, 3287–3301. [CrossRef] [PubMed]
22. Sui, X.; Li, M.; Frey, B.; Dai, G.; Yang, L.; Li, M.H. Effect of elevation on composition and diversity of fungi in the rhizosphere of a population of Deyeuxia angustifolia on Changbai Mountain, northeastern China. *Front. Microbiol.* **2023**, *14*, 1087475. [CrossRef]
23. Guerrero-Galan, C.; Calvo-Polanco, M.; Zimmermann, S.D. Ectomycorrhizal symbiosis helps plants to challenge salt stress conditions. *Mycorrhiza* **2019**, *29*, 291–301. [CrossRef]
24. Treseder, K.K.; Lennon, J.T. Fungal traits that drive ecosystem dynamics on land. *Microbiol. Mol. Biol. Rev.* **2015**, *79*, 243–262. [CrossRef] [PubMed]
25. Liang, M.; Liu, X.; Gilbert, G.S.; Zheng, Y.; Luo, S.; Huang, F.; Yu, S. Adult trees cause density-dependent mortality in conspecific seedlings by regulating the frequency of pathogenic soil fungi. *Ecol. Lett.* **2016**, *19*, 1448–1456. [CrossRef] [PubMed]
26. Egan, C.P.; Callaway, R.M.; Hart, M.M.; Pither, J.; Klironomos, J. Phylogenetic structure of arbuscular mycorrhizal fungal communities along an elevation gradient. *Mycorrhiza* **2017**, *27*, 273–282. [CrossRef]
27. Ren, L.; Jeppesen, E.; He, D.; Wang, J.; Liboriussen, L.; Xing, P.; Wu, Q.L. pH influences the importance of niche-related and neutral processes in lacustrine bacterioplankton assembly. *Appl. Environ. Microbiol.* **2015**, *81*, 3104–3114. [CrossRef]
28. Siles, J.A.; Margesin, R. Abundance and Diversity of Bacterial, Archaeal, and Fungal Communities Along an Altitudinal Gradient in Alpine Forest Soils: What Are the Driving Factors? *Microb. Ecol.* **2016**, *72*, 207–220. [CrossRef]
29. Liu, D.; Liu, G.; Chen, L.; Wang, J.; Zhang, L. Soil pH determines fungal diversity along an elevation gradient in Southwestern China. *Sci. China Life Sci.* **2018**, *61*, 718–726. [CrossRef]
30. Kerfahi, D.; Guo, Y.; Dong, K.; Wang, Q.; Adams, J.M. pH is the major predictor of soil microbial network complexity in Chinese forests along a latitudinal gradient. *Catena* **2024**, *234*, 107595. [CrossRef]
31. Hu, Y.; Veresoglou, S.D.; Tedersoo, L.; Xu, T.; Ge, T.; Liu, L.; Chen, Y.; Hao, Z.; Su, Y.; Rillig, M.C.; et al. Contrasting latitudinal diversity and co-occurrence patterns of soil fungi and plants in forest ecosystems. *Soil Biol. Biochem.* **2019**, *131*, 100–110. [CrossRef]
32. Lee, S.-C.; Choi, S.-H.; Kang, H.-M.; Cho, H.-S.; Cho, J.-W. The change and structure of altitudinal vegetation on the east side of Hallasan National Park. *Korean J. Environ. Ecol.* **2010**, *24*, 26–36.
33. Yim, Y.; Kim, J. *The Vegetation of Mt. Chiri National Park*; The Chungang University Press: Seoul, Republic of Korea, 1992; 466p. (In Korean)
34. Choi, S.-W.; An, J.-S. What we know and do not know about moth diversity from seven-year-monitoring in Mt. Jirisan National Park, South Korea. *J. Asia-Pac. Entomol.* **2013**, *16*, 401–409. [CrossRef]
35. Kim, J.; Lim, J.H.; Yun, C. Dynamics of *Abies nephrolepis* Seedlings in Relation to Environmental Factors in Seorak Mountain, South Korea. *Forests* **2019**, *10*, 702. [CrossRef]
36. Lee, M.H.; Song, J.H.; Byeon, S.Y.; Lee, J.E.; Kim, H.J.; Chae, S.B.; Yun, C.W.; Kim, J.D. The species range-size patterns for vascular plants of Seorak Mountain (Korea): Relationship between group of life forms and phytogeography affinity along the elevational gradient. *Ecol. Evol.* **2021**, *11*, 12872–12881. [CrossRef] [PubMed]
37. Yu, Z.; Zou, S.; Li, N.; Kerfahi, D.; Lee, C.; Adams, J.; Kwak, H.J.; Kim, J.; Lee, S.S.; Dong, K. Elevation-related climatic factors dominate soil free-living nematode communities and their co-occurrence patterns on Mt. Halla, South Korea. *Ecol. Evol.* **2021**, *11*, 18540–18551. [CrossRef]
38. Yu, Z.; Lee, C.; Kerfahi, D.; Li, N.; Yamamoto, N.; Yang, T.; Lee, H.; Zhen, G.; Song, Y.; Shi, L.; et al. Elevational dynamics in soil microbial co-occurrence: Disentangling biotic and abiotic influences on bacterial and fungal networks on Mt. Seorak. *Soil Ecol. Lett.* **2024**, *6*, 240246. [CrossRef]
39. Zou, S.; Adams, J.; Yu, Z.; Li, N.; Kerfahi, D.; Tripathi, B.; Lee, C.; Yang, T.; Moroenyane, I.; Chen, X.; et al. Stochasticity dominates assembly processes of soil nematode metacommunities on three Asian mountains. *Pedosphere* **2023**, *33*, 331–342. [CrossRef]
40. Rong, S.; Fu-Liang, Q.; Yi-Ting, C.; Fa-Ping, Z.; Wei, D.; Ya-Xian, L.; Zhi-Pang, H.; Xiao-Yan, Y.; Wen, X. Soil sampling methods for microbial study in montane regions. *Glob. Ecol. Conserv.* **2023**, *47*, e02679. [CrossRef]
41. Dickie, I.A.; Boyer, S.; Buckley, H.L.; Duncan, R.P.; Gardner, P.P.; Hogg, I.D.; Holdaway, R.J.; Lear, G.; Makiola, A.; Morales, S.E.; et al. Towards robust and repeatable sampling methods in eDNA-based studies. *Mol. Ecol. Resour.* **2018**, *18*, 940–952. [CrossRef]
42. Chun, J.H.; Lee, C.B. Partitioning the regional and local drivers of phylogenetic and functional diversity along temperate elevational gradients on an East Asian peninsula. *Sci. Rep.* **2018**, *8*, 2853. [CrossRef]
43. Turenne, C.Y.; Sanche, S.E.; Hoban, D.J.; Karlowsky, J.A.; Kabani, A.M. Rapid identification of fungi by using the ITS2 genetic region and an automated fluorescent capillary electrophoresis system. *J. Clin. Microbiol.* **1999**, *37*, 1846–1851. [CrossRef] [PubMed]
44. Schloss, P.D.; Westcott, S.L.; Ryabin, T.; Hall, J.R.; Hartmann, M.; Hollister, E.B.; Lesniewski, R.A.; Oakley, B.B.; Parks, D.H.; Robinson, C.J.; et al. Introducing mothur: Open-source, platform-independent, community-supported software for describing and comparing microbial communities. *Appl. Environ. Microbiol.* **2009**, *75*, 7537–7541. [CrossRef] [PubMed]
45. Edgar, R.C. Accuracy of taxonomy prediction for 16S rRNA and fungal ITS sequences. *PeerJ* **2018**, *6*, e4652. [CrossRef] [PubMed]
46. Taylor, D.L.; Walters William, A.; Lennon Niall, J.; Bochicchio, J.; Krohn, A.; Caporaso, J.G.; Pennanen, T. Accurate Estimation of Fungal Diversity and Abundance through Improved Lineage-Specific Primers Optimized for Illumina Amplicon Sequencing. *Appl. Environ. Microbiol.* **2016**, *82*, 7217–7226. [CrossRef] [PubMed]
47. Tedersoo, L.; Anslan, S.; Bahram, M.; Põlme, S.; Riit, T.; Liiv, I.; Kõljalg, U.; Kisand, V.; Nilsson, H.; Hildebrand, F.; et al. Shotgun metagenomes and multiple primer pair-barcode combinations of amplicons reveal biases in metabarcoding analyses of fungi. *MycoKeys* **2015**, *10*, 1–43. [CrossRef]

48. Abarenkov, K.; Henrik Nilsson, R.; Larsson, K.-H.; Alexander, I.J.; Eberhardt, U.; Erland, S.; Høiland, K.; Kjøller, R.; Larsson, E.; Pennanen, T.; et al. The UNITE database for molecular identification of fungi—Recent updates and future perspectives. *New Phytol.* **2010**, *186*, 281–285. [CrossRef] [PubMed]
49. Nguyen, N.H.; Song, Z.; Bates, S.T.; Branco, S.; Tedersoo, L.; Menke, J.; Schilling, J.S.; Kennedy, P.G. FUNGuild: An open annotation tool for parsing fungal community datasets by ecological guild. *Fungal Ecol.* **2016**, *20*, 241–248. [CrossRef]
50. Borcard, D.; Legendre, P.; Drapeau, P. Partialling out the Spatial Component of Ecological Variation. *Ecology* **1992**, *73*, 1045–1055. [CrossRef]
51. Burnham, K.P.; Anderson, D.R. *Model Selection and Multimodel Inference: A Practical Information-Theoretic Approach*; Springer: Berlin/Heidelberg, Germany, 2002.
52. Oksanen, J. *Vegan: An Introduction to Ordination*; University of Helsinki: Helsinki, Finland, 2008.
53. Xu, S.; Dong, K.; Lee, S.; Ogwu, M.C.; Undrakhbold, S.; Singh, D.; Ariunzaya, D.; Enkhmandal, O.; Spence, L.A.; Sharkhuu, A.; et al. Metagenetics of fairy rings reveals complex and variable soil fungal communities. *Pedosphere* **2023**, *33*, 567–578. [CrossRef]
54. Wang, M.; Shi, S.; Lin, F.; Jiang, P. Response of the soil fungal community to multi-factor environmental changes in a temperate forest. *Appl. Soil Ecol.* **2014**, *81*, 45–56. [CrossRef]
55. Miyamoto, Y.; Nakano, T.; Hattori, M.; Nara, K. The mid-domain effect in ectomycorrhizal fungi: Range overlap along an elevation gradient on Mount Fuji, Japan. *ISME J.* **2014**, *8*, 1739–1746. [CrossRef] [PubMed]
56. Geml, J.; Morgado, L.N.; Semenova-Nelsen, T.A.; Schilthuizen, M. Changes in richness and community composition of ectomycorrhizal fungi among altitudinal vegetation types on Mount Kinabalu in Borneo. *New Phytol.* **2017**, *215*, 454–468. [CrossRef]
57. Colwell, R.K.; Lees, D.C. The mid-domain effect: Geometric constraints on the geography of species richness. *Trends Ecol. Evol.* **2000**, *15*, 70–76. [CrossRef] [PubMed]
58. Ping, Y.; Han, D.; Wang, N.; Hu, Y.; Mu, L.; Feng, F. Vertical zonation of soil fungal community structure in a Korean pine forest on Changbai Mountain, China. *World J. Microbiol. Biotechnol.* **2017**, *33*, 12. [CrossRef]
59. Koranda, M.; Rinnan, R.; Michelsen, A. Close coupling of plant functional types with soil microbial community composition drives soil carbon and nutrient cycling in tundra heath. *Plant Soil* **2023**, *488*, 551–572. [CrossRef]
60. Dasila, K.; Pandey, A.; Samant, S.S.; Pande, V. Endophytes associated with Himalayan silver birch (*Betula utilis* D. Don) roots in relation to season and soil parameters. *Appl. Soil Ecol.* **2020**, *149*, 103513. [CrossRef]
61. Fu, F.; Li, J.; Li, S.; Chen, W.; Ding, H.; Xiao, S.; Li, Y. Elevational distribution patterns and drivers of soil microbial diversity in the Sygera Mountains, southeastern Tibet, China. *Catena* **2023**, *221*, 106738. [CrossRef]
62. Wang, J.-T.; Cao, P.; Hu, H.-W.; Li, J.; Han, L.-L.; Zhang, L.-M.; Zheng, Y.-M.; He, J.-Z. Altitudinal Distribution Patterns of Soil Bacterial and Archaeal Communities along Mt. Shegyla on the Tibetan Plateau. *Microb. Ecol.* **2015**, *69*, 135–145. [CrossRef]
63. Djukic, I.; Zehetner, F.; Mentler, A.; Gerzabek, M.H. Microbial community composition and activity in different Alpine vegetation zones. *Soil Biol. Biochem.* **2010**, *42*, 155–161. [CrossRef]
64. Pan, J.; Guo, Q.; Li, H.; Luo, S.; Zhang, Y.; Yao, S.; Fan, X.; Sun, X.; Qi, Y. Dynamics of Soil Nutrients, Microbial Community Structure, Enzymatic Activity, and Their Relationships along a Chronosequence of Pinus massoniana Plantations. *Forests* **2021**, *12*, 376. [CrossRef]
65. Maestre, F.T.; Delgado-Baquerizo, M.; Jeffries, T.C.; Eldridge, D.J.; Ochoa, V.; Gozalo, B.; Quero, J.L.; García-Gómez, M.; Gallardo, A.; Ulrich, W. Increasing aridity reduces soil microbial diversity and abundance in global drylands. *Proc. Natl. Acad. Sci. USA* **2015**, *112*, 15684–15689. [CrossRef]
66. Tedersoo, L.; Bahram, M.; Põlme, S.; Kõljalg, U.; Yorou, N.S.; Wijesundera, R.; Ruiz, L.V.; Vasco-Palacios, A.M.; Thu, P.Q.; Suija, A. Global diversity and geography of soil fungi. *Science* **2014**, *346*, 1256688. [CrossRef] [PubMed]
67. Delgado-Baquerizo, M.; Reith, F.; Dennis, P.G.; Hamonts, K.; Powell, J.R.; Young, A.; Singh, B.K.; Bissett, A. Ecological drivers of soil microbial diversity and soil biological networks in the Southern Hemisphere. *Ecology* **2018**, *99*, 583–596. [CrossRef] [PubMed]
68. Viscarra Rossel, R.A.; Yang, Y.; Bissett, A.; Behrens, T.; Dixon, K.; Nevil, P.; Li, S. Environmental controls of soil fungal abundance and diversity in Australia's diverse ecosystems. *Soil Biol. Biochem.* **2022**, *170*, 108694. [CrossRef]
69. Bahram, M.; Kõljalg, U.; Courty, P.E.; Diédhiou, A.G.; Kjøller, R.; Põlme, S.; Ryberg, M.; Veldre, V.; Tedersoo, L.; Wurzburger, N. The distance decay of similarity in communities of ectomycorrhizal fungi in different ecosystems and scales. *J. Ecol.* **2013**, *101*, 1335–1344. [CrossRef]
70. Coince, A.; Cordier, T.; Lengelle, J.; Defossez, E.; Vacher, C.; Robin, C.; Buee, M.; Marcais, B. Leaf and root-associated fungal assemblages do not follow similar elevational diversity patterns. *PLoS ONE* **2014**, *9*, e100668. [CrossRef] [PubMed]
71. Jarvis, S.G.; Woodward, S.; Taylor, A.F.S. Strong altitudinal partitioning in the distributions of ectomycorrhizal fungi along a short (300 m) elevation gradient. *New Phytol.* **2015**, *206*, 1145–1155. [CrossRef]
72. Frey, S.D.; Drijber, R.; Smith, H.; Melillo, J. Microbial biomass, functional capacity, and community structure after 12 years of soil warming. *Soil Biol. Biochem.* **2008**, *40*, 2904–2907. [CrossRef]
73. Meng, H.; Li, K.; Nie, M.; Wan, J.R.; Quan, Z.X.; Fang, C.M.; Chen, J.K.; Gu, J.D.; Li, B. Responses of bacterial and fungal communities to an elevation gradient in a subtropical montane forest of China. *Appl. Microbiol. Biotechnol.* **2013**, *97*, 2219–2230. [CrossRef]
74. Wang, J.-T.; Zheng, Y.-M.; Hu, H.-W.; Zhang, L.-M.; Li, J.; He, J.-Z. Soil pH determines the alpha diversity but not beta diversity of soil fungal community along altitude in a typical Tibetan forest ecosystem. *J. Soils Sediments* **2015**, *15*, 1224–1232. [CrossRef]

75. Rousk, J.; Brookes, P.C.; Bååth, E. Fungal and bacterial growth responses to N fertilization and pH in the 150-year 'Park Grass' UK grassland experiment. *FEMS Microbiol. Ecol.* **2011**, *76*, 89–99. [CrossRef] [PubMed]
76. Yang, Y.; Gao, Y.; Wang, S.; Xu, D.; Yu, H.; Wu, L.; Lin, Q.; Hu, Y.; Li, X.; He, Z.; et al. The microbial gene diversity along an elevation gradient of the Tibetan grassland. *ISME J.* **2014**, *8*, 430–440. [CrossRef] [PubMed]
77. Wu, H.; Li, Y.; Zhang, J.; Niu, L.; Zhang, W.; Cai, W.; Zhu, X. Sediment bacterial communities in a eutrophic lake influenced by multiple inflow-rivers. *Environ. Sci. Pollut. Res. Int.* **2017**, *24*, 19795–19806. [CrossRef] [PubMed]
78. Li, J.; Wang, X.; Wu, J.H.; Sun, Y.X.; Zhang, Y.Y.; Zhao, Y.F.; Huang, Z.; Duan, W.H. Climate and geochemistry at different altitudes influence soil fungal community aggregation patterns in alpine grasslands. *Sci. Total Environ.* **2023**, *881*, 163375. [CrossRef] [PubMed]
79. Verbruggen, E.; Van Der Heijden, M.G.; Weedon, J.T.; Kowalchuk, G.A.; Roling, W.F. Community assembly, species richness and nestedness of arbuscular mycorrhizal fungi in agricultural soils. *Mol. Ecol.* **2012**, *21*, 2341–2353. [CrossRef] [PubMed]
80. Cox, F.; Barsoum, N.; Lilleskov, E.A.; Bidartondo, M.I. Nitrogen availability is a primary determinant of conifer mycorrhizas across complex environmental gradients. *Ecol. Lett.* **2010**, *13*, 1103–1113. [CrossRef] [PubMed]
81. Beauregard, M.S.; Hamel, C.; Atul, N.; St-Arnaud, M. Long-Term Phosphorus Fertilization Impacts Soil Fungal and Bacterial Diversity but not AM Fungal Community in Alfalfa. *Microb. Ecol.* **2010**, *59*, 379–389. [CrossRef] [PubMed]
82. Siciliano, S.D.; Palmer, A.S.; Winsley, T.; Lamb, E.; Bissett, A.; Brown, M.V.; van Dorst, J.; Ji, M.; Ferrari, B.C.; Grogan, P.; et al. Soil fertility is associated with fungal and bacterial richness, whereas pH is associated with community composition in polar soil microbial communities. *Soil Biol. Biochem.* **2014**, *78*, 10–20. [CrossRef]
83. Bhalla, K.; Qu, X.; Kretschmer, M.; Kronstad, J.W. The phosphate language of fungi. *Trends Microbiol.* **2022**, *30*, 338–349. [CrossRef]
84. Rousk, J.; Baath, E.; Brookes, P.C.; Lauber, C.L.; Lozupone, C.; Caporaso, J.G.; Knight, R.; Fierer, N. Soil bacterial and fungal communities across a pH gradient in an arable soil. *ISME J.* **2010**, *4*, 1340–1351. [CrossRef]
85. Liu, Y.; Mao, L.; Li, J.; Shi, G.; Jiang, S.; Ma, X.; An, L.; Du, G.; Feng, H. Resource availability differentially drives community assemblages of plants and their root-associated arbuscular mycorrhizal fungi. *Plant Soil* **2014**, *386*, 341–355. [CrossRef]
86. van der Gast, C.J.; Gosling, P.; Tiwari, B.; Bending, G.D. Spatial scaling of arbuscular mycorrhizal fungal diversity is affected by farming practice. *Environ. Microbiol.* **2011**, *13*, 241–249. [CrossRef]
87. Caruso, T. Disentangling the factors shaping arbuscular mycorrhizal fungal communities across multiple spatial scales. *New Phytol.* **2018**, *220*, 954–956. [CrossRef] [PubMed]
88. Tedersoo, L.; Bahram, M.; Cajthaml, T.; Polme, S.; Hiiesalu, I.; Anslan, S.; Harend, H.; Buegger, F.; Pritsch, K.; Koricheva, J.; et al. Tree diversity and species identity effects on soil fungi, protists and animals are context dependent. *ISME J.* **2016**, *10*, 346–362. [CrossRef] [PubMed]
89. Wu, B.; Tian, J.; Bai, C.; Xiang, M.; Sun, J.; Liu, X. The biogeography of fungal communities in wetland sediments along the Changjiang River and other sites in China. *ISME J.* **2013**, *7*, 1299–1309. [CrossRef]
90. Bayranvand, M.; Akbarinia, M.; Salehi Jouzani, G.; Gharechahi, J.; Kooch, Y.; Baldrian, P. Composition of soil bacterial and fungal communities in relation to vegetation composition and soil characteristics along an altitudinal gradient. *FEMS Microbiol. Ecol.* **2021**, *97*, fiaa201. [CrossRef]
91. Zhao, S.; Liu, J.-J.; Banerjee, S.; White, J.F.; Zhou, N.; Zhao, Z.-Y.; Zhang, K.; Hu, M.-F.; Kingsley, K.; Tian, C.-Y. Not by Salinity Alone: How Environmental Factors Shape Fungal Communities in Saline Soils. *Soil. Sci. Soc. Am. J.* **2019**, *83*, 1387–1398. [CrossRef]

Disclaimer/Publisher's Note: The statements, opinions and data contained in all publications are solely those of the individual author(s) and contributor(s) and not of MDPI and/or the editor(s). MDPI and/or the editor(s) disclaim responsibility for any injury to people or property resulting from any ideas, methods, instructions or products referred to in the content.

Journal of *Fungi*

MDPI

Article

Dominant Tree Species and Litter Quality Govern Fungal Community Dynamics during Litter Decomposition

Wenjing Meng [1,2], Lin Chang [1], Zhaolei Qu [1], Bing Liu [1,3], Kang Liu [1], Yuemei Zhang [1], Lin Huang [1,*] and Hui Sun [1,2,*]

[1] Collaborative Innovation Center of Sustainable Forestry in Southern China, College of Forestry, Nanjing Forestry University, Nanjing 210037, China; mengwenjing@njfu.edu.cn (W.M.); linchang@njfu.edu.cn (L.C.); qzl941211@njfu.edu.cn (Z.Q.); 202404324@163.com (B.L.); liukang@njfu.edu.cn (K.L.); zymei23394@njfu.edu.cn (Y.Z.)

[2] Department of Forest Sciences, Faculty of Agriculture and Forestry, University of Helsinki, 00790 Helsinki, Finland

[3] College of Landscape and Horticulture, Yangzhou Polytechnic College, Yangzhou 225009, China

* Correspondence: lhuang@njfu.edu.cn (L.H.); hui.sun@helsinki.fi (H.S.); Tel.: +86-(25)-85427303 (L.H.); +358-442109439 (H.S.)

Abstract: Litter decomposition is a crucial biochemical process regulated by microbial activities in the forest ecosystem. However, the dynamic response of the fungal community during litter decomposition to vegetation changes is not well understood. Here, we investigated the litter decomposition rate, extracellular enzyme activities, fungal community, and nutrient cycling-related genes in leaf and twig litters over a three-year decomposition period in a pure *Liquidamabar formosana* forest and a mixed *L. formosana*/*Pinus thunbergii* forest. The result showed that during the three-year decomposition, twig litter in the mixed forest decomposed faster than that in the pure forest. In both leaf litter and twig litter, β-cellobiosidase and N-acetyl-glucosamidase exhibited higher activities in the mixed forest, whereas phosphatase, β-glucosidase, and β-xylosidase were higher in the pure forest. The fungal α-diversity were higher in both litters in the pure forest compared to the mixed forest, with leaf litter showing higher α-diversity than twig litter. Fungal species richness and α-diversity within leaf litter increased as decomposition progressed. Within leaf litter, Basidiomycota dominated in the mixed forest, while Ascomycota dominated in the pure forest. Funguild analysis revealed that Symbiotroph and ectomycorrhizal fungi were more abundant in the mixed forest compared to the pure forest. In the third-year decomposition, genes related to phosphorus cycling were most abundant in both forests, with the pure forest having a higher abundance of *cex* and *gcd* genes. Fungal community structure, predicted functional structure, and gene composition differed between the two forest types and between the two litter types. Notably, the fungal functional community structure during the first-year decomposition was distinct from that in the subsequent two years. These findings suggest that dominant tree species, litter quality, and decomposition time all significantly influence litter decomposition by attracting different fungal communities, thereby affecting the entire decomposition process.

Keywords: litter decomposition; enzyme activity; fungal community function; nutrient cycling; forest types

1. Introduction

In the forest ecosystem, litter decomposition plays important roles in nutrient cycling, linking biogeochemical processes above and below the ground [1,2]. Leaf and other organic matter, including twigs, stems, and propagative structures, accounts for 70% and 30% of aboveground litterfall, respectively [3]. As litter decomposes, soluble compounds leach into the soil, converting organic matter into accessible nutrients for plants [4], thereby maintaining a balance between soil carbon storage and atmospheric CO_2 release [5]. This

process significantly influences forest soil fertility and nutrient cycling, especially microbial nutrient absorption and utilization [6,7].

Litter decomposition is a dynamic process [8] and is influenced by environmental conditions, litter quality, and microbial communities involved in decomposition [4,9]. Different forest types influence the decomposition rate through variations in litter quality. In subtropical forests, the litter decomposition rate rank is as follows: pure *Cinnamomum camphora* forest > mixed *C. camphora* and *Pinus massoniana* forest > pure *P. massoniana* forest [10]. Studies have shown notable variations in decomposition rates among different forest types. For instance, *Populus davidiana*-dominated forests exhibited a higher decomposition rate than *Quercus liaotungensis*-dominated climax forests, primarily due to lower litter quality [11]. Additionally, research indicates that broadleaf forests potentially facilitated litter to decompose faster compared to coniferous forests in British Columbia [12].

Fungi are the main agents in litter decomposition, whereas bacteria participate in the decomposition to a lesser extent in forest ecosystems [13,14]. Fungi are primary decomposers, breaking down organic polymers through the release of hydrolytic and oxidative enzymes [15–17]. These fungi frequently encode enzymes such as acidic phosphatase, β-glucosidase, and N-acetylglucosaminidase, while enzymes like hemicellulases or laccase are less common [18]. The extracellular enzyme activities, in turn, could reflect the litter decomposition pattern at a biochemical level in that they are closely associated with element cycling, especially carbon dynamics [19,20]. Significant correlations were observed between mass loss and cellobiohydrolase and polyphenol oxidase activity in a two-year decomposition experiment conducted in Hawaii, USA [21]. Also, a study on leaf litter decomposition in a wet tropical forest reported that 35% of the variance in leaf litter decomposition could be explained by the enzymes [22]. Moreover, from the fungal predicted guild level, saprotrophic fungi can directly modify or decompose recalcitrant lignin [16,23,24], whereas other fungi, including mycorrhizal fungi, pathogens, endophytes, can metabolize organic matter [5,25].

During decomposition, fungal community composition undergoes substratum succession [26]. These changes correspond to evolving catabolic abilities required at different stages of decomposition, influenced by continuous variations in litter quality [27–29]. Research indicates that active fungi species richness peaks near the end of the degradation, with ectomycorrhizal fungi becoming the dominant group [30]. Similar microbial succession patterns have been detected in the fungal community during the decomposing of beech leaf litter, where Basidiomycetes dynamically replace Ascomycetes [31]. A 24-month study on decaying *Q. petraea* leaves also confirmed an increase in the abundance of Basidiomycetes over time and enhanced fungal diversity in the fourth month [32]. Research also suggests a strong link between shifts in forest vegetation and changes in fungal communities. The composition of fungal communities in both litter and soil is profoundly modulated by the prevailing tree species, underscoring their significant ecological influence [33,34]. Conifer–broadleaf forests exhibit greater diversity in saprotrophs and other functional groups associated with carbon and nitrogen cycling compared to pure conifer forests [11]. Changes in dominant tree species in mixed boreal forests lead to shifts in soil fungal communities [35], with diverse litter types shaping the saprotrophic fungi group [36,37]. These findings underscore the significance of understanding shifts in fungal communities that correlate with dominant tree species within forest ecosystems.

The original conifer forests are located in Zijin Mountain, Nanjing, China, and have undergone significant successions due to pine wilt disease [38]. Currently, the forest types include mixed broadleaved and coniferous forests dominated by *P. massoniana*, *P. thunbergii*, *Quercus variabilis*, and *Liquidamabar formosana* [39]. Additionally, there are deciduous broadleaved forests dominated by *L. formosana*, *Q. acutissima*, and *Q. fabri* [40]. The transition from pure conifer to mixed conifer and broadleaved forest, and eventually to broadleaved forest, is still ongoing [39,41].

Although changes in fungal communities in different forests are reported frequently, few studies have focused on the internal relationships in the fungal community composition

and their actual enzyme productions and gene potentials in the field of litter decomposition. To better understand how fungal communities respond to decomposition time and changes in dominant tree species, we selected a pure broadleaved forest dominated by *L. formosana*, as well as a mixed forest dominated equally by *L. formosana* and *P. thunbergii* to conduct a three-year decomposition experiment. This study tests two hypotheses: (1) decomposition time and changes in dominant tree species influence enzyme activities and fungal community structures during decomposition; and (2) correlations exist between decomposition rate, enzyme activities, and fungal community composition. The findings offer a unique perspective on fungal communities in litter, as most studies focus on microbial communities within the soil.

2. Materials and Methods

2.1. Study Sites, Litter Bag Embedding, and Sample Collection

The study site (32°16′15″ N, 118°48′00″ W) is situated in the Linggu Temple Scenic Area at the southeastern foot of Zijin Mountain in Nanjing, Jiangsu, China. Zijin Mountain rises 448.9 m and covers an area of 2970 hm^2. This area has a subtropical monsoon climate, with an annual precipitation of 1000–1050 mm and an average temperature of 15.4 °C [42,43].

In this study, we selected two sites: one mixed forest dominated by *L. formosana* and *P. thunbergii* and one pure broadleaved forest dominated by *L. formosana*, situated more than 500 m apart. To avoid self-correlation, we selected three subplots (50 × 80 m) in each forest, located at a distance of 50 m away from each other. In each subplot, we randomly chose three *L. formosana* trees which were good in health status as the sampling trees, therefore generating nine sample trees in the mixed forest and nine sample trees in the pure forest. We assessed the litter degradation by using the traditional mesh bag method [44]; the detailed process is as follows. In October 2017, we set the nylon mesh on the forest floor near each sampling tree to gather the fresh falling *L. formosana* litter for three weeks.

The collected litter was dried at 65 °C until it reached a stable weight. Subsequently, 20 g of *L. formosana* leaves or 7 g of *L. formosana* twigs was placed into each nylon mesh bag (25 × 25 cm, with 2 mm mesh size). In November 2017, six bags of leaves and six bags of twigs were buried beneath the humus layer around each sample tree after removing the existing litter near these trees. This setup resulted in a total of 216 litter bags, with 108 bags placed in the pure forest and 108 bags in the mixed forest.

After one, two, and three years of litter decomposition, two bags of leaves and two bags of twigs were taken to the laboratory in ice boxes. The litters from one leaf bag and one twig bag were dried at 65 °C until the weight stayed stable to determine the decomposition rate, which is the ratio of weight loss in the current year to the original weight. The first-year decomposition rate was calculated by

$$R = \frac{W0 - W1}{W0},$$

while the second-year decomposition rate was calculated by

$$R = \frac{W1 - W2}{W0},$$

and the third-year decomposition rate was calculated by

$$R = \frac{W2 - W3}{W0}$$

The R stands for decomposition rate, while W1, W2, and W3 represent the litter constant weight after the drying process for the first, second, and third year, respectively. W0 is the original weight, 20 g for the leaves and 7 g for the twigs. The litter from the other

two mesh bags was stored at +4 °C and −20 °C for enzyme activity measurements and DNA extraction, respectively.

2.2. DNA Extraction, Amplification of ITS2 Region, and Sequencing

Plant genomic DNA kits (Tiangen Biotech Company, Beijing, China) were used to extract the genomic DNA from each litter sample according to the manufacturer's protocol [45]. Then the extracted DNA was tested on a NanoDrop ND-1000 spectrophotometer (Thermo Fisher Scientific, Waltham, MA, USA) for DNA quality and concentration. The fungal internal transcribed spacer 2 region (ITS2) was amplified by polymerase chain reaction (PCR) using the forward primer ITS1F (5′-CTTGGTCATTTAGAGGAAGTAA-3′) and the reverse primer ITS2 (5′-GCTGCGTTCTTCATCGATGC-3′) [46]. The triplicate 50 μL reaction mixture utilized for the PCR was provided by TransGen Biotech Company, Beijing, China, and comprised 25 μL of 2× Premix Taq, 1 μL of forward primer at a concentration of 10 μM, 1 μL of reverse primer at an equivalent concentration, 10 ng of template DNA, and an appropriate volume of nuclease-free water to reach the final reaction volume. A PCR control with sterile water instead of DNA was used to check for contamination. The PCR program included the following: 3 min at 95 °C for denaturation followed by 36 cycles of 30 s at 95 °C, 30 s at 55 °C for annealing, 45 s at 72 °C for elongation, and a final extension at 72 °C for 10 min. The product was analyzed using 2% agarose gel electrophoresis, then purified and quantified with a spectrophotometer. The amplicons underwent sequencing on an Illumina MiSeq platform (PE = 300) at Majorbio Company (Shanghai, China). The resulting raw sequence data were deposited in the National Center for Biotechnology Information (https://www.ncbi.nlm.nih.gov/) Sequence Read Archive under the project accession number PRJNA1056890, accessed on 26 December 2023.

2.3. Enzyme Activity Measurements

The activities of eight enzymes involved in carbon degradation, namely, β-xylosidase (XYL), β-d-glucuronidase (GLR), β-cellobiosidase (CEL), β-glucosidase (GLS), and laccase, along with enzymes implicated in nitrogen degradation (N-acetyl-glucosamidase, NAG), organic phosphorus degradation (phosphatase, PHO), and organic sulfur hydrolysis (sulfatase, SUL) were systematically measured and quantified after being stored at +4 °C for seven days after sample collection. The enzyme activities were quantified fluorometrically using 4-methylumbelliferone-linked (4-MUB) substrates [47]. For each sample, 0.45 g of litter was placed into three filter tubes and centrifuged following incubation in 600 μL of culture solution. The reaction was initiated by adding 200 μL of suspension containing 50 μL of the substrate to each well. The fluid was transferred to 5 mL tubes and adjusted to a volume of 3.5–4 mL with culture buffers to create enzyme-active samples. A negative control group was prepared by heating 1 mL of the sample fluid. Following the addition of fluorogenic substrate working solutions, the plates were incubated in the dark at 22 °C with shaking at 160 RPM for 15 min (for GLS and NAG) or 30 min (for all other enzymes except laccase). To terminate the reactions, 10 μL of 1 M NaOH was added. Fluorescence was measured using a Thermo Scientific Multiskan SkyHigh with excitation and emission filters set to 365 nm and 450 nm, respectively [48]. Enzyme activity was calculated based on the amount of MUB released from the litter samples over a specified period, expressed as $nmol \cdot g^{-1} \cdot h^{-1}$. For laccase measurements, ABTS solution was added to the sample plates, which were then incubated in the dark at 22 °C with shaking at 160 RPM for 60 min. The emission wavelength for laccase was set to 420 nm.

2.4. Quantitative Microbial Element Cycling

Quantitative Microbial Element Cycling (QMEC) employs a high-throughput quantitative PCR-based chip to assess and quantify the genetic potential of microbiota in transforming essential nutrients, including carbon, nitrogen, phosphorus, and sulfur [49]. The chip comprises 72 primer pairs targeting 64 microbial functional genes involved in carbon, nitrogen, phosphorus, and sulfur cycling, as well as methane metabolism. Twig litter from

the third year of decomposition was selected for analysis. QMEC was conducted using a WaferGen Smart Chip Real-Time PCR system at Majorbio Company (Shanghai, China). Each primer set was run in triplicate, with a non-template negative control included in each run. The qPCR process included the first denaturation step at 95 °C for 5 min, followed by 40 cycles of denaturation at 95 °C for 30 s, annealing at 58 °C for 30 s, and extension at 72 °C for 30 s. Data quality control was performed using the Ct values for each gene, as analyzed with Canoco software 5 [49].

2.5. Sequence Data Processing and Statistical Analysis

Sequence processing was conducted on Mothur (v. 1.39.5), referring to the operating procedures described previously [50]. Initially, paired-end sequences were merged into contigs, followed by error correction using the chimera and PCR.seq commands. The corrected sequences were then assigned to operational taxonomic units (OTUs) with a 97% similarity threshold, employing the neighbor-joining algorithm [51]. Representative sequences from each OTU were classified using the UNITE database version 8.0, applying a bootstrap cutoff value of 80 [52]. Non-fungal sequences were eliminated using the 'remove.lineage' command. The sequence information after sequence denoising and quality filtering is shown in the supplementary table (Table S1). For data normalization, the smallest sample sizes with a sequence number were randomly subsampled for calculating the diversity indices and further analysis of fungal community structure. The OTUs were subsequently classified into ecological guilds: Saprotroph, Symbiotroph, and Pathotroph, based on FUNGuild, a functional annotation tool which uses a curated database to assign fungal taxa to guilds [53].

Across different decomposition years, one-way analysis of variance was utilized to assess significant differences in litter weight loss rates, enzyme activities, fungal community diversity, and fungal functional groups within the same litter type in SPSS v26.0 (Chicago, IL, USA). To compare these variables between different forests, the Kruskal–Wallis H test was utilized in SPSS v26.0. Spearman correlation analysis was utilized to test the correlation between diversity indices and enzyme activities in SPSS v26.0. Correlation heatmaps between genus abundance and enzyme activities and between genus abundance and gene abundance were generated on the Hiplot website (https://hiplot.com.cn, accessed on 24 September 2024). Graphpad Prism was utilized to visualize the results and to calculate R-square values and F-statistics within the framework of linear regression analysis. Principal coordinate analysis (PCoA) and PERMANOVA were employed to detect the significant differences in fungal community structure and fungal functional structure over three years, as well as the fungal functional gene community structure within twig litter from the third year, using Primer 7 software [54].

3. Results

3.1. Decomposition Rate and Enzyme Activities during Litter Decomposition

The decomposition rate of leaf litter did not exhibit significant differences between pure and mixed forest stands over the three-year period (Figure 1a). However, in the third year, the decomposition rate in twig litter was significantly higher in the mixed forest compared to the pure forest ($p < 0.05$) (Figure 1b). Both leaf and twig litters showed a similar trend over the 3-year period, with the highest decomposition rate in the first year ($p < 0.05$) and the lowest in the second year. Moreover, the leaf litter was decomposed faster than the twig litter in the first year ($p < 0.05$) (Table S2), but no difference in decomposition rates was observed between leaf and twig litters in the second and third years.

In the first year of leaf decomposition, the activity of β-cellobiosidase (CEL) was significantly higher in the mixed forest (MLF) compared to the pure forest (PLF), whereas laccase activity was significantly higher in the pure forest ($p < 0.05$) (Figure 2a). During the second year, glucosidase (GLS) and phosphatase (PHO) activity in leaf litter were higher in the pure forest than in the mixed forest ($p < 0.05$) (Figure 2a). In the second year of twig decomposition, laccase and N-acetylglucosaminidase (NAG) activities were higher in the

mixed forest, while sulfase (SUL) activity was higher in the pure forest ($p < 0.05$) (Figure 2b). In the third year of twig decomposition, CEL and SUL activity were higher in the mixed forest, while xylanase (XYL) activity was higher in the pure forest ($p < 0.05$) (Figure 2b).

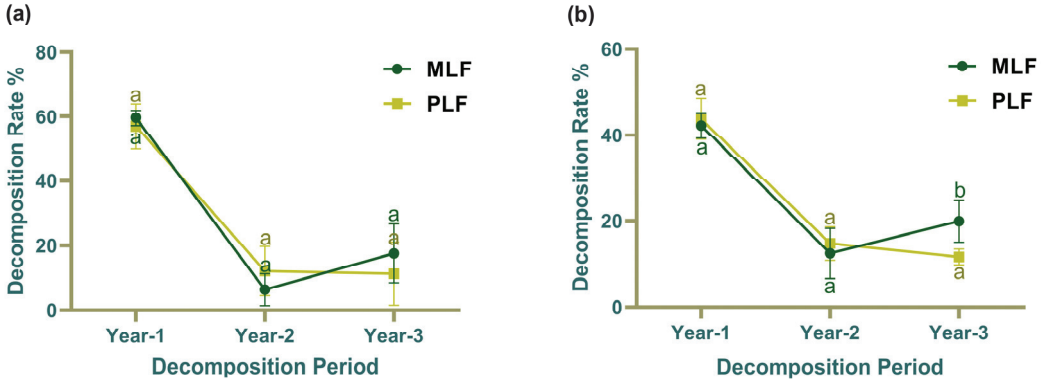


Figure 1. The litter decomposition rate of leaf (**a**) and twig (**b**) in mixed *Liquidambar formosana* forest (MLF) and pure *L. formosana* forest (PLF) over a 3-year period. Lowercase letters above the bars indicate statistically significant differences ($p < 0.05$) between the forests.

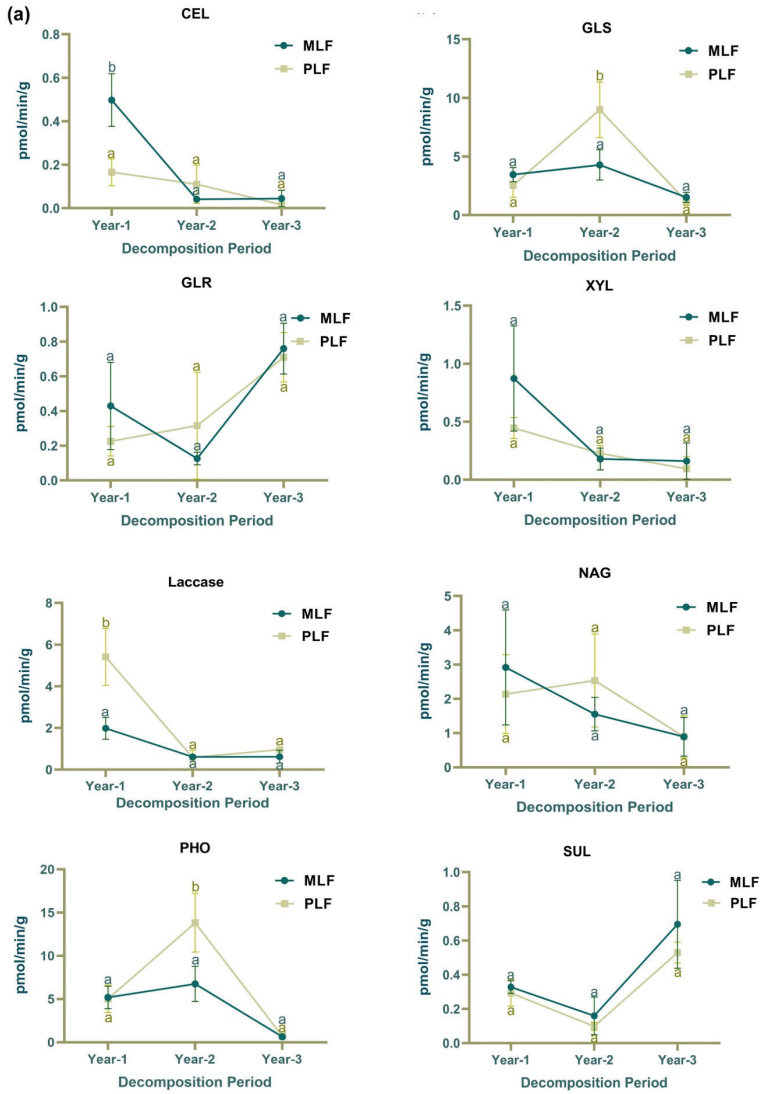


Figure 2. *Cont.*

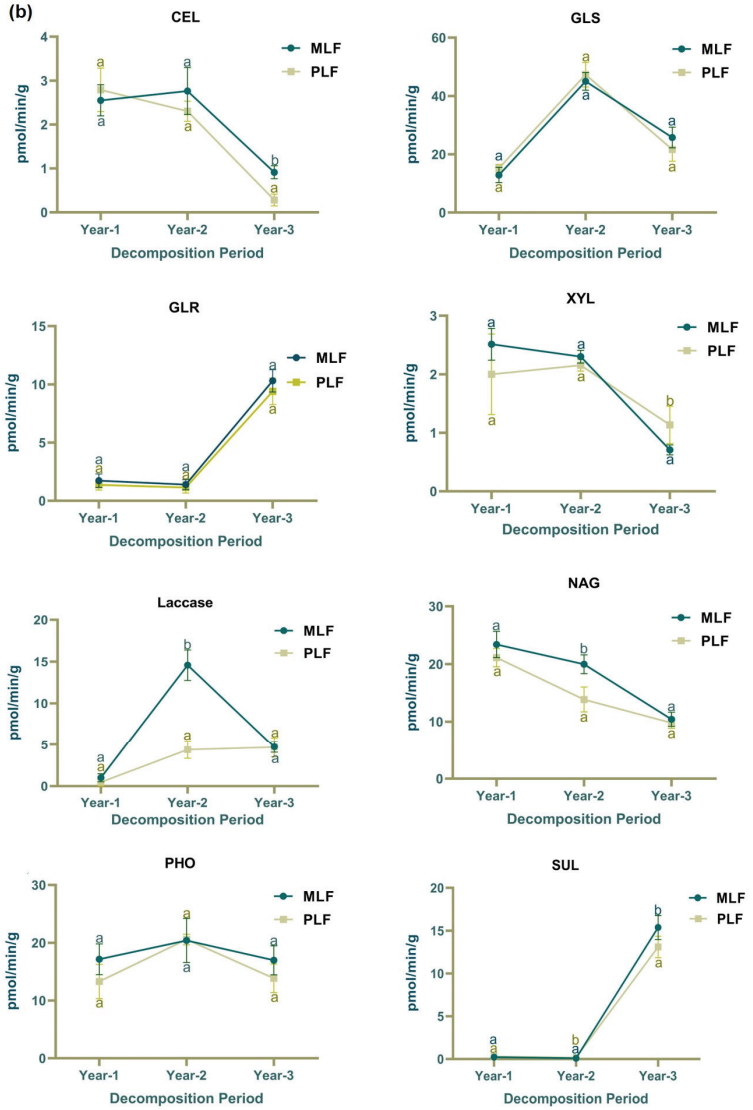


Figure 2. The activities of extracellular enzymes associated with carbon degradation, including β-cellobiosidase (CEL), β-glucosidase (GLS), β-D-glucuronidase (GLR), β-xylosidase (XYL), and laccase; nitrogen cycling (chitin decomposition N-acetyl-glucosamidase (NAG)); organic phosphorus decomposition (PHO); and sulfur hydrolysis (SUL) in leaf litter (**a**) and twig litter (**b**), respectively, in mixed *Liquidambar formosana* forest (MLF) and pure *L. formosana* forest (PLF) during the 3-year decomposition period. Lowercase letters above the bars indicate statistically significant differences ($p < 0.05$) between the forests.

In the mixed forest, the activities of CEL, XYL, and NAG in leaf litter decreased over the decomposition period (Table S3). In leaf litter, GLS and PHO activities increased in the second year and decreased in the third year, while SUL activity demonstrated the opposite pattern ($p < 0.05$) (Figure 2a). In twig litter, the activities of CEL, XYL, and NAG in the mixed forest also showed decreasing trends over time (Table S3), as did CEL and NAG activity in the pure forest (Table S3). GLS, laccase, and PHO activities increased in the second-year and decreased in the third-year twig decomposition ($p < 0.05$) (Figure 2b).

In the first-year decomposition, laccase activity was higher in leaf litter compared to twig litter, while all other enzymes except for SUL showed higher activities in twig litter ($p < 0.05$). In the second and third years, all tested enzymes showed higher activities in twig litter compared to leaf litter ($p < 0.05$)

The decomposition rate of leaf litter was positively correlated with the activities of CEL, XYL, and laccase ($p < 0.01$) (Table S4), while the decomposition rate of twig litter was

positively correlated with CEL and NAG activities ($p < 0.05$) but negatively correlated with GLS and laccase activities ($p < 0.01$) (Table S5).

3.2. Fungal Community α-Diversity during Litter Decomposition

Fungal species richness (Sobs) within leaf litter did not differ between the pure and mixed forests over the three-year decomposition period (Figure 3a). However, the diversity (Inver Simpson index) was significantly higher in the pure forest compared to the mixed forest over the three years, with higher evenness (Simpsoneven) observed in the second year ($p < 0.05$) (Figure 3b,c). Within twig litter, the species richness was higher in the pure forest than in the mixed forest in the third-year decomposition (Figure 3d), and in the first-year decomposition, the diversity and evenness were higher in the pure forest as well ($p < 0.05$) (Figure 3e,f).

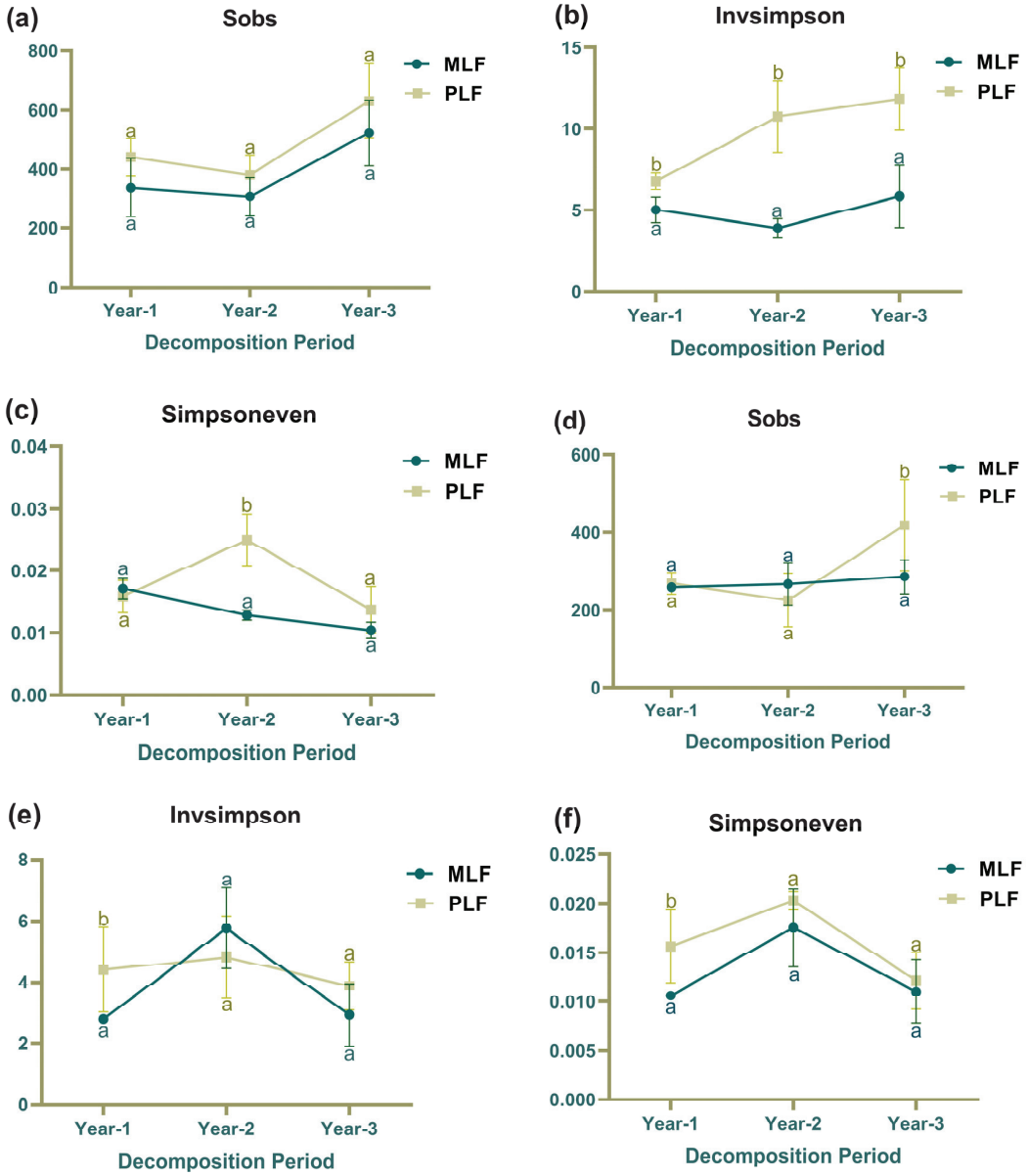


Figure 3. The fungal community richness (Sobs), fungal community diversity (Invsimpson), and fungal community evenness (Simpsoneven) within leaf litter (**a**–**c**) and twig litter (**d**–**f**) in mixed *Liquidambar formosana* forest (MLF) and pure *L. formosana* forest (PLF). Lowercase letters above the bars indicate statistically significant differences ($p < 0.05$) between the forests.

In the pure forest, fungal community diversity within leaf litter increased over the decomposition period (R^2 = 0.63, F = 12.24) (Figure 3b). Fungal community evenness, however, exhibited decreasing trend in mixed forest (R^2 = 0.8499, F = 39.62) (Figure 3c). Within twig litter, fungal community diversity and evenness in both forests experienced an increase followed by a decrease, while fungal community richness increased in the third year in the pure forest ($p < 0.05$) (Figure 3d,f).

In addition, compared to twig litter, leaf litter exhibited higher fungal community diversity in the first year of decomposition in both forests. However, in the third year, leaf litter harbored higher fungal species richness in the mixed forest ($p < 0.05$).

Fungal community richness demonstrated a positive correlation with GLR and SUL activities in both leaf and twig litters (Tables S4 and S5). During leaf decomposition, fungal community evenness showed a positive correlation with GLS, NAG, and PHO activities but a negative correlation with SUL activity (Table S2). Within twig litter, positive and negative correlations were observed between fungal community evenness with GLS and GLR activities, respectively (Table S5).

3.3. Fungal Composition at Taxonomic Level during Litter Decomposition

Ascomycota (48.28%) and Basidiomycota (38.94%) were the two most abundant phyla out of the nine detected phyla across the three-year decomposition, followed by Mortierellomycota (0.83%), Kickxellomycota (0.08%), and Glomeromycota (0.06%). Within leaf litter, the abundance of Ascomycota was higher in the pure forest compared to the mixed forest in the second and third years of decomposition ($p < 0.05$), while Basidiomycota had a higher abundance in the mixed forest during the first and second years ($p < 0.05$) (Figure 4a).

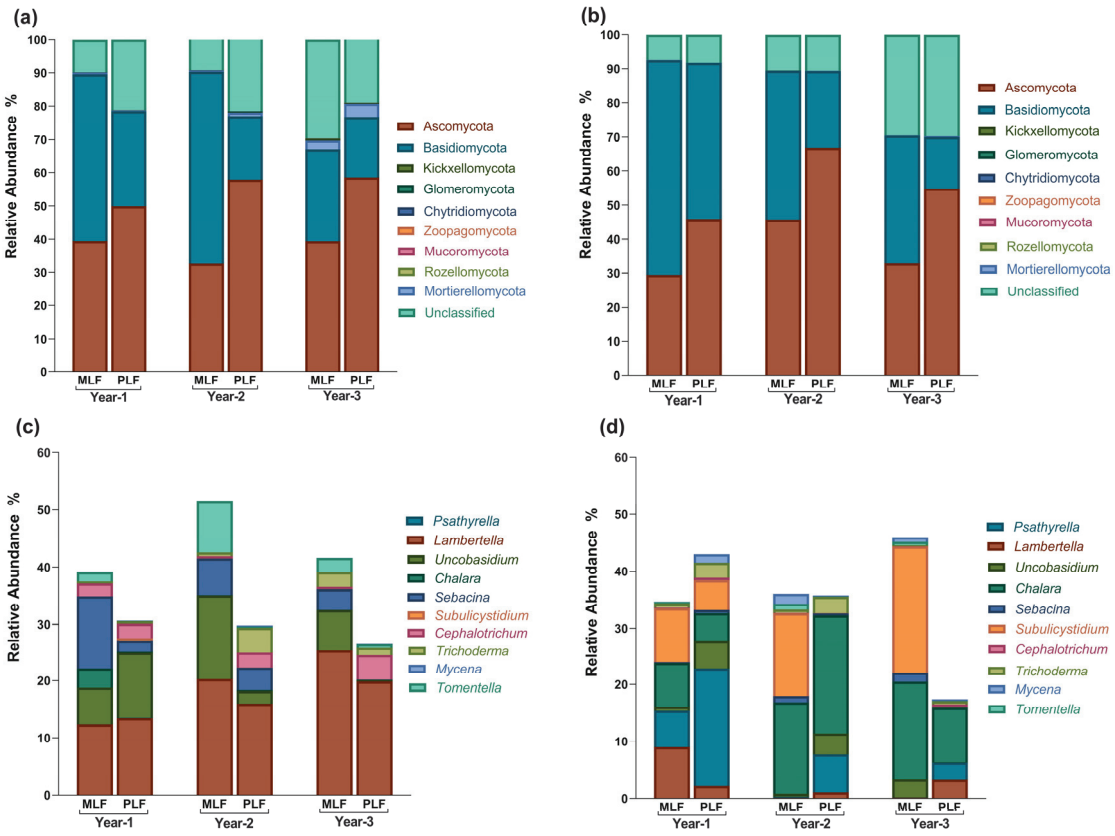


Figure 4. The relative abundance of fungal phyla and the top 10 genera in leaf litter (**a**,**c**) and twig litter (**b**,**d**) during decomposition in the mixed *L. formosana* forest (MLF) and pure *L. formosana* forest (PLF).

At the genus level, 359 genera were classified based on the identified OTU over three years. *Lambertella* and *Chalara* were the most abundant genera in leaf and twig litters,

respectively. During leaf litter decomposition, *Chalara* and *Tomentella* were more abundant in the mixed forest compared to the pure forest in the first year and the first two years, respectively ($p < 0.05$) (Figure 4c). *Tomentella* and *Sebacina* were found to be richer in the second year and third year of twig decomposition in the mixed forest than in the pure forest ($p < 0.05$) (Figure 4c). Regarding leaf decomposition, the relative abundance of *Chalara* and *Uncobasidium* dropped in the second year ($p < 0.05$). *Lambertella*, *Sebacina*, *Tomentella*, *Uncobasidium*, and *Cephalotrichum* were richer in abundance in leaf litter, while *Chalara*, *Subulicystidium*, and *Psathyrella* held higher abundance in twig litter ($p < 0.05$).

Chalara showed positive correlations with the activities of laccase, CEL, GLS, XYL, and NAG ($p < 0.05$) (Figure 5). *Subulicystidium* correlated positively with CEL, GLR, NAG, and PHO, whereas *Psathyrella* correlated positively with CEL and NAG. *Mycena* was found to build positive correlations with laccase, GLS, and XYL ($p < 0.05$) (Figure 5). The relative abundance of *Lambertella* was negatively correlated with the activities of laccase, GLS, GLR, XYL, and PHO ($p < 0.05$) (Figure 5). *Uncobasidium* and *Cephalotrichum* were negatively correlated with NAG, as was *Sebacina* with GLS, NAG, and PHO ($p < 0.05$) (Figure 5).

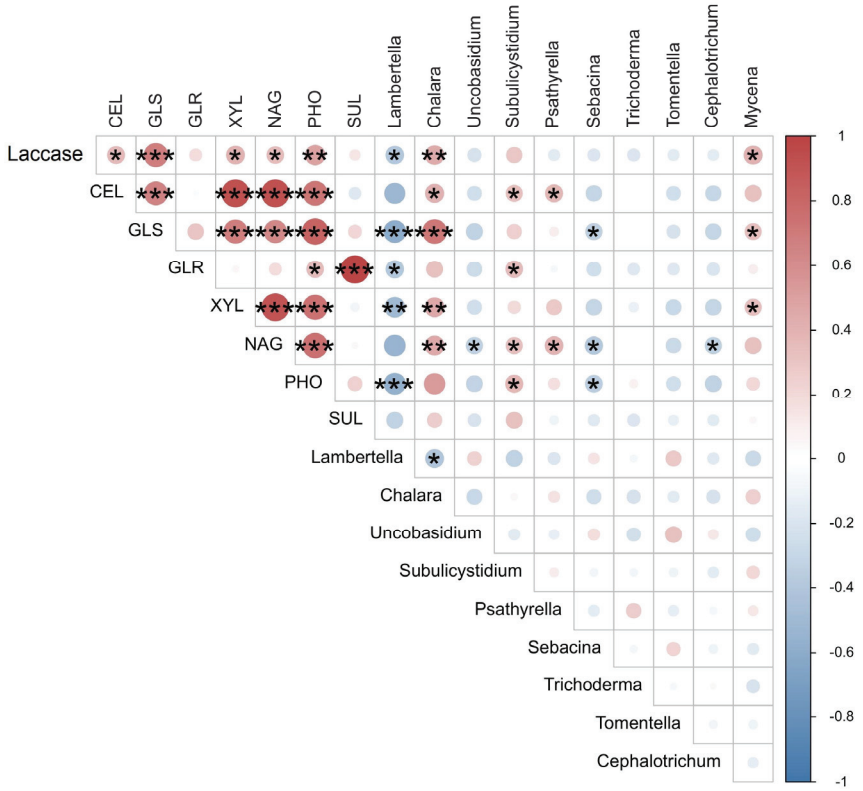


Figure 5. The correlation heatmap of the relative abundance of top ten genera and enzyme activities. A blue circle represents a negative correlation, and a red circle represents a positive correlation, with the color shade expressing the correlation value (from −1 to 1). A single asterisk (*) represents a *p*-value < 0.05, two asterisks (**) represent a *p*-value < 0.01, and three asterisks (***) represent a *p*-value < 0.001.

The principal coordinate analysis (PCoA) constructed based on fungal OTU abundance indicated that the fungal community structures during the decomposition differed between the two forests within the same litter and between the two litters within the same forest (Figure 6a). The separation of fungal community structures was observed between different decomposition years (Figure 6a). These differences among community structures were subsequently confirmed by PERMANOVA results ($p < 0.05$ for each pair) (Table S6).

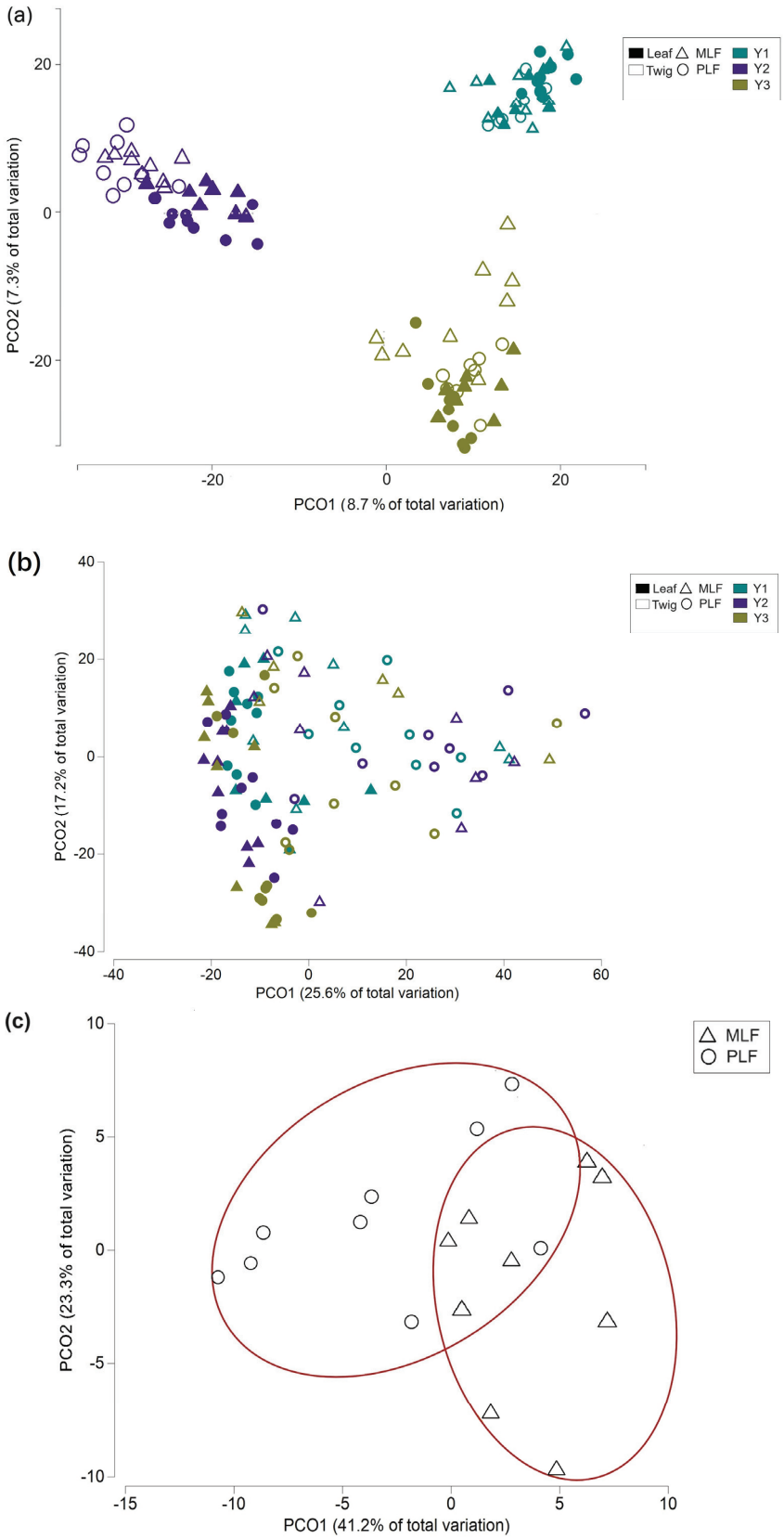


Figure 6. Principal coordinate analysis (PCoA) representing the fungal community structure (**a**), the fungal functional structure (**b**) within leaf and twig litters during the 3-year decomposition, and fungal genes within twig litter in the third decomposition year (**c**) in the mixed *Liquidambar formosana* forest (MLF) and the pure *L. formosana* forest (PLF). The red circles represent the separation of fungal genes between forest types.

3.4. Fungal Functional Structure during Litter Decomposition

In the FUNGuild analysis, 3983 OTUs (39.47%) were classified into seven trophic modes. Saprotroph was the most abundant group, covering 55.00% of the assigned OTUs, followed by Pathotroph–Saprotroph–Symbiotroph (23.15%), Saprotroph–Symbiotroph (8.82%), Symbiotroph (6.05%), Pathotroph–Saprotroph (5.51%), Pathotroph (1.20%), and Pathotroph–Symbiotroph (0.26%) (Figure 7).

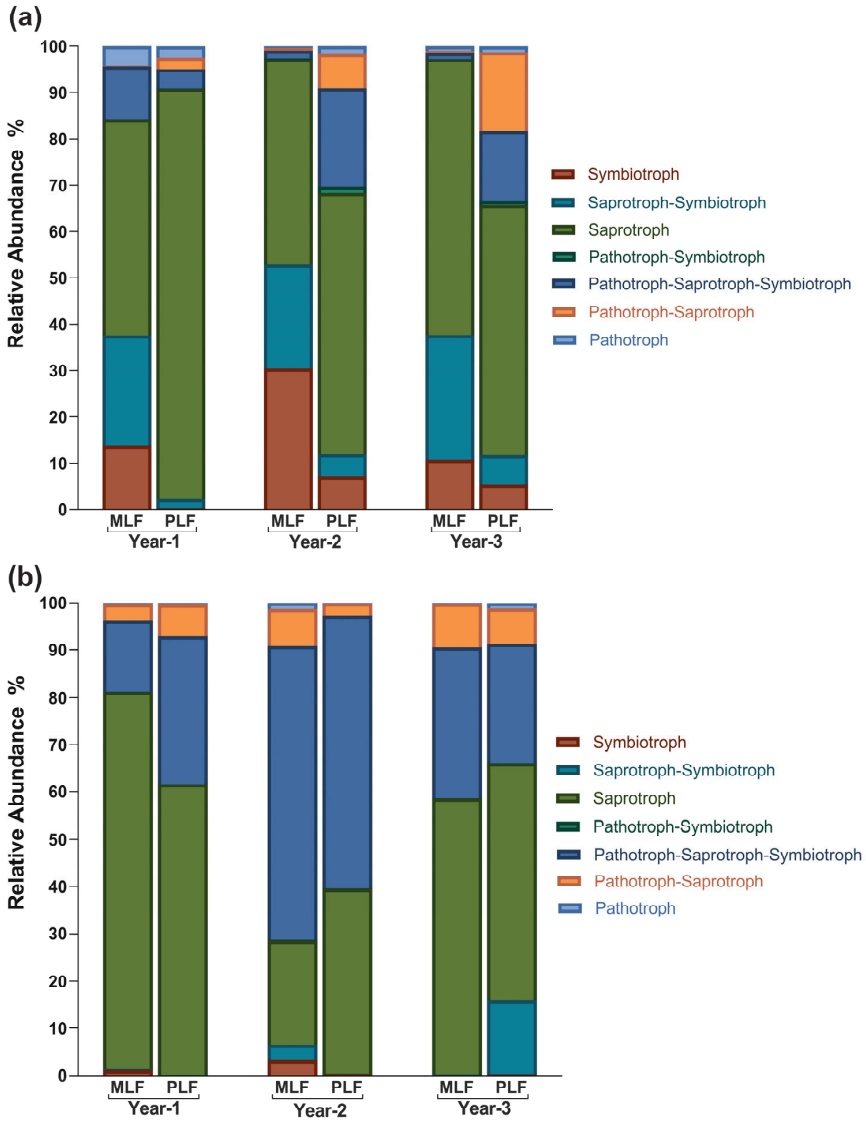


Figure 7. The relative abundance of fungal trophic modes based on FUNGuild analysis during the leaf litter decomposition (**a**) and twig litter decomposition (**b**).

Within leaf litter, Saprotroph–Symbiotroph and Symbiotroph had a higher abundance in the mixed forest during the decomposition period, while the pure forest had a higher abundance of Saprotroph, Pathotroph–Symbiotroph, and Pathotroph–Saprotroph ($p < 0.05$) (Figure S1a). Within twig litter, the abundance of Saprotroph in the mixed forest was higher in the first year but lower in the second year compared to the pure forest. Additionally, Symbiotroph had higher abundance in the mixed forest ($p < 0.05$) (Figure S1b).

Within leaf litter, the relative abundance of Symbiotroph, Pathotroph–Symbiotroph, and Pathotroph–Saprotroph increased significantly in the second year, while Saprotroph and Pathotroph decreased simultaneously ($p < 0.05$) (Figure S1a). In the third year of leaf decomposition, the relative abundance of Pathotroph–Symbiotroph and Symbiotroph dropped, while Saprotroph increased ($p < 0.05$) (Figure S1a). During twig decomposi-

tion, Symbiotroph, Pathotroph–Symbiotroph, and Pathotroph–Symbiotroph–Saprotroph all experienced an increase followed by decrease, peaking in the second year ($p < 0.05$) (Figure S1b). The relative abundance of Saprotroph, however, decreased and reached the lowest value in the second year of twig decomposition in both forests ($p < 0.05$) (Figure S1b).

In both forests, Symbiotroph, Saprotroph–Symbiotroph, and Pathotroph–Symbiotroph were more abundant within leaf litter during decomposition compared to twig litter, while Pathotroph–Symbiotroph–Saprotroph exhibited higher abundance within twig litter ($p < 0.05$).

PCoA based on the functional trophic modes showed distinct fungal trophic structures between the mixed and pure forests in each decomposition period, between the leaf and twig litters in each forest, and between the first-year decomposition and the subsequent period (Figure 6b). The differences in fungal trophic structures were later proved by PERMANOVA ($p < 0.05$ between all pairs) (Table S7).

3.5. Fungal Function Gene Structure in Twig Litter in the Third-Year Decomposition

A total of 19 functional genes associated with carbon degradation, carbon fixation, and phosphorus cycling were found in the twig litter. In both forests, genes participating in P cycling (43.22%) were the most abundant, followed by those involved in C degradation (36.76%) and C fixation (20.02%) (Figure 8a). Among individual genes, the top three were *phoD* (20.99%), *abfA* (18.72%), and *aclB* (16.01%), involved in carbon degradation, carbon fixation, and phosphorus cycling, respectively (Figure 8b).

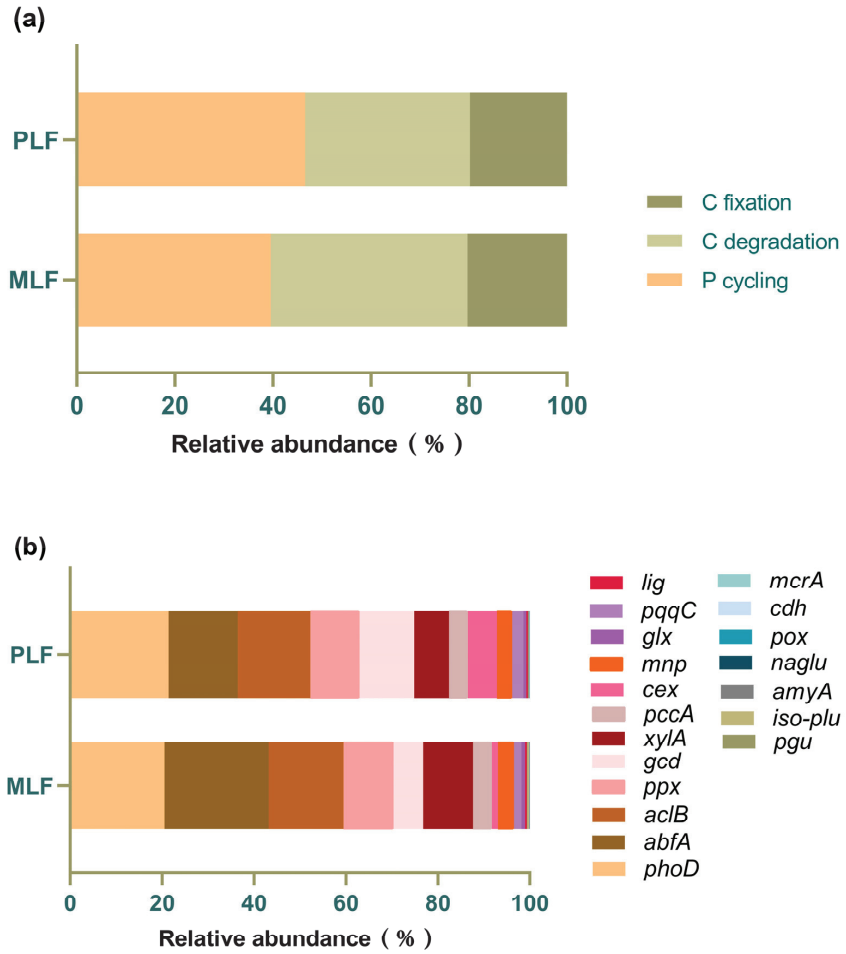


Figure 8. The relative abundance of fungal functional genes associated with C and P cycles (**a**) and individual fungal functional genes (**b**) in twig litter in the third-year decomposition in the mixed *Liquidambar formosana* forest (MLF) and the pure *L. formosana* forest (PLF).

The relative abundance of the gene *cex*, involved in carbon degradation, and the gene *gcd*, involved in phosphorus cycling, were both higher in the pure forest than those in the mixed forest ($p < 0.05$).

PCoA showed differences in the fungal functional gene structure in the twig litter between the mixed and pure forests (Figure 6c), which was further proved by PERMANOVA analysis ($p < 0.001$) (Table S8).

Trichoderma was found to be correlated positively with *cex*, *pgu*, *mcrA*, and *pqqC*, whereas *Tomentella* was found to be correlated positively with *lig* and *iso-plu* ($p < 0.05$) (Figure 9). *Lambertella*, *Chalara*, and *Subulicystidium* were correlated positively with *pox*, *glx*, and *xylA*, respectively ($p < 0.05$) (Figure 9). The gene *pox* was positively correlated with both *Psathyrella* and *Cephalotrichum* ($p < 0.05$) (Figure 9). One negative correlation was found between *Tomentella* and *pccA* ($p < 0.05$) (Figure 9).

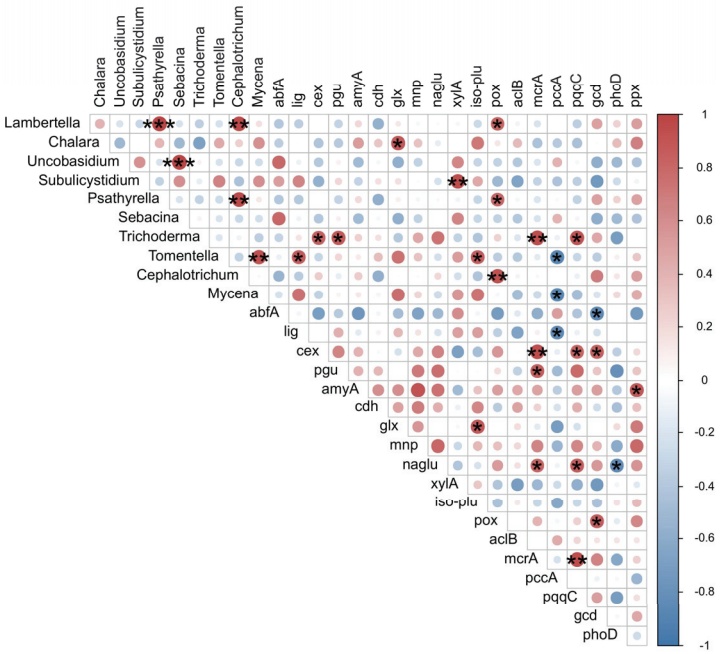


Figure 9. The correlation heatmap of the relative abundance of top ten genera and the relative abundance of genes. A blue circle represents a negative correlation, and a red circle represents a positive correlation, with the color shade expressing the correlation value (from −1 to 1). A single asterisk (*) represents a *p*-value < 0.05, two asterisks (**) represent a *p*-value < 0.01, and three asterisks (***) represent a *p*-value < 0.001.

4. Discussion

The mixed forest exhibited a higher twig litter weight loss rate compared to the pure forest. This difference can be attributed to variations in the decomposer communities present in the two forests, as local decomposer communities significantly influence litter degradation [55]. Tree species impact litter decomposition not only through litter qualities but also by the specific conditions and decomposer communities in their forest floor [56]. Dominant plant species significantly affect both abiotic and biotic soil properties [57,58], which subsequently shape the litter decomposition by altering the decomposer assembly [59]. The litter decomposition rate decreased significantly from the first to the second year, reflecting the common temporal dynamic that the decomposition rate declines over time and stabilizes around a critical value [60]. Initially, microorganisms decompose small, readily available substances, while more complex macromolecular substances persist until the presence of some specific microorganisms which are capable of degrading them at a later stage [61,62]. The higher decomposition rate of leaf litter compared to twig in the first year suggests a difference in the initial qualities of readily degradable substances between leaf and twig litters.

In both leaf litter and twig litter, the mixed forest exhibited elevated β-cellobiosidase and N-acetyl-glucosamidase activities, whereas the pure forest showed higher activities of phosphatase, β-glucosidase, and β-xylosidase. These differences suggest that forest type does influence enzyme activity. Forests with specific tree species compositions impact soil properties through leaf litter and root exudates deposition [63]. Consequently, variations in tree species attributes lead to distinct soil environments [64], significantly affecting microbial activities through altering soil physical and chemical properties [65,66]. Enzyme activities, including β-cellobiosidase, β-xylosidase, and N-acetyl-glucosamidase, showed decreasing trends throughout decomposition in both litter types, consistent with the overall decline in decomposition rate. The activities of laccase within twig litter peaked in the second year, aligning with the previous research indicating high ligninolytic enzyme activity after 24 months of decomposition [67]. Laccases target aromatic moieties in lignin, with a preference for phenolic structures [68]. The peak in laccase activities suggests that significant decomposition of twig lignin occurred during the second year, indicating lignin removal following the decomposition of other components [67,69]. Higher enzyme activities were observed within twig litter compared to leaf, likely due to the presence of more refractory substances such as polyphenols, nitrogen, and lignin in twigs [70]. These substances attract a fungal community with higher enzyme production abilities. Strong positive correlations were found between the leaf litter decomposition rate and the activities of β-xylosidase, β-cellobiosidase, and laccase. β-xylosidase and β-cellobiosidase are extracellular hydrolytic enzymes related to hemicellulose and cellulose decomposition, respectively [71,72], breaking down the long chains of xylans and cellulose [68]. Thus, our results suggest that the loss of cellulose, hemicellulose, and lignin constitutes a significant proportion of the leaf litter mass loss in this study.

All three fungal α-diversity indices were higher in the pure forest. This suggests that tree species identity significantly influences the diversity and composition of the microbial community in organic soil [73], with conifer litter providing a poor substrate for microbial growth [22]. Consequently, the pure broadleaf forest likely offers a more favorable decomposing environment, assembling a decomposer community with higher diversity. Although more diverse microbe communities are hypothesized to enhance decomposition due to their ability to target various substrates and potentially include strong decomposers [74,75], increased diversity can also lead to competition or inhibition among fungal species [76]. This could explain the inhibited twig decomposition rate in the pure forest, attributed to adverse interactions within a diverse fungal community. The observed increase in fungal community species richness in the final year aligns with the peak richness of active fungi in logs at an advanced stage of decay [30]. Fungal community composition tends to shift rapidly with changing litter quality, driven by factors such as nutrient availability, other nutritional requirements, and the competitive abilities of individual taxa [32]. Competition likely diminishes as decomposition reaches its final phase, when nutrients become less available, leading to higher fungal species richness in the third year. Fungal species richness was positively correlated with β-d-glucuronidase and sulfatase activities, indicating that fungi vary in their enzyme production capabilities [77]. Community with more species tend to harbor higher enzyme activities, as a diverse community is more likely to include fungi that produce a broader range of enzymes targeting different components.

Within leaf litter, the pure forest exhibited a higher abundance of Ascomycota, while the mixed forest had more abundant Basidiomycota. Basidiomycota can synthesize enzymes essential for decomposition of complex polymers [78] and cause the loss of lignin and carbohydrates in variable proportions [79], making Basidiomycetes well suited for the more complex litter input in the mixed forest. In contrast, Ascomycota selectively decompose cellulose over lignin [32]. As the main wood decay fungi [80], Basidiomycota decreased in abundance along with twig decomposition as the decomposition process slowed. *Lambertella*, the most abundant genus in leaf litter, is known as a plant parasitic fungus capable of secreting lignin-degrading enzymes, including Mn-peroxidase and lac-

case [81,82]. Species of the genus *Chalara* predominantly thrive as litter saprotrophs, with a notable prevalence on coniferous litter [83], explaining its higher abundance in the mixed forest. Furthermore, *Chalara* built positive correlations with most of the enzymes involved in C degradation and was also positively correlated with the gene *glx*, responsible for lignin degradation [84]. Another study reported that *Chalara longipes* possessed a high content of genes involved in cell wall polysaccharide decomposition [85]. It thus could be inferred that *Chalara* could act as the key decomposers by facilitating enzyme production from a gene coding level. *Tomentella*, an ectomycorrhizal genus, can secrete extracellular enzymes that facilitate the decomposition of proteins, polysaccharides, and organic phosphorus compounds through root tips [86,87]. Another ectomycorrhizal genus, *Sebacina*, was also more abundant in the mixed forest [88]. The higher abundance of *Tomentella* and *Sebacina* in the mixed forest may be attributed to their ectomycorrhizal characteristics, allowing them to form mutualistic symbioses with various tree species [89].

Symbiotrophic and ectomycorrhizal fungi showed higher abundance in the mixed forest, whereas saprotrophic did not show a clear preference for either forest type. In forest ecosystems, nutrient constraints in soil have driven tree species to engage in mutualistic relationships with mycorrhizal fungi, which play a significant role in plant symbiosis [90]. High concentrations of polyphenols in conifer trees [91] potentially enhance the diversity of symbiotrophic fungi [92], leading to their prevalence in mixed forests. Evolutionarily, symbiotrophic fungi, compared to saprotrophs, have shifted from producing degrading enzymes to fulfilling new symbiotic functions, though they still retain some saprotrophic abilities such as producing cellobiohydrolases, ligninolytic MnP-ESD peroxidases, proteases, and laccases [93–96]. Ectomycorrhiza build associations with trees as the primary symbiosis [97] and use mycorrhizal hyphae extending from tree roots to reach the upper soil and litter layer and obtain essential nutrients, including inorganic and organic nitrogen and phosphate compounds [98,99]. The increased activity of N-acetyl-glucosamidase, involved in the nitrogen cycle and chitin degradation, could partly be due to the richer ectomycorrhiza presence in the mixed forest.

Microorganisms enhance nutrient cycling within ecosystems through diverse functional gene expression pathways [100]. After three-year decomposition, the fungal community in the pure forest emphasized phosphorus turnover more than carbon cycling at the gene level. This is logical given phosphorus's essential and limiting role in soil fertility [101]. In our study, the most abundant genes in the mixed forest and pure forest were *abfA* and *phod*, respectively. The gene *abfA* encodes α-L-arabinofuranosidase (α-L-AFase), which catabolizes arabinoside and utilizes carbohydrates [102,103], while *phod* encodes alkaline phosphatase, participating in the mineralization of organic phosphorus [49]. In addition, the pure forest held higher abundance of *cex* and *gcd* genes, which are involved in cellulose hydrolysis [104] and solubilizing inorganic phosphorus, coding for quinoprotein glucose dehydrogenase [105,106], respectively. The divergence in gene structure between the two forests highlights the distinctiveness of fungal functional community at a deeper level. The correlation analysis of genus abundance and gene abundance revealed that most of the correlations were positive, indicating the contribution of the main occupying fungal taxa in mediating the practical nutrient cycling. The genus *Trichoderma*, which was reported to be a main source of biological beneficial agents in agriculture [107,108], was found to be correlated positively with the most genes, including cellulose hydrolysis gene *cex*, pectin degradation gene *pgu*, methane production gene *mcrA*, and *pqqC* [109–111]. Another genus, *Tomentella*, was positively correlated with *lig* and *iso-plu*, which are a lignin degradation gene and a starch degradation gene, respectively [112,113].

Based on OTU abundance, predicted functional modes, and fungal genes, distinct fungal communities and functional structures were formed in different forest types, emphasizing the influence of dominant tree species on the litter decomposing microbial community. Previous studies have reported a close association between aboveground plants and belowground fungal communities [48,114]. As plant characteristics change with the dominant tree species at a site, soil microbial communities can be influenced by micro-

climate variations, litter production (both above- and belowground), herbivore interactions, root exudate production, and symbiotic associations such as mycorrhizal fungi [114]. In our study, the drying process removed previously colonized microbes, making the litter microbial community closely associated with the soil microbial community, as soil microbes serve as a primary source of litter-degrading microorganisms [115]. In the Abitibi region, diverse microbial communities, both functionally and genetically distinct, were also observed in forest stand floors dominated by different tree species [116]. Microbial communities related to litter decomposition are shaped by substrate characteristics, which determine the capacity of different taxa to obtain and utilize distinct structural substrates [14,31,61]. Therefore, the different decomposing conditions provided by various forest types shape the distinct microbial communities. The first-year decomposition exhibited a distinct functional community structure compared to the following two years, corresponding with the dynamic pattern of the decomposition rate. This demonstrates the interaction between fungal community structure and litter decomposition patterns. As expected, twig and leaf harbored separate fungal communities, reflecting the sensitivity of fungal communities to litter qualities [117].

5. Conclusions

The litter decomposition rate differed significantly in the third year of twig decomposition, which could be supported by the different higher enzyme activities in the mixed *L. formosana* forest (β-cellobiosidase and N-acetyl-glucosamidase) and the pure forest (phosphatase, β-xylosidase, and β-glucosidase). Fungal community species richness, diversity, and evenness were higher in the pure forest owing to its more favorable condition. The genus *Chalara* and *Trichoderma* were positively correlated with enzyme activities and gene abundance, suggesting their key roles in litter decomposition. Functionally, symbiotrophic fungi and ectomycorrhizal fungi were more abundant in the mixed forest, supporting the litter decomposition in a potential way. In the third year of twig decomposition, genes associated with phosphorus cycling were the most abundant. Different forest types harbored distinct fungal community structure at community, functional, and gene levels. These findings suggest that forest types strongly influence litter decomposition by recruiting different fungal communities. Additionally, decomposition time and litter quality affect the decomposition by shifting substrate characteristics.

Supplementary Materials: The following supporting information can be downloaded at: https://www.mdpi.com/article/10.3390/jof10100690/s1. Figure S1: The relative abundance of the main trophic modes of Symbiotroph, Saprotroph-Symbiotroph, Saportroph, Pathotroph-Symbiotroph, Pathotroph-Saprotroph-Symbiotroph, Pathotroph-Saprotroph, Pathotroph in leaf litter (a) and twig litter (b) in the mixed *Liquidambar formosana* forest (MLF), and the pure *L. formosana* forest (PLF). Lowercases above represent the significant difference ($p < 0.05$) between different forests; Table S1: Sequences information after denoising and quality filtering; Table S2: Independent-samples Kruskal-Wallis tests showing the difference of decomposition rate from different litter qualities (leaf and twig) in the same forest; Table S3: R square and F value showing the decreasing trend of the enzyme activities along the three-year decomposition; Table S4: Correlation analysis of decomposition rate and fungal diversity indices with enzyme activities within leaf litter; Table S5: Correlation analysis of fungal diversity indices with enzyme activities within twig litter; Table S6: PERMANOVA results showing the difference in fungal community structure; Table S7: PERMANOVA results showing the difference in fungal community functional structure; Table S8: PERMANOVA results showing the difference in fungal gene structure.

Author Contributions: Conceptualization, B.L. and H.S.; Methodology, Z.Q., B.L. and H.S.; Software, Y.Z. and H.S.; Validation, W.M.; Formal analysis, W.M. and K.L.; Investigation, W.M., L.C., Z.Q. and K.L.; Resources, L.C. and H.S.; Data curation, W.M.; Writing—original draft, W.M.; Writing—review & editing, H.S.; Visualization, W.M.; Supervision, H.S.; Project administration, H.S.; Funding acquisition, L.H. and H.S. All authors have read and agreed to the published version of the manuscript.

Funding: The study was supported by the National Key R & D Program of China (2023YFD1401304), the National Natural Science Foundation of China (31870474), and the funding for the Jiangsu

Specially Appointed Professorship (project 163010219). The CSC–IT Center for Science (Finland) is gratefully acknowledged for the computational resource support.

Institutional Review Board Statement: Not applicable.

Informed Consent Statement: Not applicable.

Data Availability Statement: The data analyzed in this study are accessible upon request from the corresponding author. Additionally, the raw sequence data have been deposited in the NCBI Sequence Read Archive (SRA) and are available under the project accession number PRJNA1056890.

Conflicts of Interest: The authors declare no conflict of interest.

References

1. Prescott, C.E.; Vesterdal, L. Decomposition and Transformations along the Continuum from Litter to Soil Organic Matter in Forest Soils. *For. Ecol. Manag.* **2021**, *498*, 119522. [CrossRef]
2. Latterini, F.; Dyderski, M.K.; Horodecki, P.; Picchio, R.; Venanzi, R.; Lapin, K.; Jagodziński, A.M. The Effects of Forest Operations and Silvicultural Treatments on Litter Decomposition Rate: A Meta-Analysis. *Curr. For. Rep.* **2023**, *9*, 276–290. [CrossRef]
3. Robertson, G.P.; Paul, E.A. Decomposition and Soil Organic Matter Dynamics. In *Methods in Ecosystem Science*; Sala, O.E., Jackson, R.B., Mooney, H.A., Howarth, R.W., Eds.; Springer: New York, NY, USA, 2000; pp. 104–116. ISBN 978-1-4612-1224-9.
4. Krishna, M.P.; Mohan, M. Litter Decomposition in Forest Ecosystems: A Review. *Energ. Ecol. Environ.* **2017**, *2*, 236–249. [CrossRef]
5. van der Wal, A.; Geydan, T.D.; Kuyper, T.W.; de Boer, W. A Thready Affair: Linking Fungal Diversity and Community Dynamics to Terrestrial Decomposition Processes. *FEMS Microbiol. Rev.* **2013**, *37*, 477–494. [CrossRef]
6. Guo, J.; Yang, Y.; Chen, G.; Lin, P.; Xie, J. A Review on Litter Decomposition in Forest Ecosystem. Available online: http://html.rhhz.net/linyekexue/html/20060417.htm (accessed on 5 October 2023).
7. Keller, A.B.; Phillips, R.P. Leaf Litter Decay Rates Differ between Mycorrhizal Groups in Temperate, but Not Tropical, Forests. *New Phytol.* **2019**, *222*, 556–564. [CrossRef]
8. Jing, H.; Wang, G. Temporal Dynamics of Pinus Tabulaeformis Litter Decomposition under Nitrogen Addition on the Loess Plateau of China. *For. Ecol. Manag.* **2020**, *476*, 118465. [CrossRef]
9. Dechaine, J.; Ruan, H.; Sanchez-de Leon, Y.; Zou, X. Correlation between Earthworms and Plant Litter Decomposition in a Tropical Wet Forest of Puerto Rico. *Pedobiologia* **2005**, *49*, 601–607. [CrossRef]
10. Farooq, T.H.; Li, Z.; Yan, W.; Shakoor, A.; Kumar, U.; Shabbir, R.; Peng, Y.; Gayathiri, E.; Alotaibi, S.S.; Wróbel, J.; et al. Variations in Litterfall Dynamics, C:N:P Stoichiometry and Associated Nutrient Return in Pure and Mixed Stands of Camphor Tree and Masson Pine Forests. *Front. Environ. Sci.* **2022**, *10*, 903039. [CrossRef]
11. Bai, Y.; Zhou, Y.; Chen, X.; An, Z.; Zhang, X.; Du, J.; Chang, S.X. Tree Species Composition Alters the Decomposition of Mixed Litter and the Associated Microbial Community Composition and Function in Subtropical Plantations in China. *For. Ecol. Manag.* **2023**, *529*, 120743. [CrossRef]
12. Prescott, C.E.; Zabek, L.M.; Staley, C.L.; Kabzems, R. Decomposition of Broadleaf and Needle Litter in Forests of British Columbia: Influences of Litter Type, Forest Type, and Litter Mixtures. *Can. J. For. Res.* **2000**, *30*, 1742–1750. [CrossRef]
13. Baldrian, P. Forest Microbiome: Diversity, Complexity and Dynamics. *FEMS Microbiol. Rev.* **2017**, *41*, 109–130. [CrossRef] [PubMed]
14. Bani, A.; Pioli, S.; Ventura, M.; Panzacchi, P.; Borruso, L.; Tognetti, R.; Tonon, G.; Brusetti, L. The Role of Microbial Community in the Decomposition of Leaf Litter and Deadwood. *Appl. Soil Ecol.* **2018**, *126*, 75–84. [CrossRef]
15. Baldrian, P.; Valásková, V. Degradation of Cellulose by Basidiomycetous Fungi. *FEMS Microbiol. Rev.* **2008**, *32*, 501–521. [CrossRef] [PubMed]
16. Floudas, D.; Binder, M.; Riley, R.; Barry, K.; Blanchette, R.A.; Henrissat, B.; Martínez, A.T.; Otillar, R.; Spatafora, J.W.; Yadav, J.S.; et al. The Paleozoic Origin of Enzymatic Lignin Decomposition Reconstructed from 31 Fungal Genomes. *Science* **2012**, *336*, 1715–1719. [CrossRef]
17. Chávez-Vergara, B.; Rosales-Castillo, A.; Merino, A.; Vázquez-Marrufo, G.; Oyama, K.; García-Oliva, F. Quercus Species Control Nutrients Dynamics by Determining the Composition and Activity of the Forest Floor Fungal Community. *Soil Biol. Biochem.* **2016**, *98*, 186–195. [CrossRef]
18. Eichlerová, I.; Homolka, L.; Žifčáková, L.; Lisá, L.; Dobiášová, P.; Baldrian, P. Enzymatic Systems Involved in Decomposition Reflects the Ecology and Taxonomy of Saprotrophic Fungi. *Fungal Ecol.* **2015**, *13*, 10–22. [CrossRef]
19. Tian, L.; Dell, E.; Shi, W. Chemical Composition of Dissolved Organic Matter in Agroecosystems: Correlations with Soil Enzyme Activity and Carbon and Nitrogen Mineralization. *Appl. Soil Ecol.* **2010**, *46*, 426–435. [CrossRef]
20. Xu, Z.; Yu, G.; Zhang, X.; Ge, J.; He, N.; Wang, Q.; Wang, D. The Variations in Soil Microbial Communities, Enzyme Activities and Their Relationships with Soil Organic Matter Decomposition along the Northern Slope of Changbai Mountain. *Appl. Soil Ecol.* **2015**, *86*, 19–29. [CrossRef]
21. Allison, S.D.; Vitousek, P.M. Extracellular Enzyme Activities and Carbon Chemistry as Drivers of Tropical Plant Litter Decomposition. *Biotropica* **2004**, *36*, 285–296. [CrossRef]

22. Waring, B.G. Exploring Relationships between Enzyme Activities and Leaf Litter Decomposition in a Wet Tropical Forest. *Soil Biol. Biochem.* **2013**, *64*, 89–95. [CrossRef]
23. Osono, T.; To-Anun, C.; Hagiwara, Y.; Hirose, D. Decomposition of Wood, Petiole and Leaf Litter by Xylaria Species from Northern Thailand. *Fungal Ecol.* **2011**, *4*, 210–218. [CrossRef]
24. Eastwood, D.C.; Floudas, D.; Binder, M.; Majcherczyk, A.; Schneider, P.; Aerts, A.; Asiegbu, F.O.; Baker, S.E.; Barry, K.; Bendiksby, M.; et al. The Plant Cell Wall-Decomposing Machinery Underlies the Functional Diversity of Forest Fungi. *Science* **2011**, *333*, 762–765. [CrossRef] [PubMed]
25. Sun, X.; Zheng, Y.; Xu, G.; Guo, Q.; Tan, J.; Ding, G. Fungal Diversity within the Phyllosphere of Pinus Massoniana and the Possible Involvement of Phyllospheric Fungi in Litter Decomposition. *Fungal Biol.* **2021**, *125*, 785–795. [CrossRef] [PubMed]
26. Osono, T. Ecology of Ligninolytic Fungi Associated with Leaf Litter Decomposition. *Ecol. Res.* **2007**, *22*, 955–974. [CrossRef]
27. Frankland, J.C. Fungal Succession—Unravelling the Unpredictable. *Mycol. Res.* **1998**, *102*, 1–15. [CrossRef]
28. Dilly, O.; Bartsch, S.; Rosenbrock, P.; Buscot, F.; Munch, J.C. Shifts in Physiological Capabilities of the Microbiota during the Decomposition of Leaf Litter in a Black Alder (*Alnus glutinosa* (Gaertn.) L.) Forest. *Soil Biol. Biochem.* **2001**, *33*, 921–930. [CrossRef]
29. Osono, T. Role of Phyllosphere Fungi of Forest Trees in the Development of Decomposer Fungal Communities and Decomposition Processes of Leaf Litter. *Can. J. Microbiol.* **2006**, *52*, 701–716. [CrossRef]
30. Rajala, T.; Peltoniemi, M.; Hantula, J.; Mäkipää, R.; Pennanen, T. RNA Reveals a Succession of Active Fungi during the Decay of Norway Spruce Logs. *Fungal Ecol.* **2011**, *4*, 437–448. [CrossRef]
31. Purahong, W.; Wubet, T.; Lentendu, G.; Schloter, M.; Pecyna, M.J.; Kapturska, D.; Hofrichter, M.; Krüger, D.; Buscot, F. Life in Leaf Litter: Novel Insights into Community Dynamics of Bacteria and Fungi during Litter Decomposition. *Mol. Ecol.* **2016**, *25*, 4059–4074. [CrossRef]
32. Voříšková, J.; Baldrian, P. Fungal Community on Decomposing Leaf Litter Undergoes Rapid Successional Changes. *ISME J.* **2013**, *7*, 477–486. [CrossRef]
33. Urbanová, M.; Šnajdr, J.; Baldrian, P. Composition of Fungal and Bacterial Communities in Forest Litter and Soil Is Largely Determined by Dominant Trees. *Soil Biol. Biochem.* **2015**, *84*, 53–64. [CrossRef]
34. Sun, H.; Terhonen, E.; Kovalchuk, A.; Tuovila, H.; Chen, H.; Oghenekaro, A.O.; Heinonsalo, J.; Kohler, A.; Kasanen, R.; Vasander, H.; et al. Dominant Tree Species and Soil Type Affect the Fungal Community Structure in a Boreal Peatland Forest. *Appl. Environ. Microbiol.* **2016**, *82*, 2632–2643. [CrossRef] [PubMed]
35. Nagati, M.; Roy, M.; Manzi, S.; Richard, F.; Desrochers, A.; Gardes, M.; Bergeron, Y. Impact of Local Forest Composition on Soil Fungal Communities in a Mixed Boreal Forest. *Plant Soil* **2018**, *432*, 345–357. [CrossRef]
36. Treseder, K.K.; Bent, E.; Borneman, J.; McGuire, K.L. Shifts in Fungal Communities during Decomposition of Boreal Forest Litter. *Fungal Ecol.* **2014**, *10*, 58–69. [CrossRef]
37. Foudyl-Bey, S.; Brais, S.; Drouin, P. Litter Heterogeneity Modulates Fungal Activity, C Mineralization and N Retention in the Boreal Forest Floor. *Soil Biol. Biochem.* **2016**, *100*, 264–275. [CrossRef]
38. Qu, Z.-L.; Liu, B.; Ma, Y.; Xu, J.; Sun, H. The Response of the Soil Bacterial Community and Function to Forest Succession Caused by Forest Disease. *Funct. Ecol.* **2020**, *34*, 2548–2559. [CrossRef]
39. Chen, X.; Yuan, Z.; Jin, X.; Zhu, J.; Xu, H.; Zhao, C.; Chen, B.; Guan, Q. Spatial Distribution Pattern and Interspecific Association of Dominant Tree Species in a Broad-Leaved Mixed Forest on Zijin Mountain. *J. Nanjing For. Univ.* **2018**, *61*, 84. [CrossRef]
40. Deng, J.; Yin, Y.; Luo, J.; Zhu, W.; Zhou, Y. Different Revegetation Types Alter Soil Physical-Chemical Characteristics and Fungal Community in the Baishilazi Nature Reserve. *PeerJ* **2019**, *6*, e6251. [CrossRef]
41. Liu, K.; Meng, W.; Qu, Z.; Zhang, Y.; Liu, B.; Ma, Y.; Chang, L.; Sun, H. Changes in Bacterial Communities and Functions Associated with Litter Degradation during Forest Succession Caused by Forest Disease. *Phytobiomes J.* **2023**, *7*, 491–499. [CrossRef]
42. Chen, X.; Yuan, Z.; Jin, X.; Guan, Q.; Zhu, J.; Dai, K.; Zhao, C. Characteristics of Coniferous and Broad-Leaved Mixed Forest Community on Zijin Mountain. *J. Cent. South Univ. For. Technol.* **2020**, *40*, 113–119.
43. Jiang, A.; Wan, F.; Hu, F. Study on Soil Anti-Erodibility in Different Forests in Spirit Valley of Mount Zijin in Nanjing. Available online: http://stbcyj.paperonce.org/oa/DArticle.aspx?id=20180103 (accessed on 7 November 2023).
44. Anderson, J.M. The Breakdown and Decomposition of Sweet Chestnut (*Castanea sativa* Mill.) and Beech (*Fagus sylvatica* L.) Leaf Litter in Two Deciduous Woodland Soils: I. Breakdown, Leaching and Decomposition. *Oecologia* **1973**, *12*, 251–274. [CrossRef] [PubMed]
45. Ma, Y.; Qu, Z.-L.; Liu, B.; Tan, J.-J.; Asiegbu, F.O.; Sun, H. Bacterial Community Structure of *Pinus Thunbergii* Naturally Infected by the Nematode *Bursaphelenchus xylophilus*. *Microorganisms* **2020**, *8*, 307. [CrossRef] [PubMed]
46. Smith, D.P.; Peay, K.G. Sequence Depth, Not PCR Replication, Improves Ecological Inference from next Generation DNA Sequencing. *PLoS ONE* **2014**, *9*, e90234. [CrossRef] [PubMed]
47. Sinsabaugh, R.L.; Saiya-Cork, K.; Long, T.; Osgood, M.P.; Neher, D.A.; Zak, D.R.; Norby, R.J. Soil Microbial Activity in a Liquidambar Plantation Unresponsive to CO2-Driven Increases in Primary Production. *Appl. Soil Ecol.* **2003**, *24*, 263–271. [CrossRef]
48. Xu, J.; Liu, B.; Qu, Z.-L.; Ma, Y.; Sun, H. Age and Species of Eucalyptus Plantations Affect Soil Microbial Biomass and Enzymatic Activities. *Microorganisms* **2020**, *8*, 811. [CrossRef]
49. Zheng, B.; Zhu, Y.; Sardans, J.; Peñuelas, J.; Su, J. QMEC: A Tool for High-Throughput Quantitative Assessment of Microbial Functional Potential in C, N, P, and S Biogeochemical Cycling. *Sci. China Life Sci.* **2018**, *61*, 1451–1462. [CrossRef]

50. Schloss, P.D.; Westcott, S.L.; Ryabin, T.; Hall, J.R.; Hartmann, M.; Hollister, E.B.; Lesniewski, R.A.; Oakley, B.B.; Parks, D.H.; Robinson, C.J.; et al. Introducing Mothur: Open-Source, Platform-Independent, Community-Supported Software for Describing and Comparing Microbial Communities. *Appl. Environ. Microbiol.* **2009**, *75*, 7537–7541. [CrossRef]
51. Tedersoo, L.; Nilsson, R.H.; Abarenkov, K.; Jairus, T.; Sadam, A.; Saar, I.; Bahram, M.; Bechem, E.; Chuyong, G.; Kõljalg, U. 454 Pyrosequencing and Sanger Sequencing of Tropical Mycorrhizal Fungi Provide Similar Results but Reveal Substantial Methodological Biases. *New Phytol.* **2010**, *188*, 291–301. [CrossRef]
52. Abarenkov, K.; Henrik Nilsson, R.; Larsson, K.-H.; Alexander, I.J.; Eberhardt, U.; Erland, S.; Høiland, K.; Kjøller, R.; Larsson, E.; Pennanen, T.; et al. The UNITE Database for Molecular Identification of Fungi--Recent Updates and Future Perspectives. *New Phytol.* **2010**, *186*, 281–285. [CrossRef]
53. Nguyen, N.H.; Song, Z.; Bates, S.T.; Branco, S.; Tedersoo, L.; Menke, J.; Schilling, J.S.; Kennedy, P.G. FUNGuild: An Open Annotation Tool for Parsing Fungal Community Datasets by Ecological Guild. *Fungal Ecol.* **2016**, *20*, 241–248. [CrossRef]
54. Anderson, M. *Permanova+ for Primer: Guide to Software and Statistical Methods*; Primer-E Limited: Plymouth, UK, 2008.
55. Jackrel, S.L.; Gilbert, J.A.; Wootton, J.T. The Origin, Succession, and Predicted Metabolism of Bacterial Communities Associated with Leaf Decomposition. *mBio* **2019**, *10*, e01703-19. [CrossRef] [PubMed]
56. Laganière, J.; Paré, D.; Bradley, R.L. How Does a Tree Species Influence Litter Decomposition? Separating the Relative Contribution of Litter Quality, Litter Mixing, and Forest Floor Conditions. *Can. J. For. Res.* **2010**, *40*, 465–475. [CrossRef]
57. Kamau, S.; Barrios, E.; Karanja, N.K.; Ayuke, F.O.; Lehmann, J. Dominant Tree Species and Earthworms Affect Soil Aggregation and Carbon Content along a Soil Degradation Gradient in an Agricultural Landscape. *Geoderma* **2020**, *359*, 113983. [CrossRef]
58. Wang, X.; Xiao, S.; Yang, X.; Liu, Z.; Zhou, X.; Du, G.; Zhang, L.; Guo, A.; Chen, S.; Nielsen, U.N. Dominant Plant Species Influence Nematode Richness by Moderating Understory Diversity and Microbial Assemblages. *Soil Biol. Biochem.* **2019**, *137*, 107566. [CrossRef]
59. Yang, X.; Wang, X.; Xiao, S.; Liu, Z.; Zhou, X.; Du, G.; Liu, K.; Wang, Y.; Chen, S.; Nielsen, U.N. Dominant Plants Affect Litter Decomposition Mainly through Modifications of the Soil Microbial Community. *Soil Biol. Biochem.* **2021**, *161*, 108399. [CrossRef]
60. Yue, K.; Yang, W.; Peng, C.; Peng, Y.; Zhang, C.; Huang, C.; Tan, Y.; Wu, F. Foliar Litter Decomposition in an Alpine Forest Meta-Ecosystem on the Eastern Tibetan Plateau. *Sci. Total Environ.* **2016**, *566–567*, 279–287. [CrossRef]
61. Bray, S.R.; Kitajima, K.; Mack, M.C. Temporal Dynamics of Microbial Communities on Decomposing Leaf Litter of 10 Plant Species in Relation to Decomposition Rate. *Soil Biol. Biochem.* **2012**, *49*, 30–37. [CrossRef]
62. Gołębiewski, M.; Tarasek, A.; Sikora, M.; Deja-Sikora, E.; Tretyn, A.; Niklińska, M. Rapid Microbial Community Changes During Initial Stages of Pine Litter Decomposition. *Microb. Ecol.* **2019**, *77*, 56–75. [CrossRef]
63. Cheng, F.; Peng, X.; Zhao, P.; Yuan, J.; Zhong, C.; Cheng, Y.; Cui, C.; Zhang, S. Soil Microbial Biomass, Basal Respiration and Enzyme Activity of Main Forest Types in the Qinling Mountains. *PLoS ONE* **2013**, *8*, e67353. [CrossRef]
64. Ayres, E.; Steltzer, H.; Berg, S.; Wallenstein, M.D.; Simmons, B.L.; Wall, D.H. Tree Species Traits Influence Soil Physical, Chemical, and Biological Properties in High Elevation Forests. *PLoS ONE* **2009**, *4*, e5964. [CrossRef]
65. Bauhus, J.; Paré, D.; Côtéc, L. Effects of Tree Species, Stand Age and Soil Type on Soil Microbial Biomass and Its Activity in a Southern Boreal Forest. *Soil Biol. Biochem.* **1998**, *30*, 1077–1089. [CrossRef]
66. Aciego Pietri, J.C.; Brookes, P.C. Substrate Inputs and pH as Factors Controlling Microbial Biomass, Activity and Community Structure in an Arable Soil. *Soil Biol. Biochem.* **2009**, *41*, 1396–1405. [CrossRef]
67. Šnajdr, J.; Cajthaml, T.; Valášková, V.; Merhautová, V.; Petránková, M.; Spetz, P.; Leppänen, K.; Baldrian, P. Transformation of Quercus Petraea Litter: Successive Changes in Litter Chemistry Are Reflected in Differential Enzyme Activity and Changes in the Microbial Community Composition. *FEMS Microbiol. Ecol.* **2011**, *75*, 291–303. [CrossRef] [PubMed]
68. Steffen, K.T.; Cajthaml, T.; Šnajdr, J.; Baldrian, P. Differential Degradation of Oak (*Quercus petraea*) Leaf Litter by Litter-Decomposing Basidiomycetes. *Res. Microbiol.* **2007**, *158*, 447–455. [CrossRef]
69. Berg, B.; McClaugherty, C. Decomposition as a Process—Some Main Features. In *Plant Litter: Decomposition, Humus Formation, Carbon Sequestration*; Berg, B., McClaugherty, C., Eds.; Springer International Publishing: Cham, Switzerland, 2020; pp. 13–43. ISBN 978-3-030-59631-6.
70. Lehmann, J.; Schroth, G.; Zech, W. Decomposition and Nutrient Release from Leaves, Twigs and Roots of Three Alley-Cropped Tree Legumes in Central Togo. *Agroforest Syst.* **1995**, *29*, 21–36. [CrossRef]
71. Cai, Y.J.; Chapman, S.J.; Buswell, J.A.; Chang, S. Production and Distribution of Endoglucanase, Cellobiohydrolase, and β-Glucosidase Components of the Cellulolytic System of Volvariella Volvacea, the Edible Straw Mushroom. *Appl. Environ. Microbiol.* **1999**, *65*, 553–559. [CrossRef]
72. Kähkönen, M.A.; Lankinen, P.; Hatakka, A. Hydrolytic and Ligninolytic Enzyme Activities in the Pb Contaminated Soil Inoculated with Litter-Decomposing Fungi. *Chemosphere* **2008**, *72*, 708–714. [CrossRef]
73. Chen, L.; Xiang, W.; Wu, H.; Ouyang, S.; Zhou, B.; Zeng, Y.; Chen, Y.; Kuzyakov, Y. Tree Species Identity Surpasses Richness in Affecting Soil Microbial Richness and Community Composition in Subtropical Forests. *Soil Biol. Biochem.* **2019**, *130*, 113–121. [CrossRef]
74. Loreau, M. Microbial Diversity, Producer–Decomposer Interactions and Ecosystem Processes: A Theoretical Model. *Proc. R. Soc. London Ser. B Biol. Sci.* **2001**, *268*, 303–309. [CrossRef]
75. Loreau, M.; Hector, A. Partitioning Selection and Complementarity in Biodiversity Experiments. *Nature* **2001**, *412*, 72–76. [CrossRef]

76. LeBauer, D.S. Litter Degradation Rate and β-Glucosidase Activity Increase with Fungal Diversity. *Can. J. For. Res.* **2010**, *40*, 1076–1085. [CrossRef]
77. Novotný, Č.; Svobodová, K.; Erbanová, P.; Cajthaml, T.; Kasinath, A.; Lang, E.; Šašek, V. Ligninolytic Fungi in Bioremediation: Extracellular Enzyme Production and Degradation Rate. *Soil Biol. Biochem.* **2004**, *36*, 1545–1551. [CrossRef]
78. Baldrian, P. Chapter 2 Enzymes of Saprotrophic Basidiomycetes. In *British Mycological Society Symposia Series*; Boddy, L., Frankland, J.C., van West, P., Eds.; Ecology of Saprotrophic Basidiomycetes; Academic Press: Cambridge, MA, USA, 2008; Volume 28, pp. 19–41.
79. Geethanjali, P.A.; Jayashankar, M. A Review on Litter Decomposition by Soil Fungal Community. *IOSR J. Pharm. Biol. Sci.* **2016**, *11*, 01–03. [CrossRef]
80. Lundell, T.K.; Mäkelä, M.R.; de Vries, R.P.; Hildén, K.S. Chapter Eleven—Genomics, Lifestyles and Future Prospects of Wood-Decay and Litter-Decomposing Basidiomycota. In *Advances in Botanical Research*; Martin, F.M., Ed.; Fungi; Academic Press: Cambridge, MA, USA, 2014; Volume 70, pp. 329–370.
81. Hirose, A.; Kudo, S.; Murakami, T.; Tanaka, K.; Harada, Y.; Hashimoto, M. Lambertellin System, the Mechanism for Fungal Replacement of *Monilinia fructigena* with *Lambertella corni-maris* without Competitive Inhibition on Agar Media. *Bioorganic Med. Chem.* **2014**, *22*, 2489–2495. [CrossRef] [PubMed]
82. Becarelli, S.; Chicca, I.; Siracusa, G.; La China, S.; Gentini, A.; Lorenzi, R.; Munz, G.; Petroni, G.; Levin, D.B.; Di Gregorio, S. Hydrocarbonoclastic Ascomycetes to Enhance Co-Composting of Total Petroleum Hydrocarbon (TPH) Contaminated Dredged Sediments and Lignocellulosic Matrices. *N. Biotechnol.* **2019**, *50*, 27–36. [CrossRef]
83. Koukol, O. New Species of Chalara Occupying Coniferous Needles. *Fungal Divers.* **2011**, *49*, 75–91. [CrossRef]
84. Vanden Wymelenberg, A.; Sabat, G.; Mozuch, M.; Kersten, P.J.; Cullen, D.; Blanchette, R.A. Structure, Organization, and Transcriptional Regulation of a Family of Copper Radical Oxidase Genes in the Lignin-Degrading Basidiomycete Phanerochaete Chrysosporium. *Appl. Environ. Microbiol.* **2006**, *72*, 4871–4877. [CrossRef]
85. Barbi, F.; Kohler, A.; Barry, K.; Baskaran, P.; Daum, C.; Fauchery, L.; Ihrmark, K.; Kuo, A.; LaButti, K.; Lipzen, A.; et al. Fungal Ecological Strategies Reflected in Gene Transcription—A Case Study of Two Litter Decomposers. *Environ. Microbiol.* **2020**, *22*, 1089–1103. [CrossRef]
86. Tedersoo, L.; Bahram, M.; Toots, M.; Diédhiou, A.G.; Henkel, T.W.; Kjøller, R.; Morris, M.H.; Nara, K.; Nouhra, E.; Peay, K.G.; et al. Towards Global Patterns in the Diversity and Community Structure of Ectomycorrhizal Fungi. *Mol. Ecol.* **2012**, *21*, 4160–4170. [CrossRef]
87. Fernandez, C.W.; See, C.R.; Kennedy, P.G. Decelerated Carbon Cycling by Ectomycorrhizal Fungi Is Controlled by Substrate Quality and Community Composition. *New Phytol.* **2020**, *226*, 569–582. [CrossRef]
88. Tedersoo, L.; Bahram, M.; Ryberg, M.; Otsing, E.; Kõljalg, U.; Abarenkov, K. Global Biogeography of the Ectomycorrhizal /Sebacina Lineage (Fungi, Sebacinales) as Revealed from Comparative Phylogenetic Analyses. *Mol. Ecol.* **2014**, *23*, 4168–4183. [CrossRef] [PubMed]
89. Anderson, I.C.; Cairney, J.W.G. Ectomycorrhizal Fungi: Exploring the Mycelial Frontier. *FEMS Microbiol. Rev.* **2007**, *31*, 388–406. [CrossRef] [PubMed]
90. Strullu-Derrien, C.; Selosse, M.-A.; Kenrick, P.; Martin, F.M. The Origin and Evolution of Mycorrhizal Symbioses: From Palaeomycology to Phylogenomics. *New Phytol.* **2018**, *220*, 1012–1030. [CrossRef] [PubMed]
91. Popescu, D.I.; Frum, A.; Dobrea, C.M.; Cristea, R.; Gligor, F.G.; Vicas, L.G.; Ionete, R.E.; Sutan, N.A.; Georgescu, C. Comparative Antioxidant and Antimicrobial Activities of Several Conifer Needles and Bark Extracts. *Pharmaceutics* **2024**, *16*, 52. [CrossRef]
92. Simon, J.; Dörken, V.M.; L.-M.-Arnold, A.; Adamczyk, B. Environmental Conditions and Species Identity Drive Metabolite Levels in Green Leaves and Leaf Litter of 14 Temperate Woody Species. *Forests* **2018**, *9*, 775. [CrossRef]
93. Kusuda, M.; Ueda, M.; Miyatake, K.; Terashita, T. Characterization of the Carbohydrase Productions of an Ectomycorrhizal Fungus, Tricholoma Matsutake. *Mycoscience* **2008**, *49*, 291–297. [CrossRef]
94. Kohler, A.; Kuo, A.; Nagy, L.G.; Morin, E.; Barry, K.W.; Buscot, F.; Canbäck, B.; Choi, C.; Cichocki, N.; Clum, A.; et al. Convergent Losses of Decay Mechanisms and Rapid Turnover of Symbiosis Genes in Mycorrhizal Mutualists. *Nat. Genet.* **2015**, *47*, 410–415. [CrossRef]
95. Miyauchi, S.; Kiss, E.; Kuo, A.; Drula, E.; Kohler, A.; Sánchez-García, M.; Morin, E.; Andreopoulos, B.; Barry, K.W.; Bonito, G.; et al. Large-Scale Genome Sequencing of Mycorrhizal Fungi Provides Insights into the Early Evolution of Symbiotic Traits. *Nat. Commun.* **2020**, *11*, 5125. [CrossRef]
96. Looney, B.; Miyauchi, S.; Morin, E.; Drula, E.; Courty, P.-E.; Kohler, A.; Lindquist, E.; Kuo, A.; Labutti, K.; Pangilinan, J.; et al. Evolutionary Priming and Transition to the Ectomycorrhizal Habit in an Iconic Lineage of Mushroom-Forming Fungi: Is Preadaptation a Requirement? *bioRxiv* **2021**. [CrossRef]
97. Lebreton, A.; Zeng, Q.; Miyauchi, S.; Kohler, A.; Dai, Y.-C.; Martin, F.M. Evolution of the Mode of Nutrition in Symbiotic and Saprotrophic Fungi in Forest Ecosystems. *Annu. Rev. Ecol. Evol. Syst.* **2021**, *52*, 385–404. [CrossRef]
98. Nehls, U.; Plassard, C. Nitrogen and Phosphate Metabolism in Ectomycorrhizas. *New Phytol.* **2018**, *220*, 1047–1058. [CrossRef] [PubMed]
99. Lindahl, B.D.; Ihrmark, K.; Boberg, J.; Trumbore, S.E.; Högberg, P.; Stenlid, J.; Finlay, R.D. Spatial Separation of Litter Decomposition and Mycorrhizal Nitrogen Uptake in a Boreal Forest. *New Phytol.* **2007**, *173*, 611–620. [CrossRef] [PubMed]

100. Hug, L.A.; Co, R. It Takes a Village: Microbial Communities Thrive through Interactions and Metabolic Handoffs. *mSystems* **2018**, *3*, e00152-17. [CrossRef] [PubMed]
101. Siles, J.A.; Starke, R.; Martinovic, T.; Parente Fernandes, M.L.; Orgiazzi, A.; Bastida, F. Distribution of Phosphorus Cycling Genes across Land Uses and Microbial Taxonomic Groups Based on Metagenome and Genome Mining. *Soil Biol. Biochem.* **2022**, *174*, 108826. [CrossRef]
102. Matsumura, K.; Obata, H.; Hata, Y.; Kawato, A.; Abe, Y.; Akita, O. Isolation and Characterization of a Novel Gene Encoding α-L-Arabinofuranosidase from Aspergillus Oryzae. *J. Biosci. Bioeng.* **2004**, *98*, 77–84. [CrossRef]
103. Rodionov, D.A.; Rodionova, I.A.; Rodionov, V.A.; Arzamasov, A.A.; Zhang, K.; Rubinstein, G.M.; Tanwee, T.N.N.; Bing, R.G.; Crosby, J.R.; Nookaew, I.; et al. Transcriptional Regulation of Plant Biomass Degradation and Carbohydrate Utilization Genes in the Extreme Thermophile Caldicellulosiruptor Bescii. *mSystems* **2021**, *6*, e0134520. [CrossRef]
104. Zhang, Y.; Li, X.; Xiao, M.; Feng, Z.; Yu, Y.; Yao, H. Effects of Microplastics on Soil Carbon Dioxide Emissions and the Microbial Functional Genes Involved in Organic Carbon Decomposition in Agricultural Soil. *Sci. Total Environ.* **2022**, *806*, 150714. [CrossRef]
105. Li, M.; Hao, Y.; Yan, Z.; Kang, E.; Wang, J.; Zhang, K.; Li, Y.; Wu, H.; Kang, X. Long-term Degradation from Marshes into Meadows Shifts Microbial Functional Diversity of Soil Phosphorus Cycling in an Alpine Wetland of the Tibetan Plateau. *Land. Degrad. Dev.* **2022**, *33*, 628–637. [CrossRef]
106. Zhou, S.; Li, Y.; Wang, J.; He, L.; Wang, J.; Guo, Y.; Zhao, F. Contrasting Soil Microbial Functional Potential for Phosphorus Cycling in Subtropical and Temperate Forests. *Forests* **2022**, *13*, 2002. [CrossRef]
107. Kashyap, P.L.; Rai, P.; Srivastava, A.K.; Kumar, S. Trichoderma for Climate Resilient Agriculture. *World J. Microbiol. Biotechnol.* **2017**, *33*, 155. [CrossRef]
108. Zhang, F.; Huo, Y.; Cobb, A.B.; Luo, G.; Zhou, J.; Yang, G.; Wilson, G.W.T.; Zhang, Y. Trichoderma Biofertilizer Links to Altered Soil Chemistry, Altered Microbial Communities, and Improved Grassland Biomass. *Front. Microbiol.* **2018**, *9*, 848. [CrossRef] [PubMed]
109. Hallam, S.J.; Girguis, P.R.; Preston, C.M.; Richardson, P.M.; DeLong, E.F. Identification of Methyl Coenzyme M Reductase A (mcrA) Genes Associated with Methane-Oxidizing Archaea. *Appl. Environ. Microbiol.* **2003**, *69*, 5483–5491. [CrossRef] [PubMed]
110. Naumova, E.S.; Borovkova, A.N.; Shalamitskiy, M.Y.; Naumov, G.I. Natural Polymorphism of Pectinase PGU Genes in the Saccharomyces Yeasts. *Microbiology* **2021**, *90*, 349–360. [CrossRef]
111. Hua, Z.; Liu, T.; Han, P.; Zhou, J.; Zhao, Y.; Huang, L.; Yuan, Y. Isolation, Genomic Characterization, and Mushroom Growth-Promoting Effect of the First Fungus-Derived Rhizobium. *Front. Microbiol.* **2022**, *13*, 947687. [CrossRef]
112. Granja-Travez, R.S.; Persinoti, G.F.; Squina, F.M.; Bugg, T.D.H. Functional Genomic Analysis of Bacterial Lignin Degraders: Diversity in Mechanisms of Lignin Oxidation and Metabolism. *Appl. Microbiol. Biotechnol.* **2020**, *104*, 3305–3320. [CrossRef]
113. Zhang, Y.; He, G.; Yang, L.; Wen, S.; Yan, J.; Min, B.; Peng, T.; Ji, L. Phosphorus Fertilizer Application Shifts the Rhizosphere Bacterial Community and Their Carbon, Nitrogen and Phosphorus-Cycle Genes in a *Phoebe bournei* Young Plantation. *Appl. Soil Ecol.* **2024**, *198*, 105391. [CrossRef]
114. Prescott, C.E.; Grayston, S.J. Tree Species Influence on Microbial Communities in Litter and Soil: Current Knowledge and Research Needs. *For. Ecol. Manag.* **2013**, *309*, 19–27. [CrossRef]
115. Wu, X.; Shi, Y.; Zhu, J.; Sun, L.; Ma, X. Impacts of Global Warming on Forest Litters. Available online: http://www.sjlyyj.com/article/doi/10.13348/j.cnki.sjlyyj.2022.0079.y (accessed on 28 December 2023).
116. Lamarche, J.; Bradley, R.L.; Hooper, E.; Shipley, B.; Simao Beaunoir, A.-M.; Beaulieu, C. Forest Floor Bacterial Community Composition and Catabolic Profiles in Relation to Landscape Features in Québec's Southern Boreal Forest. *Microb. Ecol.* **2007**, *54*, 10–20. [CrossRef]
117. Habtewold, J.Z.; Helgason, B.L.; Yanni, S.F.; Janzen, H.H.; Ellert, B.H.; Gregorich, E.G. Litter Composition Has Stronger Influence on the Structure of Soil Fungal than Bacterial Communities. *Eur. J. Soil Biol.* **2020**, *98*, 103190. [CrossRef]

Disclaimer/Publisher's Note: The statements, opinions and data contained in all publications are solely those of the individual author(s) and contributor(s) and not of MDPI and/or the editor(s). MDPI and/or the editor(s) disclaim responsibility for any injury to people or property resulting from any ideas, methods, instructions or products referred to in the content.

Journal of *Fungi*

MDPI

Article

Discovery of *Gibellula floridensis* from Infected Spiders and Analysis of the Surrounding Fungal Entomopathogen Community

Ross A. Joseph [1], Abolfazl Masoudi [1], Mateo J. Valdiviezo [2] and Nemat O. Keyhani [1,*]

[1] Department of Biological Sciences, University of Illinois at Chicago, Chicago, IL 60607, USA; rossj@uic.edu (R.A.J.); amasou7@uic.edu (A.M.)
[2] Department of Microbiology and Cell Science, University of Florida, Gainesville, FL 32611, USA; mvaldiviezo@ufl.edu
* Correspondence: keyhani@uic.edu

Abstract: Characterization of fungal spider pathogens lags far behind their insect counterparts. In addition, little to nothing is known concerning the ecological reservoir and/or fungal entomopathogen community surrounding infection sites. Five infected spider cadavers were identified in the neotropical climate of north-central Florida, USA, from three of which viable cultures were obtained. Multi-locus molecular phylogenetic and morphological characterization identified one isolate as a new *Gibellula* species, here named, *Gibellula floridensis*, and the other isolates highly similar to *Parengyodontium album*. The fungal entomopathogen community surrounding infected spiders was sampled at different habitats/trophic levels, including soil, leaf litter, leaf, and twig, and analyzed using ITS amplicon sequencing. These data revealed broad but differential distribution of insect-pathogenic fungi between habitats and variation between sites, with members of genera belonging to *Metarhizium* and *Metacordyceps* from Clavicipitaceae, *Purpureocillium* and *Polycephalomyces* from Ophiocordyceps, and *Akanthomyces* and *Simplicillium* from Cordycipitaceae predominating. However, no sequences corresponding to *Gibellula* or *Parengyodontium*, even at the genera levels, could be detected. Potential explanations for these findings are discussed. These data highlight novel discovery of fungal spider pathogens and open the broader question regarding the environmental distribution and ecological niches of such host-specific pathogens.

Keywords: spider; insect and spider fungal pathogens; *Gibellula*; habitat; amplicon sequencing

1. Introduction

Spiders (Arachnida: Araneae) are highly diverse predatory arthropods characteristic for their use of silk and venom to capture and immobilize prey [1–3]. Occupying a wide range of ecosystems, these organisms play critical ecological roles by feeding on species of insects, fish, reptiles, and even birds and mammals [4–6]. Similar to insects, a major driver of spider mortality appears to be infection by entomopathogenic fungi, including species in the Cordycipitaceae, Ophiocordycipitaceae, and Clavicipitaceae families [7–11]. Among spider-infecting fungi, *Gibellula* (Cordycipitaceae) is a genus of specialized obligate spider-infecting pathogens with ~31 species described thus far, mainly from tropical and temperate environments [12–18]. These fungi are often characterized by causing their spider hosts to attach themselves to the undersides of leaves during the infection process, where the fungus kills it, covering the cadaver in a thick layer of mycelia and sprouting synnemata which produce conidia that are released to "rain" down on new unsuspecting victims [19]. Thus far, *Gibellula* species have been described to infect over 15 different spider families, although identifying spider hosts can be challenging as the fungus envelops the spider body, obscuring morphological features of the infected organism [13]. Despite the apparent global distribution of this genus, knowledge concerning the diversity of *Gibellula*

species in many geographic regions are lacking, with most described species isolated from tropical regions of either Southeast Asia or South America [13–15,20–23]. Indeed, to date, only two *Gibellula* species have been reported from North America, *G. leiopus* and *G. pulchra*, primarily from infected spiders of the Trachelidae and Salticidae families [13,24].

Aside from a lack of knowledge concerning *Gibellula* species diversity in many areas of the world, almost nothing is known concerning their environmental prevalence and/or the fungal community dynamics surrounding infection sites. Some genera of entomopathogenic fungi, particularly generalist facultative fungi of the Cordycipitaceae and Clavicipitaceae families, such as *Beauveria* and *Metarhizium* sp., which have broad host ranges, readily grow in vitro on mycological media and can be found outside of their insect hosts in environmental reservoirs such as soil and/or can be associated in the plant rhizosphere or even as plant epi-/endophytes [25–28]. In contrast, specialized insect pathogenic fungi of the order Entomophthorales, e.g., *Massospora cicadina*, *Arthrophaga myriapodina*, and *Entomophthora muscae*, are obligate insect pathogens and are not readily culturable (if at all) in vitro [29–31]. Some of these latter fungi, e.g., *Massospora* sp., produce resting spores that can persist in the soil [32–34]. *Gibellula* sp. present an in between phenotype, where they can be cultured in vitro, i.e., can grow saprophytically, but have narrow, specialized host ranges. Furthermore, though poorly examined, *Gibellula* infection apparently includes some level of manipulation of host behavior, as part of its extended phenotype is to cause their hosts to become fixed to the underside of leaves and other plant material, often at an elevated position above the ground [35,36]. This presumably facilitates the spread spores onto the surrounding area in order to infect other hosts. However, to our knowledge, to date there are no reports attempting to detect *Gibellula* outside of their spider hosts and/or to examine the fungal community surrounding infected hosts. Such studies are important as little is known concerning any potential reservoir for host-specific insect fungal pathogens and/or the fungal community dynamics that may affect infection, persistence, and/or transmission/spread of the fungus.

In the present study, we found the cadavers of five fungal infected spiders in two forested locations surrounding the University of Florida in Gainesville, Florida: Lake Alice Natural Area and Loblolly Woods Nature Park. Based on visible morphological characteristics, all spider hosts appeared to be of a single genus, *Trachelas*, and all were found to have fixed their bodies in similar positions and on similar substrates: to bark on the undersides of tree branches and trunks one to two meters above the ground. These specimens were collected, and cultures were obtained from three of the five cadavers. Through phylogenetic characterization of cultured isolates using ITS, LSU, SSU, and TEF1a loci as well as morphological characterization, one isolate was confirmed as a new *Gibellula* species, herein described as *Gibellula floridensis* and the other two isolates as *Parengyodontium album* (Cordycipitaceae). The morphology of these isolates was characterized on different growth media, and the characters of the *Gibellula* isolate are described. *Gibellula floridensis* is most closely related to *G. leiopus* but differs by the appearance of their synnemata, as well as the length of their conidiophores, metulae, and conidia. To determine the presence and prevalence of these isolates outside of their spider host, a systematic survey of the fungal communities of samples derived from four trophic levels, namely, soil, leaf litter, leaves, and twigs, from areas surrounding the location of the spider cadavers was performed via amplicon sequencing of the ITS1 region. These areas were found to contain high abundances and diversity of entomopathogenic fungi, particularly in soil samples, with differential distribution between the trophic levels examined. However, sequences corresponding to the *Gibellula* or *Parengyodontium* species isolated in our survey were not detected in these samples, nor, surprisingly, were sequences corresponding to other *Gibellula* or *Parengyodontium* species observed in our dataset. Potential explanations for failure to detect the characterized isolates are discussed. This study adds to the known diversity of *Gibellula* species in North America and opens questions of the presence, prevalence, and distribution of *Gibellula* and other entomopathogenic fungi outside of their arthropod hosts.

2. Materials and Methods

2.1. Infected Spider Location and Collection

Spiders infected by fungal pathogens were located and collected from the Lake Alice and Loblolly natural areas in Gainesville, Florida, United States over the course of several months between March and August 2023. During each collection, the trunks, branches, twigs, and leaves of trees were carefully examined for the presence of spider cadavers. Once located, cadavers were photographed in situ prior to removal. Cadavers were collected from locations on tree trunks and branches using a knife to remove a small amount of the bark to which the spiders had become firmly attached. Collected samples were stored in Falcon tubes or sealed Petri dishes until they could be returned to the lab for further investigation. Once in the lab, samples were stored in a cool dark environment for further photographic documentation and culturing of the infecting fungi.

2.2. Culturing from Infected Spiders and Assessing Growth on Different Media Types

Pure cultures were obtained from infected spider cadavers by lightly touching the conidiophores forming at the ends of synnemata growing from the spiders with a sterilized inoculation loop and then streaking this loop in quadrants onto a potato dextrose agar (PDA) plate containing 200 μg/mL of streptomycin and ampicillin. The plates were monitored for the presence of fungal colonies, and, once appearing, these colonies were touched with an inoculation loop and spread onto a new plate as above for single-spore isolation of cultures. Single-spore isolation was repeated three times for each culture to obtain pure cultures, characterized by morphologically uniform growth. This technique produced pure cultures of a single fungal isolate from spiders 3, 4, and 5, with the isolates being designated UFSI_3, UFSI_4, and UFSI_5, respectively. Once pure cultures of each isolate were obtained, plates containing PDA, Sabouraud dextrose agar (SDA), malt extract agar (MEA), and Czapek–Dox solution agar (CZA) were prepared, and 1 mm plugs of all isolates were taken from the edges of actively growing cultures and inoculated into the center of these plates. Colony growth and morphology were assessed over the course of 1 month for each isolate on each of the above media types to determine growth rates and substrate preferences.

2.3. Environmental Sampling

Soil samples were collected at the locations shown (Supplementary Figure S1), and the soil-sampling sites were assigned coordinates via the Global Positioning System (GPS). The two areas sampled where infected spiders were found were (1) Lake Alice (LA) (29°38′31.14″ N, 82°21′29.20″ W) and (2) Loblolly Woods Nature Park (LB) (29°39′34.74″ N, 82°22′7.27″ W) both in Gainesville, Florida. The LA region was treated as a single site, from which 3 soil, 3 plant litter, 2 twig, and 2 leaf samples were collected. The LB region was divided into four sites, from which 3 soil and 3 plant litter samples were collected from each site, along with 1 twig and 1 leaf sample per site. From the LB region, a total of 12 soil samples, 12 plant litter samples, 4 twig samples, and 4 leaf samples were collected. In total, 42 samples were collected from both regions. Sample collection followed a standard protocol [26]. Briefly, at each location, soil sampling involved marking out five transects spaced ~100 m apart. Along each line, the soil was sampled at five points, each 10 m apart, starting 50 m from the beginning of the line. Samples were taken from the topsoil down to a depth of 30–50 cm and had a diameter of 30 cm. These subsamples were collected using clean shovels and combined in a plastic bag to create a single mixed sample per line. Efforts were made to remove large roots and gravel bigger than 0.5 cm from the samples. The shovels were rinsed with 70% alcohol and dried before moving to the next location. Subsamples of the mixed soil were then packed into individually labeled zip-lock bags (10 cm × 12 cm), and for each site, five of these bagged samples were stored in a large, sealable polyethylene bag and kept cool in a cooler. The schematic for the soil sampling is presented in Supplementary Figure S1.

For isolation of the microbial communities, samples from the plant litter, leaves, and twigs were entirely submerged in 500 mL of distilled water and agitated for three hours at 140 revolutions per minute (rpm) to solubilize the microbial communities from the environmental sample surfaces into the water. Suspensions were filtered through a 0.22 µm pore-size mixed-cellulose esters (MCEs) membrane filter (MF-Millipore™, Tullagreen, Carrigtwohill, Ireland) to collect the microbial community. Filters were immediately frozen and stored at −80 °C.

2.4. DNA Extraction, PCR, and Sequencing

To extract DNA from cultured isolates, a small plug of actively growing hyphae at the edge of a culture plate was removed and placed into a flask containing 50 mL of potato dextrose broth (PDB) to initiate liquid cultures. Liquid cultures were grown at 25 °C with 250 rpm orbital shaking for 7 d, at which point small balls of hyphae could be noted at the bottom of the culture medium. Hyphae were separated from the culture medium by filtration through a 0.7 µm filter and washed with sterile distilled water to remove any residual culture media. Filtered hyphae were then collected into 2 mL tubes along with a sterile glass bead and lyophilized overnight until all water had been removed from the tissues. Lyophilized tissue was powdered by bead beating using an MP FastPrep-24 (MP Biomedicals, Irvine, CA, USA) at 4.0 m/s for 60 s. DNA was extracted from powdered tissues using the Norgen Biotek Plant/Fungi DNA Isolation Kit (Norgen Biotek, Thorold, ON, Canada) according to manufacturer's instructions. Concentration and purity of extracted DNA was assessed using an NP80 nanophotometer (Implemen, Munich, Germany). To amplify loci for downstream sequencing and phylogenetic analysis, the primer sets ITS1F (5′-CTTGGTCATTTAGAGGAAGTAA-3′)/ITS4 (5′-TCCTCCGCTTATTGATATGC-3′) (ITS region), LROR-F (5′-ACCCGCTGAACTTAAGC-3′)/LR5-R (5′-TCCTGA GGGAAACTTCG-3′) (LSU region), NS1-F (5′-GTAGTCATATGCTTGTCTC-3′)/NS4-R (5′-CTTCCGTCAATTC CTTTAAG-3′) (SSU region), and EF1-728F (5′-CATCGAGAAGTTCGAGAAGG-3′)/TEF1LL Erev (5′-AACTTGCAGGCAATGTGG-3′) (TEF1a region) were used in conjunction with taq 5x master mix (New England Biosciences, Ipswich, MA, USA) according to manufacturer instructions. The success of all polymerase chain reactions (PCRs) were verified by gel electrophoresis to visually confirm the presence of a single amplified band. PCR products were purified using GeneJET PCR Purification Kit (Thermo Scientific, Waltham, MA, USA) according to manufacturer instructions, and the concentration was verified by nanophotometer as above prior to sending samples for sequencing. PCR products were sequenced using Oxford Nanopore-sequencing technology (Plasmidsaurus, Eugene, OR, USA). The consensus sequences received from the nanopore-sequencing results were assessed by BLAST searching and examining CDS features to determine sequence quality, strandedness, and the presence of introns. Sequences for each isolate were deposited in Genbank under the following accession numbers: UFSI_3: PP915745 (ITS), PP915999 (LSU), PP916007 (SSU); UFSI_4: PP915746 (ITS), PP916000 (LSU), PP916008 (SSU); UFSI_5: PP915747 (ITS), PP916001 (LSU), PP916009 (SSU), PP938454 (TEF1a).

For environmental samples (soil, leaves, leaf litter, and twigs), total DNA from soil and those from samples collected on 0.22 µm filters (as above) were extracted using the DNeasy® PowerSoil® Pro kit (Qiagen, GmbH, Hilden, Germany) or DNeasy® PowerWater® kit (Qiagen, GmbH, Hilden, Germany), respectively, according to the manufacturer's instructions. Genomic DNA purity and integrity were determined by using NanoPhotometer® NP80 (IMPLEN, Munich, Germany). DNA was diluted to 1 ng/µL using sterile Mili-Q ddH_2O, based on the concentration. Amplification of the DNA samples was performed using ITS1F (5′-CTTGGTCATTTAGAGGAAGTAA-3′) and ITS2R (5′-GCTGCGTTCTTCATCGATGC-3′) primers, which target ~500 bp of the fungal rRNA gene internal transcribed spacer (ITS) region. PCR cycling conditions were as follows: 94 °C for 1 min as initial denaturation, 35 cycles of 94 °C for 30 s, 52 °C for 30 s, and 68 °C for 30 s, and a 10 min incubation at 68 °C. The PCR products were purified using GeneJET™ Gel Extraction Kit (Thermo Fisher Scientific, Waltman, MA, USA) and quantified by Nanodrop 2000 (Thermo Fisher Scien-

tific). Amplicon sequencing was performed at the University of Illinois at Chicago (UIC) genome research core for next-generation Illumina Miseq (Illumina, San Diego, CA, USA) sequencing (paired-ended 2 × 300 base sequencing reads). The raw sequences produced in the current study can be accessed through the National Center for Biotechnology (NCBI) under BioProject PRJNA1119211, accession SUB14498584.

2.5. Phylogenetic Analysis

Phylogenetic analyses of multiple loci were carried out in order to determine the taxonomic identity of the three cultured isolates from spider cadavers. Sequence data generated from loci from the cultured isolates, as well as sequences obtained from Genbank encompassing representative genera in the family Cordycipitaceae, and the outgroup genus *Trichoderma*, were organized such that sequences for each locus were grouped together into lists of FASTA sequences. Multiple sequence alignments were generated for sequences of each locus individually using the program MAFFT v7.520 [37] with default parameters set. Following alignment, sequences were trimmed using the program GBLOCKS v0.91b [38] with a minimum block length of 3. Following trimming, sequences from the different loci were concatenated using the concat function in the Seqkit v2.4.0 program [39]. Concatenated sequences were used to generate a phylogeny using the program RAxML v8.2.12 [40] with four partitions in the dataset, GTRGAMMA as the model, a rapid bootstrap random number seed of 6669, a parsimony random seed of 2539, and 2000 bootstrap replicates. The hypocrealean fungus, *Trichoderma harzianum*, was used as an outgroup for this tree. To determine how distinct isolate UFSI_5 was from other sequenced *Gibellula* isolates, a second tree was generated using the UFSI_5 ITS sequence and ITS sequences from all available *Gibellula* isolates deposited in genbank. For this tree, sequences were aligned in MAFFT, with no trimming with GBLOCKS to prevent the removal of excessive sequence from the alignment. RAxML was performed as above but without any partitioning of the single locus. For this tree, *Metarrhizium anisopliae* was used as an outgroup. Both trees were visualized using FigTree v1.4.4 [41]. Bootstrap values greater than 70 are displayed on the nodes.

2.6. Amplicon Sequence Variants (ASVs) Cluster and Sequence Analyses

Sequences were provided by UIC as fastq files, which were processed through the DADA2 pipeline in the DADA2 R package to assign reads to ASVs using the Majorbio Cloud platform (https://cloud.majorbio.com/, accessed on 15 May 2024) for high-throughput omics data [42]. This process includes filtering and trimming reads with quality scores < 30, constructing an ASV table, removing chimeras, and assigning taxonomy [43]. ASVs were assigned a taxonomic group using the curated fungal database (UNITE) (https://unite.ut.ee/, 20 May 2024) [44], and any ASV with fewer than 2 occurrences was removed [45]. The sampling effectiveness was evaluated with a rarefaction analysis of data subsets using the rank abundance curve (Supplementary Figure S2). Since entomopathogenic fungi (EFs) were considered in this study, only three families of the Hypocreales order and those with the potential of being spider-specific pathogens were chosen to generate the abundance plots, and the rest of the sequences were removed.

2.7. Microscopy and Whole-Organism Photography

Following collection, whole infected spiders were imaged using a Zeiss Stemi 305 dissecting microscope (Zeiss, Jena, Germany) and a Keyence VHX digital microscope. On the Keyence VHX digital microscope, automated focus stacking was performed for optimal focus and resolution across the entire surface of spider cadavers. This microscope was also used to image colony growth on Petri dishes. For higher magnification imaging, a Zeiss LSM 800 confocal microscope, a Motic BA310E with a Moticam X3 camera attached (Motic Instruments, Schertz, TX, USA), and a Keyence BZX 800 (Keyence, Itasca, IL, USA) were used. To image the conidiophores, spores, and hyphae from the infected spiders, tissue was carefully removed using a scalpel and forceps and placed onto a drop of water on a

microscope slide. A small amount of lactophenol cotton blue was then added to this drop, and the tissue was allowed to sit in the stain for one minute, after which the liquid was wicked away using a Kim Wipe, and a fresh drop of water was added. A cover slip was then added, and the sample was imaged for identifying features using a Keyence BZX 800 and Motic BA310E. To image the morphological features from cultures, a small amount of tissue was removed from plates and wet mounts were prepared as above, but without lactophenol blue staining. The tissue samples were imaged using a Zeiss LSM 800 confocal microscope to image features such as spores, conidiophores, and hyphae. Morphological features were measured using ImageJ.js [46].

3. Results

3.1. Sampling, Spider Identity, and Isolation from Infected Spiders

In total, five infected spiders were located across the two sampling sites, Lake Alice Natural Area and Loblolly Woods, in Gainesville, FL, USA, between the months of March and August 2023. The location of each spider cadaver was noted to be fixed to the bark on the underside of branches and slanted trunks of trees (Figure 1). The position and body arrangement of the spiders all appeared similar, with the front two pairs of legs tucked around the cephalothorax and the abdomen pressed tightly against the tree substrate with a tan to bright yellow mat of hyphae covering most of the arachnid body and affixing it to the tree. Several club-shaped synnemata were observed growing from this mat of hyphae primarily on the abdomen, but also, from the legs and cephalothorax, masses of purple-pigmented conidia were seen forming toward the clubbed ends of these structures. Conidiophores were also noted forming directly from the hyphal mat which covered the body of the spider. Infected spiders were collected using a knife by removing a small piece of the bark to which the cadaver was attached. Spiders were then transported to the lab and stored in sterile, sealed Petri dishes in the dark. Isolations of the infecting fungus were attempted from each of the infected spiders by lightly touching the conidiophores with a sterile inoculating loop and streaking this loop on a PDA plate containing streptomycin and ampicillin for isolation. Using this technique, actively growing cultures were obtained from three of the five infected spiders, S3, S4, and S5, and these cultures were single-spore purified three times to achieve pure cultures as detailed in the Methods section. These isolates were designated UFSI_3, UFSI_4, and UFSI_5, respectively. Based upon the visible morphology of spider hosts (areas not covered by fungal hyphae), including the arrangement of eyes, the color of cephalothorax carapace, and the arrangement of legs, all infected spiders collected appear to belong to the genus *Trachelas* (family Trachelidae).

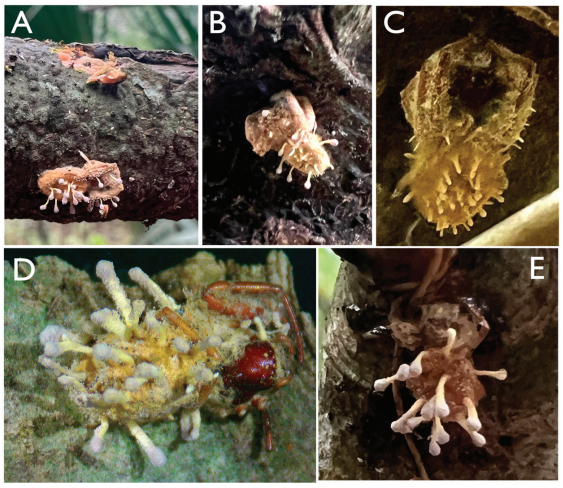


Figure 1. In situ photographs of spider cadavers. (**A**) Spider cadaver S1. (**B**) Spider cadaver S2. (**C**) Spider cadaver S3. (**D**) Spider cadaver S4. (**E**) Spider cadaver S5. Cultivatable fungi were able to be isolated and single-spore purified from cadavers S3–S5 (**C**–**E**).

3.2. Growth and Morphology on Different Media Types

To determine media preference and relative rates of growth, 5 mm plugs of actively growing hyphae from each isolate were cut out of established cultures and placed into the center of plates containing potato dextrose agar (PDA), Czapek–Dox solution agar (CZA), malt extract agar (MEA), and Sabouraud dextrose agar (SDA) and allowed to grow for one month, after which the cultures were examined for their extent of growth and colony morphology (Figure 2). Of the four media types examined, CZA yielded the least amount of growth for all isolates with UFSI_3, UFSI_4, and UFSI_5 showing colony diameters of 7.0, 5.4, and 7.0 mm after 30 d of growth, respectively (Figure 2). Colony morphology on CZA was similar for the three isolates, with dense white mycelia covering the original plug and growing out onto the plate in a thin layer of hyphae. Isolate UFSI_5 showed some small projections growing from the plug on this medium, but no conidiophores or pigmented conidia were noted in any of the plates examined. On the MEA plates, all isolates displayed slightly more robust growth, with UFSI_3, UFSI_4, and UFSI_5 showing 12.9, 9.9, and 18.1 mm colony diameters after 30 d of growth, respectively. On MEA, isolates UFSI_3 and UFSI_4 displayed dense, cottony white to tan mycelia, while the growth of UFSI_5 on this medium appeared tan to yellow, with hyphae forming a much flatter and, in some places, submerged, appearance on plates. On the SDA plates, UFSI_3, UFSI_4, and UFSI_5 grew to a diameter of 9.9, 15.4, and 37.8 mm after 30 d of growth, respectively. The colony morphologies of UFSI_3 and UFSI_4 appeared largely similar, with dense white to tan hyphae spreading from the inoculating plug and growing onto the medium to form a flat colony with irregular edges. A slight darkening of the surrounding medium was noted (Figure 2), suggesting that, under these nutritional conditions, these isolates may be secreting pigmented compounds into the surrounding media. Isolate UFSI_5 displayed a dramatically different morphology on SDA compared to the other isolates as well as to the morphology of UFSI_5 observed on the other media tested. On the SDA, UFSI_5 growth appeared flat to crust-like, with sparse hyphae forming and a submerged irregular appearance, especially at the margins of the colony. The colony displayed an orange to brown coloration which differed from that observed on the other media tested. Of the four media tested, all three isolates displayed the most robust growth on PDA with UFSI_3, UFSI_4, and UFSI_5 showing colony diameters of 25.1, 23.9, and 44.0 mm after 30 d of growth, respectively. On the PDA, isolates UFSI_3 and UFSI_4 displayed largely similar colony morphologies characterized by tan to yellow velvety hyphal growth extending in an irregular margin onto the plate and with some discoloration of the surrounding medium, similar to the discoloration observed on SDA plates. Isolate UFSI_5 grew on PDA as flat to somewhat cottony mycelium with regular margins and a somewhat submerged appearance at the edges of colonies. UFSI_5 on PDA showed dramatic morphological features not observed on other growth media tested, which including the formation of rudimentary synnemata which produced conidiophores and purple-pigmented conidia (Figure 3).

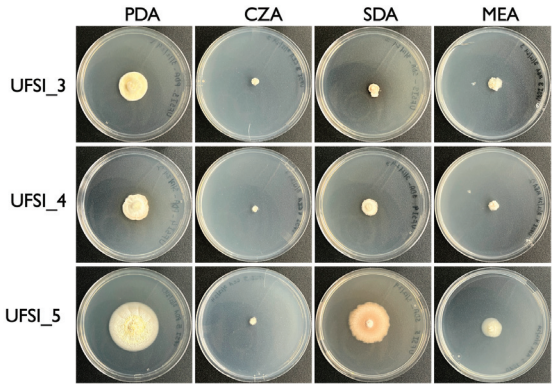


Figure 2. Colony morphology of fungal isolates (UFSI_3, UFSI_4, and UFSI_5) grown on potato dextrose agar (PDA), Czapek–Dox agar (CZA), malt extract agar (MEA), and Sabouraud dextrose agar (SDA) for 30 d at 25 °C.

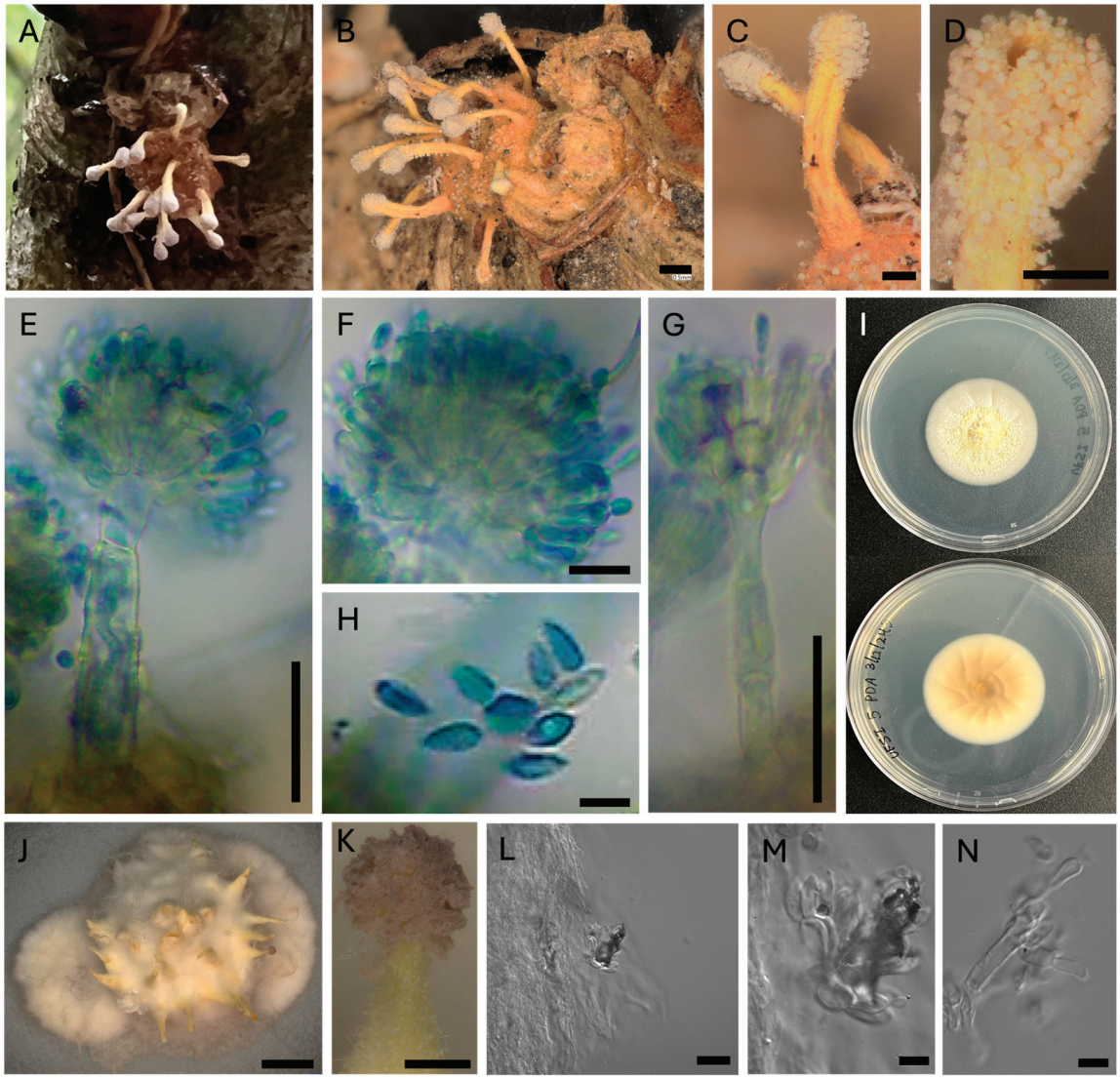


Figure 3. Macroscopic and microscopic morphological characters of *Gibellula* isolate on spider cadavers and in culture. (**A**,**B**) Appearance of spiders (assigned to *Trachelas*) infected by fungal (*Gibellula*) isolates S4 and S5, respectively. (**C**) Synnemata emerging from infected spider cadavers. (**D**) Synnemata head showing purple-pigmented conidiophores. (**E**) Lactophenol blue staining of conidiophore from synnemata showing aspergillus-like morphology. (**F**) Close up of conidiophore head displaying vesicle, metulae, phialides, and conidia. (**G**) Lactophenol blue stained Granulomanus-like asexual morph conidiophore. (**H**) Conidia originating from aspergillus-like asexual morph conidiophores. (**I**) Front and back appearance of *Gibellula* isolate in culture on PDA. (**J**) Gibellula isolate in culture on PDA showing synnema. (**K**) Closeup of synnema produced in culture showing purple-pigmented conidiophores forming at the end. (**L**) Conidiophore forming on synnema produced in culture. (**M**) Closeup of conidiophore produced on synnema in culture. (**N**) Possible Granulomanus-like conidiophore produced in culture. Scale bars in images are as follows: (**A**,**B**) 500 µm, (**C**) 200 µm, (**D**) 200 µm, (**E**) 25 µm, (**F**) 10 µm, (**G**) 25 µm, (**H**) 5 µm, (**J**) 2000 µm, (**K**) 200 µm, (**L**) 20 µm, (**M**) 5 µm, (**N**) 5 µm.

3.3. Microscopic Morphology of Fungal Infected Spider Cadavers and in Culture

Morphological structures of the fungal isolate present on spider cadavers S4 and S5, as well as whole spiders, were imaged using dissecting and compound microscopes (Figure 3A,B). Synnemata appeared numerous, yellow fading to tan with age, clavate (Figure 3C,D). The synnemata were curved and were observed to be covered in conidiophores, particularly at their ends, which appeared purple in color. To better view these

microscopic structures, synnemata were carefully removed from spider cadavers and stained with lactophenol cotton blue before mounting on microscope slides and imaging (Figure 3E–G). Under a compound microscope, two asexual morphs were noted, *Gibellula*-like asexual morphs which presented aspergillus-like morphologies and Granulomanus-like asexual morphs. The presence of sexual morphs were not noted on any spider cadaver examined. *Gibellula*-like asexual morph conidiophores, vesicles on *Gibellula*-like asexual morphs, metulae, and phialides on conidiophores were observed. The culture grown on PDA appeared off-white to tan, with synnema and purple-pigmented conidiophores visible (Figure 3I–K). Conidiophore forming on synnema produced in culture and possible Granulomanus-like conidiophores produced in culture were noted (Figure 3L–N).

3.4. Phylogenetic Placement of Fungal Isolates—Molecular Description of a New Gibellula Species, G. floridensis

To determine the molecular taxonomic identity of the fungal isolates cultured from the infected spider cadavers, genomic DNA was extracted from UFSI_3, UFSI_4, and UFSI_5, and respective ITS, LSU, SSU, and TEF1a loci were amplified and sequenced as detailed in the Methods section (Genbank accession numbers, Supplemental Table S1). Sequences for the above-listed loci corresponding to representative species of the major genera in the family Cordycipitaceae were collected from Genbank, and together with the sequences determined as part of this study, were used to generate a multilocus maximum likelihood phylogenetic tree using RAxML (Figure 4). Following alignment and trimming, 268 bp of ITS, 404 bp of LSU, 237 bp of SSU, and 279 bp of TEF1a were concatenated for a total of 1188 characters used the phylogenetic analysis. In the resulting phylogenetic tree, isolate UFSI_3 grouped closely with the *Parengyodontium album* strain NRRL 28022 with a bootstrap support value of 90%. Isolate UFSI_4 grouped most closely with an isolate labeled as *Hevansia cinnereus* NHJ 3510; however, both isolates together were observed to cluster in the same clade as the above-listed *P. album* isolate and UFSI_3 and between these two isolates and another *Parengyodontium album* strain, UTHSCSA R-4523. This phylogenetic placement, as well as the morphological similarities observed in culture, suggest that the identity of UFSI_4 is likely also *Parengyodontium album* and that the closely clustered *H. cinereus* isolate may represent a *P. album* isolate mislabeled as a species in the genus *Hevansia*. Isolate UFSI_5 clustered within the genus *Gibellula*, with its closest clustering relatives being a clade containing *G. pilosa*, *G. unica*, *G. solita*, *G. pulchra*, and *G. brevistipitata* isolates. However, UFSI_5 formed a distinct branch separate from this clade with a bootstrap support value of 97%, suggesting strong support for this isolate as distinct from these other *Gibellula* species. To better determine the phylogenetic placement of this isolate within a more comprehensive framework of *Gibellula* isolates, a second tree was generated using all available ITS sequences for taxa returned as *Gibellula* in Genbank (Figure 5, Supplementary Table S2). This search yielded a total of 234 sequences, of which 16 were removed after observing preliminary trees due to their abnormally long branch lengths and phylogenetic distance from UFSI_5, indicating that their inclusion was not essential for determining the phylogenetic placement of this isolate. In this *Gibellula*-restricted ITS tree, isolate UFSI_5 cluster with an undescribed *Gibellula* species, *Gibellula* sp. 'CA02' isolate CA FUNDIS iNaturalist 170575944., within a clade containing *G. leiopus*, *G. brevistipitata*, *G. pilosa*, *G. solita*, and *G. unica*. However, again, isolate UFSI_5 occupied a neighboring branch which was distinct from this clade with a bootstrap support value of 99%. A comparison of the major morphological characteristics of the isolate with available information for *G. leiopus* and *G. pulchra* was performed (Supplemental Table S3). Given its molecular phylogenetic placements within these two trees coupled to its distinct morphological features and geographical separation from any previously described *Gibellula* species, we identify this *Gibellula* isolate as a new species, *Gibellula floridensis*. Cultures of this *Gibellula* species, as well as of the *P. album* strains UFSI_3 and UFSI_4, have been deposited in the USDA entomopathogenic fungi culture collection ARSEF under the accession numbers 14,792, 14,693, and 14,794, respectively.

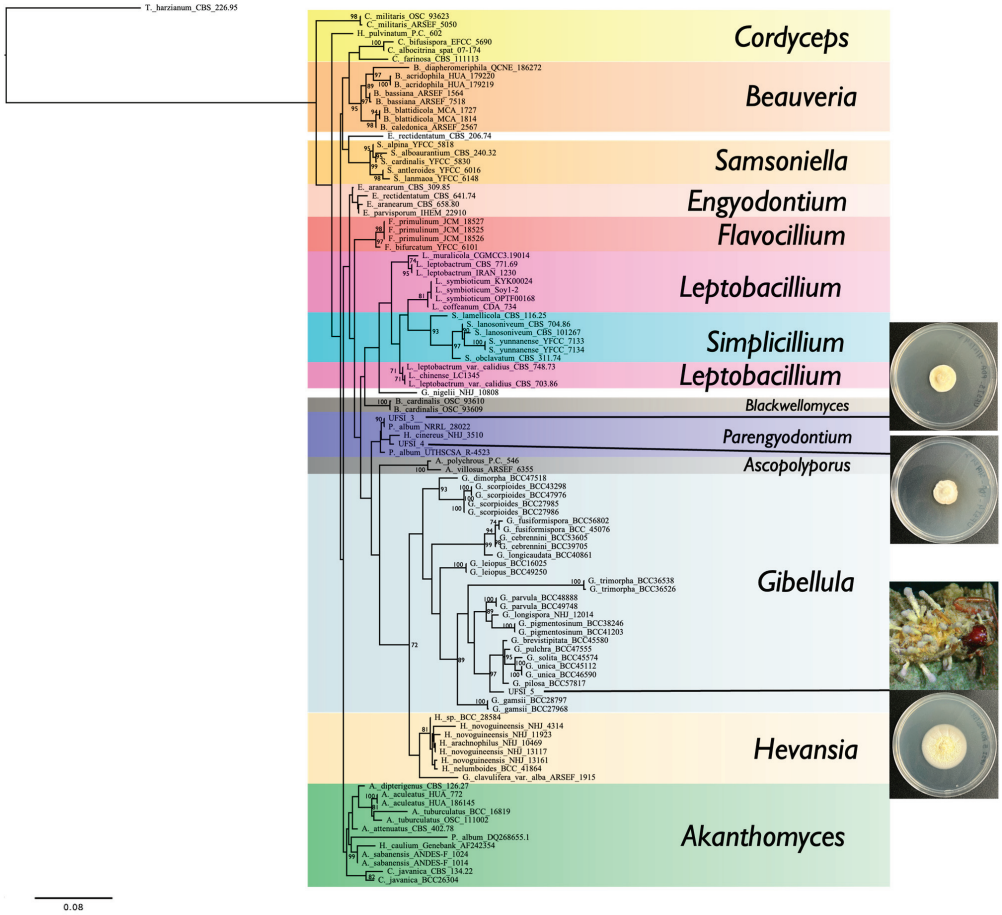


Figure 4. Multilocus maximum likelihood tree of the Cordycipitaceae family generated by RAxML with 2000 bootstrap replicates and containing concatenated ITS, LSU, SSU, and TEF1a sequences to determine the phylogenetic placement of isolates UFSI_3, UFSI_4, and UFSI_5. Bootstrap support values greater than or equal to 70 are displayed on tree nodes.

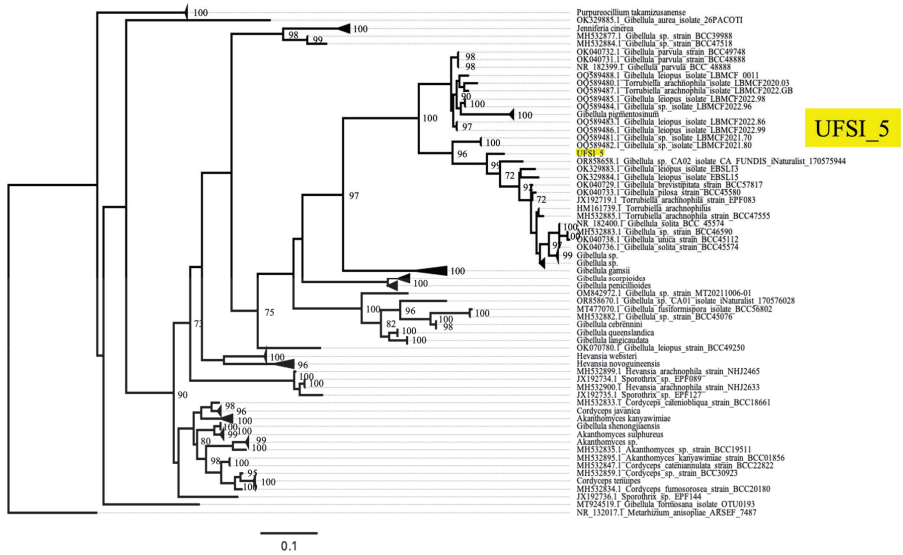


Figure 5. Maximum likelihood ITS tree of UFSI_5 and *Gibellula* sequences downloaded from Genbank. This tree was generated using RAxML with 2000 bootstrap replicates. Bootstrap support values greater than or equal to 70 are displayed on the nodes of the tree. Clades containing many isolates of the same species are collapsed and appear as triangles at the tips of the tree. Isolate UFSI_5 is highlighted in yellow to emphasize its phylogenetic placement among other *Gibellula* species.

3.5. Taxonomy

Gibellula floridensis sp. nov. R. Joseph and N.O. Keyhani, (Figures 3–5).

MycoBank: 856032.

Etymology: Named after state of Florida where the fungus was collected.

Holotype: USA, Florida, University of Florida, Gainesville 29°39′7.47″ N, 82°19′30.25″ W, from infected Trachelidae spiders, March 2023, R. Joseph (ex-type living culture ARSEF 14792).

Description: Infecting spiders in the family Trachelidae, covering the body with a mat of yellow hyphae, fading to tan with age. Producing synnemata from the abdomen and legs, 438–577 μm long by 46–82 μm wide, yellow, curved, isolated to branching, with clavate ends. Conidiophores bearing purple-pigmented spores forming along synnemata, primarily at ends. *Gibellula*-like asexual morphs of conidiophores 64–100 μm in height and 7–16 μm in width at the widest point of the stalk. Conidial heads measuring 30–50 μm in height and 41–56 μm in width. Vesicles of *Gibellula*-like asexual morphs 11–17 μm in height and 7–9 μm in width. Metulae measuring 8–14μm in height, 3–7 μm in width. Phialides measuring 8–11 μm in length and 2–4 μm in width. Conidia from *Gibellula*-like asexual morphs of conidiophores appearing elongated, curved on one end and tapering to a point at the other end, 5–7 μm in length, 1.5–3 μm in width. Granulomanus morphs of conidiophores measured 54–68 μm in height, 5–7 μm width. Conidial heads measured 29–47 μm in height, 24–40 μm in width. Vesicles measured 9–17 μm in height, 6–8 μm in width. Metulae measured 7–9 μm height, 3–6 μm width. Phialides measuring 7–11 μm length, 2–4 μm width. Conidia measuring 4–7 μm length, 2–4 μm width. No sexual structures were noted on spider cadavers.

Culture characteristics: On potato dextrose agar, cultures appeared white to yellow, with a darkened color visible on the reverse side of the plate and grew to 44.0 mm after 30 d at 25 °C, with colonies displaying flat to somewhat cottony mycelia with regular margins and a somewhat submerged appearance at the edges of colonies, producing sparse, rudimentary synnemata, adorned with conidiophores and purple-pigmented conidia.

Material examined: USA, Florida, University of Florida, Gainesville 42°14′.084″ N, 117°8′.124″ E, from infected Trachelidae spiders, March 2023. Collected specimens destroyed during processing by contaminating fungi, ex-type living culture serving as holotype: ARSEF 14792

Notes: Based on distinct morphological features and multilocus molecular phylogenetic analyses, the strain of the genus *Gibellula* was identified as a new species; nucleotide comparison of ITS, LSU, and *tef1-α* showed differences with the sequences of *Gibellula leiopus* BCC49250, similarities were 80.53% (513/637), 93.4% (726/777), and 94% (695/743). Nucleotide comparisons with the ITS region of *G. leiopus* EBSL13 showed similarities of 93.54% (478/511).

3.6. Environmental Sampling of the Fungal Communities Surrounding the Fungal-Infected Cadavers

To address questions concerning the distribution, environmental location/reservoir, and/or occurrence of isolated fungi within the greater fungal community surrounding the infected spiders, samples were collected from four habitat/trophic levels, namely (i) soil (S), (ii) plant litter (PL), (iii) twigs (T), and (iv) leaves (LV) as detailed in the Methods section (outlined in Supplemental Figure S1). Samples were from two locations: (1) Lake Alice (LA) and (2) Loblolly Woods Nature Park (LB) in north-central (Gainesville) Florida. A total of 3 soil, 3 plant litter, 2 twig, and 2 leaf samples were collected from the LA site, with the LB region was divided into four sites. At each of these sites 3 soil, 3 plant litter 1 twig, and 1 leaf samples were collected for a total of 12 soil, 12 plant litter, 4 twig, and 4 leaf samples (for LB). In total, for both LA and LB, 42 samples were collected. Each soil sample consisted of a pool of 5 soil cores along 4 lines (20 cores) in a grid-like pattern as detailed in the Methods section. Each plant litter, twig, and leaf sample consisted of material (~150–200 g) gathered within a ~10 m^2 area surrounding the infected spiders.

3.7. Amplicon-Sequencing Data Output

Environmental samples were processed for ITS amplicon sequencing as detailed in the Methods section. A total of 1,681,793 reads were obtained from the 42 environmental samples; 1,586,552 high-quality reads with an average length of 589 bp were retained after length filtering as well as removal of chimeric sequences. The minimum and maximum read length was 581 to 592 bp, respectively (Supplemental Table S4). Finally, the reads were sorted into samples via barcodes detection/analyses using the global fungal database (UNITE). Data for genera corresponding to insect pathogenic fungi for the families Clavicipitaceae, Cordycipitaceae, and Ophiocordycipitaceae (Hypocrealeas), and other potential specific-spider pathogens were extracted and used for further analysis. This resulted in 30,780 sequence reads corresponding to insect fungal pathogens within these groups with: 18,001 sequence reads found within the Clavicipitaceae, 2160 sequence reads within the Cordycipitaceae, and 9011 sequence reads within the Ophiocordycipitaceae, which were clustered into 112 Amplicon Sequence Variants (ASVs). No sequences corresponding to entomopathogenic fungi belonging to the Entomophthora order were found in our dataset.

3.8. Taxonomic Abundance Analysis of EFs

The four habitat/trophic types: soils (S), plant litter (PL), twigs (T), and leaves (LV) corresponding to the 42 environmental samples were divided into eight groups, namely Lake Alice (LA-): (1) LAS, (2) LAPL, (3) LAT, and (4) LALV, and Loblolly (LB-): (5) LBS, (6) LBPL, (7) LBT, and (8) LBLV for visualization of the data. The average relative abundance of entomopathogenic fungi from the overall fungal community in terms of the sampling site and habitat revealed was LAS >LBS >LBT > LBLV > LBPL > LAT > LAPL > LALV (representing 6.99, 3.42, 1.73, 0.64, 0.45, 0.14, 0.101, and 0.09% of the total fungal sequences, respectively) (Supplementary Figure S3). Insect–fungal pathogen sequences belonged mainly to Clavicipitaceae (63.81%), followed by Ophiocordycipitaceae (29.19%) and Cordycipitaceae (6.99%) (Figure 6A) across the three families analyzed. Soil, twig, and leaf habitats showed the highest proportion of Clavicipitaceae, whereas plant litter habitats showed a lower proportion of EF families irrespective of sampling locations (Figure 6B).

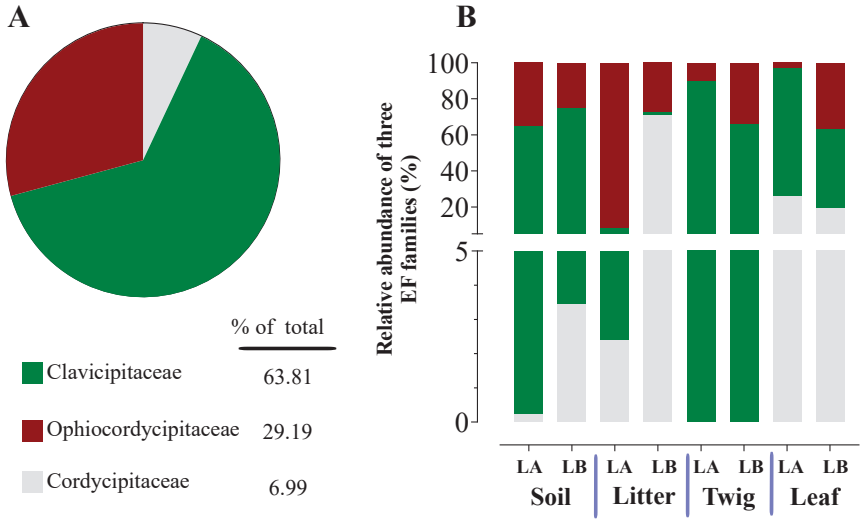


Figure 6. Relative taxonomic abundance of soil-inhabiting entomopathogenic fungi. (**A**) Total percentages of Ophiocordycipitaceae, Clavicipitaceae, and Cordycipitaceae from environmental samples. (**B**) Relative abundances of the three families were detected by amplicon sequencing within each environmental sample type at the two different sampling sites Lake Alice and Loblolly (LA and LB).

Within the Cordycipitaceae family, a total of 9 genera (Figure 7A) and 12 species (Figure 8A) were identified. The genus *Akanthomyces* represented the highest proportion within Cordycipitaceae, accounting for 54.07%, whereas the species *Simplicillium lanosoniveum* was the most prevalent, constituting 43.53% of the species detected. In terms

of habitat distribution, the genus *Simplicillium* and the species *S. lanosoniveum* were most abundant on twigs at the Loblolly site (78.82%) and in plant litter at the Lake Alice site (100%), respectively (Figures 7 and 8). In the Clavicipitaceae family, 8 genera (Figure 4) and an equivalent number of species (Figure 9) were observed. Among these, the genus *Metarhizium* showed the highest relative abundance, comprising 70.5% of the detected genera, with *M. indigoticum* being the most dominant species at 70.12%. Notably, both the *Metarhizium* genus and *M. indigoticum* species were found exclusively on twigs at the Lake Alice site, with a 100% occurrence in this habitat type (Figures 9 and 10). The Ophiocordycipitaceae family was represented by 7 genera (Figure 11) and 9 species (Figure 12). Within this family, *Purpureocillium* was the most abundant genus, constituting 32.3% of the total genera detected, while *Tolypocladium album* was the most prevalent species, accounting for 22.89%. The *Ophiocordyceps* genus and *T. album* species exhibited the highest abundance on leaf surfaces (100%) and twigs (81.03%) at the Lake Alice site, respectively (Figures 11 and 12).

3.9. Spider-Specific Pathogens in the ITS-Amplicon Dataset

Our dataset contained only two fungal pathogens that could be assigned on the species level that are considered specific to spiders: *Acrodontium crateriforme* (Mycosphaerellales, Teratosphaeriaceae) and *Akanthomyces araneogenus* [47]. *Akanthomyces araneogenus* was detected exclusively in plant litter at the Loblolly site, where it constituted 58.62% of the total entomopathogenic fungal community (Figure 13). In contrast, *Acrodontium crateriforme* was found in all environmental samples except soil at the Lake Alice site. The highest proportion (31.74%) of the total entomopathogenic fungal community of *A. crateriforme* was seen in plant litter at Lake Alice. These findings suggest that plant litter may serve as a favorable habitat for these pathogens. No sequences corresponding to *Gibelulla* or *Paraengyodontium* were detected, nor were any sequences found in our ITS dataset for the known major spider fungal pathogens reported in North America [47], including *Akanthomyces lacanii*, *Cordyceps* (*Isaria*/*Paecilomyces farinosus*), *Cordyceps thaxteri*, *Cordyceps* spp., *Hevansia* cf. *aranearum*, *Hevansia* sp., *Ophiocordyceps verrucosa*, *Purpureocillium atypicola* (*Nomuraea atypicola*), *Cladosporium cladosporioides*, *Conidiobolus coronatus*, *Mucor fragilis*, *Sporodiniella umbellata*, and *Cryptococcus depauperatus*.

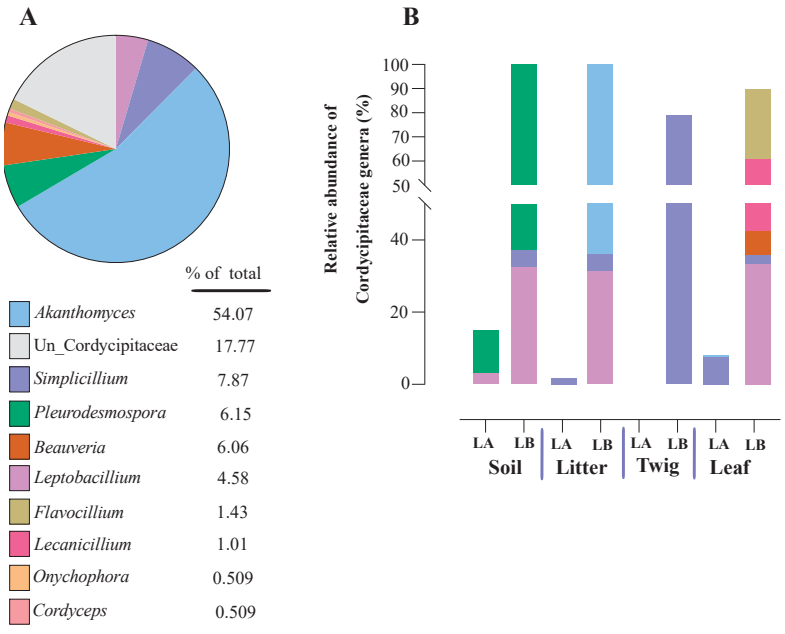


Figure 7. Relative abundance of entomopathogenic fungi in the Cordycipitaceae family from environmental samples. (**A**) Total percentages of Cordycipitaceae genera among all samples. (**B**) Relative abundances of Cordycipitaceae genera from the different environmental samples at both sampling sites (LA and LB).

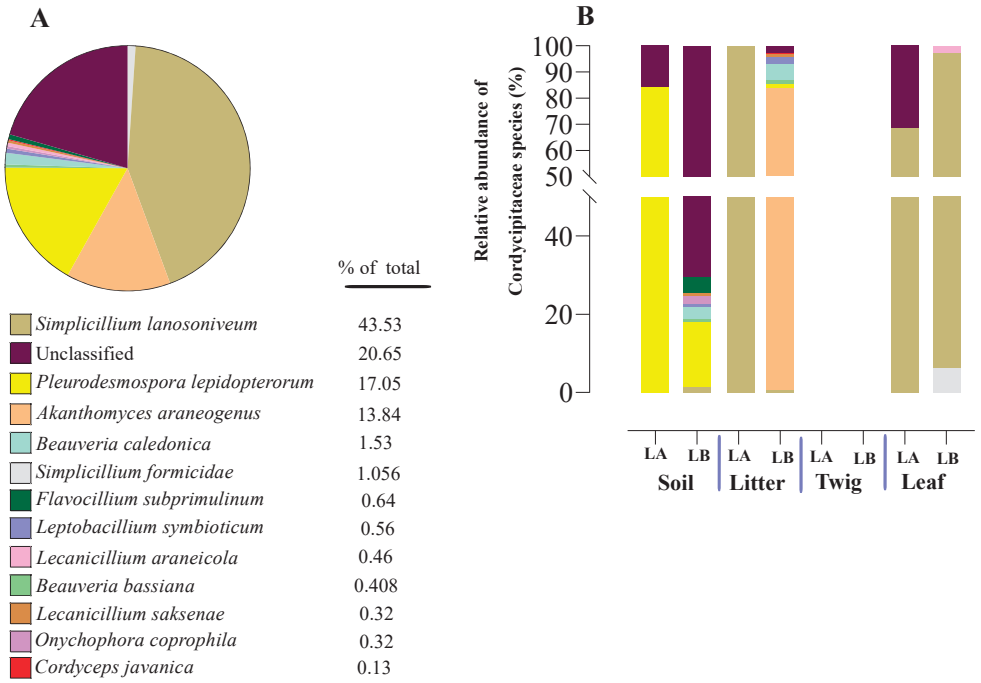


Figure 8. Relative abundance of entomopathogenic fungal species in the family Cordcypitaceae from environmental samples. (**A**) Total percentages of species within the Corcycipitaceae. (**B**) Relative abundances of species within the Cordycipitaceae within environmental sample types and across sample locations (LA and LB).

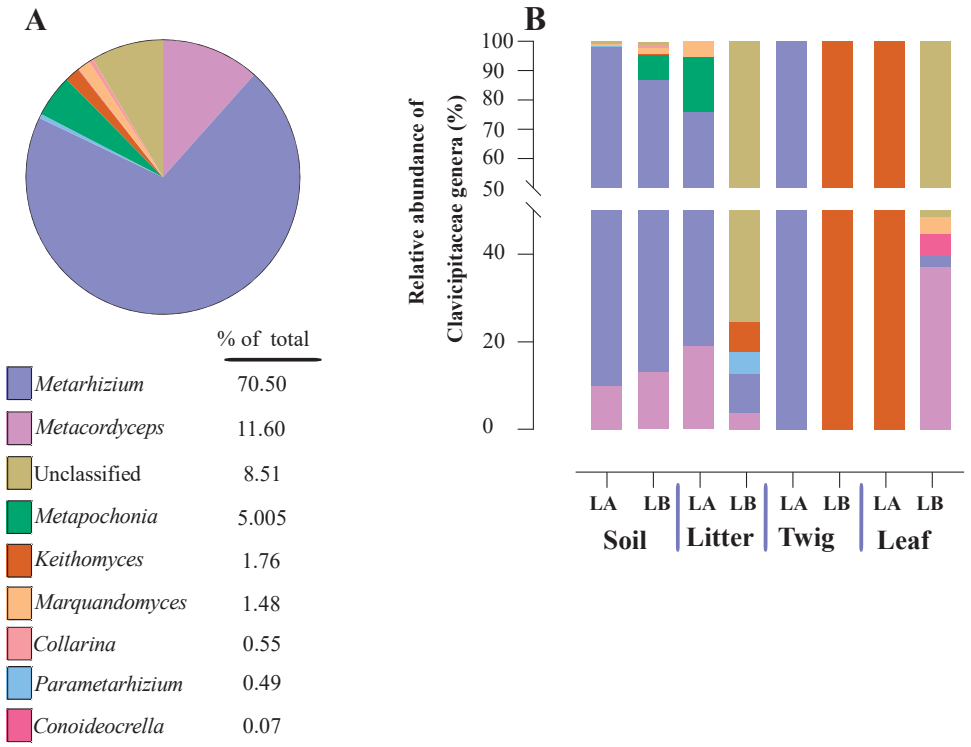


Figure 9. Relative abundance of entomopathogenic fungi in the Clavicipitaceae family from environmental samples. (**A**) Total percentage of Clavicipitaceae genera within all environmental samples. (**B**) Relative abundance of Clavicipitaceae genera for each of the environmental sample types and at the two different sampling locations (LA and LB).

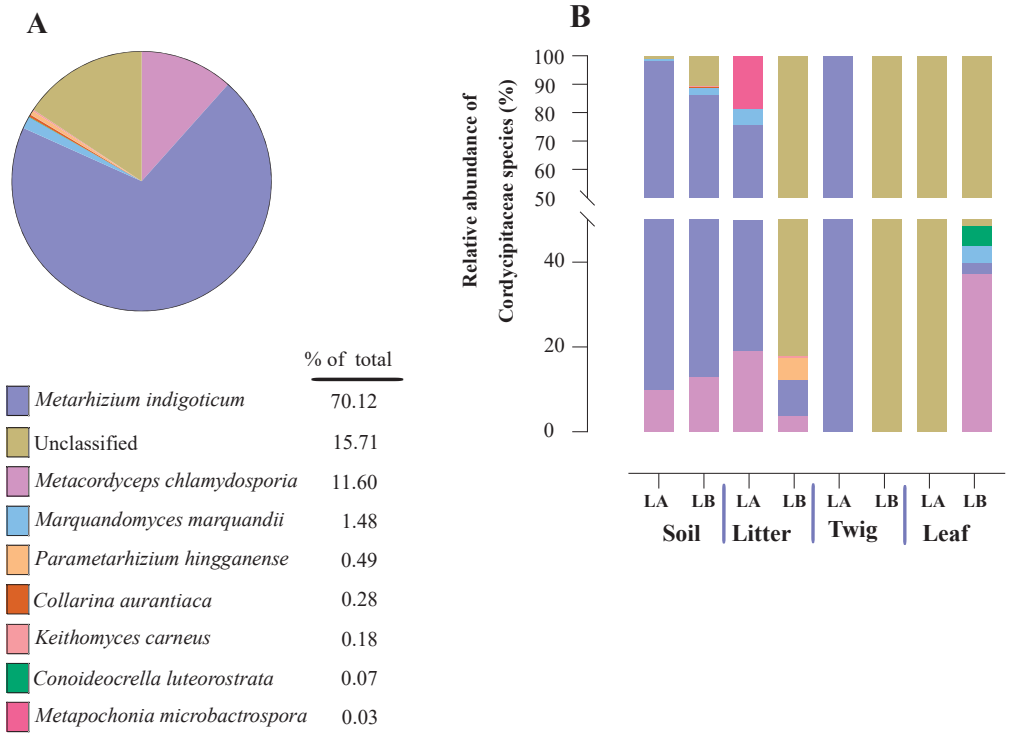


Figure 10. Relative abundances of entomopathogenic fungal species in the Clavicipitaceae from environmental samples. (**A**) Total percentages of Clavicipitaceae fungal species detected in environmental samples. (**B**) Relative abundance of fungal species in the Clavicipitaceae at each environmental sample type and across the two sampling sites (LA and LB).

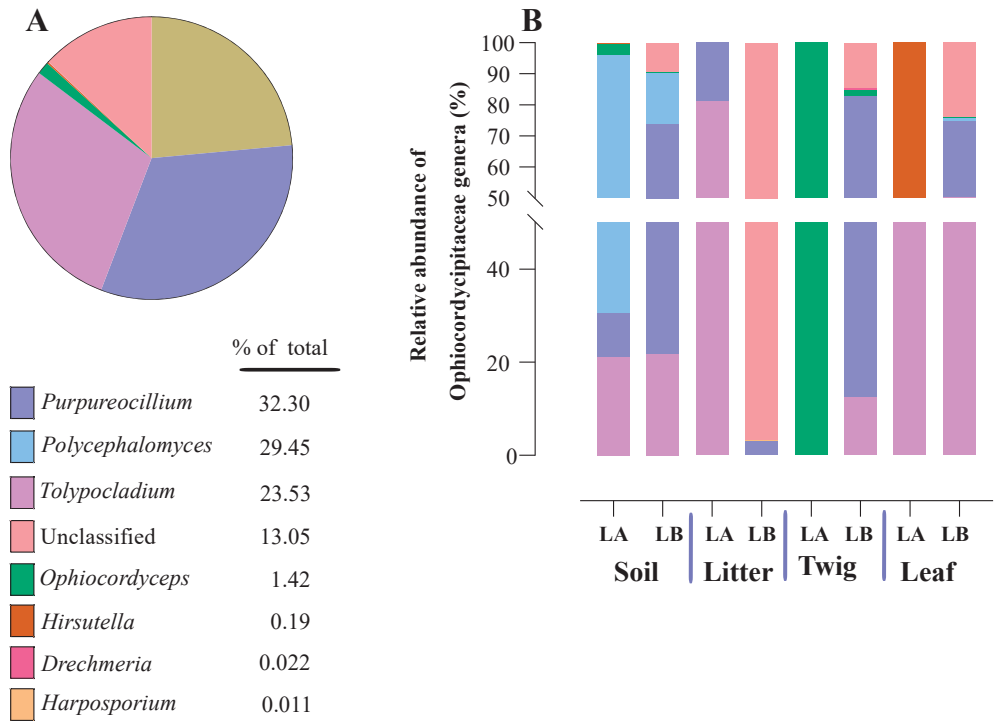


Figure 11. Relative abundances of entomopathogenic fungal genera in the Ophiocordycipitaceae family detected in environmental samples. (**A**) Total percentages of Ophiocordycipitaceae genera detected from environmental samples. (**B**) Relative abundance of Ophiocordycipitaceae genera detected at each environmental sample type from each of the two sampling locations (LA and LB).

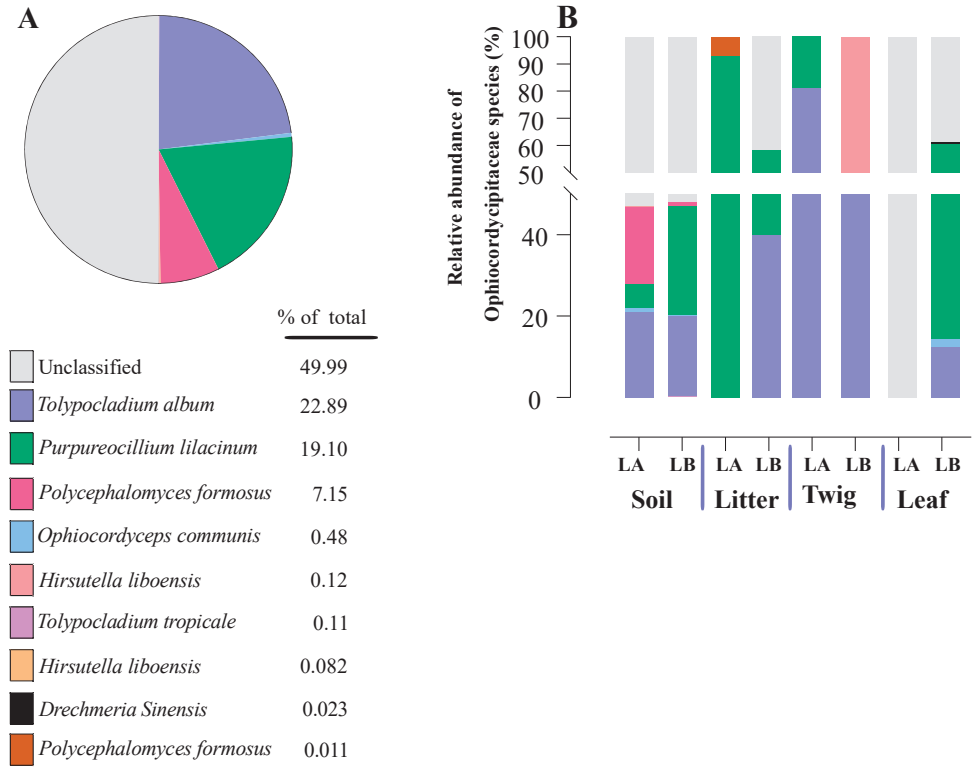


Figure 12. Relative abundances of entomopathogenic fungal species in the Ophiocordycipitaceae detected from environmental samples. (**A**) Total percentages of fungal species in the Ophiocordycipitaceae detected across all environmental samples. (**B**) Relative abundance of fungal species in the Ophiocordycipitaceae detected at each environmental sample type and across the two sampling locations (LA and LB).

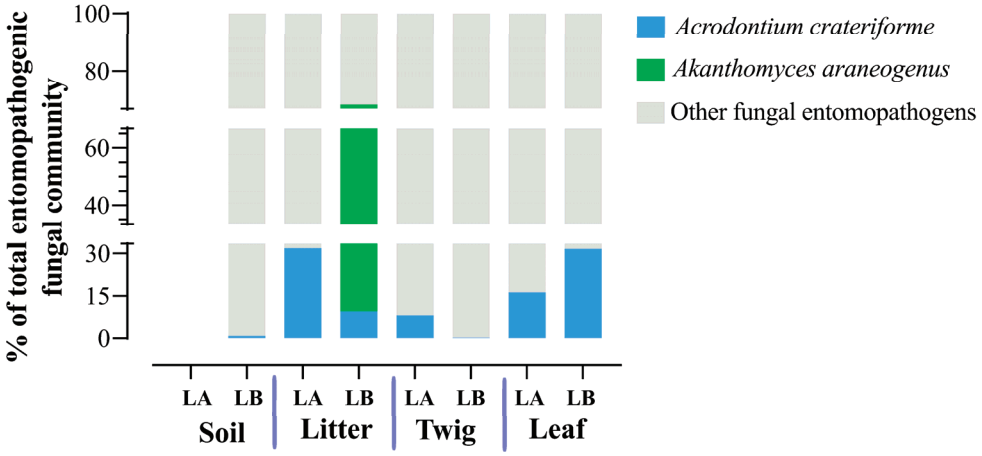


Figure 13. The total percentages of two spider-specific pathogens within the entomopathogenic fungal communities were identified across all environmental sample types and both sampling locations (LA and LB).

4. Discussion

Interest in insect pathogenic fungi and their related cousins for pest control has garnered significant attention [48,49]; however, thus far, only a relatively small number of spider (Araneae) fungal pathogens have been characterized relative to their insect cousins. Most spider-pathogenic fungi characterized to data are found in the Ascomycota, Hypocreales order [8]. A few generalist, i.e., broad host range, insect fungal pathogens from several genera, e.g., *Beauveria*, *Isaria*, *Hirsutella*, have described species isolated from infected spiders, although the extent to which these represent specialized spider pathogens

remains unclear. Members of the *Akanthomyces* genera are typically generalists; however, *A. araneogenus* appears to be spider-specific. The most widely characterized, apparent, and more specific Araneae fungal pathogens are found in the *Gibellula* (sexual morph *Torrubiella*) genera, of which up to 60 species (~30 *Gibellula*, ~28 *Torrubiella*) have been described as capable of infecting at least 25 different spider families.

Here, we identified five spider cadavers apparently infected with fungi in an area of north-central Florida. This region's climate is defined as humid subtropical, with tropical-like summers, warm to hot shoulder seasons, and mild winters. The area around the sampled regions includes a range of wetlands and aquatic vegetation: grasses, mosses, and other moisture-loving plants, as well as live oaks and palm trees (Lake Alice). The plant canopy in the Loblolly state park zone is mixed hardwood, including loblolly pine (*Pinus taeda*), slash pine (*Pinus elliottii*), laurel oak (*Quercus laurifolia*), water oak (*Quercus nigra*), red maple (*Acer rubrum*), Carolina laurel cherry (*Prunus caroliniana*), sweetgum (*Liquidambar styraciflua*), wax myrtle (*Morella cerifera*), swamp tupelo (*Nyssa biflora*), and sugarberry (*Celtis laevigata*). Based on morphological features and consistent with their range/habitats, the spiders appeared to belong to the genus *Trachelas*. Spider cadavers were found fixed to bark on the underside of branches and trunks, facing downwards. This is consistent with reports of infection mechanisms of above-ground spiders, which normally forage or live close to the ground or soil, by fungal pathogens which result in summit disease, i.e., elevation seeking/negative gravitropism, as the spider host dies. Such behavioral manipulation of the host is considered to maximize spore discharge from the dead spider from heights that would allow for dispersal of infectious spores over a wide area to hosts found in lower trophic levels.

Of the five fungal infected spider cadavers collected, and all had preliminary morphological features consistent with *Gibellula*; however, fungi could only be cultured from three. It is possible that either the fungi on the two specimen from which we could not recovered active fungi were either no longer viable or else fastidious and could not be readily cultured. Of the three fungal isolates that could be cultured and were subsequently single spore purified, two were found to likely represent the same species, and closely matched *Parengyodontium album* NRRL28022 (LSU/SSU 100% match UFSI_3, 98.28% match UFSI_4) and *Parengyodontium album* UTHSCSA_R-4523 (ITS/LSU 99.70% match UFSI_3 and UFSI_4). The third was grouped within *Gibellula*, with its closest match to *G. leiopus* EBSL13 (80% query cover, 93.54% identity) and what has only been listed as *Gibellula* sp. CA02 (ITS, 97% query cover 91.64% identity), albeit both multilocus and greater depth ITS phylogenetic reconstruction indicated the isolate to be distinct. We therefore describe this as a new species, *G. floridensis*, based on combined morphological (Supplementary Table S3) and multilocus molecular phylogenetic characterization. To the best of our knowledge, this is the first description of *Gibellula* from Florida and the broader southeastern United States. Members of the *Gibellula* genera are well known pathogens of a range of spiders [13–15,20], and *Gibellula leiopus*/*Gibellula* sp. have been found infecting members of the *Anyphaenidae*, *Araneidae*, *Corinnidae*, *Linyphiidae*, *Pholcidae*, *Salticidae*, *Sparassidae*, *Theridiidae*, *Thomisidae*, and *Zodariidae* families, but not *Trachelidae*, as reported here. For the *Gibellula* sp. isolate that grouped most closely with our isolate, this was found in California, and the host spider identity was not listed [36,50], and these regions are significantly separated from the southeastern US. In addition, multilocus data for *G. leiopus* separated it from *G. floridensis* further than what was seen in the ITS tree, indicating our isolate remains distinct at both the molecular and morphological levels.

P. album has a curious distribution and reporting. Originally *Tritirachium* album, then *Beauveria alba*, *Engyodontium album*, it now has its own genera (*Parengyodontium*), with *P. album* as its sole described species, although it is unclear the extent to which various *P. album* isolates have been confirmed via molecular phylogenetic analyses. It is reported to be globally distributed, including from geographically diverse deteriorated (cultural heritage) sites, potentially adapted to salty, moist environments, as well as being an opportunistic mammalian pathogen [51–59]. An isolate found on floating plastic debris in

the North Pacific Subtropical Gyre has been shown to be able to mineralize plastic [52,60]. *P. album* has been isolated from spider cadavers [61–63], but it has not been definitively proven to be a pathogen and not a saprotroph or secondary infection in these cases. Similarly, we cannot make any definitive conclusions concerning whether our isolate is a spider pathogen, and the fact that we isolated *P. album* by performing single-spore isolation from the synnemata and conidiophores from two of the collected spiders was surprising but might point to some kind of secondary association between *P. album* and spider cadavers, or even *P. album* and *Gibellula* species. Additional sampling and/or infection assays are needed to examine this point and/or complete Koch's postulate.

Knowledge concerning soil fungal communities is an important aspect of understanding effects on forestry and agriculture [64–66], and can impact use of entomopathogenic fungi in crop pest protection [67]. An open question concerning facultative, yet specialized insect/arachnid fungal pathogens concerns their environmental distribution (aside from on the host), and at which trophic levels in the environment they can be found. To address this, we performed a systematic sampling of the areas surrounding the spider cadavers, separating our collection into four trophic levels, namely: soil, leaf litter, leaves, and twigs. Sampling was performed following a grid-like pattern that extended the scope to an area of ~10 × 10 m, with multiple sample points for each level that were pooled and subjected to genomic DNA extraction and subsequent amplicon ITS sequencing. Entomopathogenic fungi were found to represent ~1.92% of the total reads generated, and within the three major families, Clavicipitaceae predominated (64%), followed by Ophiocordyceps (29%) and Cordycipitaceae (7%). Important differences between trophic levels were seen, with soil showing the highest diversity, followed by some variation between twigs, leaves, and leaf litter, as well as site (Lake Alice vs. Loblolly nature park). Of note, Cordycipitaceae was found to represent a greater proportion than the others at the leaf trophic level, whereas Clavicipitaceae predominated at the soil and twig levels. For leaf litter, Ophiocordycipitaceae predominated at the Lake Alice site, whereas Cordycipitaceae was found more prevalent in the leaf litter of the Loblolly site. Important differences were also seen at the genera level across the trophic levels and sites, with *Akanthomyces*, *Metarhizium*, *Purpueocillium*, *Tolypocladium*, and *Polycephalomyces* highly abundant. At the species level: *Simplicillium lanosoniveum*, *Pleurodesmonspora lepiopterorum*, and *A. araneogenus* (Cordycipitaceae), *Metarhizium indigoticum* and *Metacordyceps chlamydosporia* (Clavicipitaceae), *Tolypocladium album*, *Purpueocillium lilacinum*, and *Polycephalus formosus* could be identified as highly prevalent. However, it should be noted that a significant portion (9–20%) of our ITS dataset, while categorized at the family level, could not be placed in any described genera, and of those that could be placed into genera, 15–50% could not be assigned at the species level. This indicates significant room for discovery and addition to available databases.

Surprisingly, despite obtaining >1.5 million ITS reads, direct BLAST analysis with the ITS sequences obtained from *G. floridensis* and *P. album*, no hits were obtained. Furthermore, on a broader level, we could not detect any *Gibellula* or *Parengyodontium* even at the genera level in our dataset. There are several potential explanations for these results. First, it cannot be excluded that we did not sample enough, despite examining both areas where the spider cadavers were found and looking at the surrounding soil, leaf litter, leaves, and twigs. Second, our collection excluded insects or other animals in the samples. In tropical areas where spiders are active year-round, it is possible for direct spider to spider transmission of *Gibellula* to account for the full life cycle of this fungus. Another possibility is that other insects can act as a reservoir for the fungus even if they are not hosts, *i.e.*, no disease is caused on these "carriers". In temperate regions where many species of spider and other arthropod go dormant during the winter, other strategies besides potential spider to spider transmission may be necessary for the fungus to survive this period, including potentially reducing pathogenicity to overwinter with infected individuals or surviving outside of their host in as yet unidentified environmental reservoirs [68]. As Florida is subtropical, direct or carrier-based transmission may prevail, in which case *Gibellula* may be below the detection

limit of our sampling. In addition, persistence/survival of *Gibellula* or *Parengyodontium* in the sampled environments may be low. As the cadavers were found after full infection and likely dispersal of any spores, if persistence is low (days to weeks timeframe), the fungi could have been gone by the time we sampled the surrounding environment. We could, however, detect two fungal spider pathogens, *A. crateriforme* and *A. araneogenus* [47]. The latter was found only in the plant litter at the Loblolly but at a high proportion (59%) of the total entomopathogenic fungal community. *A. crateriforme* was widely distributed in all environmental habitats examined except for Lake Alice soil. Wed did not detect any other major spider fungal pathogens described in North America [47]. These data indicate the prevalence of a small subset of spider-specific fungal pathogens in the environment examined. However, some caution should be taken in interpreting any results, and as more species are described and the (ITS) database expands, additional members may be identified. In addition, it is worth noting that we could not detect sequences belonging to members of the Entomophthorales order, which could be due to their lack of presence in our samples but could also be a result of poor efficiency of obtaining such sequences using the ITS amplicon strategy employed which relies on a "universal" primer. Thus, it is possible that ITS amplicon sequencing using such universal primers may poorly target some fungal families and thus bias the data, although this would not affect our ability to detect *Gibellula* or *Parengyodontium*, as these could be readily amplified.

5. Conclusions

We have identified a new fungal pathogen of spiders (*Trachelas*), which we have named *Gibellula floridensis* as well as *P. album* from spider cadavers. It is unclear whether the *P. album* represents a true spider pathogen or, as we suspect, an unexamined aspect of secondary associations between *P. album*-spider cadavers or *P. album-Gibellula* sp. We further examined the surrounding fungal entomopathogen community across different habitat/trophic levels. To the best of our knowledge, our data represent the first such environmental sampling aimed towards delineating where in the environment these fungi may occur and particularly highlights critical gaps in our understanding of the ecology of more host-specific and/or fastidious insect fungal pathogens. It is recommended that, during future collection and discovery of fungal-infected insects/arachnids, surrounding environmental samples are also collected and analyzed to more broadly begin to address these issues.

Supplementary Materials: The following supporting information can be downloaded at: https://www.mdpi.com/article/10.3390/jof10100694/s1, Figure S1: Outline of sample habitats/trophic levels, sample #s and replicates, and geolocation of samples; Figure S2: The rank-abundance curves illustrate the distribution and relative abundance of fungal taxa identified across sampling sites; Figure S3: The proportion of the EF OTUs in comparison with the whole fungal OTU compositions based on percentages; Table S1: Species and Genbank Accession IDs used in construction of multilocus phylogenetic tree; Table S2: Species, isolate codes, Genbank accession IDs, and references for species used in construction of the ITS phylogenetic tree; Table S3: Comparative measurements and morphological characteristics for G. floridensis, G. leiopus, and G. pulchra; Table S4: Overview of raw sequencing data.

Author Contributions: Conceptualization, R.A.J., A.M. and N.O.K.; methodology, R.A.J., A.M. and N.O.K.; formal analysis, R.A.J. and A.M; investigation, R.A.J., A.M. and N.O.K.; resources, N.O.K.; data curation, R.A.J. and A.M.; writing—original draft preparation, R.A.J. and A.M.; writing—review and editing, R.A.J., A.M. and N.O.K.; visualization, R.A.J., A.M. and M.J.V.; supervision, N.O.K.; project administration, N.O.K.; funding acquisition, N.O.K. All authors have read and agreed to the published version of the manuscript.

Funding: This research was funded in part by US National Science Foundation (NSF), grant number IOS-2418026 to N.O.K.

Institutional Review Board Statement: Not applicable.

Informed Consent Statement: Not applicable.

Data Availability Statement: All data are available in the manuscript itself or have been deposited with accession numbers in the appropriate data repositories.

Conflicts of Interest: The authors declare no conflict of interest.

References

1. Lüddecke, T.; Herzig, V.; von Reumont, B.M.; Vilcinskas, A. The Biology and Evolution of Spider Venoms. *Biol. Rev.* **2022**, *97*, 163–178. [CrossRef] [PubMed]
2. Platnick, N.I. *Spiders of the World: A Natural History*; Princeton University Press: Princeton, NJ, USA, 2020; ISBN 978-0-691-20498-7.
3. Sanggaard, K.W.; Bechsgaard, J.S.; Fang, X.; Duan, J.; Dyrlund, T.F.; Gupta, V.; Jiang, X.; Cheng, L.; Fan, D.; Feng, Y.; et al. Spider Genomes Provide Insight into Composition and Evolution of Venom and Silk. *Nat. Commun.* **2014**, *5*, 3765. [CrossRef] [PubMed]
4. Valdez, J.W. Arthropods as Vertebrate Predators: A Review of Global Patterns. *Glob. Ecol. Biogeogr.* **2020**, *29*, 1691–1703. [CrossRef]
5. Nyffeler, M.; Gibbons, J.W. Spiders (Arachnida: Araneae) Feeding on Snakes (Reptilia: Squamata). *J. Arachnol.* **2021**, *49*, 1–27. [CrossRef]
6. Dimitrov, D.; Hormiga, G. Spider Diversification Through Space and Time. *Annu. Rev. Entomol.* **2021**, *66*, 225–241. [CrossRef] [PubMed]
7. Mongkolsamrit, S.; Noisripoom, W.; Tasanathai, K.; Kobmoo, N.; Thanakitpipattana, D.; Khonsanit, A.; Petcharad, B.; Sakolrak, B.; Himaman, W. Comprehensive Treatise of *Hevansia* and Three New Genera Jenniferia, *Parahevansia* and *Polystromomyces* on Spiders in Cordycipitaceae from Thailand. *MycoKeys* **2022**, *91*, 113–149. [CrossRef]
8. Evans, H.C. Fungal Pathogens of Spiders. In *Spider Ecophysiology*; Nentwig, W., Ed.; Springer: Berlin/Heidelberg, Germany, 2013; pp. 107–121, ISBN 978-3-642-33989-9.
9. Chen, W.-H.; Liang, J.-D.; Ren, X.-X.; Zhao, J.-H.; Han, Y.-F.; Liang, Z.-Q. Phylogenetic, Ecological and Morphological Characteristics Reveal Two New Spider-Associated Genera in Clavicipitaceae. *MycoKeys* **2022**, *91*, 49–66. [CrossRef]
10. Shrestha, B.; Kubátová, A.; Tanaka, E.; Oh, J.; Yoon, D.-H.; Sung, J.-M.; Sung, G.-H. Spider-Pathogenic Fungi within Hypocreales (Ascomycota): Their Current Nomenclature, Diversity, and Distribution. *Mycol. Prog.* **2019**, *18*, 983–1003. [CrossRef]
11. Wang, T.; Li, J.; Chang, X.; Li, Z.; Hywel-Jones, N.L.; Huang, B.; Chen, M. Morphology and Multigene Phylogeny Reveal Three New Species of *Samsoniella* (Cordycipitaceae, Hypocreales) from Spiders in China. *MycoKeys* **2024**, *101*, 329–346. [CrossRef]
12. Mains, E.B. The Genus *Gibellula* on Spiders in North America. *Mycologia* **1950**, *42*, 306–321. [CrossRef]
13. Mendes-Pereira, T.; de Araújo, J.P.M.; Kloss, T.G.; Costa-Rezende, D.H.; de Carvalho, D.S.; Góes-Neto, A. Disentangling the Taxonomy, Systematics, and Life History of the Spider-Parasitic Fungus *Gibellula* (Cordycipitaceae, Hypocreales). *J. Fungi* **2023**, *9*, 457. [CrossRef] [PubMed]
14. Chen, M.; Wang, T.; Lin, Y.; Huang, B. Morphological and Molecular Analyses Reveal Two New Species of *Gibellula* (Cordycipitaceae, Hypocreales) from China. *MycoKeys* **2022**, *90*, 53–69. [CrossRef] [PubMed]
15. Kuephadungphan, W.; Tasanathai, K.; Petcharad, B.; Khonsanit, A.; Stadler, M.; Luangsa-ard, J.J. Phylogeny- and Morphology-Based Recognition of New Species in the Spider-Parasitic Genus *Gibellula* (Hypocreales, Cordycipitaceae) from Thailand. *MycoKeys* **2020**, *72*, 17–42. [CrossRef] [PubMed]
16. Sánchez-Peña, S.R. Some Insect and Spider Pathogenic Fungi from Mexico with Data on Their Host Ranges. *Fla. Entomol.* **1990**, *73*, 517–522. [CrossRef]
17. Mendes-Pereira, T.; Araújo, J.P.M.D.; Mendes, F.C.; Fonseca, E.O.; Alves, J.E.D.R.; Sobczak, J.F.; Góes-Neto, A. *Gibellula aurea* Sp. Nov. (Ascomycota, Cordycipitaceae): A New Golden Spider-Devouring Fungus from a Brazilian Atlantic Rainforest. *Phytotaxa* **2022**, *573*, 85–102. [CrossRef]
18. Kuephadungphan, W.; Phongpaichit, S.; Luangsa-ard, J.J.; Rukachaisirikul, V. Antimicrobial Activity of Invertebrate-Pathogenic Fungi in the Genera *Akanthomyces* and *Gibellula*. *Mycoscience* **2014**, *55*, 127–133. [CrossRef]
19. Arruda, I.D.P.; Villanueva-Bonilla, G.A.; Faustino, M.L.; Moura-Sobczak, J.C.M.S.; Sobczak, J.F. Behavioral Manipulation of the Spider *Macrophyes pacoti* (Araneae: Anyphaenidae) by the Araneopathogenic Fungus *Gibellula* Sp. (Hypocreales: Cordycipitaceae). *Can. J. Zool.* **2021**, *99*, 401–408. [CrossRef]
20. Kuephadungphan, W.; Petcharad, B.; Tasanathai, K.; Thanakitpipattana, D.; Kobmoo, N.; Khonsanit, A.; Samson, R.A.; Luangsaard, J.J. Multi-Locus Phylogeny Unmasks Hidden Species within the Specialised Spider-Parasitic Fungus, *Gibellula* (Hypocreales, Cordycipitaceae) in Thailand. *Stud. Mycol.* **2022**, *101*, 245–286. [CrossRef]
21. Samson, R.A.; Evans, H.C. New Species of *Gibellula* on Spiders (Araneida) from South America. *Mycologia* **1992**, *84*, 300–314. [CrossRef]
22. Tzean, S.S.; Hsieh, L.S.; Wu, W.J. The Genus *Gibellula* on Spiders from Taiwan. *Mycologia* **1997**, *89*, 309–318. [CrossRef]
23. Chen, W.-H.; Han, Y.-F.; Liang, Z.-Q.; Zou, X. Morphological Traits, DELTA System, and Molecular Analysis for *Gibellula clavispora* Sp. Nov. from China. *Mycotaxon* **2016**, *131*, 111–121. [CrossRef]
24. Strongman, D.B. *Gibellula Pulchra* from a Spider (Salticidae) in Nova Scotia, Canada. *Mycologia* **1991**, *83*, 816–817. [CrossRef]
25. Chen, W.; Xie, W.; Cai, W.; Thaochan, N.; Hu, Q. Entomopathogenic Fungi Biodiversity in the Soil of Three Provinces Located in Southwest China and First Approach to Evaluate Their Biocontrol Potential. *J. Fungi* **2021**, *7*, 984. [CrossRef] [PubMed]

26. Masoudi, A.; Wang, M.; Zhang, X.; Wang, C.; Qiu, Z.; Wang, W.; Wang, H.; Liu, J. Meta-Analysis and Evaluation by Insect-Mediated Baiting Reveal Different Patterns of Hypocrealean Entomopathogenic Fungi in the Soils from Two Regions of China. *Front. Microbiol.* **2020**, *11*, 1133. [CrossRef] [PubMed]
27. Murindangabo, Y.T.; Kopecký, M.; Perná, K.; Konvalina, P.; Bohatá, A.; Kavková, M.; Nguyen, T.G.; Hoang, T.N. Relevance of Entomopathogenic Fungi in Soil–Plant Systems. *Plant Soil* **2024**, *495*, 287–310. [CrossRef]
28. Quesada Moraga, E. Entomopathogenic Fungi as Endophytes: Their Broader Contribution to IPM and Crop Production. *Biocontrol Sci. Technol.* **2020**, *30*, 864–877. [CrossRef]
29. Macias, A.M.; Geiser, D.M.; Stajich, J.E.; Łukasik, P.; Veloso, C.; Bublitz, D.C.; Berger, M.C.; Boyce, G.R.; Hodge, K.; Kasson, M.T. Evolutionary Relationships among *Massospora* Spp. (Entomophthorales), Obligate Pathogens of Cicadas. *Mycologia* **2020**, *112*, 1060–1074. [CrossRef]
30. Hodge, K.T.; Hajek, A.E.; Gryganskyi, A. The First Entomophthoralean Killing Millipedes, *Arthrophaga Myriapodina* n. Gen. n. Sp., Causes Climbing before Host Death. *J. Invertebr. Pathol.* **2017**, *149*, 135–140. [CrossRef]
31. Elya, C.; De Fine Licht, H.H. The Genus Entomophthora: Bringing the Insect Destroyers into the Twenty-First Century. *IMA Fungus* **2021**, *12*, 34. [CrossRef]
32. Duke, L.; Steinkraus, D.C.; English, J.E.; Smith, K.G. Infectivity of Resting Spores of *Massospora Cicadina* (Entomophthorales: Entomophthoraceae), an Entomopathogenic Fungus of Periodical Cicadas (*Magicicada* Spp.) (Homoptera: Cicadidae). *J. Invertebr. Pathol.* **2002**, *80*, 1–6. [CrossRef]
33. Anderson, J.A.; Corbin, E.M.; Lovett, B.; Kasson, M.T.; LaDouceur, E.E.B. Histologic Findings of *Massospora cicadina* Infection in Periodical Cicadas (Magicicada Septendecim). *Vet. Pathol.* **2023**, *60*, 704–708. [CrossRef]
34. Lovett, B.; Macias, A.; Stajich, J.E.; Cooley, J.; Eilenberg, J.; de Licht, H.H.F.; Kasson, M.T. Behavioral Betrayal: How Select Fungal Parasites Enlist Living Insects to Do Their Bidding. *PLOS Pathog.* **2020**, *16*, e1008598. [CrossRef] [PubMed]
35. Hughes, D.P.; Araújo, J.P.M.; Loreto, R.G.; Quevillon, L.; de Bekker, C.; Evans, H.C. Chapter Eleven—From So Simple a Beginning: The Evolution of Behavioral Manipulation by Fungi. In *Advances in Genetics*; Genetics and Molecular Biology of Entomopathogenic Fungi; Lovett, B., St. Leger, R.J., Eds.; Academic Press: Cambridge, MA, USA, 2016; Volume 94, pp. 437–469.
36. Costa, P.P. *Gibellula spp. Associadas a Aranhas da Mata do Paraíso, Viçosa-MG*; Universidade Federal de Viçosa: Viçosa, Brazil.
37. Katoh, K.; Standley, D.M. MAFFT Multiple Sequence Alignment Software Version 7: Improvements in Performance and Usability. *Mol. Biol. Evol.* **2013**, *30*, 772–780. [CrossRef] [PubMed]
38. Castresana, J. Selection of Conserved Blocks from Multiple Alignments for Their Use in Phylogenetic Analysis. *Mol. Biol. Evol.* **2000**, *17*, 540–552. [CrossRef] [PubMed]
39. Shen, W.; Le, S.; Li, Y.; Hu, F. SeqKit: A Cross-Platform and Ultrafast Toolkit for FASTA/Q File Manipulation. *PLoS ONE* **2016**, *11*, e0163962. [CrossRef]
40. Stamatakis, A. RAxML Version 8: A Tool for Phylogenetic Analysis and Post-Analysis of Large Phylogenies. *Bioinformatics* **2014**, *30*, 1312–1313. [CrossRef] [PubMed]
41. FigTree. Available online: http://tree.bio.ed.ac.uk/software/figtree/ (accessed on 16 August 2024).
42. Ren, Y.; Yu, G.; Shi, C.; Liu, L.; Guo, Q.; Han, C.; Zhang, D.; Zhang, L.; Liu, B.; Gao, H.; et al. Majorbio Cloud: A One-Stop, Comprehensive Bioinformatic Platform for Multiomics Analyses. *iMeta* **2022**, *1*, e12. [CrossRef]
43. Wu, C.; Wang, M.; Wang, C.; Zhao, X.; Liu, Y.; Masoudi, A.; Yu, Z.; Liu, J. Reed Biochar Improved the Soil Functioning and Bacterial Interactions: A Bagging Experiment Using the Plantation Forest Soil (*Fraxinus Chinensis*) in the Xiong'an New Area, China. *J. Clean. Prod.* **2023**, *410*, 137316. [CrossRef]
44. Nilsson, R.H.; Larsson, K.-H.; Taylor, A.F.S.; Bengtsson-Palme, J.; Jeppesen, T.S.; Schigel, D.; Kennedy, P.; Picard, K.; Glöckner, F.O.; Tedersoo, L.; et al. The UNITE Database for Molecular Identification of Fungi: Handling Dark Taxa and Parallel Taxonomic Classifications. *Nucleic Acids Res.* **2019**, *47*, D259–D264. [CrossRef]
45. Wang, M.; Wang, C.; Yu, Z.; Wang, H.; Wu, C.; Masoudi, A.; Liu, J. Fungal Diversities and Community Assembly Processes Show Different Biogeographical Patterns in Forest and Grassland Soil Ecosystems. *Front. Microbiol.* **2023**, *14*, 1036905. [CrossRef]
46. Schneider, C.A.; Rasband, W.S.; Eliceiri, K.W. NIH Image to ImageJ: 25 Years of Image Analysis. *Nat. Methods* **2012**, *9*, 671–675. [CrossRef] [PubMed]
47. Nyffeler, M.; Hywel-Jones, N. Diversity of Spider Families Parasitized by Fungal Pathogens: A Global Review 2023. *bioRxiv* **2023**. bioRxiv 2023.05.11.540451.
48. Wang, L.; Keyhani, N.; Xia, Y.; Xie, J. The Potential and Limitations of Entomopathogenic Fungi as Biocontrol Agents for Insect Pest Management. *Entomol. Gen.* **2024**, *44*, 797–811. [CrossRef]
49. Joseph, R.; Darrisaw, C.; Lloyd, A.; Hoel, D.; Keyhani, N.O. Isolation of a Novel *Pythium* Species, *P. Thermoculicivorax*, and *Trichoderma* Sp. from Natural Enzootic Mosquito Larval Infections. *J. Fungi* **2024**, *10*, 199. [CrossRef] [PubMed]
50. Saltamachia, S.J. Theoretical and Empirical Evidence for Extended Phenotypes in a Specialized Parasite of Spiders. *Authorea Prepr.* 2022; *preprint*.
51. Wu, F.; Tian, T.; Wenxia, M. A Brief Introduction on Microbial Deterioration of ca. 1500-Year-Old Tomb Wall Paintings. International Biodeterioration and Biodegradation-Newsletter December 2021, 23–24. Available online: https://www.researchgate.net/profile/Fasi-Wu/publication/359647902_A_brief_introduction_on_microbial_deterioration_of_ca_1500-year-old_tomb_wall_paintings/links/624675a18068956f3c5e941a/A-brief-introduction-on-microbial-deterioration-of-ca-1500-year-old-tomb-wall-paintings.pdf (accessed on 30 August 2024).

52. Leplat, J.; François, A.; Bousta, F. *Parengyodontium Album*, a Frequently Reported Fungal Species in the Cultural Heritage Environment. *Fungal Biol. Rev.* **2020**, *34*, 126–135. [CrossRef]
53. Leplat, J.; François, A.; Bousta, F. Diversity of *Parengyodontium* Spp. Strains Isolated from the Cultural Heritage Environment: Phylogenetic Diversity, Phenotypical Diversity, and Occurrence. *Mycologia* **2022**, *114*, 825–840. [CrossRef] [PubMed]
54. Kanegae, H.; Tomino, N.; Nakamura, Y.; Minakawa, T.; Yaguchi, T.; Izawa, T.; Sano, A.; Itano, E.N.; Ueda, K. *Parengyodontium album* Isolated from Cutaneous Lesions of a Pacific White-Sided Dolphin (Lagenorhynchus Obliquidens) During Treatment for *Paracoccidioidomycosis ceti*. *Mycopathologia* **2020**, *185*, 1021–1031. [CrossRef]
55. Mohamed, N.; Ding, C.H.; Wahab, A.A.; Tzar, M.N.; Hassan, M. Isolation of an Obscure Fungus, *Parengyodontium album,* from the Blood of a Severely Neutropenic Patient: The First Reported Case from Malaysia. *J. Infect. Dev. Ctries.* **2022**, *16*, 1668–1670. [CrossRef]
56. Tsang, C.-C.; Chan, J.F.W.; Pong, W.-M.; Chen, J.H.K.; Ngan, A.H.Y.; Cheung, M.; Lai, C.K.C.; Tsang, D.N.C.; Lau, S.K.P.; Woo, P.C.Y. Cutaneous Hyalohyphomycosis Due to *Parengyodontium album* Gen. et Comb. Nov. *Med. Mycol.* **2016**, *54*, 699–713. [CrossRef]
57. Bastian, F.; Alabouvette, C.; Saiz-Jimenez, C. The Impact of Arthropods on Fungal Community Structure in Lascaux Cave. *J. Appl. Microbiol.* **2009**, *106*, 1456–1462. [CrossRef]
58. Gorbushina, A.A.; Petersen, K. Distribution of Microorganisms on Ancient Wall Paintings as Related to Associated Faunal Elements. *Int. Biodeterior. Biodegrad.* **2000**, *46*, 277–284. [CrossRef]
59. Saarela, M.; Alakomi, H.-L.; Suihko, M.-L.; Maunuksela, L.; Raaska, L.; Mattila-Sandholm, T. Heterotrophic Microorganisms in Air and Biofilm Samples from Roman Catacombs, with Special Emphasis on Actinobacteria and Fungi. *Int. Biodeterior. Biodegrad.* **2004**, *54*, 27–37. [CrossRef]
60. Vaksmaa, A.; Vielfaure, H.; Polerecky, L.; Kienhuis, M.V.M.; van der Meer, M.T.J.; Pflüger, T.; Egger, M.; Niemann, H. Biodegradation of Polyethylene by the Marine Fungus *Parengyodontium Album*. *Sci. Total Environ.* **2024**, *934*, 172819. [CrossRef] [PubMed]
61. Trovão, J.; Mesquita, N.; Paiva, D.S.; Paiva de Carvalho, H.; Avelar, L.; Portugal, A. Can Arthropods Act as Vectors of Fungal Dispersion in Heritage Collections? A Case Study on the Archive of the University of Coimbra, Portugal. *Int. Biodeterior. Biodegrad.* **2013**, *79*, 49–55. [CrossRef]
62. Suryanarayanan, T. Occurrence of *Beauveria alba* on a Spider. *Curr. Sci.* **1981**, *50*, 284.
63. Martynenko, S.V.; Kondratyuk, T.O.; Sukhomlyn, M. A Hyphomycete, *Engyodontium album* (Limber) de Hoog, Attacking Spiders in Underground Headings of Kyiv-city. *Ukrainian Botanical Journal* **2020**, *69*, 423–432.
64. Jibola-Shittu, M.Y.; Heng, Z.; Keyhani, N.O.; Dang, Y.; Chen, R.; Liu, S.; Lin, Y.; Lai, P.; Chen, J.; Yang, C.; et al. Understanding and Exploring the Diversity of Soil Microorganisms in Tea (*Camellia Sinensis*) Gardens: Toward Sustainable Tea Production. *Front. Microbiol.* **2024**, *15*, 1379879. [CrossRef]
65. Xu, X.; Lin, W.; Keyhani, N.O.; Liu, S.; Li, L.; Zhang, Y.; Lu, X.; Wei, Q.; Wei, D.; Huang, S.; et al. Properties and Fungal Communities of Different Soils for Growth of the Medicinal Asian Water Plantain, *Alisma orientale*, in Fujian, China. *J. Fungi* **2024**, *10*, 187. [CrossRef]
66. Liu, S.; Xiong, C.; Lin, L.; Keyhani, N.O.; Zhu, M.; Zhao, Z.; Zhang, W.; Yang, C.; Su, H.; Liu, P.; et al. Assessing the Structure and Diversity of Fungal Community in Plant Soil under Different Climatic and Vegetation Conditions. *Front. Microbiol.* **2023**, *14*, 1288066. [CrossRef]
67. Hong, M.; Peng, G.; Keyhani, N.O.; Xia, Y. Application of the Entomogenous Fungus, *Metarhizium anisopliae*, for Leafroller (Cnaphalocrocis Medinalis) Control and Its Effect on Rice Phyllosphere Microbial Diversity. *Appl. Microbiol. Biotechnol.* **2017**, *101*, 6793–6807. [CrossRef]
68. Potts, L.J.; Koštál, V.; Simek, P.; Teets, N.M. Energy Balance and Metabolic Changes in an Overwintering Wolf Spider, *Schizocosa Stridulans*. *J. Insect Physiol.* **2020**, *126*, 104112. [CrossRef] [PubMed]

Disclaimer/Publisher's Note: The statements, opinions and data contained in all publications are solely those of the individual author(s) and contributor(s) and not of MDPI and/or the editor(s). MDPI and/or the editor(s) disclaim responsibility for any injury to people or property resulting from any ideas, methods, instructions or products referred to in the content.

Journal of *Fungi*

MDPI

Article

What Quality Suffices for Nanopore Metabarcoding? Reconsidering Methodology and Ectomycorrhizae in Decaying *Fagus sylvatica* Bark as Case Study

Glen Dierickx [1,2,*], Lowie Tondeleir [1], Pieter Asselman [1], Kris Vandekerkhove [2] and Annemieke Verbeken [1]

[1] Research Group Mycology, Ghent University, 9000 Gent, Belgium
[2] Research Institute for Nature and Forest, 9500 Geraardsbergen, Belgium
* Correspondence: glen.dierickx@ugent.be

Abstract: Nanopore raw read accuracy has improved to over 99%, making it a potential tool for metabarcoding. For broad adoption, guidelines on quality filtering are needed to ensure reliable taxonomic unit recovery. This study aims to provide those guidelines for a fungal metabarcoding context and to apply them to a case study of ectomycorrhizae in the decaying bark of *Fagus sylvatica*. We introduce the eNano pipeline to test two standard metabarcoding approaches: (1) Reference-based mapping leveraging UNITE's species hypothesis system (SH approach); (2) Constructing 98% OTUs (OTU approach). Our results demonstrate that both approaches are effective with Nanopore data. When using a reference database, we recommend strict mapping criteria rather than Phred-based filtering. Leveraging the SH-system further enhances reproducibility and facilitates cross-study communication. For the 98% OTUs, filtering reads at ≥Q25 is recommended. Our case study reveals that the decay gradient is a primary determinant of community composition and that specific mycorrhizal fungi colonize decaying bark. Complementing our metabarcoding results with root tip morphotypification, we identify *Laccaria amethystina* and *Tomentella sublilacina* as key ectomycorrhizae of saplings on decaying logs. These findings demonstrate that Nanopore sequencing can provide valuable ecological insights and support its broader use in fungal metabarcoding as read quality continues to improve.

Keywords: Nanopore; deadwood; ectomycorrhiza; *Fagus sylvatica*; quality filtering; Phred score; eNano pipeline; natural regeneration; metabarcoding

1. Introduction

1.1. Fungal Metabarcoding

A significant hurdle in fungal ecology is that most species elude visual detection. This especially affects community ecological studies where the aim is to include all community members. While second-generation sequencing propelled fungal ecology forward by enabling large-scale metabarcoding, the taxonomic resolution using the dominant Illumina platform is constrained by short amplicon lengths at a maximum of 2 × 300 base-pairs (bp). This hampers the exploitation of the fungal barcode region, the Internal Transcribed Spacer (ITS), which ranges between 250 and 1500 bp [1–3]. Third-generation sequencing technologies, such as Nanopore (Oxford Nanopore Technologies Inc., Oxford, UK) and PacBio SMRT (Pacific BioSciences Inc., Menlo Park, CA, USA), have overcome read length limitations, enabling the targeting of the full-length ITS region. While Nanopore initially lagged in quality, advancements in chemistry (V14) and algorithms (transformer model-based architecture, dorado ≥ v0.7) are closing this gap. Raw read accuracy now exceeds 99% correct base call probability [4]. This accuracy surpasses the interspecific distances typically observed for the ITS region [5], making Nanopore a potentially viable tool in fungal metabarcoding.

Despite these advancements, studies on the application of Nanopore sequencing in fungal metabarcoding remain limited, with conclusions varying from unsuitable to feasible for simple communities, depending on the version of the technology used [6–11]. A critical step in sequence data processing is quality control. Typically, this involves setting a minimum read quality threshold, expressed in terms of Phred score (Q), which indicates the probability of an incorrect base call. For example, Q10 represents a 90% accuracy (1 in 10 chance of error), while Q30 represents a 99.9% accuracy (1 in 1000 chance of error).

The most widely adopted approach in metabarcoding is generating operational taxonomic units (OTUs) de novo from raw data. However, this method has been considered unfeasible with Nanopore data due to high error rates that significantly impact clustering. Typically, the OTU approach involves setting a minimum Phred score of Q28, as recommended in FASTQC [12], and clustering the filtered reads at a predefined similarity threshold. Currently, enforcing a Q28 threshold results in a near-total reduction of usable data, which has limited the adoption of this approach.

To address the issue of read quality, two approaches have thus far been used. The first approach improves sequence quality by drafting consensus sequences from clusters [6,9,11], as implemented in tools like Decona, ONTrack2, and CONCOMPRA [13–15]. While these tools are far more sophisticated than simple clustering, they need fine-tuning of more parameters, adding complexity to their use. Similar to OTU clustering, consensus sequence generation bypasses the need for a reference database, offering an advantage for taxonomic units absent from databases.

The second approach aligns raw reads against a reference database, retaining reads that can be confidently mapped [7,9,10]. This approach depends on the comprehensiveness and accuracy of the reference database and shifts the quality issue to defining what constitutes a confidently mapped read.

In all these approaches, setting a minimum Phred score is standard practice. Therefore, establishing a robust minimal quality threshold for each approach is crucial for the reliable recovery of taxonomic units, which underpins all subsequent analyses. However, guidelines for determining an appropriate threshold are sparse, complicating the analysis of Nanopore data and raising the question of what read quality suffices in the context of metabarcoding.

In this paper, we aim to provide guidelines for the quality filtering of Nanopore metabarcoding data using simple OTU-clustering and reference-based approaches. We detail our experiences with analyzing Nanopore data from a mock community and share our bioinformatics pipeline, eNano.

Building on these insights, we apply our methods to a case study. Specifically, we focus on an often overlooked microsite—the fungal community within decaying bark of European beech (*Fagus sylvatica* L. (1753))—and validate our results through the morphotypification of ectomycorrhizal mantles.

1.2. Case Study: Deadwood Bark Ectomycorrhizae

A specific aspect of habitat creation by deadwood is the case where large logs in intermediate to advanced decay stages act as a tree regeneration site (Figure 1). In mycorrhizal research, these logs are of particular interest because the excavation of root systems can confirm the establishment of ectomycorrhizal fungi (EcM) through morphotypification.

While EcM are abundant in soil and readily mycorrhize roots after germination [16], they are initially absent or scarce in deadwood. Their prevalence increases as the wood decays and becomes more penetrable [17–21]. Eventually, the fungal community in deadwood transitions to resemble that in soil, completing a full ecological transformation [20]. In contrast to fruitbody-based inventories, metabarcoding techniques have detected EcM surprisingly early in the decay process. For example, Rajala et al. [19] found metabolically active EcM in slightly decayed *Picea abies* (L.) H. Karst. (1881) logs, which suggests a continuum of tree regeneration in old natural forests. Several reasons for colonization have

been put forward, including nutrient mining [22–24], the elevation of fruiting positions, and associating with sapling roots in decaying logs [21,25].

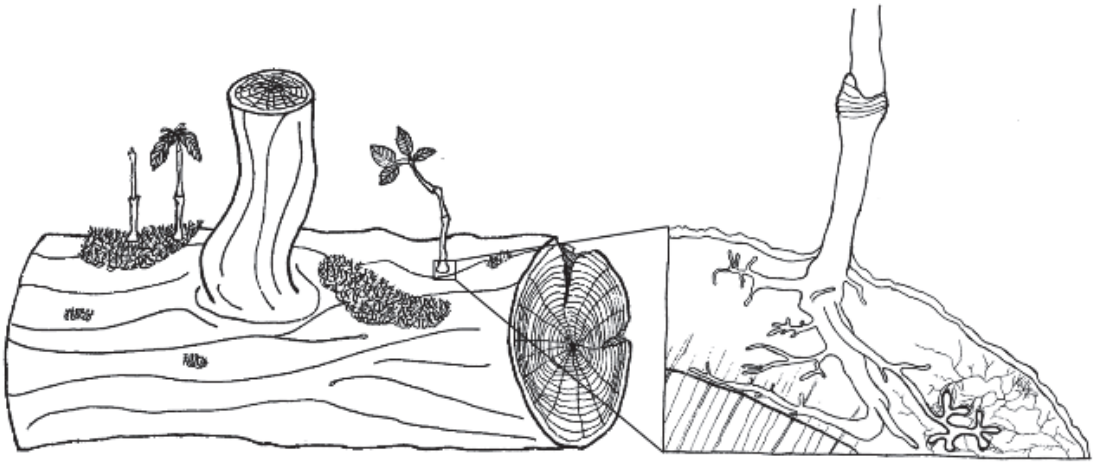


Figure 1. Schematic representation of *Fagus sylvatica* deadwood microsite for regeneration. Seedlings root in the soft, decaying outer layer, the inner bark. Ectomycorrhizal fungi may also proliferate in this substrate, helping seedlings grow.

From a seedling's perspective, associating with EcM is believed to be crucial for survival, especially in environments where nutrients are hard to access, such as recent deadwood [26]. For example, in North America, *Tsuga heterophylla* (Raf.) Sarg. (1899) regenerating on deadwood is known to associate with a wide range of EcM species [16,27,28]. In Europe, Tedersoo et al. [25,29] studied sapling EcM in mixed Estonian forests and found the most frequent species on roots in deadwood to also be common in soil, which is consistent with metabarcoding results.

Over the past decade, we have occasionally observed seedlings of European beech growing on relatively fresh deadwood. These seedlings primarily root in the decaying inner bark—comprising the secondary phloem and nutrient-rich cambium—rather than in the denser wood underneath (Figure 1). This layer, often overlooked except in studies on bark beetles (e.g., [30]), offers a potentially favorable environment for EcM colonization due to its higher moisture content, higher nutrient availability, less compact nature, and faster decay rate [31–34]. Such conditions could facilitate the penetration of sapling roots and EcM originating either from soil or from propagules. However, there is limited literature available to contextualize our observations, making it an intriguing case study for this underexplored EcM niche.

2. Materials and Methods

2.1. Study Site and Log Selection

Sampling was conducted in the Joseph Zwaenepoel forest reserve (Brussels, Belgium). This forest reserve is dominated by European beech (*Fagus sylvatica*) and has been left unmanaged since 1983. Further information on the study site can be found in Vandekerkhove et al. [35] and De Keersmaeker et al. [36]. For this study, we specifically searched for large beech logs of intermediate decay stage (Log decay stage 2–3 according to Renvall et al. [37]) bearing newly established saplings. This means that the wood is still mostly hard, and the bark is still present but starts to loosen. We selected 24 suitable logs; an overview of the sampled logs is given in Table S1.

2.2. Root Tip Morphotypification and Sanger Barcoding

From the selected logs, a set of 23 beech saplings were collected in September–November 2022 (Table S1). Sapling age was approximated by counting the number of leaf bud scar zones along the dominant axis. To extract saplings from the logs, a knife was

used to pry away the outer bark (periderm). Then, the roots were carefully pulled out of the decaying bark (secondary phloem). Saplings were transported separately, with their roots wrapped in aluminum foil to prevent contamination and desiccation of EcM mantles. In addition, five saplings growing on soil in close proximity to the log were collected to serve as a baseline. All plants were stored at 4 °C and processed within three days from collection.

We morphotypified the EcM mantles using the work of Agerer [38–44]. Mantle coverage was estimated by sectioning the fine root tips (⌀ < 1 mm) into fragments of approximately 5 mm. Each fragment was inspected for mantle presence to estimate total coverage, expressed as the ratio of colonized to total root tips. Mantle micromorphology was assessed using brightfield microscopy. For each morphotype, three root tips were separately preserved for Sanger sequencing.

Kruskal–Wallis rank sum and Dunn's tests (*stats 4.2.3*, *FSA 0.9.4*) were used to test for differences in EcM species richness and colonization rates between bark- and soil-growing saplings.

Genomic DNA was isolated from the mycorrhized root tips of the collected saplings following a modified cetyltrimethylammonium bromide (CTAB) method [45] Homogenized mantles were suspended in CTAB extraction buffer and incubated on a heat block at 55 °C for at least two hours. The lysate was purified with two rounds of chloroform:isoamyl alcohol cleanups and precipitated using isopropanol (0.54×) | ammonium acetate (0.08×). The ITS region was amplified using Dream Taq Mastermix (Thermo Fisher, Waltham, MA, USA) and primer pair ITS1F/ITS4 (10 µM) [3,46,47]. Amplification conditions were the following: initial denaturation at 94 °C for 5 min; 30 cycles of 94 °C for 30 s, 55 °C for 30 s, and 72 °C for 45 s; and a final extension at 70 °C for 7 min. Amplicons were purified using EXOFastAP (Thermo Fisher, Waltham, MA, USA) and sequenced by Macrogen™ (Amsterdam, The Netherlands).

2.3. Nanopore Metabarcoding

2.3.1. Mock Community

We constructed a mock community comprising 16 taxa that represent major ectomycorrhizal lineages and are phylogenetically diverse. Moreover, we included some closely related species to assess the sensitivity of our run at lower taxonomic levels. DNA extracts were sourced from previous collections [48–51] and opportunistically pooled without prior quality control. Included taxa are detailed in Table S2.

2.3.2. Bark Sampling

We gathered decaying inner bark of 13 beech logs with beech regeneration, with two of these logs sampled at three distinct locations on the log to assess community turnover at the log level. Three logs without regeneration were selected as a control group, resulting in 20 samples for metabarcoding.

We assessed inner bark decay stage (bark DS) on a 3-level scale from early to late, as described in Table 1.

Table 1. Decay stages of inner bark layer in European beech (Fagus sylvatica) deadwood. Note that bark decay stage (DS) may differ within the same log.

Bark Decay Stage	Description
Early	Layer (incl. inner bark) is difficult to penetrate with a metal spoon (force needed), and almost all fibers are intact and dark yellow in color. This corresponds to log decay stage (DS) 1 or early 2.
Intermediate	Layer crumbles and can be scooped up with a metal spoon. They crumble with minimal force between fingers, some fibers intact, light brown in color. This corresponds to a late log DS 2 or early 3.
Late	Layer is almost fully decayed, penetrable without force; it easily disintegrates between fingertips–resembles soil, no fibers intact, (dark) brown in color. Corresponds to a late log DS 3 or 4.

Each substrate sample constitutes a pool of 4 subsamples. Each subsample was taken at a 30° angle from the top of the log, half a meter apart, repeated in two places and on both sides of the log. A sterile knife was used to cut out a 25 cm × 25 cm square in the outer bark layer (periderm) that was carefully peeled back. In each subsample area, three tablespoons of degraded inner bark were added to a sterile Ziplock bag and pooled with other subsamples. The spoon and knife were disinfected between samples by wiping and burning with EtOH. To assess background soil diversity, three soil samples were collected according to the protocol of Tedersoo et al. [52]. All samples were transferred to the lab in a cooling box. Samples were airdried at 40 °C and homogenized by vigorously rubbing in a Ziplock bag. Two grams of sample material were used for DNA extraction.

2.3.3. Wet Lab

Samples were ground under liquid nitrogen. gDNA was isolated as previously described and cleaned using 0.8× SPRI beads (Beckman Coulter, Pasadena, CA, USA).

15 µL PCR reactions were run in duplicate. Each reaction mix consisted of 200 µM dNTPs, 0.5 µM of each primer, 1× Q5 reaction buffer, 0.02 U/µL Q5 HIFI polymerase (New England Biolabs, Ipswich, MA, USA), and 1 µL sample DNA. Cycling conditions were as follows: (1) Initial denaturation for 30 s at 98 °C; (2) 30 cycles of denaturation for 30 s at 98 °C, annealing for 20 s at 60 °C, with an extension for 20 s at 72 °C; (3) Final extension for 2 min at 72 °C. Amplicons were purified using SPRI beads and quantified on a Qubit Fluorometer (Invitrogen, Carlsbad, CA, USA).

Amplicons were normalized to 200 fmol, assuming an average amplicon size of 700 bp, and barcoded using the Native Barcoding kit 96 V14 (SQK-NBD114.96, Oxford Nanopore Technologies Inc., Oxford, UK). 25 fmol was loaded on an R10.4.1 MinION flowcell (Oxford Nanopore Technologies Inc., Oxford, UK). Sequencing ran for 72 h at 260 bp/s.

2.4. Bioinformatics

2.4.1. Reference Database

We used the SINTAX-formatted version of UNITEv10 [53]. Fasta header taxonomy annotation was manipulated to include UNITE species hypotheses (SH) by replacing or adding species-level annotations with the RefSeq's associated SH code (e.g., >UDB05341741; tax=d:Fungi,p:Rozellomycota,s:SH0910702.10FU;). This file can be found on the eNano GitHub page (see Section 2.4.2).

Nine reference sequences were added as dummy SH codes (e.g., SH0000001.10FU) for easier downstream manipulation (Table S2). Three previously generated sanger sequences that did not match any SH. Two references for taxa in the *Russula nigrifacta* species complex: *Russula ustulata* De Lange & Verbeken (2021) as it is part of our mock community, and *R. ambusta* De Lange, Adamčík & F. Hampe (2021) to serve as a control for false positives (GenBank accession number MW172301). In addition, because some of our root tip Sanger sequences did not confidently match any SH, references for *Tomentella sublilacina* (Ellis & Holw.) Wakef. (1962) and *Laccaria amethystina* Cooke (1884) were added. Finally, two large *Laccaria* zOTUs identified in the SH approach were also added (see Section 3.2.4).

2.4.2. eNano Pipeline

Demultiplexed fastq files, as outputted by MinKow (v. 22.10.7), were run through our eNano pipeline, which is opensource and available on the GitHub page of the Research Group Mycology (https://github.com/MycoMatics/eNano (accessed on 4 January 2024)). The pipeline takes a directory with subfolders (each representing sample barcodes) containing fastq files and a SINTAX formatted database as input. It outputs a (LULU-curated) OTU table with assigned taxonomy. Processing steps are detailed in the README file on GitHub. In short, Porechop v. 0.2.4 [54] trims adapters and barcodes, Cutadapt v. $\geq$ 2.8 [55] reorients sequences and cuts primers, Chopper v. $\geq$ 0.9 [56] quality filters on average Phred score, Vsearch v. $\geq$ 2.21 [57] appends sample information and performs clustering, chimera detection, creates a LULU match list and assigns taxonomy with the SINTAX algorithm [58].

LULU-curation [59] is run using the MUMU algorithm v. ≥ 1.0.2 [60], and taxonomic units are aggregated at the species level.

We explored two metabarcoding approaches for processing read data, here explained as the SH approach (reference-based) and the OTU approach (de novo clustering).

2.4.3. SH Approach

Reads were deduplicated into zero-radius Operational Taxonomic Units (zOTUs) and classified into species hypotheses (SH). Given that our mock community comprises databased taxa, which are theoretically classifiable, we established the threshold for the SINTAX classification algorithm by plotting the distribution of SINTAX confidence scores across Phred scores in Figure S1. Using high-quality reads (≥Q28), the SINTAX threshold was determined based on the density of the right tail, which shows an increase starting at 0.80 and a slight dip between 0.90 and 0.95. We therefore set the threshold for singletons at 0.95 and relaxed the criterion for multiton zOTUs to 0.8, considering that such reads are less likely to contain sequencing errors. zOTUs meeting this criterium were retained, and their conspecific abundances were aggregated for each SH. This method prioritizes read classifiability over read quality and is hereafter referred to as the 'SH approach'.

2.4.4. OTU Approach

Given that not all taxa are represented in databases, and thus, not all reads are classifiable, we also evaluated whether our datasets could support a traditional approach of quality filtering and clustering into 98% OTUs. This method allows the incorporation of sequence clusters that have no obvious match in databases but might be large and influential in driving ecological patterns and is hereafter referred to as the 'OTU approach'.

2.4.5. Minimum Quality Evaluation

To determine the minimum acceptable quality threshold, we divided the reads from our mock and bark communities based on their average Phred scores. We subsampled Phred-specific datasets to read count at Q28 (4245 mock and 42,560 bark reads per Phred score for Q14–28) and ran eNano on each set. The minimum Phred score for quality filtering was determined as the point where the recovery of taxonomic units (either 98% OTUs or SHs) stabilized. Due to the probabilistic nature of several steps, including chimera removal, clustering, and classification, we ran each dataset one hundred times. Additionally, because singleton exclusion is a common practice in quality filtering but problematic in Nanopore data due to high error rates resulting in many singletons, we also evaluated the effect of singleton taxonomic unit exclusion for both approaches. Finally, to assess species turnover between Phred-specific datasets, Beta-diversity (Bray–Curtis distance) is visualized in Figure S2.

2.4.6. Bark Metabarcoding

Sequence data were processed using insights from both the SH- and OTU approaches. For the SH approach, eNano was run with clustering at 100% identity (--id 1), without a quality threshold (--q 0), using our modified version of the UNITEv10 database. zOTUs were filtered based on SINTAX threshold (0.95 for singletons, 0.8 multitons), and conspecific abundances were aggregated into an SH-table used in all subsequent analyses.

For the OTU approach, eNano was run with a clustering identity of 98% (--id 0.98), a quality threshold of Q25 (--q 25), and a SINTAX threshold of 0.80 (--sintax 0.8) with LULU-curation (--skip-lulu 0). Singleton SHs and OTUs were excluded from analysis.

Tables with taxonomic units were handled using phyloseq 1.42.0 [61], metagMisc 0.5.0 [62], and vegan v. 2.6.4 [63]. Alpha diversity indices—species richness, Shannon-Wiener, and Simpson—were analyzed using a generalized linear model (GLM) with sequencing depth as a covariate to assess variations across bark decay stages. Read abundances were converted to Aitchison distances for Non-metric Multidimensional Scaling (NMDS) and Principal Coordinates Analysis (PCoA). Variable selection for PERMANOVA

was conducted through forward and backward selection using AICcPermanova 0.0.2 [64] while considering factors such as decay stages of the log and bark (DS Log, DS Bark) and the presence of regeneration. Indicator species analysis was carried out with the indicspecies package 1.7.13 [65], applying Pearson's phi coefficient for association (fidelity) and the standard Invdal.g function. Ecological guild assignments were made using FUNGuildR version 0.2.0.9000 [66]. Data processing was performed on the HPC of Ghent University, using eNano v 0.1and R 4.2.3 [67]

3. Results

3.1. Morphotyping

Saplings growing on logs were primarily found in the intermediate (n = 6) and late (n = 17) stages of bark decay. Although seedlings were occasionally observed in early bark decay stages, their delicate root systems were not successfully retrieved.

For this study, 23 beech saplings growing on 22 distinct logs were selected for root tip morphotyping analysis (Tables S1 and S3). Additionally, five saplings growing in soil were included as a reference group. We constructed ten morphotypes, eight of which were identified by sanger sequencing (Table S4). Two others failed sequencing and were identified based on morphology, the jet-black *Cenococcum geophilum* Fr. (1829) and *Elaphomyces* cf. *muricatus* Fr. (1829), which is recognizable by the spindle shape of the emanating hyphae.

Among the log-based saplings, 13 were colonized by EcM (Table S3). Specifically, two EcM species, *Laccaria amethystina* and *Tomentella sublilacina* were identified, with the former being dominant. In contrast, all soil-grown saplings were colonized by EcM. Also, species diversity is higher in soil, with nine species identified in total (*Laccaria amethystina*, *Lactarius subdulcis* (Pers.) Gray (1821), *Xerocomellus pruinatus* (Fr.) Šutara (2008), *Cenococcum geophilum*, *Russula ochroleuca* Fr. (1829), *Melanogaster* cf. *intermedius* (Berk) Zeller & C.W. Dodge (1937), *Scleroderma citrinum* Pers. (1801), *Inocybe napipes* J.E. Lange (1917) and *Elaphomyces* cf. *muricatus*). EcM coverage (proportion of colonized root tips) and EcM species richness are significantly higher for those saplings growing in soil (Dunn test, resp. $p = 0.02$ and $p = 0.001$). Ten log-based saplings were not colonized; eight of these were estimated to be only two years old. The two older saplings did not show accumulation of EcM, with no EcM present for the 8-year-old sampling and only *Laccaria amethystina* present for the 9-year-old sapling (Table S3).

3.2. Metabarcoding

SH and OTU tables for mock and bark datasets can be found in File S1. The negative control was sequenced to account for potential contaminants. Two OTUs mapped to *Malassezia* spp.; these were removed in further analysis.

The average Phred score was 15.3, but it is best re-evaluated after trimming the low-quality, non-informative adapter region. With the first 20 bp trimmed, the average Phred score increased to Q17.3. The median amplicon size was 709 bp.

3.2.1. Minimum Quality Evaluation

Both approaches demonstrated stabilization in taxonomic unit recovery, with consistent patterns observed for mock and bark datasets. Recovery in the bark community was consistently slower with increasing quality, highlighting the complexity of the dataset (Figure 2b,c).

For the 98% OTU approach, the stabilization in taxonomic unit recovery began at Q24 but never fully plateaued, with 26 and 2605 OTUs recovered at Q28 in the mock and bark communities, respectively (Figure 2b). This trend persisted when excluding singleton OTUs, yielding 15 and 1770 OTUs at Q28.

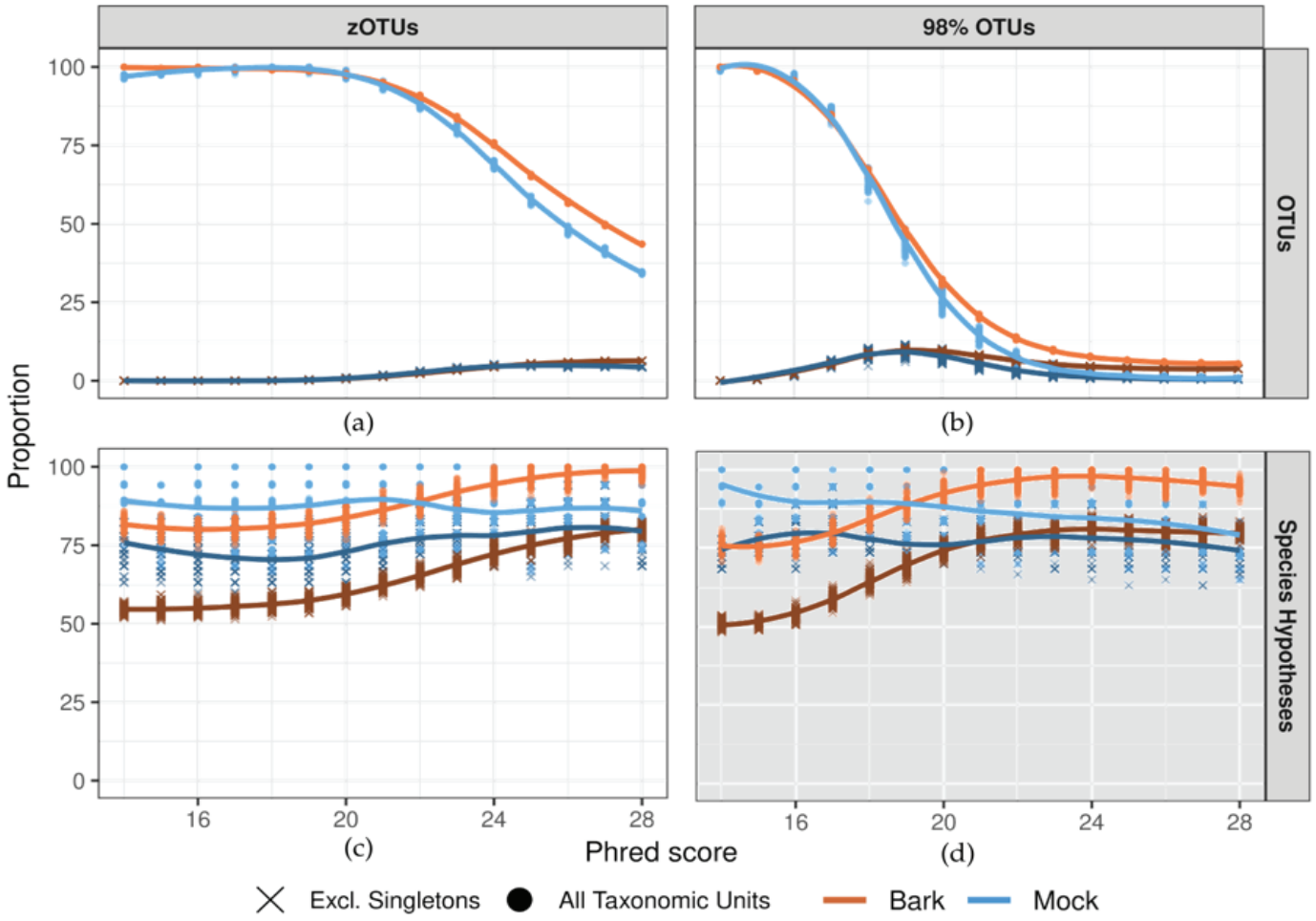


Figure 2. Taxonomic unit recovery using all reads and excluding singleton units (zOTUs, 98% OTUs or SHs), Phred-specific datasets subsampled to amount of reads at Q28. Each datapoint represents 4245 reads for the mock dataset and 42,560 for the bark dataset. Dark and light brown represent Bark data, dark and light blue represent Mock data. Lines represent a loess smoother to visualize trends. (**a**) Intermediate zOTU step in SH approach. (**b**) OTU approach. (**c**) SH approach. (**d**) merging 98% OTUs into SHs was excluded a priori (gray-shaded), shown for completeness. Graphs standardized by maximum recovered units for each analysis and dataset. Nmax-zOTU-bark = 39,382; Nmax-zOTU-mock = 3818; Nmax-98%OTU-bark = 39,348; Nmax-98%OTU-mock = 3722; Nmax-SH-bark = 546; Nmax-SH-mock = 20.

In the SH approach, the intermediate zOTUs step did not show any signs of stabilizing before Q28, indicating that the sequence error is too impactful to reach a stable number of taxonomic (Figure 2a). When singleton zOTUs were excluded, zOTU recovery slowed at Q25 but never stabilized. At Q28, singleton zOTUs accounted for 28.6% and 37.2% of reads in mock and bark, respectively. The SH approach exhibited stable recovery of SHs across all Phred scores for both datasets, with a slight increase when using higher quality reads in the bark dataset (Figure 2c). At Q28, excluding singleton SHs resulted in fewer SHs in the bark community, reflecting the presence of rare SHs. In the mock community, the average difference when excluding singleton SHs was one SH, *Curvibasidium cygneicollum* (14 vs. 15, Figure 2c).

Merging 98% OTUs into SHs was excluded a priori because clustering at 98% blurs taxonomic resolution well beyond the minimum difference of 0.5% between SHs and the 1.5% clustering threshold of the dynamic UNITE release (Figure 2d).

3.2.2. Mock Community

The OTU approach resulted in 188 OTUs, of which 107 were identified to SH, corresponding to 18 unique SH codes. Fourteen taxa from our input mock were recovered, as well as four contaminant OTUs.

The SH approach generated 127,075 zOTUs, of which 46% could be mapped to SH. 44 SHs were recovered, 17 of which are singletons. 75% of total reads were classified into SHs, and unmatched reads (not detected as fungal) occurred only at Q5–7 (0.27%). Classification rates show a rapid increase up until Q16, after which the increase slows down and finally stabilizes at Q27 (88 ± 0.2% of reads/Phred classified). This pattern was partly repeated for the more complex bark community, whose classification rates stabilized at Q16, as seen in Figure S3.

Taxon recovery at each Phred score is depicted in Figure 3. Our mock community showed high recovery, with all taxa (excl. *Lactifluus russulisporus* Dierickx & De Crop (2019)) recovered at Phred scores up to Q27. *L. russulisporus* is detected at Q16 (3 reads) and Q20 (2 reads), showing that it was picked up in low abundances. Next to our 16 mock taxa, 28 contaminant SHs were picked up, most of which are singletons.

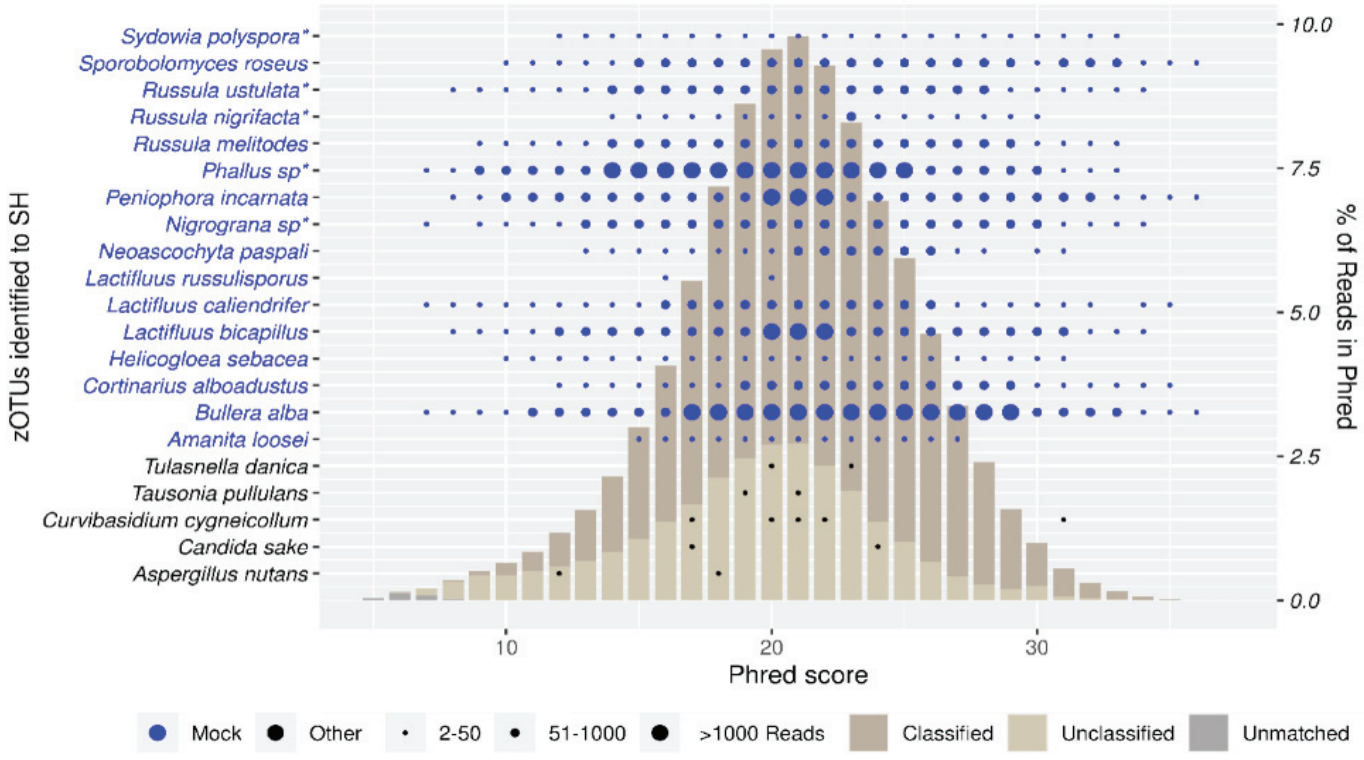


Figure 3. Mock community recovered at different Phred scores using SH approach. * Reference sequences added to database.

3.2.3. Bark Substrate Community

The OTU approach produced 2431 OTUs out of 332,874 reads (9.4% of total reads), while the SH approach used 758,755 reads (24.4%) to recover 901 species hypotheses, including two contaminants and 62 singleton SHs.

At the phylum level, recovery of both methods was similar, with most taxonomic units belonging to Ascomycota, then Basidiomycota and Rozellomycota (Figure 4). The OTU approach produced more units that belonged to Mortierellomycota and more units that could not be classified. The SH approach recovered relatively more Basidiomycota and Rozellomycota. Because the main target of our study was to identify ectomycorrhizal taxa, most of which we assume to be recorded in the UNITE database for our study area, the metabarcoding results and discussion focus mostly on our SH approach.

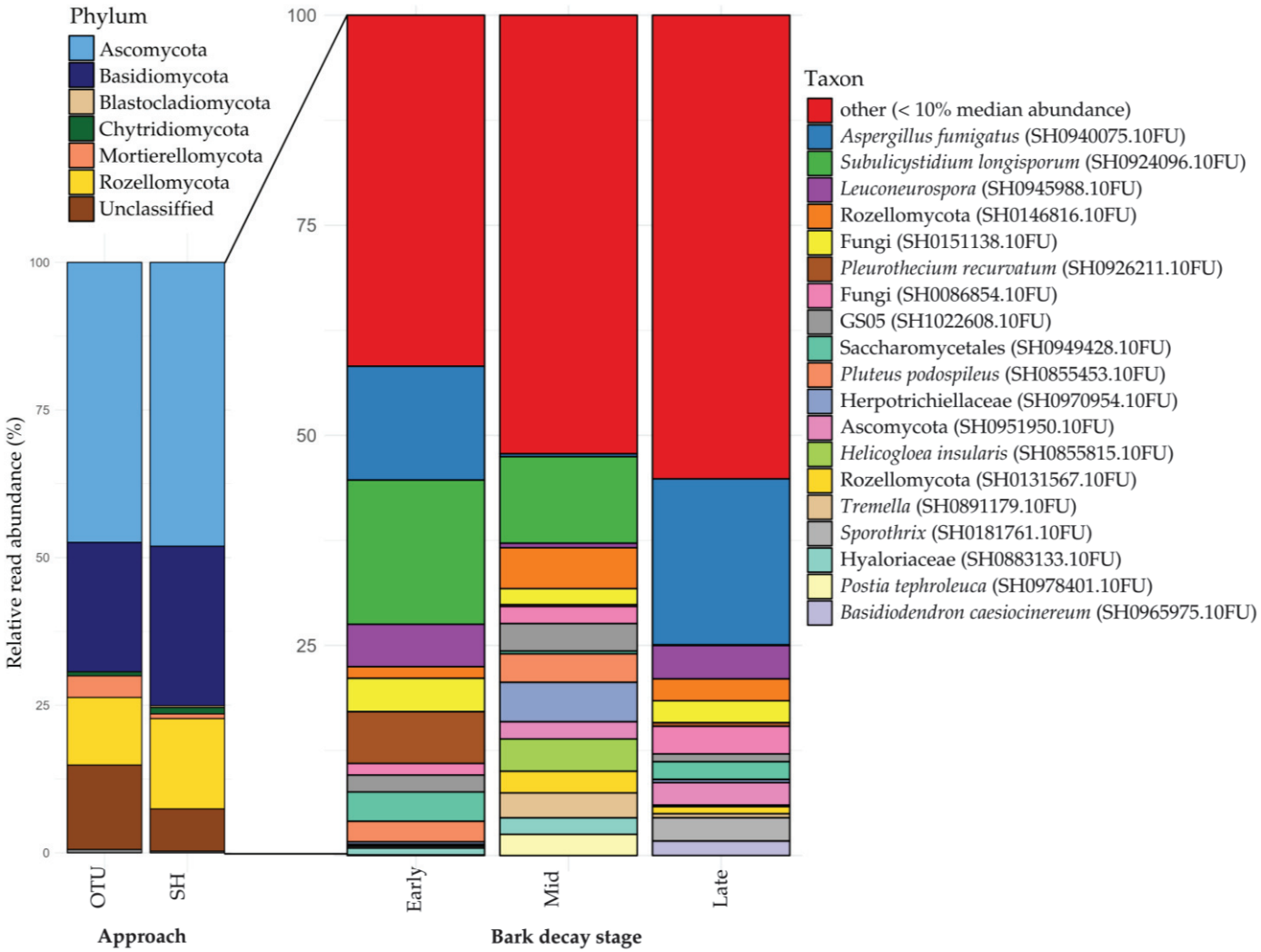


Figure 4. Left: Taxonomic composition across approaches. Right: Composition in each bark decay stage for the SH approach. Phyla with median abundance < 1% not shown (Glomeromycota, Olpidiomycota, Kickxellomycota, Zoopagomycota, Mucoromycota, Entomophthoromycota, Sanchytriomycota, Aphelidiomycota, and 'GS01_phy_Incertae_sedis').

The inner bark samples were composed of 778 SHs. *Subulicystidium longisporum* (SH0924096.10FU) is the most common SH, with high abundance in both early and intermediate bark decay stages (Figure 4). 19 SHs represent the most common taxa, most of which have no associated species name, for example, two Rozellomycota SHs (SH0131567.10FU and SH0146816.10FU) (Figure 4).

Species richness (SR) increased with bark decay from 106 ± 21 SHs in early decay to 125 ± 27 and 135 ± 28 SHs in intermediate and late decay stages, respectively. Observed and Shannon diversity differed significantly between early and late bark decay stages (Tukey's HSD, p = 0.02 and 0.05, respectively) but not between other pairs. Simpson diversity was similar for all bark decay stages. While richness patterns were consistent in both approaches, significance was more pronounced in the OTU approach.

Both NMDS and PCoA ordination reveal clustering of samples according to the bark decay stage (Figure 5), with the most overlap between early and intermediate bark decay stages.

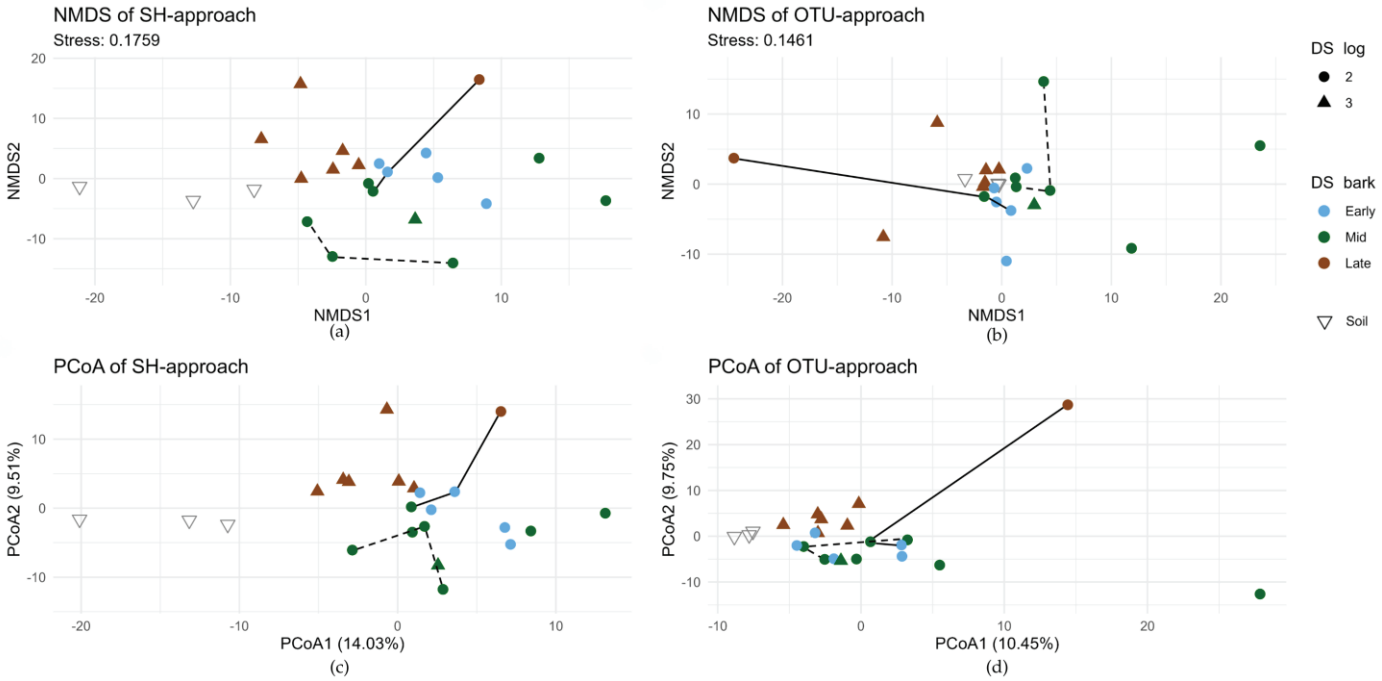


Figure 5. Ordination of both approaches on Aitchison distances. Samples originating from the same logs are connected by the same line types. (**a**) NMDS of SH approach; (**b**) NMDS of OTU approach; (**c**) PCoA of SH approach; (**d**) PCoA of OTU approach.

A notable exception is the NMDS on OTU approach, which shows little data structure with decay (Figure 5b). Two outlier samples (ZF321_1 and ZF327) can be identified in the PCoA of OTU approach (Figure 5d). ZF321_1 is dominated by a single OTU, mapping to a species of Saccharomycetales (66% sample reads). ZF327 contains an OTU that does not occur in any other sample, identified as *Pluteus podospileus* (SH0855453.10FU). This SH is present across multiple samples in the SH approach, thereby not producing an outlier by common absence. As explained before, for two logs, three separate composite samples were taken at several meters distance on the same log. These samples from the same log exhibit greater dissimilarity in ordination space than those from different logs, as illustrated in (Figure 5). Stepwise model selection indicated that the bark decay stage is the best predictor of community composition. PERMANOVA analysis showed that the bark decay stage explains 15.60% of the variance (p = 0.001). The effect of the log decay stage was less pronounced, explaining an additional 7.41% (p = 0.005). The presence of regeneration (p = 0.4) was a non-significant predictor.

In the OTU approach, 50.18% of reads could not be assigned at the species level, including many large clusters. The two largest of these OTUs account for 7% of reads, and both belong to Saccharomycetales. Another 4.5% of reads can be assigned to three OTUs in the Sordariales. Other large OTUs belong to *Trichoderma* (1.6% reads), *Mortierella* (1.4% reads), and Helotiales (1.3% reads).

Fidelity analysis identified 27 and 65 taxa in the SH- and OTU approach, respectively. Results at the 0.01 significance level are presented in Table 2. Of the OTUs identified at the SH level, 18 were shared with those identified by the SH approach. Additionally, 14 SH-level high-fidelity OTUs were exclusive to the OTU approach, with only one (*Rhinocladiella*, SH0970950.10FU) surpassing the 0.01 significance threshold. In addition, indicator analysis (Indval.g function) corroborated these high-fidelity taxa as indicators at the 0.01 level and additionally identified *Pleurothecium recurvatum* (SH0926211.10FU) as an indicator for early bark decay across both approaches.

Table 2. High-fidelity taxa for the OTU- and SH approaches that met a significance threshold of $p < 0.01$. Fidelity scores are those from SH approach if taxon is present in both approaches.

DS Bark	Lowest Taxon Name	Fidelity	p	SH	OTU
Early	Chaetosphaeriaceae (SH0980871.10FU)	0.798	0.001	•	•
	Tulasnella (OTU 1097)	0.728	0.003		•
	Sordariales (SH0840221.10FU)	0.779	0.008	•	•
	Pleurothecium recurvatum (SH0926211.10FU) *	0.950	0.007	•	•
Mid	*Ganoderma adspersum* (SH0762773.10FU)	0.839	0.001	•	
	Hydnodontaceae (OTU 448)	0.729	0.004		•
	Herpotrichiellaceae (SH0970954.10FU)	0.751	0.005	•	•
	Rhinocladiella (OTU 75 | SH0970950.10FU)	0.697	0.005		•
	Helotiales (OTU 474)	0.729	0.006		•
	Mortierella (SH0960682.10FU)	0.745	0.008	•	•
	Serendipita (SH0743656.10FU)	0.730	0.008	•	•
	Chaetosphaeria decastyla (SH0980872.10FU)	0.655	0.010	•	
Late	Hyaloscyphaceae (SH0973189.10FU)	0.707	0.006	•	•
	Rozellomycota (SH0910702.10FU)	0.707	0.006	•	
	Ilyonectria mors-panacis (SH1450888.10FU)	0.707	0.007	•	
	Rozellomycota (OTU 1883)	0.711	0.007		•
	Pezizomycotina (SH0755218.10FU)	0.808	0.008	•	•
	Trichoderma (OTU 4045)	0.707	0.008		•
	Hypocreales (OTU 2917)	0.707	0.009		•
	Leotiomycetes (SH0948543.10FU)	0.707	0.010	•	•

* Additional taxon identified using Indval.g function in multiipatt (indicspecies 1.7.13); fidelity value is the indicator statistic.

3.2.4. Mycorrhizae in Decaying Beech Inner Bark

Our SH-dataset was filtered for reads of mycorrhizal taxa, which were low in abundance. Their relative read abundances in each sample are visualized in Figure 6. Ectomycorrhizal SHs accounted for slightly fewer reads than endomycorrhizal SHs (1.18% and 1.4% respectively). In soil, 3.6% of reads are considered mycorrhizal. Four Glomeromycotan and six ectomycorrhizal taxa are identified: *Lactarius subdulcis* and *Russula nigricans* (Russulaceae), *Inocybe maculata* (Inocybaceae), *Paxillus involutus* (Paxillaceae), *Tomentella sublilacina* (Thelephoraceae), and three *Laccaria* species (Hydnangiaceae). Two of these were detected as large *Laccaria* zOTUs, containing 36 and 12 sequences in our SH approach, but failed to align with our included reference sequence for *Laccaria amethystina*. At the same time, they BLASTn match with more than 99% identity to different *Laccaria* taxa. The pairwise distance between these three sequences ranges from 1.4 to 2.2%. Consequently, we incorporated these zOTUs into our reference database (SH0000009-10.10FU) and conducted a re-analysis with the updated database. These two additional references are only present in a single sample (ZF321_1), while *Laccaria amethystina* occurs in six other samples.

We detected no correlation between the presence of regeneration on logs and the number of mycorrhizal reads ($r = -0.16$). PERMANOVA on mycorrhizal taxa confirmed that the presence of regeneration ($R^2 = 0.08$, $p = 0.47$), the decay stage of bark ($R^2 = 0.11$, $p = 0.75$), and the decay stage of the log ($R^2 = 0.03$, $p = 0.93$) did not have significant effects on mycorrhizal community composition.

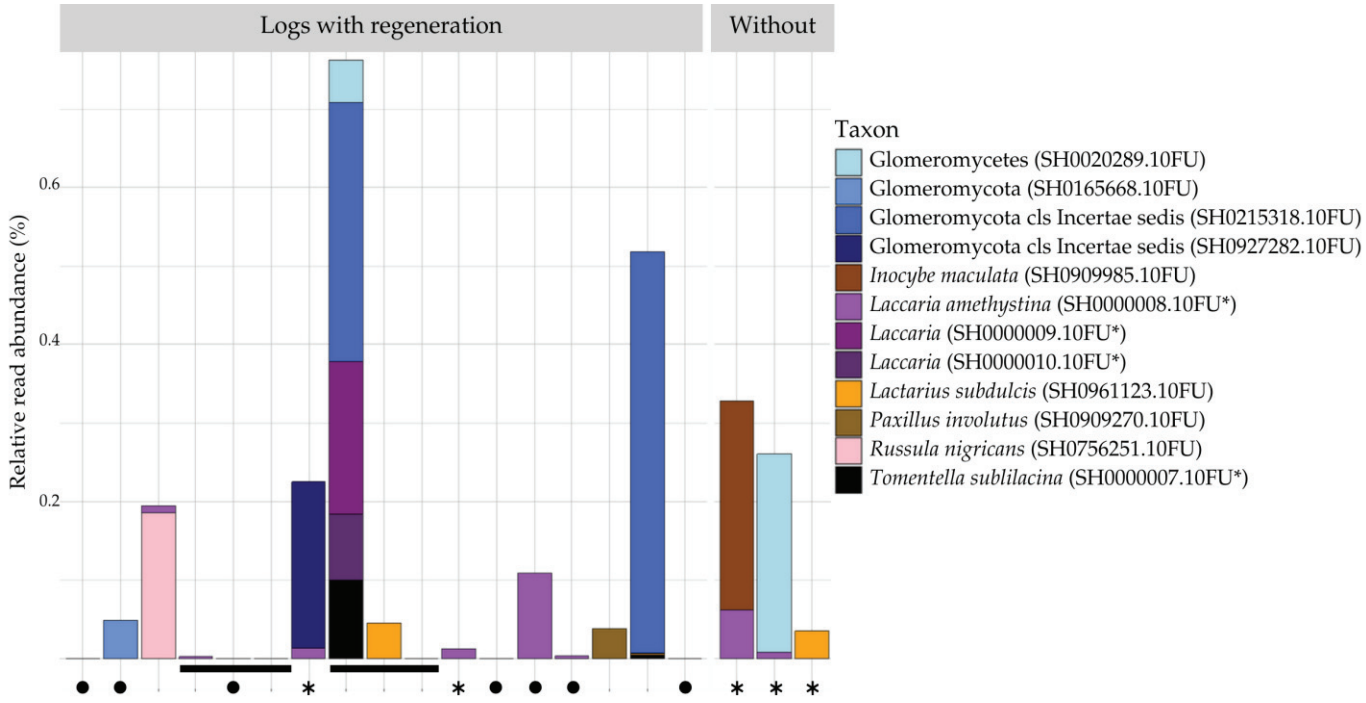


Figure 6. Relative read abundance of EcM species in bark according to presence of regeneration. Bars indicate samples from the same log. Circles indicate logs where EcM were found by morphotyping. Large asterisks under bars indicate samples not used in morphotyping. Sample names from left to right: ZF031, ZF302, ZF311, ZF319_1, ZF319_2, ZF319_3, ZF320, ZF321_1, ZF321_2, ZF321_3, ZF322, ZF323, ZF324, ZF325, ZF326, ZF327, ZF'681', ZF317, ZF328, and ZF401. * dummy SH codes.

4. Discussion

4.1. Minimum Quality Evaluation

We evaluated Nanopore sequencing for fungal metabarcoding using the full-length ITS region. We defined acceptable read quality as the point where taxonomic unit recovery stabilized, indicated by consistent recovery rates for 98% OTUs (OTU approach) or zOTUs aggregated into SHs (SH approach). While we acknowledge that annotation accuracy might improve with even fewer sequence errors, we believe such changes would be minimal and unlikely to impact biodiversity patterns in community ecology studies.

Beta-diversity comparisons of OTU tables from Q24 and higher-quality reads showed minimal differences, supporting the robustness of this threshold (Figure S2). Furthermore, the difference in OTU numbers with and without singleton exclusion remained stable within this range, indicating consistent clustering. As illustrated in Figure 2b, the number of recovered 98% OTUs declines rapidly when sequencing accuracy exceeds the clustering threshold (Q17 for 98% OTUs) and stabilizes at Q24–25, where errors minimally impact clustering.

The SH approach bypasses Phred-based filtering by prioritizing read classifiability over average base call quality. Surprisingly, the proportion of classified reads is only partly correlated to the Phred score, with a strong increase at the low end of quality up to Q16, especially in more complex datasets like our bark community (Figure S3). For higher Phred scores, classifiability is independent of the average Phred score. Therefore, beyond Q16, the average Phred score does not reliably predict classifiability.

Our experimental results demonstrate that both the SH- and OTU approach are viable and complementary due to their distinct quality filtering methods. The SH approach avoids signal loss from Phred score filtering and does not blur biological signals by predefining clustering thresholds, using mapping confidence as the quality filter instead. Because SH recovery remains stable regardless of Phred score, also when singleton zOTUs are included, the SH approach eliminates the need for Phred score filtering and singleton zOTU exclusion

Our results show that raw Nanopore data, when appropriately filtered, can support a traditional metabarcoding approach without needing to generate consensus sequences or use complex protocols like Unique Molecular Identifiers [68,69] or Rolling Circle Amplification [70]. We recommend filtering at Q25 for 98% OTUs and to re-evaluate for other clustering thresholds or marker genes. While this currently still loses much data, it effectively identifies larger OTUs, likely key drivers of ecological patterns. Moreover, this threshold can be maintained with expected improvements in Nanopore data quality [71].

While the presented methods of quality filtering are effective, there remains an unoccupied space for more sophisticated techniques. Projecting the zOTU trend (Figure 2a) suggests that Phred scores of >Q30 are necessary for zOTUs to serve as a reliable analysis unit. If such a quality threshold is reached, it opens up the possibility to use Amplicon Sequence Variants (ASVs) with DADA2-like error correction techniques, which assumes that the data contain a non-trivial fraction of error-free reads [72].

4.2. Mock Community

Both approaches on the mock community yielded similar results in terms of identified taxa. The OTU approach' shortcomings of both low data retention and a priori clustering are obvious, with *Lactifluus russulisporus* filtered out due to low abundance (no presence at ≥Q25) and *Russula nigrifacta* and *R. ustulata* being merged to a single taxon (*R. ustulata*) as they differ less than the clustering threshold.

In contrast, the SH approach demonstrated a higher resolution, with 46% of zOTUs being confidently mapped to SH, accounting for 75% of total reads (Figure S3). Classification rates increased rapidly up to a Phred score of Q16, confirming that even modest-quality reads can be reliably classified.

The taxon recovery graph (Figure 3) reveals that nearly all taxa were effectively recovered at Phred scores up to Q27. We attribute the low recovery of *L. russulisporus* to poor DNA extract quality and PCR bias [48]. Despite expecting some false positives, our analysis found no misidentifications, demonstrating the robustness of our classification thresholds.

Our study demonstrated the effectiveness of the SH approach, rather than the OTU approach, in accurately identifying closely related taxa. This is shown by the consistent detection of all species from the included *Lactifluus* and *Russula* groups across various Phred scores. We did not pick up any false positives; for example, no zOTUs matched the reference sequence for the closely related *R. ambusta*.

We recommend the routine use of mock communities as positive controls. Their use offers a low-effort strategy to evaluate both qualitative and quantitative aspects of sequencing runs. A more sophisticated mock should include taxa that are not present in the sample's locality to ensure that index-switching and cross-contamination can be attributed to the control [1]. An interesting extension of this concept are non-biological, synthetic spike-in controls, like SynMock, which mimic biological diversity without the risk of overlapping with natural taxa [73].

4.3. Inner Bark Community

Both approaches classified less than a quarter of the bark dataset reads. While the SH approach still manages to use more than double the amount of reads than the OTU approach, it is obvious that in complex and natural communities, many reads cannot be matched to a database confidently. Even with high-quality reads (Q28), only 36% of reads (31% of zOTUs, Figure S3) were identifiable at the SH level.

At the phylum level, both approaches produced broadly similar outcomes (Figure 4). However, the OTU approach detected a notably higher proportion of Mortierellomycota, largely due to two large OTUs (*Linnemannia amoeboidea*, 4099 reads; *Mortierella* sp., 3058 reads). In contrast, the SH approach yielded a greater recovery of Basidiomycota and Rozellomycota. The subtle nature of these differences suggests both approaches adequately

capture diversity. Unless stated otherwise, the species-level results discussed hereafter pertain to the SH approach.

In our bark samples, across decay stages, we found a co-dominating mix of typical soil (e.g., *Aspergillus fumigatus*) and wood-inhabiting fungi (e.g., *Subulicystidium longisporum*, *Pluteus podospileus*, and *Postia tephroleuca*). This mix reflects our characterization of the substrate as 'soil-like wood'. A significant number of reads were assignable to taxa capable of growing as yeasts (Saccharomycetales) and known mycoparasites (*Tremella*), alongside some less clearly defined taxa such as the enigmatic Rozellomycetous 'GS05' and a Hyaloriaceae SH. Interestingly, the latter is also present in the OTU approach, and a manual BLASTn search suggests these sequences likely originate from *Myxarium podlachicum* (Bres.) Raitv. (1971), a common jelly fungus in the reserve. Interestingly, members of our lab have described a mycoparasite inhabiting this species, *Slooffia micra* (Bourdot & Galzin) (Schoutteten 2023) [74], which, despite targeted efforts, has not been found in the sampled area. *S. micra* was incorporated in the latest version of UNITE [53]) as SH0867261.10FU and was recovered in relatively high abundance (213 and 64 reads in the SH- and OTU approaches, respectively). This surprising result hints that this species has part of its life cycle outside of its host basidiomes (fruitbodies were excluded from samples). Indeed, *Slooffia* spp. have been isolated as yeasts from soils, litter, and insect feces [74]. Nevertheless, at the time of writing, it had not been observed in eDNA samples on UNITE. Additionally, several species typically associated with beech deadwood, such as *Simocybe centunculus*, *Coprinellus micaceus,* and eight species of *Pluteus,* were found. Strangely, *Mycena* species, expected to be diverse and abundant, were conspicuously absent from our bark dataset. This is particularly striking given that *Mycena galericulata* and *M. haematopus* are among the most prevalent fungi on deadwood in the reserve [75,76]. The findings outlined in this paragraph highlight the added value of solid field knowledge when interpreting eDNA data.

We observed significant changes in species richness and composition corresponding to bark decay. Species richness (SR) and Shannon diversity metrics varied between early and late decay stages but never with intermediate decay. This pattern suggests that early and late decay stages represent opposite ends of a decay continuum characterized by a gradual species gain and turnover. As the bark decays, it becomes more soil-like, as demonstrated in Figure 5. However, it does not fully converge to resemble the soil community. We attribute this to the presence of colonization barriers and greater environmental fluctuations, such as variations in temperature.

The bark decay stage best explains variation in beta diversity, accounting for 15.6% of the variation, while a model incorporating both the bark and log decay stage explains approximately 23% of the variation. This suggests that the decay gradient is a primary determinant of community composition and aligns with patterns in coarse woody debris, where fungal communities vary significantly between decay stages due to shifting abiotic conditions attracting different specialized species [21,76,77]. We observed high community turnover, with intra-log communities exhibiting greater beta-diversity than those across different logs (Figure 5). This suggests that our sampling was insufficient to capture the bark community at the log level, and we hypothesize that bark volume is an important factor for community richness, provided an adequate surface is sampled.

Both fidelity and indicator analyses underscore the utility of the OTU- and SH approaches in pinpointing critical taxa, with all but one SH-level taxon being shared at a significance level of $p \leq 0.01$ (Table 2). Simultaneously, these analyses also emphasize the importance of incorporating OTUs at all taxonomic levels, as OTU-only indicators were detected at each stage of bark decay (early: *Tulasnella*; mid: Hydnodontaceae, *Rhinocladiella*, and Helotiales; late: Rozellomycota, *Trichoderma*, and Hypocreales).

The identification of decay stage-specific indicators further underpins the successional nature of bark fungal communities.

4.4. Ectomycorrhizal Colonization of Beech Deadwood

In the morphotyping analysis, around half of the investigated saplings growing on logs were colonized by EcM fungi. EcM coverage, species diversity, and the proportion of colonized saplings were significantly lower compared to the saplings growing in soil. Only two species could be identified forming associations with the saplings growing on deadwood: *Laccaria amethystina* and *Tomentella sublilacina*. *Tomentella* is a multistage, highly competitive ECM genus in mature forests [78]. *T. sublilacina* is a corticoid species forming basidiomes on wood and was also identified by Tedersoo et al. [25,79] on saplings growing on decaying logs of *Betula pendula* Roth (1788), *Picea abies* and *Nothofagus cunninghamii* (Hook.f.) Oerst (1871). Baldrian et al. [17] metabarcoded course woody debris in a beech-dominated forest and found the species to be the second most common EcM at 0.45% of reads. Interestingly, only one sapling was colonized with both *L. amethystina* and *T. sublilacina*, which hints at competitive exclusion. Indeed, *T. sublilacina* has been found to be capable of competitive exclusion of, e.g., *Tylospora fibrillosa* (Burt) Donk (1960) [25] and *Lactarius* spp. [26].

Laccaria amethystina is considered a late successional species In Europe [80] and can form basidiomes on decaying wood of beech [76], Norway spruce [81] and Silver fir [82]. This species produces small, short-lived genets dedicated to the production of meiospores [83]. Moreover, it prefers to associate with beech saplings within our study area [84]. Supporting this, Grebenc et al. [85] found a positive association between the occurrence of *L. amethystina* and the number of beech seedlings, and Hortal et al. [86] demonstrated that beech roots can be simultaneously colonized by multiple *L. amethystina* genets. These characteristics underscore its classification as an R-strategist, adept at spore production and dispersal, which explains its propensity to rapidly colonize new microsites within its late successional habitat.

Despite the relatively low abundance of mycorrhizal reads, several mycorrhizal SHs were detected. Ectomycorrhizal (EcM) species accounted for 1.18% of the total reads, while endomycorrhizal species made up a slightly higher proportion at 1.4%, as illustrated in Figure 6. We visually confirmed the presence of arbuscular mycorrhizal fungi by staining *Acer* saplings growing on certain beech logs (Personal oberservation, staining method according to Vierheilig et al. [87]). Supporting our observations, Baldrian et al. [17] found EcM fungi in similarly low abundances across early and intermediate log decay stages of beech, only becoming more abundant in late log DS. Our analysis revealed no significant correlation between the presence of logs with and without regeneration. This suggests that while specific mycorrhizal taxa are effectively colonizing decaying bark, their distribution is independent of sapling presence. The absence of correlation indicates that other environmental or biological factors have a more pronounced impact on shaping these mycorrhizal communities. Our metabarcoding results offered limited insights into the presence of ectomycorrhizal (EcM) fungi in deadwood. In contrast, morphotyping is per definition more detailed as it also demonstrates successful establishment. Like the results of our morphotyping analysis, EcM read abundance and diversity are higher in soil than in bark, with EcM diversity in bark being a subset of that in soil. Thus, both methods indicate that soil is the more beneficial habitat for mycorrhization.

Across our analyses, *L. amethystina* and *T. sublilacina* are identified as the key EcM in bark. In terms of EcM establishment, two critical factors can be identified: the source of the inoculum (via propagules or mycelium emerging from the soil) and the timing of arrival (before or after seedlings arrive). Mycelia in the soil may respond to the presence of deadwood by initiating growth into it. Initially, wood is resistant to penetration, but inner bark, with its softer consistency and quicker degradation, may serve as an early colonization pathway for soil-based EcM. Another possibility is that mycelium grows out of the soil regardless, as some fungi, such as *Tomentella* spp., are known to use wood as a substrate for fruiting. Alternatively, EcM can establish within deadwood bark through propagules, deposited either from the air or vectored by arthropods. The latter route

benefits from direct deposition into the decaying substrate, a process well-supported by studies demonstrating the effectiveness of arthropods as fungal vectors [88–90].

While EcM are able to colonize deadwood, their viability in the absence of seedlings remains uncertain. Without seedlings, deadwood could act as a refuge from intense competition in the soil among well-established mycelia linked within the EcM network, especially among mature beeches. Such EcM may utilize delignified carbohydrates as a carbon source while awaiting their symbiotic partners [91,92], although such capabilities are now questioned [23]. Still, several studies suggest that certain EcM can contribute to decomposition [93,94]. This process is likely not targeted at carbon acquisition but rather helps mobilize nitrogen from organic matter [23,95], which could enhance seedling establishment. Thus, the formation of common mycelial networks prior to the arrival of saplings could explain the enhanced sapling establishment sometimes observed in these specific forest microhabitats [25]. Alternatively, successful EcM establishment might require germination in the presence of roots, raising questions about whether the EcM reads detected in logs without seedlings are from spores, mycelia doomed to perish, or necromass. Our data present mixed signals. First, there is no evidence that EcM accumulation correlates with the bark decay stage (DS), suggesting either that establishment is difficult after early bark DS or, more likely, that EcM do not accumulate in time. Second, the absence of a signal of beech regeneration on mycorrhizal reads indicates that they occur independently of their partners. This dual pattern supports our belief that colonization can happen in the absence of seedlings, but forming symbiosis is crucial for the continued survival of mycorrhizae in decaying bark. Mechanistic experiments (e.g., Fukasawa and Kitabatake [96]) or sampling forests without natural regeneration would enhance our understanding.

4.5. Database

By prioritizing the classifiability of our data within the SH framework, our study demonstrates that sequences, even those with moderate average quality, can be accurately classified. User-defined references can also be included if existing SHs are inadequate, as demonstrated in our analysis of mock and bark samples. For example, we added references for mock and ectomycorrhizal taxa that could not be confidently assigned to a SH. Unfortunately, incorporating such references also hampers cross-study communication of taxa. In that regard, the nascent SH-matching tool [97] deserves further attention as it makes the public assignment of new SH possible, but we did not extensively test it.

We assumed EcM in our sampling area to be well documented in the database, and indeed, many reference sequences are available for, e.g., *Laccaria amethystina*. Nevertheless, we encountered difficulties in mapping zOTUs of *Laccaria* and *Tomentella* to SH, as well as issues with the interpretation of some taxon names in SHs with many associated voucher sequences. These problems may stem from the proliferation of sequence data and inconsistent sequence annotations, which complicate the precise definition and annotation of SHs. Addressing these challenges will require manual curation, a daunting task at the scale of UNITE.

We recommend leveraging reference-based approaches, such as the SH approach, in well-characterized communities, i.e., in regions or substrates that have been extensively sampled. A significant benefit of this approach is superior data retention and aggregation at the SH level, facilitating communication and comparisons of taxonomic units across analyses and studies and enhancing reproducibility.

4.6. Nanopore Metabarcoding

We found Nanopore to be a suitable platform for metabarcoding, although currently, only a fraction of the generated data meet the quality required for broad-scale adoption. Despite these limitations, the platform offers unique advantages beyond the elimination of traditional read length constraints, making it particularly advantageous in the field of mycology, which heavily involves citizen scientists [98,99]. The low initial capital investment and the presence of an active user community contribute to its accessibility,

which makes it a practical option for both amateurs and smaller research groups. Moreover, the ability to conduct in-house sequencing eliminates the need for outsourcing, thereby providing autonomy over workflows and data, empowering especially citizen scientists.

The Nanopore metabarcoding field is experiencing rapid growth, with a variety of tools and analysis strategies being developed. We built eNano to be a simple-to-understand tool with straightforward integration of standard metabarcoding steps. Therefore, it is not designed to outperform emerging tools but rather to serve as a valuable baseline for comparison. The simple installation process (a single binary file) and the clarity of the procedures make eNano also suitable for educational purposes.

Considering the dynamic nature of this field, we recommend that researchers also explore other strategies like implementing Unique Molecular Identifiers [68,69] or tools such as EMU [100] and PIMENTA [101]. Noteworthy alternatives such as Decona [13] and CONCOMPRA [15] do not require reference databases to generate taxonomic units and have been demonstrated to be viable alternatives [11,15,102]. Regardless of the approach, benchmarking tools should ideally include a baseline for comparison in the form of a properly quality-filtered OTU table generated using the OTU approach.

5. Conclusions

This study evaluates the effectiveness of Nanopore sequencing for fungal metabarcoding using the full-length ITS region through the analysis ofboth a mock and natural community. We demonstrate that both the reference-based SH approach (mapping reads to a database) and the OTU approach (de novo clustering) are viable options. The SH approach ensures stable taxonomic unit recovery and is only minimally impacted by low Phred scores (<Q16) when strict mapping criteria are applied. The OTU approach is feasible but requires stricter quality filtering, which currently results in significant data loss. However, it is capable of identifying taxonomic units that are not represented in existing databases. We recommend using reads with a quality score of $\geq$Q25 when constructing 98% OTUs.

Our analysis of fungal communities in decaying bark emphasizes the decay gradient as a primary determinant of community composition. Ectomycorrhizal fungi are found to be less diverse and abundant in bark compared to soil, indicating that soil provides a more favorable environment for mycorrhization. Despite this, *Laccaria amethystina* and *Tomentella sublilacina* are identified as key species colonizing decaying bark and capable of successful establishment. These findings suggest that decaying bark can serve as a microhabitat for specific mycorrhizal species, providing a potential explanation for the presence of mycorrhizae, which are observed in early decay stages in other metabarcoding studies on deadwood.

We introduce the eNano tool, which offers a simple baseline approach to Nanopore metabarcoding and is suitable for broad adoption. Overall, Nanopore offers a promising platform for fungal metabarcoding, with the potential to yield valuable ecological insights and engage a wider audience of researchers and citizen scientists. As read quality continues to improve, the use of Nanopore data in a more classical metabarcoding fashion, whether through reference databases or by constructing OTUs, is likely to take hold.

Supplementary Materials: The following supporting information can be downloaded at https://www.mdpi.com/article/10.3390/jof10100708/s1, Figure S1. Density histogram of SINTAX confidence values at SH-level; Figure S2. Heatmaps of Beta diversity in Bray–Curtis distance between subsampled Phred-specific datasets; Figure S3. Classification rates of zOTUs in SH-approach; Table S1. Overview of sampled logs; Table S2. Mock community composition; Table S3. Mycorrhization and morphotyping results; Table S4. Sanger sequencing results of root tip morphotypes; File S1. OpenDocument Spreadsheet with OTU-tables.

Author Contributions: Conceptualization, G.D., K.V. and A.V.; Formal analysis, G.D. and L.T.; Funding acquisition, G.D., K.V. and A.V.; Investigation, G.D. and L.T.; Methodology, G.D., L.T. and P.A.; Project administration, G.D., K.V. and A.V.; Resources, K.V. and A.V.; Software, G.D. and P.A.;

Supervision, K.V. and A.V.; Visualization, G.D.; Writing—original draft, G.D. and L.T.; Writing—review and editing, G.D., L.T., P.A., K.V. and A.V. All authors have read and agreed to the published version of the manuscript.

Funding: This research was funded by Research Foundation Flanders (Belgium), grant numbers 1126221N and 1126223N, the Research Institute for Nature and Forest (INBO), and Research Group Mycology at Ghent University.

Data Availability Statement: The original contributions presented in the study are included in the article and Supplementary Materials. Sequence data can be accessed as fastq files at the NCBI Sequence Read Archive under BioProject ID PRJNA1151640.

Acknowledgments: We thank the forest ecology and management team at INBO for providing data on deadwood.

Conflicts of Interest: The authors declare no conflicts of interest. The funders had no role in the design of the study, in the collection, analyses, or interpretation of data, in the writing of the manuscript, or in the decision to publish the results.

References

1. Tedersoo, L.; Bahram, M.; Zinger, L.; Nilsson, R.H.; Kennedy, P.G.; Yang, T.; Anslan, S.; Mikryukov, V. Best Practices in Metabarcoding of Fungi: From Experimental Design to Results. *Mol. Ecol.* **2022**, *31*, 2769–2795. [CrossRef]
2. Nilsson, R.H.; Tedersoo, L.; Ryberg, M.; Kristiansson, E.; Hartmann, M.; Unterseher, M.; Porter, T.M.; Bengtsson-Palme, J.; Walker, D.M.; De Sousa, F.; et al. A Comprehensive, Automatically Updated Fungal ITS Sequence Dataset for Reference-Based Chimera Control in Environmental Sequencing Efforts. *Microbes Environ.* **2015**, *30*, 145–150. [CrossRef]
3. Schoch, C.L.; Seifert, K.A.; Huhndorf, S.; Robert, V.; Spouge, J.L.; Levesque, C.A.; Chen, W.; Bolchacova, E.; Voigt, K.; Crous, P.W.; et al. Nuclear Ribosomal Internal Transcribed Spacer (ITS) Region as a Universal DNA Barcode Marker for Fungi. *Proc. Natl. Acad. Sci. USA* **2012**, *109*, 6241–6246. [CrossRef]
4. Oxford Nanopore Technologies. Available online: https://nanoporetech.com/platform/accuracy (accessed on 4 January 2024).
5. Wilson, A.W.; Eberhardt, U.; Nguyen, N.; Noffsinger, C.R.; Swenie, R.A.; Loucks, J.L.; Perry, B.A.; Herrera, M.; Osmundson, T.W.; DeLong-Duhon, S.; et al. Does One Size Fit All? Variations in the DNA Barcode Gaps of Macrofungal Genera. *J. Fungi* **2023**, *9*, 788. [CrossRef]
6. Davidov, K.; Iankelevich-Kounio, E.; Yakovenko, I.; Koucherov, Y.; Rubin-Blum, M.; Oren, M. Identification of Plastic-Associated Species in the Mediterranean Sea Using DNA Metabarcoding with Nanopore MinION. *Sci. Rep.* **2020**, *10*, 17533. [CrossRef]
7. Kaire, L.; Kalev, A.; Mohammad, B.; Rasmus, P.; Sten, A.; Riinu, K.; Rein, D. Tedersoo Leho Relative Performance of MinION (Oxford Nanopore Technologies) versus Sequel (Pacific Biosciences) Third-Generation Sequencing Instruments in Identification of Agricultural and Forest Fungal Pathogens. *Appl. Environ. Microbiol.* **2019**, *85*, e01368-19. [CrossRef]
8. Theologidis, I.; Karamitros, T.; Vichou, A.-E.; Kizis, D. Nanopore-Sequencing Metabarcoding for Identification of Phytopathogenic and Endophytic Fungi in Olive (*Olea Europaea*) Twigs. *J. Fungi* **2023**, *9*, 1119. [CrossRef]
9. Langsiri, N.; Worasilchai, N.; Irinyi, L.; Jenjaroenpun, P.; Wongsurawat, T.; Luangsa-ard, J.J.; Meyer, W.; Chindamporn, A. Targeted Sequencing Analysis Pipeline for Species Identification of Human Pathogenic Fungi Using Long-Read Nanopore Sequencing. *IMA Fungus* **2023**, *14*, 18. [CrossRef]
10. Groben, G.; Clarke, B.B.; Kerkhof, L.J.; Bonos, S.A.; Meyer, W.A.; Qu, Y.; Luo, J.; Walsh, E.; Zhang, N. Mycobiome Analysis of Tall Fescue Grass under Drought Stress Using the Illumina MiSeq and Oxford Nanopore Technology MinION. *Phytobiomes J.* **2023**, *7*, 413–423. [CrossRef]
11. Lysenko, L.; Griem, E.; Wagener, P.; Langer, E.J. Fungi Associated with Fine Roots of Fraxinus Excelsior Affected by Ash Dieback Detected by Next-Generation Sequencing. *J. Plant Dis. Prot.* **2024**. [CrossRef]
12. Andrews, S. FastQC: A Quality Control Tool for High Throughput Sequence Data. 2010. Available online: http://www.bioinformatics.babraham.ac.uk/projects/fastqc (accessed on 4 January 2024).
13. Oosterbroek, S.; Doorenspleet, K.; Nijland, R.; Jansen, L. Decona: From Demultiplexing to Consensus for Nanopore Amplicon Data. *ARPHA Conf. Abstr.* **2021**, *4*, e65029. [CrossRef]
14. Maestri, S.; Cosentino, E.; Paterno, M.; Freitag, H.; Garces, J.M.; Marcolungo, L.; Alfano, M.; Njunjić, I.; Schilthuizen, M.; Slik, F.; et al. A Rapid and Accurate MinION-Based Workflow for Tracking Species Biodiversity in the Field. *Genes* **2019**, *10*, 468. [CrossRef] [PubMed]
15. Stock, W.; Rousseau, C.; Dierickx, G.; D'hondt, S.; Martínez, L.A.; Dittami, S.M.; van der Loos, L.; Clerck, O.D. Breaking Free from References: A Consensus-Based Approach for Community Profiling with Long Amplicon Nanopore Data. *bioRxiv* **2024**. [CrossRef]
16. Christy, E.J.; Sollins, P.; Trappe, J.M. First-Year Survival of Tsuga Heterophylla without Mycorrhizae and Subsequent Ectomycorrhizal Development on Decaying Logs and Mineral Soil. *Can. J. Bot.* **1982**, *60*, 1601–1605. [CrossRef]
17. Baldrian, P.; Zrůstová, P.; Tláskal, V.; Davidová, A.; Merhautová, V.; Vrška, T. Fungi Associated with Decomposing Deadwood in a Natural Beech-Dominated Forest. *Fungal Ecol.* **2016**, *23*, 109–122. [CrossRef]

18. Kubartová, A.; Ottosson, E.; Dahlberg, A.; Stenlid, J. Patterns of Fungal Communities among and within Decaying Logs, Revealed by 454 Sequencing. *Mol. Ecol.* **2012**, *21*, 4514–4532. [CrossRef]
19. Rajala, T.; Peltoniemi, M.; Hantula, J.; Mäkipää, R.; Pennanen, T. RNA Reveals a Succession of Active Fungi during the Decay of Norway Spruce Logs. *Fungal Ecol.* **2011**, *4*, 437–448. [CrossRef]
20. Mäkipää, R.; Rajala, T.; Schigel, D.; Rinne, K.T.; Pennanen, T.; Abrego, N.; Ovaskainen, O. Interactions between Soil- and Dead Wood-Inhabiting Fungal Communities during the Decay of Norway Spruce Logs. *ISME J.* **2017**, *11*, 1964–1974. [CrossRef]
21. Rajala, T.; Tuomivirta, T.; Pennanen, T.; Mäkipää, R. Habitat Models of Wood-Inhabiting Fungi along a Decay Gradient of Norway Spruce Logs. *Fungal Ecol.* **2015**, *18*, 48–55. [CrossRef]
22. Bödeker, I.T.M.; Nygren, C.M.R.; Taylor, A.F.S.; Olson, A.; Lindahl, B.D. ClassII Peroxidase-Encoding Genes Are Present in a Phylogenetically Wide Range of Ectomycorrhizal Fungi. *ISME J.* **2009**, *3*, 1387–1395. [CrossRef]
23. Lindahl, B.D.; Tunlid, A. Ectomycorrhizal Fungi–Potential Organic Matter Decomposers, yet Not Saprotrophs. *New Phytol.* **2015**, *205*, 1443–1447. [CrossRef]
24. Lindahl, B.; Stenlid, J.; Olsson, S.; Finlay, R. Translocation of 32P between Interacting Mycelia of a Wood-Decomposing Fungus and Ectomycorrhizal Fungi in Microcosm Systems. *New Phytol.* **1999**, *144*, 183–193. [CrossRef]
25. Tedersoo, L.; Suvi, T.; Jairus, T.; Kõljalg, U. Forest Microsite Effects on Community Composition of Ectomycorrhizal Fungi on Seedlings of Picea Abies and Betula Pendula. *Environ. Microbiol.* **2008**, *10*, 1189–1201. [CrossRef]
26. Poznanovic, S.K.; Lilleskov, E.A.; Webster, C.R. Sharing Rotting Wood in the Shade: Ectomycorrhizal Communities of Co-Occurringbirch and Hemlock Seedlings. *Mycorrhiza* **2015**, *25*, 153–164. [CrossRef]
27. Kropp, B.R. Fungi from Decayed Wood as Ectomycorrhizal Symbionts of Western Hemlock. *Can. J. For. Res.* **1982**, *12*, 36–39. [CrossRef]
28. Orrego, G. Western Hemlock Regeneration on Coarse Woody Debris Is Facilitated by Linkage into a Mycorrhizal Network in an Old-Growth Forest. Master's Thesis, The University of British Columbia, Vancouver, BC, Canada, 2018.
29. Tedersoo, L.; Kõljalg, U.; Hallenberg, N.; Larsson, K.-H. Fine Scale Distribution of Ectomycorrhizal Fungi and Roots across Substrate Layers Including Coarse Woody Debris in a Mixed Forest. *New Phytol.* **2003**, *159*, 153–165. [CrossRef] [PubMed]
30. Kluting, K.; Strid, Y.; Six, D.; Rosling, A. Forest Fire Influence on Tomicus Piniperda-Associated Fungal Communities and Phloem Nutrient Availability of Colonized Pinus Sylvestris. *Microb. Ecol.* **2023**, *86*, 224–239. [CrossRef]
31. Rumpf, S.; Schönfelder, E.; Ahrends, B. 3 Biometrische Schätzmodelle für Nährelementgehalte in Baumkompartimenten. *Freibg. Forstl. Forsch.* **2018**, *101*, 33–73.
32. Mussche, S.; Bussche, B.; De Schrijver, A.; Neirynck, J.; Nachtergale, L.; Lust, N. Nutrient Uptake of a Mixed Oak/Beech Forest in Flanders (Belgium). *Silva Gandav.* **1998**, *63*, 120–133. [CrossRef]
33. André, F.; Jonard, M.; Ponette, Q. Biomass and Nutrient Content of Sessile Oak (*Quercus Petraea* (Matt.) Liebl.) and Beech (*Fagus sylvatica* L.) Stem and Branches in a Mixed Stand in Southern Belgium. *Sci. Total Environ.* **2010**, *408*, 2285–2294. [CrossRef]
34. Ahrends, B.; Von Wilpert, K.; Weis, W.; Vonderach, C.; Kändler, G.; Zirlewagen, D.; Sucker, C.; Puhlmann, H. Merits and Limitations of Element Balances as a Forest Planning Tool for Harvest Intensities and Sustainable Nutrient Management—A Case Study from Germany. *Soil Syst.* **2022**, *6*, 41. [CrossRef]
35. Vandekerkhove, K.; Deforce, K.; Bastiaens, J. Historic-Ecological Position of Beech in the Area of the Sonian Forest and an Overview of Beech-Forest-Related Biodiversity Present in the Forest. In *Onderzoeksrapport*; Instituut voor Natuur- en Bosonderzoek: Brussels, Belgium, 2018.
36. De Keersmaeker, L.; Esprit, M.; Goessens, S.; Anja, L.; Thomaes, A.; Van de Kerckhove, P.; Vandekerkhove, K. Monitoring Programme on Strict Forest Reserves in Flanders (Belgium)—Site Level Stand Structure, Regeneration and Vegetation Data. In *Onderzoeksrapport*; Instituut voor Natuur- en Bosonderzoek: Brussels, Belgium, 2023.
37. Renvall, P. Community Structure and Dynamics of Wood-Rotting Basidiomycetes on Decomposing Conifer Trunks in Northern Finland. *Karstenia* **1995**, *35*, 1–51. [CrossRef]
38. Agerer, R. Studies on Ectomycorrhizae II. Introducing Remarks on Characterisation and Identification. *Mycotaxon* **1986**, *26*, 473–492.
39. Agerer, R. Studies on Ectomycorrhizae III. Mycorrhizae Formed by Four Fungi in the Genera Lactarius and Russula on Spruce. *Mycotaxon* **1986**, *27*, 1–59.
40. Agerer, R. (Ed.) *Colour Atlas of Ectomycorrhizae*, 1st–11th ed.; Einhorn: Schwäbisch Gmünd, Germany, 1987.
41. Agerer, R. Characterisation of Ectomycorrhiza. In *Methods in Microbiology*; Norris, J.R., Read, D.J., Varma, A.K., Eds.; Academic Press Limited: New York, NY, USA, 1991; Volume 23, pp. 25–73.
42. Agerer, R. Anatomical Characteristics of Identified Ectomycorrhizas: An Attempt towards a Natural Classification. In *Mycorrhiza: Structure, Function, Molecular Biology and Biotechnology*; Springer: Berlin/Heidelberg, Germany, 1995.
43. Agerer, R.; Danielson, R.M.; Egli, S.; Ingleby, K.; Luoma, D.; Treu, R. *Descriptions of Ectomycorrhizae*; Einhorn: Schwäbisch Gmünd, Germany, 1996.
44. Nuytinck, J.; Verbeken, A. Lactarius Sanguifluus versus Lactarius Vinosus—Molecular and Morphological Analyses. *Mycol. Prog.* **2003**, *2*, 227–234. [CrossRef]
45. Doyle, J.J.; Doyle, J.L. A rapid DNA isolation procedure for small quantities of fresh leaf tissue. *Phytochem. Bull.* **1987**, *19*, 11–15.
46. Gardes, M.; Bruns, T.D. ITS primers with enhanced specificity for basidiomycetes-application to the identification of mycorrhizae and rusts. *Mol. Ecol.* **1993**, *2*, 113–118. [CrossRef]

47. White, T.J.; Bruns, T.; Lee SJ, W.T.; Taylor, J. Amplification and direct sequencing of fungal ribosomal RNA genes for phylogenetics. In *PCR Protocols: A Guide to Methods and Applications*; Academic Press, Inc.: New York, NY, USA, 1990; Volume 18, pp. 315–322.
48. Dierickx, G.; Froyen, M.; Halling, R.; Wisitrassameewong, K.; Delgat, L.; De Crop, E.; Verbeken, M. Updated Taxonomy of Lactifluus Section Luteoli: *L. Russulisporus* from Australia and *L. Caliendrifer* from Thailand. *Mycokeys* **2019**, *56*, 13–32. [CrossRef]
49. De Lange, R.; Adamčík, S.; Adamčíkova, K.; Asselman, P.; Borovička, J.; Delgat, L.; Hampe, F.; Verbeken, A. Enlightening the Black and White: Species Delimitation and UNITE Species Hypothesis Testing in the Russula Albonigra Species Complex. *IMA Fungus* **2021**, *12*, 20. [CrossRef]
50. De Crop, E.; Lescroart, J.; De Lange, R.; Van de Putte, K.; Verbeken, A. *Lactifluus bicapillus* (Russulales, Russulaceae), a new species from the Guineo-Congolian rainforest. *MycoKeys* **2019**, *45*, 25. [CrossRef]
51. Malysheva, V.; Spirin, V.; Schoutteten, N.; De Lange, R.; Pennanen, J.; Larsson, K.H. New and noteworthy species of Helicogloea (Atractiellomycetes, Basidiomycota) from Europe. In *Annales Botanici Fennici*; Finnish Zoological and Botanical Publishing Board: Helsinki, Finland, 2020; Volume 57, No. 1–3, pp. 1–7.
52. Tedersoo, L.; Bahram, M.; Ryberg, M.; Otsing, E.; Koljalg, U.; Abarenkov, K. Global Biogeography of the Ectomycorrhizal /Sebacina Lineage (Fungi, Sebacinales) as Revealed from Comparative Phylogenetic Analyses. *Mol. Ecol.* **2014**, *23*, 4168–4183. [CrossRef]
53. Abarenkov, K.; Nilsson, R.H.; Larsson, K.-H.; Taylor, A.F.S.; May, T.W.; Frøslev, T.G.; Pawlowska, J.; Lindahl, B.; Põldmaa, K.; Truong, C.; et al. The UNITE Database for Molecular Identification and Taxonomic Communication of Fungi and Other Eukaryotes: Sequences, Taxa and Classifications Reconsidered. *Nucleic Acids Res.* **2024**, *52*, D791–D797. [CrossRef] [PubMed]
54. Wick, R. Porechop: Adapter Trimmer for Oxford Nanopore Reads. 2018. Available online: https://github.com/rrwick/Porechop (accessed on 4 January 2024).
55. Martin, M. Cutadapt Removes Adapter Sequences from High-Throughput Sequencing Reads. *EMBnet. J.* **2011**, *17*, 10–12. [CrossRef]
56. De Coster, W.; Rademakers, R. NanoPack2: Population-Scale Evaluation of Long-Read Sequencing Data. *Bioinformatics* **2023**, *39*, btad311. [CrossRef]
57. Rognes, T.; Flouri, T.; Nichols, B.; Quince, C.; Mahé, F. VSEARCH: A Versatile Open Source Tool for Metagenomics. *PeerJ* **2016**, *4*, e2584. Available online: https://www.ncbi.nlm.nih.gov/pmc/articles/PMC5075697/pdf/peerj-04-2584.pdf (accessed on 4 January 2024). [CrossRef]
58. Edgar, R.C. SINTAX: A Simple Non-Bayesian Taxonomy Classifier for 16S and ITS Sequences. *bioRxiv* **2016**. [CrossRef]
59. Frøslev, T.G.; Kjøller, R.; Bruun, H.H.; Ejrnæs, R.; Brunbjerg, A.K.; Pietroni, C.; Hansen, A.J. Algorithm for Post-Clustering Curation of DNA Amplicon Data Yields Reliable Biodiversity Estimates. *Nat. Commun.* **2017**, *8*, 1188. [CrossRef]
60. Frederic-Mahe/Mumu: C++ Implementation of Lulu, a R Package for Post-Clustering Curation of Metabarcoding Data. Available online: https://github.com/frederic-mahe/mumu (accessed on 5 October 2024).
61. McMurdie, P.J.; Holmes, S. Phyloseq: An R Package for Reproducible Interactive Analysis and Graphics of Microbiome Census Data. *PLoS ONE* **2013**, *8*, e61217. [CrossRef]
62. Mikryukov, V. metagMisc: Miscellaneous Functions for Metagenomic Data Analysis. 2018. Available online: https://github.com/vmikk/metagMisc (accessed on 4 January 2024).
63. Oksanen, J.; Blanchet, F.G.; Kindt, R.; Legendre, P.; Minchin, P.R.; O'hara, R.; Simpson, G.L.; Solymos, P.; Stevens, M.H.H.; Wagner, H. Package 'Vegan'. *Community Ecol. Package Version* **2013**, *2*, 1–295.
64. Corcoran, D. AICcPermanova: Model Selection of PERMANOVA Models Using AICc (Version 0.0.2). R Package. 2023. Available online: https://cran.r-project.org/package=AICcPermanova (accessed on 4 January 2024).
65. De Cáceres, M.; Legendre, P. Associations between species and groups of sites: Indices and statistical inference. *Ecology* **2009**, *90*, 3566–3574. [CrossRef]
66. Nguyen, N.H.; Song, Z.; Bates, S.T.; Branco, S.; Tedersoo, L.; Menke, J.; Schilling, J.S.; Kennedy, P.G. FUNGuild: An Open Annotation Tool for Parsing Fungal Community Datasets by Ecological Guild. *Fungal Ecol.* **2016**, *20*, 241–248. [CrossRef]
67. R Core Team. *R: A Language and Environment for Statistical Computing*; R Foundation for Statistical Computing: Vienna, Austria, 2022.
68. Karst, S.M.; Ziels, R.M.; Kirkegaard, R.H.; Sørensen, E.A.; McDonald, D.; Zhu, Q.; Knight, R.; Albertsen, M. Enabling High-Accuracy Long-Read Amplicon Sequences Using Unique Molecular Identifiers with Nanopore or PacBio Sequencing. *Nat. Methods* **2021**, *18*, 165–169. [CrossRef]
69. Lin, X.; Waring, K.; Tyson, J.; Ziels, R.M. High-Accuracy Meets High-Throughput for Microbiome Profiling with near Full-Length 16S rRNA Amplicon Sequencing on the Nanopore Platform. *bioRxiv* **2023**. [CrossRef]
70. Baloğlu, B.; Chen, Z.; Elbrecht, V.; Braukmann, T.; MacDonald, S.; Steinke, D. A Workflow for Accurate Metabarcoding Using Nanopore MinION Sequencing. *Methods Ecol. Evol.* **2021**, *12*, 794–804. [CrossRef]
71. Oxford Nanopore Announces Breakthrough Technology Performance to Deliver Complete Human Genome Assemblies and Richer Multiomic Data in London Calling. Available online: https://nanoporetech.com/news/oxford-nanopore-announces-breakthrough-technology-performance-to-deliver-complete-human-genomes-and-richer-multiomic-data-in-london-calling-tech-update (accessed on 26 August 2024).
72. Callahan, B.J.; McMurdie, P.J.; Rosen, M.J.; Han, A.W.; Johnson, A.J.A.; Holmes, S.P. DADA2: High-Resolution Sample Inference from Illumina Amplicon Data. *Nat. Methods* **2016**, *13*, 581–583. [CrossRef]

73. Palmer, J.M.; Jusino, M.A.; Banik, M.T.; Lindner, D.L. Non-Biological Synthetic Spike-in Controls and the AMPtk Software Pipeline Improve Mycobiome Data. *PeerJ* **2018**, *6*, e4925. [CrossRef]
74. Schoutteten, N.; Yurkov, A.; Leroux, O.; Haelewaters, D.; Van Der Straeten, D.; Miettinen, O.; Boekhout, T.; Begerow, D.; Verbeken, A. Diversity of Colacosome-Interacting Mycoparasites Expands the Understanding of the Evolution and Ecology of Microbotryomycetes. Available online: https://www.ingentaconnect.com/content/wfbi/sim/pre-prints/content-a2_sim_vol106_art2;jsessionid=1tl834f1c8ks.x-ic-live-03# (accessed on 3 August 2023).
75. Walleyn, R.; Vandekerkhove, K. Diversiteit, Ecologie en Indicatorwaarde van Paddestoelen op Groot Dood Beukenhout in Het Bosreservaat Kersselaerspleyn (Zoniënwoud). In *Onderzoeksrapport*; Instituut voor Bosbouw en Wildbeheer: Brussels, Belgium, 2002.
76. Ódor, P.; Heilmann-Clausen, J.; Christensen, M.; Aude, E.; van Dort, K.W.; Piltaver, A.; Siller, I.; Veerkamp, M.T.; Walleyn, R.; Standovár, T.; et al. Diversity of Dead Wood Inhabiting Fungi and Bryophytes in Semi-Natural Beech Forests in Europe. *Biol. Conserv.* **2006**, *131*, 58–71. [CrossRef]
77. Heilmann-Clausen, J.; Christensen, M. Fungal Diversity on Decaying Beech Logs—Implications for Sustainable Forestry. *Biodivers. Conserv.-Biodivers Conserv.* **2003**, *12*, 953–973. [CrossRef]
78. Burke, D.J.; López-Gutiérrez, J.C.; Smemo, K.A.; Chan, C.R. Vegetation and Soil Environment Influence the Spatial Distribution of Root-Associated Fungi in a Mature Beech-Maple Forest. *Appl. Environ. Microbiol.* **2009**, *75*, 7639–7648. [CrossRef]
79. Tedersoo, L.; Gates, G.; Dunk, C.W.; Lebel, T.; May, T.W.; Kõljalg, U.; Jairus, T. Establishment of Ectomycorrhizal Fungal Community on Isolated Nothofagus Cunninghamii Seedlings Regenerating on Dead Wood in Australian Wet Temperate Forests: Does Fruit-Body Type Matter? *Mycorrhiza* **2009**, *19*, 403–416. [CrossRef] [PubMed]
80. Vincenot, L.; Nara, K.; Sthultz, C.; Labbé, J.; Dubois, M.; Tedersoo, L.; Martin, F.; Selosse, M. Extensive Gene Flow over Europe and Possible Speciation over Eurasia in the Ectomycorrhizal Basidiomycete *Laccaria Amethystina* Complex. *Mol. Ecol.* **2012**, *21*, 281–299. [CrossRef]
81. Holec, J.; Kučera, T.; Běťák, J.; Hort, L. Macrofungi on Large Decaying Spruce Trunks in a Central European Old-Growth Forest: What Factors Affect Their Species Richness and Composition? *Mycol. Prog.* **2020**, *19*, 53–66. [CrossRef]
82. Holec, J.; Kučera, T. Richness and Composition of Macrofungi on Large Decaying Trees in a Central European Old-Growth Forest: A Case Study on Silver Fir (*Abies Alba*). *Mycol. Prog.* **2020**, *19*, 1429–1443. [CrossRef]
83. Fiore-Donno, A.-M.; Martin, F. Populations of Ectomycorrhizal Laccaria Amethystina and Xerocomus Spp. Show Contrasting Colonization Patterns in a Mixed Forest. *New Phytol.* **2001**, *152*, 533–542. [CrossRef] [PubMed]
84. Boeraeve, M.; Everts, T.; Vandekerkhove, K.; De Keersmaeker, L.; Van de Kerckhove, P.; Jacquemyn, H. Partner Turnover and Changes in Ectomycorrhizal Fungal Communities during the Early Life Stages of European Beech (*Fagus sylvatica* L.). *Mycorrhiza* **2021**, *31*, 43–53. [CrossRef]
85. Grebenc, T.; Christensen, M.; Vilhar, U.; Cater, M.; Martin, M.P.; Simoncic, P.; Kraigher, H. Response of Ectomycorrhizal Community Structure to Gap Opening in Natural and Managed Temperate Beech-Dominated Forests. *Can. J. For. Res.* **2009**, *39*, 1375–1386. [CrossRef]
86. Hortal, S.; Trocha, L.K.; Murat, C.; Chybicki, I.J.; Buée, M.; Trojankiewicz, M.; Burczyk, J.; Martin, F. Beech Roots Are Simultaneously Colonized by Multiple Genets of the Ectomycorrhizal Fungus Laccaria Amethystina Clustered in Two Genetic Groups. *Mol. Ecol.* **2012**, *21*, 2116–2129. [CrossRef]
87. Vierheilig, H.; Coughlan, A.P.; Wyss, U.; Piche, Y. Ink and Vinegar, a Simple Staining Technique for Arbuscular-Mycorrhizal Fungi. *Appl. Environ. Microbiol.* **1998**, *64*, 5004–5007. [CrossRef]
88. Lilleskov, E.A.; Bruns, T.D. Spore Dispersal of a Resupinate Ectomycorrhizal Fungus, *Tomentella Sublilacina*, via Soil Food Webs. *Mycologia* **2005**, *97*, 762–769. [CrossRef]
89. Persson, Y.; Ihrmark, K.; Stenlid, J. Do Bark Beetles Facilitate the Establishment of Rot Fungi in Norway Spruce? *Fungal Ecol.* **2011**, *4*, 262–269. [CrossRef]
90. Seibold, S.; Müller, J.; Baldrian, P.; Cadotte, M.W.; Šťursová, M.; Biedermann, P.H.W.; Krah, F.-S.; Bässler, C. Fungi Associated with Beetles Dispersing from Dead Wood—Let's Take the Beetle Bus! *Fungal Ecol.* **2019**, *39*, 100–108. [CrossRef]
91. Frank, A. Die Bedeutung Der Mykorrhiza-Pilze Für Die Gemeine Kiefer. *Forstwiss. Cent.* **1894**, *16*, 185–190.
92. Kuyper, T.W. De rol van ectomycorrhiza-schimmels in de nutriëntenkringloop. *Coolia* **1990**, *33*, 32–37.
93. Courty, P.-E.; Pritsch, K.; Schloter, M.; Hartmann, A.; Garbaye, J. Activity Profiling of Ectomycorrhiza Communities in Two Forest Soils Using Multiple Enzymatic Tests. *New Phytol.* **2005**, *167*, 309–319. [CrossRef]
94. Phillips, L.A.; Ward, V.; Jones, M.D. Ectomycorrhizal Fungi Contribute to Soil Organic Matter Cycling in Sub-Boreal Forests. *ISME J.* **2014**, *8*, 699–713. [CrossRef]
95. Rineau, F.; Roth, D.; Shah, F.; Smits, M.; Johansson, T.; Canbäck, B.; Olsen, P.B.; Persson, P.; Grell, M.N.; Lindquist, E.; et al. The Ectomycorrhizal Fungus *Paxillus Involutus* Converts Organic Matter in Plant Litter Using a Trimmed Brown-rot Mechanism Involving Fenton Chemistry. *Environ. Microbiol.* **2012**, *14*, 1477–1487. [CrossRef]
96. Fukasawa, Y.; Kitabatake, H. Which Is the Best Substrate to Regenerate? A Comparative Pot Experiment for Tree Seedling Growth on Decayed Wood and in Soil. *Forests* **2022**, *13*, 1036. [CrossRef]
97. Abarenkov, K.; Kõljalg, U.; Nilsson, R.H. UNITE Species Hypotheses Matching Analysis. *Biodivers. Inf. Sci. Stand.* **2022**, *6*, e93856. [CrossRef]

98. Haelewaters, D.; Quandt, C.A.; Bartrop, L.; Cazabonne, J.; Crockatt, M.E.; Cunha, S.P.; De Lange, R.; Dominici, L.; Douglas, B.; Drechsler-Santos, E.R.; et al. The Power of Citizen Science to Advance Fungal Conservation. *Conserv. Lett.* **2024**, *17*, e13013. [CrossRef]
99. Heilmann-Clausen, J.; Bruun, H.H.; Ejrnæs, R.; Frøslev, T.G.; Læssøe, T.; Petersen, J.H. How Citizen Science Boosted Primary Knowledge on Fungal Biodiversity in Denmark. *Biol. Conserv.* **2019**, *237*, 366–372. [CrossRef]
100. Curry, K.D.; Wang, Q.; Nute, M.G.; Tyshaieva, A.; Reeves, E.; Soriano, S.; Wu, Q.; Graeber, E.; Finzer, P.; Mendling, W.; et al. Emu: Species-Level Microbial Community Profiling of Full-Length 16S rRNA Oxford Nanopore Sequencing Data. *Nat. Methods* **2022**, *19*, 845–853. [CrossRef]
101. van der Vorst, V.; Thijssen, M.; Fronen, B.J.; de Groot, A.; Maathuis, M.A.M.; Nijhuis, E.; Polling, M.; Stassen, J.; Voorhuijzen-Harink, M.M.; Jak, R. PIMENTA: PIpeline for MEtabarcoding through Nanopore Technology Used for Authentication. *bioRxiv* **2024**. [CrossRef]
102. Doorenspleet, K.; Jansen, L.; Oosterbroek, S.; Kamermans, P.; Bos, O.; Wurz, E.; Murk, A.; Nijland, R. The Long and the Short of It: Nanopore Based eDNA Metabarcoding of Marine Vertebrates Works; Sensitivity and Specificity Depend on Amplicon Lengths. *bioRxiv* **2023**. [CrossRef]

Disclaimer/Publisher's Note: The statements, opinions and data contained in all publications are solely those of the individual author(s) and contributor(s) and not of MDPI and/or the editor(s). MDPI and/or the editor(s) disclaim responsibility for any injury to people or property resulting from any ideas, methods, instructions or products referred to in the content.

Journal of *Fungi*

MDPI

Article

A Treasure Trove of Urban Microbial Diversity: Community and Diversity Characteristics of Urban Ancient *Ginkgo biloba* Rhizosphere Microorganisms in Shanghai

Jieying Mao [1,2,3], Qiong Wang [1,2], Yaying Yang [1,2,4], Feng Pan [5], Ziwei Zou [1,2], Xiaona Su [1,2], Yi Wang [1,2], Wei Liu [1,2,*] and Yaohua Tang [6,*]

[1] Jiangxi Provincial Key Laboratory of Conservation Biology, Nanchang 330045, China; 15757555875@163.com (J.M.); wangqiong881004@163.com (Q.W.); yangyy0725@163.com (Y.Y.); zzwei0911@163.com (Z.Z.); 13561584223@163.com (X.S.); 18207000523@163.com (Y.W.)
[2] School of Art and Landscape, College of Forestry, Jiangxi Agricultural University, Nanchang 330045, China
[3] Ningbo Yongneng Biomass Energy Development Co., Ltd., Ningbo 315000, China
[4] Ganzhou Vegetable and Flower Rrerarch Institute, Ganzhou 341413, China
[5] Jiangxi Academy of Water Science and Engineering, Nanchang 330029, China; panfeng_1987@163.com
[6] Shanghai Municipal Landscape Management and Guidance Station, Shanghai 200020, China
* Correspondence: w_liu08@163.com (W.L.); 13397089185@163.com (Y.T.)

Abstract: Rapid urbanization has exerted immense pressure on urban environments, severely constraining the growth of ancient trees. The growth of ancient trees is closely linked to the microbial communities in their rhizospheres, and studying their community characteristics may provide new insights into promoting the growth and rejuvenation of ancient trees. In this study, the rhizosphere soil and root systems of ancient *Ginkgo biloba* trees (approximately 200 years old) and adult *G. biloba* trees (approximately 50 years old) in Shanghai were selected as research subjects. Phospholipid fatty acid (PLFA) analysis and high-throughput sequencing were employed to investigate the diversity of microbial communities in the *G. biloba* rhizosphere. The results indicated that the 19 PLFA species selected to characterize the soil microbial community structure and biomass were present in the rhizosphere soil of both ancient and adult *G. biloba* trees. However, the total microbial biomass and the microbial biomass in the rhizosphere soil of ancient *G. biloba* were lower than the microbial biomass in the rhizosphere soil of adult *G. biloba*. The biomasses of Gram-negative bacteria (G^-), arbuscular mycorrhizal fungi (AMF), and protozoans (P) were significantly different. Total phosphorus, organic matter, and pH may be the key factors influencing the soil microbial community in the rhizosphere zone of ancient *G. biloba*. An in-depth study of AMF showed that the roots and rhizosphere soil of *G. biloba* contained abundant AMF resources, which were assigned to 224 virtual taxa using the MaarjAM reference database, belonging to four orders, ten families, and nineteen genera. The first and second most dominant genera were *Glomus* and *Paraglomus*, respectively. *Archaeospora* and *Ambispora* were more dominant in the rhizosphere than the roots. Furthermore, the abundance of live AMF was significantly higher in ancient *G. biloba* than in adult *G. biloba*. Therefore, future research should focus on the improvement of soil environmental characteristics and the identification and cultivation of indigenous dominant AMF in the rhizosphere of ancient *G. biloba*, aiming for their effective application in the rejuvenation of ancient trees.

Keywords: ancient *Ginkgo biloba*; phospholipid fatty acid; high-throughput sequencing technology; microorganism; arbuscular mycorrhizal fungi; community characteristics

1. Introduction

According to China's National Technical Regulations for the Census of Ancient and Famous Trees, published in 2001, ancient trees are defined as trees that are 100 years old and older [1]. These trees carry important historical memories and research value, making them

a valuable natural and cultural heritage resource [2]. However, the vigor of ancient trees gradually weakens after a long period of growth. Natural disasters, pests, and diseases are likely to cause harm to ancient trees. Moreover, old trees that grow in cities have an even less optimistic outlook. *Ginkgo biloba* is an endemic tree species in China that only blossoms and bears fruit after about 20 years [3]. The development of flowers occurs when *G. biloba* reaches adulthood [4]. With a large population, *G. biloba* is an important ancient and famous tree resource in China. *G. biloba* is the most abundant ancient tree species in Shanghai [5]. However, according to the Shanghai Municipal Administration of Greening and Amenities, approximately one-third of ancient *G. biloba* in Shanghai exhibit signs of poor growth owing to natural and anthropogenic influences.

Soil quality is among the most important factors affecting the growth of ancient trees. Problems such as soil compaction, heavy metal pollution, mineral nutrient scarcity, and imbalances in rationing affect the health of ancient trees, resulting in the slow growth of their root systems and an insufficient supply of nutrients. The most active components of the soil are microorganisms, which can interact with the soil. The soil microbiota is also an important indicator of soil quality [6]. Therefore, there is a strong link between the soil microbiota and the growth of ancient trees. However, studies have shown that there are significant differences in the structure of the microbiota between the rhizosphere and non-rhizosphere soils of *G. biloba*, and the profile of soil fungi is complex and inconsistent between these soils [7].

Arbuscular mycorrhizal fungi (AMF) are a group of endophytic fungi widely distributed in terrestrial ecosystems [8]. AMF are present in the soil as spores and mycelia. AMF account for the largest proportion of the fungal biomass in soil and directly affect the microbial community structure through mycelial secretions that cause changes in plant root secretions [9]. Previous studies have confirmed that AMF infesting the root system of *G. biloba* is a common phenomenon that forms a mutually beneficial symbiotic system with the host. Fontana [10] found that *G. biloba* on the campus of the Università degli Studi di Torino, Italy, exhibited numerous intracellular mycelia. Wu and Wei [11] found that the development of clumped mycorrhizae in grafted *G. biloba* seedlings was significantly better than that seen in live seedlings grown through seed germination. Yuan et al. [12] determined that the AMF of *G. biloba* growing on artificial coasts exhibited a P-type structure. In a symbiotic system formed with the host plant, AMF can absorb mineral nutrients through mycelial extensions into soil crevices that are inaccessible to the plant root system for transfer to the host plant [13,14]. Additionally, AMF have various beneficial effects on soil, including improving the physical structure, stabilizing organic carbon, activating nutrients, and maintaining pore space [15,16].

Tong et al. [17] applied exogenous mycorrhizal fungi to ancient *G. biloba* in Shanghai and found that AMF inoculation significantly promoted the growth of ancient trees, with enhanced soil fertility detected four years later. This suggests that mycorrhizal fungi can promote the rejuvenation of ancient *G. biloba*. In fact, indigenous mycorrhizal fungi in the rhizosphere soil of plants may be more adaptable to the soil environment and function more efficiently than exogenous mycorrhizal fungi because they have a closer relationship with the host plants [18]. Therefore, exploring the diversity of microbial communities, especially AMF communities, may provide a new direction for promoting the growth of ancient *G. biloba* and for salvage and rejuvenation.

After hundreds or even thousands of years of growth, ancient *G. biloba* may have a more stable microbial community in its rhizosphere than younger adult *G. biloba*. In this study, it was hypothesized that (1) ancient *G. biloba* trees accumulate more microbial species and numbers in the rhizosphere soil than younger adult *G. biloba*; and (2) AMF are present in both the roots and rhizosphere soils of *G. biloba* but may differ considerably in terms of species and number between ancient and younger adult *G. biloba*.

To test these hypotheses, phospholipid fatty acid (PLFA) technology was employed to detect microbial taxa in the rhizosphere soil of ancient and younger adult *G. biloba* in Shanghai. High-throughput sequencing technology was utilized to reveal the community

composition and diversity of AMF in the rhizosphere of *G. biloba* in depth. It is hoped that this study will provide a research basis for identifying microbial taxa in the rhizosphere soils of ancient *G. biloba*, as well as for the preparation of mycorrhizal agents to promote the growth and rejuvenation of ancient trees.

2. Materials and Methods

2.1. Site and Experimental Design

The sampling sites were located in the Jiading District and Qingpu District (31°9′14″ N–31°23′3″ N, 121°8′35″ E–121°27′5″ E) of Shanghai, China (Figure 1). The region has a northern subtropical monsoon climate with warm weather and ample precipitation. The average annual temperature is 17.7 °C, and precipitation is concentrated from April through October, with an average annual precipitation of 1726 mm.

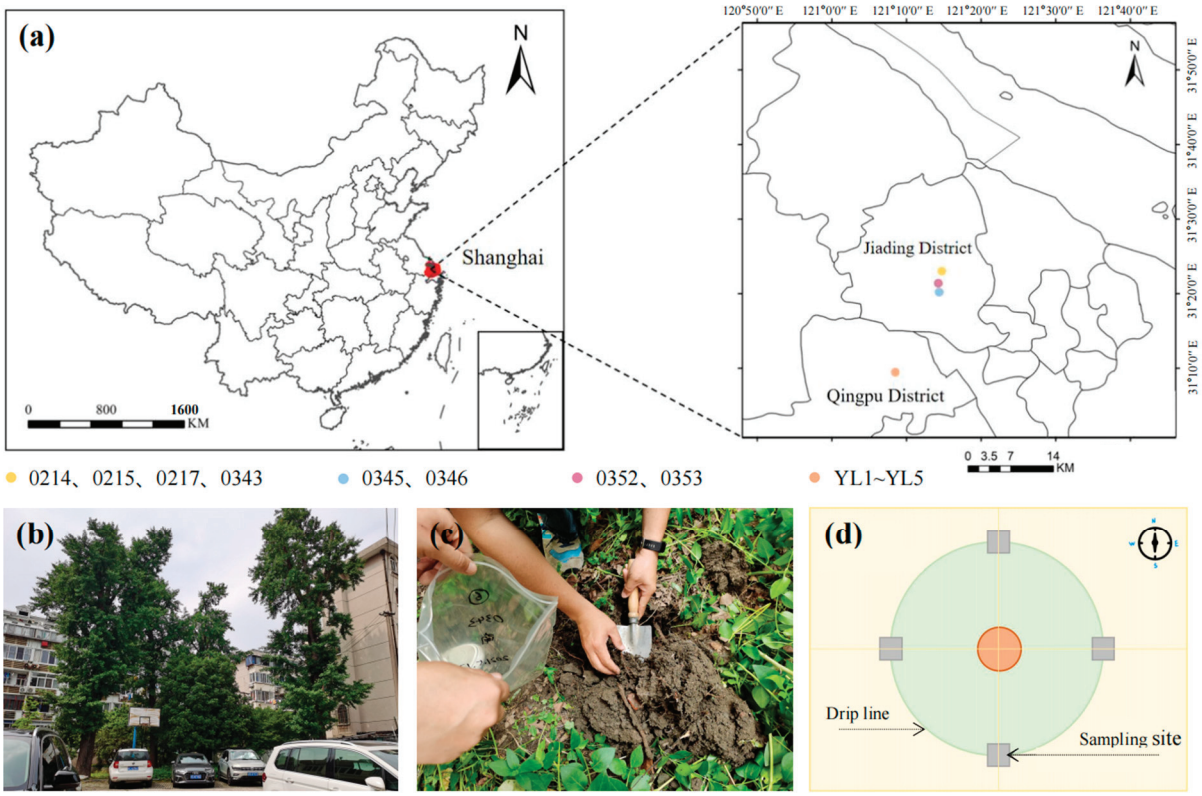


Figure 1. Sampling positions and process. (**a**) Map of study sites; (**b**) sampling sites; (**c**) sampling process; and (**d**) sampling diagram.

To explore the symbiosis between AMF and *G. biloba*, two types of *G. biloba* were selected for the study: eight ancient *G. biloba* approximately 200 years old, and five adult *G. biloba* approximately 50 years old. The ages of ancient *G. biloba* trees were determined according to the times recorded on the protection plates for ancient and famous trees established by the Shanghai Municipal Administration of Greening and Amenities, which were obtained through a literature review [19]. The ages of adult *G. biloba* trees were estimated based on the landscaping projects implemented by the Shanghai Municipal Administration of Greening and Amenities at that time. None of these trees were treated with mycorrhizal fungicides. Fieldwork was performed on 17 May 2021 and 15 September 2022, and the relevant information about each tree was recorded (Table 1). The drip lines of *G. biloba* were located in four directions: east, west, south, and north. During sample collection, 150 g of mixed soil and roots were collected to a depth of approximately 30 cm. Samples from all four directions were placed on a newspaper sheet to remove plant debris and stones. The samples were then mixed thoroughly in a sealing bag to form a composite

sample, and this process was repeated three times for each tree. To prevent contamination, the shovel was cleaned to remove soil particles and disinfected with 70% ethanol before and after digging, and sterile gloves were utilized during the removal of plant debris and stones.

Table 1. Overview of *Ginkgo biloba* habitat survey and soil sampling sites.

Category	Number	Tree Age/Years	Longitude and Latitude	Site	Growth Status	Growth Environment Characteristics
Ancient *G. biloba*	0214	250	31°23′3″ N, 121°14′46″ E	Liuyi Community	normal	Within the green area, there is a cluster of ancient trees, surrounded by residential areas and parking lots. There is a considerable amount of construction and household waste in the vicinity.
	0215	250			normal	
	0217	250			normal	
	0343	180			normal	
	0345	180	31°20′37″ N, 121°14′11″ E	Ziqi Donglai Park	normal	In the park, grass is regularly removed under the trees, and the surrounding area is covered with white clover vegetation.
	0346	180			normal	
	0352	180	31°21′24″ N, 121°14′6″ E	Near Shengxin Road Suspension Binhai Bridge	normal	Lakeside area with exposed ground, protected by a fence.
	0353	180			normal	
Adult *G. biloba*	YL1	50	31°9′14″ N, 121°8′35″ E	Hua Le Road	normal	Adjacent to the main urban thoroughfare, limited growing space.
	YL2	50			normal	
	YL3	50			normal	
	YL4	50			normal	
	YL5	50			normal	

Note: The growth status of ancient *G. biloba* was judged according to the People's Republic of China LY/T 3073-2018 "Technical regulations for the management and conservation of old and notable trees". The growth of adult *G. biloba* was judged by the same industry standards.

For sample preservation, it was necessary to separate the roots from the soil in each sample and rinse the root surface. The samples were labeled as the roots of ancient *G. biloba* (GYXG), the rhizosphere soil of ancient *G. biloba* (GYXT), the roots of adult *G. biloba* (XYXG), and the rhizosphere soil of adult *G. biloba* (XYXT). Each soil sample was equally divided into three parts, one of which was given to the South China Botanical Garden for the PLFA assay based on the methodology referenced from Bossio et al. [20] and analyzed using the MIDI Sherlock® Microbial Identification System 6.0. Another part, together with the roots of *G. biloba*, was sent to Novogene for high-throughput sequencing. As the samples were not immediately available for PLFA and high-throughput sequencing assays, they were stored temporarily at −20 °C. The final part was used to determine the chemical properties, stored at room temperature (20–25 °C), sieved (2 mm), spread flat in the laboratory, and allowed to dry naturally.

2.2. Experimental Methods

2.2.1. Soil Chemical Analyses

The soil was digested using the $HClO_4$-H_2SO_4 decoction method before the analysis of the total nitrogen (TN), total phosphorus (TP), and total potassium (TK) contents. The TN was analyzed using a flow analyzer (AutoAnalyzer III, Bran + Luebbe GmbH, Hamburg, Germany). The TP was measured using the molybdenum antimony anti-colorimetric method [21], and the TK was determined using a flame photometer (FP640, Jingke, Shanghai, China). The potassium dichromate-potassium external heating method was employed to determine the organic matter (OM) content. The soil pH was measured using a pH meter (PB-10, Sartorius AG, Göttingen, Germany), and the soil conductivity was measured using

a conductivity meter (DDS-307, Yidian Corporation, Shanghai, China). Each soil sample was replicated three times with a blank control.

2.2.2. PLFA Analysis

The quantified internal standard, normal nonadecanoic acid (19:0), was employed to dissolve the extracted and processed fatty acid methyl esters obtained from the soil samples. Gas chromatography (Agilent 7890A, Santa Clara, CA, USA) was utilized to obtain the response values for the characteristic peaks of each fatty acid region [22]. A reference to previously compiled PLFA markers [23] was used to select 19 specific types (Table 2) to characterize the structure and biomass of the soil microbial community. Additionally, the total microbial biomass (T-PLFA) for the six microbial groups was calculated, and ratios including the ratio of Gram-positive bacteria to Gram-negative bacteria (G^+/G^-), the environmental pressure (cy17:0c/16:1ω7c), and the ratio of fungi to bacteria (F/B) were determined.

Table 2. Characteristic microbes of phospholipid fatty acids (PLFAs).

Characterization of Microbial Taxa	PLFA Species
Fungi (F)	18:1ω9c, 18:2ω6c, and 18:3ω6c
Gram-positive bacteria (G^+)	i14:0, i15:0, a15:0, i16:0, a17:0, and i17:0
Gram-negative bacteria (G^-)	16:1ω7c, cy 17:0c, 18: 1ω7c, and cy 19:0c
Actinomycetes (A)	10Me16:0, 10Me17:0, and 10Me18:0
Arbuscular mycorrhizal fungi (AMF)	16:1ω5c
Protozoa (P)	20:3ω6c and 20:4ω6c

Note: i, a, cy, and Me represent isopropyl, anti-isopropyl, cyclopropyl, and methyl-branched fatty acids, respectively; ω and c represent methyl terminal and homeotropic space structures, respectively.

2.2.3. High-Throughput Sequencing Methods for AMF

Five grams each of soil and root samples were used for DNA extraction. A total of 1000 μL of cetyltrimethylammonium bromide (CTAB) lysate, 20 μL of lysozyme, and 1 μL of RNase A were used to extract the DNA of AMF from roots and soil according to the CTAB method [24]. There were three biological replicates for each sample. The quality of DNA extraction was analyzed using 1.2% agarose gel electrophoresis [25,26]. DNA was amplified using polymerase chain reaction (PCR) with a target fragment length of 280 bp. The AMF-specific primers AMV4.5NF (5′-AAG CTC GTA GTT GAA TTT CG-3′) and AMDGR (5′-CCC AAC TAT CCC TAT TAA TCA T-3′) were utilized to accomplish this process [27–29]. Gel electrophoresis was performed on the amplification products to obtain valid samples for the amplification of specific fragments. The assay conditions were a 2% gel concentration, 80 V, and 40 min of electrophoresis time.

Paired-end sequencing was performed on the samples using a sequencer (Illumina NovaSeq 6000, San Diego, CA, USA). Due to the possibility of sequencing misalignment in the raw data, splicing and filtering were performed to obtain valid data. DADA2 was employed for denoising, and sequences with an abundance of less than five were filtered out. Amplicon sequence variant (ASV) feature sequences with nearly 100% similarity were obtained through clustering [30]. Each ASV feature sequence was aligned with the Nt database to eliminate non-Glomeromycota sequences. This was followed by a BLAST comparison of the remaining representative sequences on MaarjAM (https://maarjam.botany.ut.ee/, accessed on 10 March 2023) to attribute the sequences to the AMF virtual taxa and determine the genus information [31,32]. This classification was a virtual classification based on small subunit rRNA genes in the MaarjAM database [33]. A virtual taxon was the classification unit, representing a well-supported monophyletic clade with sequence similarity within the clade exceeding a threshold of 97% [34]. Analyses including the ASV abundance, Venn diagrams, alpha diversity, and beta diversity were performed to obtain information on the absolute and relative abundances, shared and unique ASVs, and diversity indices, including the species richness (Chao1), Shannon diversity (Shannon), Simpson's diversity (Simpson), and evenness (Pielou_e) indices [35].

2.3. Data Analysis

Zone mapping was performed using ArcGIS 10.8 (Environmental Systems Research Institute, Redlands, CA, USA). An independent samples *t*-test was utilized to analyze the variability of the soil microbial biomass and soil microbial community structure ratio. One-way analysis of variance (ANOVA) and Duncan's multiple comparisons were used to complete the analysis of the AMF community data within the roots and soil of *G. biloba*, including the soil chemical, absolute, and relative abundances, shared and unique ASVs, and diversity indices such as Chao1, Shannon, Simpson, and Pielou_e. Differences were considered significant at $p < 0.05$ and highly significant at $p < 0.01$. Pearson's coefficients were used to analyze the soil microbial biomass and correlation factors representing habitat conditions, as well as between AMF species and correlation factors representing habitat conditions. All statistical analyses were performed using SPSS version 22 (IBMSPSS Statistics, Armonk, NY, USA). These statistics were used to complete a drawing in Origin Pro 2022 (OriginLab, Hampden, MA, USA). Principal coordinate analysis (PCoA) was performed using the online platform Novogene Cloud (https://magic.novogene.com/ accessed on 27 July 2024) [36].

3. Results

3.1. Soil Environmental Traits

As displayed in Table 3, the results of soil chemical analyses indicated that there were significant differences between GYXT and XYXT. Except for the TN and OM, all other indices exhibited significant differences ($p < 0.05$). GYXT had significantly higher TN and TK contents than XYXT ($p < 0.05$), where the difference in TK was highly significant ($p < 0.01$). However, the TP, OM, pH, and electrical conductivity (EC) were lower in GYXT than in XYXT, with significant differences in the TP and EC ($p < 0.05$) and highly significant differences in pH ($p < 0.01$).

Table 3. Soil chemical analyses of the rhizosphere soil of *Ginkgo biloba*.

Soil	TN ($g \cdot kg^{-1}$)	TP ($g \cdot kg^{-1}$)	TK ($g \cdot kg^{-1}$)	OM ($g \cdot kg^{-1}$)	pH	EC ($mS \cdot cm^{-1}$)
XYXT	1.34 ± 0.08 a	2.02 ± 0.15 a	4.10 ± 0.32 b	30.85 ± 3.51 a	8.23 ± 0.03 a	0.17 ± 0.014 a
GYXT	2.00 ± 0.28 a	1.39 ± 0.22 b	5.78 ± 0.19 a	29.29 ± 4.32 a	7.79 ± 0.05 b	0.13 ± 0.005 b

Note: XYXT represents the rhizosphere soil of adult *Ginkgo biloba*, and GYXT represents the rhizosphere soil of ancient *Ginkgo biloba*. Different lowercase letters indicate significant differences ($p < 0.05$). The following is the same.

3.2. Microbial Biomass of the Rhizosphere Soil of G. biloba

In total, 19 specific PLFAs were detected in the 13 soil samples examined, and the same microbial species were present in XYXT and GYXT; however, there were large differences in their contents (Figure 2). XYXT had a higher biomass of F, G^+, G^-, A, AMF, and P than GXYT, and all except for G^- were significantly different ($p < 0.05$). Among them, the biomass of G^+, AMF, and P showed highly significant differences ($p < 0.01$). Calculating the total microbial biomass revealed that the total microbial biomass of GYXT was 82.61 $nmol \cdot g^{-1}$, which was highly significant ($p < 0.01$) and lower than that of XYXT. The highest content of PLFA biomarkers in XYXT and GYXT was found in G^+, which accounted for 36.40% and 33.16% of the total PLFA biomarkers in the soils, respectively, and had the greatest predominance in the soils. The content of AMF in XYXT accounted for 5.14% of T-PLFA, which was slightly higher than that detected in GYXT (4.54%).

3.3. Relationship Between Soil Environmental Traits and Microbial Biomass

Pearson's correlation analysis showed a significant correlation ($p < 0.05$) between the soil environmental traits and the microbial community structure. However, large differences in the soil environmental factors had significant effects on the microbial community structure in both ancient and adult *G. biloba* soils (Figure 3). In XYXT, the TK was significantly negatively correlated with AMF and P ($p < 0.05$), whereas the EC was significantly

negatively correlated with F ($p < 0.05$) and significantly negatively correlated with G^+ ($p < 0.05$). In GYXT, the TP and OM were significantly negatively correlated with F, G^+, G^-, AC, AMF, P, and the T-PLFA ($p < 0.05$). pH was significantly negatively correlated with P ($p < 0.05$) and highly negatively correlated with F, G^+, G^-, AC, AMF, and the T-PLFA ($p < 0.01$).

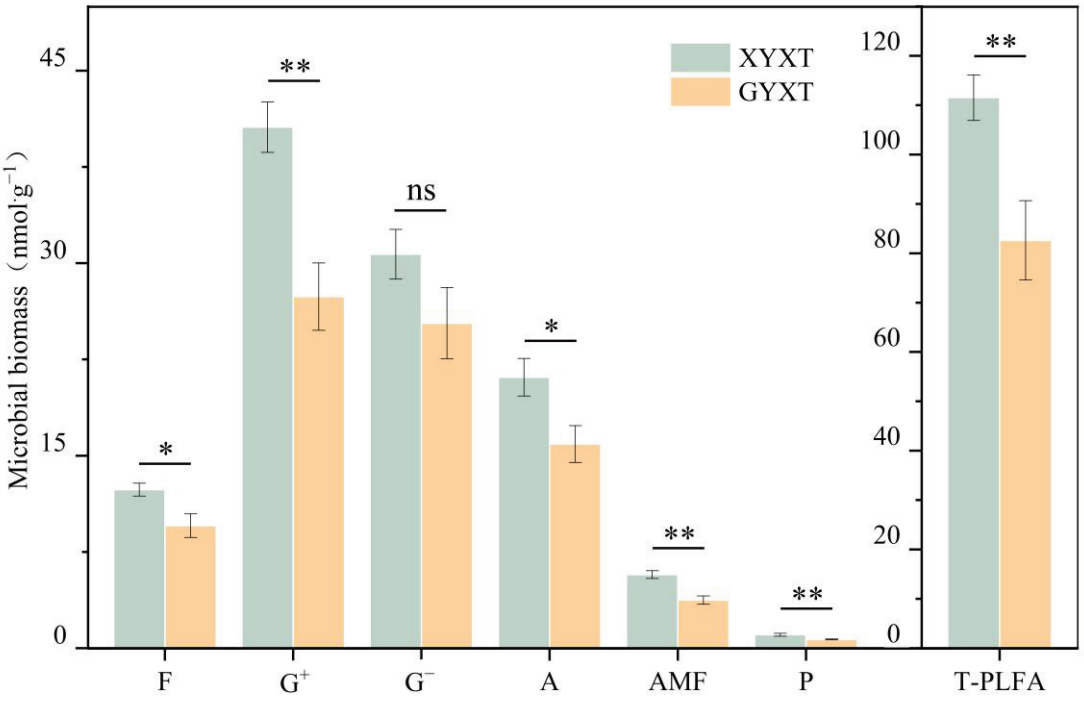


Figure 2. Microbial biomass in the rhizosphere soil of *Ginkgo biloba*. ns indicates $p > 0.05$, * indicates $p < 0.05$, ** indicates $p < 0.01$. The following is the same.

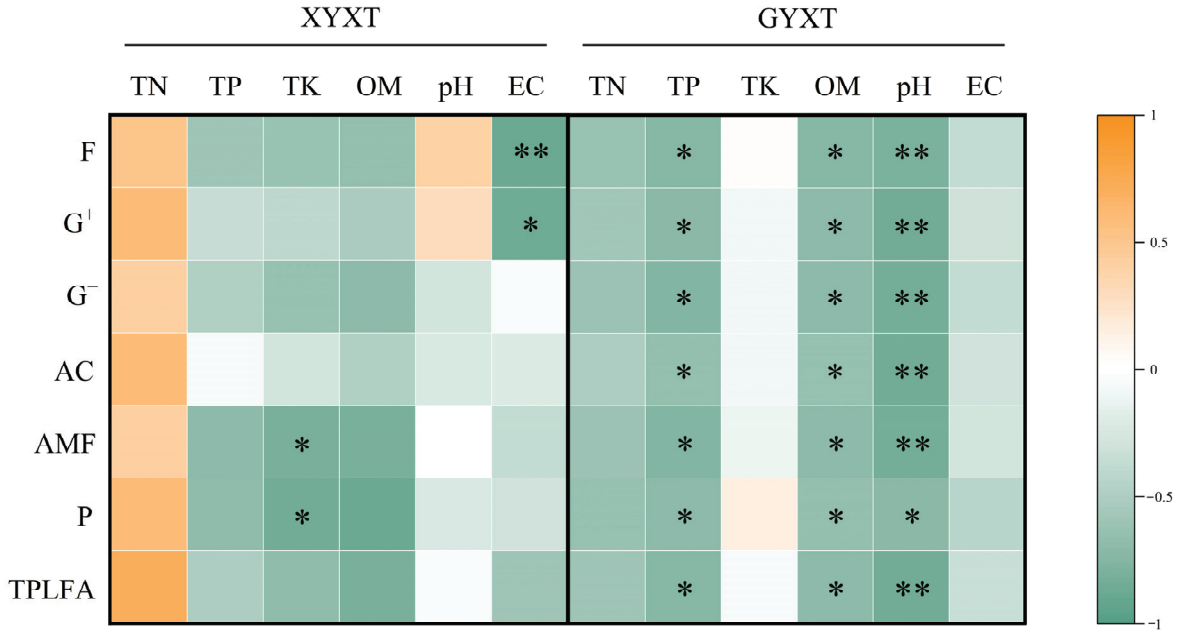


Figure 3. Analysis of soil environmental traits and microbial biomass. * indicates $p < 0.05$, ** indicates $p < 0.01$.

Fungi and bacteria are the most dominant microbial groups in soil, and the F/B and G^+/G^- ratios can indirectly respond to the survival environment of soil microorganisms

and the diversity characteristics of bacterial communities. As shown in Table 4, the F/B ratio of GXYT was 0.009 higher than that of XYXT, and the G^+/G^- ratio was 0.246 lower than that of XYXT. The environmental pressure of GXYT was 0.360, which was significantly lower than that of XYXT ($p < 0.05$).

Table 4. Soil microbial community structure ratios of *Ginkgo biloba*.

Treatments	F/B	G^+/G^-	cy17:0c/16:1ω7c
XYXT	0.173 ± 0.004 a	1.346 ± 0.122 a	0.599 ± 0.006 a
GYXT	0.182 ± 0.004 a	1.100 ± 0.027 a	0.360 ± 0.012 b

Different lowercase letters indicate significant differences ($p < 0.05$).

3.4. Analysis of the AMF Community in the Roots and Rhizosphere Soil of G. biloba

3.4.1. Composition of the AMF Community

Abundant AMF resources were found in the roots and rhizosphere soil of *G. biloba* (Table 5). In total, 224 AMF virtual taxa were obtained from all samples using high-throughput sequencing. These taxa belonged to four orders, ten families, and nineteen genera. Among them, the genus with the most identified species was *Scutellospora*, with five species, followed by *Rhizophagus* with four species, *Paraglomus* and *Ambispora* with three species, and *Glomus*, *Septoglomus*, *Sclerocystis*, *Claroideoglomus*, and *Acaulospora* with two species. Furthermore, *Funneliformis*, *Dominikia*, *Kamienskia*, *Geosiphon*, *Diversispora*, *Redeckera*, *Gigaspora*, *Dentiscutata*, and *Pacispora* all had only one species.

Table 5. Virtual taxa of AMF in the root and rhizosphere soil of *Ginkgo biloba* obtained via high-throughput sequencing.

Order	Family	Genus	Virtual Taxa
Glomerales	Glomeraceae		G. *microaggregatum* VTX00104, *G. hoi* VTX00199
		Glomus	VTX00053, VTX00066, VTX00068, VTX00070, VTX00072–VTX00074, VTX00076, VTX00077, VTX00079, VTX00080, VTX00082–VTX00084, VTX00088, VTX00089, VTX00093, VTX00096, VTX00098, VTX00109, VTX00112, VTX00120–VTX00122, VTX00124–VTX00127, VTX00137, VTX00140, VTX00143, VTX00150, VTX00151, VTX00154, VTX00156, VTX00159, VTX00166, VTX00167, VTX00174, VTX00175, VTX00178–VTX00184, VTX00186, VTX00188, VTX00189, VTX00191, VTX00194, VTX00197, VTX00200, VTX00202, VTX00206, VTX00209, VTX00212, VTX00214, VTX00216, VTX00219, VTX00223, VTX00224, VTX00234, VTX00235, VTX00253, VTX00259, VTX00270, VTX00290–VTX00292, VTX00294, VTX00301, VTX00304, VTX00305, VTX00309, VTX00312, VTX00316, VTX00317, VTX00319, VTX00322–VTX00327, VTX00329, VTX00331, VTX00333, VTX00342–VTX00344, VTX00359, VTX00360, VTX00362, VTX00364, VTX00366, VTX00368–VTX00373, VTX00382–VTX00384, VTX00386–VTX00390, VTX00392, VTX00393, VTX00395, VTX00397–VTX00399, VTX00404, VTX00409, VTX00411–VTX00413, VTX00416, VTX00419, VTX00420, VTX00422, VTX00423, VTX00426, VTX00427, VTX00432, VTX00436, VTX00437, VTX00441–VTX00443, VTX00448, VTX00452, and VTX00453
Glomerales		*Rhizophagus*	*R. clarus* VTX00090, *R. proliferus* VTX00099, *R. intraradices* VTX00105, and *R. irregularis* VTX00114
		Septoglomus	*S. viscosum* VTX00063 and *S. constrictum* VTX00064
		Sclerocystis	*S. sinuosa* VTX00069 and *S. coremioides* VTX00268
		Funneliformis	*F. mosseae* VTX00067
		Dominikia	*D. indica* VTX00222
		Kamienskia	*K. perpusilla* VTX00287

Table 5. *Cont.*

Order	Family	Genus	Virtual Taxa
Glomerales	Claroideoglomeraceae	*Claroideoglomus*	*C. lamellosum* VTX00193 and *C. claroideum* VTX00225 and VTX00279
			VTX00055–VTX00057, VTX00237, VTX00276–VTX00278, VTX00297, VTX00340, VTX00357, VTX00358, and VTX00402
Paraglomerales	Paraglomeraceae	*Paraglomus*	*P. brasilianum* VTX00239, *P. laccatum* VTX00281, and *P. majewskii* VTX00335
			VTX00001, VTX00002, VTX00308, VTX00337, VTX00348–VTX00352, VTX00375, VTX00433, VTX00435, VTX00444, and VTX00446
Archaeosporales	Ambisporaceae	*Ambispora*	*A. leptoticha* VTX00242, *A. fennica* VTX00283, *A. granatensis* VTX00339
			VTX00405
Archaeosporales	Archaeosporaceae	*Archaeospora*	VTX00004–VTX00009, VTX00051, VTX00338, VTX00376, and VTX00450
	Geosiphonaceae	*Geosiphon*	*G. pyriformis* VTX00241
Diversisporales	Diversisporaceae	*Diversispora*	*D. epigaea* VTX00061
			VTX00040, VTX00306, VTX00354–VTX00356, VTX00380, and VTX00401
		Redeckera	*R. fulvum* VTX00262
	Acaulosporaceae	*Acaulospora*	*A. spinosa* VTX00026 and *A. longula* VTX00028
			VTX00013, VTX00015, VTX00016, VTX00227, VTX00231, VTX00272, and VTX00328
	Gigasporaceae	*Scutellospora*	*S. dipurpurescens* VTX00049, *S. nodosa* VTX00052, *S. spinosissima* VTX00254, *S. projecturata* VTX00260, and *S. nodosa* VTX00261
			VTX00318
		Gigaspora	*G. decipiens* VTX00039
		Dentiscutata	*D. heterogama* VTX00255
	Pacisporaceae	*Pacispora*	*P. scintillans* VTX00284
			VTX00011

The most numerous virtual taxon was *Glomus* with 137 species, accounting for 72.49% of the total virtual taxa. There were 14 species of *Paraglomus*, 12 species of *Claroideoglomus*, 10 species of *Archaeospora*, 7 species of *Acaulospora* and *Diversispora*, and 1 each of *Scutellospora*, *Ambispora*, and *Pacispora*.

3.4.2. Abundance Analysis of AMF Community

The genus-level composition of the AMF community in the root and rhizosphere soils of *G. biloba* is shown in Figure 4. *Glomus* was the most dominant genus in all treatments, with the number of ASVs ranging from 225 to 267 across treatments and the relative species abundance ranging from 48.55% to 59.11%. The highest ASV numbers and relative species abundances were found in GYXG, and the ASV numbers and relative species abundances of *Glomus* in the roots were higher than those in the rhizosphere soil. The second most dominant genus in all treatments was *Paraglomus*, with ASV numbers ranging from 87 to 103 and a relative species abundance between 19.01% and 21.92%. In the rhizosphere soil, the third most dominant genus was *Archaeospora*, while in the roots, the third most dominant genus was *Diversispora*. *Ambispora* was the fourth most dominant genus in

GYXT and XYXT, while the fourth most dominant genera in GYXG and XYXG were *Archaeospora* and *Claroideoglomus*, respectively. Additionally, *Gigaspora*, *Acaulospora*, *Geosiphon*, *Scutellospora*, *Septoglomus*, *Dominikia*, *Sclerocystis*, *Rhizophagus*, *Funneliformis*, *Dentiscutata*, *Redeckera*, *Pacispora*, and *Kamienskia* were present in small amounts in all treatments.

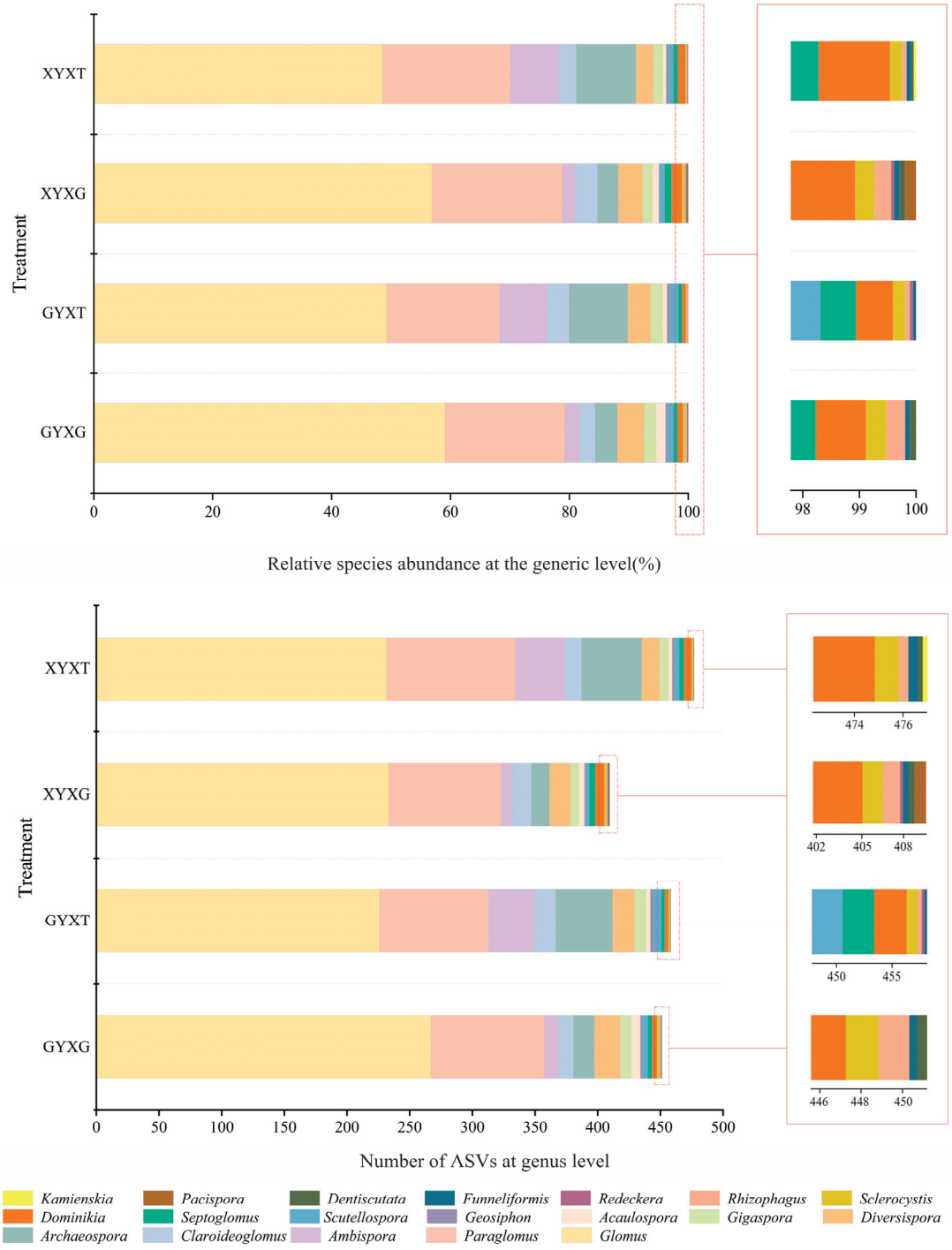


Figure 4. Arbuscular mycorrhizal fungi (AMF) community composition of the root and rhizosphere soil of *Ginkgo biloba* at the genus level. XYXG represents the roots of adult *Ginkgo biloba*, XYXT represents the rhizosphere soil of adult *Ginkgo biloba*, GYXG represents the roots of ancient *Ginkgo biloba*, and GYXT represents the rhizosphere soil of ancient *Ginkgo biloba*.

3.4.3. Venn Diagram Analysis of AMF Community

As shown in the Venn diagram, the numbers of total and unique ASVs in ancient *G. biloba* were greater than the corresponding ASV numbers detected in adult *G. biloba* (Figure 5). The highest numbers of total and unique ASVs in all treatments were found in GYXG, followed by GYXT and XYXT, and the lowest were found in XYXG. In addition, the number of shared ASVs in all treatments was low at only 244, accounting for 4.38% of the total number of ASVs. The highest number of shared ASVs between GYXT and XYXT was 725, and the lowest number of shared ASVs between XYXT and GYXG was 501.

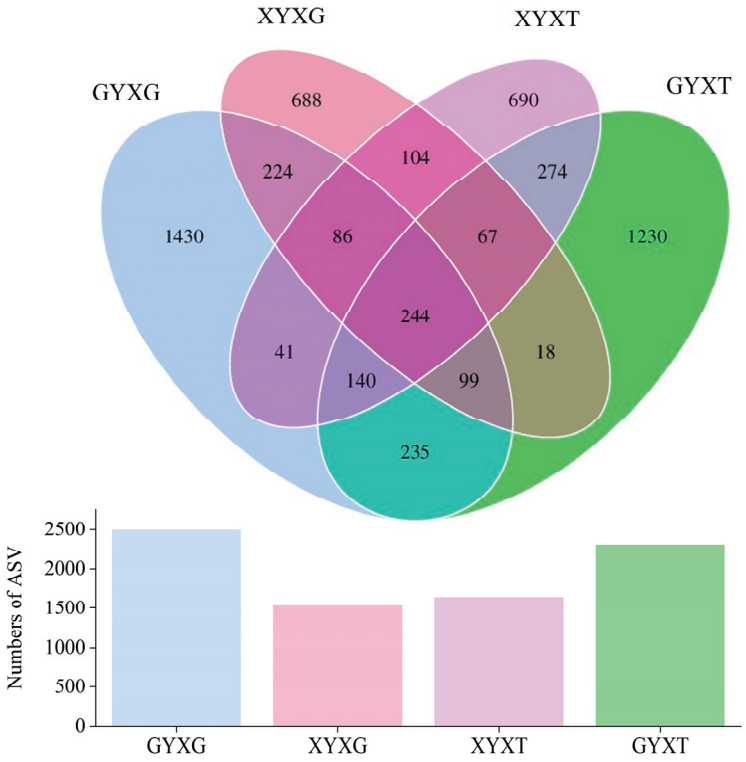


Figure 5. Venn diagram of arbuscular mycorrhizal fungi (AMF) community in the root and rhizosphere soil of *Ginkgo biloba*.

3.4.4. Diversity of AMF Community

The diversity of the AMF community can be assessed using diversity indices such as Shannon, Simpson, Chao1, and Pielou_e (Figure 6). As shown in Figure 6, the median Chao1 index and median Shannon index of soil samples were higher than those of the root samples. The median Simpson index of adult *G. biloba* was higher than that of ancient *G. biloba*. The Pielou's evenness index median was highest in XYXT (0.741) and lowest in XYXG (0.631), with a slight difference of 0.003 between the ancient *G. biloba* roots and the rhizosphere soil. However, there were no significant differences in the four diversity indices among treatments. Additionally, looking at the overall picture of the four indices, the dispersion of the indices in ancient *G. biloba* was greater than that in adult *G. biloba*. The skewness was stronger, and most were negatively skewed.

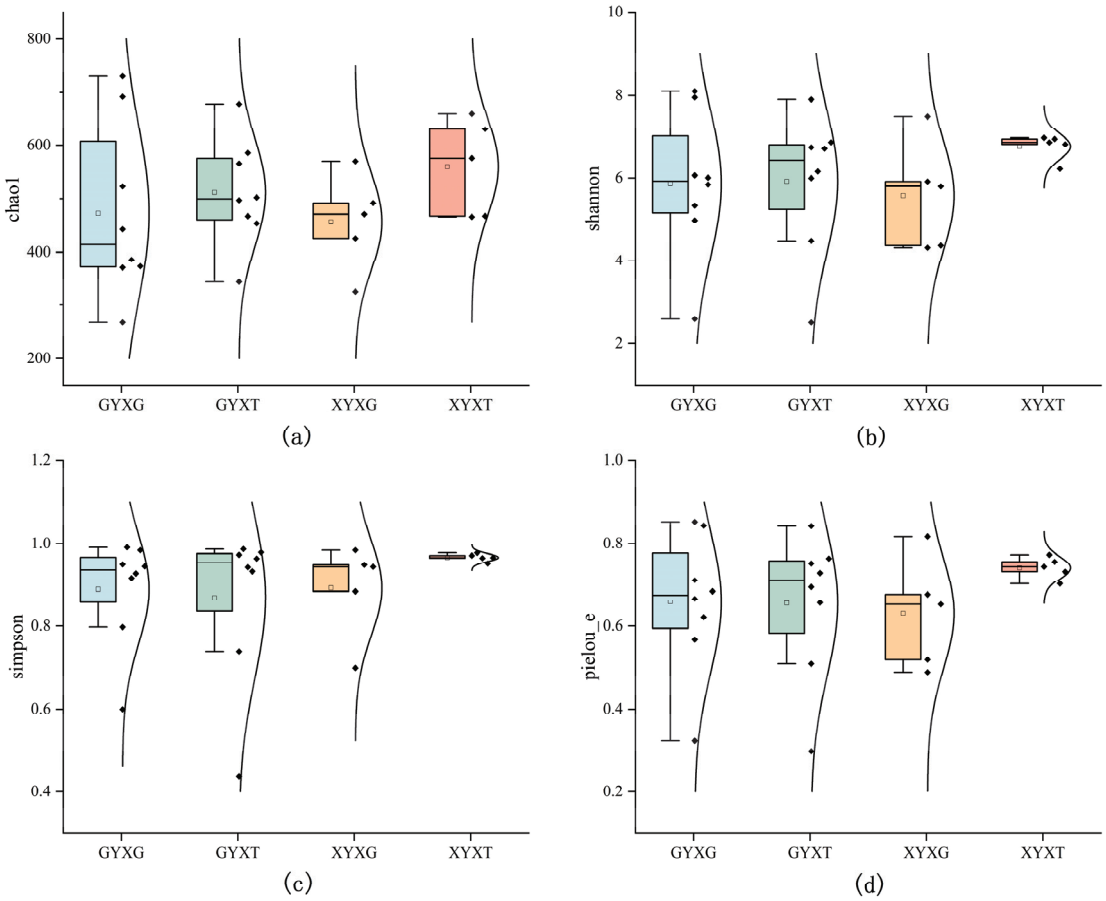


Figure 6. Diversity analysis of the arbuscular mycorrhizal fungi (AMF) community in the root and rhizosphere soil of *Ginkgo biloba*. (**a**) the chart of Chao1 data analysis; (**b**) the chart of Shannon analysis; (**c**) the chart of Simpson analysis; (**d**) the chart of Pielou's evenness analysis. Each point in the graph represents the data for each sample.

3.4.5. PCoA of the AMF Community

PCoA using the unweighted UniFrac distance matrix algorithm revealed that the AMF community structures in the root and rhizosphere soils of *G. biloba* were significantly different (Figure 7). The AMF community structures of GYXG and XYXG were more similar, and those of GYXT and XYXT were more similar. The PCoA results indicated that a small number of widely differing biological replicates appeared in GYXG and XYXG, but all were clustered in the first and second quadrants, were positively correlated with PC1, and were basically negatively correlated with PC2. The biological replicates of GYXT and XYXT were all well clustered together, clustered in the third and fourth quadrants, were negatively correlated with PC1, and were basically positively correlated with PC2.

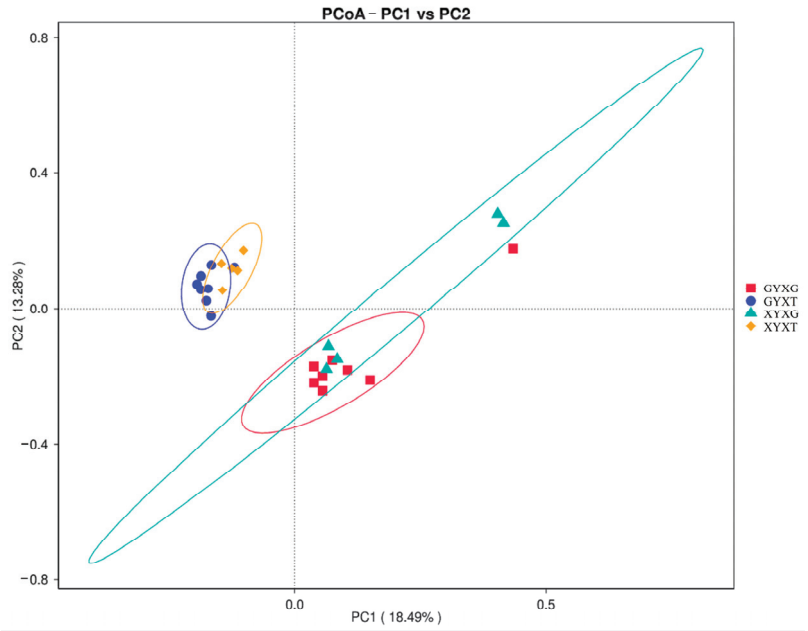


Figure 7. Principal coordinate analysis (PCoA) of arbuscular mycorrhizal fungi (AMF) community diversity in the root and rhizosphere soil of *Ginkgo biloba*.

3.4.6. Cluster Analysis of AMF Community

As shown in the cluster analysis heat map, the genera with relatively high abundances varied among all treatments (Figure 8). In the root treatments, seven genera had relatively high abundances in GYXG, namely *Paraglomus*, *Claroideoglomus*, *Septoglomus*, *Sclerocystis*, *Diversispora*, *Gigaspora*, and *Acaulospora*, whereas relatively high abundances of *Dominikia* and *Pacispora* were observed in XYXG. In the soil treatments, the relatively high abundance of *Geosiphon* in GYXT differed from that in XYXT, which had relatively high abundances of *Ambispora*, *Archaeospora*, *Funneliformis*, and *Kamienskia*.

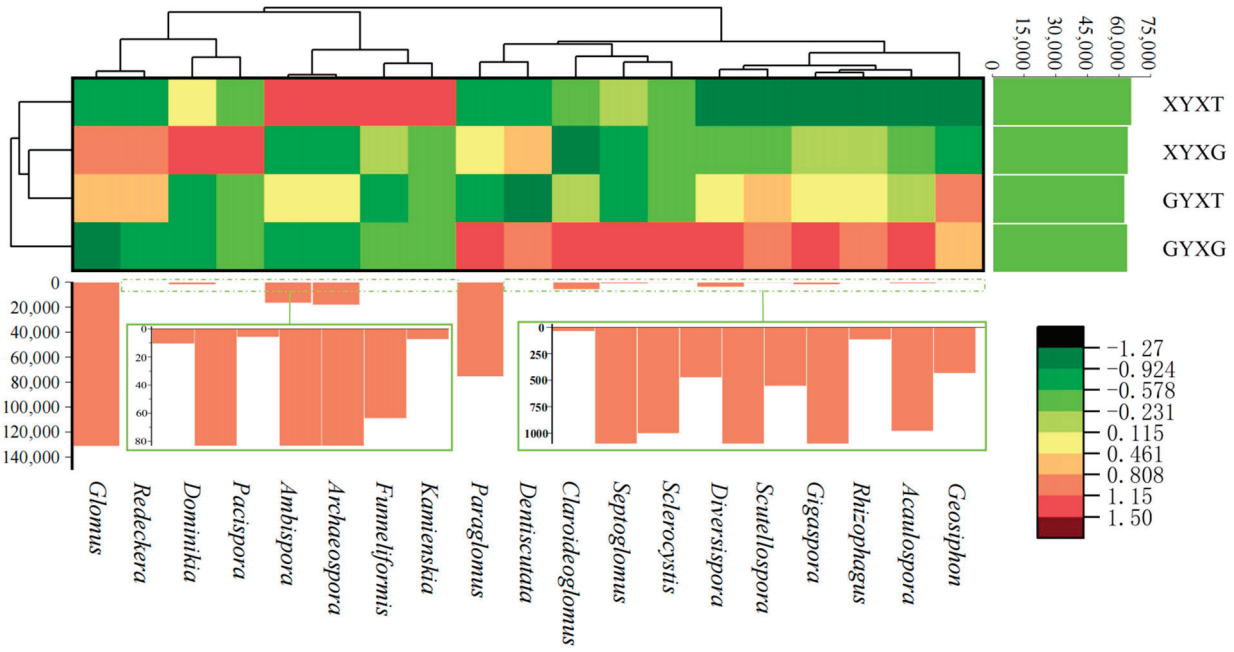


Figure 8. Species clustering heat map of the arbuscular mycorrhizal fungi (AMF) community in the root and rhizosphere soil of *Ginkgo biloba*.

3.4.7. Relationship between Soil Environmental Traits and the AMF Community

Soil environmental factors were significantly correlated ($p < 0.05$) with AMF community structure (Figure 9). The soil environmental factors that significantly affected the AMF species composition in the soils of ancient and adult *G. biloba* were quite different. In XYXT, *Gigaspora* was significantly negatively correlated with the TP and TK ($p < 0.05$), and *Dentiscutata* was significantly negatively correlated with the TN and TP ($p < 0.05$). In GYXT, *Geosiphon* was significantly positively correlated with the TN and TP ($p < 0.05$), while *Sclerocystis* was significantly positively correlated with the TN and OM ($p < 0.01$).

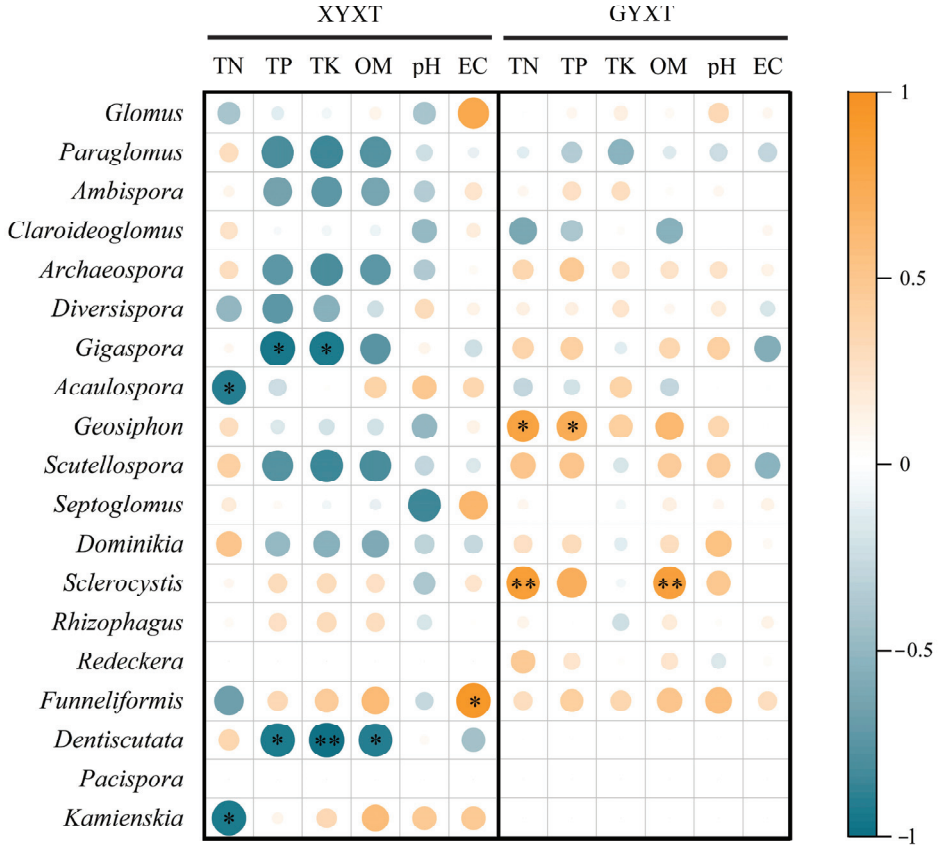


Figure 9. Analysis of soil environmental traits and the arbuscular mycorrhizal fungi (AMF) community. * indicates $p < 0.05$, ** indicates $p < 0.01$.

4. Discussion

Ruan et al. [7] reported a complex relationship between *G. biloba* and soil microbial communities. In the present study, similar to most tree species, bacteria contributed the greatest proportion of the microbial biomass of *G. biloba* rhizosphere soil, followed by actinomycetes and fungi, and the lowest proportion was that of protozoa. The T-PLFA in the rhizosphere soil is an indicator of microbial community richness. A high total amount represents a rich microbial community structure with a large number of microbial species and populations, which is favorable for nutrient uptake by plants [37]. In the present study, the 19 PLFAs chosen to characterize the soil microbial community structure and biomass were present in the rhizosphere soils of ancient and adult *G. biloba*, which was inconsistent with hypothesis (1). Moreover, contrary to hypothesis (1), the microbial biomass in the rhizosphere soil of ancient *G. biloba* was significantly lower than that of adult *G. biloba*. Previous studies have demonstrated that soil microbial biomass and diversity tend to decrease with increasing tree age, especially for the bacteria and actinomycetes involved in cycling soil substances. In contrast, fungi, which have lower metabolic capabilities, may increase in quantity or in terms of the proportion of the total microbial biomass [38]. The F/B ratio of ancient *G. biloba* in the present study was slightly higher than that of adult

G. biloba, confirming this hypothesis. There is a possibility that the rhizosphere soil of ancient *G. biloba* may change from a "bacterial" to a "fungal" pattern with the increase of planting time. The F/B ratio reflects the stability of the microbial community; the larger the F/B ratio, the greater the stability [39]. This indicated that the rhizosphere soil microbial community of ancient *G. biloba* was more stable than that of adult *G. biloba*. The G^+/G^- ratio reflects the soil nutrient status, where the higher the value, the higher the nutrient stress [40], suggesting that adult *G. biloba* trees experience stronger nutrient stress.

Diax et al. [41] concluded that the distribution of the soil microbial population was affected by the combination of local climatic conditions, hydrothermal conditions, soil nutrient status, soil texture, and vegetation composition. According to the correlation analysis between the soil microbial biomass and environmental factors in the present study, soil microorganisms are extremely sensitive to environmental changes, and TP, OM, and pH may be the key factors influencing the soil microbial community in the rhizosphere zone of ancient *G. biloba*. Tan et al. [42] and Lauber et al. [43] found that changes in the TP content of the soil affected the diversity of the soil bacterial and fungal communities. Accordingly, the significantly lower TP content in ancient *G. biloba* than in adult *G. biloba* may be the main reason for the lower microbial biomass in ancient *G. biloba*. In addition, the soil microbial biomass is related to the soil fertility. The rhizosphere soil of adult *G. biloba* in this study had a higher organic matter content, and the density of soil bacteria and actinomycetes was also high, which was consistent with the findings of Liu et al. [44]. Although *G. biloba* has less stringent requirements for soil pH, the metabolic processes of microorganisms have optimal pH ranges. The results of this study suggest that microorganisms in the *G. biloba* rhizosphere prefer alkaline soils. Therefore, improving the TP, OM, and pH of the soil can increase the microbial biomass in the rhizosphere soil of ancient *G. biloba*, enhance the microbial community diversity, and promote the absorption of nutrients by ancient trees.

Tong et al. [17] found that inoculation with mycorrhizal fungi could promote the growth of ancient trees and increase soil fertility in practical applications. Therefore, this study examined AMF, which contributes the largest proportion of fungal biomass, in greater depth. Cai et al. [45] also demonstrated that inoculation with AMF treatments also increased the growth and reproduction of phosphate-dissolving bacteria, fungi, and actinomycetes in the soil, but there were significant differences in the increase of the soil microbial population of different AMF. Owing to its ability to generate large amounts of amplicon data, high-throughput sequencing technology is considered one of the most effective molecular techniques for studying community structures and identifying AMF species. It is worth mentioning that this experiment is the first study to employ high-throughput sequencing technology to investigate the diversity of AMF communities in adult *G. biloba*. This is different from most applications of high-throughput sequencing technology in relation to *G. biloba* transcriptome, whole genome, and molecular genetic marker discovery [46]. The results indicated the presence of a rich diversity of AMF in *G. biloba* roots and rhizosphere soil (four orders, ten families, and nineteen genera), which were assigned to 224 virtual taxa. This provides a more comprehensive evaluation than the morphological identification results of nine species from four genera of AMF in *G. biloba* rhizosphere in Zhejiang Province. Additionally, the present study detected a higher number of ASVs in ancient *G. biloba* than in adult *G. biloba*, suggesting closer mutualistic symbiosis between ancient *G. biloba* and AMF. This aligned with the findings of Pei et al. [47], who reported an increasing trend in the number of AMF operational taxonomic units in the rhizosphere soil of *Panax notoginseng* with increasing planting years. Interestingly, this contradicted the results of the PLFA analysis, which indicated a significantly lower soil microbial biomass in the rhizosphere of ancient *G. biloba* than in the rhizosphere soil of adult *G. biloba*. This suggests that although AMF resources are abundant in the rhizosphere soil of ancient *G. biloba*, there may be an accumulation of dead but not fully decomposed AMF over long-term growth, leading to a lower biomass of live AMF.

In contrast, in terms of the AMF species composition and community structure, the situation was broadly similar in the roots and rhizosphere soil of ancient and adult *G. biloba*.

The first and second most dominant genera were *Glomus* and *Paraglomus*, respectively, in the roots and rhizosphere soils of *G. biloba*, which was consistent with results reported in different ecosystems by other researchers. *Glomus*, in particular, is ecologically adaptable, extremely widespread, and a dominant genus in most ecosystems [48–50]. Some studies have reported that *Paraglomus* is the second most dominant genus after *Glomus* in some studies [51,52]. In contrast, *Archaeospora* and *Ambispora* were dominant in the rhizosphere, whereas *Diversispora* and *Claroideoglomus* were dominant in the roots. Furthermore, cluster analysis indicated that seven genera had a closer relationship with ancient *G. biloba* roots, namely *Paraglomus*, *Claroideoglomus*, *Septoglomus*, *Sclerocystis*, *Diversispora*, *Gigaspora*, and *Acaulospora*, whereas *Dominikia* and *Pacispora* had a closer relationship with younger adult *G. biloba* roots. These findings imply that the application of *Diversispora* and *Claroideoglomus* as mycorrhizal fungi in the rhizosphere of ancient *G. biloba* may improve the mycorrhizal infestation rate.

As evidenced by the aforementioned results, hypothesis (2) is valid. Next, the soil environments of the sampling sites were explored. Differences were found in the effects of different soil factors on AMF. In the rhizosphere soil of adult *G. biloba*, the results suggest that TN may be the main influencing factor for *Acaulospora* and *Kamienskia*, EC may be the main influencing factor for *Funneliformis*, and TP and TK may be the main influencing factors for *Gigaspora* and *Dentiscutata*. *Dentiscutata* may also be influenced by OM. *Geosiphons* may be affected by TN and TP in the rhizosphere soil of ancient *G. biloba*, *Geosiphon* may be affected by TN and TP, and *Sclerocystis* may be influenced by TN and OM. Rhizosphere soil factors are important ecological factors that have complex effects on AMF species, diversity, and abundance. However, none of the six soil factors tested had a significant effect on either *Claroideoglomus* or *Diversispora*, which can infest the roots of *G. biloba*. In future research, additional soil factors should be investigated to explore the driving factors and provide a more suitable soil environment.

Furthermore, it will be necessary to isolate and identify the dominant strains in the rhizosphere soil of ancient *G. biloba* through wet screening, cultivation, and propagation. In addition, the rhizosphere soil should be inoculated with suitable AMF agents to increase the biomass of living AMF in the rhizosphere of ancient trees and improve the mycorrhizal infestation rate and root vigor of ancient *G. biloba*. This might produce a more obvious effect than the application of exogenous fungi. It is hoped that self-produced mycorrhizal agents obtained from indigenous fungi can reduce the cost of rejuvenation and realize the great potential of using AMF as biofertilizers. This will promote the localized application of suitable AMF to ancient *G. biloba*, provide more products and choices for the protection and rejuvenation of ancient trees, and play a role in promoting the sustainable protection of ancient trees.

Author Contributions: Conceptualization, J.M. and W.L.; methodology, J.M., F.P., Z.Z., and W.L.; software, J.M. and X.S.; validation, J.M., Y.Y., and Y.W.; formal analysis, J.M.; investigation, J.M., Y.T. and W.L.; resources, Y.T. and W.L.; data curation, J.M. and Y.Y.; writing—original draft, J.M., Q.W., Y.Y., F.P., Z.Z., X.S., and Y.W.; writing—review and editing, Q.W., J.M., F.P., Z.Z. and W.L.; visualization, J.M. and Y.Y.; supervision, Y.T. and W.L.; project administration, Y.T. and W.L.; funding acquisition, Y.T. and W.L. All authors have read and agreed to the published version of the manuscript.

Funding: This work was supported by the Special Fund for Scientific Research of Shanghai Landscaping and City Appearance Administrative Bureau (No. G230505) and the Central Finance Forestry Science and Technology Promotion Demonstration Project (No. JXTG [2024] 25).

Institutional Review Board Statement: Not applicable.

Informed Consent Statement: Not applicable.

Data Availability Statement: The following information was supplied regarding data availability: Data is available at NCBI BioProject accession number PR]NA1142869 (SAMN42966095, SAMN42966096, SAMN42966097, SAMN42966098, SAMN42966099, SAMN42966100, SAMN42966101, SAMN42966102, SAMN42966103, SAMN42966104, SAMN42966105, SAMN42966106, SAMN42966107, SAMN42966108,

SAMN42966109, SAMN42966110, SAMN42966111, SAMN42966112, SAMN42966113, SAMN42966114, SAMN42966115, SAMN42966116, SAMN42966117, SAMN42966118, SAMN42966119, SAMN42966120.

Conflicts of Interest: Author Jieying Mao was employed by the company Ningbo Yongneng Biomass Energy Development Co., Ltd. The remaining authors declare that the research was conducted in the absence of any commercial or financial relationships that could be construed as a potential conflict of interest.

References

1. Liu, J.J.; Lindenmayer, D.B.; Yang, W.J.; Ren, Y.; Campbell, M.J.; Wu, C.P.; Luo, Y.Q.; Zhong, L.; Yu, M.J. Diversity and density patterns of large old trees in China. *Sci. Total Environ.* **2019**, *655*, 255–262. [CrossRef] [PubMed]
2. Nolan, V.; Reader, T.; Gilbert, F.; Atkinson, N. Historical maps confirm the accuracy of zero-inflated model predictions of ancient tree abundance in english wood-pastures. *J. Appl. Ecol.* **2021**, *58*, 2661–2672. [CrossRef]
3. Wu, C.F.; Guo, J.; Wang, G.B. Morphological and physiological responses of male and female *Ginkgo biloba* to temperature changes. *J. Nanjing For. Univ. (Nat. Sci. Ed.)* **2024**, *48*, 150.
4. Dunberg, A. Jubenility, maturation, ageing and rejuvenation in woodyplants. In *Vegetative Propagation of Forest Tree-Physiology and Practice*; Symp: Uppsala, Sweden, 1977; pp. 55–64.
5. Liang, Z.J.; Le, X.W.; Li, X.S. Research on health evaluation index system of ancient *Ginkgo biloba* in Shanghai based on analytic hierarchy process. *For. Environ. Sci.* **2023**, *39*, 89–96.
6. Comer, J.; Perkins, L. Resistance of the soil microbial community to land-surface disturbances of high-intensity winter grazing and wildfire. *J. Environ. Manag.* **2021**, *279*, 111596. [CrossRef] [PubMed]
7. Ruan, R.J.; Jiang, Z.F.; Wu, Y.H.; Xu, M.J.; Ni, J. High-throughput sequence analysis reveals variation in the relative abundance of components of the bacterial and fungal microbiota in the rhizosphere of *Ginkgo biloba*. *PeerJ* **2019**, *7*, e8051. [CrossRef]
8. Smith, F.A.; Smith, S.E. Structural diversity in (vesicular)–arbuscular mycorrhizal symbioses. *New Phytol.* **1997**, *137*, 373–388. [CrossRef]
9. Fierer, N.; Jackson, R.B. The diversity and biogeography of soil bacterial communities. *Proc. Natl. Acad. Sci. USA* **2006**, *103*, 626–631. [CrossRef]
10. Fontana, A. Vesicular-Arbuscular mycorrhizas of *Ginkgo biloba* L. in natural and controlled conditions. *New Phytol.* **1985**, *99*, 441–447. [CrossRef]
11. Wu, Q.S.; Qa, W. Arbuscular mycorrhizae of *Ginkgo biloba* and its correlation with soil available phosphorus. *J. Yangtze Univ. (Nat. Sci. Ed.) Agric. Sci. Vol.* **2008**, *3*, 49–51+112.
12. Yuan, Z.M.; Cheng, X.F.; Wang, J.P.; Zhu, L.J.; Ma, S.L.; Zhang, J.C.; Chu, D.S. Effects of edaphic factors on arbuscular mycorrhizal fungi colonization in muddy coastal area of northern Jiangsu province. *J. Northeast. For. Univ.* **2019**, *47*, 123–129. [CrossRef]
13. Soares, C.R.F.S.; Siqueira, J.O. Mycorrhiza and phosphate protection of tropical grass species against heavy metal toxicity in multi-contaminated soil. *Biol. Fertil. Soils* **2008**, *44*, 833–841. [CrossRef]
14. Huang, Z.; Zou, Z.R.; He, C.X.; He, Z.Q.; Zhang, Z.B.; Li, J.M. Physiological and photosynthetic responses of melon (*Cucumis melo* L.) seedlings to three *Glomus* species under water deficit. *Plant Soil* **2011**, *339*, 391–399. [CrossRef]
15. Li, Z.; Wu, S.L.; Liu, Y.J.; Yi, Q.; You, F.; Ma, Y.Y.; Thomsen, L.; Chan, T.S.; Lu, Y.R.; Hall, M.; et al. Arbuscular mycorrhizal symbiosis enhances water stable aggregate formation and organic matter stabilization in Fe ore tailings. *Geoderma* **2022**, *406*, 115528. [CrossRef]
16. Pauwels, R.; Graefe, J.; Bitterlich, M. An arbuscular mycorrhizal fungus alters soil water retention and hydraulic conductivity in a soil texture specific way. *Mycorrhiza* **2023**, *33*, 165–179. [CrossRef]
17. Tang, Y.H.; Le, X.W.; Liu, J.L. Research on endogenous mycorrhizal fungi to Shanghai ancient *Ginkgo* soil function. *Shanghai Constr. Sci. Technol.* **2021**, *93*, 113–115.
18. Labidi, S.; Ben Jeddi, F.; Tisserant, B.; Yousfi, M.; Sanaa, M.; Dalpe, Y.; Sahraoui, A.L.-H. Field application of mycorrhizal bio-inoculants affects the mineral uptake of a forage legume (*Hedysarum coronarium* L.) on a highly calcareous soil. *Mycorrhiza* **2015**, *25*, 297–309. [CrossRef]
19. Gao, X. Research Progress on the Identification Methodsof the Age of Ancient Trees. *J. Green Sci. Technol.* **2023**, *25*, 163–168+172. [CrossRef]
20. Bossio, D.A.; Scow, K.M.; Gunapala, N.; Graham, K.J. Determinants of soil microbial communities: Effects of agricultural management, season, and soil type on phospholipid fatty acid profiles. *Microb. Ecol.* **1998**, *36*, 1–12. [CrossRef]
21. Zeng, Q.C.; Jia, P.L.; Wang, Y.; Wang, H.L.; Li, C.C.; An, S.S. The local environment regulates biogeographic patterns of soil fungal communities on the Loess Plateau. *Catena* **2019**, *183*, 104220. [CrossRef]
22. Willers, C.; van Rensburg, P.J.J.; Claassens, S. Phospholipid fatty acid profiling of microbial communities-a review of interpretations and recent applications. *J. Appl. Microbiol.* **2015**, *119*, 1207–1218. [CrossRef] [PubMed]
23. Yao, X.D.; Wang, W.; Zeng, H. Application of phospholipid fatty acid method in analyzing soil microbial community composition. *Microbiol. China* **2016**, *43*, 2086–2095. [CrossRef]
24. Murray, M.G.; Thompson, W.F. Rapid isolation of high molecular weight plant DNA. *Nucleic Acids Res.* **1980**, *8*, 4321–4325. [CrossRef]

25. Abe, B.T.; Wesselhoeft, R.A.; Chen, R.; Anderson, D.G.; Chang, H.Y. Circular RNA migration in agarose gel electrophoresis. *Mol. Cell* **2022**, *82*, 1768–1777.e3. [CrossRef] [PubMed]
26. Liu, S.; Wang, P.F.; Wang, C.; Chen, J.; Wang, X.; Hu, B.; Yuan, Q.S. Ecological insights into the disturbances in bacterioplankton-communities due to emerging organic pollutants from differentanthropogenic activities along an urban river. *Sci. Total Environ.* **2021**, *796*, 148973. [CrossRef] [PubMed]
27. Lumini, E.; Orgiazzi, A.; Borriello, R.; Bonfante, P.; Bianciotto, V. Disclosing arbuscular mycorrhizal fungal biodiversity in soil through a land-use gradient using a pyrosequencing approach. *Environ. Microbiol.* **2010**, *12*, 2165–2179. [CrossRef]
28. Lin, X.G.; Feng, Y.Z.; Zhang, H.Y.; Chen, R.R.; Wang, J.H.; Zhang, J.B.; Chu, H.Y. Long-Term balanced fertilization decreases arbuscular mycorrhizal fungal diversity in an arable soil in north China revealed by 454 pyrosequencing. *Environ. Sci. Technol.* **2012**, *46*, 5764–5771. [CrossRef]
29. Bi, Y.L.; Xiao, L.; Guo, C.; Christie, P. Revegetation type drives rhizosphere arbuscular mycorrhizal fungi and soil organic carbon fractions in the mining subsidence area of northwest China. *Catena* **2020**, *195*, 104791. [CrossRef]
30. Li, M.J.; Shao, D.T.; Zhou, J.C.; Gu, J.H.; Qin, J.J.; Chen, W.; Wei, W.Q. Signatures within esophageal microbiota with progression of esophageal squamous cell carcinoma. *Chin. J. Cancer Res.* **2020**, *32*, 755–767. [CrossRef]
31. Koskey, G.; Avio, L.; Turrini, A.; Cristiana, S.; Paolo, B. Durum wheat-lentil relay intercropping enhances soil mycorrhizal activity but does not alter structure of arbuscular mycorrhizal fungal community within roots. *Agric. Ecosyst. Environ.* **2023**, *357*, 108696. [CrossRef]
32. John, D.; Mari, M.; Marina, S.; Binte, A.S.; Talaat, A.; Asem, A.A.; Juha, M.A.; Saleh, A.-Q.; Elena, A.; Sten, A.; et al. Temperature and pH define the realised niche space of arbuscular mycorrhizal fungi. *New Phytol.* **2021**, *231*, 763–776. [CrossRef]
33. Öpik, M.; Vanatoa, A.; Vanatoa, E.; Moora, M.; Davison, J.; Kalwij, J.M.; Reier, U.; Zobel, M. The online database MaarjAM reveals global and ecosystemic distribution patterns in arbuscular mycorrhizal fungi (Glomeromycota). *New Phytol.* **2010**, *188*, 223–241. [CrossRef] [PubMed]
34. Öpik, M.; Davison, J. Uniting species-and community-oriented approaches to understand arbuscular mycorrhizal fungal diversity. *Fungal Ecol.* **2016**, *24*, 106–113. [CrossRef]
35. Deng, J.J.; Yu, D.P.; Zhou, W.M.; Li, Z.; Zhu, W.X. Variations of Phyllosphere and Rhizosphere Microbial Communities of Pinus koraiensis Infected by Bursaphelenchus xylophilus. *Microb. Ecol.* **2022**, *84*, 285–301. [CrossRef] [PubMed]
36. Wang, Y.; Pan, F.; Wang, Q.; Luo, J.; Zhang, Q.; Pan, Y.Y.; Wu, C.L.; Liu, W. The Effect of Different Remediation Treatments on Soil Fungal Communities in Rare Earth Tailings Soil. *Forests* **2022**, *13*, 1987. [CrossRef]
37. Bååth, E.; Anderson, T.H. Comparison of soil fungal/bacterial ratios in a pH gradient using physiological and PLFA-based techniques. *Soil Biol. Biochem.* **2003**, *35*, 955–963. [CrossRef]
38. Fu, X.Q.; Huang, W.X. Analysis on microbial diversity in the rhizosphere of Nanfeng tangerine of different tree-age. *Acta Hortic. Sin.* **2014**, *41*, 631–640. [CrossRef]
39. de Vries, F.T.; Hoffland, E.; van Eekeren, N.; Brussaard, L.; Bloem, J. Fungal/bacterial ratios in grasslands with contrasting nitrogen management. *Soil Biol. Biochem.* **2006**, *38*, 2092–2103. [CrossRef]
40. Hammesfahr, U.; Heuer, H.; Manzke, B.; Smalla, K.; Thiele-Bruhn, S. Impact of the antibiotic sulfadiazine and pig manure on the microbial community structure in agricultural soils. *Soil Biol. Biochem.* **2008**, *40*, 1583–1591. [CrossRef]
41. Díaz-Raviña, M.; Acea, M.J.; Carballas, T. Seasonal changes in microbial biomass and nutrient flush in forest soils. *Biol. Fertil. Soils* **1995**, *19*, 220–226. [CrossRef]
42. Tan, H.; Barret, M.; Mooij, M.J.; Rice, O.; Morrissey, J.P.; Dobson, A.; Griffiths, B.; O'gara, F. Long-term phosphorus fertilisation increased the diversity of the total bacterial community and the phoD phosphorus mineraliser group in pasture soils. *Biol. Fertil. Soils* **2013**, *49*, 661–672. [CrossRef]
43. Lauber, C.L.; Strickland, M.S.; Bradford, M.A.; Fierer, N. The influence of soil properties on the structure of bacterial and fungal communities across land-use types. *Soil Biol. Biochem.* **2008**, *40*, 2407–2415. [CrossRef]
44. Liu, G.Q.; Bian, X.M.; Zhang, W.; Li, S. Eficets of long-term continuous cropping of colon and retuming cotton stalk into field on soil biological activities. *Chin. J. Appl. Ecol.* **2008**, *19*, 1027–1032.
45. Cai, X.B.; Feng, G.; Qian, C.; Gai, J.P. Effects of AM fungi on steppe plants and soil environment in Tibet plateau. *Acta Pedol. Sin.* **2007**, *44*, 63–72. [CrossRef]
46. Ruan, R.J.; Wang, L.J.; Ni, J. Application of high-throughput sequencing in the research of *Ginkgo biloba*. *J. Hangzhou Norm. Univ. (Nat. Sci. Ed.)* **2021**, *20*, 137–142. [CrossRef]
47. Pei, Y.; Yin, M.; Li, Q.H.; Zhang, Y.F.; Zhong, Y.; Chen, X.; Zhang, Y.P.; Huang, B.; Ren, Z. Diversity and community structure of arbuscular mycorrhizal fungi (AMF) in the rhizospheric soil of *Panax notoginseng* in different ages. *Eurasian Soil Sci.* **2023**, *56*, 329–339. [CrossRef]
48. Jing, Y.B.; Li, T.; Cui, H.L.; Li, L.F.; Allen, S.C.; Chen, L.; Li, Y.P.; Zhao, Z.W. Shifts in the arbuscular mycorrhizal fungal community composition of *Betula alnoides* along young, middle-aged plantation and adjacent natural forest. *Iforest-Biogeosci. For.* **2020**, *13*, 447–455. [CrossRef]
49. Alimi, A.A.; Ezeokoli, O.T.; Adeleke, R.; Moteetee, A. Arbuscular mycorrhizal fungal communities colonising the roots of indigenous legumes of South Africa as revealed by high-throughput DNA metabarcoding. *Rhizosphere* **2021**, *19*, 100405. [CrossRef]
50. Yu, X.-Y.; Wang, B.-T.; Jin, L.; Ruan, H.-H.; Lee, H.-G.; Jin, F.-J. Impacts of biogas slurry fertilization on arbuscular mycorrhizal fungal communities in the rhizospheric soil of poplar plantations. *J. Fungi* **2022**, *8*, 1253. [CrossRef]

51. Wang, Z.J.; Ma, K.; Cui, H.Z.; Li, G.W.; Yu, H.Q.; Jiang, Q. Correlations between arbuscular mycorrhizal fungi and distribution of main grassland types in Ningxia. *Acta Pratacult. Sin.* **2020**, *29*, 150–160.
52. Gao, T.T.; Wang, Z.K.; He, Y.L.; Li, G.F.; Lv, X.H.; Zhuang, L. Comparative study of rhizospheric arbuscular mycorrhizal fungi from three medicinal licorice plants of Xinjiang. *Acta Bot. Boreali-Occident. Sin.* **2021**, *41*, 643–653.

Disclaimer/Publisher's Note: The statements, opinions and data contained in all publications are solely those of the individual author(s) and contributor(s) and not of MDPI and/or the editor(s). MDPI and/or the editor(s) disclaim responsibility for any injury to people or property resulting from any ideas, methods, instructions or products referred to in the content.

Journal of *Fungi*

MDPI

Article

The Fungal Community Structure Regulates Elevational Variations in Soil Organic Carbon Fractions in a Wugong Mountain Meadow

Jinping Wang [1], Jihong Yuan [2,*], Qiong Ren [2,*], Liyin Zhou [2], Huanhuan Zeng [2], Lujun Miao [2], Zhiyong Sun [2], Fang Wan [2] and Yuanying Yan [2]

[1] Jiangxi Key Laboratory for Intelligent Monitoring and Integrated Restoration of Watershed Ecosystem, Nanchang Institute of Technology, 289 Tianxiang Road, Nanchang 330099, China; wangjp0107@nit.edu.cn
[2] National Ecosystem Research Station of Jiangxi Wugong Mountain Meadow, Wetland Ecological Resources Research Center, Jiangxi Academy of Forestry, 1629 West Fenglin Street, Nanchang 330032, China; zhouly@jxlky.cn (L.Z.); zenghuanhuan1124@163.com (H.Z.); miaolujun@126.com (L.M.); andyd@163.com (Z.S.); zly800907@126.com (F.W.); yuanjh040@nenu.edu.cn (Y.Y.)
* Correspondence: yuanjh0107@jxlky.cn (J.Y.); jane5872@126.com (Q.R.); Tel.: +86-170-0703-1718 (J.Y.); +86-136-8791-6228 (Q.R.)

Abstract: Soil organic carbon (SOC) fractions are vital intrinsic indicators of SOC stability, and soil fungi are the key drivers of soil carbon cycling. However, variations in SOC fractions along an elevational gradient in mountain meadows and the role of the fungal community in regulating these variations are largely unknown, especially in subtropical areas. In this study, an elevation gradient experiment (with experimental sites at 1500, 1700, and 1900 m) was set up in a *Miscanthus sinensis* community in a meadow on Wugong Mountain, Southeast China, to clarify the effects of elevation on soil fungal community composition, microbial residue carbon, and SOC fractions. The results showed that the contribution of soil microbial residue carbon to SOC was only 16.1%, and the contribution of soil fungal residue carbon to SOC (15.3%) was far greater than that of bacterial residue carbon (0.3%). An increase in elevation changed the fungal community structure and diversity, especially in the topsoil (0–20 cm depth) compared with that in the subsoil (20–40 cm depth), but did not affect fungal residue carbon in the two soil layers. When separating SOC into the fractions mineral-associated organic carbon (MAOC) and particulate organic carbon (POC), we found that the contribution of MAOC (66.6%) to SOC was significantly higher than that of POC (20.6%). Although an increased elevation did not affect the SOC concentration, it significantly changed the SOC fractions in the topsoil and subsoil. The soil POC concentration and its contribution to SOC increased with an increasing elevation, whereas soil MAOC showed the opposite response. The elevational variations in SOC fractions and the POC/MAOC ratio were co-regulated by the fungal community structure and total nitrogen. Our results suggested that SOC stabilization in mountain meadows decreases with an increasing elevation and is driven by the fungal community structure, providing scientific guidance for SOC sequestration and stability in mountain meadows in subtropical areas.

Keywords: SOC fractions; mountain meadow; elevation; fungal community; microbial residue carbon

1. Introduction

Since the beginning of the 20th century, global air temperature has risen due to the rise in atmospheric concentrations of CO_2 and other greenhouse gases. The increase in global average temperature is over 1.1 °C now, and might reach 1.4–5.8 °C by the end of the 21st century [1], with the increases being greater in high-latitude and high-elevation regions. Disastrous consequences will occur without mitigating the global warming trend. Soil is the largest terrestrial organic carbon (C) reserve [2] and is central to climate change mitigation and ecosystem sustainability [3]. Globally, more activated C is stored in the

soil than in the atmosphere and vegetation combined [4]. Therefore, small changes in soil organic carbon (SOC) have marked effects on atmospheric CO_2 concentrations and, hence, on global climate [5]. Soil C decomposition caused by climate warming leads to a faster transfer of soil-stored C into the air, triggering a positive feedback loop of climate warming [6]. Enhancing soil C sequestration is a key strategy for mitigating the climate crisis [7]. The formation, decomposition, and transformation of soil C directly affect SOC sequestration [8], and SOC fractions directly affect the rate of soil C decomposition, thereby determining the stabilization of SOC [9,10]. Hence, research on the variation in SOC sources and SOC fractions is essential for understanding global C cycling and management of soil C sequestration.

The SOC can be separated into two physical fractions: particulate organic carbon (POC) and mineral-associated organic carbon (MAOC) [11]. POC is mainly formed from incompletely decomposed plant residues and is composed of lightweight fragments made up of large polymers [12], whereas MAOC is formed from single small molecules that originate from dead microbial biomass or leachate from plant residues and roots and is associated with silt- and clay-sized minerals [13,14]. Therefore, the stability of POC is low and it is easily decomposed by microorganisms, whereas MAOC has the opposite properties. Scientists have studied the effects of atmospheric CO_2 concentration increases [15], climate warming [16], rainfall increases [17], and nitrogen deposition [18] on soil POC and MAOC and found that POC was more responsive to global change, whereas MAOC was generally less responsive [19]. However, these studies rarely involved variations in microbial communities even though microorganisms play a key role in soil C cycling. Microorganisms promote the formation and transformation of POC and MAOC, and microbial residues and secretions are important stable C sources for the soil C pool [20,21]. Microorganisms regulate the SOC quantity and quality, including the transformation of plant-derived C, the formation of microbial C, and the stabilization of microbial C [22]. There are two routes for transferring plant-derived C by microorganisms: first, microorganisms decompose and transform high-molecular-weight plant-derived substrates into low-molecular-weight compounds that can accumulate steadily in the soil by secreting extracellular enzymes; second, microorganisms synthesize their own biomass by assimilating plant-derived substrates; and ultimately, part of their necromass is stabilized in the soil. Hence, variations in microbial community structure, composition, and metabolic activities affect plant-derived C transformation and microbe-derived C formation [23,24], thus regulating SOC fractions and ultimately affecting soil C cycling and stabilization [25]. However, the effects of microbial community variations on microbial C generation and SOC fraction accumulation in changing environments remain unclear.

Microorganisms have key ecological functions in terrestrial ecosystems, and fungi play pivotal roles in organic matter decomposition and soil C cycling [26]. Compared with bacteria, fungi have a higher C/N ratio and some fungi species like white rot fungi tend to decompose complex substrates, such as lignin [27]. Among the soil fungi, saprotrophic fungi decompose soil organic substrates and release CO_2 into the atmosphere, whereas mutualistic mycorrhizal fungi have the opposite effect, leading to enhanced C sequestration [28]. Numerous studies have indicated that the contribution of fungi to SOC accumulation is greater than that of bacteria [24,29–31], particularly in grassland ecosystems [32]. A meta-analysis conducted by Wang et al. [33] found that the accumulation efficiency of soil microbial residue C was higher in grasslands and farmlands than in forests; the contributions of microbial residue C to SOC were grassland (47–54%) > farmland (24–51%) > forests (34–44%), while fungal residue C contributed more to SOC (>65%) than bacterial residue C (32–36%). This latter observation could be attributed to the greater biomass of fungi and the lower decomposition rate of fungal cell compounds compared to those of bacteria [33]. Therefore, fungi play a key role in soil C storage and stabilization.

The ecological function, biomass production, and community distribution of fungi are readily affected by environmental changes [34,35] because environmental changes trigger variations in vegetation type and soil physicochemical properties, including soil

water content, pH, C/N ratio, and temperature [36–39]. Variations in fungal community composition and ecological functions lead to changes in fungal residue C storage [40]. Different elevational gradients have significantly different climate, soil, and vegetation characteristics, thus creating complex environmental conditions, and are regarded as natural experiments for research on the ecological and evolutionary responses of microbial communities to changing environments [41–43]. The shift in the fungal community caused by changes in the environment along elevational gradients may lead to significant changes in litter decomposition and nutrient transformation [44,45], thus affecting the SOC fractions. Although the response of the fungal community composition and its biomass to elevation is clear, our knowledge of the relationship between the fungal community and fungal residue C at high elevations, which is the key to understanding how fungal communities affect SOC fractions, is limited.

Global grasslands cover approximately 40.5% of the Earth's terrestrial area and store 34% of the terrestrial C stock [46]. Because of their large area and potential for C sequestration, grasslands are critical for the global C cycle [47]. Approximately 90% of the C in grasslands is stored belowground as root biomass and SOC, which are highly vulnerable to human disturbance and climate change [48]. Globally, grasslands have undergone severe degradation, and their biodiversity and ecosystem functions are declining, leading to reductions in SOC storage [49–52]. Much research has focused on the climatic effects on SOC variation, including warming, precipitation, drought, and nitrogen deposition, to slow the speed of soil C loss from grasslands [46,53,54]. However, such research has mainly been conducted in temperate regions because approximately 67% of global grasslands are distributed in temperate regions with arid, semi-arid, and cold climates [55]. The effect of elevation on SOC has been neglected in mountain meadows in subtropical humid regions, which is not helpful for an overall understanding of SOC variation in grasslands. Mountain meadows are special ecosystems with complex substrates that are dominant in soils and rely more on decomposition by fungi [56]. In addition, fungi are better adapted to the low-N and high-elevation environments of mountain meadows [57]. Recent research has found that increased fungal diversity promotes the stabilization efficiency of grass-litter-derived particulate organic matter (POM) but reduces that of mineral-associated organic matter (MAOM) [58], thus affecting SOC storage. Theoretically, variations in fungal metabolism and community composition caused by elevation inevitably affect the formation and stabilization of SOC; however, the processes at play are largely unknown.

The Wugong Mountain meadow is a typical subtropical mountain meadow distributed at an elevation range of 1500 to 1918 m. In this study, we investigated variations in the fungal community, microbial residue C, and SOC fractions in two soil layers (topsoil and subsoil) in response to elevational gradients in the Wugong Mountain meadow. We hypothesized that (i) elevation changes the fungal community diversity and structure, (ii) variation in fungal and bacterial residue C leads to a significant difference in SOC concentration along elevation gradients, (iii) the responses of the concentrations of the SOC fractions POC and MAOC to elevation are different along elevation gradients, and (iv) the difference in fungal community diversity or structure along elevation gradients alters the accumulation of SOC fractions. The goals of this study were to clarify the variations in SOC fractions along elevation gradients and reveal the fungal regulation of SOC fractions in subtropical mountain meadows. This study improves our understanding of the relationships between fungal communities and SOC fractions in humid mountain meadow ecosystems.

2. Materials and Methods

2.1. Study Area Description

Wugong Mountain is a national park in China located on the north side of the Luoxiao Mountains, reaching an elevation of 1918 m. It has a warm and humid monsoon climate zone. The climate in this region exhibits clear seasonal differences. The mean annual temperature is 15 °C, with the highest and lowest recorded temperatures of 39.7 °C and

−9.3 °C. The average annual precipitation is approximately 1800 mm and the frost-free period is more than 200 days. The mountain meadow ecosystem is distributed on Wugong Mountain at an elevation of more than 1500 m, with a total area of 1569.24 hectares. The dominant herbaceous species are *Miscanthus sinensis* Andersson., *Miscanthus floridulus* (Labill.) Warburg ex K. Schumann., *Arundinella hirta* Steud., *Agrostis sozanensis* Hayata., *Pennisetum alopecuroides* (L.) Spreng., *Aster ageratoides* Turcz., *Osmunda japonica* hunb., *Spiraea japonica* L. f., *Senecio nemorensis* L., and *Anaphalis margaritacea* (L.) Benth. & Hook. f.

2.2. Experimental Design and Soil Sampling

We conducted our research in November 2022 at the Grassland Ecological Research Station of Wugong Mountain, Pingxiang, China. Samples were collected at three elevations (1500, 1700, and 1900 m) at approximately 200 m intervals on the sunny slope of Wugong Mountain. The dominant herbaceous *M. sinensis* community along an elevation gradient was selected as the sampling site. Three independent replicate sites (each 10 m × 10 m) were established at each elevation to account for the effects of elevation. The distance between replicate sites at the same elevation was greater than 50 m. Soil samples were collected from the topsoil (0–20 cm depth) and subsoil (20–40 cm depth) layers at each site. After litter removal, triplicate soil samples were collected from the same soil layer at each site and mixed to represent one pooled soil sample. Eighteen mixed soil samples (three elevations × three replicates × two soil layers) were collected in self-sealing bags for preservation. Each of the 18 soil samples was divided into two parts in the laboratory, one part being stored at −80 °C to measure fungal community diversity and structure, and one part being air-dried prior to measure SOC fractions and soil physicochemical properties.

2.3. Soil Physicochemical Analyses

The soil physicochemical properties were determined following the protocols of Ren et al. [59]. The soil pH was determined in a 1: 5 dilution of soil: water using a pH meter (PHS-3D, Shanghai Leica Instrument Co., Ltd., Shanghai, China). Soil total nitrogen (TN) was determined using an elemental analyzer (Vario MACRO cube; Elementar Trading Shanghai, Shanghai, China). Soil total phosphorus (TP) samples were digested with $HClO_4$–H_2SO_4 and determined using molybdenum blue colorimetry. The OM and SOC concentrations were determined using potassium dichromate colorimetry.

2.4. SOC Fraction Analysis

Soil POC and MAOC were extracted using 5 g/L sodium hexametaphosphate according to the method described by Cambardella and Elliott [11]. Air-dried soil was sieved through a 2 mm sieve. A sub-sample (20 g) of sieved soil was placed in a plastic bottle. Then, 100 mL of sodium hexametaphosphate (5 g/L) was added, and a soil suspension was obtained after shaking for 18 h at 90 rpm. The soil suspension was passed through a 53 μm sieve and the residue repeatedly rinsed with distilled water until the water was clear. The materials that remained in the sieve and that passed through the sieve were collected and dried at 60 °C to a constant weight, representing POC and MAOC, respectively. Finally, the proportions of their contents relative to the soil dry weight were calculated.

2.5. Soil Microbial Residue C Analyses

Muramic acid (MurN) is uniquely derived from bacterial peptidoglycans and glucosamine (GluN) predominantly originates from chitin in fungal cell walls. Hence, the bacterial and fungal residue C concentrations were calculated from the MurN and GluN concentrations, respectively. The concentrations of individual amino sugars (MurN, GluN, and galactosamine (GalN)) were determined according to the method described by Indorf et al. [60]. A sub-sample (0.2 g) of air-dried soil was placed in a hydrolytic tube, and 5 mL of HCl (6 mol/L) was added. The hydrolytic tube was incubated in an oven at 105 °C for 48 h to fully hydrolyze the soil sub-sample. Chromatographic separations were performed on a HyperClone C_{18} column (150 mm length × 4.6 mm diameter) at 35 °C, using an

Agilent 6890 gas chromatograph with a flame ionization detector set at 445 nm emission and 330 nm excitation wavelengths. The concentrations of individual amino sugars (MurN, GluN, and GalN) were quantified using the internal standard, myo-inositol.

2.6. Soil DNA Extraction, PCR Amplification, and Illumina Sequencing

Soil fungal DNA was extracted from three independent 0.50 g sub-samples of soil, which had been stored at −80 °C, using a metagenomic DNA Extraction Kit (GENErary), according to the protocol of the manufacturer. The quality and concentration of the extracted DNA were assessed using 1% agarose gel electrophoresis and UV spectrophotometry (AA900T; Perkin Elmer, Norwalk, CA, USA), respectively. The DNA extracts were diluted and stored at −20 °C. The fungal rRNA internal transcribed spacer ITS-1 region was amplified using the primers ITS1F (5′-CTTGGTCATTTAGAGGAAGTAA-3′) and ITS2 (5′-GCTGCGTTCTTCATCGATGC-3′) [61]. PCR amplification was performed as described by Ren et al. [59]. The amplicons were sequenced using an Illumina MiSeq platform (EDC-810; Beijing Bai Mai Biotechnology Co., Ltd., Beijing, China).

Raw sequence data (FASTQ files) were quality-filtered using the Trimmomatic tool and merged using FLASH v1.2.11 software according to three criteria [62]. Sequences with ambiguous bases were excluded from the analysis. Trimmed and unique sequences were clustered using USEARCH at a 97% similarity level to generate operational taxonomic units (OTUs). The taxonomic identity of each phylotype was assigned using a QIIME2 comparison against the UNITE database (https://unite.ut.ee/ (accessed on 18 July 2023)). The diversity and richness indices (Chao1, Simpson, Shannon, and Pielou) of the fungal communities were calculated using QIIME2.

2.7. Statistical Analysis

Duncan's multiple range test ($p < 0.05$) was performed on SOC fractions, microbial residue C, fungal α-diversity indices, the relative abundances of fungal species, and soil physicochemical properties at different elevations in topsoil or subsoil. Multivariate two-way (interaction) analysis of variance (MANOVA) was used to analyze the effects of elevation and soil depth on SOC fractions, microbial residual C, and the microbial residual C: SOC ratio. The results were expressed as the mean ± standard error ($n = 3$). Fungal OTU numbers were normalized using log (OTUs + 1), and redundancy analysis (RDA) of the fungal community and soil chemical factors was conducted using a Monte Carlo test based on an axis length of <4. The statistical significance test included 999 permutations. Non-metric multidimensional scaling (NMDS) was used to illustrate the clustering of different samples and further reflect the fungal community structure based on Bray–Curtis distances at the OTU level.

The relationship between SOC fractions and functional groups of fungi, fungal community composition, and fungal α-diversity indices were investigated using the "pheatmap" package in R, while the correlation coefficients between SOC fractions and soil physicochemical properties were determined using the "corrplot" package in R. Structural equation modeling (SEM) was used to estimate the influence pathway of elevation on SOC fractions and the POC/MAOC ratio. All analyses were conducted using R (v3.6.2).

3. Results

3.1. Variation in Soil Physicochemical Properties Along an Elevation Gradient

Elevation had no significant effect on soil pH or OM concentration but significantly affected soil TN concentration, TP concentration, and the C/N ratio, especially in the topsoil (0–20 cm) compared with the subsoil (20–40 cm) (Table 1). Soil TN and TP concentrations decreased with an increasing elevation, and the decreases were significant at elevations of 1700 and 1900 m ($p < 0.05$) compared with that at 1500 m, while the soil C/N ratio increased with an increasing elevation. The SOC, TN, and TP concentrations in the topsoil were significantly higher than those in the subsoil.

Table 1. Soil physicochemical properties along an elevation gradient in a mountain meadow.

Soil Depth	Elevation	pH	OM (g/kg)	TN (g/kg)	TP (g/kg)	C:N
0–20 cm	1500 m	5.31	127.44	4.80 a	0.82 a	15.62 b
	1700 m	5.46	129.61	3.68 b	0.53 b	20.43 a
	1900 m	5.43	127.59	3.40 b	0.55 b	21.73 a
20–40 cm	1500 m	5.49	79.18	2.88	0.59 a	16.00 b
	1700 m	5.48	87.36	2.62	0.35 b	19.34 a
	1900 m	5.49	88.63	2.54	0.44 ab	20.18 a

Note: SOC, soil organic carbon; TN, total nitrogen; TP, total phosphorus; the same lowercase letter indicates no significant differences ($p < 0.05$) among elevation gradients within the same soil layer.

3.2. Variation in SOC Fractions Along an Elevation Gradient

Although an increasing elevation did not significantly affect the SOC concentration, it did significantly affect the SOC fractions (Figure 1A–C). As for the SOC fraction, the POC concentration increased, and the MAOC concentration decreased in response to an increasing elevation. This trend was more evident in the topsoil (0–20 cm) than in the subsoil (20–40 cm) (Figure 1A,B). In the topsoil, the soil POC concentration increased significantly, whereas the soil MAOC concentration decreased significantly at an elevation of 1700 m compared with that at 1500 m. The increase in the contribution of POC to SOC (POC/SOC ratio) and the decrease in the contribution of MAOC to SOC (MAOC/SOC ratio) reached significant levels at an elevation of 1900 m compared to that at 1500 m (Figure 1D,E). However, in the subsoil, the increase in POC concentration and decrease in the MAOC/SOC ratio reached significant levels when the elevation reached 1700 m and 1900 m, respectively. The soil layer significantly affected the SOC and its fractions, indicating that the concentrations of SOC and its fractions were higher in the topsoil than in the subsoil. The average contribution of MAOC to SOC was 66.6% (ranging from 34.3% to 97.4%), whereas that of POC to SOC was 20.6% (ranging from 7.6% to 44.3%). The POC/MAOC ratio increased with an increasing elevation, and the increased value reached a significant level at an elevation of 1900 m compared with that at 1500 m in the topsoil (Figure 1F).

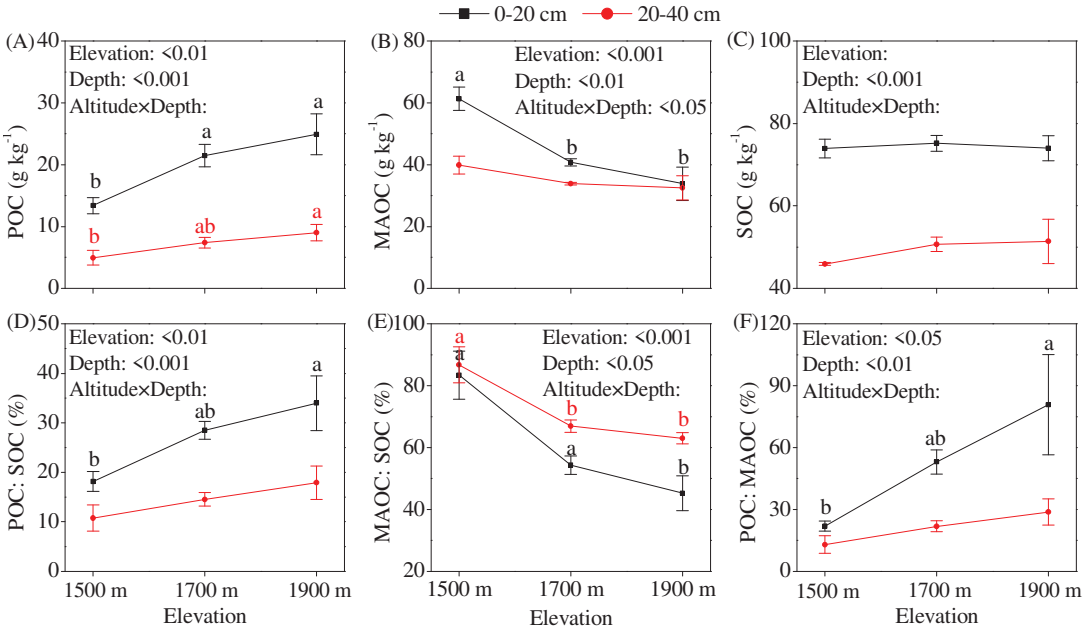


Figure 1. Variation in soil organic carbon (SOC) fractions along an elevation gradient in a mountain meadow. (**A**) POC concentration, (**B**) MAOC concentration, (**C**) SOC concentration, (**D**) POC: SOC ratio, (**E**) MAOC: SOC ratio, (**F**) POC: MAOC ratio. Note: POC, particulate organic carbon; MAOC, mineral-associated organic carbon; the same lowercase letter indicates no significant differences ($p < 0.05$) among elevation gradients within the same soil layer.

3.3. Variation in Soil Microbial Residue C Along an Elevation Gradient

The effects of elevation on soil microbial, fungal, and bacterial residue C were not significant (Figure 2A–C). The fungal/bacterial residue C ratio decreased in the topsoil in response to an increasing elevation, reaching a significant level at an elevation of 1900 m compared to that at 1500 m (Figure 2D). The soil layer had significant effects on microbial and fungal residue C but had no significant effect on bacterial residue C, with the concentrations of microbial and fungal residue C being significantly higher in the topsoil than in the subsoil. The contributions of microbial residue C to SOC were not significantly affected by elevation (Figure 3A–C). The contributions averaged 16.1% (ranging from 6.8% to 20.7%) (Figure 3C), and 98.1% of microbial residue C was contributed by fungal residue C. The contribution of fungal residue C to SOC (15.8%) was far higher than that of bacterial residue C (0.3%) (Figure 3A,B).

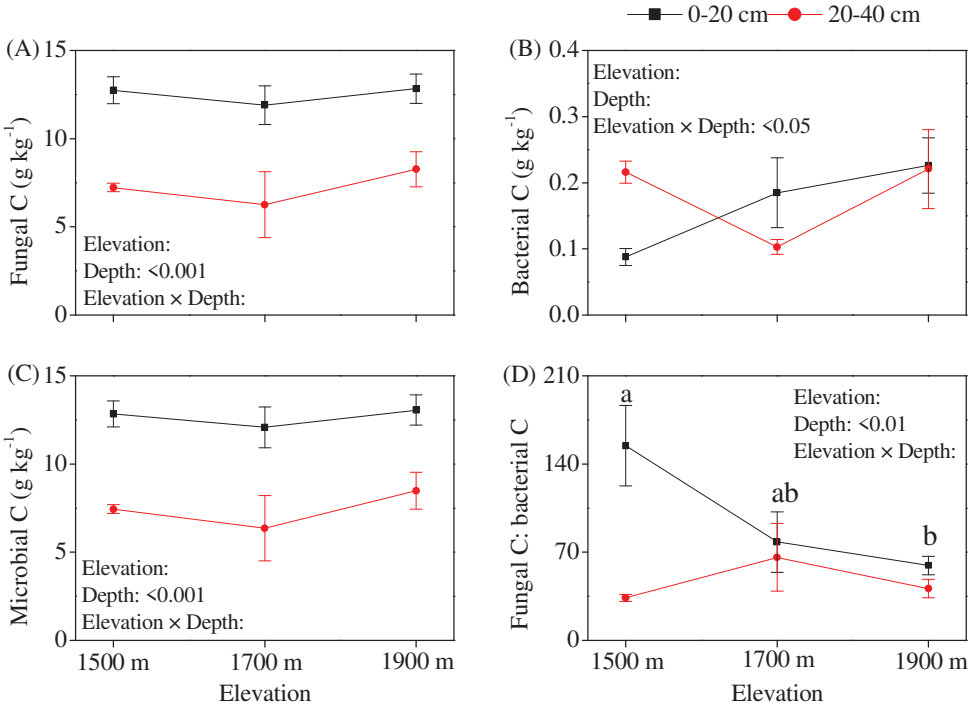


Figure 2. Variation in soil microbial residue C along an elevation gradient in a mountain meadow. (**A**) Fungal residue C concentration, (**B**) Bacterial residue C concentration, (**C**) Microbial residue C concentration, (**D**) Fungal residue C: Bacterial residue C ratio. Note: The same lowercase letter indicates no significant differences ($p < 0.05$) among elevation gradients within the same soil layer.

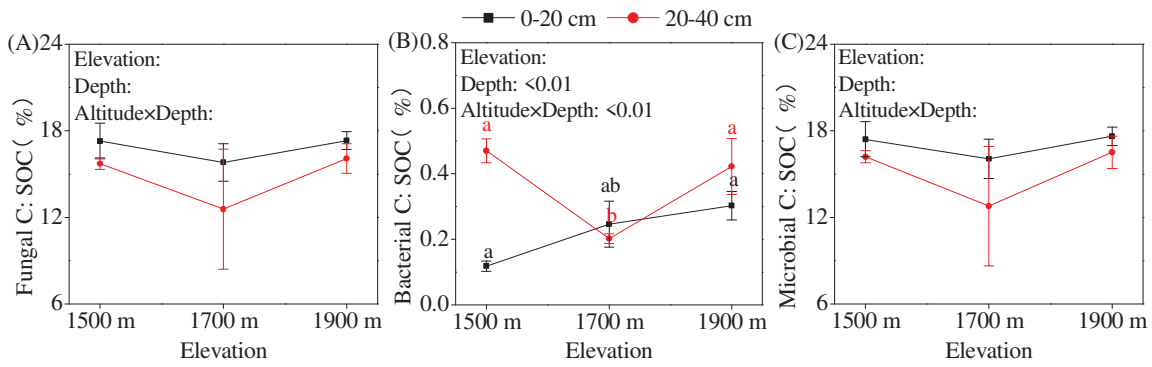


Figure 3. The contribution of soil microbial residue C to soil organic carbon (SOC). (**A**) Fungal residue C: SOC ratio, (**B**) Bacterial residue C: SOC ratio, (**C**) Microbial residue C: SOC ratio. Note: The same lowercase letter indicates no significant differences ($p < 0.05$) among elevation gradients within the same soil layer.

3.4. Variation in Soil Fungal Community α-Diversity Along an Elevation Gradient

Soil fungal community diversity was significantly affected by elevation, especially in the topsoil (Table 2). In the topsoil, the fungal community Chao1 index increased with an increasing elevation, reaching a significant level at an elevation of 1700 m compared with that at 1500 m. The Simpson and Pielou indices of the fungal community decreased significantly at an elevation of 1900 m, while the Shannon index increased significantly at an elevation of 1700 m compared with that at 1500 m. In the subsoil, only the Chao1 index showed significant differences among the different elevations, and the response of the Chao1 index to an increasing elevation in the subsoil was similar to that of the topsoil; however, the increased value of the Chao1 index reached significance only when the elevation reached 1900 m when compared with that at 1500 m.

Table 2. Soil fungal community α-diversity along an elevation gradient in a mountain meadow.

Indices	0–20 cm			20–40 cm			Significance		
	1500 m	1700 m	1900 m	1500 m	1700 m	1900 m	Elevation	Depth	Elevation × Depth
Chao1	292 b	378 a	430 a	213 b	275 b	386 a	0.000	0.001	0.420
Simpson	0.979 a	0.981 a	0.965 b	0.948	0.892	0.929	0.729	0.084	0.639
Shannon	6.445 b	6.908 a	6.421 b	5.712	5.149	5.682	0.993	0.011	0.432
Pielou	1.136 a	1.166 a	1.059 b	1.065	0.917	0.956	0.497	0.045	0.492

Note: The same lowercase letter indicates no significant differences ($p < 0.05$) among elevation gradients within the same soil layer.

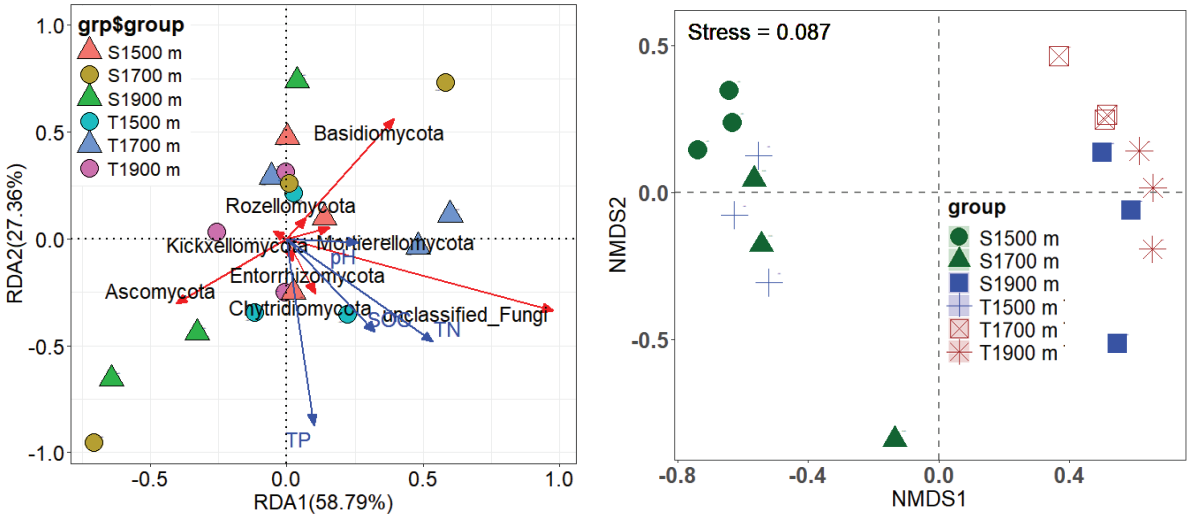
3.5. Variations in Soil Fungal Community Composition and Structure Along an Elevation Gradient

Analysis of the seven main fungi identified at the phylum level revealed that the relative abundances of *Ascomycota* and *Mortierellomycota* in the topsoil were significantly different among the various elevations; the value of *Ascomycota* was the lowest, and that of *Mortierellomycota* was the highest at an elevation of 1700 m (Table 3). In the subsoil, the abundance of *Kickxellomycota* was affected by elevation, with the relative abundance of *Kickxellomycota* increasing with an increasing elevation and the increased value reaching a significant level at an elevation of 1900 m compared with that at 1500 m. *Glomeromycota* was not detected in soil. RDA showed that 87.15% of the variation in fungal community composition could be explained by soil chemical properties, with the fungal community composition mainly affected by soil TN and SOC (Figure 4A). Among the fungal phyla, the abundances of *Chytridiomycota* and unclassified_Fungi were positively correlated with soil TN and SOC ($p < 0.05$), whereas that of *Kickxellomycota* was negatively correlated with soil TN and SOC ($p < 0.05$).

Table 3. Variation in soil fungal phyla along an elevation gradient in a mountain meadow.

Phylum	0–20 cm			20–40 cm			Significance		
	1500 m	1700 m	1900 m	1500 m	1700 m	1900 m	Elevation	Depth	Elevation × Depth
Ascomycota	72.98 a	64.69 b	73.02 a	70.90	71.96	77.33	0.45	0.47	0.67
Basidiomycota	19.18	24.13	20.41	21.82	21.24	17.39	0.71	0.77	0.78
Mortierellomycota	1.90 b	3.24 a	2.41 b	2.10	1.97	2.44	0.20	0.21	0.08
Chytridiomycota	0.17	0.32	0.16	0.03	0.02	0.06	0.12	0.00	0.03
Kickxellomycota	0.09	0.16	0.21	0.04 b	0.10 ab	0.12 a	0.02	0.03	0.81
Rozellomycota	0.00	0.00	0.00	0.09	0.00	0.00	0.40	0.34	0.40
Entorrhizomycota	0.01	0.01	0.01	0.02	0.00	0.00	0.62	0.95	0.41
unclassified_Fungi	5.66	7.46	3.77	5.00	4.71	2.66	0.13	0.19	0.72

Note: The same lowercase letter indicates no significant differences ($p < 0.05$) among elevation gradients within the same soil layer.



(**A**) RDA (**B**) NMDS

Figure 4. Redundancy analysis (RDA) and non-metric multidimensional scaling (NDMS) analysis of soil fungal community structure at different elevations. (**A**) RDA analysis, (**B**) NMDS analysis. Note: SOC, soil organic carbon; TN, total nitrogen; TP, total phosphorus.

The stress value of the NMDS analysis based on the Bray–Curtis distance was 0.087. The fact that this value was <0.200 indicates the reliability of the analysis. For the fungal community structure of the topsoil, the soil samples collected at an elevation of 1700 m were close to those collected at 1900 m but relatively far from those collected at 1500 m. Meanwhile, in the subsoil, the distances between the soil samples collected at an elevation of 1700 m were close to those collected at 1500 m but relatively far from those collected at 1900 m. Hence, elevation had important effects on soil fungal community structure, with the effects being greater in the topsoil than in the subsoil (Figure 4B).

3.6. Factor Analysis of SOC Fractions

Heat map analysis showed that soil MAOC was positively correlated with the relative abundance of saprophytic fungi, such as plant pathogen–undefined saprotrophs ($r = 0.599$, $p < 0.01$), endophyte–litter saprotroph–wood saprotrophs ($r = 0.521$, $p < 0.05$), and lichenized–undefined saprotrophs (r = 0.511, $p < 0.05$) (Figure 5). The relative abundances of these saprophytic fungi were negatively affected by an increase in elevation. Correlation analysis showed that soil POC and SOC were positively correlated with the fungal Chao1 index ($r = 0.649$, $p < 0.01$; $r = 0.540$, $p < 0.05$, respectively), Shannon index ($r = 0.510$, $p < 0.05$; $r = 0.579$, $p < 0.05$, respectively), the abundance of the fungal phylum *Chytridiomycota* ($r = 0.769$, $p < 0.01$; $r = 0.769$, $p < 0.01$, respectively), and the abundance of *Kickxellomycota* ($r = 0.533$, $p < 0.05$; $r = 0.483$, $p < 0.05$, respectively). Furthermore, fungal residue C was positively correlated with the fungal Shannon index ($r = 0.606$, $p < 0.01$), Simpson index ($r = 0.573$, $p < 0.05$), Pielou index ($r = 0.536$, $p < 0.05$), *Chytridiomycota* abundance ($r = 0.505$, $p < 0.05$), and *Kickxellomycota* abundance ($r = 0.505$, $p < 0.05$) (Figure 6A).

Correlation analysis between SOC fractions and soil physicochemical properties indicated that MAOC was positively correlated with TP ($r = 0.780$, $p < 0.01$) and TN ($r = 0.874$, $p < 0.01$) but negatively correlated with the pH value ($r = -0.524$, $p < 0.05$) and C/N ratio ($r = -0.641$, $p < 0.01$). Soil POC was positively correlated with the C/N ratio ($r = 0.525$, $p < 0.05$), whereas SOC was positively correlated with TP ($r = 0.477$, $p < 0.05$) and TN ($r = 0.742$, $p < 0.01$) (Figure 6B). Structural equation modeling (SEM) showed that the elevational variation in the POC: MAOC ratio was regulated by soil fungal community structure, while the elevational variations in POC and MAOC were co-regulated by soil fungal community structure and TN (Figure 7A–C).

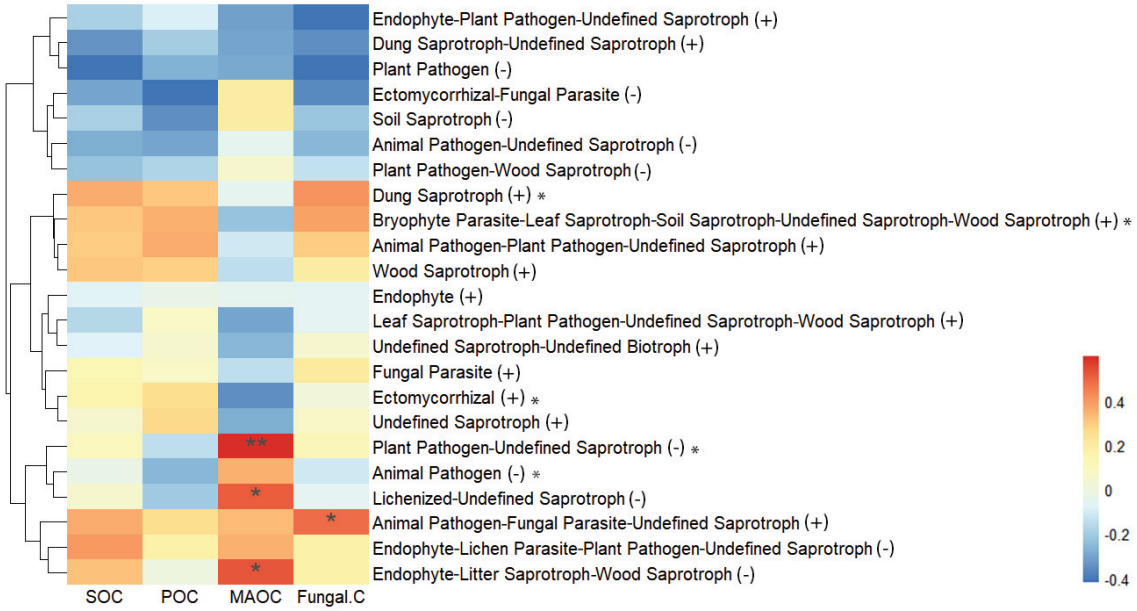
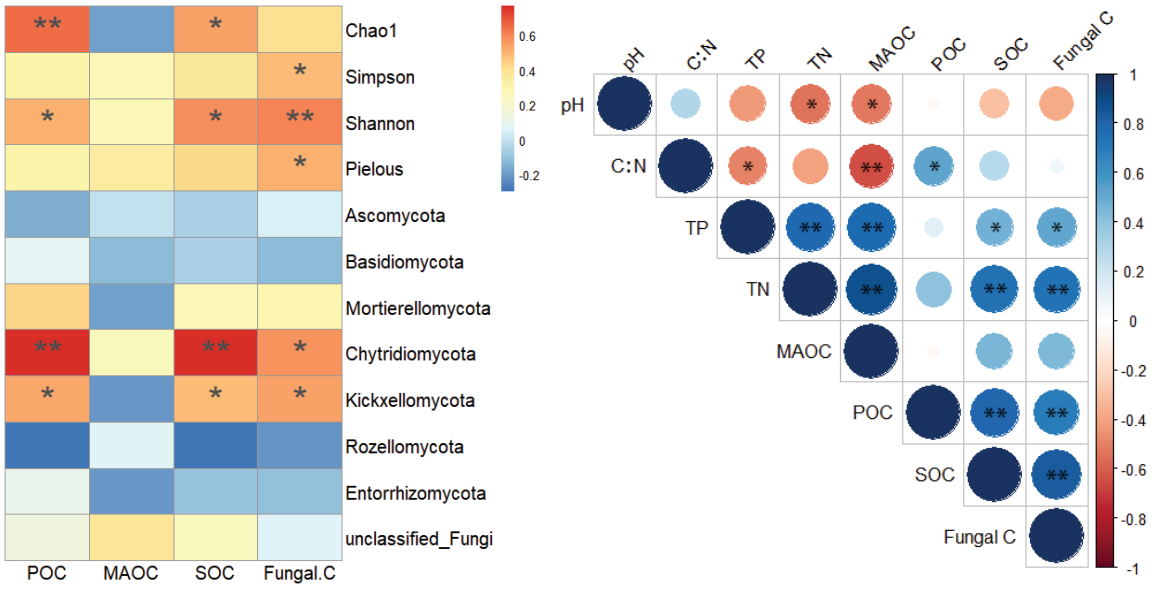


Figure 5. Correlation analysis between soil organic carbon (SOC) fractions and functional groups of fungi. Note: POC, particulate organic carbon; MAOC, mineral-associated organic carbon; symbol between parentheses describes the effect of elevation on fungal functional groups, "−" denotes a negative relationship between fungal functional group and increasing elevation, "+" means a positive relationship, and "*" outside parentheses means the elevation effect was significant; "*" and "**" in the heat map indicate the correlation are significant at 0.05 and 0.01.



(**A**) SOC fractions vs. fungal community (**B**) SOC fractions vs. soil factor

Figure 6. Correlation analysis between soil organic carbon (SOC) fractions and fungal community or soil factor. Note: POC, particulate organic carbon; MAOC, mineral-associated organic carbon; TN, total nitrogen; TP, total phosphorus; *, $p < 0.05$; **, $p < 0.01$.

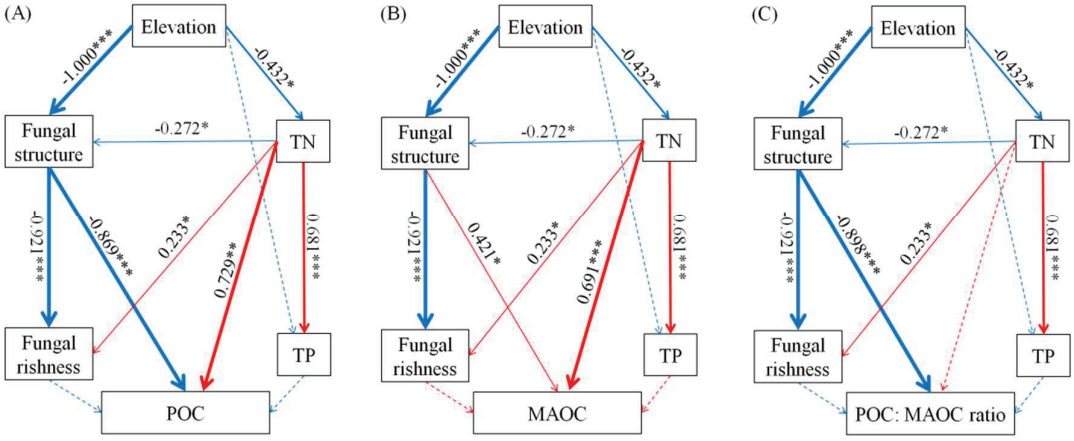


Figure 7. Structural equation model (SEM) of soil organic carbon fractions. Note: POC, particulate organic carbon; MAOC, mineral-associated organic carbon; TN, total nitrogen; TP, total phosphorus; *, $p < 0.05$; **, $p < 0.01$; ***, $p < 0.001$; (**A**) $X^2 = 5.429$, CMIN/DF = 1.357, $p = 0.246$, GFI = 0.920, CFI = 0.985, RMSEA = 0.145; (**B**) $X^2 = 5.688$, CMIN/DF = 1.422, $p = 0.224$, GFI = 0.917, CFI = 0.984, RMSEA = 0.158; (**C**) $X^2 = 5.729$, CMIN/DF = 1.2432, $p = 0.220$, GFI = 0.916, CFI = 0.980, RMSEA = 0.159.

4. Discussion

4.1. Contribution of Fungi to the Soil C Pool Was Far Higher than That of Bacteria

The soil C pool is mainly derived from plant and microbial residue C, and most studies have found that the contribution of soil microbial residue C to SOC is equivalent to or even greater than that of plant residue C [32,63,64]. However, the published results for soil MAOC are open to debate, as stable isotopes reveal that fungal residues contribute more to mineral-associated organic matter (MAOM) pools than plant residues [63]. The stoichiometric approach showed that the contribution of plant residues to MAOM (53–66%) exceeds that of microbial residues (34–47%) [65]. The present study showed that the contribution of microbial residue C to SOC was only 16.1%, indicating that more C was derived from plant-derived C inputs (Figure 3C), which is consistent with the results of previous studies [65,66]. Generally, plant residues are less well assimilated by microorganisms in harsh ecosystems (e.g., under cold or hypoxic conditions), leading to increased plant-derived C storage in the soil [67]. In the mountain meadow, the low temperature reduced microbial activity, leading to a lower assimilation of plant residues. Most studies have shown that fungal residue C contributes more to the soil C pool than bacterial residue C [32]. Our study showed that the contribution of fungal residue C to SOC was much higher than that of bacterial residue C (Figure 3A,B). This discrepancy might be attributed to the lower decomposition rate of cellular compounds and the higher C-use efficiency of fungi than that of bacteria [21]. Moreover, fungi readily decompose grass litter with a high lignin content, which is difficult to decompose, and hence are better adapted to low-nutrient environments [4,27], leading to far higher fungal biomass than bacterial biomass, resulting in far higher fungal residue C than bacterial residue C in a mountain meadow. However, a study conducted in an alpine meadow (elevation of 4750 m) on the Tibetan Plateau showed that the contributions of fungal and bacterial residues to the soil C pool (5.7% and 7.5%, respectively) were not very different [68]. A possible explanation is that the harsh climatic environment created by a very high elevation inhibits plant growth and greatly reduces the C input from plants to the soil system [69]; however, most fungi cannot survive such harsh environments.

4.2. Elevation Changed the Soil Fungal Community Structure and Diversity

Microorganisms are important in regulating biogeochemical cycling and maintaining ecosystem functions [70]. Fungi maintain various ecosystem processes, including belowground C transportation, plant litter decomposition, and plant growth [71–73]. Compared

with bacteria, fungi can decompose recalcitrant organic materials better [26] and adapt better to soil conditions of low nitrogen and high C:N ratios [57]. Fungi are sensitive to environmental changes [74], and variations in the soil fungal community can affect soil C storage [63]. Published reports on the effects of elevation on soil fungal communities are inconsistent and may be related to different ecosystem types. In forest ecosystems, elevation has little effect on soil fungal community composition [75] or affects soil fungal community structure but not diversity [76]. Elevation affects soil fungal communities in a meadow ecosystem [77], which is consistent with the results of our study. The variations in fungal community diversity, composition, and structure with an increasing elevation verified hypothesis (i) (Tables 2 and 3, Figure 4B). The effect of elevation on the soil fungal community structure is driven by vegetation type, soil properties, and climate change [76,77]. Among the soil properties, SOC, TP, TN, the C/N ratio, pH, temperature, humidity, and bulk density significantly affect soil fungal community composition [75–78]. In the present study, elevation-based changes in soil fungal community structure were driven by soil TN and SOC (Figure 4A). Nitrogen is the most important element in microbial cells; therefore, the lower soil TN concentration at higher elevations increases the C/N value, leading to greater constraints on microbial growth and reproduction by soil nitrogen (N), ultimately changing the soil fungal community. We also found that soil fungal community diversity was significantly and positively correlated with soil POC (Figure 6A). POC is composed of plant residues that are easily decomposed, with higher soil POC concentrations at higher elevations indicating that more C is available for fungi, which can relieve competitive pressure on fungi and lead to an increase in fungal community diversity. In addition, we found that the fungal community diversity in the topsoil was higher than that in the subsoil (Table 2), a finding which was consistent with that of Yang et al. [79], who found that, except for nutrient factors, the subsoil created an enclosed microhabitat, which blocked the immigration of exogenous fungal species, maintaining an ecologically specialized and less diverse local community. Topsoil is more susceptible to external environmental changes, such as plant litter input and temperature changes; therefore, the effect of elevation on fungal community structure and diversity was higher in topsoil than in subsoil in the present study.

4.3. Elevation Did Not Change Soil Fungal Residue C Concentration

Generally, harsher environments created at higher elevations will regulate the fungal community, decrease fungal C-use efficiency, and reduce plant residue decomposition by fungi, ultimately leading to a decrease in fungal biomass and fungal residue C. Interestingly, no variation in fungal residue C concentrations was found in response to an elevation gradient (Figure 3A). However, the fungal community changed in our study, a finding which was inconsistent with hypothesis (ii). Accumulation of fungal residue C in soil is caused by the formation of fungal residues and by the decomposition of fungal residues [21]. Soil temperature decreased with an increasing elevation, which reduced the formation of fungal residue; however, the decomposition of fungal residue was also reduced. Therefore, the accumulation efficiency of fungal residue increased [56]; ultimately, the soil fungal residue C concentration did not change along the elevation gradients. Furthermore, we found that soil fungal residue C was significantly and positively correlated with fungal community diversity and some saprophytic fungi such as *Kickxellomycota* (Figures 5 and 6A). Hence, we hypothesized that certain fungal phyla, such as *Kickxellomycota*, adapted well to the environment at higher elevations and compensated for the decrease in fungal residues caused by the biomass reduction in other fungi. *Zoosporic* fungi phylum *Chytridiomycota* was not affected by elevation, but it was significantly and positively correlated with soil fungal residue C, indicating that *Chytridiomycota* might be one of the main fungal phyla that produce fungal residue C at higher elevations. *Glomeromycota* is an important fungal phylum that contributes to soil carbon sequestration in grassland. However, it was not detected, which was attributed to the primers used in our study. Fungal community richness (Chao1 index) and the relative abundance of the phyla *Kickxellomycota* and *Chytridiomycota*

increased, whereas the Simpson index decreased, and the fungal community structure changed significantly at higher elevations (Tables 2 and 3, Figure 4B). Soil properties are considered important factors affecting the accumulation of fungal residue C. A meta-analysis showed that the soil C/N ratio controls the accumulation of soil microbial residue C [80]. However, no significant correlation was observed between soil microbial residue C and the C/N ratio in our study (Figure 6B). Recently, a comprehensive global analysis found that soil N is one of the most important factors affecting the accumulation of microbial residual C [81]. Our study results also showed that the accumulation of fungal residue C was significantly correlated with soil N concentration (Figure 6B).

4.4. Elevation Did Not Change SOC Concentration but Significantly Affected SOC Fractions

The relative concentrations of the SOC fractions are different among terrestrial ecosystems, which reflects SOC stabilization. More SOC is stored as POM in forest ecosystems, whereas more SOC is stored as MAOC in grassland ecosystems [27]. Our study showed that 66.6% of SOC was stored as MAOC in the mountain meadows (Figure 1D), confirming the findings of Cotrufo et al. [27]. The effects of elevation on the SOC concentrations were variable. Garten and Hanson [82] found that SOC storage increased with an increasing elevation, while Djukic et al. [83] reported that SOC storage increased with an increasing elevation below 1500 m but decreased with an increasing elevation above 1500 m. The elevation of the mountain meadow in our study ranged from 1500 m to 1900 m, and our data showed that SOC and microbial residue C concentrations did not increase or decrease with an increasing elevation (Table 1, Figure 3C). The effect of elevation on soil C concentration may be related to vegetation type; the soil C concentration increased with an increasing elevation in bamboo forests, but this trend was not observed in grasslands [84]. Although elevation did not change the SOC concentration in the present study, it significantly affected SOC fractions, increasing the POC concentration and POC/MAOC ratio, while decreasing the MAOC concentration with an increasing elevation (Figure 1A, B, and F). This indicated that SOC stabilization decreased with an increasing elevation in subtropical mountain meadows, thus verifying hypothesis (iii).

The SOC fraction POC mostly comprises undecomposed or semi-decomposed macromolecular plant structural materials such as lignin and semi-lignin [12,85]. Lignin turnover is mainly controlled by temperature and requires moderate-to-high temperatures [86]. The lower soil temperature at higher elevations decreased lignin decomposition by fungi, leading to a greater accumulation of macromolecular plant structural materials; thus, the soil POC concentration increased with an increasing elevation. The SOC fraction, MAOC, consists of low-molecular-weight compounds derived from microorganisms and plants, such as microbial residues, plant lipids, and polysaccharides [13,14]. Decreases in soil temperature, weathering, and N supply at higher elevations slow the rates of microbial decomposition and C-use efficiency, decreasing the decomposition of macromolecular plant residues. Therefore, more macromolecular plant residues were stored in the soil, and fewer low-molecular-weight plant residues were formed and stored in the soil at high elevations, ultimately contributing to increased soil POC concentrations and decreased soil MAOC concentrations at higher elevations. Moreover, higher POC concentrations at higher elevations might be attributed to the increase in fungal community diversity, because greater diversity can promote the stabilization efficiency of grass-litter-derived POM [58]. In our study, SEM analysis verified that elevation affected SOC fractions and the POC/MAOC ratio by changing the fungal community structure and decreasing the soil TN content (Figure 7A–C), thus verifying hypothesis (iv).

Generally, the soil C/N ratio is inversely proportional to the decomposition rate of organic matter by microorganisms. The increase in the soil C/N ratio with an increasing elevation in our study (Table 1) indicates that the decomposition rate of organic matter by microorganisms was lower at higher elevations. This might be attributed to the decrease in the abundance of certain saprophytic fungi, such as endophyte–litter saprotroph–wood saprotrophs, because the abundance of this fungus was negatively affected by an increasing

elevation (Figure 5). Lower N contents and soil temperatures at higher elevations limit the survival of saprophytic fungi. A significant and positive correlation between MAOC concentration and endophyte–litter saprotroph–wood saprotroph abundance suggested that the decrease in soil MAOC concentration at higher elevations was related to the decreased amount of endophyte–litter saprotroph–wood saprotrophs (Figure 5). Moreover, the accumulation of MAOC in the soil is related to soil mineral preservation, the rate of which increases with an increasing degree of weathering [87]. Lower concentrations of soil nutrients P and N (Table 1) indicated lower rates of soil weathering and organic matter decomposition at higher elevations, respectively, and lower soil weathering rates resulted in fewer active minerals (clay and metal oxides), which is not conducive to the formation and storage of MAOC. Furthermore, our results showed that the soil C/N ratio was significantly and positively correlated with POC but negatively correlated with MAOC (Figure 6B). This is not surprising because the main POC materials such as lignin have high C/N ratios (10–40), whereas the organic matter of MAOC has low C/N ratios [12,88,89].

5. Conclusions

Although considerable literature exists on the response of grassland SOC to environmental changes, the effects of elevation on SOC fractions and microbe-driven mechanisms in subtropical mountain meadows are relatively unclear. We designed the experiments described in the current study to address this shortcoming and obtained interesting results. We found that the contribution of microbial residue C to SOC and MAOC was less than 20%, largely due to fungal residue C, and not bacterial residue C, suggesting that the decomposition and transformation of SOC in subtropical mountain meadows were largely dominated by fungi rather than bacteria. Generally, variations in microbial communities affect the accumulation of microbial residues. However, in our study, an increased elevation significantly affected the fungal community composition, while it did not affect the accumulation of fungal residue C, suggesting that the change in the microbial community did not necessarily affect the accumulation of microbial residues. Furthermore, we found that an increased elevation significantly affected SOC fractions but did not affect the SOC concentration. The variation in the fungal community structure and TN with an increasing elevation maintained the accumulation of the fungal residue but altered the SOC fractions and stabilization.

Author Contributions: Conceptualization, J.W., J.Y. and Q.R.; Methodology, J.W., L.Z., L.M., H.Z. and F.W.; Software, Z.S.; Validation, Q.R.; Formal Analysis, J.W. and J.Y.; Investigation, J.W., J.Y. and L.Z.; Resources, Q.R.; Data Curation, J.Y.; Writing—Original Draft, J.W.; Writing—Review and Editing, J.Y.; Visualization, J.W.; Supervision, Y.Y.; Project Administration, J.Y.; Funding Acquisition, J.Y. and Q.R. All authors have read and agreed to the published version of the manuscript.

Funding: This work was financially supported by the Jiangxi Province Forestry Innovation Special Project (Grant No. 2023 (25)), Jiangxi Academy of Forestry Basic and Talent Research Special Project (2022516601, 2023512301, and 2024512301), National Natural Science Foundation of China (42467044), Jiangxi Provincial Natural Science Foundation (20224BAB215032), Science of Technology Research Project of the Education Department of Jiangxi Province (GJJ201924), and Jiangxi Academy of Forestry Youth Science and Technology Talent Training Project.

Institutional Review Board Statement: Not applicable.

Informed Consent Statement: Not applicable.

Data Availability Statement: The original contributions presented in this study are included in the article, and further inquiries can be directed to the corresponding authors.

Conflicts of Interest: The authors declare no conflicts of interest.

References

1. IPCC. *IPCC Fourth Assessment Report: Climatic Change 2007: The Physical Science Basis: Contribution of Working Group I to the Fourth Assessment Report of the Intergovernmental Panel on Climate Change*; Cabridge University Press: New York, NY, USA, 2007.

2. Schlesinger, W.H.; Andrews, J.A. Soil respiration and the global carbon cycle. *Biogeochemistry* **2000**, *48*, 7–20. [CrossRef]
3. Georgiou, K.; Jackson, R.B.; Vinduková, O.; Abramoff, R.Z.; Ahlstrm, A.; Feng, W.; Harden, J.W.; Pellegrini, A.F.A.; Polley, H.W.; Soong, J.L.; et al. Global stocks and capacity of mineral-associated soil organic carbon. *Nat. Commun.* **2022**, *13*, 3797. [CrossRef] [PubMed]
4. Angst, G.; Mueller, K.E.; Nierop, K.G.J.; Simpson, M.J. Plant- or microbial-derived? A review on the molecular composition of stabilized soil organic matter. *Soil Biol. Biochem.* **2021**, *156*, 108189. [CrossRef]
5. Galy, V.; Peucker-Ehrenbrink, B.; Eglinton, T. Global carbon export from the terrestrial biosphere controlled by erosion. *Nature* **2015**, *521*, 204–207. [CrossRef] [PubMed]
6. Davidson, E.A.; Janssens, I.A. Temperature sensitivity of soil carbon decomposition and feedbacks to climate change. *Nature* **2006**, *440*, 165–173. [CrossRef] [PubMed]
7. Bossio, D.A.; Cook-Patton, S.C.; Ellis, P.W.; Fargione, J.; Sanderman, J.; Smith, P.; Wood, S.; Zomer, R.J.; von Unger, M.; Emmer, I.M.; et al. The role of soil carbon in natural climate solutions. *Nat. Sustain.* **2020**, *3*, 391–398. [CrossRef]
8. Schmidt, M.W.I.; Torn, M.S.; Abiven, S.; Dittmar, T.; Guggenberger, G.; Janssens, I.A.; Kleber, M.; Koegel-Knabner, I.; Lehmann, J.; Manning, D.A.C.; et al. Persistence of soil organic matter as an ecosystem property. *Nature* **2011**, *478*, 49–56. [CrossRef]
9. Guan, S.; An, N.; Zong, N.; He, Y.t.; Shi, P.l.; Zhang, J.J.; He, N.P. Climate warming impacts on soil organic carbon fractions and aggregate stability in a Tibetan alpine meadow. *Soil Biol. Biochem.* **2018**, *116*, 224–236. [CrossRef]
10. Lehmann, J.; Hansel, C.M.; Kaiser, C.; Kleber, M.; Maher, K.; Manzoni, S.; Nunan, N.; Reichstein, M.; Schimel, J.P.; Torn, M.S.; et al. Persistence of soil organic carbon caused by functional complexity. *Nat. Geosci.* **2020**, *13*, 529–534. [CrossRef]
11. Cambardella, C.A.; Elliott, E.T. Particulate Soil Organic-Matter Changes across a Grassland Cultivation Sequence. *Soil Sci. Soc. Am. J.* **1992**, *56*, 777–783. [CrossRef]
12. Williams, E.K.; Fogel, M.L.; Berhe, A.A.; Plante, A.F. Distinct bioenergetic signatures in particulate versus mineral-associated soil organic matter. *Geoderma* **2018**, *330*, 107–116. [CrossRef]
13. Sokol, N.W.; Sanderman, J.; Bradford, M.A. Pathways of mineral- associated soil organic matter formation: Integrating the role of plant carbon source, chemistry, and point of entry. *Global Change Biol.* **2019**, *25*, 12–24. [CrossRef]
14. Buckeridge, K.M.; Creamer, C.; Whitaker, J. Deconstructing the microbial necromass continuum to inform soil carbon sequestration. *Funct. Ecol.* **2022**, *36*, 1396–1410. [CrossRef]
15. Hofmockel, K.S.; Zak, D.R.; Moran, K.K.; Jastrow, J.D. Changes in forest soil organic matter pools after a decade of elevated CO_2 and O_3. *Soil Biol. Biochem.* **2011**, *43*, 1518–1527. [CrossRef]
16. Poeplau, C.; Thomas, K.T.; Leblans, N.I.W.; Sigurdsson, B.D. Sensitivity of soil carbon fractions and their specific stabilization mechanisms to extreme soil warming in a subarctic grassland. *Global Change Biol.* **2017**, *23*, 1316–1327. [CrossRef] [PubMed]
17. Song, B.; Niu, S.L.; Zhang, Z.; Yang, H.J.; Li, L.H.; Wan, S.Q. Light and heavy fractions of soil organic matter in response to climate warming and increased precipitation in a temperate steppe. *PLoS ONE* **2012**, *7*, e33217. [CrossRef]
18. Chen, J.G.; Xiao, W.; Zheng, C.Y.; Zhu, B. Nitrogen addition has contrasting effects on particulate and mineral-associated soil organic carbon in a subtropical forest. *Soil Biol. Biochem.* **2020**, *142*, 107708. [CrossRef]
19. Rocci, K.; Lavalle, J.M.; Stewart, C.E.; Cotrufo, M.F. Soil organic carbon response to global environmental change depends on its distribution between mineral-associated and particulate organic matter: A meta-analysis. *Sci. Total Environ.* **2021**, *793*, 148569. [CrossRef]
20. Georgiou, K.; Abramoff, R.Z.; Harte, J.; Riley, W.J.; Torn, M.S. Microbial community-level regulation explains soil carbon responses to long-term litter manipulations. *Nat. Commun.* **2017**, *8*, 1223. [CrossRef] [PubMed]
21. Wang, C.; Wang, X.; Pei, G.T.; Xia, Z.W.; Peng, B.; Sun, L.F.; Gao, D.C.; Chen, S.D.; Liu, D.W.; Dai, W.W.; et al. Stabilization of microbial residues in soil organic matter after two years of decomposition. *Soil Biol. Biochem.* **2020**, *141*, 107687. [CrossRef]
22. Liang, C.; Schimel, J.P.; Jastrow, J.D. The importance of anabolism in microbial control over soil carbon storage. *Nat. Microbiol.* **2017**, *2*, 17105. [CrossRef] [PubMed]
23. Jia, S.; Liu, X.; Lin, W.; Li, X.; Yang, L.; Sun, S.; Hui, D.; Guo, J.; Zou, X.; Yang, Y. Tree roots exert greater influence on soil microbial necromass carbon than above-ground litter in subtropical natural and plantation forests. *Soil Biol. Biochem.* **2022**, *173*, 108811. [CrossRef]
24. Tian, P.; Zhao, X.; Liu, S.; Wang, Q.; Zhang, W.; Guo, P.; Razavi, B.S.; Liang, C. Differential responses of fungal and bacterial necromass accumulation in soil to nitrogen deposition in relation to deposition rate. *Sci. Total Environ.* **2022**, *847*, 157645. [CrossRef]
25. Liang, C.; Cheng, G.; Wixon, D.L.; Balser, T.C. An Absorbing Markov Chain approach to understanding the microbial role in soil carbon stabilization. *Biogeochemistry* **2011**, *106*, 303–309. [CrossRef]
26. Clipson, N.; Otte, M.; Landy, E. Biogeochemical roles of fungi in marine and estuaring habitats. In *Fungi in Biogeochemical Cycles*; Gadd, G.M., Ed.; Cambridge University Press: New York, NY, USA, 2006; pp. 436–461.
27. Cotrufo, M.F.; Ranalli, M.G.; Haddix, M.L.; Six, J.; Lugato, E. Soil carbon storage informed by particulate and mineral-associated organic matter. *Nat. Geosci.* **2019**, *12*, 989–994. [CrossRef]
28. Clemmensen, K.E.; Bahr, A.; Ovaskainen, O.; Dahlberg, A.; Ekblad, A.; Wallander, H.; Stenlid, J.; Finlay, R.D.; Wardle, D.A.; Lindahl, B.D. Roots and associated fungi drive long-term carbon sequestration in boreal forest. *Science* **2013**, *339*, 1615–1618. [CrossRef]

29. Li, N.; Xu, Y.Z.; Han, X.Z.; He, H.B.; Zhang, X.D.; Zhang, B. Fungi contribute more than bacteria to soil organic matter through necromass accumulation under different agricultural practices during the early pedogenesis of a Mollisol. *Eur. J. Soil Biol.* **2015**, *67*, 51–58. [CrossRef]
30. Li, T.; Zhang, J.; Wang, X.; Hartley, I.P.; Zhang, Y. Fungal necromass contributes more to soil organic carbon and more sensitive to land use intensity than bacterial necromass. *App. Soil Ecol.* **2022**, *176*, 104492. [CrossRef]
31. Wang, X.X.; Zhou, L.Y.; Fu, Y.L.; Jiang, Z.; Jia, S.X.; Song, B.Q.; Liu, D.G.; Zhou, X.H. Drought-induced changes in rare microbial community promoted contribution of microbial necromass C to SOC in a subtropical forests. *Soil Biol. Biochem.* **2024**, *189*, 109252. [CrossRef]
32. Liang, C.; Amelung, W.; Lehmann, J.; Kastner, M. Quantitative assessment of microbial necromass contribution to soil organic matter. *Global Change Biol.* **2019**, *25*, 3578–3590. [CrossRef]
33. Wang, B.R.; An, S.S.; Liang, C.; Yang, L.; Yakov, K. Microbial necromass as the source of soil organic carbon in global ecosystems. *Soil Biol. Biochem.* **2021**, *162*, 108422. [CrossRef]
34. Parmesan, C. Ecological and evolutionary responses to recent climate change. *Annu. Rev. Ecol. Evol. Syst.* **2006**, *37*, 637–669. [CrossRef]
35. Pecl, G.T.; Araujo, M.B.; Bell, J.D.; Blanchard, J.; Bonebrake, T.C.; Chen, I.; Clark, T.D.; Colwell, R.K.; Danielsen, F.; Evengard, B.; et al. Biodiversity redistribution under climate change: Impacts on ecosystems and human well-being. *Science* **2017**, *355*, 6332. [CrossRef] [PubMed]
36. Myers, R.T.; Zak, D.R.; White, D.C.; Peacock, A. Landscape-level patterns of microbial community composition and substrate use in upland forest ecosystems. *Soil Sci. Am. J.* **2001**, *65*, 359–367. [CrossRef]
37. Treseder, K.K. A meta-analysis of mycorrhizal responses to nitrogen, phosphorus, and atmospheric CO_2 in field studies. *New Phytol.* **2004**, *164*, 347–355. [CrossRef] [PubMed]
38. Castro, H.F.; Classen, A.T.; Austin, E.E.; Norby, R.J.; Schadt, C.W. Soil microbial community responses to multiple experimental climate change drivers. *Appl. Environ. Microb.* **2010**, *76*, 999–1007. [CrossRef]
39. Wakelin, S.A.; Colloff, M.J.; Harvey, P.R.; Marschner, P.; Gregg, A. The effects of stubble retention and nitrogen application on soil microbial community structure and functional gene abundance under irrigatedmaize. *FEMS Microbiol. Ecol.* **2007**, *59*, 661–670. [CrossRef]
40. Butler, O.M.; Manzoni, S.; Warren, C.R. Community composition and physiological plasticity control microbial carbon storage across natural and experimental soil fertility gradients. *ISME J.* **2023**, *17*, 2259–2269. [CrossRef] [PubMed]
41. Körner, C. The use of 'altitude' in ecological research. *Trends Ecol. Evol.* **2007**, *22*, 569–574. [CrossRef] [PubMed]
42. Siles, J.A.; Margesin, R. Seasonal soil microbial responses are limited to changes in functionality at two alpine forest sites differing in altitude and vegetation. *Sci. Rep.* **2017**, *7*, 2204. [CrossRef] [PubMed]
43. Sundqvist, M.K.; Sanders, N.J.; Wardle, D.A. Community and ecosystem responses to elevational gradients: Processes, mechanisms, and insights for global change. *Annu. Rev. Ecol. Evol. Syst.* **2013**, *44*, 261–280. [CrossRef]
44. Bragazza, L.; Bardgett, R.D.; Mitchell, E.A.D.; Buttler, A. Linking soil microbial communities to vascular plant abundance along a climate gradient. *New Phytol.* **2015**, *205*, 1175–1182. [CrossRef] [PubMed]
45. Deng, Q.; Cheng, X.L.; Hui, D.F.; Zhang, Q.; Li, M.; Zhang, Q.F. Soil microbial community and its interaction with soil carbon and nitrogen dynamics following afforestation in central China. *Sci. Total Environ.* **2016**, *541*, 230–237. [CrossRef] [PubMed]
46. Bai, Y.F.; Cotrufo, M.F. Grassland soil carbon sequestration: Current understanding, challenges, and solution. *Science* **2022**, *377*, 603–608. [CrossRef] [PubMed]
47. Abdalla, M.; Hastings, A.; Chadwick, D.R.; Jones, D.L.; Evans, C.D.; Jones, M.B.; Rees, R.M.; Smith, P. Critical review of the impacts of grazing intensity on soil organic carbon storage and other soil quality indicators in extensively managed grasslands. *Agric. Ecosyst. Environ.* **2018**, *253*, 62–81. [CrossRef]
48. Lugato, E.; Lavallee, J.M.; Haddix, M.L.; Panagos, P.; Cotrufo, M.F. Different climate sensitivity of particulate and mineral-associated soil organic matter. *Nat. Geosci.* **2021**, *14*, 295–300. [CrossRef]
49. Zhou, W.; Gang, C.C.; Zhou, L.; Chen, Y.; Li, J.L.; Ju, W.M.; Odeh, I. Dynamic of grassland vegetation degradation and its quantitative assessment in the northwest China. *Acta Oecol.* **2014**, *55*, 86–96. [CrossRef]
50. Deng, L.; Shangguan, Z.P.; Wu, G.L.; Chang, X.F. Efects of grazing exclusion on carbon sequestration in China's grassland. *Earth-Sci. Rev.* **2017**, *173*, 84–95. [CrossRef]
51. Yang, Y.; Tilman, D.; Furey, G.; Lehman, C. Soil carbon sequestion accelerated by restoration of grassland biodiversity. *Nat. Commun.* **2019**, *10*, 718. [CrossRef]
52. Bardgett, R.D.; Bullock, J.M.; Lavorel, S.; Manning, P.; Schaffner, U.; Ostle, N.; Chomel, M.; Durigan, G.; Fry, E.L.; Johnson, D.; et al. Combatting global grassland degredation. *Nat. Rev. Earth Env.* **2021**, *2*, 720–735. [CrossRef]
53. Aronson, E.L.; Goulden, M.L.; Allison, S.D. Greenhouse gas fluxes under drought and nitrogen addition in a Southern California grassland. *Soil Biol. Biochem.* **2019**, *131*, 19–27. [CrossRef]
54. Wang, M.M.; Sun, X.; Cao, B.C.; Chiariello, N.R.; Docherty, K.M.; Field, C.B.; Gao, Q.; Gutknecht, J.L.M.; Guo, X.; He, G.H.; et al. Long-term elevated precipitation induces grassland soil carbon loss via microbe-plant–soil interplay. *Global Change Biol.* **2023**, *29*, 5429–5444. [CrossRef] [PubMed]
55. White, R.P.; Murray, S.; Rohweder, M. *Pilot Analysis of Global Ecosystems: Grassland Ecosystems*; World Resources Institute: Washington, DC, USA, 2000.

56. Wang, C.; Qu, L.R.; Yang, L.M.; Liu, D.W.; Morrissey, E.; Miao, R.H.; Liu, Z.P.; Wang, Q.K.; Fang, Y.T.; Bai, E. Large-scale importance of microbial carbon use efficiency and necromass to soil organic carbon. *Global Change Biol.* **2021**, *27*, 2039–2048. [CrossRef] [PubMed]
57. Strickland, M.S.; Rousk, J. Considering fungal: Bacterial dominance in soils methods, controls, and ecosystem implications. *Soil Biol. Biochem.* **2010**, *42*, 1385–1395. [CrossRef]
58. Cotrufo, M.F.; Haddix, M.L.; Kroeger, M.E.; Stewart, C.E. The role of plant input physical-chemical properties, and microbial and soil chemical diversity on the formation of particulate and mineral-associated organic matter. *Soil Biol. Biochem.* **2022**, *168*, 108648. [CrossRef]
59. Ren, Q.; Yuan, J.H.; Wang, J.P.; Liu, X.; Ma, S.L.; Zhou, L.Y.; Miao, L.J.; Zhang, J.C. Water level has higher influence on soil organic carbon and microbial community in Poyang lake wetland than vegetation type. *Microorganisms* **2022**, *10*, 131. [CrossRef]
60. Indorf, C.; Dyckmans, J.; Khan, K.S.; Joergensen, T.G. Optimisation of amino sugar quantification by HPLC in soil and plant hydrolysates. *Biol. Fertil. Soils* **2011**, *47*, 387–396. [CrossRef]
61. Kang, E.; Li, Y.; Zhang, X.D.; Yan, Z.Q.; Wu, H.D.; Li, M.; Yan, L.; Zhang, K.R.; Wang, J.Z.; Kang, X.M. Soil pH and nutrients shape the vertical distribution of microbial communities in an alpine wetland. *Sci. Total Environ.* **2021**, *774*, 145780. [CrossRef]
62. Caporaso, J.G.; Lauber, C.L.; Walters, W.A.; Berg-Lyons, D.; Huntley, J.; Fierer, N.; Owens, S.M.; Betley, J.; Fraser, L.; Bauer, M. Ultra-high-throughput microbial community analysis on the Illumina HiSeq and MiSeq platforms. *ISME J.* **2012**, *6*, 1621–1624. [CrossRef] [PubMed]
63. Klink, S.; Keller, A.B.; Wild, A.J.; Baumert, V.L.; Gube, M.; Lehndorff, E.; Meyer, N.; Mueller, C.W.; Phillips, R.P.; Pausch, J. Stable isotopes reveal that fungal residues contribute more to mineral-associated organic matter pools than plant residues. *Soil Biol. Biochem.* **2022**, *168*, 108634. [CrossRef]
64. Yang, Y.; Dou, Y.X.; Wang, B.R.; Wang, Y.Q.; Liang, C.; An, S.S.; Soromotin, A.; Kuzyakov, Y. Increasing contribution of microbial residues to soil organic carbon in grassland restoration chronosequence. *Soil Biol. Biochem.* **2022**, *170*, 108688. [CrossRef]
65. Chang, Y.; Sokol, N.W.; Groenigen, K.J.V.; Bradford, M.A.; Ji, D.C.; Crowther, T.W.; Liang, C.; Luo, Y.Q.; Kuzyakov, Y.; Wang, J.K.; et al. Stoichiometric approach to estimate sources of mineral-associated soil organic matter. *Global Change Biol.* **2024**, *30*, e17092. [CrossRef] [PubMed]
66. Angst, G.; Mueller, K.E.; Kögel-Knabner, I.; Freeman, K.H.; Mueller, C.W. Aggregation controls the stability of lignin and lipids in claysized particulate and mineral associated organic matter. *Biogeochemistry* **2017**, *132*, 307–324. [CrossRef]
67. Keiluweit, M.; Wanzek, T.; Kleber, M.; Nico, P.; Fendorf, S. Anaerobic microsites have an unaccounted role in soil carbon stabilization. *Nat. Commun.* **2017**, *8*, 1771. [CrossRef] [PubMed]
68. Chang, R.; Liu, S.G.; Chen, L.Y.; Li, N.; Bing, H.J.; Wang, T.; Chen, X.P.; Li, Y.; Wang, G.X. Soil organic carbon becomes newer under warming at a permafrost site on the Tibetan Plateau. *Soil Biol. Biochem.* **2021**, *152*, 108074. [CrossRef]
69. Podwojewski, P.; Poulenard, J.; Nguyet, M.L.; de Rouw, A.; Nguyen, V.T.; Pham, Q.H.; Tran, D.T. Climate and vegetation determine soil organic matter status in an alpine inner-tropical soil catena in the Fan Si Pan Mountain, Vietnam. *Catena* **2011**, *87*, 226–239. [CrossRef]
70. Chen, Y.L.; Deng, Y.; Ding, J.Z.; Hu, H.W.; Xu, T.L.; Li, F.; Yang, G.B.; Yang, Y.H. Distinct microbial communities in the active and permafrost layers on the Tibetan Plateau. *Mol. Ecol.* **2017**, *26*, 6608–6620. [CrossRef]
71. Parniske, M. Arbuscular mycorrhiza: The mother of plant root endosymbioses. *Nat. Rev. Microbiol.* **2008**, *6*, 763–775. [CrossRef]
72. Voriskova, J.; Baldrian, P. Fungal community on decomposing leaf litter undergoes rapid successional changes. *ISME J.* **2013**, *7*, 477–486. [CrossRef] [PubMed]
73. Klein, T.; Siegwolf, R.T.; Korner, C. Belowground carbon trade among tall trees in a temperate forest. *Science* **2016**, *352*, 342–344. [CrossRef]
74. Shen, C.C.; Ni, Y.Y.; Liang, W.J.; Wang, J.J.; Chu, H.Y. Distinct soil bacterial communities along a small-scale elevational gradient in alpine tundra. *Front. Microbiol.* **2015**, *6*, 582. [CrossRef] [PubMed]
75. Ren, C.J.; Zhang, W.; Zhong, Z.K.; Han, X.H.; Yang, G.H.; Feng, Y.Z.; Ren, G.X. Differential responses of soil microbial biomass, diversity, and compositions to altitudinal gradients depend on plant and soil characteristics. *Sci. Total Environ.* **2018**, *610*, 750–758. [CrossRef]
76. Gui, Y.X.; Bing, H.J.; Fang, L.C.; Wu, Y.H.; Yu, J.L.; Shen, G.T.; Jiang, M.; Wang, X.; Zhang, X.C. Diversity patterns of the rhizosphere and bulk soil microbial communities along an altitudinal gradient in an alpine ecosystem of the eastern Tibetan Plateau. *Geoderma* **2019**, *338*, 118–127.
77. Li, J.; Wang, X.; Wu, J.H.; Sun, Y.X.; Zhang, Y.Y.; Zhao, Y.F.; Huang, Z.; Duan, W.H. Climate and geochemistry at different altitudes influence soil fungal community aggregation patterns in alpine grasslands. *Sci. Total Environ.* **2023**, *881*, 163375. [CrossRef] [PubMed]
78. Wang, M.; Shi, S.; Lin, F.; Jiang, P. Response of the soil fungal community to multi-factor environmental changes in a temperate forest. *Appl. Soil Ecol.* **2014**, *81*, 45–56. [CrossRef]
79. Yang, T.; Adams, J.M.; Shi, Y.; Sun, H.B.; Cheng, L.; Zhang, Y.J.; Chu, H.Y. Fungal community assemblages in a high elevation desert environment: Absence of dispersal limitation and edaphic effects in surface soil. *Soil Biol. Biochem.* **2017**, *115*, 393–402. [CrossRef]
80. Hao, Z.G.; Zhao, Y.F.; Wang, X.; Wu, J.H.; Jiang, S.L.; Xiao, J.J.; Wang, X.H.; Liu, H.Y.; Li, J.; Sun, Y.X. Thresholds in aridity and soil carbon-to-nitrogen ratio govern the accumulation of soil microbial residues. Commun. *Earth Environ.* **2021**, *2*, 236. [CrossRef]

81. Xu, S.; Song, X.Y.; Zeng, H.; Wang, J.J. Soil microbial necromass carbon in forests: A global synthesis of patterns and controlling factors. *Soil Ecol. Lett.* **2024**, *6*, 240237. [CrossRef]
82. Garten, C.T., Jr.; Hanson, P.J. Measured forest soil C stocks and estimated turnover times along an elevation gradient. *Geoderma* **2006**, *136*, 342–352. [CrossRef]
83. Djukic, I.; Zehetner, F.; Tatzber, M.; Gerzabek, M.H. Soil organic-matter stocks and characteristics along an Alpine elevation gradient. *J. Plant Nutr. Soil Sci.* **2010**, *173*, 30–38. [CrossRef]
84. Tian, G.; Justicia, R.; Coleman, D.C.; Carroll, C.R. Assessment of soil and plant carbon levels in two ecosystems (woody bamboo and pasture) in Montane Ecuador. *Soil Sci.* **2007**, *173*, 459–468. [CrossRef]
85. Six, J.; Guggenberger, G.; Paustian, K.; Haumaier, L.; Elliott, E.T.; Zech, W. Sources and composition of soil organic matter fractions between and within soil aggregates. *Eur. J. Soil Sci.* **2001**, *52*, 607–618. [CrossRef]
86. Jia, J.; Liu, Z.; Haghipour, N.; Wacker, L.; Zhang, H.; Sierra, C.A.; Ma, T.; Wang, Y.; Chen, L.; Luo, A.; et al. Molecular ^{14}C evidence for contrasting turnover and temperature sensitivity of soil organic matter fractionss. *Ecol. Lett.* **2023**, *26*, 778–788. [CrossRef] [PubMed]
87. Zhu, E.X.; Liu, Z.G.; Ma, L.X.; Luo, J.N.; Kang, E.Z.; Wang, Y.; Zhao, Y.P.; Jia, J.; Feng, X.J. Enhanced mineral preservation rather than microbial residue production dictates the accrual of mineral associated organic carbon along a weathering gradient. *Geophys. Res. Lett.* **2024**, *51*, e2024GL108466. [CrossRef]
88. Jilling, A.; Keiluweit, M.; Contosta, A.R.; Frey, S.; Schimel, J.; Schnecker, J.; Smith, R.G.; Tiemann, L.; Grandy, A.S. Minerals in the rhizosphere: Overlooked mediators of soil nitrogen availability to plants and Microorganisms. *Biogeochemistry* **2018**, *139*, 103–122. [CrossRef]
89. Lavallee, J.M.; Soong, J.L.; Cotrufo, M.F. Conceptualizing soil organic matter into particulate and mineral-associated forms to address global change in the 21st century. *Global Change Biol.* **2020**, *26*, 261–273. [CrossRef] [PubMed]

Disclaimer/Publisher's Note: The statements, opinions and data contained in all publications are solely those of the individual author(s) and contributor(s) and not of MDPI and/or the editor(s). MDPI and/or the editor(s) disclaim responsibility for any injury to people or property resulting from any ideas, methods, instructions or products referred to in the content.

Journal of *Fungi*

MDPI

Article

New Species and Records Expand the Checklist of Cellular Slime Molds (Dictyostelids) in Jilin Province, China

Zhaojuan Zhang [1], Liang He [1], Yuqing Sun [1], Zhuang Li [2], Yingkun Yang [1,3], Chao Zhai [1], Steven L. Stephenson [4], Xiangrui Xie [1], Yu Li [1] and Pu Liu [1,*]

[1] Engineering Research Center of Edible and Medicinal Fungi, Ministry of Education, Jilin Agricultural University, Changchun 130118, China; 17843098488@163.com (Z.Z.); 15844982685@163.com (L.H.); y3050644744@126.com (Y.S.); yangyingkun2020@163.com (Y.Y.); zhai13029119483@163.com (C.Z.); 18381823422@163.com (X.X.); fungi966@126.com (Y.L.)
[2] Shandong Provincial Key Laboratory for Biology of Vegetable Diseases and Insect Pests, College of Plant Protection, Shandong Agricultural University, Tai'an 271018, China; liz552@126.com
[3] Science and Technology Research Center of Edible Fungi, Qingyuan 323800, China
[4] Department of Biological Sciences, University of Arkansas, Fayetteville, AR 72701, USA; slsteph@uark.edu
* Correspondence: pul@jlau.edu.cn

Abstract: Dictyostelids represent a crucial element in the protist community, and their abundant presence in Jilin Province underscores their indispensable role in biodiversity conservation. In the present study, a resource survey of dictyostelids used random sampling to collect 28 soil samples from five localities in Changbai Korean Autonomous County, Jilin Province. In addition, a compilation of dictyostelid species reported from Jilin Province was developed, based on a thorough review of the literature. The survey yielded fifteen isolates of dictyostelids, comprising six species from four genera. Notably, two new species (*Dictyostelium longigracilis* sp. nov. and *Dictyostelium macrosoriobrevipes* sp. nov.) were described using morphological characteristics and SSU gene-based phylogenetic analyses. One other species (*Polysphondylium patagonicum*) was recorded as new for China, while another (*Cavenderia aureostipes*) was recorded as a new record for Jilin Province. The dictyostelid assemblage in Jilin Province is dominated by the genus *Dictyostelium* (51.4%), with a total of 35 species, which represent 59.3% of the current total known for all of China. These findings provide a scientific basis for the protection of species diversity and resource utilization of dictyostelids in Jilin Province.

Keywords: dictyostelids; biodiversity; new taxa; resource utilization

1. Introduction

Species richness, specifically referring to the variety of plant, animal, and microbial species (hereafter referred to as 'biodiversity'), is crucial to human existence as it underpins ecological balance, sustains natural processes, provides food, medicine, and numerous resources, and serves as a foundation for scientific research and esthetic appreciation [1–3]. For example, soil harbors a broad diversity of microorganisms that are well recognized drivers of key processes such as nutrient cycling and plant growth [4,5]. Just like aboveground animal and plant communities, the diversity and composition of soil-dwelling microbial communities can vary markedly across the globe [6]. As is known, protists actively participate in belowground ecosystems, both in absolute density (a single gram of soil contains tens of thousands or more individuals) and in the level of energy transfer they provide [7–9].

Dictyostelid cellular slime molds (dictyostelids or heterotrophic amoebae [10]) comprise a group of sorocarp-forming eukaryotic protists that inhabit the surface layers of soils worldwide [11–13]. However, they have received far less attention than other components of the soil microbiome. Due to their small size, their study is currently limited to laboratory culture [14]. As the second largest group of slime molds [15], dictyostelids encompass

almost 200 described species, second only to the true slime molds (myxomycetes [16]). As such, these organisms are an important component of biodiversity. In addition, as bacterial predators, they potentially play important roles in soil ecology and promote soil and plant health by performing top–down control on ecosystem processes (e.g., decomposition) in which bacterial populations are involved. Since dictyostelids are essentially indistinguishable, their identification and taxonomy have traditionally been based on the morphology of their sorocarps and related characters, but this has recently been augmented by molecular phylogeny. They are particularly well known and widely studied for their lifestyle, which alternates between uni- and multicellular (sorocarpic) stages and represents one of nature's tractable system to resolve the evolution of cell-type specialization and inventions of multicellularity [17,18].

In recent years, research on the diversity of dictyostelids and their environmental impact has attracted the attention of scholars in China and abroad. China covers a vast territory characterized by a large number of terrestrial slime molds (*Catalogue of Life China: 2024 Annual Checklist*, http://www.sp2000.org.cn, accessed on 12 July 2024; [19]). During the period from 1983 to 2024, 59 taxa of dictyostelids (58 species and 1 variety) from 2 orders and 4 families were reported from samples collected from 25 provincial administrative regions, covering 4 climate zones (tropical, subtropical, temperate, and alpine regions) [20–22]. Among these, Jilin is the province with the richest dictyostelid diversity due to its diverse topography, temperate continental monsoon climate, and abundant ecosystems. Extensive research has been undertaken to explore the diversity of dictyostelids within Jilin Province [21,23,24].

The classification system of dictyostelids has undergone considerable change in the past decade, and numerous families have been classified and revised [25–27]. The objective of this study was to systematically summarize and organize existing reports on species of dictyostelids from Jilin Province according to the latest classification system and subsequently conduct appropriate supplementary investigations based on this baseline of data.

2. Materials and Methods

2.1. Study Area

Changbai Korean Autonomous County is located in the southeast of Baishan City and southeast of Jilin Province, China (40°37′ N–41°05′ N, 127°17′ E–128°29′ E) (Figure 1a). Changbai Korean Autonomous County has a sub-frigid continental monsoon climate, featuring uneven temperatures in the spring, warm and rainy conditions in the summer, clear and crisp days in the autumn, and cold and long days in the winter. The rainfall is abundant and concentrated. The average annual precipitation is 605.8 mm, of which 374.2 mm falls from June to August, accounting for 57% of the annual precipitation. The average annual frost-free period is 123 d, the annual sunshine duration is 2458.7 h, the average annual wind speed is 2.1 m per second, and the most frequent wind direction is northeasterly. The annual number of days with thunderstorms is 37.4 (available online: http://changbai.gov.cn/cbgk/zrgk/201801/t20180108_257149.html; http://www.dajilin.com/mobile/node_6043.html accessed on 12 July 2024).

2.2. Sampling, Isolation, and Cultivation

Briefly, 28 soil samples were collected from five localities (L1–L5) in Changbai Korean Autonomous County, representing four vegetation types (coniferous forest, broadleaf forest, mixed forest, and farmland) in July 2021 (Table 1). L1 includes coniferous forest; L2 includes farmland and broadleaf forest; L3 includes mixed forest, broadleaf forest, and farmland; L4 and L5 include broadleaf forest (Figure 1a). Each sample consisted of 30 to 40 g from surface soil (0–10 cm in depth) based on a random sampling method and was placed in a sterile Whirl-Pak plastic bag. Within a few hours of collection, all samples were transported to a laboratory. The samples were numbered and recorded in the laboratory soil sample database and then stored at 4 °C.

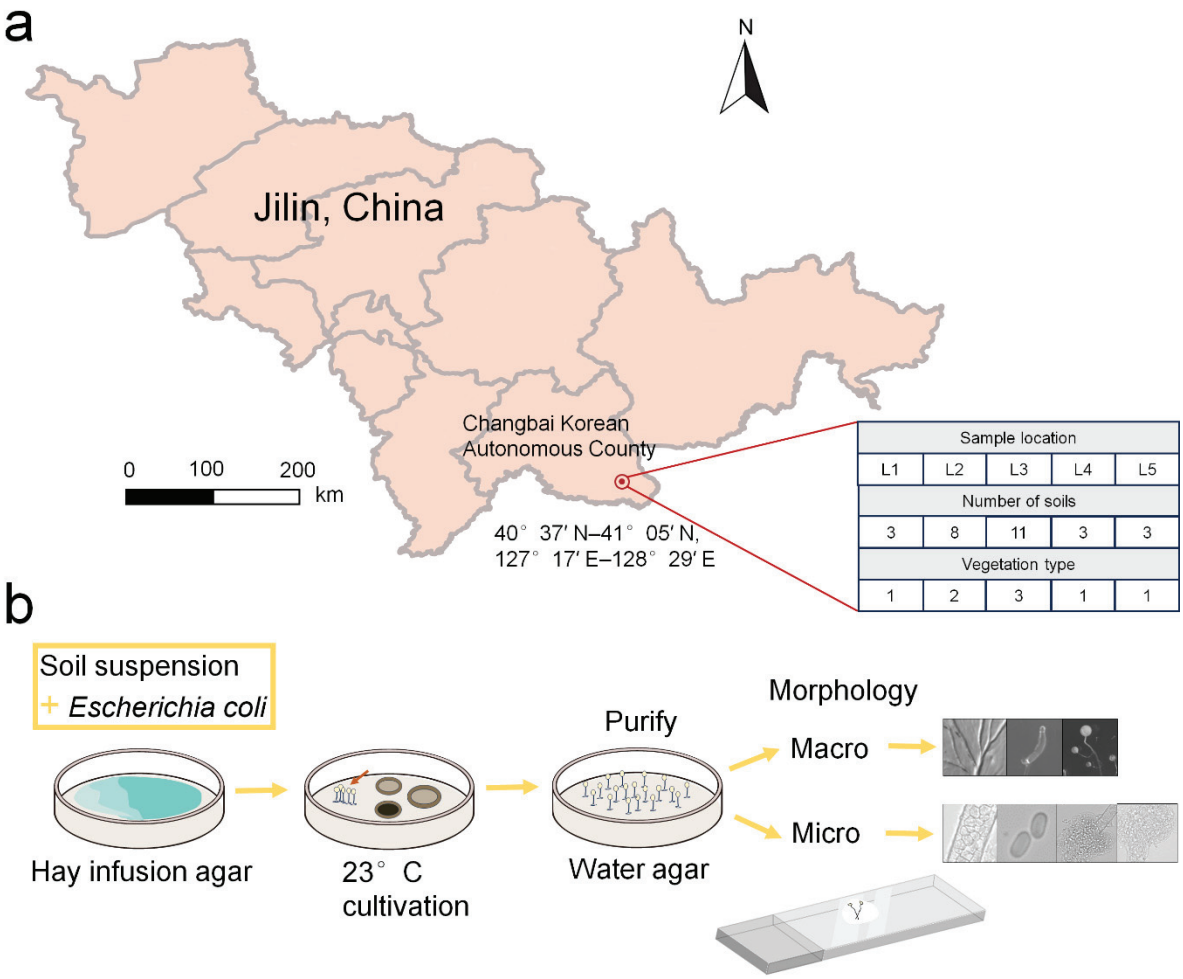


Figure 1. Study area and location of the sampling sites in Changbai Korean Autonomous County, Jilin Province, China (**a**). Outline of the experimental workflow used to isolate dictyostelids from the collected soil samples (**b**), the arrow indicates the step-by-step progression of the experiment. Note: the map was drawn using ArcGIS 10.8 [28] software. Details of the samples (e.g., sample location, number of soil samples, and vegetation types) are shown in Table 1.

Table 1. Sample location information and dictyostelid species isolated from Changbai Korean Autonomous County, Jilin Province.

Soil Nos.	Localities	Vegetation	Coordinates	Elevation (m)	Temperature	Dictyostelid Species
6693	Tashan Park [L1]	Coniferous forest	41°25′27″ N, 128°11′36″ E	833	19–27 °C	——
6694			41°25′29″ N, 128°11′36″ E	854.62	19–27 °C	——
6695			41°25′3″ N, 128°11′35″ E	849	19–27 °C	——
6696	Fifteen Gap [L2]	Farmland (soybean field)	41°28′1″ N, 127°56′28″ E	655	19–27 °C	——
6697			41°28′02″ N, 127°56′27″ E	652	19–27 °C	——
6698			41°28′02″ N, 127°56′27″ E	655	19–27 °C	——

Table 1. *Cont.*

Soil Nos.	Localities	Vegetation	Coordinates	Elevation (m)	Temperature	Dictyostelid Species
6699	Fifteen Gap [L2]	Broadleaf forest	41°27′02″ N, 127°56′18″ E	644	19–27 °C	——
6700			41°28′03″ N, 127°56′26″ E	651	19–27 °C	*** *Dictyostelium longigracilis* (3), *Dictyostelium robusticaule* (1)
6701			41°27′17″ N, 127°56′26″ E	648	19–27 °C	——
6702			41°27′17″ N, 127°56′13″ E	644	19–27 °C	——
6703			47°28′0″ N, 127°56′26″ E	655.64	19–27 °C	——
6704	Wangtian'e New Village [L3]	Mixed forest	41°27′27″ N, 127°56′41″ E	682	19–30 °C	——
6705			41°27′26″ N, 127°56′41″ E	686	19–30 °C	——
6706			41°22′25″ N, 127°56′42″ E	732.13	19–30 °C	——
6707		Broadleaf forest	41°27′27″ N, 127°56′41″ E	678	19–30 °C	——
6708		Farmland (scallion field)	41°27′41″ N, 127°56′32″ E	654	19–30 °C	——
6709		Farmland (scallion field)	41°27′44″ N, 127°56′31″ E	630	19–30 °C	* *Cavenderia aureostipes* (1)
6710		Farmland (corn field)	41°27′40″ N, 127°56′32″ E	680	19–30 °C	——
6711		Farmland (corn field)	41°27′41″ N, 127°56′32″ E	671	19–30 °C	——
6712		Farmland (corn field)	41°27′41″ N, 127°56′33″ E	675	19–30 °C	——
6713		Farmland (Chinese chives field)	41°27′44″ N, 127°56′31″ E	675	19–30 °C	——
6714		Farmland (soybean field)	41°27′42″ N, 127°56′32″ E	652	19–30 °C	——
6715	Lishui Manor [L4]	Broadleaf forest	41°31′23″ N, 127°56′58″ E	795	19–30 °C	*Heterostelium candidum* (1), * *Cavenderia aureostipes* (1)
6716			41°31′22″ N, 127°57′0″ E	798.47	19–30 °C	* *Cavenderia aureostipes* (3)
6717			41°31′24″ N, 127°57′1″ E	787	19–30 °C	——

Table 1. *Cont.*

Soil Nos.	Localities	Vegetation	Coordinates	Elevation (m)	Temperature	Dictyostelid Species
6718	Primary Protection Zone of Drinking Water Sources [L5]	Broadleaf forest	41°29′17″ N, 127°56′32″ E	717.85	19–30 °C	* *Cavenderia aureostipes* (1), ** *Polysphondylium patagonicum* (2), *** *Dictyostelium macrosoriobrevipes* (1)
6719		Broadleaf forest	41°29′17″ N, 127°56′34″ E	729.46	19–30 °C	* *Cavenderia aureostipes* (1)
6720		Broadleaf forest	41°29′16″ N, 127°56′34″ E	693.39	19–30 °C	——

Numbers (1), (2), and (3) indicate the number of species clones/strains obtained from the soil samples (n). * refers to a species new to Jilin Province. ** refers to a species new to China. *** refers to a species new to science.

The isolation protocols used in this research followed those described by Cavender and Raper [29] (Figure 1b). Each sample was weighed, and enough ddH_2O was added for an initial dilution (1:10). This dilution was shaken to disperse the soil particles and suspend the amoebae, microcysts, and spores of dictyostelids. Afterward, an 0.5 mL aliquot of this dilution and 0.4 mL *Escherichia coli* (food source) were dispensed into three duplicate culture plates prepared with hay infusion agar. The plates were incubated at 23 °C with a 12 h light-and-darkness cycle.

For a period of two weeks following the initial emergence of aggregations, each plate was carefully inspected at least once daily. Each isolate recovered from one of the plates was purified and cultivated for taxonomic studies and preservation on non-nutrient water agar plates with *E. coli* pre-grown for 12 to 24 h. Spores from these plates were frozen in a HL5 [30] medium and stored at −80 °C in the herbarium of the Mycological Institute of Jilin Agricultural University (HMJAU), Changchun, China.

2.3. Observation of Morphological Features

Morphological characteristics in the life cycle were described as proposed by Hagiwara [31] and Raper [12]. Under a stereoscopic microscope, isolates were observed and features of their morphology documented. This features included growth habit, branching, color, sorocarp characteristics, and sizes/shapes of aggregates and pseudoplasmodia. All these features were observed under a fluorescent stereo microscope (Leica M165FC; Leica, Wetzlar, Germany). In each instance, a viable and morphologically normal-appearing dictyostelid isolate, referred to as a "healthy" isolate, was selected under a dissecting microscope, mounted on a slide with sterile water, covered, and then observed under an optical microscope. The microscopic features observed were spore size/shape, polar granules, sorophore, cell rows, and sorophore tips/bases. These were observed using a Zeiss light microscope (Axio Imager A2; Zeiss, Oberkochen, Germany), with 10 ocular and 10, 40, and 100 (oil) objectives. Photographs were taken with a Zeiss AxioCam 506 color microscope camera.

We compared the recorded information and photographs of dictyostelids with the morphological characteristics documented in the original literature, which was referenced in Index Fungorum [32] (http://www.indexfungorum.org/names/Names.asp, accessed on 7 May 2022), to accurately identify the species isolated in the present study.

2.4. DNA Isolation, PCR Amplification, Sequencing, and Phylogenetic Analysis

The molecular methods employed in this study followed those described by Liu et al. [33]. The spores of each isolate were collected with a sterile tip and mixed with the lysis buffer of the MiniBEST universal genomic DNA extraction kit ver.5.0 (TaKaRa Bio Inc.,

Kusatsu, Japan) according to the manufacturer's protocol. The genomic DNA solution was used directly for PCR amplification using the primers [34] 18S-FA (5′-AACCTGGTTGATCC TGCCAG-3′) and 18S-RB (5′-TGATCCTTCTGCAGGTTCAC-3′). The 25 µL reaction volume consisted of 12.5 µL Premix Taq™ (Ex Taq™ Version 2.0), 1 µL of each forward and reverse primer, 1 µL template genomic DNA (about 10 ng/µL), and 8.5 µL ddH_2O. PCR products were visually inspected on agarose electrophoresis gels and compared with band intensities of 1600–1800 bp DNA ladders.

PCR products were sent to Sangon Bio-tech Co., Ltd. (Shanghai, China), for sequencing. Following thorough verification, the fifteen newly generated sequences were confirmed to be accurate and were subsequently submitted to GenBank. All sequences of related species were downloaded from GenBank for phylogenetic analysis to determine their phylogenetic relationships with other taxa in the group (Table 2).

Table 2. Sequences used in phylogenetic analysis based on SSU.

Species Name	Strain Number	SSU Accession Numbers	Species Name	Strain Number	SSU Accession Numbers
Cavenderia amphispora	BM9A	HQ141521.1	*T. lacteum*		AM168045.1
C. antarctica	NZ43B	AM168080.1	*T. menorah*	M1	AM168073.1
C. aureostabilis	TH10B	MH745571.1	*T. montium*	57a	JF892717.1
C. aureostipes	YA6	AM168083.1	*T. simplex*	OH598	JF892720.1
C. aureostipes	B15A	KF662199.1	*T. unicornutum*	OH599	JF892725.1
C. aureostipes	OH396	KF662201.1	*Hagiwaraea coeruleostipes*	CRLC53B	AM168036.1
C. aureostipes	**S2-2A**	**PQ222850**	*H. lavandula*	B15	AM168047.1
C. aureostipes	**S1-3A**	**PQ222849**	*H. radiculata*	ML5A	HQ141494.1
C. aureostipes	**L2-113B**	**PQ222848**	*H. rhizopodium*	AusKY-4	AM168063.1
C. aureostipes	**L2-113A**	**PQ222847**	*H. tenebrica*	Ong2	MH762956.1
C. aureostipes	**L2-1A**	**PQ222846**	*H. vinaceofusca*	CC4	AM168062.1
C. aureostipes	**L1-2L**	**PQ222845**	*Raperostelium australe*	NZ80B	AM168029.1
C. aureostipes	**6709-2**	**PQ222842**	*R. capillare*	37A	JF892721.1
C. aureostipes var. *helvetia*	HM592	KF662214.1	*R. crispum*	Eden2	MH762957.1
C. basinodulosa	Mad5-1A	MN338955.1	*R. cymosum*	Krug15A	MH762958.1
C. bhumiboliana	THC11X	HQ141523.1	*R. filiforme*	OH603	JF892724.1
C. bifurcata	UK5	AM168084.1	*R. gracile*	TNS-C-183	AM168078.1
C. boomerangispora	K26B	HQ141520.1	*R. ibericum*	214rjb	HQ141495.1
C. canoespora	Mad14-3C	MN338956.1	*R. maeandriforme*	OH604	JF892719.1
C. delicata	TNS-C-226	AM168093.1	*R. minutum*	71-2	AM168051.1
C. deminutiva	MexM19A	AM168092.1	*R. monochasioides*	HAG653	AM168052.1
C. exigua	TNS-C-199	AM168085.1	*R. ohioense*	Okla4C	HQ141493.1
C. fasciculata	SmokOW9A	AM168086.1	*R. potamoides*	FP1A	AM168069.1
C. fasciculata	SH3	AM168087.1	*R. reciprocatum*	38A	JF892718.1
C. fasciculoidea		GQ496157.1	*R. reciprocatum* var. *transitum*	OH601	JF892723.1
C. fulva	Krug6-5A	MH762953.1	*R. stabile*	M12A	MN338957.1
C. granulophora	CHII-4	AM168072.1	*R. tenue*	Pan52	AM168076.1
C. helicoidea	Landolt TH19B	OM677255.1	*R. tenue*	PJ6	AM168094.1
C. macrocarpa	MGE2	HQ141519.1	*R. tenue*	PR4	AM168075.1
C. medusoides	OH592	AM168088.1	*Speleostelium caveatum*	WS695	AM168077.1
C. mexicana	MexTF4B1	AM168089.1	*Dictyostelium ammophilum*	KBK4A	HQ141478.1
C. microspora	TNS-C-38	AM168090.1	*D. aureocephalum*	TNS-C-180	AM167876.1
C. minima	Eden1	MH762954.1	*D. aureum*	SL1	AM168028.1
C. multistipes	UK26b	AM168070.1	*D. austroandinum*		GQ496158.1
C. myxobasis	NT2A	HQ141522.1	*D. barbarae*	1-5	MK322959.1
C. parvibrachiata	Landolt TH20C	OM677256.1	*D. barbibulus*	Sweden-4R	JX173878.1
C. parvibrachiata	Landolt 2019 TH20C	OM677257.1	*D. brefeldianum*	TNS-C-115	AM168030.1
C. parvispora	OS126	AM168091.1	*D. brunneum*	WS700	AM168031.1
C. protodigitata	TH18BA	MH745572.1	*D. capitatum*	91HO-50	AM168032.1
C. protumula	Landolt TH20A	OM677258.1	*D. chordatum*		GQ496159.1
C. pseudoaureostipes	TH39A	HQ141518.1	*D. citrinum*	OH494	AM168033.1
C. stellata	SAB7B	AM168081.1	*D. clavatum*	TNS-C-189	AM168034.1
C. subdiscoidea	TH1A	HQ141515.1	*D. clavatum*	TNS-C-220	AM168035.1
C. ungulata	Landolt TH18B	OM677259.1	*D. crassicaule*	93HO-33	AM168037.1
Acytostelium amazonicum	Landolt X	HQ141510.1	*D. dimigraformum*	AR5b	AM168038.1
A. amazonicum	HN1B1	HQ141511.1	*D. discoideum*	NC4	AM168071.1
A. anastomosans	PP1	AM168115.1	*D. discoideum*	V34	AM168039.1
A. digitatum	OH517	AM168114.1	*D. firmibasis*	TNS-C-14	AM168041.1

Table 2. *Cont.*

Species Name	Strain Number	SSU Accession Numbers	Species Name	Strain Number	SSU Accession Numbers
A. leptosomum	212rjb	HQ141512.1	*D. gargantuum*		GQ496161.1
A. leptosomum	FG12	AM168111.1	*D. giganteum*	WS589	AM168042.1
A. longisorophorum	DB10A	AM168109.1	***D. longigracilis***	**6709C**	**PQ287291**
A. magnisorum	08A	HQ141513.1	***D. longigracilis***	**6709L**	**PQ287298**
A. serpentarium	SAB3A	AM168113.1	***D. longigracilis***	**6709M**	**PQ287299**
A. singulare	FDIB	HQ141514.1	*D. implicatum*	93HO-1	AM168043.1
A. subglobosum	LB1	AM168110.1	*D. insulinativitatis*		MK322958.1
Rostrostelium ellipticum	AE2	AM168112.1	*D. intermedium*	PJ11	AM168044.1
Heterostelium album	PN500	AM168104.1	*D. leptosomopsis*	Araucaria 1	HM159992.1
H. ampliverticillatum		KP167480.1	*D. leptosomum*	NZN49A	HQ141480.1
H. anisocaule	NZ47B	AM168096.1	*D. longosporum*	TNS-C-109	AM168048.1
H. arachnoideum	YA1	AM168102.1	*D. macrocephalum*	B33	AM168049.1
H. asymetricum	OH567	AM168097.1	*D. medium*	TNS-C-205	AM168050.1
H. asymetricum	HN20C	HQ141503.1	*D. minimum*	2794	MG490369.1
H. australicum	NB1AP	HQ141508.1	*D. brefeldianum*	S28b	AM168054.1
H. boreale	BSB10A	HQ141499.1	*D. mucoroides* var. *stoloniferum*	FOII-1	AM168055.1
H. candidum	bsb6b	HQ141498.1	*D. multiforme*	4007	MG490370.1
H. candidum		AY040337.1	*D. pseudobrefeldianum*	91HO-8	AM168059.1
H. candidum	**L1-1B**	**PQ222844**	*D. purpureum*	QSpu1	FJ424829.1
H. colligatum	HN13C1	HQ141505.1	*D. purpureum*	QSpu2	FJ424839.1
H. colligatum	OH538	AM168098.1	*D. purpureum*	QSpu23	FJ424832.1
H. cumulocystum		KP167479.1	*D. purpureum*	QSpu28	FJ424836.1
H. equisetoides	B7JB	AM168099.1	*D. purpureum*		DQ340386.1
H. filamentosum	SU-1	AM168100.1	*D. purpureum*	QSpu4	FJ424826.1
H. flexuosum	AU4B	HQ141500.1	*D. purpureum*		AY040335.1
H. gloeosporum	TCK52	AM168074.1	*D. purpureum*	QSpu36	FJ424828.1
H. granulosum	MF5A	HQ141502.1	*D. purpureum*	C143	AM168060.1
H. irregularibrachiatum	Krug6-5B	MH762955.1	*D. purpureum*	WS321	AM168061.1
H. lapidosum		KP167477.1	*D. purpureum*	cavender	HQ141481.1
H. luridum	LR-2	AM168101.1	*D. purpureum var. pseudosessile*	MR273 (4637)	MH280022.1
H. migratissimum		KP167481.1	*D. purpureum var. pseudosessile*	MR273 (4446)	MH280023.1
H. multicystogenum	AS2	HQ141506.1	*D. quercibrachium*	NZ201B	HQ141479.1
H. oculare		HQ141497.1	*D. robusticaule*	5729-bai-2021	MW931857.1
H. oculare	DB4B	AM168079.1	*D. robusticaule*	5729-huang -2021	MW931856.1
H. pallidum	PPHU8	EU004605.1	***D. robusticaule***	**6700D**	**PQ237105**
H. pallidum	TNS-C-98	AM168103.1	***D. macrosoriobrevipes***	**6718S1-2B**	**PQ304778**
H. parvimigratum		KP167483.1	*D. robustum*	TNS-C-219	AM168064.1
H. plurimicrocystogenum		KP167475.1	*D. rosarium*	M45	AM168065.1
H. pseudocandidum	TNS-C-91	AM168107.1	*D. septentrionale*	IY49	AM168066.1
H. pseudocolligatum		KP167474.1	*D. septentrionale*	AK2	AM168067.1
H. pseudoplasmodiofascium		KP167482.1	*D. sphaerocephalum*	GR11	AM168068.1
H. pseudoplasmodiomagnum		KP167472.1	*D. valdivianum*		GQ496155.1
H. racemiferum		KP167476.1	*D. brevicaule*	SMA	
H. radiatum	M26B	MN338953.1	*Polysphondylium fuscans*	Sweden-11D	JX173877.1
H. rotatum	QC2C	HQ141501.1	*P. laterosorum*	AE4	AM168046.1
H. stolonicoideum	K12A	HQ141507.1	*P. patagonicum*		GQ496156.1
H. tenuissimum	TNS-C-97	AM168105.1	***P. patagonicum***	**6718-Z2**	**PQ236756**
H. tenuissimum		AY040339.1	***P. patagonicum***	**6718-zi**	**PQ236757**
H. tikalense	OH595	AM168106.1	*P. violaceum*	209	HQ141486.1
H. tikalense	HN1C1	HQ141509.1	*P. violaceum*	P6	AM168108.1
H. unguliferum		KP167473.1	*P. acuminatum*	OH500 SML	
H. versatile	Mad52	MN338954.1	*Coremiostelium polycephalum*	Landolt # 1130 SS3B	HQ141488.1
H. violaceotypum		KP167478.1	*C. polycephalum*	Landolt # 2132 B-9c	HQ141489.1
H. recretum	5756-1-17	MW857293.1	*C. polycephalum*	Landolt # 1675 GUAM	HQ141490.1
H. multibrachiatum	5916lun	MN752217.1	*C. polycephalum*	MY1-1	AM168056.1
H. naviculare	JC SMA		*Synstelium polycarpum*	VE1b	AM168057.1
Tieghemostelium angelicum	38B0	JF892716.1	*S. polycarpum*	OhioWILDS	AM168058.1
T. dumosum	OH602	JF892722.1	*Physarum polycephalum*		X13160.1

Newly generated sequences are shown in bold.

All SSU sequences were aligned and compared separately using the ClustalW Multiple alignment [35], then manually adjusted in BioEdit version 7.0.9.0 [36]. Maximum-likelihood

analyses (ML analyses) were performed using IQTREE v.1.6.12 [37], with 10,000 replicates of ultrafast-likelihood bootstrapping to obtain node support values with the "-bb 10,000" option and further optimized using a hill-climbing nearest-neighbor interchange (NNI) with the "-bnni" option [38]. We also used the SH-aLRT test to obtain the confidence limit of the topology with the "-alrt 1000" option [39]. The "-nt AUTO" option was used to automatically determine the best number of cores given the current data. We used ModelFinder as implemented within IQ-TREE to determine the best substitution model based on Bayesian information criteria (BIC) [40]. We used a myxomycete sequence (*Physarum polycephalum*, accession no. X13160.1/NC_002508.1) as the outgroup with the "-o X13160.1"/"-o NC_002508.1" option. The phylogenetic tree was beautified using iTOL [41] for display, manipulation, and annotation purposes.

3. Results

Fifteen isolates representing six species of dictyostelids were recovered from soil samples collected at four localities (L2–L5) in Changbai Korean Autonomous County, out of a total of twenty-eight samples gathered from five localities (Table 1, Figure 1). Four isolates (*Dictyostelium longigracilis* and *Dictyostelium macrosoriobrevipes*) (Figures 2 and 3) from localities L2 and L5 were new to science. The species *Dictyostelium robusticaule* (Figure 4) from L2 had been reported from Jilin Province previously. Two isolates (*Polysphondylium patagonicum*) (Figure 5) from locality (L5) were new records from China. The species *Heterostelium candidum* (Figure 6) from L4 had been reported from Jilin Province previously. Seven isolates (*Cavenderia aureostipes*) (Figure 7) from localities (L3–L5) were new records for Jilin Province. One locality (L1) did not yield any isolates. Furthermore, phylogenetic studies of the ribosomal small subunit (SSU) further support the taxonomic placement of all six species recorded from the Changbai Korean Autonomous County (Figures 8–11). All isolates and soil samples of the species considered herein were deposited in the mycological herbarium of Jilin Agricultural University.

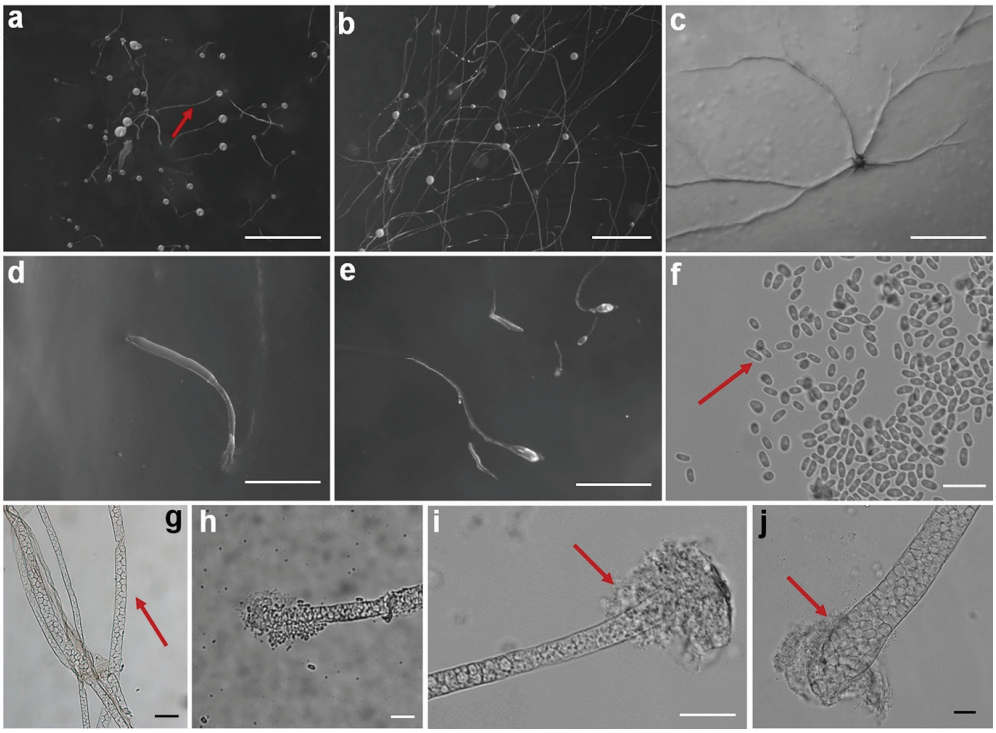


Figure 2. Morphological features of *Dictyostelium longigracilis*: (**a**,**b**) sorocarps; (**c**) aggregation; (**d**,**e**) pseudoplasmodia; (**f**) spores; (**g**) sorophores; (**h**,**i**) sorophore tips; and (**j**) sorophore base. Scale bars: (**a**–**c**) = 2 mm; (**d**,**e**) = 1 mm; (**f**,**i**,**j**) = 20 μm; (**g**) = 50 μm; and (**h**) = 10 μm. The red arrows refer to the key distinguishing characteristics.

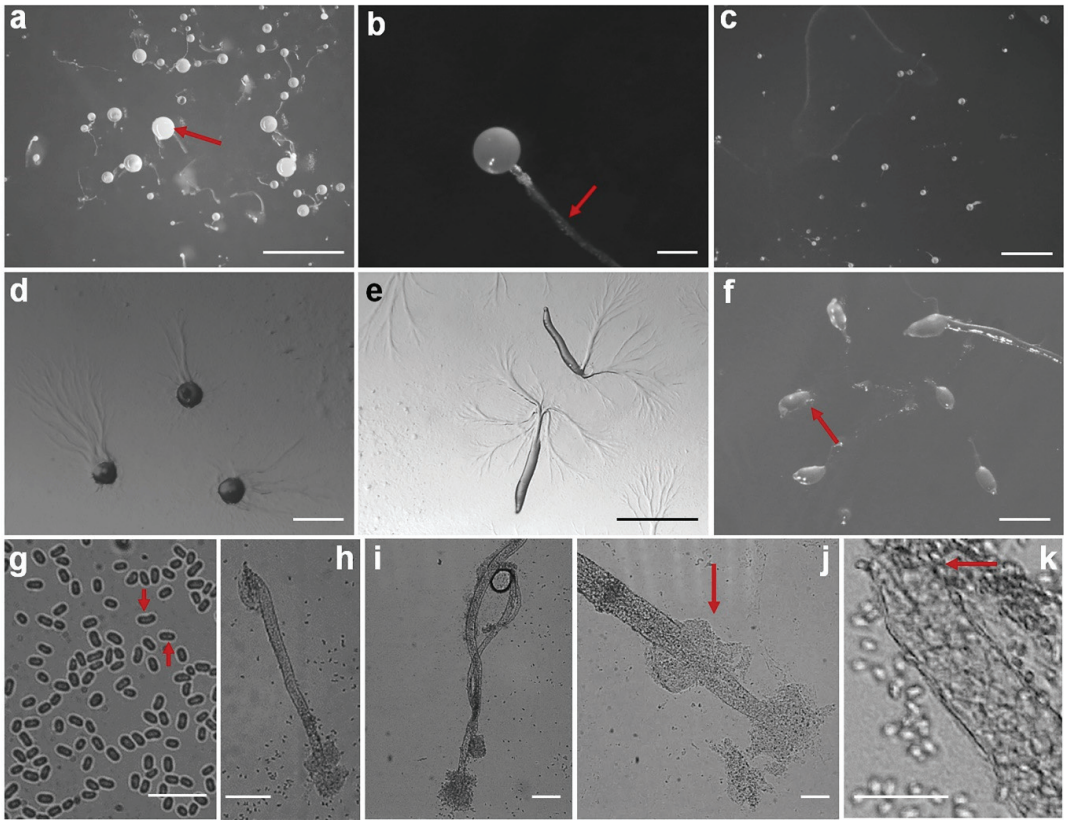


Figure 3. Morphological features of *Dictyostelium macrosoriobrevipes*: (**a**–**c**) sorocarps; (**d**) aggregations; (**e**) pseudoplasmodia; (**f**) sorogens; (**g**) spores; (**h**,**i**) sorophores; (**j**) tip of sorophore; and (**k**) base of sorophore. Scale bars: (**a**,**c**) = 2 mm; (**b**) = 200 µm; (**d**,**f**) = 500 µm; (**e**) = 1 mm; (**g**–**j**) = 50 µm; and (**k**) = 20 µm. The red arrows refer to the key distinguishing characteristics.

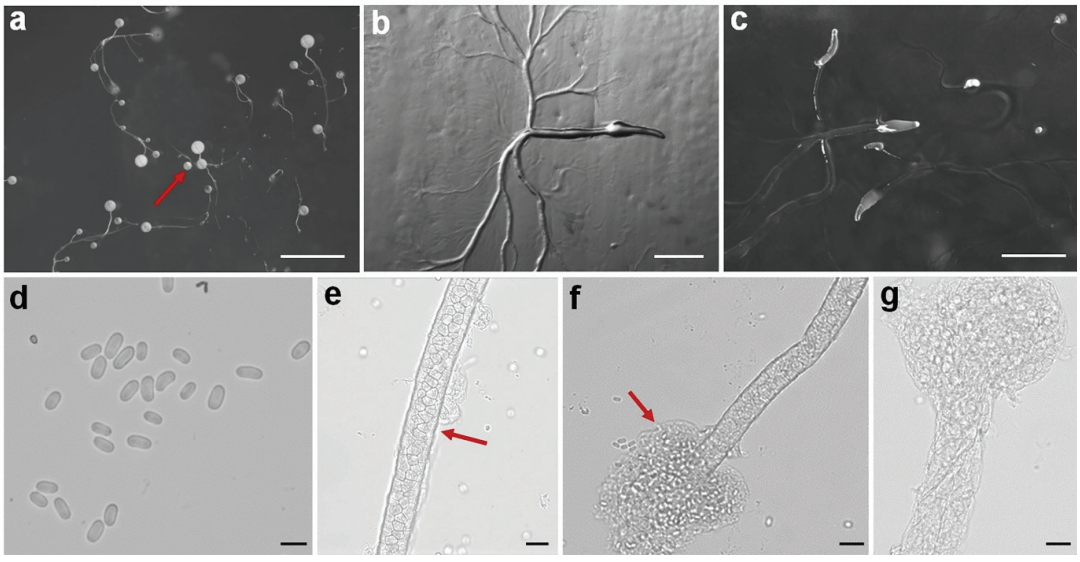


Figure 4. Morphological features of *Dictyostelium robusticaule*: (**a**) sorocarps; (**b**) aggregations; (**c**) pseudoplasmodia; (**d**) spores; (**e**) sorophore; (**f**) sorophore tip; and (**g**) sorophore base. Scale bars: (**a**) = 2 mm; (**b**,**c**) = 1 mm; and (**d**–**g**) = 20 µm. The red arrows refer to the key distinguishing characteristics.

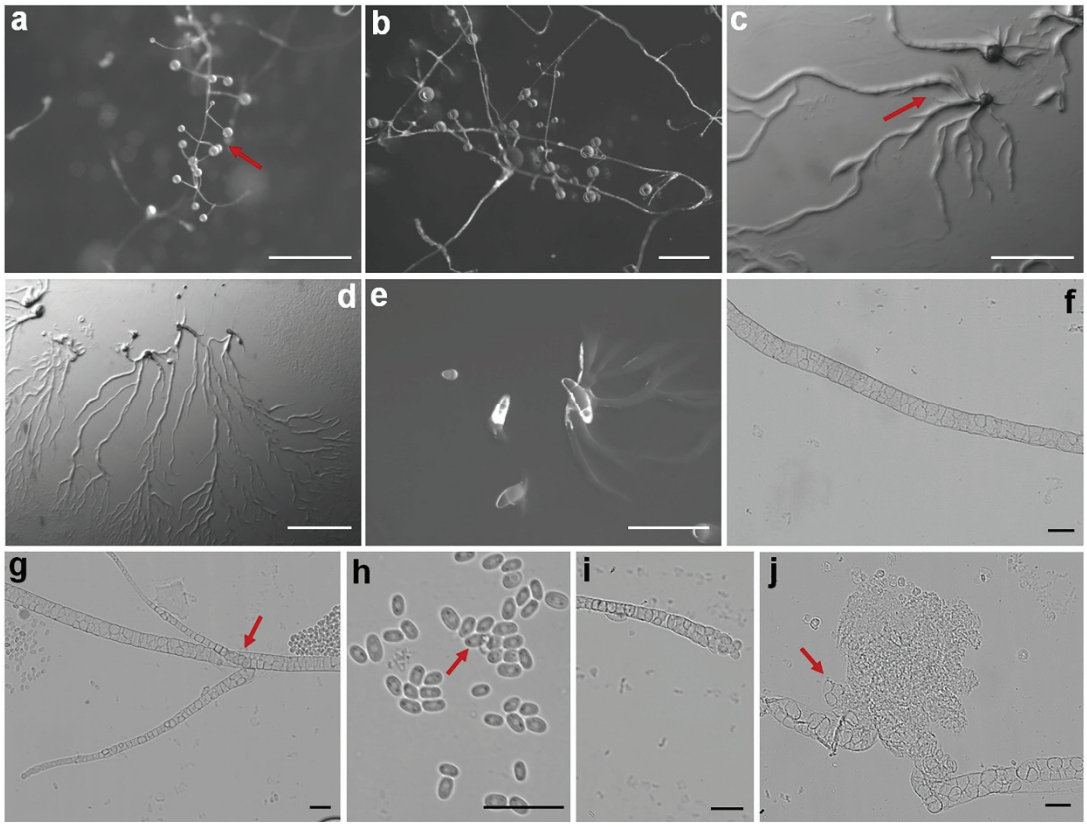


Figure 5. Morphological features of *Polysphondylium patagonicum*: (**a**,**b**) sorocarps; (**c**,**d**) aggregations; (**e**) pseudoplasmodia; (**f**) sorophore; (**g**) branches; (**h**) spores; (**i**) sorophore tip; and (**j**) sorophore base. Scale bars: (**a**,**c**) = 1 mm; (**b**,**e**) = 500 µm; (**d**) =2 mm; and (**f**–**j**) = 20 µm. The red arrows refer to the key distinguishing characteristics.

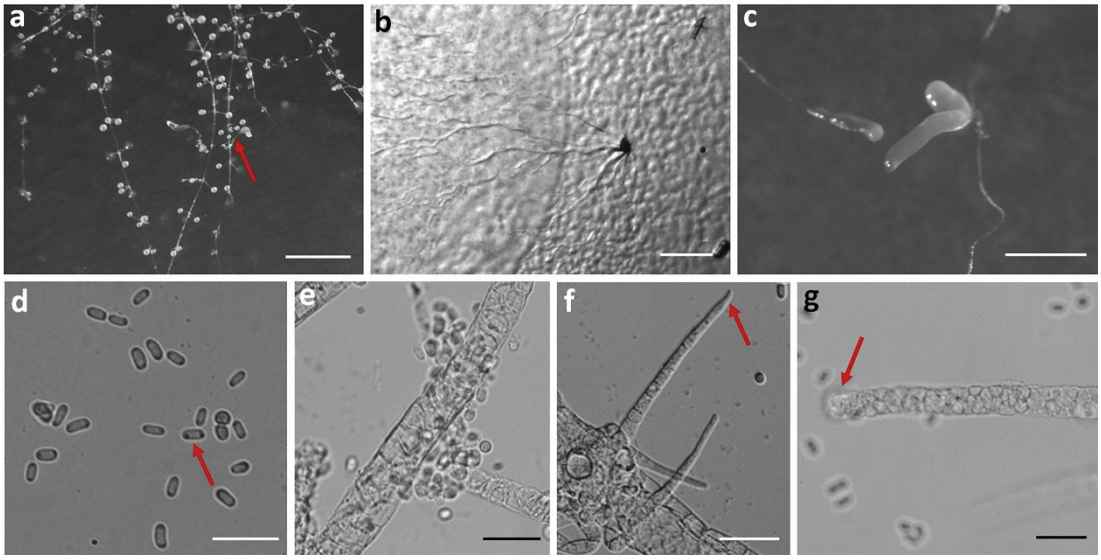


Figure 6. Morphological features of *Heterostelium candidum*: (**a**) sorocarps; (**b**) aggregations; (**c**) pseudoplasmodia; (**d**) spores; (**e**) sorophore; (**f**) sorophore tip; and (**g**) sorophore base. Scale bars: (**a**,**b**) = 1 mm; (**c**) = 500 µm; (**d**) = 20 µm; (**e**) = 10 µm; (**f**) = 50 µm; and (**g**) = 20 µm. The red arrows refer to the key distinguishing characteristics.

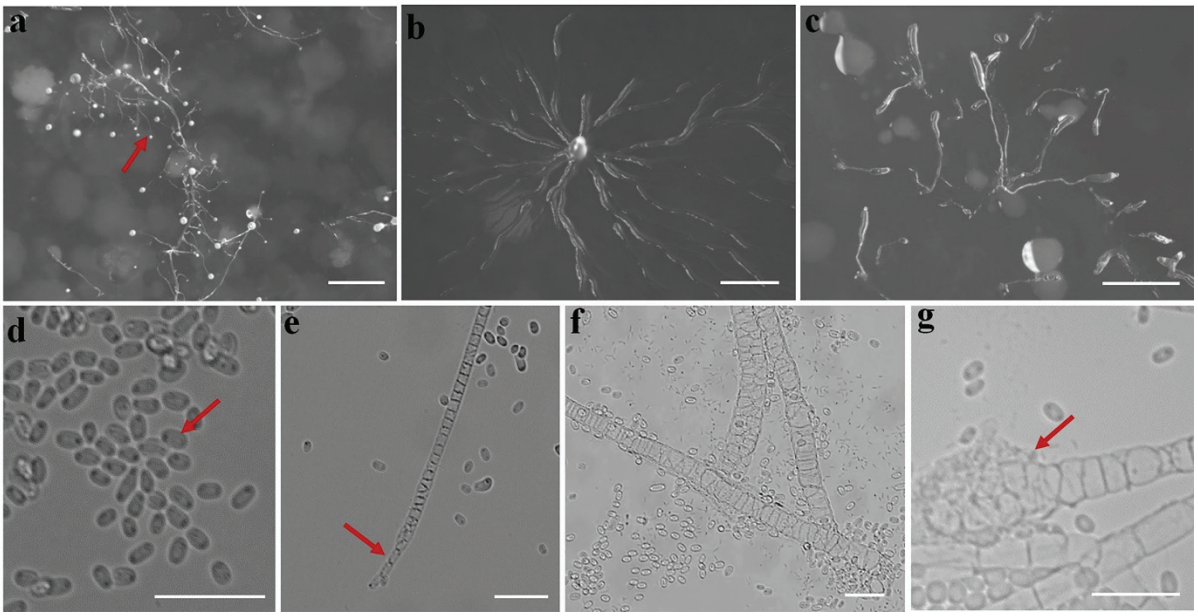


Figure 7. Morphological features of *Cavenderia aureostipes*: (**a**) sorocarps; (**b**) aggregations; (**c**) pseudoplasmodia; (**d**) spores; (**e**) sorophore tip; (**f**) sorophore; and (**g**) sorophore base. Scale bars: (**a**,**c**) = 1 mm; (**b**) = 500 μm; and (**d**–**g**) = 20 μm. The red arrows refer to the key distinguishing characteristics.

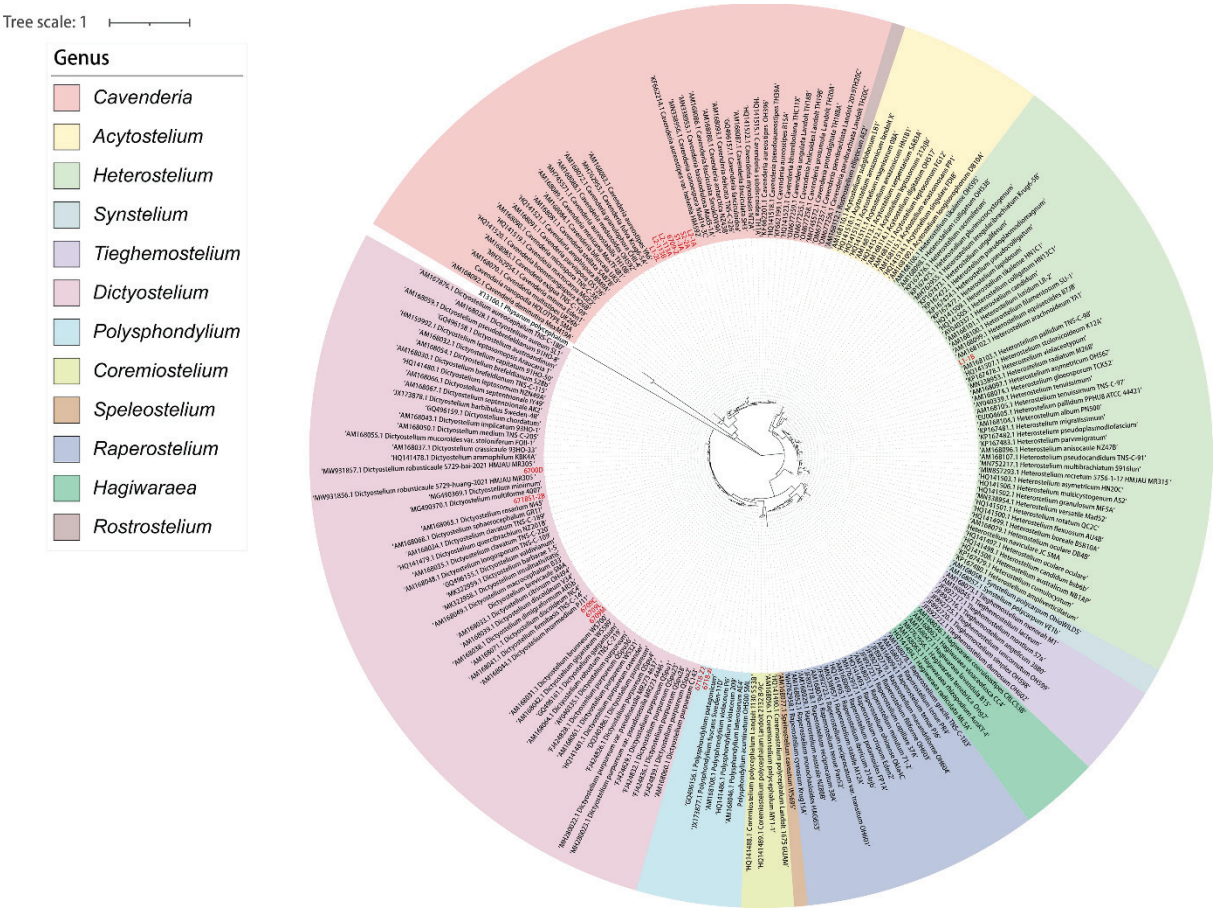


Figure 8. Phylogeny of all known species of dictyostelids based on SSU rDNA. Newly generated sequences are indicated in red.

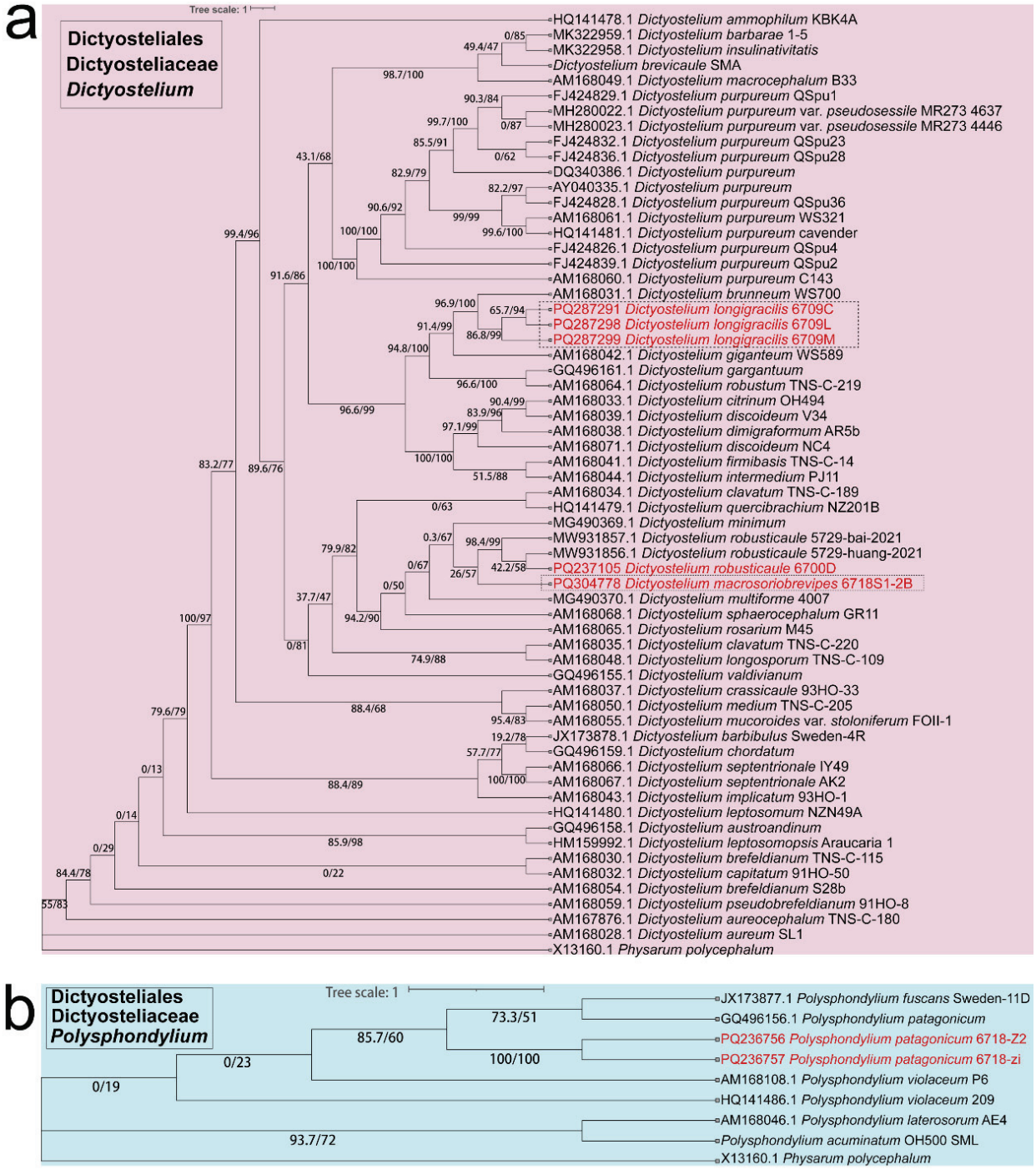


Figure 9. SSU phylogeny of *Dictyostelium* (**a**) and *Polysphondylium* (**b**) sequences in the order Dictyosteliales and the family Dictyosteliaceae. Numbers in parentheses are SH-aLRT support (%)/ultrafast bootstrap support (%). Newly generated sequences are indicated in red and the new species are framed in black.

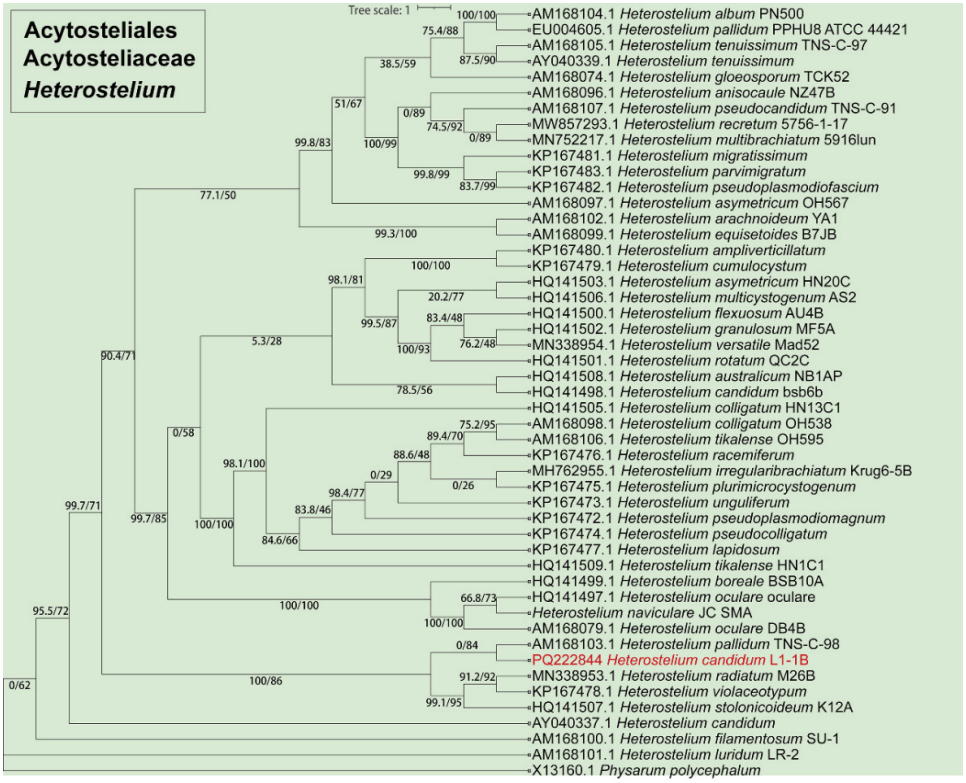


Figure 10. SSU phylogeny of *Heterostelium* sequences in the order Acytosteliales and the family Acytosteliaceae. Numbers in parentheses are SH-aLRT support (%)/ultrafast bootstrap support (%). Newly generated sequences are indicated in red.

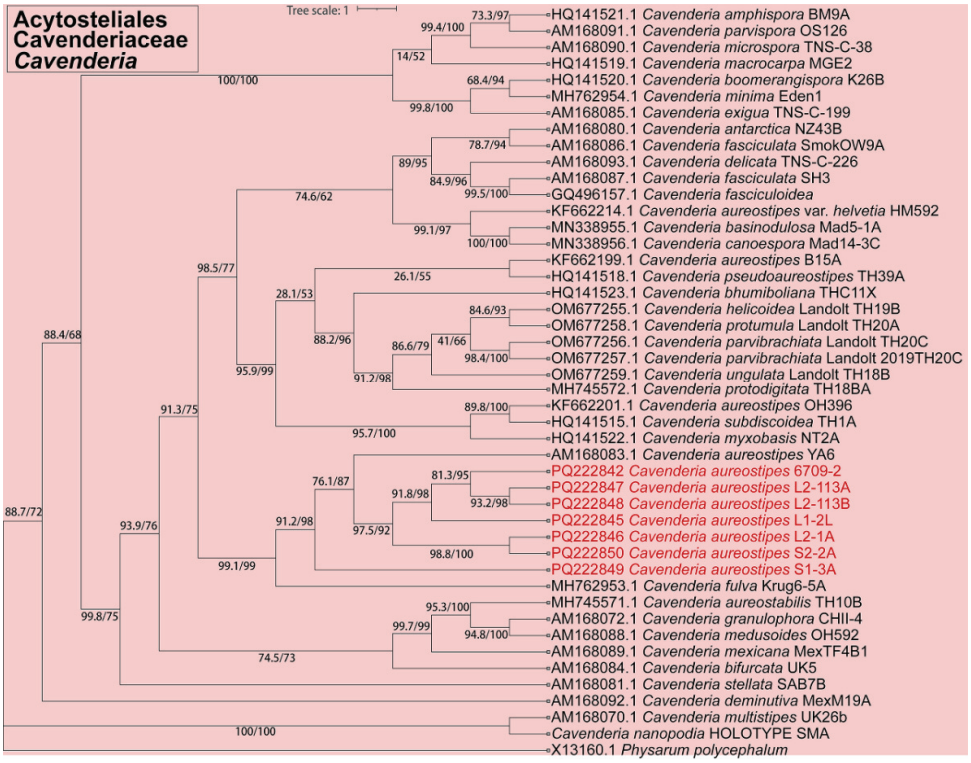


Figure 11. SSU phylogeny of *Cavenderia* sequences in the order Acytosteliales and the family Cavenderiaceae. Numbers in parentheses are SH-aLRT support (%)/ultrafast bootstrap support (%). Newly generated sequences are indicated in red.

3.1. Taxonomy and Molecular Phylogeny

Dictyostelium longigracilis, found by Z.J. Zhang, P. Liu, and Y. Li sp. nov., is shown in Figure 2.

MycoBank: FN 572069.

When cultured at 23 °C on non-nutrient agar with *Escherichia coli*, the **sorocarps** are solitary, erect, or inclined, sometimes prostrate on the medium, unbranched, strongly phototropic, with a relatively fast growth rate, reaching 10 mm in 48 h, fragile and prone to lodging on the medium, 2.375–10.710 mm high. The **sorophores** are colorless and slender, consisting of two to four tiers of cells, 6.539–17.767 μm wide. The **sorophore tips** are capitate, surrounded by a slimy substance, 5.539–8.011 μm in diameter. The **sorophore bases** are rounded, surrounded with a slimy substance, 16.922–39.985 μm in diameter. The **sori** is globose or lemon-shaped, hyaline or creamy white, transparent and hyaline in the early stage, and gradually tends to be milky white with time, 0.158–0.426 mm in diameter, mostly 0.284–0.313 mm in diameter. The **spores** are oblong or elliptical, elongated, 5.673–9.330 × 3.050–3.814 μm, without polar granules. The **aggregations** exhibit radiate streaming. The **pseudoplasmodia** migrate with the stalks.

Etymology: This name refers to the slender sorophores.

Holotype: HMJAU MR 430, HMJAU MR 431, and HMJAU MR 432 (strain 6709C, strain 6709L, and strain 6709M) were isolated from a soil sample collected in China, Jilin Province, Baishan City, Changbai Korean Autonomous County, Wangtian'e New Village (soil no. 6709; elevation 630 m; coordinates 41°27′44″ N, 127°56′31″ E), on 21 July 2021 in a scallion farmland.

The GenBank accession numbers for the SSU sequences are PQ287291, PQ287298, and PQ287299.

Known distribution: Currently, it is believed to be found only in China.

Commentary: The proliferation rate of this species is remarkable, with mature sorocarps emerging within a mere 48 h of cultivation. These sorocarps exhibit a distinctive feature—a notably elongated sorophore, which leads to the easy collapse of the sorocarps. Molecular phylogeny based on SSU rRNA supported the position of this species in the genus *Dictyostelium* [25] (Figure 9a). It forms a clade together with *D. brunneum* and *D. giganteum* [12,31].

However, the sorophore of *D. giganteum* is hyaline and sparsely branched, whereas *D. longigracilis* is unbranched. The spores of *D. longigracilis* (5.673–9.330 × 3.050–3.814 μm) are longer than those of *D. giganteum* (5.0–6.5 × 3.0–3.5 μm). Compared to *D. brunneum* (color of sori off-white to cream-colored when young, becoming tan to dull brown with age), the sori in *D. longigracilis* is colorless or milky white. Moreover, in terms of sorocarp size, it is worth noting the differences between *D. longigracilis* and another species, *D. longosporum*. The sorocarps of *D. longosporum* are 0.5–5.1 (−30) mm, whereas, in *D. longigracilis*, they are larger, ranging from 2.375 to 10.710 mm. This comparison highlights the variability in sorocarp size among different species within the genus.

Dictyostelium macrosoriobrevipes, found by Z.J. Zhang, P. Liu, and Y. Li sp. nov., is shown in Figure 3.

Fungal Names: FN 572068.

When cultured at 23 °C on non-nutrient agar with *Escherichia coli*, the **sorocarps** are mostly solitary, occasionally clustered, erect, semi-erect, or inclined, without branches or occasional branches, 0.483–1.389 mm high. The **sorophores** are thick and short, consisting of two to five tiers of cells, tapering from the base to the top, 18.653–27.520 μm wide. The **sorophore tips** are obtuse, with a collar structure, with two to three tiers of cells, relatively thick, 10.616–19.303 μm in diameter. The **sorophore bases** are clavate, 14.860–22.027 μm in diameter. The **sori** is globose, hyaline or milky white, 0.065–0.578 mm in diameter, but mostly 0.216–0.348 mm in diameter. The **spores** are oblong or reniform, 9.282–17.484 × 4.527–6.382 μm, without polar granules. The **aggregations** exhibit radiate streaming, and the sorocarps are pulled up from the center of the aggregations or

the end of the aggregations. The **sorogens** are colorless, 0.416–1.619 mm in length. The **pseudoplasmodia** migrate with the stalks.

Etymology: This name refers to the large sori and the short sorophores.

Holotype: HMJAU MR433 (Strain 6718S1-2B) was isolated from a soil sample from China, Jilin Province, Baishan City, Changbai Korean Autonomous County, Primary Protection Zone of Drinking Water Sources (soil no. 6718; elevation 717.85 m; coordinates 41°29′17″ N, 127°56′32″ E), collected on 23 July 2021, in a broadleaf forest.

The GenBank accession number for the SSU sequence is PQ304778.

Known distribution: Currently, it is believed to be found only in China.

Commentary: *Dictyostelium macrosoriobrevipes* is characterized by a collar-like structure at the tip of the sorocarps, large sori, and a short sorophore compared to its large sori. A molecular phylogeny study based on SSU rRNA supported the position of this species in the genus *Dictyostelium* [25] (Figure 9a). This species forms a clade with *D. robusticaule* [21] and *D. minimum* [42]. However, the sorocarps of *D. robusticaule* are 0.3–2.4 mm or 0.1–0.2 mm, whereas those of *D. macrosoriobrevipes* are 0.483–1.389 mm. Radiate aggregations occur in *D. macrosoriobrevipes*, whereas those of *D. minimum* are mounds, and *D. multiforme* aggregations are mound-like and minutum-type. The spores of *D. robusticaule* (5.0–7.2 × 3.2–4.7 μm or 4.7–6.5 × 3.0–4.3 μm) and *D. minimum* (3.7–5.4 μm) are smaller than in *D. macrosoriobrevipes* (9.282–17.484 × 4.527–6.382 μm).

Dictyostelium robusticaule, found by Y. Li, P. Liu, and Y. Zou and described by Zou, Hou, Guo, Li, Li, Stephenson, Pavlov, Liu and Lia in *Microbiology Spectrum* 10 (5): 8 (2022), is shown in Figure 4.

When cultured at 23 °C on non-nutrient agar with *Escherichia coli*, the **sorocarps** are erect or twisted in the medium, with branches or with branches which are not obvious in the early stage; sometimes, branches will appear in the later stage. They are 1.601–3.182 mm high. The **sorophores** are colorless, consisting of three to four tiers of cells, 19.235–21.152 μm wide. The **sorophore bases** are clavate, while the **sorophore tips** have a collar structure. The **sori** is large, globose, hyaline or milk white, 0.126–0.432 mm in diameter. The **spores** are oblong or elliptical, 7.156–9.612 × 4.449–6.249 μm, without polar granules. The **aggregations** have a radiate pattern, and **pseudoplasmodia** migration occurs with the sorophore.

Holotype: HMJAU MR 434 (strain 6700D) was isolated from a soil sample from China, Jilin Province, Baishan City, Changbai Korean Autonomous County, Fifteen Gap (soil no. 6700; elevation 651 m; coordinates 41°28′03″ N, 127°56′26″ E), collected on July 20, 2021, in a broadleaf forest.

The GenBank accession number for the SSU sequence is PQ237105.

Known distribution: Currently, it is believed to only be found in China, specifically in Guizhou [22] and Jilin [21].

Polysphondylium patagonicum, described by Vadell, Cavender, Romeralo, and S.L. Stephenson in *Mycologia* 103 (1): 113 (2011), is shown in Figure 5.

When cultured at 23 °C on non-nutrient agar with *Escherichia coli*, the **sorocarps** are solitary or gregarious, erect or semi-erect, often prostrate on the medium, unbranched or with 2–8 whorled branches, each whorl with 2–5 spaced nodes, nearly 2.85–6.32 mm high. The **sorophores** are purplish red, consisting of several tiers of cells. The **sorophore tips** are clavate, 6.45–11.79 μm in diameter. The **sorophore bases** are round or clavate, 10.14–21.99 μm in diameter. The **sori** is globose, light purple or purplish red, 0.075–0.233 mm in diameter. The **spores** are elliptical, mostly 5.47–6.75 × 3.084–4.314 μm, with consolidated polar granules. The **aggregations** have a radiate pattern. The **pseudoplasmodia** migrate with the stalks.

Holotype: HMJAU MR 435 and HMJAU MR 436 (strain 6718-Z2, strain 6718-zi) were isolated from a soil sample of China, Jilin Province, Baishan City, Changbai Korean Autonomous County, Primary Protection Zone of Drinking Water Sources (soil no. 6718; elevation 717.85 m; coordinates 41°29′17″ N, 127°56′32″ E), collected on 23 July 2021 in a broadleaf forest.

The GenBank accession numbers for the SSU sequences are PQ236756 and PQ236757.

Known distribution: It can be found in Patagonia [43], Argentina, Russia [44], and China, specifically in Jilin.

Heterostelium candidum (H. Hagiw.), described by S. Baldauf, S. Sheikh, and Thulin, in Sheikh, Thulin, Cavender, Escalante, Kawakami, Lado, Landolt, Nanjundiah, Queller, Strassmann, Spiegel, Stephenson, Vadell, and Baldauf, *Protist* 169: 14 (2018), is shown in Figure 6.

When cultured at 23 °C on non-nutrient agar with *Escherichia coli*, the **sorocarps** are solitary, sometimes clustered, inclined or prostrate on the medium, 1.367–5.574 mm high. The **sorophores** are colorless, consisting of one to two tiers of cells, with about 3–7 whorled branches, each whorl bearing 2–4 sori. The **sorophore bases** are clavate, their branch end conical. The **sori** is globose, white, and transparent; the terminal sori measures 65.27–100.92 μm in diameter, while the lateral sori is 34.19–82.27 μm in diameter. The **spores** are elliptical to oblong, 7.116–10.426 × 3.266–5.959 μm, with polar granules. The **aggregations** have a radiate pattern. The **pseudoplasmodia** migrate with the stalks.

Holotype: HMJAU MR 437 (strain L1-1B) was isolated from soil samples collected in China, Jilin Province, Baishan City, Changbai Korean Autonomous County, Lishui Manor (soil no. 6715; elevation 795 m; coordinates 41°31′23″ N, 127°56′58″ E), on 22 July 2021 in a broadleaf forest.

The GenBank accession number for the SSU sequence is PQ222844.

Known distribution: It can be found in Japan, United States, and China, specifically in Hubei, Henan [45], and Jilin.

Cavenderia aureostipes (Cavender), found by S. Baldauf, S. Sheikh and Thulin and described in Sheikh, Thulin, Cavender, Escalante, Kawakami, Lado, Landolt, Nanjundiah, Queller, Strassmann, Spiegel, Stephenson, Vadell, and Baldauf, *Protist* 169: 19 (2018), is shown in Figure 7.

When cultured at 23 °C on non-nutrient agar with *Escherichia coli*, the **sorocarps** are solitary or clustered, erect or semi-erect, with irregular branches, strongly phototropic, and nearly 3.81–7.53 mm high. The **sorophores** are golden yellow, with 5–23 irregular branches, 392.52–749.81 μm wide. The **sorophore tips** are obtuse, 7.48–10.82 μm in diameter. The **sorophore bases** are clavate, consisting of several tiers of cells, 23.26–27.79 μm in diameter. The **sori** is white and globose; the terminal sori is 140.71–194.48 μm in diameter, while the lateral sori measures 36.14.78–82.81 μm in diameter. The **spores** are elliptical to oblong, mostly 4.733–6.281 × 2.881–4.251 μm, with consolidated polar granules. The **aggregations** have a radiate pattern. The **pseudoplasmodia** migrate with the stalks.

Holotype: HMJAU MR 438 (strain 6709-2) was isolated from a soil sample collected in China, Jilin Province, Baishan City, Changbai Korean Autonomous County, Wangtian'e New Village (soil no. 6709; elevation 630 m; coordinates 41°27′44″ N, 127°56′31″ E), on 21 July 2021, on scallion farmland. HMJAU MR 439 (strain L1-2L) was isolated from soil samples from China, Jilin Province, Baishan City, Changbai Korean Autonomous County, Lishui Manor (soil no. 6715; elevation 795 m; coordinates 41°31′23″ N, 127°56′58″ E), collected on 22 July 2021, in a broadleaf forest. HMJAU MR 440, HMJAU MR 441, and HMJAU MR 442 (strain L2-1A, strain L2-113A, and strain L2-113B) were isolated from soil samples collected in China, Jilin Province, Baishan City, Changbai Korean Autonomous County, Lishui Manor (soil no. 6716; elevation 798.47 m; coordinates 41°31′22″ N, 127°57′0″ E), on 22 July 2021, in a broadleaf forest. HMJAU MR 443 and HMJAU MR 444 (strain S1-3A and strain S2-2A) were isolated from soil samples from China, Jilin Province, Baishan City, Changbai Korean Autonomous County, Primary Protection Zone of Drinking Water Sources (soil no. 6718; elevation 717.85 m; coordinates 41°29′17″ N, 127°56′32″ E; and soil no. 6719; elevation 729.46 m; coordinates 41°29′17″ N, 127°56′34″ E), collected on 23 July 2021, in broadleaf forests.

The GenBank accession numbers for the SSU sequences are PQ222850, PQ222849, PQ222848, PQ222847, PQ222846, PQ222845, and PQ222842.

Known distribution: It is found in Switzerland, the United States, Japan, India, Nepal, Russia, and China, specifically on the Qinghai–Tibet Plateau [42] and in Jilin.

3.2. Assemblage of Dictyostelids in Jilin Province

Based on the identification, collation, and statistical analysis carried out in this study, a total of 35 species of dictyostelids, classified under 6 genera, 4 families, and 2 orders, are known to occur in Jilin Province (Supplementary Table S1, Figure 12a). Their primary ecological niche is soil, with a minority occurring in decaying leaves and humus (Supplementary Table S1). The dominant order within this group is the Dictyosteliales (Figure 12b), featuring 1 predominant family (>10 species) (Figure 12c), encompassing 20 species, accounting for 57% of the total species count. Within the group in Jilin Province, there are 2 dominant genera (>5 species) (Figure 12d), comprising 25 species, dominated by *Dictyostelium* and *Polysphondylium*, which, together, represent 71% of the total species diversity.

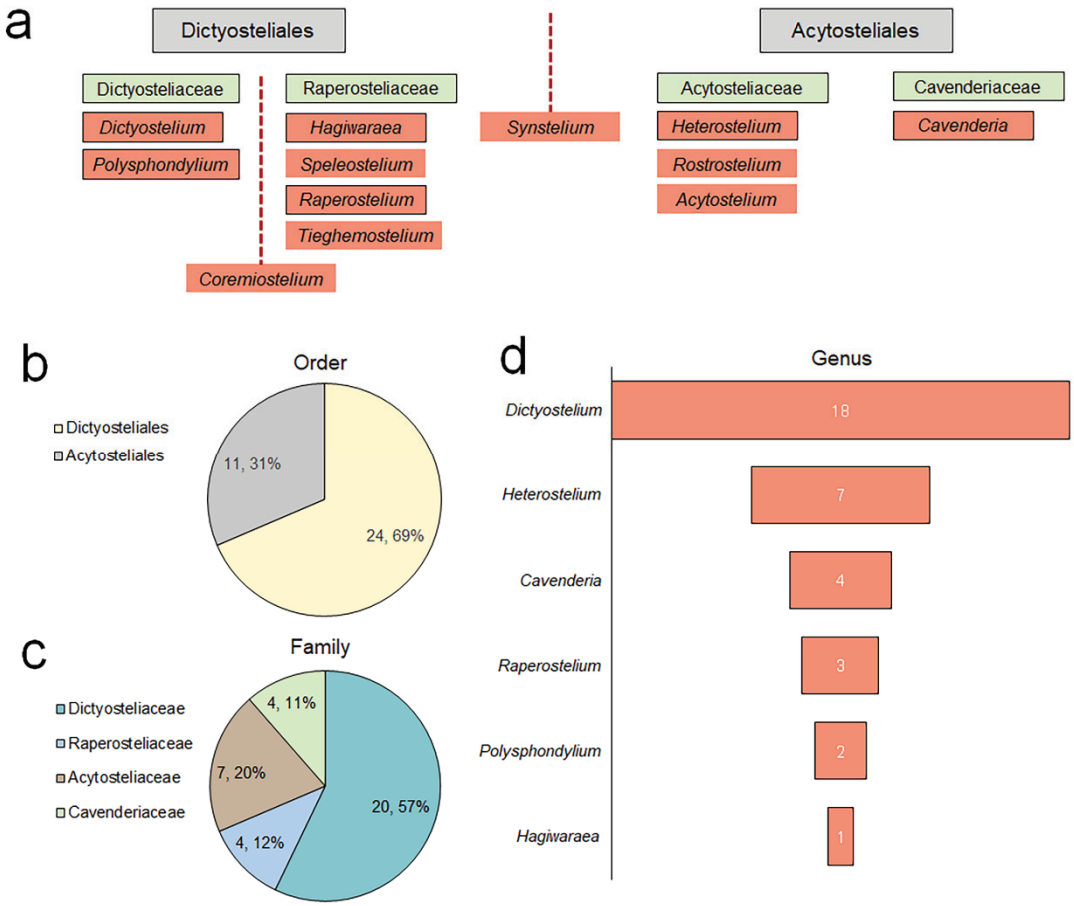


Figure 12. The new classification as indicated by nuclear small subunit (18S) [25] rDNA sequences, displayed with a black border (**a**) and numbers of dictyostelid species within the order (**b**), family (**c**), and genus (**d**) in Jilin Province, China.

4. Discussion

4.1. Species Distribution and Geographic Uniqueness

As a hotspot for ecological diversity conservation in Northeast China, Changbai Korean Autonomous County [46] (Figure 1a) in Jilin Province boasts a unique geographical location (nestled in the heart of Changbai Mountain, featuring a mild and humid climate with four distinct seasons) and a complex terrain (encompassing various ecosystems such as mountains, forests, and wetlands), providing an ideal habitat for microorganisms like dictyostelids.

In this study, we collected 28 soil samples from five localities in Changbai Korean Autonomous County, Jilin Province (Table 1), and employed a combined approach of morphological [12,31] (Figures 2–7) and the latest molecular systematic [25] (Figures 8–11) identification methods, yielding 15 dictyostelid isolates belonging to 6 species from 4 genera, with the family Dictyosteliaceae occupying a dominant position (66.67%). The family Dictyosteliaceae [47], the most species-rich group within the class Dictyosteliales, primarily comprises the genera *Dictyostelium* and *Polysphondylium* [25]. Due to the special geographical location and terrain of Jilin Province, it is characterized by some unique species of dictyostelids, including two new species and two new records, not only reflecting the abundance of dictyostelid resources in this region but also underlining its significance in microbial diversity conservation.

4.2. Ecological Significance and Species Diversity

The terrain of Changbai Korean Autonomous County is dominated by mountains and hills, with elevations ranging from 500 to 2691 m. The total forest area of Changbai Korean Autonomous County is 232,895.6 hectares, representing a forest coverage of 92%, ranking among the forefront in the province and even the country (http://changbai.gov.cn/cbgk/zrzy/201801/t20180108_257152.html, accessed on 11 May 2023). Dictyostelids, as a crucial component of soil ecosystems, engage in processes such as organic matter decomposition and nutrient cycling, thereby playing a pivotal role in maintaining ecological balance and soil health [22,48].

The five localities investigated encompassed four vegetation types: coniferous forest, broadleaf forest, mixed forest, and farmland. Overall, the density and fruiting body abundance of dictyostelids in broadleaf forests was up to 19.44 clones/g, followed by farmland with 1.67 clones/g. No isolates were recovered from the coniferous forest at L1 in this study, and no isolates were obtained from any of the sampled mixed forests. Previous research by Zou et al. [21] and Zhang et al. [11] indicated that mixed forests yielded more isolates, whereas our findings revealed the highest species richness in broadleaf forests. As is generally known, the growth and reproduction of soil protists depend largely on the habitat and substrate provided by plants [49]. However, the composition and quantity of protozoa communities vary significantly under different vegetation types [50], highlighting the notable impact of vegetation type on the richness of dictyostelids at sampling sites.

4.3. Composition and Distribution of Dictyostelid Species in Jilin Province

Furthermore, this study primarily relied on comprehensive literature sources such as mycological treatises [51] and the published literature to provide a detailed inventory of dictyostelid distributions at the county and city levels. Corresponding voucher information is also provided for each species' occurrence in Jilin Province, encompassing specimens, substrate numbers, vegetation types, strain numbers, geographical locations, and references. These voucher details serve as verifiable evidence for researchers to examine.

Notably, in 1984, Bai [52] first reported five species of dictyostelids from Jilin Province. To date, Jilin Province is known to have 35 species, belonging to 6 genera, 4 families, and 2 orders (Supplementary Table S1). Among them, the dominant family is the Dictyosteliaceae, and the dominant genus is *Dictyostelium* (Figure 12). Swanson et al. [53] divided the global distribution of 65 species of forest soil dictyostelids into 4 categories—cosmopolitan, disjunct, restricted, and pantropical. The dictyostelid species in Jilin Province are abundant, and, in terms of the geographical composition of families and genera, they are dominated by restricted species, forming a complex and diverse assemblage. This is also consistent with the distribution of Madagascar species reported by Cavender et al. [54], indicating that species distribution is sometimes regional.

5. Conclusions

The present study underscores the significance of dictyostelids within the protist community, particularly in Jilin Province, China. Through a comprehensive resource

survey employing random sampling at five localities in Changbai Korean Autonomous County, we identified a rich diversity of dictyostelids, including the description of two novel species based on morphological and genetic analyses. The dominance of the genus *Dictyostelium* in the dictyostelid assemblage of Jilin Province, coupled with the discovery of new records for China and Jilin Province, highlights the region's importance as a hotspot for these organisms. Our findings not only contribute to the understanding of dictyostelid diversity and distribution but also provide valuable insights into their ecological roles and potential applications. The compilation of dictyostelid species reported in Jilin Province represents an important step towards developing effective conservation strategies and promoting sustainable resource utilization of these fascinating organisms.

Supplementary Materials: The following supporting information can be downloaded at https://www.mdpi.com/article/10.3390/jof10120834/s1: Table S1: A checklist of dictyostelids in Iilin province, China [21,23–25,51,52,55–59].

Author Contributions: Z.Z.: writing—original draft, data curation, software, and conceptualization. L.H.: methodology and formal analysis. Y.S.: validation and data curation. Z.L.: writing—review and editing. Y.Y.: resources. C.Z.: software. S.L.S.: writing—review and editing. X.X.: validation. Y.L.: supervision and project administration. P.L.: writing—review and editing, project administration, and funding acquisition. All authors have read and agreed to the published version of the manuscript.

Funding: The research reported herein was supported by funding supplied by the National Natural Science Foundation of China (nos. 32070009 and 32370020), the Natural Science Foundation of Jilin Province (no. 20220101187JC), and the Program of Creation and Utilization of Germplasm of Mushroom Crop of "111" Project (no. D17014).

Institutional Review Board Statement: Not applicable.

Informed Consent Statement: Not applicable.

Data Availability Statement: The original contributions presented in the study are included in the article and Supplementary Material, further inquiries can be directed to the corresponding author.

Conflicts of Interest: The authors declare no conflict of interest.

References

1. Landi, P.; Minoarivelo, H.O.; Brannstrom, A.; Hui, C.; Dieckmann, U. Complexity and stability of ecological networks: A review of the theory. *Popul. Ecol.* **2018**, *60*, 319–345. [CrossRef]
2. Nelson, G.; Ellis, S. The history and impact of digitization and digital data mobilization on biodiversity research. *Philos. Trans. R. Soc. B-Biol. Sci.* **2019**, *374*, 20170391. [CrossRef] [PubMed]
3. Fairchild, T.P.; Weedon, J.; Griffin, J.N. Species diversity enhances perceptions of urban coastlines at multiple scales. *People Nat.* **2022**, *4*, 931–948. [CrossRef]
4. Chen, G.; Zhu, H.; Zhang, Y. Soil microbial activities and carbon and nitrogen fixation. *Res. Microbiol.* **2003**, *154*, 393–398. [CrossRef]
5. Matsuoka, S.; Kobayashi, Y.; Hobara, S.; Osono, T. Identifying microbial drivers promoting plant growth on soil amended with composted aquatic plant: Insight into nutrient transfer from aquatic to terrestrial systems. *Limnology* **2020**, *21*, 443–452. [CrossRef]
6. Mishustin, E.N. Microbial associations of soil types. *Microb. Ecol.* **1975**, *2*, 97–118. [CrossRef]
7. Xiong, W.; Jousset, A.; Guo, S.; Karlsson, I.; Zhao, Q.; Wu, H.; Kowalchuk, G.A.; Shen, Q.; Li, R.; Geisen, S. Soil protist communities form a dynamic hub in the soil microbiome. *ISME J.* **2018**, *12*, 634–638. [CrossRef]
8. Ceja-Navarro, J.A.; Wang, Y.; Ning, D.; Arellano, A.; Ramanculova, L.; Yuan, M.M.; Byer, A.; Craven, K.D.; Saha, M.C.; Brodie, E.L.; et al. Protist diversity and community complexity in the rhizosphere of switchgrass are dynamic as plants develop. *Microbiome* **2021**, *9*, 2–18. [CrossRef] [PubMed]
9. Oliverio, A.M.; Geisen, S.; Delgado-Baquerizo, M.; Maestre, F.T.; Turner, B.L.; Fierer, N. The global-scale distributions of soil protists and their contributions to belowground systems. *Sci. Adv.* **2020**, *6*, eaax8787. [CrossRef]
10. Shadwick, L.L.; Spiegel, F.W.; Shadwick, J.D.L.; Brown, M.W.; Silberman, J.D. Eumycetozoa Amoebozoa: SSUrDNA phylogeny of protosteloid slime molds and its significance for the Amoebozoan supergroup. *PLoS ONE* **2009**, *4*, e6754. [CrossRef]
11. Zhang, Z.; Yang, Y.; Zhao, J.; Li, Y.; Stephenson, S.L.; Qiu, J.; Liu, P. Environmental factors influencing the diversity and distribution of dictyostelid cellular slime molds in forest and farmland soils of western China. *Microbiol. Spectr.* **2023**, *11*, e01732-23. [CrossRef] [PubMed]
12. Raper, K.B. *The Dictyostelids*; Princeton University Press: Princeton, NJ, USA, 1984. [CrossRef]

13. Perrigo, A.L.; Baldauf, S.L.; Romeralo, M. Diversity of dictyostelid social amoebae in high latitude habitats of Northern Sweden. *Fungal Divers.* **2013**, *58*, 185–198. [CrossRef]
14. Baldauf, S.L.; Romeralo, M.; Fiz-Palacios, O.; Heidari, N. A deep hidden diversity of dictyostelia. *Protist* **2018**, *169*, 64–78. [CrossRef] [PubMed]
15. Stephenson, S.L.; Feest, A. Ecology of soil Eumycetozoans. *Acta Protozool.* **2012**, *51*, 201–208. [CrossRef]
16. Rao, G.; Chen, S. Advancements in the taxonomic study of myxomycetes (Myxogastrea) in China. *Mycology* **2023**, *14*, 316–325. [CrossRef]
17. Romeralo, M.; Skiba, A.; Gonzalez-Voyer, A.; Schilde, C.; Lawal, H.; Kedziora, S.; Cavender, J.C.; Gloeckner, G.; Urushihara, H.; Schaap, P. Analysis of phenotypic evolution in dictyostelia highlights developmental plasticity as a likely consequence of colonial multicellularity. *Proc. R. Soc. B-Biol. Sci.* **2013**, *280*, 20130976. [CrossRef]
18. Schaap, P. Evolution of developmental signalling in dictyostelid social amoebas. *Curr. Opin. Genet. Dev.* **2016**, *39*, 29–34. [CrossRef]
19. Li, Y.; Liu, P.; Zhao, M.J. *Species Catalogue of China: Volume 3 Fungi (Slime Molds, Water Molds)*; Science Press: Beijing, China, 2018.
20. Liu, P.; Zhang, S.; Zou, Y.; Li, Z.; Stephenson, S.L.; Li, Y. Distribution and ecology of dictyostelids in China. *Fungal Biol. Rev.* **2020**, *34*, 170–177. [CrossRef]
21. Zou, Y.; Hou, J.; Guo, S.; Li, C.; Li, Z.; Stephenson, S.L.; Pavlov, I.N.; Liu, P.; Li, Y. Diversity of dictyostelid cellular slime molds, including two species new to science, in forest soils of Changbai Mountain, China. *Microbiol. Spectr.* **2022**, *10*, e02402-22. [CrossRef]
22. Zhang, Z.; Li, M.; Zhang, S.; Qin, Y.; Zhao, J.; Li, Y.; Stephenson, S.L.; Qiu, J.; Liu, P. Diversity of cellular slime molds (dictyostelids) in the Fanjing Mountain Nature Reserve and geographical distribution comparisons with other representative nature reserves in different climate zones of China. *Microorganisms* **2024**, *12*, 1061. [CrossRef]
23. Liu, P.; Li, Y. Dictyostelids from Jilin Province, China. I. *Phytotaxa* **2014**, *183*, 279–283. [CrossRef]
24. Liu, P.; Li, Y. Dictyostelids from Jilin Province, China II. *Phytotaxa* **2017**, *323*, 77–82. [CrossRef]
25. Sheikh, S.; Thulin, M.; Cavender, J.C.; Escalante, R.; Kawakami, S.-I.; Lado, C.; Landolt, J.C.; Nanjundiah, V.; Queller, D.C.; Strassmann, J.E.; et al. A new classification of the dictyostelids. *Protist* **2018**, *169*, 1–28. [CrossRef]
26. Schaap, P.; Winckler, T.; Nelson, M.; Alvarez-Curto, E.; Elgie, B.; Hagiwara, H.; Cavender, J.; Milano-Curto, A.; Rozen, D.E.; Dingermann, T.; et al. Molecular phylogeny and evolution of morphology in the social amoebas. *Science* **2006**, *314*, 661–663. [CrossRef]
27. Romeralo, M.; Cavender, J.C.; Landolt, J.C.; Stephenson, S.L.; Baldauf, S.L. An expanded phylogeny of social amoebas (dictyostelia) shows increasing diversity and new morphological patterns. *BMC Evol. Biol.* **2011**, *11*, 84. [CrossRef] [PubMed]
28. Wu, L.; Li, L.; Liu, H.; Cheng, X.; Zhu, T. Application of ArcGIS in geography teaching of secondary school: A case study in the practice of map teaching. *Wirel. Pers. Commun.* **2018**, *102*, 2543–2553. [CrossRef]
29. Cavender, J.C.; Raper, K.B. The Acrasieae in nature. I. isolation. *Am. J. Bot.* **1965**, *52*, 294–296. [CrossRef] [PubMed]
30. Cocucci, S.M.; Sussman, M. RNA in cytoplasmic and nuclear fractions of cellular slime mold amebas. *J. Cell Biol.* **1970**, *45*, 399–407. [CrossRef]
31. Hagiwara, H. *The Taxonomic Study of Japanese Dictyostelid Cellular Slime Molds*; National Science Museum: Tokyo, Japan, 1989.
32. Redhead, S.A.; Norvell, L.L. MycoBank, Index Fungorum, and Fungal Names recommended as official nomenclatural repositories for 2013. *IMA Fungus* **2012**, *3*, 44–45. [CrossRef]
33. Liu, P.; Zou, Y.; Li, W.; Li, Y.; Li, X.; Che, S.; Stephenson, S.L. Dictyostelid cellular slime molds from Christmas Island, Indian Ocean. *Msphere* **2019**, *4*, 10-1128. [CrossRef]
34. Medlin, L.; Elwood, H.J.; Stickel, S.; Sogin, M.L. The characterization of enzymatically ampliffed eukaryotic 16S-like rRNA-coding regions. *Gene* **1988**, *71*, 491–499. [CrossRef] [PubMed]
35. Thompson, J.D.; Higgins, D.G.; Gibson, T.J. CLUSTAL W: Improving the sensitivity of progressive multiple sequence alignment through sequence weighting, position-specific gap penalties and weight matrix choice. *Nucleic Acids Res.* **1994**, *22*, 4673–4680. [CrossRef] [PubMed]
36. Tippmann, H.-F. Analysis for free: Comparing programs for sequence analysis. *Brief. Bioinform.* **2004**, *5*, 82–87. [CrossRef]
37. Minh, B.Q.; Schmidt, H.A.; Chernomor, O.; Schrempf, D.; Woodhams, M.D.; von Haeseler, A.; Lanfear, R. IQ-TREE 2: New models and efficient methods for phylogenetic inference in the Genomic Era. *Mol. Biol. Evol.* **2020**, *37*, 1530–1534. [CrossRef]
38. Diep Thi, H.; Chernomor, O.; von Haeseler, A.; Minh, B.Q.; Le Sy, V. UFBoot2: Improving the ultrafast bootstrap approximation. *Mol. Biol. Evol.* **2018**, *35*, 518–522. [CrossRef]
39. Shimodaira, H.; Hasegawa, M. Multiple comparisons of Log-Likelihoods with applications to phylogenetic inference. *Mol. Biol. Evol.* **1999**, *16*, 1114–1116. [CrossRef]
40. Kalyaanamoorthy, S.; Bui Quang, M.; Wong, T.K.F.; von Haeseler, A.; Jermiin, L.S. ModelFinder: Fast model selection for accurate phylogenetic estimates. *Nat. Methods* **2017**, *14*, 587–589. [CrossRef] [PubMed]
41. Letunic, I.; Bork, P. Interactive Tree of Life (iTOL) v5: An online tool for phylogenetic tree display and annotation. *Nucleic Acids Res.* **2021**, *49*, W293–W296. [CrossRef]
42. Liu, P.; Zou, Y.; Li, S.; Stephenson, S.L.; Wang, Q.; Li, Y. Two new species of dictyostelid cellular slime molds in high-elevation habitats on the Qinghai-Tibet Plateau, China. *Sci. Rep.* **2019**, *9*, 5. [CrossRef]

43. Vadell, E.M.; Cavender, J.C.; Romeralo, M.; Edwards, S.M.; Stephenson, S.L.; Baldauf, S.L. New species of dictyostelids from Patagonia and Tierra del Fuego, Argentina. *Mycologia* **2011**, *103*, 101–117. [CrossRef]
44. Li, W.; Wei, Y.; Zou, Y.; Liu, P.; Li, Z.; Gontcharov, A.A.; Stephenson, S.L.; Wang, Q.; Zhang, S.; Li, Y. Dictyostelid cellular slime molds from the Russian Far East. *Protist* **2020**, *171*, 125756. [CrossRef] [PubMed]
45. Li, C.; Liu, P.; Li, Y. Studies on dictyostelid cellular slime molds in Henan Province. *J. Fungal Res.* **2014**, *12*, 148–153. [CrossRef]
46. Zhu, L.Y.; Zhang, D.H. Forest ecological carrying capacity evaluation on Changbai County in Jilin Province. *Ecol. Sci.* **2016**, *35*, 176–182. [CrossRef]
47. Singh, B.N. Studies on soil Acrasieae; distribution of species of *Dictyostelium* in soils of Great Britain and the effect of bacteria on their development. *J. Gen. Microbiol.* **1947**, *1*, 11–21. [CrossRef]
48. Huang, W.; Zhao, Y.; Zhang, L.; Shi, Y.; Wang, Z.; Mai, Y.; Shu, L. Soil physical structure drives N-glycan mediated trophic interactions in soil amoebae: Mechanisms and environmental implications. *Sci. Total Environ.* **2024**, *906*, 167509. [CrossRef] [PubMed]
49. Singer, D.; Seppey, C.V.W.; Lentendu, G.; Dunthorn, M.; Bass, D.; Belbahri, L.; Blandenier, Q.; Debroas, D.; de Groot, G.A.; de Vargas, C.; et al. Protist taxonomic and functional diversity in soil, freshwater and marine ecosystems. *Environ. Int.* **2021**, *146*, 106262. [CrossRef] [PubMed]
50. Ferreira de Araujo, A.S.; Mendes, L.W.; Lemos, L.N.; Lopes Antunes, J.E.; Aguiar Beserra, J.E., Jr.; Catanho Pereira de Lyra, M.d.C.; Barreto Figueiredo, M.d.V.; de Almeida Lopes, A.C.; Ferreira Gomes, R.L.; Bezerra, W.M.; et al. Protist species richness and soil microbiome complexity increase towards climax vegetation in the Brazilian Cerrado. *Commun. Biol.* **2018**, *1*, 135. [CrossRef]
51. Li, Y.; Wang, Q.; Liu, P.; Zhang, B. *Compilation and Research on the Biological Diversity of Jilin Province: The Volume of Fungi in Gymnomycota*; Jilin Education Press: Changchun, China, 2019.
52. Bai, R.L. A study on some species of Acrasiomycetes. *Acta Mycol. Sin.* **1983**, *2*, 173–178. [CrossRef]
53. Swanson, A.R.; Vadell, E.M.; Cavender, J.C. Global distribution of forest soil dictyostelids. *J. Biogeogr.* **1999**, *26*, 133–148. [CrossRef]
54. Cavender, J.C.; Landolt, J.C.; Vadell, E.M.; Perrigo, A.L.; Stephenson, S.L.; De Basanta, D.W.; Lado, C.; Liu, P. Distribution and ecology of dictyostelids in Madagascar. *Phytotaxa* **2021**, *505*, 176–186. [CrossRef]
55. He, X.L.; Li, Y. Three new records of dictyostelids in China. *Mycosystema* **2008**, *27*, 532–537.
56. He, X.-L.; Li, Y. A new species of *Dictyostelium*. *Mycotaxon* **2008**, *106*, 379–383.
57. Ren, Y.Z.; Liu, P.; Li, Y. New records of dictyostelids from China. *Nova Hedwig.* **2014**, *99*, 233–237. [CrossRef]
58. Liu, P.; Zhang, S.; Zou, Y.; Kang, X.; Li, Y. Dictyostelids from Jilin Province, China 3: New *Cavenderia* and *Dictyostelium* records. *Mycotaxon* **2019**, *134*, 613–618. [CrossRef]
59. Zhu, H.; Guo, S.; Xue, Q.; Li, Z.; Kang, X.; Wei, Y.; Liu, P.; Wang, Q.; Li, Y. Dictyostelids from Jilin Province, China, 4. *Mycotaxon* **2021**, *136*, 445–489. [CrossRef]

Disclaimer/Publisher's Note: The statements, opinions and data contained in all publications are solely those of the individual author(s) and contributor(s) and not of MDPI and/or the editor(s). MDPI and/or the editor(s) disclaim responsibility for any injury to people or property resulting from any ideas, methods, instructions or products referred to in the content.

Journal of *Fungi*

MDPI

Article

Phytophthora Species and Their Associations with Chaparral and Oak Woodland Vegetation in Southern California

Sebastian N. Fajardo [1,*], Tyler B. Bourret [1,2], Susan J. Frankel [3] and David M. Rizzo [1]

[1] Department of Plant Pathology, University of California, Davis, CA 95616, USA; tyler.bourret@usda.gov (T.B.B.); dmrizzo@ucdavis.edu (D.M.R.)
[2] Mycology and Nematology Genetic Diversity and Biology Laboratory, United States Department of Agriculture, Agricultural Research Service, Beltsville, MD 20705, USA
[3] United States Forest Service, Pacific Southwest Research Station, Albany, CA 94710, USA; susan.frankel@usda.gov
* Correspondence: snfajardo@ucdavis.edu

Abstract: Evidence of unintended introductions of *Phytophthora* species into native habitats has become increasingly prevalent in California. If not managed adequately, *Phytophthora* species can become devastating agricultural and forest plant pathogens. Additionally, California's natural areas, characterized by a Mediterranean climate and dominated by chaparral (evergreen, drought-tolerant shrubs) and oak woodlands, lack sufficient baseline knowledge on *Phytophthora* biology and ecology, hindering effective management efforts. From 2018 to 2021, soil samples were collected from Angeles National Forest lands (Los Angeles County) with the objective of better understanding the diversity and distribution of *Phytophthora* species in Southern California. Forty sites were surveyed, and soil samples were taken from plant rhizospheres, riverbeds, and off-road vehicle tracks in chaparral and oak woodland areas. From these surveys, fourteen species of *Phytophthora* were detected, including *P. cactorum* (subclade 1a), *P. multivora* (subclade 2c), *P.* sp. *cadmea* (subclade 7a), *P.* taxon 'oakpath' (subclade 8e, first reported in this study), and several clade-6 species, including *P. crassamura*. *Phytophthora* species detected in rhizosphere soil were found underneath both symptomatic and asymptomatic plants and were most frequently associated with *Salvia mellifera*, *Quercus agrifolia*, and *Salix* sp. *Phytophthora* species were present in both chaparral and oak woodland areas and primarily in riparian areas, including detections in off-road tracks, trails, and riverbeds. Although these Mediterranean ecosystems are among the driest and most fire-prone areas in the United States, they harbor a large diversity of *Phytophthora* species, indicating a potential risk for disease for native Californian vegetation.

Keywords: Mediterranean vegetation; oomycete; plant pathogen

1. Introduction

The oomycete genus *Phytophthora*, family Peronosporaceae, kingdom Straminipila [1], includes several species that are significant plant pathogens worldwide [2–6]. In forests and natural ecosystems, invasive *Phytophthora* species can destabilize ecosystems with detrimental effects on biodiversity and on ecosystem services [7–11]. Since its detection in the mid-1990s in Northern California [12], *P. ramorum*, the causal agent of sudden oak death, is now present in 16 counties in California and has expanded its distribution to over 318.5 km^2 in Oregon [11,13,14]. Western Australia has been severely affected by the

"biological bulldozer" *P. cinnamomi*, which is capable of infecting 40% of the 5710 species of native flora [15,16].

Since the 1960s, there has been an exponential rise in devastating tree and shrub diseases caused by invasive *Phytophthora* species in natural ecosystems in Australia, Europe, and North America [17,18]. This is likely due to a combination of factors, including increased ecosystem disturbance associated with population growth and expanded plant cultivation and trade [19,20]. Studies focused on dispersal risk have shown that the inadvertent outplanting of infested nursery stock is a primary route for the unintended introduction of *Phytophthora* species into natural areas [7,21,22], with many recorded cases in native ecosystems in California [23–28]. Eradication efforts, however, are generally unsuccessful despite requiring labor-intensive management and incurring high associated costs, as well as increased surveys and improved diagnostic techniques [27,29,30].

California is one of the five main Mediterranean climate regions in the world, together with the European and North African Mediterranean Basin, Southern and Southwestern Australia, Cape Province in South Africa, and central coastal Chile [31–36]. These areas are biodiversity hot spots of endemic flora and fauna, containing about one sixth of the vascular plant species in the world in just 2.2% of the world's land area [9,37–39]. Mediterranean climates support vegetation that provides essential ecosystem services such as climate amelioration, flood and erosion control, nutrient cycling, carbon sequestration, and wildlife habitat [40]. Furthermore, these areas are culturally significant to local indigenous people [41]. In California, a major representative of Mediterranean vegetation is the chaparral biome. These plant communities account for 9% of the vegetation land-cover, with a distribution that extends from the lower elevations of the coastal ranges and western slopes of the Sierra Nevada to the Transverse and Peninsular ranges in the Southern part of the state [42]. Chaparral comprises drought-tolerant evergreen sclerophyllous shrubs, with *Adenostoma* spp. (chamise and red-shanks, Rosaceae), *Arctostaphylos* spp. (manzanita, Ericaceae), and *Ceanothus* spp. (Rhamnaceae) being common representatives [43,44]. These species are prone to frequent wildfires but have evolved disturbance-resilient traits, such as resprouting, germination from persistent seed banks, and the development of deep tap roots [45–47]. Frequent fires and other human disturbances can severely degrade chaparral and other Mediterranean landscapes, often hindering their ability to recover completely [31,32,48,49]. To address this challenge, restoration activities are employed across various landscapes in California. These efforts may involve herbicide application, weeding, the outplanting of nursery-reared plants, seeding, or other treatments aimed at restoring impacted areas [32].

Restoration projects have historically relied on native plant container nursey stock as a primary source for materials. Many nurseries in California specialize in providing stock for restoration (CALSCAPE, https://calscape.org/plant_nursery.php (accessed on 3 December 2024)). However, pathogen surveys and sampling in nurseries have demonstrated that *Phytophthora* species are prevalent in horticultural settings, especially when sanitation best management practices are not adequately implemented [50–54]. *Phytophthora cactorum*, *P. crassamura*, *P. rosacearum*, and *P.* ×*cambivora* are the most frequently detected *Phytophthora* species in Californian restoration areas, with *P. cactorum* being amongst the most common in horticultural and forest settings across the state [28]. The risk of pathogen introductions is increasing due to intensifying restoration efforts in response to more wide-spread land degradation due to increased fire frequency and other natural and/or anthropogenic disturbances, and plantings aimed at reducing climate change.

The Angeles National Forest (ANF), in Southern California, USA, utilizes thousands of nursery-grown container native plants for the restoration of areas disturbed by fires,

invasive plants, recreation activities (e.g., off-road vehicle use), and other special uses [34]. Surveys including pathogen testing determined that plants being grown in Southern California nurseries and outplanted at ANF restoration sites were contaminated with *Phytophthora* species [26]. However, the risk those introductions posed to restoration plantings and adjacent natural vegetation remained unknown. The main objective of the current study was to obtain an understanding of the current distribution patterns and diversity of *Phytophthora* species within ANF lands. This will serve as a baseline for comparison and indicate whether these introductions are damaging to adjacent vegetation and if the introduced *Phytophthora* species survive on outplanted native plants. This knowledge will aid in the monitoring and prevention of future pathogen introductions, enabling a more targeted approach to the development of best management practices and conservation efforts [55]. These goals prompted a National Fish and Wildlife Foundation (NFWF)-funded collaborative project between The United States Forest Service (USFS), ANF, and the Pacific Southwest Research Station (PSW), along with the University of California, Davis, Plant Pathology. The main objective of this initiative was to determine the distribution and diversity of *Phytophthora* species located on previously burned ANF lands that were being considered for restoration. This study presents the main outcomes and the potential risks associated with the presence of these *Phytophthora* species in the arid lands of Southern California.

2. Materials and Methods

2.1. Study Area and Sampling

The ANF is a 283,280 ha. protected area spanning the San Gabriel and Sierra Pelona Mountains managed by the USFS in Los Angeles County, USA (34°32′ N, 118°30′ W). The primary vegetation types are chamise chaparral and coastal sage scrub, dominated by shrub species including *Adenostoma fasciculatum* (chamise), *Eriogonum fasciculatum* (California buckwheat), *Eriodictyon crassifolium* (thickleaf yerba santa), and *Salvia mellifera* (black sage), which are often surrounded by native and exotic grasses (Figure 1A–C). In addition, larger shrubs can be found in this vegetation type, such as *Heteromeles arbutifolia*, *Rhus integrifolia*, and *Prunus ilicifolia*. In areas adjacent to natural waterways or rivers, *Quercus agrifolia* and the endangered *Berberis nevinii* grow together with other riparian plants, for example *Populus fremontii, Baccharis salicifolia*, and other *Salix* species (Figure 1D).

The ANF is characterized by having a Mediterranean climate, with average temperatures ranging from 8–20 °C in winter to 15–33 °C during the dry summer months, with a yearly average precipitation of 566 mm, which varies by elevation. Elevations range from 365 m to 3067 m above sea level, with Mt. Baldy Notch being among the areas with the highest elevation, where the average yearly snowfall is 334 cm.

Three past wildfires, the Copper (2002), Ranch (2006) and Sayre (2008) fires, have affected over 16,187 ha of the ANF [56]. Land disturbances can be observed within the three fire areas. Despite barriers and signage aimed to prohibit off-road vehicle use, vehicles tracks were observed, passing through grasslands and oak woodlands with several crossings or following through stream beds. Fencing has been erected to reduce grazing; however, evidence of cattle intrusion was commonly observed. Construction debris and soil movement were also observed in areas where powerlines or oil pipelines had been extended or repaired.



Figure 1. Examples of areas of the Angeles National Forest from which soil samples were taken to determine the presence of *Phytophthora* species. These include transition areas between chaparral and oak woodland areas (**A**), montane chaparral areas (**B**), rip riparian areas with dry and wet riverbeds (**C**), and oak woodlands (**D**). *Adenostoma* fasciculatum, *Eriodictyon crassifolium*, *Salvia mellifera*, and *Quercus agrifolia* were the most sampled native plant species in these areas.

2.2. Site Selection and Sampling

Three areas across the ANF were evaluated in this study (Figure 2): (1) the northwestern area (NWA), characterized by montane chaparral; (2) the northeastern area (NEA) where oak woodlands and chamise chaparral dominate; and (3) the southwestern area (SWA), predominantly montane chaparral. Twenty-eight sites were selected based on ANF botanists' criteria used for suitability for potential restoration. Twelve additional sites were added to the surveyed area to broaden the scope of the study and better represent chaparral and oak woodlands. Sites were surveyed for *Phytophthora* species over five field visits: May 2018, December 2018, March 2019, March 2020, and May 2021. Sampling in the NWA was discontinued in the last three field surveys as requested by the funder due to administrative changes.

Two of the NEA sites had been outplanted with restoration nursery stock prior to 2018, and restoration activities had been initiated in 2019 in three sites. Additionally, one restoration site in both the SWA and the NWA areas was sampled. Digital elevation models and flowlines for perennial and ephemeral streams were obtained from the United States Geological Services (USGS) databases, fire perimeters were obtained from the Fire and Resource Assessment Program (FRAP, CAL FIRE), and road and trails were obtained from a USFS database.

At each site, 10 to 15 soil samples were taken either from plant (rhizosphere)-associated soil or bulk soil (from off-road vehicle trails, river basins, or bare-ground). Plant species were selected for sampling based on their relative dominance at the site. Plant individuals were sampled if they presented typical *Phytophthora*-associated symptoms (dieback, wilting, or chlorosis). Asymptomatic plants were also sampled to determine the possibility of the presence of *Phytophthora* species without associated symptoms. The sampling scheme was based on previous surveys conducted in other regions of the world which aimed to unveil

Phytophthora diversity [57–60]. Each sample consisted of approximately 1000 mL of soil collected from 1–30 cm below the soil line [61,62]. Roots were included in the sample when present. For each sample, GPS location, vegetation class (chaparral or oak woodland), sample category (upland or stream bed), and plant health were recorded. Plant health was assessed for all sampled trees and shrubs by a general rating, ranging from 1 (healthy), to 2 (50% or less affected canopy), 3 (75% of canopy affected), and 4 (dead). Samples were maintained in sealed, 1-gallon plastic bags in coolers with ice packs for transport to the Rizzo laboratory, UC Davis, for processing. Across all field visits, a total of 576 soil samples were collected among the three areas.

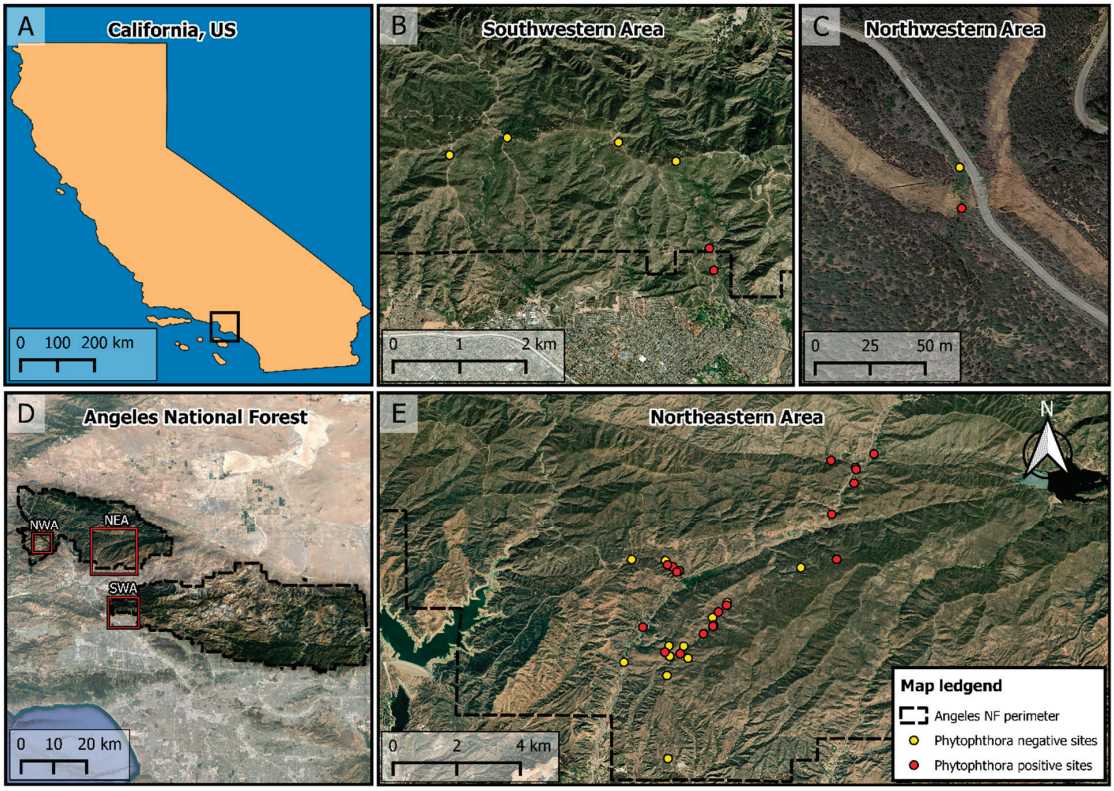


Figure 2. Location of the 40 sites sampled in the Angeles National Forest (ANF). Three main areas were sampled: the southwestern (SWA, **B**) area, with six sites; the northwestern (NWA, **C**) area, with two sites; and the northeastern (NEA, **E**) area, with 32 sites. Red dots indicate *Phytophthora*-positive sites, and yellow indicate *Phytophthora*-negative sites (**B**,**C**,**E**). Map (**A**) displays the location of the ANF in Southern California, with black box indicating Los Angeles County, and map (**D**) shows the general location of the sampling areas.

2.3. Baiting, Isolation, Identification, and Isolate Storage

Phytophthora baiting was conducted according to Erwin and Ribeiro [63]. A green D'Anjou pear and a rhododendron leaf were placed in each soil sample bag. Double-distilled water (ddH2O) was added to the sample bags until the water level was about 3 cm above the soil surface, ensuring both baits were in contact with the water. Baited soils were maintained at 20–22 °C with indirect natural light for 6–7 days. Once lesions appeared, pears were removed from the baiting bag and isolations were made from the lesions. Pear lesions were individually excised and submerged in CMA-PARP (modified from Erwin and Ribeiro [63]: 15 g/L corn meal agar; 0.025 g/L pentachloronitrobenzene; 0.25 g/L ampicillin; 0.01 g/L rifampicin; 0.01 g/L pimaricin). For rhododendron baits, leaves were surface-sterilized for 1 min in 5% bleach and rinsed with ddH2O. Twelve to fifteen 0.5 cm

diameter leaf discs were excised from leaves and plated on CMA-PARP. Isolation plates were incubated in the dark at 18 °C for two weeks and checked periodically for growth. *Phytophthora*-like growth from pear lesions and rhododendron leaf disks were subcultured onto CMA-PARP and maintained in the dark at 20 °C. Isolates were morphotyped based on cultural morphology. Indistinguishable isolates from the same sample were "dereplicated", and a representative isolate was selected.

The pure cultures of each isolate were transferred to a sterile 1 mL pea broth solution and grown at 20 °C for at least 48 h for DNA extraction [64]. A tuft of growing mycelium from the pea broth vials was removed with a sterile needle and placed in 100 µL of PrepMan Ultra kit (Thermo Fisher Scientific, Waltham, MA, USA), and DNA was extracted according to the manufacturer's instructions. The oomycete-specific primer pair FRiz + ITS4TT was used to amplify the internal transcribed spacer (ITS) locus of the isolates according to previously reported conditions [64]. PCR products were prepared for Sanger sequencing with Exo-SAP IT (Thermo Fisher, Waltham, MA, USA) according to the manufacturer's instructions, and sequencing was performed with PCR primers by the UC Davis College of Biological Sciences, DNA Sequencing Facility. Contigs and finished sequences were formed from the sequencing runs, as previously described [64].

ITS sequences were compared to those available in the GenBank nucleotide collection using BLAST searches (https://blast.ncbi.nlm.nih.gov/Blast.cgi (last accessed on 24 October 2024)). Positive determinations were made based on 100% matches to sequences from strains of verifiable identity, and additional loci were consulted for the remaining isolates [65]. For the long-term storage of representative isolates, 4–5-day pure cultures in 1/3 strength clarified V8 agar were transferred to sterile vials containing 1 mL water in duplicate and stored at 14 °C and 20 °C.

2.4. Phylogenetic Inference

Additional sequences were obtained for selected isolates to clarify ambiguous phylogenetic relationships for which ITS was not sufficient for species determination. The molecular determination of clade-7 and clade-8 isolates was, as described by Bourret et al. [66], based on the phylogenetic analysis of two single-locus datasets that were composed of ITS and mt cox1 (Supplementary Table S1). For clade-7 isolates, two strains produced ITS sequences that suggested an affinity to subclade 7a and a close relationship to *P. abietivora* but could not be determined as a previously described species. The ITS and mt cox1 datasets were created featuring verified members of subclade 7a using *P. sojae* and *P. cinnamomi* as outgroups and representatives of subclades 7b and 7c, respectively. For clade 8, the ITS sequence of a single strain suggested a phylogenetic placement in subclade 8e, with proximity to *P. marrasii*. For this, the ITS and mt. cox1 datasets were put together with verified members of clade 8, with *P. ilii* from clade 11 and *P. stricta* from clade 17 as the outgroups.

Phylogenetic analyses were conducted as described in Bourret et al. [23]. Datasets were aligned using MAFT L-ins-l [67] within AliView v1.28 [68]. Maximum likelihood trees were inferred by using IQTREE2 v2.3.6 [69]. TreeGraph2 v2.15.0 [70] was used to apply Bayesian posterior probabilities to maximum likelihood trees, which were later annotated with Inkscape (www.inkscape.org, accessed on 2 December 2024).

3. Results

3.1. Phytophthora Species Incidence

Phytophthora species were detected at 22 of the 40 sampled sites, encompassing all three areas. Of the 576 samples, 73 (~12%) were positive for *Phytophthora* (Supplementary Table S2), 308 were positive for *Pythium* spp. sensu lato (including *Globisporangium* spp.,

Phytopythium spp. and *Pythium* spp. s.s.), and 195 were negative for oomycetes. Positive *Phytophthora* samples were collected from 475 m to 1011 m above sea level, and across all 5 survey dates with a 5.3% *Phytophthora* positivity rate out of 56 samples in May 2018, 6.2% of 161 samples in December 2018, 18% of 199 in March 2019, 16% of 53 in March 2020, and 14% of 107 during May 2021. The GenBank accessions numbers of the ITS sequences of representative isolates of all fourteen species of *Phytophthora* and additional *P. cactorum* ITS haplotypes are given in Table 1.

Table 1. *Phytophthora* species isolated from the Angeles National Forest, including sample source or host, sample type, and a representative isolate of each *Phytophthora* species.

Phytophthora Species	Sub Clade	No. of Isolates	Vegetation Type	Sample	Source/Host	ANF Area
cactorum (CAC3)	1a	3	Oak woodland	Rhizosphere	*Quercus agrifolia*, *Hazardia squarrosa*	NEA
cactorum (CAC1)	1a	2	Chaparral	Rhizosphere	*Salix* sp., *Eriodictyon crassifolium*	NEA, SWA
chlamydospora	6b	3	Chaparral	Bulk	Riverbed	NEA, SWA
crassamura	6b	14	Chaparral, Oak woodland	Rhizosphere, Bulk	*Artemisia californica*, *B. salicifolia*, Grass [1], OHV tracks [2], *Q. agrifolia*, *Salvia mellifera*, Riverbed [3],	NEA, SWA, NWA
gonapodyides	6b	23	Chaparral, Oak woodland	Rhizosphere, Bulk	*Adenostoma fasciculatum*, *B. salicifolia*, Grass, OHV tracks, *Populus fremontii*, *Q. agrifolia*, Riverbed	NEA, SWA
inundata	6a	7	Chaparral, Oak woodland	Rhizosphere, Bulk	*B. salicifolia*, Riverbed,	NEA
lacustris	6d	6	Chaparral, Oak woodland	Bulk	Riverbed, *Salix* sp.	NEA
lacustris x riparia	6d	1	Oak woodland	Rhizosphere, Bulk	*B. salicifolia*, Riverbed	NEA
megasperma	6b	3	Oak woodland	Rhizosphere, Bulk	*Diplacus auricantus*, Riverbed	NEA
multivora	2c	6	Chaparral	Rhizosphere, Bulk	*E. crassifolium*, *Eriogonum fasciculatum*, Riverbed, *S. mellifera*, *Toxicodendron diversilobum*	SWA
riparia	6d	9	Oak woodland	Rhizosphere, Bulk	Grass, OHV, *Q. agrifolia*, Riverbed, *Salix* sp.	NEA
rosacearum	6a	3	Chaparral	Rhizosphere, Bulk	Grass, Riverbed	NEA
sp. *cadmea*	7a	2	Chaparral, Oak woodland	Rhizosphere, Bulk	Grass, Riverbed	NEA
sp. 'pocumtuck'	6b	4	Chaparral, Oak woodland	Rhizosphere, Bulk	*B. salicifolia*, OHV, Riverbed	NEA
taxon 'oakpath'	8e	1	Oak woodland	Bulk	OHV	NEA

[1] Native and exotic grasses (*Bromus* spp., *Avena* spp.). [2] Tracks left by off-highway vehicles (OHV). [3] Areas with evidence that water passes through, ephemerally or perennially.

3.2. Phytophthora Community Composition

From the 73 *Phytophthora*-positive samples, 87 *Phytophthora* isolates were obtained (Figure 3). The most frequently detected *Phytophthora* species were in clade 6b, *P. gonapodyides* (23 isolates matching strain P-1905, Gen Bank accession n° MK908981.1), followed by *P. crassamura* (14 isolates, strain CPHST BL 151 Gen bank accession n° MG865482.1), *P. megasperma* (three isolates, strain WPC: P6957, GU258767.1), and *P. chlamydospora* (three isolates, strain Ex-type CPHST BL 156, MG865471.1) from clade 6c (Table 1). In lesser frequency, isolates presenting two distinct ITS haplotypes of *P. cactorum* (clade 1a) were detected. Two *P. cactorum* isolates (haplotype CAC1) matched CBS voucher isolate 108.09, Gen bank accession N°KJ128036.1. The other three *P. cactorum* isolates (haplotype CAC3) differed by 2 bp from CAC1, with two polymorphisms in positions 616 and 717. All six isolates of *P. multivora* (clade 2c) differed by 1 bp from strain ex-type CPHST BL 104. The clade with most representatives was clade 6, with *P. inundata* (seven isolates matching strain CPHST BL 130, MG865517.1) and *P. rosacearum* (three isolates, differing by two bp from CBS:124696, GU259045.1) from subclade-6a, and *P. lacustris* (six isolates, differed one bp form ex-type P245 AF266793.2), *P. lacustris* x *riparia* (one isolate, matching strain SM15APR_ARG, MG696509.1) and *P. riparia* (nine isolates, differing by 1bp from strain CPHST ex-type BL 111, MG865583.1) from subclade 6d.

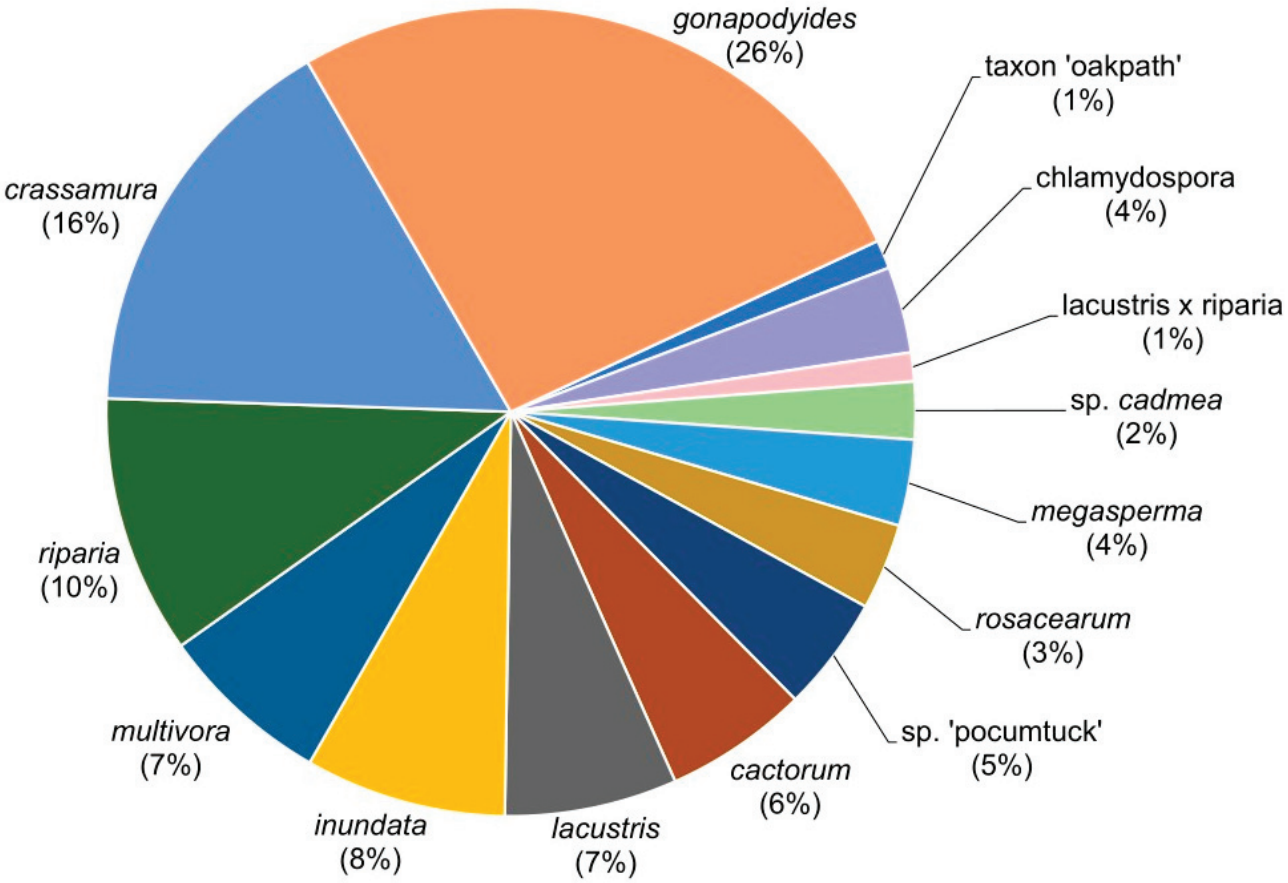


Figure 3. Diversity and frequency of *Phytophthora* taxa isolated from surveys of burnt areas of the Angeles National Forest from 2018 through 2021. Upland areas and streams beds were sampled in chaparral and oak woodlands, including restoration areas. Multiple isolates of a *Phytophthora* taxon from the same sample were considered as one record.

Three *Phytophthora* species that did not match any previously described species were also detected. Four isolates were recovered of *P*. sp. 'pocumtuck' (matching strain Rizzo Lab N°: SM08FEB_FLZ1, MG696351.1) from subclade-6b [71]. Additionally, ITS sequences from two isolates indicated a previously undescribed species closely related to *P. europaea* of subclade 7a. Upon further analysis, these two isolates were found to be 100% homologous to two strains detected in previous Rizzo Lab surveys of restoration areas in Santa Clara, County, CA (Rizzo Lab N°: SCVWD235, MG707801.1 and SCVWD621, MG707855.1). The two strains in the current study, plus the two strains from Santa Clara County, were given the provisional name of *P*. sp. *cadmea.* ITS phylogenies indicate that these strains cluster within subclade 7a and cannot be distinguished from *P. abietivora* (Figure 4). However, the mt. cox1 tree shows a phylogenetic distinction between *P.* sp. *cadmea* and most strains of *P. abietivora,* including the ex-type, as well as other species of subclade 7a (Figure 5). Lastly, a single record was made of a phylogenetically clade 8 strain. Phylogenetic inference of both ITS (Figure 6) and mt. cox1 (Figure 7) loci placed this isolate, introduced as a new provisional species, namely, *P.* taxon 'oakpath', within subclade 8e, with a distinct position from the only other species in the subclade, *P. marrasii*.

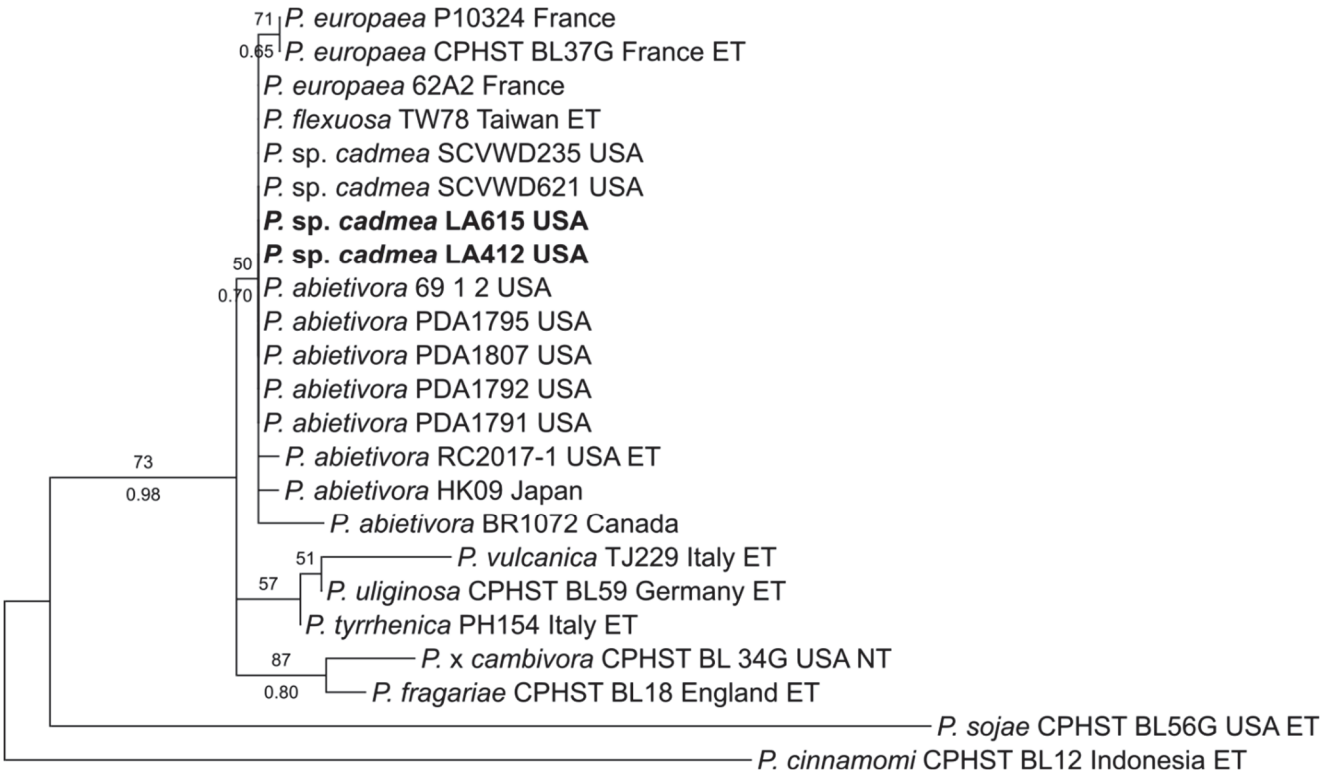


Figure 4. Maximum likelihood tree of *Phytophthora* subclade 7a. The tree is inferred with IQ-TREE 2 from single-locus ITS rDNA alignment. Support values above the branches are ultrafast bootstrap approximations $\geq$ 50, and those below are posterior probabilities $\geq$ 0.90, according to an analysis with MrBayes v2.3.7a. The isolates in bold are from this study.

Thirteen of the fourteen *Phytophthora* species were detected in NEA sites, but *P. multivora* was only detected in SWA. Alongside *P. multivora*, SWA sites also yielded *P. cactorum*, *P. crassamura*, and *P. gonapodyides*. Only two *Phytophthora*-positive samples were recorded for the NWA, with both samples being positive for *P. crassamura*.

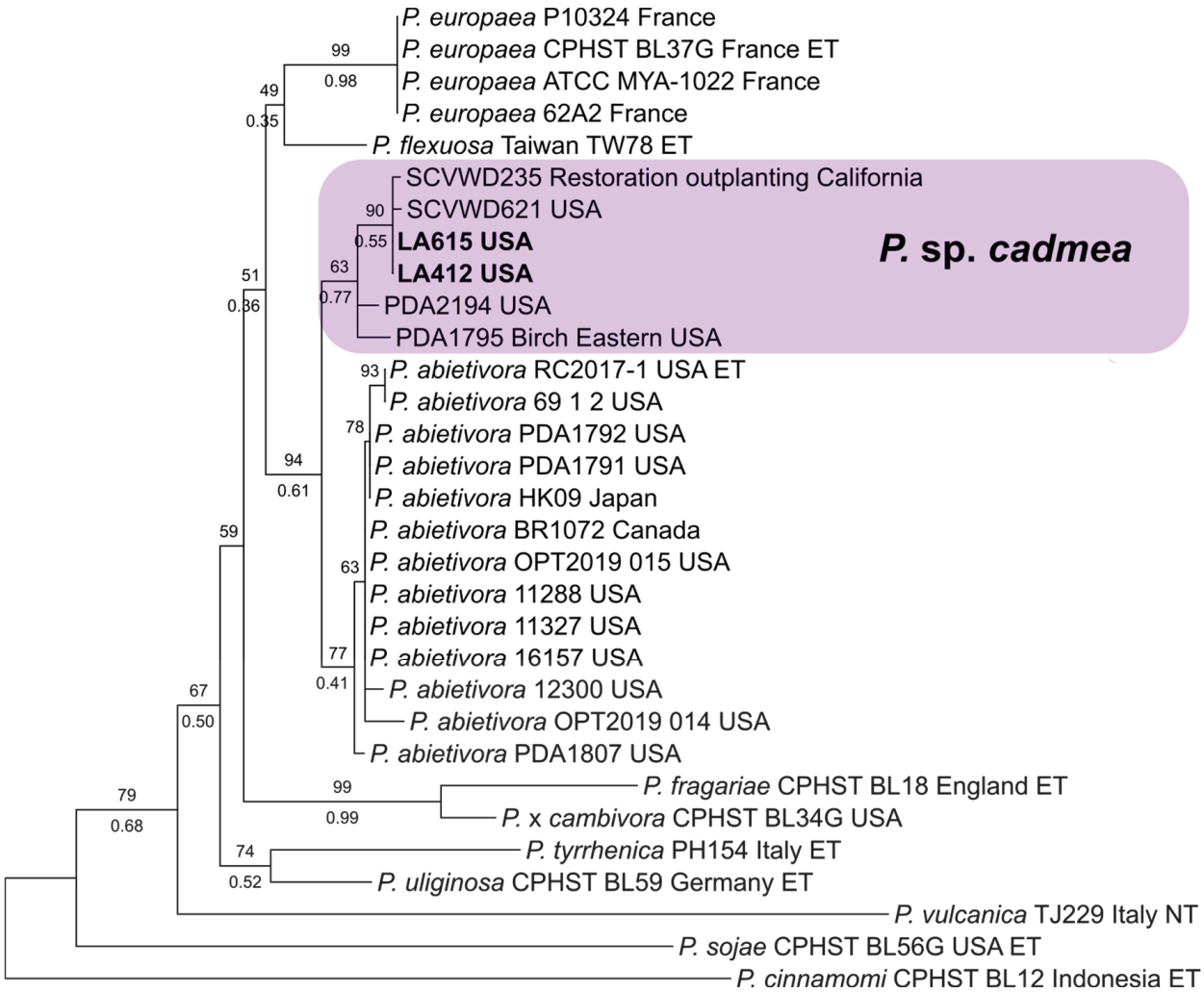


Figure 5. Maximum likelihood tree of *Phytophthora* subclade 7a. The tree is inferred with IQ-TREE 2 from a mitochondrial cox1 alignment. Support values above the branches are ultrafast bootstrap approximations ≥ 50, and those below are posterior probabilities ≥ 0.90, according to an analysis with MrBayes v2.3.7a. Isolates in bold are from this study. Isolates PDA2194 and PDA1795 were uploaded as *P. abietivora* and are included in the original description of the species.

Twenty-two plant species were sampled from fourteen plant families in oak woodland areas, primarily *B. salicifolia* (Asteraceae), *Q. agrifolia* (Fagaceae), and *Populus fremontii* (Salicaceae). Less intensive sampling occurred from *Diplacus auricantus* (Phrymaceae) and *Hazardia squarrosa* (Asteraceae). Out of the 144 samples taken from upland oak woodland areas, 13% were positive for *Phytophthora* species: *P. cactorum*, *P. crassamura*, *P. gonapodyides*, *P. lacustris*, *P. lacustris* × *riparia*, *P. megasperma*, *P. riparia*, *P.* sp. *cadmea*, and *P.* sp. 'pocumtuck'. The most common *Phytophthora*-positive associated hosts were *Q. agrifolia*, from which *P. cactorum*, *P. crassamura*, *P. gonapodyides*, and *P. riparia* were found in the rhizosphere soil, as well as *P. lacustris*, *P. lacustris* × *riparia*, and *P.* sp. 'pocumtuck', which were detected underneath *Salix* sp. individuals. These subclade-6b *Phytophthora* species were also found to be present in the rhizosphere soil of grasslands and from a *B. salicifolia* with mild crown thinning.

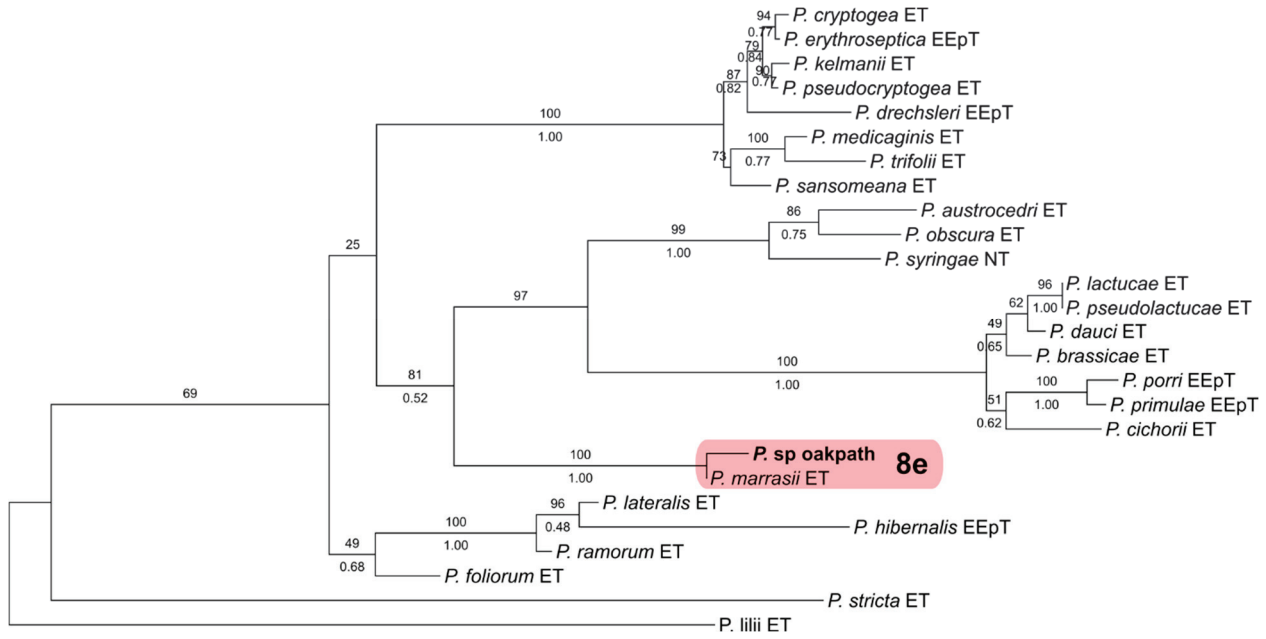


Figure 6. Maximum likelihood tree of *Phytophthora* clade 8. The tree is inferred with IQ-TREE 2 from single-locus ITS rDNA alignment. Support values above the branches are ultrafast bootstrap approximations ≥ 50, and those below are posterior probabilities ≥ 0.90, according to an analysis with MrBayes. The isolate in bold is from this study.

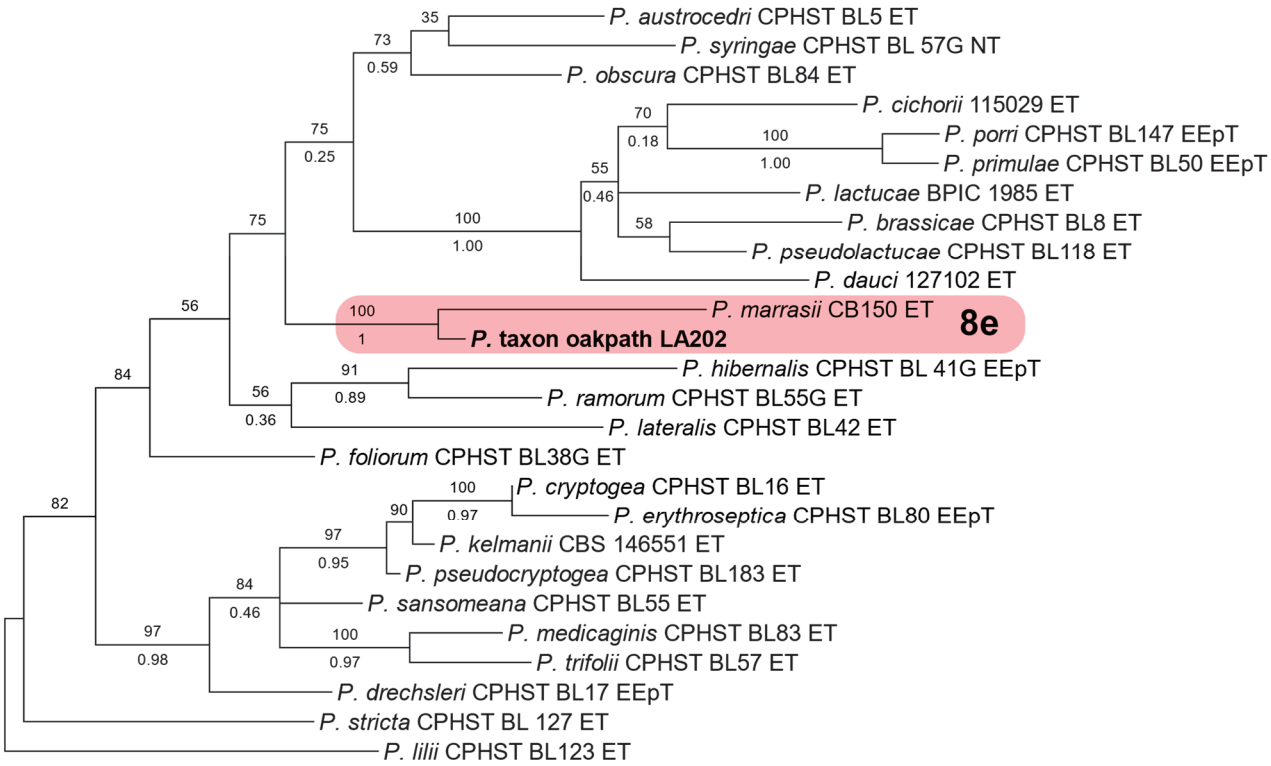


Figure 7. Maximum likelihood tree of *Phytophthora* clade 8. The tree is inferred with IQ-TREE 2 from a mitochondrial cox1 alignment. Support values above branches are ultrafast bootstrap approximations ≥ 50, and those below are posterior probabilities ≥ 0.90, according to an analysis with MrBayes v2.3.7a. The isolate in bold is from this study.

3.3. Phytophthora Species from Areas with Off-Highway Vehicle Tracks

Across all three areas, off-highway vehicle (OHV) tracks were observed in twenty sites. OHV tracks varied in terms of the severity of disturbance, which depended primarily on the vehicles used to make the tracks and the amount of use (motorbikes, heavy machinery, or trucks). In total, sixty-three samples were taken from OHV tracks, fifty-four from within chaparral, and nine from oak woodlands. These tracks had an 11% positivity-rate with seven *Phytophthora*-positive samples. *P. crassamura* was the most frequently isolated, followed by *P. gonapodyides*, *P.* sp. 'pocumtuck', *P. riparia*, and the only detection of *P.* taxon 'oakpath' (Figure 8H).



Figure 8. *Phytophthora*-positive plants and streams in fire areas of the Angeles National Forest: (**A**) *Eriodictyon crassifolium* positive for *P. cactorum*; (**B**) white arrow indicates dead *Quercus agrifolia* restoration plant positive for *P. gonapodyides*; (**C**) dead *Salvia mellifera* positive for *P. multivora*; (**D**) *E. crassifolium* with mild symptoms of crown thinning, close to a *P. crassamura*-positive stream; (**E**) thinning *Adenostoma fasciculatum* from which *P. gonapodyides* was isolated; (**F–I**) sites positive for *P. crassamura* and other clade-6 *Phytophthora* species.

3.4. Association Between Phytophthora Incidence and Disease Symptoms

In total, 450 soil samples were taken from underneath plants rated for overall health; from 48 plant species, 24 plant families, 149 samples were taken from underneath plants rated with a "1" (appeared healthy), 127 were rated with a "2" (50% or less affected canopy), 78 were rate with a "3" (75% of canopy affected), and 96 were rated with a "4" (dead).

Twenty-nine samples, from thirteen plant species, were positive for *Phytophthora* species and were associated with plants rated from 1 to 4. Plants rated with a "1-healthy" had higher *Phytophthora* species diversity when compared with symptomatic plants. *P. cactorum*, *P. crassamura*, *P. gonapodyides*, *P. lacustris* x *riparia*, *P. multivora*, *P. riparia*, *P*. sp. *cadmea*, and *P*. sp. 'pocumtuck' were all found under asymptomatic individuals from seven sites, mostly in oak woodland areas. Asymptomatic *Q. agrifolia* from two sites harbored *P. crassamura* and *P. cactorum*, while other clade-6 species were found to be associated with *Salix* sp. In the SWA, *P. multivora* was isolated from two healthy-appearing individuals of *Toxicodendron diversilobum*.

The most common symptoms observed across sampled plant species were crown thinning and branch dieback, with some individuals presenting yellowing and leaf tip necrosis. From rhizosphere soil samples under symptomatic plants (nine plant species), *P. cactorum*, *P. crassamura*, *P. gonapodyides*, *P. inundata*, *P. lacustris*, *P. megasperma*, *P. multivora*, and *P. riparia* were detected. In total, 78 dead plants were sampled, from which four individuals were positive for *Phytophthora* species, *P. crassamura*, *P. multivora*, and *P. gonapodyides*. Symptomatic *Phytophthora*-associated plants were observed at twelve sites, eight from oak woodland areas and four from chaparral areas. *Phytophthora cactorum* was isolated underneath a *H. squarrosa*, with several leaves presenting tip necrosis and *E. crassifolium* with severe yellowing, especially on its bottom branches (Figure 8A). Additionally, *P. cactorum* was isolated underneath a *Q. agrifolia* with clear symptoms of dieback of the upper crown. *P. crassamura* was detected underneath a *B. salicifolia* with sparse branches and thinning and from two dead *S. mellifera* plants. *Phytophthora gonapodyides* was the only *Phytophthora* species found in a restoration basin across the three areas. This basin had previously been planted with *Q. agrifolia*, which had a dead crown with brown leaves still attached (Figure 8B). Adjacent to this restoration basin, *P. gonapodyides* was again isolated from a cluster of thinning *A. fasciculatum* plants (Figure 8E). At other sites, *P. gonapodyides* was isolated from *B. salicifolia* and *Q. agrifolia* with mild crown dieback. Other clade-6 species were also found underneath plants with mild symptoms, with the following host associations: *P. lacustris-Salix*. sp., *P. inundata-B. salicifolia*, *P. megasperma-D. aurantiacus*, and *P. riparia-Q. agrifolia* (Table 1). Additionally, *P. multivora* was isolated underneath dead *S. mellifera* and *E. crassifolium*, and it was also detected underneath *S. mellifera* and *E. fasciculatum* with some branch dieback.

4. Discussion

This survey represents the first general *Phytophthora* survey in Southern California natural areas, and the most recent of the few studies of *Phytophthora* diversity in Mediterranean regions [57,72–77]. Across the forty sites in both chaparral and oak woodlands areas, which included riparian areas and streams, fourteen *Phytophthora* species were detected. Considering the relatively low sampling intensity and the arid nature of the region, *Phytophthora* diversity was higher than expected. The three most frequently detected species in this survey, *P. gonapodyides*, *P. crassamura*, and *P. riparia*, were found to be associated with streams in both chaparral and oak woodlands. These species, in addition to *P. cactorum* and *P. multivora*, are also commonly encountered in forest and restoration scenarios in California [23,28,78] and in natural areas in other US states [71,79–85]

A comparable *Phytophthora* survey of Mediterranean-type plant communities in the National Park of La Maddalena archipelago (Northeast Sardinia, Italy) recovered nine *Phytophthora* species [57]. Of the *Phytophthora* species associated with the Italian maquis vegetation, two were found in the current ANF survey: *P. gonapodyides*, found in Sardinia waterways; and *P. crassamura*, detected in the rhizosphere soil of *Juniperus phoenicea* (Cupressaceae). Although different flora were sampled in the two surveys, a comparison of *Phytophthora*-positive plant families can be made. In the Anacardiaceae, *T. diversilobum* in the ANF chaparral areas and *Pistacia lentiscus* (mastic) from the La Maddalena archipelago were *Phytophthora*-positive, and *Rhus integrifolia* on the ANF was negative. Only *P. multivora* was found underneath *T. diversilobum*, and *P. gonapodyides*, *P. ornamentata*, and *P. bilorbang* were all associated with *P. lentiscus* in Sardinia. In Scanu et al.'s [57] study, *Phytophthora* species were also isolated from symptomatic and declining *Asparagus albus* (Asparagaceae), *J. oxycedrus* (Cupressaceae), and *Rhamnus alaternus* (Rhamnaceae). Species in the same plant families were sampled on the ANF, but no *Phytophthora* species were detected. These ANF plant species included *Hesperoyucca whipplei* (Asparagaceae), *Calocedrus decurrens* (Cupressaceae), and *Ceanothus* sp. (Rhamnaceae). Although, in the ANF, these species were *Phytophthora*-negative, their phylogenetic relationship could indicate potential host affinity for other *Phytophthora* species.

Five distinct ITS haplotypes of *P. cactorum* are present across California [66]. Of these five, two were detected among the *P. cactorum* isolates of the ANF survey: CAC1 and CAC3. CAC1 was found in a single site in an oak woodland upland area in NEA, underneath a mildly symptomatic *Q. agrifolia* tree and *H. squarrosa* shrub. CAC3 was found in the NEA and SWA, underneath a yellowing *Er. crassifolium* and a thinning *Salix* sp. In California, CAC3 is the most commonly encountered ITS haplotype, being present in restoration outplantings in both Northern and Southern California, and it is frequently detected in native plant nurseries [66]. CAC1 has a more limited distribution, being only found in natural areas and streams of California. ANF CAC3 isolates were found to belong to a larger worldwide lineage called the "apple–oak lineage" present in Czechia, Germany, Japan, The Netherlands, New Zealand, Russia, the UK, and the USA [23,28]. This suggests that the apple–oak lineage is moving locally and worldwide through horticulture [66]. Other isolates with the CAC1 ITS haplotype did not fit into any worldwide lineages in their analysis, and more information is needed to better understand the phylogeography of *P. cactorum* in California and in a worldwide context. The widespread distribution of *P. cactorum* across the ANF and the prevalence of certain ITS haplotypes raise concerns about its adaptability and ease of establishment in diverse environments. This adaptability is evident in *P. cactorum*'s wide host range, having been detected from economically and environmentally significant plants in horticultural, agricultural, forest, and restoration contexts [28,66,86,87].

In the ANF, *P. multivora* was only found in the SWA, detected in two upland chaparral sites with detections from rhizosphere samples of a healthy *T. diversilobum* and *E. fasciculatum* and from a dead *Er. crassifolium* and *S. mellifera*. In California, *P. multivora* is considered to have a more clonal population, with a single ITS haplotype encountered in nurseries, restorations, and in natural areas [28,88]. *P. multivora* is distributed globally in natural areas and streams. In Australia, it is associated with numerous dead and dying native hosts [73,89,90], and in Europe, it is associated with the plant trade and outplantings [59]. For example, in a small Italian nature reserve, *P. multivora* was associated with vegetation types that include plant genera similar to those encountered in the ANF, *Salix* spp., *Quercus* spp., and *Populus* spp. [75].

Of the fourteen *Phytophthora* species detected, *P. crassamura* was the only one that was found in all three sampled areas, in both vegetation types, in both upland areas and in streams, and on OHV tracks. *Phytophthora crassamura* was also found beneath asymptomatic and symptomatic plants from five different plants species, including a dead *S. mellifera*. *Phytophthora crassamura*, which is among the most common *Phytophthora* species encountered in California, with strong associations with agriculture and restoration areas and to a lesser extent with nurseries [28]. Reviewing historical records, considering the recent description of *P. crassamura* from maquis vegetation in Italy and with the possibility of previous *P. megasperma* isolates having been misidentified [28,57], *P. crassamura* may have been in the US for at least 100 years [28]. Sims et al. [91] conducted a phenotypic and genotypic analysis, using cytochrome c oxidase subunit 1 (cox1) sequences, oogonia size, and mefenoxam resistance variation, and concluded that *P. crassamura* lineages found in Northern California restoration areas had originally come from nurseries and were being spread into wildlands. Follow-up analysis will be conducted to determine the lineage of the ANF *P. crassamura* isolates and potential source of introduction.

Eleven out of the fourteen species detected (79%) and 84% of the total *Phytophthora* isolates recovered from the ANF survey were in clade 6. The majority belonged to clade-6b and were more frequent in streams and oak woodlands. Except for *P. crassamura*, most clade-6 species were associated with healthy or asymptomatic plants. Only three plants from which *P. gonapodyides* was isolated showed symptoms of crown thinning. Only one was dead: a *Q. agrifolia* plant from a restoration plant basin. In California, clade-6 species are common in natural areas and streams, and many are potentially indigenous based on high levels of intraspecific diversity [23,28]. Clade-6 species also are found in streams and riparian areas in many areas of North America and Europe [75,81,92]. They are mostly associated with a saprophytic lifestyle [79,93]. However, when inoculated or present in disease conducive conditions, these species can initiate disease and damage trees [61,81,92–97]. Globally clade-6 species such as *P. gonapodyides* and *P. inundata* have been commonly detected in Mediterranean areas [57,98,99] and in other parts of California [24]. This predominant aquatic and saprophytic lifestyle in natural areas needs to be further investigated to understand the survival and potential threat these species pose in these dry and arid areas.

The subclade 7a *Phytophthora* sp. *cadmea* isolates yielded in Rizzo Lab surveys revealed that this species is associated with natural and restoration areas of both Northern and Southern California. The closely related subclade 7a *Phytophthora*, *P. abietivora*, is associated with Christmas tree nurseries in North America [28,100]. Both species' association with nurseries and/or restoration outplantings suggests that human activities are, in part, responsible for their present distributions, which may be of interest to regulators both locally and internationally. Additionally, the lack of sequences identified as *P. abietivora* covering the 5′ [101] portion of the cox1 locus and the low phylogenetic resolution of ITS in subclade 7a both likely contributed to the large number of *P. abietivora* accessions deposited as *P. europaea*, potentially underestimating the actual distribution of these species in North America. Furthermore, the intraspecific cox1 diversity observed among North American isolates of both *P. abietivora* and *P.* sp. *cadmea* suggests that these two species are native to the continent.

The sole representative of clade 8 in this current survey, *P.* taxon 'oakpath', was isolated from a bulk composite sample collected from a trail in an oak forest near a chaparral dominated area. Phylogenetically, the resolution obtained from ITS and cox1 loci clustered this species within subclade 8e and separated this isolate from *P. marrasii*. Recently identified in 2022, *P. marrasii* was associated with the decline of artichoke plants in Italy [102]. This

discovery, along with reports of *P. syringae* and *P. cryptogea* in other Mediterranean regions of the world [28,57,74,75,89], suggests that clade 8 may harbor more species associated with drier climates than previously detected, increasing the risk in natural and agricultural scenarios. As seen in refs. [103–106], new understandings of Phytophthora ecology and biology arise from analyzing newly described species, analyzing new host associations, and conducting phylogeographic analyses of populations within previously described clades.

This survey was performed in a variety of ecological niches with the goal of determining the distribution and ecology of *Phytophthora* species. Streams and oak woodland areas had the highest diversity of *Phytophthora* species, with clade-6 most prevalent. In drier areas, the upland chaparral, homothallic species *P. cactorum*, *P. multivora*, and *P. crassamura* were more common. These species can readily produce thick-walled oospores, allowing them to survive adverse environmental conditions. It is unclear why *P. multivora* had such a narrow distribution in the ANF compared to other homothallic species, being limited to a few sites and only in the SWA. This could be due to many factors. For example, waterways in SWA are fed by the Upper Los Angeles River watershed, while in the NEA, the Bouquet Canyon and Upper Santa Clara are the dominant watersheds, indicating potentially different introduction points and/or dispersal patterns through the various waterways. Further sampling is required to determine if this corresponds to a recent introduction into the area and to assess the real distribution of this species in the ANF and in other areas of Southern California.

The widespread distribution of many *Phytophthora* species in the ANF is of concern as the nature of their presence is still unknown. Periodic or seasonal *Phytophthora* sampling is recommended for monitoring potential undetected *Phytophthora* species introductions. Detection of *Phytophthora* species in OHV tracks is also of concern, indicating a potential route of dispersal through human-associated soil movement [15]. Similarly, the monitoring of waterways is also recommended to assess a baseline of *Phytophthora* diversity and because waterways are potential vectors for new introductions. Despite the absence of positive detections in established restoration areas sampled in the current ANF study, caution and monitoring should be prioritized by nursery and restoration managers to prevent introductions as *Phytophthora* species were found to be common in California native plant nurseries [25].

5. Conclusions

In recent decades, interest in *Phytophthora* sampling has increased in areas historically considered unfavorable for the pathogen's dispersal and pathogenicity, including Mediterranean plant communities [57,74,76,104,107]. These plant communities have unique ecological characteristics and support both a large diversity of flora and fauna and large human populations, making them more vulnerable to ever-increasing disturbances [31,32,108]. *Phytophthora* species in the ANF were found to be more widely distributed than anticipated, not only in dry and wet streams but also in seasonally dry uplands areas. Notably, homothallic species were more prevalent in upland habitats. This emphasizes the role these areas may have in the distribution of *Phytophthora* species and the importance of species-specific functional traits in influencing dispersal and establishment [109,110]. Soil compaction and poor drainage conditions created by OHV tracks can potentially create ideal soil conditions for proliferation and spread of *Phytophthora* species [29]. This highlights the importance of well drained soils on roads and planted areas to reduce the chances of facilitating *Phytophthora* conducive conditions. *Phytophthora* species were encountered underneath both symptomatic and asymptomatic plants, with limited detections in restoration sites, leaving the potential of overlooking *Phytophthora* infections in highly susceptible

areas. Furthermore, the use of *Phytophthora* baiting methodologies carries the risk of false negatives, potentially overlooking species present in a certain sample [111,112]. To address this limitation, continued monitoring and repeated sampling are crucial, incorporating higher resolution detection techniques such as metabarcoding to complement traditional baiting methods [113]. This study narrowed the current knowledge gap of *Phytophthora* diversity in areas of Southern California, establishing new host associations, first detections, and the discovery of novel *Phytophthora* taxa. However, further research is needed to understand the threats these *Phytophthora* species pose to the local and native flora and to develop effective strategies for their prevention and management. These should include expanded surveys within the region and pathogenicity tests on common chaparral species.

Supplementary Materials: The following supporting information can be downloaded at: https://www.mdpi.com/article/10.3390/jof11010033/s1, Table S1: Phylogeny accession and metadata; Table S2: All Phytophthora positive samples data.

Author Contributions: S.N.F. and T.B.B. were responsible for material preparation, data collection, and analysis; S.N.F. drafted the initial manuscript; and all authors contributed to subsequent revisions and approved the final version. All authors were involved in the study's conceptualization and design. All authors have read and agreed to the published version of the manuscript.

Funding: This research was supported by the National Fish and Wildlife Foundation and USFS Pacific Southwest (PSW) through grants NFWF to PSW–18-CO-11272139-006, 20-CO-112722139-011, PSW to UCD–18-JV-11272139-026, and 20-JV-11272139-025. Additionally, this study was conducted as part of a Ph.D. dissertation funded by the University of California, Davis, and the Chilean Scholarship Becas Chile of the National Association of Research and Development.

Institutional Review Board Statement: Not applicable.

Informed Consent Statement: Not applicable.

Data Availability Statement: The original contributions presented in this study are included in the article/Supplementary Materials. Further inquiries can be directed to the corresponding author.

Acknowledgments: The authors would like to thank the U.S. Forest Service and its personnel, including ANF botanists Janet Nickerman and Katie VinZandt, for their assistance in facilitating field surveys and site access. The authors would also like to acknowledge the contributions of Rizzo Lab members Evan Lozano, Chris Edelenbos, Cole Engert, Felipe Saez Cortez, and Kerri Frangioso, who assisted with field work, sample processing, and species identification. Special thanks to Ted Swiecki from Phytosphere Research for conducting preliminary sampling and providing ongoing expertise.

Conflicts of Interest: The authors declare no conflicts of interest.

References

1. Beakes, G.W.; Glockling, S.L. The Evolutionary Phylogeny of the Oomycete "Fungi". *Protoplasma* **2012**, *249*, 3–19. [CrossRef] [PubMed]
2. Davidson, J.M.; Wickland, A.C.; Patterson, H.A.; Falk, K.R.; Rizzo, D.M. Transmission of *Phytophthora ramorum* in Mixed-Evergreen Forest in California. *Phytopathology* **2005**, *95*, 587–596. [CrossRef] [PubMed]
3. Hyun, I.; Choi, W. Phytophthora Species, New Threats to the Plant Health in Korea. *Plant Pathol. J.* **2014**, *30*, 331–342. [CrossRef] [PubMed]
4. Perrine-walker, F. *Phytophthora palmivora*–Cocoa Interaction. *J. Fungi* **2020**, *6*, 167. [CrossRef] [PubMed]
5. Ivanov, A.A.; Ukladov, E.O.; Golubeva, T.S. *Phytophthora infestans*: An Overview of Methods and Attempts to Combat Late Blight. *J. Fungi* **2021**, *7*, 1071. [CrossRef]
6. Chen, Q.; Bakhshi, M.; Balci, Y.; Broders, K.D.; Cheewangkoon, R.; Chen, S.F.; Milenković, I.; Májek, T.; Jung, T.; Crous, P.W. Genera of Phytopathogenic Fungi: GOPHY 4. *Stud. Mycol.* **2022**, *564*, 417–564. [CrossRef]

7. Jung, T.; Orlikowski, L.; Henricot, B.; Abad-Campos, P.; Aday, A.G.; Aguín Casal, O.; Bakonyi, J.; Cacciola, S.O.; Cech, T.; Chavarriaga, D.; et al. Widespread *Phytophthora* Infestations in European Nurseries Put Forest, Semi-Natural and Horticultural Ecosystems at High Risk of Phytophthora Diseases. *For. Pathol.* **2016**, *46*, 134–163. [CrossRef]
8. Boyd, L.A.; Ridout, C.; O'Sullivan, D.M.; Leach, J.E.; Leung, H. Plant-Pathogen Interactions: Disease Resistance in Modern Agriculture. *Trends Genet.* **2013**, *29*, 233–240. [CrossRef]
9. Underwood, E.C.; Sa, H.D.; Molinari, N.A.; Editors, J.E.K. *Valuing Chaparral*; Springer: Berlin/Heidelberg, Germany, 2018.
10. Brasier, C.; Jung, T. Recent Developments in *Phytophthora* Diseases of Trees and Natural Ecosystems in Europe. In *Progress in Research on Phytophthora Diseases of Forest Trees*; Forest Research: Farnham, UK, 2005; pp. 5–16.
11. Grünwald, N.J.; Goss, E.M.; Press, C.M. *Phytophthora ramorum*: A Pathogen with a Remarkably Wide Host Range Causing Sudden Oak Death on Oaks and Ramorum Blight on Woody Ornamentals. *Mol. Plant Pathol.* **2008**, *9*, 729–740. [CrossRef]
12. Rizzo, D.M.; Garbelotto, M.; Davidson, J.M.; Slaughter, G.W.; Koike, S.T. *Phytophthora ramorum* as the Cause of Extensive Mortality of Quercus Spp. and Lithocarpus Densiflorus in California. *Plant Dis.* **2002**, *86*, 205–214. [CrossRef]
13. Cobb, R.C.; Haas, S.E.; Kruskamp, N.; Dillon, W.W.; Swiecki, T.J.; Rizzo, D.M.; Frankel, S.J.; Meentemeyer, R.K. The Magnitude of Regional-Scale Tree Mortality Caused by the Invasive Pathogen *Phytophthora ramorum*. *Earths Future* **2020**, *8*, e2020EF001500. [CrossRef]
14. LeBoldus, J.M.; Navarro, S.M.; Kline, N.; Ritokova, G.; Grünwald, N.J. Repeated Emergence of Sudden Oak Death in Oregon: Chronology, Impact, and Management. *Plant Dis.* **2022**, *106*, 3013–3021. [CrossRef] [PubMed]
15. Shearer, B.L.; Crane, C.E.; Cochrane, A. Quantification of the Susceptibility of the Native Flora of the South-West Botanical Province, Western Australia, to *Phytophthora cinnamomi*. *Aust. J. Bot.* **2004**, *52*, 435–443. [CrossRef]
16. Burgess, T.I.; Scott, J.K.; Mcdougall, K.L.; Stukely, M.J.C.; Crane, C.; Dunstan, W.A.; Brigg, F.; Andjic, V.; White, D.; Rudman, T.; et al. Current and Projected Global Distribution of *Phytophthora cinnamomi*, One of the World's Worst Plant Pathogens. *Glob. Change Biol.* **2017**, *23*, 1661–1674. [CrossRef]
17. Davison, E.M. Resolving Confusions about Jarrah Dieback-Don't Forget the Plants. *Australas. Plant Pathol.* **2014**, *43*, 691–701. [CrossRef]
18. Brasier, C.; Scanu, B.; Cooke, D.; Jung, T. *Phytophthora*: An Ancient, Historic, Biologically and Structurally Cohesive and Evolutionarily Successful Generic Concept in Need of Preservation. *IMA Fungus* **2022**, *13*, 12. [CrossRef]
19. Brasier, C.M. The Biosecurity Threat to the UK and Global Environment from International Trade in Plants. *Plant Pathol.* **2008**, *57*, 792–808. [CrossRef]
20. Santini, A.; Ghelardini, L.; De Pace, C.; Desprez-Loustau, M.L.; Capretti, P.; Chandelier, A.; Cech, T.; Chira, D.; Diamandis, S.; Gaitniekis, T.; et al. Biogeographical Patterns and Determinants of Invasion by Forest Pathogens in Europe. *New Phytol.* **2013**, *197*, 238–250. [CrossRef]
21. Molnar, C.; Nikolaeva, E.; Kim, S.; Olson, T.; Bily, D.; Kim, J.E.; Kang, S. *Phytophthora* Diversity in Pennsylvania Nurseries and Greenhouses Inferred from Clinical Samples Collected over Four Decades. *Microorganisms* **2020**, *8*, 1056. [CrossRef]
22. Parke, J.L.; Redekar, N.R.; Eberhart, J.L.; Funahashi, F. Hazard Analysis for *Phytophthora* Species in Container Nurseries: Three Case Studies. *Horttechnology* **2019**, *29*, 745–755. [CrossRef]
23. Bourret, T.B.; Mehl, H.K.; Aram, K.; Rizzo, D.M. Rhododendron Leaf Baiting of Coastal California Watersheds for *Phytophthora* and *Nothophytophthora*. *Mycol. Prog.* **2023**, *22*, 62. [CrossRef]
24. Garbelotto, M.; Frankel, S.J.; Scanu, B. Soil- and Waterborne *Phytophthora* Species Linked to Recent Outbreaks in Northern California Restoration Sites. *Calif. Agric. (Berkeley)* **2018**, *72*, 208–216. [CrossRef]
25. Rooney-Latham, S.; Blomquist, C.L.; Kosta, K.L.; Gou, Y.Y.; Woods, P.W. *Phytophthora* Species Are Common on Nursery Stock Grown for Restoration and Revegetation Purposes in California. *Plant Dis.* **2019**, *103*, 448–455. [CrossRef] [PubMed]
26. Swiecki, T.; Bernhardt, E. *Phytophthora* Species in California Restoration Sites and Wildlands: Ecology, Distribution, Dispersal, Management. In Proceedings of the Phytophthora species in Restoration Nurseries, Plants, and Wildlands II, San Jose, CA, USA, 18 May 2017.
27. Swiecki, T.J.; Bernhardt, E.A.; Frankel, S.J.; Benner, D.; Hillman, J. An Accreditation Program to Produce Native Plant Nursery Stock Free of Phytophthora for Use in Habitat Restoration. *Plant Health Prog.* **2021**, *22*, 348–354. [CrossRef]
28. Bourret, T.B.; Fajardo, S.N.; Frankel, S.J.; Rizzo, D.M. Cataloging *Phytophthora* Species of Agriculture, Forests, Horticulture, and Restoration Outplantings in California, U.S.A.: A Sequence-Based Meta-Analysis. *Plant Dis.* **2023**, *107*, 67–75. [CrossRef]
29. Frankel, S.J.; Alexander, J.M.; Benner, D.; Shor, A. Coordinated Response to Inadvertent Introduction of Pathogens to California Restoration Areas. *Calif. Agric.* **2018**, *72*, 205–207. [CrossRef]
30. Frankel, S.J.; Conforti, C.; Hillman, J.; Ingolia, M.; Shor, A.; Benner, D.; Alexander, J.M.; Bernhardt, E.; Swiecki, T.J. Phytophthora Introductions in Restoration Areas: Responding to Protect California Native Flora from Human-Assisted Pathogen Spread. *Forests* **2020**, *11*, 1291. [CrossRef]

31. Allen, E.B.; Brown, J.S.; Allen, M.F. Restoration of Animal, Plant, and Microbial Diversity. In *Encyclopedia of Biodiversity*, 3rd ed.; Academic Press: Cambridge, MA, USA, 2001; Volume 5, pp. V4-825–V4-840. [CrossRef]
32. Allen-diaz, B. Biodiversity Is Criticalto Future Health. *Calif. Agric. (Berkeley)* **2000**, *54*, 26–34. [CrossRef]
33. Klausmeyer, K.R.; Shaw, M.R. Climate Change, Habitat Loss, Protected Areas and the Climate Adaptation Potential of Species in Mediterranean Ecosystems Worldwide. *PLoS ONE* **2009**, *4*, e6392. [CrossRef]
34. Meyer, M.D.; Long, J.W.; Safford, H.D. *Postfire Restoration Framework for National Forests in California*; General Technical Report PSW-GTR-270; US Department of Agriculture, Forest Service, Pacific Southwest Research Station: Albany, CA, USA, 2021.
35. Rosenzweig, M.L. Other Patterns with Dynamic Roots. In *Species Diversity in Space and Time*; Cambridge University Press: Cambridge, UK, 2010; pp. 317–344. [CrossRef]
36. Veblen, T.; Young, K.; Orme, A. *The Physical Geography of South America*; Oxford University Press: Oxford, UK, 2007. [CrossRef]
37. Cowling, R.M.; Rundel, P.W.; Lamont, B.B.; Arroyo, M.K.; Arianoutsou, M. Plant Diversity in Mediterranean-Climate Regions. *Trends Ecol. Evol.* **1996**, *11*, 362–366. [CrossRef]
38. Médail, F.; Quezél, P. Linked References Are Available on JSTOR for This Article: Biodiversity Hotspots in the Mediterranean Basin: Setting Global Conservation Priorities. *Conserv. Biol.* **1999**, *13*, 1510–1513. [CrossRef]
39. Rundel, P.W. California Chaparral and Its Global Significance. In *Valuing Chaparral: Ecological, Socio-Economic, and Management Perspectives*; Springer: Cham, Switzerland, 2018; pp. 1–27. [CrossRef]
40. Valladares, F.; Matesanz, S.; Guilhaumon, F.; Araújo, M.B.; Balaguer, L.; Benito-Garzón, M.; Cornwell, W.; Gianoli, E.; van Kleunen, M.; Naya, D.E.; et al. The Effects of Phenotypic Plasticity and Local Adaptation on Forecasts of Species Range Shifts under Climate Change. *Ecol. Lett.* **2014**, *17*, 1351–1364. [CrossRef] [PubMed]
41. Millennium, T.; Assessment, E. Environmental Degradation and Human Well-Being: Report of the Millennium Ecosystem Assessment. *Popul. Dev. Rev.* **2005**, *31*, 389–398. [CrossRef]
42. Parker, T.; Pratt, B.; Keeley, J.E. Chaparral. In *Encyclopedia of Ecology*, 2nd ed.; Elsevier: Amsterdam, The Netherlands, 2019; Volume 2, pp. 420–425. [CrossRef]
43. Keeley, J.E.; Zedler, P.H. Large, High-Intensity Fire Events in Southern California Shrublands: Debunking the Fine-Grain Age Patch Model. *Ecol. Appl.* **2009**, *19*, 69–94. [CrossRef] [PubMed]
44. Kolb, K.J.; Davis, S.D. Drought Tolerance and Xylem Embolism in Co-Occurring species of coastal Sage and Chaparral. *Ecology* **2015**, *75*, 648–659. [CrossRef]
45. Rapacciuolo, G.; Maher, S.P.; Schneider, A.C.; Hammond, T.T.; Jabis, M.D.; Walsh, R.E.; Iknayan, K.J.; Walden, G.K.; Oldfather, M.F.; Ackerly, D.D.; et al. Beyond a Warming Fingerprint: Individualistic Biogeographic Responses to Heterogeneous Climate Change in California. *Glob. Change Biol.* **2014**, *20*, 2841–2855. [CrossRef]
46. Wolf, A.; Zimmerman, N.B.; Anderegg, W.R.L.; Busby, P.E.; Christensen, J. Altitudinal Shifts of the Native and Introduced Flora of California in the Context of 20th-Century Warming. *Glob. Ecol. Biogeogr.* **2016**, *25*, 418–429. [CrossRef]
47. Pratt, R.B.; Jacobsen, A.L.; Golgotiu, K.A.; Sperry, J.S.; Ewers, F.W.; Davis, S.D. Life History Type and Water Stress Tolerance in Nine California Chaparral Species (Rhamnaceae). *Ecol. Monogr.* **2007**, *77*, 239–253. [CrossRef]
48. Keeley, J.E.; Fotheringham, C.J.; Baer-Keeley, M. Factors Affecting Plant Diversity during Post-Fire Recovery and Succession of Mediterranean-Climate Shrublands in California, USA. *Divers Distrib.* **2005**, *11*, 525–537. [CrossRef]
49. Peñuelas, J.; Sardans, J.; Filella, I.; Estiarte, M.; Llusià, J.; Ogaya, R.; Carnicer, J.; Bartrons, M.; Rivas-Ubach, A.; Grau, O.; et al. Impacts of Global Change on Mediterranean Forests and Their Services. *Forests* **2017**, *8*, 463. [CrossRef]
50. Bienapfl, J.C.; Balci, Y. Movement of *Phytophthora* spp. in Maryland's Nursery Trade. *Plant Dis.* **2014**, *98*, 134–144. [CrossRef] [PubMed]
51. Balci, Y.; Balci, S.; MacDonald, W.L.; Gottschalk, K.W. Relative Susceptibility of Oaks to Seven Species of *Phytophthora* Isolated from Oak Forest Soils. *For. Pathol.* **2008**, *38*, 394–409. [CrossRef]
52. Ferguson, A.J.; Jeffers, S.N. Detecting Multiple Species of *Phytophthora* in Container Mixes from Ornamental Crop Nurseries. *Plant Dis.* **1999**, *83*, 1129–1136. [CrossRef] [PubMed]
53. Guarnaccia, V.; Hand, F.P.; Garibaldi, A.; Gullino, M.L. Bedding Plants, Production, and the Challenge of Fungal Diseases. *Plant Dis.* **2021**, *105*, 1241–1258. [CrossRef]
54. Hardy, G.; Sivasithamparam, K. Phytophthora spp. Associated with Container-Grown Plants in Nuseries in Western Australia. *Plant Dis.* **1988**, *72*, 435–437. [CrossRef]
55. Vitousek, P.M. Biological Invasions and Ecosystem Processes: Towards an Integration of Population Biology and Ecosystem Studies. *Nord. Soc. Oikos* **1990**, *57*, 7–13. [CrossRef]
56. USFS-Angeles National Forest. *Copper, Ranch, and Sayre Fires Restoration Strategy*; USFS-Angeles National Forest: Arcadia, CA, USA, 2016; pp. 1–24.

57. Scanu, B.; Linaldeddu, B.T.; Deidda, A.; Jung, T. Diversity of Phytophthora Species from Declining Mediterranean Maquis Vegetation, Including Two New Species, *Phytophthora crassamura* and *P. ornamentata* sp. nov. *PLoS ONE* **2015**, *10*, e0143234. [CrossRef]
58. Jung, T.; Durán, A.; Sanfuentes von Stowasser, E.; Schena, L.; Mosca, S.; Fajardo, S.; González, M.; Navarro Ortega, A.D.; Bakonyi, J.; Seress, D.; et al. Diversity of *Phytophthora* Species in Valdivian Rainforests and Association with Severe Dieback Symptoms. *For. Pathol.* **2018**, *48*, e12443. [CrossRef]
59. Jung, T.; Scanu, B.; Brasier, C.M.; Webber, J.; Milenković, I.; Corcobado, T.; Tomšovský, M.; Pánek, M.; Bakonyi, J.; Maia, C.; et al. A Survey in Natural Forest Ecosystems of Vietnam Reveals High Diversity of Both New and Described *Phytophthora* Taxa Including P. Ramorum. *Forests* **2020**, *11*, 93. [CrossRef]
60. Jung, T.; Chang, T.T.; Bakonyi, J.; Seress, D.; Pérez-Sierra, A.; Yang, X.; Hong, C.; Scanu, B.; Fu, C.H.; Hsueh, K.L.; et al. Diversity of *Phytophthora* Species in Natural Ecosystems of Taiwan and Association with Disease Symptoms. *Plant Pathol.* **2017**, *66*, 194–211. [CrossRef]
61. Jung, T. Beech Decline in Central Europe Driven by the Interaction between *Phytophthora* Infections and Climatic Extremes. *For. Pathol.* **2009**, *39*, 73–94. [CrossRef]
62. Pérez-Sierra, A.; Jung, M.H.; Jung, T. Survey and Monitoring of Phytophthora Species in Natural Ecosystems: Methods for Sampling, Isolation, Purification, Storage, and Pathogenicity Tests. In *Plant Pathology: Method and Protocols*; Springer: New York, NY, USA, 2022; Volume 2536. [CrossRef]
63. Erwin, D.C.; Ribeiro, O.K. *Phytophthora Diseases Worldwide*; American Phytopathology Society Press: St. Paul, MN, USA, 1996.
64. Bourret, T.B.; Choudhury, R.A.; Mehl, H.K.; Blomquist, C.L.; McRoberts, N.; Rizzo, D.M. Multiple Origins of Downy Mildews and Mito-Nuclear Discordance within the Paraphyletic Genus *Phytophthora*. *PLoS ONE* **2018**, *13*, e0192502. [CrossRef] [PubMed]
65. Abad, Z.G.; Burgess, T.I.; Redford, A.J.; Bienapfl, J.C.; Srivastava, S.; Mathew, R.; Jennings, K. IDphy: An International Online Resource for Molecular and Morphological Identification of *Phytophthora*. *Plant Dis.* **2023**, *107*, 987–998. [CrossRef]
66. Bourret, T.B.; Fajardo, S.N.; Engert, C.P.; Rizzo, D.M. A Barcode-Based Phylogenetic Characterization of *Phytophthora cactorum* Identifies Two Cosmopolitan Lineages with Distinct Host Affinities and the First Report of Phytophthora Pseudotsugae in California. *J. Fungi* **2022**, *8*, 303. [CrossRef]
67. Katoh, K.; Standley, D.M. MAFFT Multiple Sequence Alignment Software Version 7: Improvements in Performance and Usability. *Mol. Biol. Evol.* **2013**, *30*, 772–780. [CrossRef]
68. Larsson, A. AliView: A Fast and Lightweight Alignment Viewer and Editor for Large Datasets. *Bioinformatics* **2014**, *30*, 3276–3278. [CrossRef]
69. Minh, B.Q.; Schmidt, H.A.; Chernomor, O.; Schrempf, D.; Woodhams, M.D.; Von Haeseler, A.; Lanfear, R.; Teeling, E. IQ-TREE 2: New Models and Efficient Methods for Phylogenetic Inference in the Genomic Era. *Mol. Biol. Evol.* **2020**, *37*, 1530–1534. [CrossRef]
70. Stöver, B.C.; Müller, K.F. TreeGraph 2: Combining and Visualizing Evidence from Different Phylogenetic Analyses. *BMC Bioinform.* **2010**, *11*, 7. [CrossRef]
71. Brazee, N.J.; Wick, R.L.; Hulvey, J.P. Phytophthora Species Recovered from the Connecticut River Valley in Massachusetts, USA. *Mycologia* **2016**, *108*, 6–19. [CrossRef]
72. Burgess, T.I.; McDougall, K.L.; Scott, P.M.; Hardy, G.E.S.J.; Garnas, J. Predictors of *Phytophthora* Diversity and Community Composition in Natural Areas across Diverse Australian Ecoregions. *Ecography* **2019**, *42*, 565–577. [CrossRef]
73. Hüberli, D.; Hardy, G.E.S.J.; White, D.; Williams, N.; Burgess, T.I. Fishing for *Phytophthora* from Western Australia's Waterways: A Distribution and Diversity Survey. *Australas. Plant Pathol.* **2013**, *42*, 251–260. [CrossRef]
74. Pérez-Sierra, A.; López-García, C.; León, M.; García-Jiménez, J.; Abad-Campos, P.; Jung, T. Previously Unrecorded Low-Temperature *Phytophthora* Species Associated with *Quercus* Decline in a Mediterranean Forest in Eastern Spain. *For. Pathol.* **2013**, *43*, 331–339. [CrossRef]
75. Riolo, M.; Aloi, F.; La Spada, F.; Sciandrello, S.; Moricca, S.; Santilli, E.; Pane, A.; Cacciola, S.O. Diversity of *Phytophthora* Communities across Different Types of Mediterranean Vegetation in a Nature Reserve Area. *Forests* **2020**, *11*, 853. [CrossRef]
76. Scanu, B.; Linaldeddu, B.T.; Franceschini, A. First Report of *Phytophthora pseudosyringae* Associated with Ink Disease of *Castanea sativa* in Italy. *Plant Dis.* **2010**, *94*, 1068. [CrossRef] [PubMed]
77. Deidda, A.; Satta, G.G.A.; Brandano, A.; Morittu, C.; Mureddu, D.; Scanu, B. Multiple *Phytophthora* Species Associated with Declining Wild Olive Trees in Sardinia, Italy. *Plant Pathol.* 2024; *early view*. [CrossRef]
78. Aram, K.; Rizzo, D.M. Distinct Trophic Specializations Affect How *Phytophthora ramorum* and Clade 6 *Phytophthora* spp. Colonize and Persist on Umbellularia Californica Leaves in Streams. *Phytopathology* **2018**, *108*, 858–869. [CrossRef]
79. Hansen, E.M.; Reeser, P.W.; Sutton, W. *Phytophthora borealis* and *Phytophthora riparia*, New Species in *Phytophthora* ITS Clade 6. *Mycologia* **2012**, *104*, 1133–1142. [CrossRef]

80. Hong, C.; Gallegly, M.E.; Richardson, P.A.; Kong, P.; Moorman, G.W. *Phytophthora irrigata*, a New Species Isolated from Irrigation Reservoirs and Rivers in Eastern United States of America. *FEMS Microbiol. Lett.* **2008**, *285*, 203–211. [CrossRef]
81. Reeser, P.W.; Sutton, W.; Hansen, E.M.; Remigi, P.; Adams, G.C. *Phytophthora* Species in Forest Streams in Oregon and Alaska. *Mycologia* **2011**, *103*, 22–35. [CrossRef]
82. Sims, L.L.; Sutton, W.; Reeser, P.; Hansen, E.M. The *Phytophthora* Species Assemblage and Diversity in Riparian Alder Ecosystems of Western Oregon, USA. *Mycologia* **2015**, *107*, 889–902. [CrossRef]
83. Stamler, R.A.; Sanogo, S.; Goldberg, N.P.; Randall, J.J. *Phytophthora* Species in Rivers and Streams of the Southwestern United States. *Appl. Environ. Microbiol.* **2016**, *82*, 4696–4704. [CrossRef]
84. Bily, D.S.; Diehl, S.V.; Cook, M.; Wallace, L.E.; Sims, L.L.; Watson, C.; Baird, R.E. Temporal and Locational Variations of a *Phytophthora* spp. Community in an Urban Forested Water Drainage and Stream-Runoff System. *Southeast. Nat.* **2018**, *17*, 176–201. [CrossRef]
85. Hulvey, J.; Gobena, D.; Finley, L.; Lamour, K. Co-Occurrence and Genotypic Distribution of *Phytophthora* Species Recovered from Watersheds and Plant Nurseries of Eastern Tennessee. *Mycologia* **2010**, *102*, 1127–1133. [CrossRef] [PubMed]
86. Mass, J.L. *Compendium of Strawberry Diseases*, 2nd ed.; APS Press: St. Paul, MN, USA, 1998.
87. Chen, X.R.; Wen, K.; Zhou, X.; Zhu, M.Y.; Liu, Y.; Jin, J.H.; Nellist, C.F. The Devastating Oomycete Phytopathogen *Phytophthora cactorum*: Insights into Its Biology and Molecular Features. *Mol. Plant Pathol.* **2023**, *24*, 1017–1032. [CrossRef] [PubMed]
88. Tsykun, T.; Prospero, S.; Schoebel, C.N.; Rea, A.; Burgess, T.I. Global Invasion History of the Emerging Plant Pathogen Phytophthora Multivora. *BMC Genom.* **2022**, *23*, 153. [CrossRef]
89. Burgess, T.I.; Webster, J.L.; Ciampini, J.A.; White, D.; Hardy, G.E.S.; Stukely, M.J.C. Re-Evaluation of *Phytophthora* Species Isolated during 30 Years of Vegetation Health Surveys in Western Australia Using Molecular Techniques. *Plant Dis.* **2009**, *93*, 215–223. [CrossRef]
90. Scott, P.M.; Burgess, T.I.; Barber, P.A.; Shearer, B.L.; Stukely, M.J.C.; Hardy, G.E.S.J.; Jung, T. *Phytophthora multivora* sp. nov., a New Species Recovered from Declining Eucalyptus, Banksia, Agonis and Other Plant Species in Western Australia. *Persoonia Mol. Phylogeny Evol. Fungi* **2009**, *22*, 1–13. [CrossRef]
91. Sims, L.L.; Chee, C.; Bourret, T.; Hunter, S.; Garbelotto, M. Genetic and Phenotypic Variation of *Phytophthora crassamura* Isolates from California Nurseries and Restoration Sites. *Fungal Biol.* **2019**, *123*, 159–169. [CrossRef]
92. Hansen, E.; Delatour, C. *Phytophthora* Species in Oak Forests of North-East France. *Ann. For. Sci.* **1999**, *56*, 539–547. [CrossRef]
93. Brasier, C.M.; Cooke, D.E.L.; Duncan, J.M.; Hansen, E.M. Multiple New Phenotypic Taxa from Trees and Riparian Ecosystems in *Phytophthora gonapodyides*-*P. megasperma* ITS Clade 6, Which Tend to Be High-Temperature Tolerant and Either Inbreeding or Sterile. *Mycol. Res.* **2003**, *107*, 277–290. [CrossRef]
94. Greslebin, A.G.; Hansen, E.M.; Sutton, W. *Phytophthora austrocedrae* sp. nov., a New Species Associated with Austrocedrus Chilensis Mortality in Patagonia (Argentina). *Mycol. Res.* **2007**, *111*, 308–316. [CrossRef]
95. Randall, S.D.; Burns, B.R.; Bellgard, S.E.; Beever, R.E. *Fishing for Phytophthora in the Waitakere Ranges, Auckland, New Zealand*; Manaaki Whenua Landcare Research: Lincoln, New Zealand, 2009.
96. Nechwatal, J.; Bakonyi, J.; Cacciola, S.O.; Cooke, D.E.L.; Jung, T.; Nagy, Z.Á.; Vannini, A.; Vettraino, A.M.; Brasier, C.M. The Morphology, Behaviour and Molecular Phylogeny of *Phytophthora* Taxon *Salixsoil* and Its Redesignation as *Phytophthora lacustris* sp. nov. *Plant Pathol.* **2013**, *62*, 355–369. [CrossRef]
97. Brown, A.V.; Brasier, C.M. Colonization of Tree Xylem by *Phytophthora ramorum*, *P. kernoviae* and Other *Phytophthora* Species. *Plant Pathol.* **2007**, *56*, 227–241. [CrossRef]
98. Stukely, M.J.C.; Webster, J.L.; Ciampini, J.A.; Brown, E.; Dunstan, W.A.; Hardy, G.E.S.J.; Woodman, G.J.; Davison, E.M.; Tay, F.C.S. *Phytophthora inundata* from Native Vegetation in Western Australia. *Australas. Plant Pathol.* **2007**, *36*, 606–608. [CrossRef]
99. Bose, T.; Wingfield, M.J.; Roux, J.; Vivas, M.; Burgess, T.I. Community Composition and Distribution of *Phytophthora* Species across Adjacent Native and Non-Native Forests of South Africa. *Fungal Ecol.* **2018**, *36*, 17–25. [CrossRef]
100. Li, D.W.; Schultes, N.P.; LaMondia, J.A.; Cowles, R.S. *Phytophthora abietivora*, A New Species Isolated from Diseased Christmas Trees in Connecticut, U.S.A. *Plant Dis.* **2019**, *103*, 3057–3064. [CrossRef]
101. Robideau, G.P.; De Cock, A.W.A.M.; Coffey, M.D.; Voglmayr, H.; Brouwer, H.; Bala, K.; Chitty, D.W.; Désaulniers, N.; Eggertson, Q.A.; Gachon, C.M.M.; et al. DNA Barcoding of Oomycetes with Cytochrome c Oxidase Subunit I and Internal Transcribed Spacer. *Mol. Ecol. Resour.* **2011**, *11*, 1002–1011. [CrossRef]
102. Bregant, C.; Rossetto, G.; Deidda, A.; Maddau, L.; Franceschini, A.; Ionta, G.; Raiola, A.; Montecchio, L.; Linaldeddu, B.T. Phylogeny and Pathogenicity of *Phytophthora* Species Associated with Artichoke Crown and Root Rot and Description of *Phytophthora marrasii* sp. nov. *Agriculture* **2021**, *11*, 873. [CrossRef]

103. Mullett, M.S.; Harris, A.R.; Scanu, B.; Van Poucke, K.; LeBoldus, J.; Stamm, E.; Bourret, T.B.; Christova, P.K.; Oliva, J.; Redondo, M.A.; et al. Phylogeography, Origin and Population Structure of the Self-Fertile Emerging Plant Pathogen *Phytophthora pseudosyringae*. *Mol. Plant Pathol.* **2024**, *25*, e13450. [CrossRef]
104. Horta Jung, M.; Maia, C.; Mora-Sala, B.; Abad-Campos, P.; Schena, L.; Mosca, S.; Carella, G.; Moricca, S.; Nechwatal, J.; Dionísio, L.; et al. High Diversity of *Phytophthora* Species in Natural Ecosystems and Nurseries of Portugal: Detrimental Side Effect of Plant Introductions from the Age of Discovery to Modern Globalization. *Plant Pathol.* 2024; *early view*. [CrossRef]
105. Jung, T.; Milenković, I.; Balci, Y.; Janoušek, J.; Kudláček, T.; Nagy, Z.; Baharuddin, B.; Bakonyi, J.; Broders, K.D.; Cacciola, S.O.; et al. Worldwide Forest Surveys Reveal Forty-Three New Species in *Phytophthora* Major Clade 2 with Fundamental Implications for the Evolution and Biogeography of the Genus and Global Plant Biosecurity. *Stud. Mycol.* **2024**, *107*, 251–388. [CrossRef]
106. Mullett, M.S.; Van Poucke, K.; Haegeman, A.; Focquet, F.; Cauldron, N.C.; Knaus, B.J.; Horta Jung, M.; Kageyama, K.; Hieno, A.; Masuja, H.; et al. Phylogeography and Population Structure of the Global, Wide Host-Range Hybrid Pathogen *Phytophthora* × *cambivora*. *IMA Fungus* **2023**, *14*, 4. [CrossRef]
107. Jung, T.; Colquhoun, I.J.; Hardy, G.E.S.J. New Insights into the Survival Strategy of the Invasive Soilborne Pathogen *Phytophthora cinnamomi* in Different Natural Ecosystems in Western Australia. *For. Pathol.* **2013**, *43*, 266–288. [CrossRef]
108. Underwood, E. RESTORATION: Special Edition. *Fremontia* **2020**, *48*, 1–42.
109. Redondo, M.A.; Boberg, J.; Stenlid, J.; Oliva, J. Contrasting Distribution Patterns between Aquatic and Terrestrial *Phytophthora* Species along a Climatic Gradient Are Linked to Functional Traits. *ISME J.* **2018**, *12*, 2967–2980. [CrossRef] [PubMed]
110. Caballol, M.; Redondo, M.Á.; Catalán, N.; Corcobado, T.; Jung, T.; Marçais, B.; Milenković, I.; Nemesio-Gorriz, M.; Stenlid, J.; Oliva, J. Climate Acts as an Environmental Filter to Plant Pathogens. *ISME J.* **2024**, *18*, wrae010. [CrossRef]
111. Swiecki, T.J.; Bernhardt, E.A.; McClanahan, S.G. Validating and Optimizing a Method for Detecting *Phytophthora* Species by Baiting Leachate from Arrays of Container Nursery Plants. *PhytoFrontiersTM* **2024**, *4*, 14–30. [CrossRef]
112. Sarker, S.R.; McComb, J.; Hardy, G.E.S.J.; Burgess, T.I. Sample Volume Affects the Number of *Phytophthora* and *Phytopythium* Species Detected by Soil Baiting. *Eur. J. Plant Pathol.* **2023**, *166*, 303–313. [CrossRef]
113. Sarker, S.R.; Burgess, T.I.; Hardy, G.E.S.J.; McComb, J. Closing the Gap between the Number of *Phytophthora* Species Isolated through Baiting a Soil Sample and the Number Revealed through Metabarcoding. *Mycol. Prog.* **2023**, *22*, 39. [CrossRef]

Disclaimer/Publisher's Note: The statements, opinions and data contained in all publications are solely those of the individual author(s) and contributor(s) and not of MDPI and/or the editor(s). MDPI and/or the editor(s) disclaim responsibility for any injury to people or property resulting from any ideas, methods, instructions or products referred to in the content.

Journal of *Fungi*

MDPI

Article

Shifts in Soil Fungal Community and Trophic Modes During Mangrove Ecosystem Restoration

Xiaofang Shi [1], Shengyao Zhou [2,3], Lanzi Xu [2], Rajapakshalage Thashikala Nethmini [2], Yu Zhang [4], Liangliang Huang [3], Ke Dong [5], Huaxian Zhao [6,*] and Lianghao Pan [1,*]

1 Guangxi Key Lab of Mangrove Conservation and Utilization, Guangxi Academy of Marine Sciences (Guangxi Mangrove Research Center), Guangxi Academy of Sciences, Beihai 536000, China; shixiaofang_06@163.com
2 Key Laboratory of Climate, Resources and Environment in Continental Shelf Sea and Deep Sea of Department of Education of Guangdong Province, Department of Oceanography, Key Laboratory for Coastal Ocean Variation and Disaster Prediction, College of Ocean and Meteorology, Guangdong Ocean University, Zhanjiang 524000, China; syzhou001009@163.com (S.Z.); yaya942636@163.com (L.X.); nethmini1207@gmail.com (R.T.N.)
3 College of Environmental Science and Engineering, Guilin University of Technology, Guilin 541004, China; llhuang@glut.edu.cn
4 School of General Education, Guangxi Vocational University of Agriculture, Nanning 530003, China; yz1332125778@126.com
5 Department of Biological Sciences, Kyonggi University, 154-42, Gwanggyosan-ro, Yeongtong-gu, Suwon-si 16227, Gyeonggi-do, Republic of Korea; dongke-007@163.com
6 Key Laboratory of Ministry of Education for Environment Change and Resources Use in Beibu Gulf, Guangxi Key Laboratory of Earth Surface Processes and Intelligent Simulation, Nanning Normal University, Nanning 530001, China
* Correspondence: zhx343@gmail.com (H.Z.); panlh86@163.com (L.P.)

Abstract: Mangrove ecosystems are valuable coastal ecosystems; however, studies on the diversity and functional features of their soil fungal communities during restoration are limited. In this study, we examined fungal diversity and trophic modes across mudflat, young mangrove, and mature mangrove stages. We found that Ascomycota and Basidiomycota were the dominant phyla, with saprotrophs as the most abundant trophic mode. The abundance of the major phyla and trophic modes significantly varied across restoration stages. Although fungal alpha (α)-diversity remained stable among the stages, beta (β)-diversity showed significant differentiation. Spearman's analysis and partial Mantel tests revealed that total nitrogen and inorganic phosphorus significantly influenced the fungal α-diversity, whereas temperature and pH primarily shaped the fungal β-diversity. Total nitrogen and carbon were key factors affecting the trophic mode α-diversity, whereas total phosphorus and inorganic phosphorus were the main drivers of the trophic mode β-diversity. Variation partitioning analysis confirmed that nutrients, rather than soil properties, were the primary factors shaping fungal communities and trophic modes. Random forest analysis identified key bioindicators, including species such as Paraphyton cookei, and trophic modes such as saprotrophs, both of which were strongly influenced by soil carbon. These findings advance our understanding of fungal ecology in mangrove restoration.

Keywords: mangrove; restoration; soil fungi; fungal community; trophic mode; environmental effects; bioindicator

1. Introduction

Soil microbiomes represent one of the most biodiverse communities on Earth, comprising approximately one-quarter of the total biodiversity [1–3]. These microorganisms form

a vast and diverse network in soils, typically containing over 1000 kg of microbial biomass carbon per hectare [3]. They are integral to ecosystem functioning and influence critical processes, such as nutrient cycling, soil fertility, and carbon sequestration. For example, soil microbial diversity supports essential functions, such as organic matter decomposition and nutrient mineralization, that promote plant growth and ecosystem stability [4,5]. Heterogeneity in soil physicochemical properties, climate change, and human activity can alter the structure and function of soil microbial communities. For example, soil pH is a major determinant, with acidophilic and alkaline taxa displaying distinct preferences [2,6]. Temperature, water content, and other soil physicochemical properties are important drivers of microbial diversity [6,7]. Evidence suggests that the availability of soil nutrients, such as nitrogen and phosphorus, strongly influences the community structure, as microbes adjust their metabolic pathways to utilize available resources [6,8]. Human activities can alter the climate, which in turn changes the vegetation diversity and soil properties, thereby affecting soil microbial communities. Urban land use and pollution can also directly affect soil microbial composition and function [6,9–12]. However, the direct and indirect effects of environmental changes on microbial structure and function remain largely unknown.

Fungal communities are integral to soil ecosystems and act as key regulators of energy flow and nutrient transformation [10,13,14]. They play pivotal roles in organic matter decomposition and significantly influence ecosystem stability and productivity [10,13,14]. The factors driving soil fungal communities in terrestrial ecosystems have been extensively studied. For instance, in European coniferous forests, soil physical and chemical characteristics, such as the carbon to nitrogen (C:N) ratio and pH, significantly influence fungal community structure [15]. Soil fungal communities in the grasslands of the Loess Plateau are primarily shaped by factors such as ammonium-nitrogen (NH_4^+-N), water content, and dissolved organic carbon [13]. Total carbon is a critical factor influencing fungal community structure in boreal forests [16]. In current ecological research, linking specific soil microbial processes to particular microbial taxa is challenging [2]. Recent studies have shown that soil fungi can be classified into various types based on their survival strategies, such as saprotrophic, symbiotrophic, and pathotrophic [17]. Environmental changes not only affect fungal communities but may also influence their trophic modes. For instance, total carbon and nitrogen are key factors that shape the trophic modes of soil fungi in boreal forests [16]. In semi-arid grasslands in northern China, the addition of nitrogen and phosphorus significantly affected the diversity of pathogens and symbiotic fungi, whereas saprotrophic fungal diversity was primarily influenced by the addition of nitrogen [18]. Nickel contamination can alter the abundance of symbiotic fungi in agricultural soils [10]. However, the fungal diversity and trophic modes in coastal interface ecosystems remain unclear.

Mangroves are classic examples of coastal interface ecosystems, renowned for their distinctive intertidal features and important ecological roles [19]. They are vital for coastal protection and carbon sequestration but are under severe threat from global climate change and anthropogenic activities, including deforestation and urbanization [20–22]. Mangrove soil microbiomes play a critical role in maintaining biogeochemical cycles, supporting ecosystem stability in complex environments, facilitating material turnover, and linking terrestrial and marine ecosystems [23]. Several studies on fungal communities in mangrove sediments have been conducted based on high-throughput sequencing [24–26]. For example, research in New Caledonia in the South Pacific, southeastern China's mangroves, and Sanya, China has revealed the dominance of Ascomycota and Basidiomycota. The structure of mangrove soil fungal communities in Sanya was primarily influenced by factors such as salinity, total organic carbon, and NH_4^+-N [26]. Recent studies have explored the differentiation of fungal community structures and functions during mangrove succession.

Sun et al. [22] found that during the succession of Sonneratia apetala in southern China, Ascomycota and Basidiomycota were the dominant fungal phyla. Environmental factors, including effective potassium, pH, total nitrogen, NH_4^+-N, and available phosphorus, significantly influenced fungal community structure. The abundance of dung saprotrophs and undefined fungi varies significantly across different restoration stages [22]. Another study found that in mangroves formed by the conversion of receding ponds, Ascomycota was the dominant fungal phylum, fungal diversity increased, and soil saprotrophs decreased in naturally recovered mangroves [27]. However, the differentiation of fungal communities and their trophic modes across different habitats during mangrove restoration remains unclear.

Therefore, we conducted a study in the Beilun River Estuary in Dongxing City, Guangxi, within a mangrove reserve. This reserve encompasses three distinct habitats, namely mudflats, young mangroves, and mature mangroves, representing the natural successional stages from mudflats to mature mangroves. By analyzing mangrove sediment samples, we aimed to investigate the changes in fungal functions throughout the restoration and succession processes; specifically, we aimed to: (1) examine the differentiation of fungal diversity and trophic modes across different restoration and succession stages; (2) identify the key factors driving these fungal trophic modes; and (3) analyze bioindicators at different restoration stages. This study will enhance our understanding of the mechanisms that maintain fungal community diversity and functional features during mangrove restoration and provide scientific support for effective restoration and management.

2. Materials and Methods

2.1. Study Sites and Sampling Design

This study was conducted in the Beilun River Estuary in Dongxing City, Guangxi, within a mangrove restoration area (Figure S1). The restoration system encompassed three distinct habitats, namely, mudflats (MFs), young mangroves (YMs), and mature mangroves (MMs), representing the natural succession stages from mudflats to young and mature mangroves (Figure S1). MFs are characterized by open, waterlogged soil with no vegetation. YMs comprise newly established mangrove saplings and a small number of salt marsh plants. MMs feature well-developed trees. Sediment samples were collected from these habitats on 26 December 2021. Three plots were established for sampling in each habitat. Samples were collected from three depths using a three-point sampling method: surface (S; 0–5 cm), middle (M; 10–15 cm), and bottom (B; 20–25 cm). A total of 500 g of sediment was collected and homogenized at each depth. A total of 81 sediment samples were collected.

2.2. Physical and Chemical Analytical Procedures

Biochemical parameters were assessed for each sample (Figure S2). During sampling, we employed a portable salinity tester (PNT3000, STEP Systems GmbH, Nuremburg, Germany) to measure the salinity of the sediment pore water. Sediment pH and temperature were recorded using a HI98121 tester (Hanna instruments, Woonsocket, RI, USA). Water content was determined by the weight loss of wet sediment after drying at 85 °C for 24 h. Total nitrogen (TN), total carbon (TC), total organic carbon (TOC), and total inorganic carbon (TIC) were determined using an elemental analyzer (Vario MacroCube, Elementar, Langenselbold, Germany). Total phosphorus (TP) and dissolved phosphate (PO_4^{3-}) were quantified using molybdenum blue colorimetry and flame photometry. Inorganic (Pi) and organic phosphorus (Po) were determined using the method described by DeLuca et al. [22]. For the measurement of inorganic nitrogen in sediment (NH_4^+-N, NO_3^--N,

and NO_2^--N), each sample was extracted using a 2 M KCl solution at a soil-to-solution ratio of 1:4, shaken for 1 h at 200 rpm, and analyzed using a continuous flow analyzer (SAN++, Skalar, Breda, The Netherlands). Water content was gravimetrically determined by weighing the sediment samples before and after drying at 105 °C for 24 h.

2.3. DNA Extraction, Gene Amplification, and Sequencing

DNA was extracted from the samples using a PowerSoil DNA Isolation Kit (QIAGEN, Hilden, Germany) following the manufacturer's protocol. The purity and concentration of DNA were determined with a Thermo Scientific NanoDrop1000 spectrophotometer (Thermo Fisher Scientific, Wilmington, DE, USA) and stored at −80 °C. The fungal internal transcribed spacer 1 (ITS1) region was amplified by polymerase chain reaction (PCR) using the dual-bar coded primers ITS1F (5′-CTTGGTCATTTAGAGGAAGTAA-3′) and ITS2 (5′-GCTGCGTTCTTCATCGATGC-3′). Each 50 μL PCR reaction was conducted according to standard procedures for 35 cycles, with a denaturation step at 95 °C for 30 s, annealing at 55 °C for 30 s, and extension at 72 °C for 45 s. The resulting PCR products were prepared using a TruSeq DNA kit (Illumina, San Diego, CA, USA) according to the manufacturer's instructions. The purified library was prepared following the Illumina library preparation protocols and sent to Shanghai Majorbio Bio-Pharm Technology Co., Ltd. (Shanghai, China) for paired-end sequencing on an Illumina MiSeq platform (PE250, 2 × 250 bp, Illumina, San Diego, CA, USA). All the sequence data were deposited in GenBank under the BioProject Accession PRJNA1213986.

2.4. Bioinformatics and FUNGuild

The raw ITS2 sequencing data were processed using QIIME2 software (version 2020.2). The DADA2 plugin was used for quality control, denoising, chimera removal, and the generation of amplicon sequence variants (ASVs). Taxonomic annotation of fungal sequences was conducted using the Ribosomal Database Project (RDP) classifier in conjunction with a specific fungal ITS1 sequence database built by the National Center for Biotechnology Information (NCBI). For downstream analysis, only sequences classified within the kingdom of fungi were considered. The functional groups of fungi were determined using FUNGuild v1.0, namely, a flat database available on https://github.com/UMNFuN/FUNGuild (accessed on 18 March 2022). To avoid over-interpretation of fungal functional groups, we excluded entries with a confidence level of "possible" and retained only those classified as "highly probable" or "probable". Fungal communities that could not be identified—or were identified with multiple complex nutritional methods—were categorized as "undefined".

2.5. Statistical Analyses

To minimize the bias associated with sequencing coverage and enable the comparison of community patterns among samples, we normalized the number of sequences in each sample to match the smallest sample size. This resampling was conducted using the "rrarefy" function from the R package "vegan" before conducting the statistical analyses.

The majority of the statistical analyses were conducted in R, utilizing packages such as "vegan", "picante", "plspm", "ggplot2", and "Hmisc". Differences in alpha (α)-diversity and environmental parameters across different environments were assessed using a one-way analysis of variance (ANOVA). The Spearman's rank correlation method was used to calculate the correlations. Indices such as species richness, Shannon index, Simpson index, Chao1 index, and Good's coverage were calculated. In particular, the Shannon index was used to represent α-diversity, whereas the richness index indicated the species pool size. Beta (β)-diversity was assessed using the Bray–Curtis distance, and the similarity analysis

(PerMANOVA) among different groups was conducted using the "adonis" function from the "vegan" package.

A partial Mantel test, with 9999 permutations, was conducted using the "mantel.partial" function in the "vegan" package. A variation partitioning analysis (VPA) was conducted using the "varpart" function in the "vegan" package.

3. Results

3.1. Soil Fungal Diversity and Community Composition

A total of 359,632 sequence reads representing 687 fungal ASVs were retained in the fungal ITS dataset after quality filtering and discarding the rare ASVs. Good's coverage was >99.91% (Table S1) for each sample, indicating that most fungal taxa were successfully recovered. Fungal ASVs were predominantly classified as Ascomycota (56.69%), followed by Basidiomycota (33.07%), Mucoromycota (5.91%), and Zoopagomycota (1.26%) (Figures S3 and S4). The relative abundance of Ascomycota was significantly higher in the YM stage (74.31%) than in both the MF (50.03%) and MM (59.62%) stages ($p < 0.05$) (Figure S4). No significant difference was observed in the abundance of Ascomycota between the MF and MM stages. In contrast, the relative abundance of Basidiomycota was significantly higher at the MF stage (42.68%) than at the YM stage (22.89%) ($p < 0.05$), whereas no significant differences were observed between the YM and MM stages (31.05%) or MM and MF stages (Figure S4). We assessed the α-diversity of fungal communities using both the richness and Shannon indices. No significant differences were observed in either the richness or Shannon index across the different restoration stages (Figure 1A). In contrast to the α-diversity, both analyses of similarities ((ANOSIM) ($p < 0.001$) and PerMANOVA ($p < 0.001$) revealed significant differences in fungal β-diversity among the three restoration stages at the ASV level (Table S2). Non-metric multidimensional scaling (NMDS) analysis based on Bray–Curtis dissimilarities further indicated a gradual shift in the fungal community structure throughout mangrove restoration, with the MF and MM samples being clearly separated, whereas the YM samples exhibited partial overlap with both the MF and MM samples (Figure 1B).

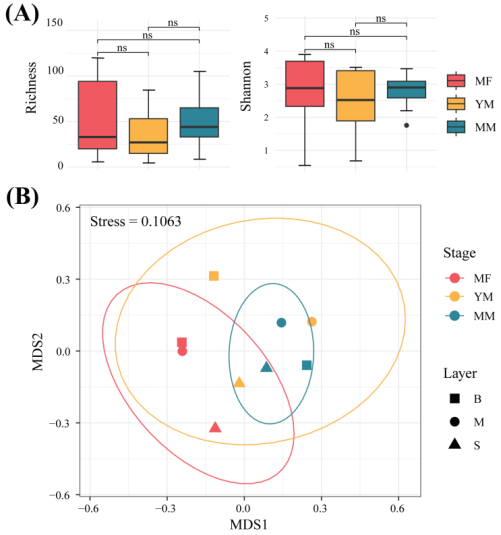


Figure 1. Alpha (α)- and beta (β)-diversities across the three restoration stages. (**A**) α-diversity (richness and Shannon index), with the median indicated by a horizontal line. (**B**) Non-metric multidimensional scaling (NMDS) plot based on the Bray–Curtis dissimilarity of fungal communities, wherein gray lines represent the within-group variability. MF: mudflat; YM: young mangrove; MM: mature mangrove.

3.2. Trophic Mode Features of the Soil Fungal Community

In this study, fungal taxa were categorized into seven trophic modes (saprotroph, pathotroph, pathotroph–saprotroph, saprotroph–symbiotroph, pathotroph–symbiotroph, pathotroph–saprotroph–symbiotroph, and saprotroph–pathotroph–symbiotroph) and 14 guilds using the FUNGuild database (Figures 2 and S5). Saprotrophs were the most predominant trophic mode, accounting for 41.62% of all the observed trophic modes (Figure 2), primarily comprising dung saprotroph–plant saprotroph–wood saprotroph and wood saprotroph guilds (Figure S5). The second most abundant trophic mode was pathotrophic-saprotrophs (34.59%) (Figure 2), primarily comprising an animal pathogen–undefined saprotroph guild (Figure S5). The top five trophic modes were saprotroph–symbiotroph (8.91%), saprotroph–pathotroph–symbiotroph (6.69%), and pathotroph–saprotroph–symbiotroph (0.62%) (Figure 2). No symbiotrophs were found in the single trophic mode, and only pathotrophs were observed, accounting for 5.26% of the fungal taxa (Figure 2). These primarily comprised plant and animal pathogen guilds (Figure S5). Significant differences ($p < 0.05$) in trophic mode abundance were observed across regions, except for the pathotroph–symbiotroph (Figure 2). The highest abundance of saprotrophs was found in the MF area, whereas pathotroph–saprotrophs peaked in the YM zone (Figure 2).

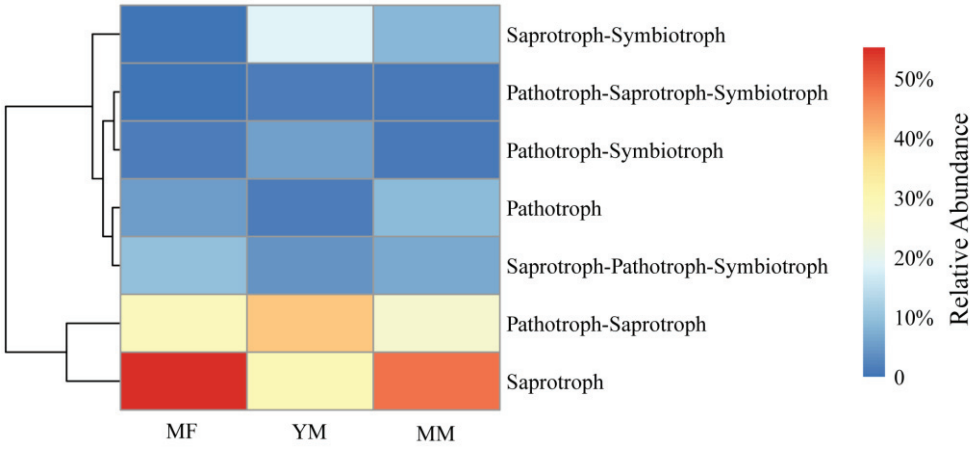


Figure 2. Relative abundance distribution of fungal trophic modes across different stages of mangrove restoration in this study.

The ASV α-diversity of the two predominant trophic modes, namely, saprotrophs and pathotroph–saprotrophs, indicated no significant differences across regions, except for the richness of saprotrophs, which differed significantly between the MF and YM regions (Figure S6).

Both ANOSIM ($p < 0.001$) and PerMANOVA ($p < 0.001$) revealed significant differences in the composition of fungal trophic modes across regions (Table 1). No significant differences were observed between the MF and MM groups (Table 1). Significant differences were observed between the YM and the other two regions (Table 1), indicating that the fungal trophic mode composition significantly changed from the MF to YM stages, and from the YM to MM stages.

Table 1. ANOSIM and PerMANOVA tests of fungal community across different mangrove restoration stages. The top-left corner presents the overall results, whereas the table presents pairwise comparisons.

0.145 ***	MF	YM
MF		
YM	0.192 ***	
MM	0.004 ***	0.238 ***
0.141 ***	MF	YM
MF		
YM	0.129 ***	
MM	0.018 ***	0.153 ***

The upper left shows the overall test results, while the table presents the results of pairwise comparisons. Values in the ANOSIM results represent the r-statistic, while values in the PerMANOVA results represent the R^2 statistic. The asterisk indicates the significance level: ***, $p < 0.001$. MF: mudflat; YM: young mangrove; MM: mature mangrove.

3.3. Environmental Effects on the Fungal Community and Trophic Modes

We examined the Spearman's correlations between the fungal community α-diversity and environmental factors (Table S3). Overall, TN and Pi were the most significant factors influencing both richness and the Shannon index ($p < 0.001$) (Table S3). However, the key factors varied across the different restoration stages (Table S3). In the MF zone, temperature was the most significant factor (Table S3). TN and TOC were the predominant factors in the YM zone (Table S3). In contrast, TN and salinity were the most influential factors in the MM zone (Table S3).

Overall, considering the α-diversity of the trophic modes, Spearman's correlation analysis revealed that TN was the most influential factor affecting richness, whereas TC had the strongest impact on the Shannon index (Table S4). In the MF zone, Pi was the most significant factor influencing both richness and the Shannon index (Table S4). In the YM zone, TOC was the predominant factor affecting both indices (Table S4). In contrast, in the MM zone, NO_2^--N was the main factor affecting richness, whereas no significant correlations were found between the Shannon index and environmental factors (Table S4).

Partial Mantel tests were conducted to examine the correlation between environmental factors and β-diversity in soil fungal communities (Figure 3 and Table S5). Overall, temperature and pH were the key factors influencing the β-diversity of fungal communities (Figure 3 and Table S5). In the MF zone, TN was the most influential factor (Table S5). In the YM zone, pH was the predominant factor (Table S5). In the MM zone, NO_2^--N and PO_4^{3-} were the most significant factors (Table S5).

Overall, TP was the most influential factor for the β-diversity of the trophic modes (Figure 3 and Table S6). TP was the most significant factor in the MF zone (Table S6). In both the YM and MM zones, NO_2^--N was identified as the most influential factor (Table S6).

We conducted variation partitioning analysis (VPA) to assess the contributions of soil physicochemical parameters (i.e., water content, salinity, pH, and temperature) and nutrient variables (i.e., TN, TC, TOC, TIC, TP, PO_4^{3-}, Pi, Po, NH_4^+-N, NO_3^--N, and NO_2^--N) to the fungal community and trophic mode composition (Figure 4). Our results revealed that both overall and across different regions, the pure effects of nutrients on the fungal community structure and trophic mode composition were greater than those of soil physicochemical parameters (Figure 4). In particular, for the fungal community structure, the pure effect of nutrients was the largest in the MF zone (61%) (Figure 4). The effect of nutrients on the fungal trophic mode composition was most pronounced in the YM zone (69%) (Figure 4).

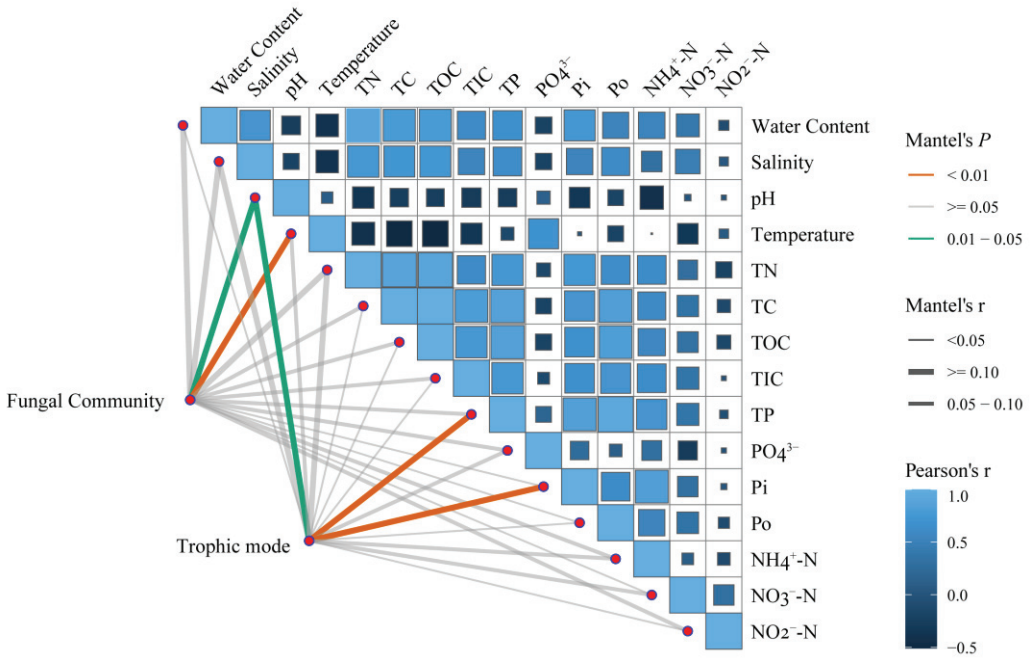


Figure 3. Pairwise correlations between environmental factors (top right) and partial Mantel tests for fungal communities and trophic modes with each environmental factor. TN: total nitrogen; TC: total carbon; TOC: total organic carbon; TIC: total inorganic carbon; TP: total phosphorus; PO_4^{3-}: dissolved phosphate; Pi: inorganic phosphorus; Po: organic phosphorus.

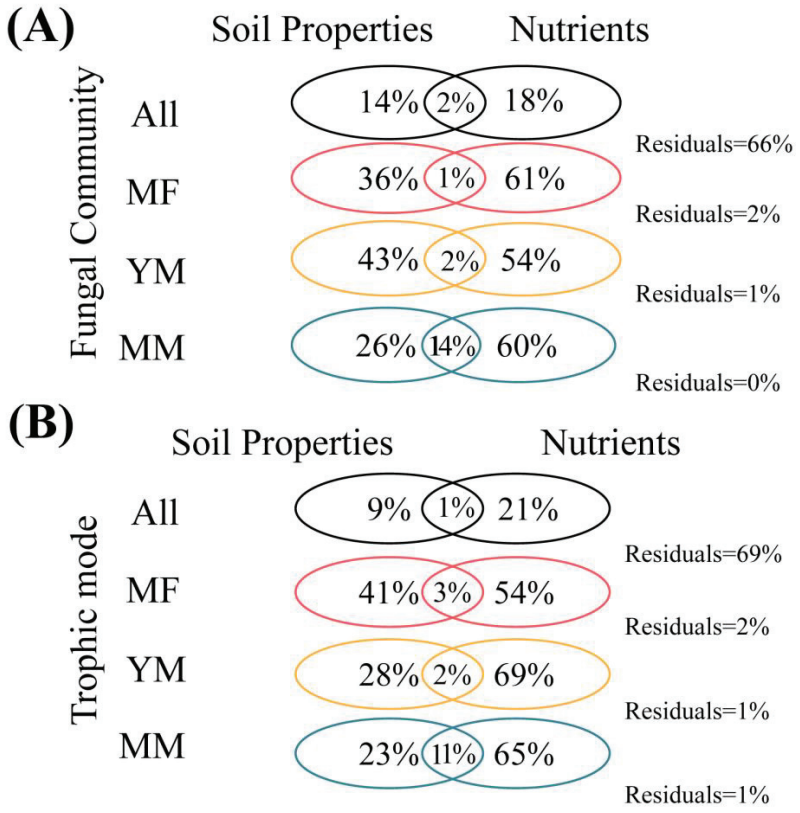


Figure 4. Variation partitioning analysis of the effects of soil properties (water content, salinity, pH, and temperature) and nutrients (TN, TC, TOC, TIC, TP, PO_4^{3-}, Pi, Po, NH_4^+-N, NO_3^--N, and NO_2^--N) in the fungal community (**A**) and trophic mode composition (**B**).

3.4. Bioindicators in Different Successional Environments

We employed a random forest approach to analyze the bioindicators across different restoration stages. Among the fungal species, *Paraphyton cookei*, *Hormographiella aspergillata*, *Candida blankii*, and *Metschnikowia bicuspidata* exhibited the highest Gini values, indicating that they were the most significant bioindicator species (Figure 5). Their abundances showed significant differences across the restoration stages (Figure 5). Spearman's correlation analysis further revealed that the abundance of most of the top 20 species was significantly correlated with various environmental factors (Figure 5). For example, *Hormographiella aspergillata* was positively correlated with TIC and Pi, whereas *Candida blankii* was significantly negatively correlated with pH and temperature (Figure 5). Among the top 20 species, TOC was significantly correlated with eight species ($p < 0.05$), making it the most frequent influencing factor (Figure 5).

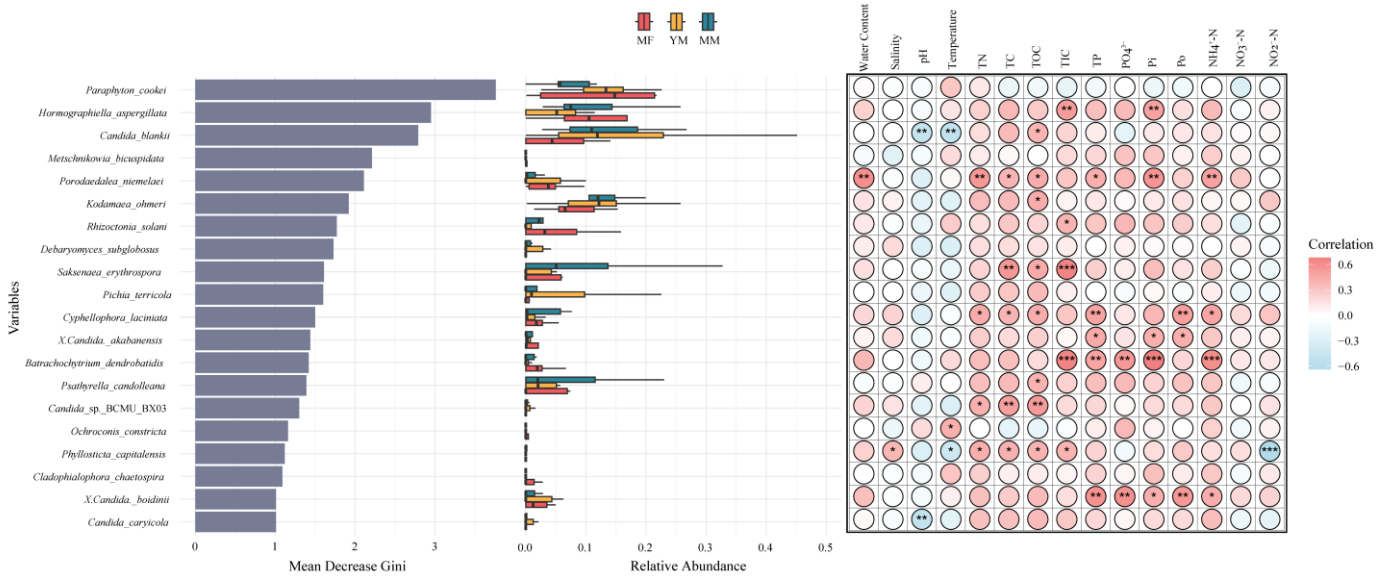


Figure 5. Bioindicators of fungal species in different mangrove restoration stages. **Left**: Gini rank of the bioindicator species, representing their importance level; **Middle**: Relative abundances of the bioindicator species; **Right**: Spearman's correlations between the relative abundances of the species and environmental and nutrient factors. The asterisk indicates the significance level: *, $p < 0.05$; **, $p < 0.01$; ***, $p < 0.001$.

Among the trophic modes, saprotrophs, pathotroph–saprotrophs, and pathotrophs exhibited the highest Gini values (Figure 6), indicating that they were the most effective indicators of environmental change across the restoration stages. Their abundances varied significantly across the stages (Figures 2 and 6). With the exception of the saprotroph–symbiotroph mode, the abundance of all trophic modes was significantly influenced by certain environmental factors (Figure 6). In particular, saprotrophs were significantly affected by TC, TOC, TIC, TP, Pi, Po, and NH_4^+-N ($p < 0.05$) (Figure 6). Both the TC and TIC were the most frequent factors affecting the abundance of the four trophic modes (Figure 6).

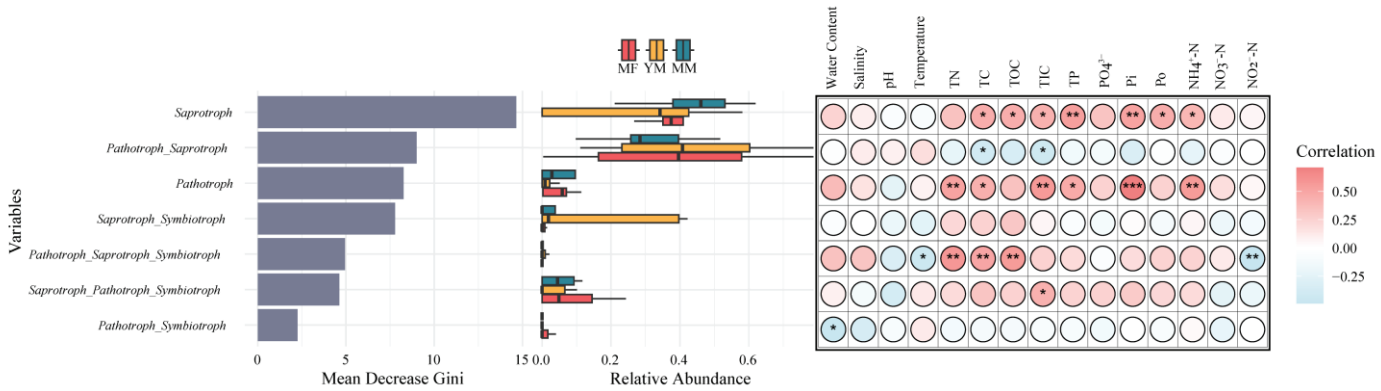


Figure 6. Bioindicators of fungal trophic modes in different mangrove restoration stages. **Left**: Gini rank of the bioindicator trophic modes, representing their importance level; **Middle**: relative abundances of the bioindicator trophic modes; **Right**: Spearman's correlations between the relative abundances of the trophic modes and environmental and nutrient factors. The asterisk indicates the significance level: *, $p < 0.05$; **, $p < 0.01$; ***, $p < 0.001$.

4. Discussion

Fungal communities play crucial roles in nutrient cycling and ecosystem functioning in mangrove environments [20,22,24]. However, our understanding of the fungal community features during the restoration of these ecosystems remains limited. In this study, we investigated the responses of fungal community diversity and trophic modes to environmental changes during different stages of anthropogenic mangrove restoration.

Consistent with the results of previous studies [22,24] on mangrove sediments, we identified Ascomycota and Basidiomycota as the dominant fungal phyla. In particular, Ascomycota has been widely recognized as the predominant fungal group in mangrove ecosystems [28]. A global comparative analysis of soil fungi revealed that individuals of the Ascomycota phylum possess a diverse array of genes associated with nutrient acquisition, such as phosphate transporters, nitrogen immobilization, and carbohydrate metabolism [29]. Similarly, Basidiomycota also plays a significant role in nutrient cycling, particularly in lignin degradation and organic matter decomposition [29,30]. These functional traits likely contribute to the dominance of both fungal phyla in mangrove environments. A previous study of the soil fungal community of *Sonneratia apetala* mangroves revealed that Ascomycota and Basidiomycota were the dominant fungal phyla, but their abundance did not vary significantly with plantation age [22]. In contrast, the mangrove communities in this study, which predominantly comprised *Avicennia marina* and *Kandelia obovata*, exhibited significant variation in the abundance of Ascomycota and Basidiomycota across different restoration stages. In particular, the abundance of Ascomycota peaked at the YM stage, whereas that of Basidiomycota peaked at the MM stage. These differences suggest that the tree species composition plays a critical role in shaping the fungal community structure, likely owing to variations in root exudates, litter input, and microhabitat conditions associated with different plant species [31,32].

We found no significant differences in the α-diversity (i.e., richness and Shannon indices) of fungal communities between the different recovery stages (Figure 1A). However, the β-diversity showed significant differences (Figure 1B). This is consistent with the results of previous studies on *Sonneratia apetala* at different plantation ages [22]. These results suggest that soil fungal α-diversity did not vary significantly during the restoration period, whereas notable changes were observed in β-diversity [22]. A previous study on coastal fungi also suggested that the response of planktonic fungi to environmental variation was more pronounced in β-diversity than in α-diversity [33]. These findings indicate

that although the overall richness and evenness of mangrove soil fungal communities remain relatively stable during ecological restoration, their specific composition is highly responsive to environmental changes and successional stages. This might be because fungi undergo adaptive adjustments at different recovery stages in response to varying environmental conditions [34]. Fungi with stronger adaptive capacities can undergo rapid proliferation even with small changes in taxonomic diversity, leading to greater community turnover [34]. We also examined the impact of environmental factors on fungal diversity and found that TN and Pi are key determinants of overall soil fungal α-diversity ($p < 0.001$) (Table S3). TN was also identified as a critical factor influencing α-diversity in mangrove soils (YM and MM) ($p < 0.01$) but had no effect in MF soils (Table S3). Mangrove ecosystems are characterized by significant nitrogen fixation owing to high organic matter input, anaerobic conditions, and microbial activity [35]. Ongoing nitrogen input, potentially influenced by human activities, such as agricultural runoff and sewage discharge, and phosphorus loss lead to phosphorus limitation, which may affect the fungal diversity [36,37]. Partial Mantel tests indicated that temperature and pH were the key drivers of soil fungal β-diversity in our study area (Figure 3).

Previous studies on *Sonneratia apetala* plantations of varying ages and mangrove ecosystems converted from ponds have indicated that pH is a critical factor in shaping the soil fungal communities in successive mangrove habitats [22,27]. However, these studies did not consider the soil temperature [22,27]. The observed influence of temperature is understandable as the presence of plants can affect sunlight exposure. In our study, vegetated areas had lower soil temperatures (Figure S2). Continental-scale research on forest soil fungal diversity has indicated that temperature and pH are universal factors shaping the fungal community structure [38], which aligns with and supports our findings. Additionally, we found that the primary factors influencing the fungal community structure varied across different stages of restoration (Table S5), reflecting the habitat-dependent nature of the environmental effects on microbial communities [39]. The environmental impact on the soil fungal community may not be independent of individual factors; therefore, we constructed VPA to explain the effects of soil properties and nutrients [40]. Our study suggests that fungal communities in coastal environments are strongly influenced by the nutrient content, which can be altered by human activities, such as agriculture or pollution.

Fungi employ various mechanisms for nutrient acquisition, leading to distinct trophic modes and functional diversities under different environmental conditions [16,41–43]. Our findings indicate that saprotrophs are the predominant trophic mode in fungal communities and that other highly abundant trophic modes also incorporate saprotrophic characteristics (Figure 2). The prominence of saprotrophs may be attributed to their crucial role in decomposition, which helps sustain nutrient cycling and carbon storage [22,27,44,45]. These fungi are prevalent in mangrove environments [22,27] and other marine ecosystems, including surface waters, intertidal zones, and deep-sea sediments [44,45]. Consistent with the results of previous studies [22,27], we found that soil saprotrophs were less abundant in successional mangrove environments than in mudflats or shrimp ponds (Figure 2). Saprotroph abundance was the lowest in the YM zone (Figure 2). Although mangrove soils are rich in organic matter [46,47], which leads to higher saprotroph abundance, vegetation characteristics also influence fungal function [43,48]. Consequently, other trophic modes (e.g., pathogens and symbiotrophic fungi) may occupy ecological niches, particularly in young mangrove zones where mangroves are still developing, leading to a reduction in the relative abundance of saprotrophs. Notably, this does not imply that the absolute abundance of saprotrophs in mangrove environments is lower than that in mudflats. Similar to fungal α-diversity, the α-diversity of the dominant trophic modes, namely, saprotrophs

and pathotroph–saprotrophs (except for saprotroph richness), indicated no significant differences across the three environments (Figure S6), suggesting that these fungal groups may adapt to the environment through community turnover rather than through changes in taxonomic diversity [49].

Considering the trophic modes of the fungal communities, we found no significant differences between the MF and MM zones, but both were significantly different from those in the YM zone (Table 1). This may be attributed to the rapid growth and development of mangrove plants in the YM region, which induce considerable changes in soil properties through the input of leaf litter, root exudates, and other organic matter. Consequently, fungal trophic modes in this environment markedly differ from those in the relatively stable coastal sediments of MFs and MMs. Notably, we found that fungal nutrient acquisition strategies were responsive to variations in multiple soil factors. The α-diversity of trophic modes was primarily influenced by TN and TC, whereas β-diversity was mainly driven by TP and Pi (Figure 3). In particular, in different zones, C-, N-, and P-related factors exerted varying degrees of influence on trophic modes (Table S6), which is consistent with findings from other soil environments [16,49]. These results highlight the significant effect of soil nutrients on the functional composition of fungal communities. The VPA results further confirmed this effect, indicating that nutrient effects outweighed those of soil properties across all the samples and in the different zones (Figure 4B).

After confirming that soil fungal communities and their trophic modes were significantly influenced by environmental heterogeneity, we applied a random forest approach to identify bioindicators across different mangrove restoration stages. Our results revealed that fungi, such as *Paraphyton cookei*, *Hormographiella aspergillata*, *Candida blankii*, and *Metschnikowia bicuspidata*, serve as key indicator species of environmental changes during mangrove succession (Figure 5). Saprotrophs were identified as the most reliable trophic mode for indicating environmental change (Figure 6). A Spearman's analysis also highlighted significant correlations between the abundance of these species and trophic mode with various environmental factors (Figures 5 and 6). TOC was the most significant factor influencing the abundance of the top indicator species (Figure 5), supporting the view that significant changes in soil organic matter during mangrove succession affect the fungal community composition [50]. Consistent with this result, we observed a progressive increase in soil TOC along a mangrove succession gradient (Figure S2). Saprotrophs are the most abundant fungal group and serve as important bioindicators, which is unsurprising considering their crucial role in the decomposition of complex organic matter [50,51]. In mangrove environments during restoration, variations in soil chemistry and physical structure, resulting from changes in vegetation and land use, can significantly shape the composition of saprotrophic communities, offering diverse ecological niches, particularly with fluctuations in soil carbon levels [50–52]. We found that the abundance of saprotrophs was influenced by multiple soil factors, including carbon, nitrogen, and phosphorus (Figure 6), highlighting their sensitivity to changes in nutrient availability. Among all the trophic mode bioindicators, TC was the most widespread influencing factor (Figure 6). Similar to TOC, the TC content increased with mangrove succession (Figure S2). These results underscore the significant association between changes in carbon content during mangrove succession and fungal bioindicators, including species and trophic modes.

5. Conclusions

This study investigated the shifts in soil fungal communities and their trophic modes during mangrove ecosystem restoration, focusing on diversity patterns, environmental drivers, and bioindicators across different restoration stages. Fungal α-diversity (rich-

ness and Shannon index) remained stable across mudflat, young mangrove, and mature mangrove stages, whereas β-diversity exhibited significant turnover. Ascomycota and Basidiomycota were the most abundant phyla, with Ascomycota dominating young mangrove soils (74.3%) and Basidiomycota peaking in mudflats (42.7%). Total nitrogen and inorganic phosphorus were the primary drivers of α-diversity, while temperature and pH governed β-diversity. Nutrients explained the majority of fungal community variation in mangrove restoration soils. *Paraphyton cookei*, *Hormographiella aspergillata*, and saprotrophs emerged as key bioindicators, with their abundances strongly linked to soil carbon dynamics. Overall, this study contributes to our understanding of the complex interactions among fungal communities, environmental factors, and ecosystem functions in mangrove ecosystems, providing a foundation for the restoration and management strategies of mangroves.

Supplementary Materials: The following supporting information can be downloaded at: https://www.mdpi.com/article/10.3390/jof11020146/s1, Figure S1: Sampling sites in the Beilun River Estuary mangrove restoration area, Dongxing City, Guangxi, China; Figure S2: Variation of soil environmental factors across different mangrove restoration areas; Figure S3: Community composition (phylum level) of soil fungi in this study; Figure S4: Community composition (phylum level) of soil fungi across different restoration stages; Figure S5: Relative abundance of functional guilds of the soil fungi; Figure S6: Alpha (α)-diversity of the most abundant trophic mode in mangrove restoration soils; Table S1: Alpha (α)-diversity index of the samples; Table S2. Results of ANOSIM and PerMANOVA tests for soil fungi community across different stages; Table S3: The Spearman's correlations of the individual environmental factor to the fungal alpha (α)-diversity; Table S4: The Spearman's correlations of the individual environmental factor to the alpha (α)-diversity of the fungal trophic modes; Table S5: The correlations of the partial Mantel test for individual environmental factor to the fungal community; Table S6: The correlations of the partial Mantel test for individual environmental factor to the fungal trophic modes.

Author Contributions: Writing—review and editing, X.S.; methodology, S.Z. and L.X.; formal analysis, R.T.N.; visualization, Y.Z.; supervision, L.H. and K.D.; conceptualization, methodology, writing—review and editing, supervision, H.Z. and L.P. All authors have read and agreed to the published version of the manuscript.

Funding: This research was funded by the Natural Science Foundation of Guangxi Province (No. 2022GXNSFBA035591); the Open Research Fund Program of Guangxi Key Lab of Mangrove Conservation and Utilization (No. GKLMC-202001); the Basic Scientific Foundation of Guangxi Mangrove Research Center (No. 2023GMRC-02); the Systematic Research Projects of the Guangxi Key Laboratory of Mangrove Conservation and Utilization (GKLMC-22A04); the project for enhancing young and middle-aged teacher's research basis ability in colleges of Guangxi (No. 2023KY1226); and the Guangdong University Innovation Team (Early warning of marine disasters) (No. 2023KCXTD015).

Institutional Review Board Statement: Not applicable.

Informed Consent Statement: Not applicable.

Data Availability Statement: All the sequence data were deposited in GenBank under the BioProject Accession PRJNA1213986.

Acknowledgments: We thank Danyi Zhao and Hailong Li for their assistance during the sample collection.

Conflicts of Interest: The authors declare no conflicts of interest.

References

1. Hartmann, M.; Six, J. Soil Structure and Microbiome Functions in Agroecosystems. *Nat. Rev. Earth Environ.* **2022**, *4*, 4–18. [CrossRef]

2. Fierer, N. Embracing the Unknown: Disentangling the Complexities of the Soil Microbiome. *Nat. Rev. Microbiol.* **2017**, *15*, 579–590. [CrossRef]
3. Sokol, N.W.; Slessarev, E.; Marschmann, G.L.; Nicolas, A.; Blazewicz, S.J.; Brodie, E.L.; Firestone, M.K.; Foley, M.M.; Hestrin, R.; Hungate, B.A.; et al. Life and Death in the Soil Microbiome: How Ecological Processes Influence Biogeochemistry. *Nat. Rev. Microbiol.* **2022**, *20*, 415–430. [CrossRef]
4. Delgado-Baquerizo, M.; Reich, P.B.; Trivedi, C.; Eldridge, D.J.; Abades, S.; Alfaro, F.D.; Bastida, F.; Berhe, A.A.; Cutler, N.A.; Gallardo, A.; et al. Multiple Elements of Soil Biodiversity Drive Ecosystem Functions across Biomes. *Nat. Ecol. Evol.* **2020**, *4*, 210–220. [CrossRef] [PubMed]
5. van der Plas, F. Biodiversity and Ecosystem Functioning in Naturally Assembled Communities. *Biol. Rev.* **2019**, *94*, 1220–1245. [CrossRef]
6. Zhang, S.; Fan, D.; Wu, J.; Zhang, X.; Zhuang, X.; Kong, W. The Interaction of Climate, Plant, and Soil Factors Drives Putative Soil Fungal Pathogen Diversity and Community Structure in Dry Grasslands. *Environ. Microbiol. Rep.* **2024**, *16*, e13223. [CrossRef] [PubMed]
7. Cui, Y.; Bing, H.; Fang, L.; Wu, Y.; Yu, J.; Shen, G.; Jiang, M.; Wang, X.; Zhang, X. Diversity Patterns of the Rhizosphere and Bulk Soil Microbial Communities along an Altitudinal Gradient in an Alpine Ecosystem of the Eastern Tibetan Plateau. *Geoderma* **2019**, *338*, 118–127. [CrossRef]
8. Lauber, C.L.; Hamady, M.; Knight, R.; Fierer, N. Pyrosequencing-Based Assessment of Soil PH as a Predictor of Soil Bacterial Community Structure at the Continental Scale. *Appl. Environ. Microbiol.* **2009**, *75*, 5111–5120. [CrossRef]
9. Nugent, A.; Allison, S.D. A Framework for Soil Microbial Ecology in Urban Ecosystems. *Ecosphere* **2022**, *13*, e3968. [CrossRef]
10. Zhang, X.; Chen, B.; Yin, R.; Xing, S.; Fu, W.; Wu, H.; Hao, Z.; Ma, Y.; Zhang, X. Long-Term Nickel Contamination Increased Soil Fungal Diversity and Altered Fungal Community Structure and Co-Occurrence Patterns in Agricultural Soils. *J. Hazard. Mater.* **2022**, *436*, 129113. [CrossRef]
11. Liu, X.; Zhang, L.; Huang, M.; Zhou, S. Plant Diversity Promotes Soil Fungal Pathogen Richness under Fertilization in an Alpine Meadow. *J. Plant Ecol.* **2021**, *14*, 323–336. [CrossRef]
12. Lladó, S.; López-Mondéjar, R.; Baldrian, P. Forest Soil Bacteria: Diversity, Involvement in Ecosystem Processes, and Response to Global Change. *Microbiol. Mol. Biol. Rev.* **2017**, *81*. [CrossRef] [PubMed]
13. Huang, Q.; Jiao, F.; Huang, Y.; Li, N.; Wang, B.; Gao, H.; An, S. Response of Soil Fungal Community Composition and Functions on the Alteration of Precipitation in the Grassland of Loess Plateau. *Sci. Total Environ.* **2021**, *751*, 142273. [CrossRef] [PubMed]
14. Nie, S.; Lei, X.; Zhao, L.; Brookes, P.C.; Wang, F.; Chen, C.; Yang, W.; Xing, S. Fungal Communities and Functions Response to Long-Term Fertilization in Paddy Soils. *Appl. Soil Ecol.* **2018**, *130*, 251–258. [CrossRef]
15. Likulunga, L.E.; Rivera Pérez, C.A.; Schneider, D.; Daniel, R.; Polle, A. Tree Species Composition and Soil Properties in Pure and Mixed Beech-Conifer Stands Drive Soil Fungal Communities. *For. Ecol. Manag.* **2021**, *502*, 119709. [CrossRef]
16. Jiang, S.; Xing, Y.; Liu, G.; Hu, C.; Wang, X.; Yan, G.; Wang, Q. Changes in Soil Bacterial and Fungal Community Composition and Functional Groups during the Succession of Boreal Forests. *Soil Biol. Biochem.* **2021**, *161*, 108393. [CrossRef]
17. Nguyen, N.H.; Song, Z.; Bates, S.T.; Branco, S.; Tedersoo, L.; Menke, J.; Schilling, J.S.; Kennedy, P.G. FUNGuild: An Open Annotation Tool for Parsing Fungal Community Datasets by Ecological Guild. *Fungal Ecol.* **2016**, *20*, 241–248. [CrossRef]
18. Yang, H.; Cheng, L.; Che, L.; Su, Y.; Li, Y. Nutrients Addition Decreases Soil Fungal Diversity and Alters Fungal Guilds and Co-Occurrence Networks in a Semi-Arid Grassland in Northern China. *Sci. Total Environ.* **2024**, *926*, 172100. [CrossRef]
19. Giri, C.; Ochieng, E.; Tieszen, L.L.; Zhu, Z.; Singh, A.; Loveland, T.; Masek, J.; Duke, N. Status and Distribution of Mangrove Forests of the World Using Earth Observation Satellite Data. *Glob. Ecol. Biogeogr.* **2011**, *20*, 154–159. [CrossRef]
20. Allard, S.M.; Costa, M.T.; Bulseco, A.N.; Helfer, V.; Wilkins, L.G.E.; Hassenrück, C.; Zengler, K.; Zimmer, M.; Erazo, N.; Mazza Rodrigues, J.L.; et al. Introducing the Mangrove Microbiome Initiative: Identifying Microbial Research Priorities and Approaches To Better Understand, Protect, and Rehabilitate Mangrove Ecosystems. *mSystems* **2020**, *5*. [CrossRef] [PubMed]
21. Ma, X.-X.; Jiang, Z.-Y.; Wu, P.; Wang, Y.-F.; Cheng, H.; Wang, Y.-S.; Gu, J.-D. Effect of Mangrove Restoration on Sediment Properties and Bacterial Community. *Ecotoxicology* **2021**, *30*, 1672–1679. [CrossRef] [PubMed]
22. Sun, D.; Huang, Y.; Wang, Z.; Tang, X.; Ye, W.; Cao, H.; Shen, H. Soil Microbial Community Structure, Function and Network along a Mangrove Forest Restoration Chronosequence. *Sci. Total Environ.* **2024**, *913*, 169704. [CrossRef]
23. Bai, S.; Li, J.; He, Z.; Van Nostrand, J.D.; Tian, Y.; Lin, G.; Zhou, J.; Zheng, T. GeoChip-Based Analysis of the Functional Gene Diversity and Metabolic Potential of Soil Microbial Communities of Mangroves. *Appl. Microbiol. Biotechnol.* **2013**, *97*, 7035–7048. [CrossRef] [PubMed]
24. Zhang, Z.-F.; Pan, Y.-P.; Liu, Y.; Li, M. High-Level Diversity of Basal Fungal Lineages and the Control of Fungal Community Assembly by Stochastic Processes in Mangrove Sediments. *Appl. Environ. Microbiol.* **2021**, *87*, e00928-21. [CrossRef]

25. Arfi, Y.; Buée, M.; Marchand, C.; Levasseur, A.; Record, E. Multiple Markers Pyrosequencing Reveals Highly Diverse and Host-Specific Fungal Communities on the Mangrove Trees Avicennia Marina and Rhizophora Stylosa. *FEMS Microbiol. Ecol.* **2012**, *79*, 433–444. [CrossRef] [PubMed]
26. Zuo, Y.; Zeng, R.; Tian, C.; Wang, J.; Qu, W. The Importance of Conditionally Rare Taxa for the Assembly and Interaction of Fungal Communities in Mangrove Sediments. *Appl. Microbiol. Biotechnol.* **2022**, *106*, 3787–3798. [CrossRef]
27. Hou, N.; Yang, X.; Wang, W.; Sardans, J.; Yin, X.; Jiang, F.; Song, Z.; Li, Z.; Tian, J.; Ding, X.; et al. Mangrove Wetland Recovery Enhances Soil Carbon Sequestration Capacity of Soil Aggregates and Microbial Network Stability in Southeastern China. *Sci. Total Environ.* **2024**, *951*, 175586. [CrossRef]
28. Devadatha, B.; Jones, E.B.G.; Pang, K.L.; Abdel-Wahab, M.A.; Hyde, K.D.; Sakayaroj, J.; Bahkali, A.H.; Calabon, M.S.; Sarma, V.V.; Sutreong, S.; et al. Occurrence and Geographical Distribution of Mangrove Fungi. *Fungal Divers.* **2021**, *106*, 137–227. [CrossRef]
29. Egidi, E.; Delgado-Baquerizo, M.; Plett, J.M.; Wang, J.; Eldridge, D.J.; Bardgett, R.D.; Maestre, F.T.; Singh, B.K. A Few Ascomycota Taxa Dominate Soil Fungal Communities Worldwide. *Nat. Commun.* **2019**, *10*, 2369. [CrossRef] [PubMed]
30. Taylor, J.D.; Cunliffe, M. Multi-Year Assessment of Coastal Planktonic Fungi Reveals Environmental Drivers of Diversity and Abundance. *ISME J.* **2016**, *10*, 2118–2128. [CrossRef]
31. Broeckling, C.D.; Broz, A.K.; Bergelson, J.; Manter, D.K.; Vivanco, J.M. Root Exudates Regulate Soil Fungal Community Composition and Diversity. *Appl. Environ. Microbiol.* **2008**, *74*, 738–744. [CrossRef]
32. Bardgett, R.D.; van der Putten, W.H. Belowground Biodiversity and Ecosystem Functioning. *Nature* **2014**, *515*, 505–511. [CrossRef]
33. Zhao, H.; Brearley, F.Q.; Huang, L.; Tang, J.; Xu, Q.; Li, X.; Huang, Y.; Zou, S.; Chen, X.; Hou, W.; et al. Abundant and Rare Taxa of Planktonic Fungal Community Exhibit Distinct Assembly Patterns Along Coastal Eutrophication Gradient. *Microb. Ecol.* **2023**, *85*, 495–507. [CrossRef]
34. Bahram, M.; Hildebrand, F.; Forslund, S.K.; Anderson, J.L.; Soudzilovskaia, N.A.; Bodegom, P.M.; Bengtsson-Palme, J.; Anslan, S.; Coelho, L.P.; Harend, H.; et al. Structure and Function of the Global Topsoil Microbiome. *Nature* **2018**, *560*, 233–237. [CrossRef] [PubMed]
35. Reef, R.; Feller, I.C.; Lovelock, C.E. Nutrition of Mangroves. *Tree Physiol.* **2010**, *30*, 1148–1160. [CrossRef]
36. Luo, L.; Meng, H.; Wu, R.; Gu, J.-D. Impact of Nitrogen Pollution/Deposition on Extracellular Enzyme Activity, Microbial Abundance and Carbon Storage in Coastal Mangrove Sediment. *Chemosphere* **2017**, *177*, 275–283. [CrossRef]
37. Saravanakumar, K.; Kathiresan, K.; MubarakAli, D.; Kayalvizhi, K.; Rajendran, N.; Hemalatha, S.; Chen, J. Soil-Microbial Communities Indexing from Mangroves Rhizosphere and Barren Sandy Habitats. *Physiol. Mol. Plant Pathol.* **2018**, *104*, 58–68. [CrossRef]
38. Zhou, J.; Deng, Y.; Shen, L.; Wen, C.; Yan, Q.; Ning, D.; Qin, Y.; Xue, K.; Wu, L.; He, Z.; et al. Temperature Mediates Continental-Scale Diversity of Microbes in Forest Soils. *Nat. Commun.* **2016**, *7*, 12083. [CrossRef]
39. Zhang, G.; Bai, J.; Zhai, Y.; Jia, J.; Zhao, Q.; Wang, W.; Hu, X. Microbial Diversity and Functions in Saline Soils: A Review from a Biogeochemical Perspective. *J. Adv. Res.* **2024**, *59*, 129–140. [CrossRef] [PubMed]
40. Verberk, W.C.E.P.; van Noordwijk, C.G.E.; Hildrew, A.G. Delivering on a Promise: Integrating Species Traits to Transform Descriptive Community Ecology into a Predictive Science. *Freshw. Sci.* **2013**, *32*, 531–547. [CrossRef]
41. Huang, J.; Zhao, H.; Yang, S.; Qin, X.; Liao, N.; Li, X.; Wei, Q.; Li, W.; Jiang, G.; Li, N.; et al. Mycoplanktonic Community Structure and Their Roles in Monitoring Environmental Changes in a Subtropical Estuary in the Beibu Gulf. *J. Mar. Sci. Eng.* **2022**, *10*, 1940. [CrossRef]
42. Li, X.; Huang, M.; Li, N.; Zhao, H.; Pu, Y.; Huang, J.; Yang, S.; Qin, X.; Dong, K.; Li, M.; et al. Effects of Environmental Factors on Mycoplankton Diversity and Trophic Modes in Coastal Surface Water. *Ecol. Indic.* **2023**, *146*, 109778. [CrossRef]
43. Zhao, H.; Zhang, F.; Wang, Y.; Wang, J.; Li, J.; Zhang, Z. Variation and Drivers of Soil Fungal and Functional Groups among Different Forest Types in Warm Temperate Secondary Forests. *Glob. Ecol. Conserv.* **2023**, *45*, e02523. [CrossRef]
44. Lacerda, A.L.d.F.; Proietti, M.C.; Secchi, E.R.; Taylor, J.D. Diverse Groups of Fungi Are Associated with Plastics in the Surface Waters of the Western South Atlantic and the Antarctic Peninsula. *Mol. Ecol.* **2020**, *29*, 1903–1918. [CrossRef] [PubMed]
45. Xu, W.; Gong, L.; Pang, K.-L.; Luo, Z.-H. Fungal Diversity in Deep-Sea Sediments of a Hydrothermal Vent System in the Southwest Indian Ridge. *Deep Sea Res. Part I Oceanogr. Res. Pap.* **2018**, *131*, 16–26. [CrossRef]
46. Xie, C.; Ma, X.; Zhao, Y.; Dai, T.; Song, W.; Qi, Q.; Feng, J.; Cui, X.; Zhou, J.; Huang, X.; et al. Nitrogen Addition and Warming Rapidly Alter Microbial Community Compositions in the Mangrove Sediment. *Sci. Total Environ.* **2022**, *850*, 157992. [CrossRef] [PubMed]
47. Crippa, M.; Guizzardi, D.; Muntean, M.; Schaaf, E.; Solazzo, E.; Monforti-Ferrario, F.; Olivier, J.G.J.; Vignati, E. *Fossil CO2 Emissions of All World Countries—2020 Report, EUR 30358 EN*; JRC121460; Publications Office of the European Union: Luxembourg, 2020; ISBN 978-92-76-21515-8. [CrossRef]

48. Purahong, W.; Sadubsarn, D.; Tanunchai, B.; Wahdan, S.F.M.; Sansupa, C.; Noll, M.; Wu, Y.-T.; Buscot, F. First Insights into the Microbiome of a Mangrove Tree Reveal Significant Differences in Taxonomic and Functional Composition among Plant and Soil Compartments. *Microorganisms* **2019**, *7*, 585. [CrossRef] [PubMed]
49. Yang, N.; Zhang, J.; Hua, J.; Song, B.; Wang, T.; Xing, W.; Wang, G.; Mao, L.; Ruan, H. Differentiation of Fungal Trophic Guilds to Long-Term Nitrogen Addition in a Poplar Plantation. *For. Ecol. Manag.* **2024**, *555*, 121699. [CrossRef]
50. Kang, P.; Pan, Y.; Ran, Y.; Li, W.; Shao, M.; Zhang, Y.; Ji, Q.; Ding, X. Soil Saprophytic Fungi Could Be Used as an Important Ecological Indicator for Land Management in Desert Steppe. *Ecol. Indic.* **2023**, *150*, 110224. [CrossRef]
51. Schmidt, R.; Mitchell, J.; Scow, K. Cover Cropping and No-till Increase Diversity and Symbiotroph:Saprotroph Ratios of Soil Fungal Communities. *Soil Biol. Biochem.* **2019**, *129*, 99–109. [CrossRef]
52. Fontaine, S.; Henault, C.; Aamor, A.; Bdioui, N.; Bloor, J.M.G.; Maire, V.; Mary, B.; Revaillot, S.; Maron, P.A. Fungi Mediate Long Term Sequestration of Carbon and Nitrogen in Soil through Their Priming Effect. *Soil Biol. Biochem.* **2011**, *43*, 86–96. [CrossRef]

Disclaimer/Publisher's Note: The statements, opinions and data contained in all publications are solely those of the individual author(s) and contributor(s) and not of MDPI and/or the editor(s). MDPI and/or the editor(s) disclaim responsibility for any injury to people or property resulting from any ideas, methods, instructions or products referred to in the content.

Journal of *Fungi*

MDPI

Article

Comparison of Rhizosphere Microbiomes Between Domesticated and Wild Wheat in a Typical Agricultural Field: Insights into Microbial Community Structure and Functional Shifts

Jie Fang [1,†], Mihal Blaschkauer [2,†], Assaf Distelfeld [3], Zihao Liu [1], Bin Song [4], Shimon Rachmilevitch [2,*] and Jonathan M. Adams [1,*]

[1] School of Geography and Ocean Science, Nanjing University, Nanjing 210023, China; fangjie961021@163.com (J.F.)
[2] The Jacob Blaustein Institute for Desert Research, Ben-Gurion University of the Negev, Sede Boker Campus, Be'er Sheva 84990, Israel; miblasch@gmail.com
[3] Department of Evolutionary and Environmental Biology, Faculty of Natural Sciences and the Institute of Evolution, University of Haifa, Haifa 3498838, Israel
[4] College of Bioscience and Biotechnology, Shenyang Agricultural University, Shenyang 110866, China
* Correspondence: rshimon@bgu.ac.il (S.R.); jonadams@nju.edu.cn (J.M.A.)
† These authors share first authorship.

Abstract: While the differences between domesticated crops and their wild relatives have been extensively studied, less is known about their rhizosphere microbiomes, which hold potential for breeding stress-resistant traits. We compared the rhizosphere microbiomes of domesticated wheat (*Triticum aestivum* L.) and its wild ancestor (*Triticum turgidum* ssp. *dicoccoides*) in a typical agricultural field using 16S rRNA and ITS gene sequencing. Our results revealed a high level of conservation in the rhizosphere microbiomes between wild and domesticated wheat, with minimal divergence in community composition and microbial network structure. However, domesticated wheat exhibited a higher prevalence of fungal pathogens and increased functional redundancy, with significant enrichment of genes involved in carbon and nitrogen cycling. The microbial community assemblies in both wheats were predominantly governed by deterministic processes. This suggests that long-term conventional agricultural practices have imposed minor effects on the compositional differences between the microbiomes of wild and domesticated wheat. Nonetheless, the lower abundance of apparent pathogens in the rhizosphere of the wild wheat suggests greater natural biota or innate host plant resistance against pathogenic fungi. This study may provide valuable insights into the host selection, assembly patterns, and functional potential of microbial communities in wild versus domesticated wheat, with implications for manipulating microbial communities in future crop breeding.

Keywords: domesticated wheat; wild ancestor; rhizosphere microbiome; functional traits; co-occurrence patterns; deterministic processes

1. Introduction

Wheat (*Triticum* sp.) occupies over 16% of global cropland and accounts for one-fifth of the food consumed by humans worldwide [1,2]. Ensuring the productivity of global wheat supplies is a major challenge in the face of global climate change, evolving diseases, and

environmental damage from intensive farming practices [3–5]. Domestication, involving the selection of desirable traits such as fertilizer responsiveness and disease resistance, remains a key strategy for ensuring food security [6], and unintentional interspecific and introgressive hybridizations with wild varieties may contribute to the emergence of subspecies better adapted to agricultural environments [7].

All crops, including wheat, are known to selectively recruit unique microbial communities on their roots, which can co-evolve with the host plant [8–11]. Previous studies have suggested that the wild ancestors of modern crops harbored microbiomes that were more active and effective in acquiring recalcitrant nutrients, thereby enhancing plant resistance to biotic and abiotic stress [2,12]. In contrast, domesticated crops may have lost the ability to sustain such a microbiome through random mutation. Furthermore, reduced carbon (C) exudation in domesticated crops favored mutant strains that produced higher yields by avoiding the costly investment in what had become an unnecessary microbiome [12–14].

Numerous studies have compared the microbiome of wild crop ancestors or traditional cultivars with those of modern high-yielding cultivars [2,15–17]. A reduction in microbial species richness has been observed in the rhizosphere microbiome of domesticated crops, accompanied by shifts in taxonomic and functional composition [16]. Modern cultivars typically exhibit a decrease in the relative abundance of Bacteroidota and an increase in Actinomycetota and Pseudomonadota [16]. Nevertheless, contrasting conclusions have been reported, with some studies suggesting that domestication increased the alpha diversity [18] or that only minor differences in rhizosphere microbial composition are associated with host genotype variations [19,20]. Our understanding of how the composition and function of the microbiome in major crops have changed throughout the history of domestication remains incomplete.

On the other hand, previous studies based on pot or plot experiments have provided only limited insight into how domestication processes have influenced the rhizosphere microbiome [16,17,19]. It is essential that studies of the microbiomes of wild crop relatives or ancestors be conducted within the crop's native region. This approach allows for a realistic understanding of the original microbiome potential of both the crop and its closest wild ancestor, considering the specific climate, soils, and biogeography of the region [18]. Such research could lead to the development of beneficial breeding and microbiome engineering programs aimed at enhancing crop resilience [21,22].

In this study, we selected a wild wheat accession 'Zavitan' (*Triticum turgidum* ssp. *dicoccoides*), commonly found as wild emmer [23], and the modern hexaploid wheat cultivar 'Galil' (*Triticum aestivum* L.) as our study subjects. Samples were collected from a high-density wheat field in Israel (Aharonson Farm), located within the geographical zone where both modern cultivated wheat and its wild ancestors originated [24–26]. This setting provides an ideal context for contrasting the microbiomes of ancestral and modern wheat varieties. We hypothesized that (1) the domestication of wheat and subsequent breeding for commercial traits would have altered the plant's phenotype, thereby influencing the microbiome they sustain. (2) Specifically, we expected the ancestral wheat to recruit a more diverse and functionally constrained root microbiome, forming more complex and stable communities that were dominated by deterministic processes, which would support the wild plants' survival under nutrient scarcity, intense abiotic stress, and pathogen attack.

2. Materials and Methods

2.1. Site Description and Soil Sampling

The wheat field studied was located at the Aharonson Farm for Agricultural Experimentation, near Atlit, Israel (32°41′14″ N, 34°56′18″ E). The field is flat and composed

of uniform loam soil, with a pH value of 7.6, organic matter of 8.2%, nitrate nitrogen of 12.3 mg kg^{-1}, ammonium nitrogen of 52.9 mg kg^{-1}, and available phosphorus of 11.2 mg kg^{-1}. The location is characterized by a typical hot summer Mediterranean climate (Csa in the Köppen–Geiger classification), with a mean annual temperature of 20.3 °C and a mean annual precipitation of 560 mm.

Whole plants were randomly harvested from a 50 m^2 field, when the grain heads of both wild (*Triticum turgidum* ssp. *dicoccoides* var. Zavitan) and domesticated (*Triticum aestivum* L. var. Galil) wheat were still green and swelling. Plants were uprooted by holding the stem and inserting a trowel into the soil about 7 cm away from the stem in a circular motion, carefully lifting the entire root ball (roots and adhering soil) from the ground. The root ball was immediately placed in a sterile bag and kept chilled, arriving at the lab within one hour of sampling. A total of 12 domesticated and 11 wild wheat plants with rhizosphere soils were collected. The plants with roots still attached were vigorously shaken to remove loose soil (outer rhizosphere). The roots were then gently rubbed using sterile gloved fingers (changing to a clean pair of gloves for each plant) to remove the closely attached soil of the middle rhizosphere.

2.2. DNA Extraction and Amplicon Sequencing

This middle rhizosphere soil was processed using a Qiagen PowerSoil® DNeasy Isolation Kit for DNA extraction. Samples were sequenced at Dalhouise University Integrated Microbiome Resource. Amplicon fragments were PCR-amplified from the DNA extracted above in duplicates using separate template dilutions (1:1 and 1:10) using high-fidelity Phusion+ polymerase. A single round of PCR was carried out using "fusion primers" (Illumina adaptors + indices + specific regions) targeting the V4-V5 sub-regions of the 16S rRNA (bacteria) and ITS2 (fungi) genes. PacBio Sequel 2 was performed as above, except full-length 16S/ITS fusion primers (PacBio adaptors + barcodes + specific regions) were used instead. PCR products were verified visually by running on a high-throughput Hamilton Nimbus Select robot using Coastal Genomics Analytical Gels. The PCR reactions from the same samples were pooled in one plate and then cleaned-up and normalized using a high-throughput Charm Biotech Just-a-Plate 96-well Normalization Kit. The primers used were as follows: 515F—GTGYCAGCMGCCGCGGTAA—926R—CCGYCAATTYMTTTRAGTTT for bacteria and TS86F—GTGAATCATCGAATCTTTGAA—ITS4R—TCCTCCGCTTATTGATATGC for fungi [27,28]. Due to high plant plasmid and mitochondrial DNA contamination, PNA blockers were added to the PCR stage (mPNA—GGCAAGTGTTCGGA for mitochondrial DNA, pPNA—GGCTCAACCCTGGACAG for plastid), as described in [29]. However, 16S rRNA and ITS gene fragments were successfully amplified from the rhizosphere soil of only 8 pairs of domesticated and wild wheat (i.e., 8 domesticated wheat samples and 8 wild wheat samples), and thus, these 8 pairs were used for subsequent analyses. The raw sequences were submitted to the NCBI Sequence Read Archive (SRA) with accession number PRJNA917337.

2.3. Bioinformatic Processing

Amplicon sequences were processed and analyzed with QIIME 2 v.2020.8 (https://qiime2.org; accessed on 14 November 2023), with quality control and actual sequence variants (ASVs) identification performed with the DADA2 pipeline [30]. An ASV table was then created and normalized according to the lowest total number of sequences in the sample to avoid the effect of uneven sequencing depth between samples [31]. Taxonomic assignment of ASVs was performed using a machine learning classifier through the classify-sklearn method in Qiime 2 [32]. The 16S rRNA gene sequences were aligned against the

SILVA 138 reference database (https://www.arb-silva.de; accessed on 18 November 2023), while the ITS gene sequences were aligned against UNITE general FASTA release for Fungi version 6.0 (https://unite.ut.ee; accessed on 18 November 2023). Because this study's focus was limited to investigating the bacterial and fungal communities, archaeal sequences were removed from the 16S rRNA sequences for the subsequent analysis.

2.4. Statistical Analysis

2.4.1. Alpha and Beta Diversity

Alpha indices, including the Chao 1, richness, Simpson, and Shannon indices, were calculated based on the normalized ASV table using the "Vegan" package in R 4.1.0 [33]. Differences in alpha diversity indices were tested by the Wilcoxon test.

To demonstrate the bacterial and fungal communities' differences between the domesticated and wild wheat rhizosphere soils, non-metric multidimensional scaling ordination (NMDS) analysis based on the Bray–Curtis dissimilarity was conducted. Permutational multivariate analysis of variance (PERMANOVA) was used to evaluate the significant differences between the domesticated and wild groups. NMDS and PERMANOVA were conducted using the "phyloseq" and "Vegan" packages in R 4.1.0, respectively [33,34].

2.4.2. Function Prediction

To investigate the potential functions of bacteria, the inferred function from soil bacterial taxonomy was evaluated based on the Functional Annotation of Prokaryotic Taxa database (FAPROTAX) [35]. The top functional groups with the average proportions of bacterial ASVs among all the samples higher than 0.1% were visualized. In addition, the Tax4Fun2 package [36] was used for the prediction of functional redundancy in the microbial community through 16S rRNA gene sequence similarity. Furthermore, the proportion of genes associated with soil C, nitrogen (N), and phosphorus (P) cycling functions based on 16S rRNA gene data was obtained, with 101, 59, and 35 genes related to soil C, N, and P cycling, respectively, being found in soils according to previous studies [37,38].

The investigation of fungal community function was performed with FUNGuild v1.0 [39], which can taxonomically parse fungal ASVs by analyzing the ecological guild of sequencing databases. Three confidence ranks, namely, "highly probable", "probable", and "possible", could be evaluated according to comparison in the fungal database, suggesting the possibility of assumed guilds. The guilds that were "highly probable" and "probable" in the assignments were selected for the purpose of not over-interpreting their data ecologically. All ASVs that did not match taxa in the database were classified as "unassigned". Then, top functional groups with the average proportions of fungal ASVs among all samples higher than 0.1% were visualized.

2.4.3. Network Analysis

Species co-occurrence networks were constructed for the domesticated and wild wheat rhizospheres, respectively, to illustrate the ecological interactions in their microbial communities. To reduce the complexity of the datasets to facilitate analysis, we constructed single networks for bacteria and fungi only using the most abundant ASVs (top 300 ASVs), respectively, and constructed a joint interdomain network combining the top 300 bacterial and fungal ASVs [40].

Pairwise correlation was calculated based on the SparCC method with default parameters, which was designed to assess correlations for compositional data and construct a non-random network [41]. Robust associations in the matrix were selected under the

threshold value of 0.6 and significance of 0.01 [42]. Network visualization was generated with Gephi version 0.9.1 (https://gephi.org; accessed on 20 November 2023), and the layout was generated using the Fruchterman–Reingold force-based algorithm [43]. Each node indicates a given ASV, and each edge represents a significant correlation between two ASVs. Topological parameters were calculated in R version 4.1.0 with the 'igraph' package [44]. Furthermore, network parameter values were assigned to each sample to estimate the complexity of the soil network (Supplementary Table S1), and the differences were tested by the Wilcoxon test, including the number of nodes and edges, average degree, and modularity [45,46]. According to the definition of these parameters, higher numbers of nodes and edges, a higher value of average degree, and a lower value of modularity suggest a more connected network, reflecting more potential complexity of soil networks [46,47].

The topological roles of nodes in each species network were identified based on their within-module connectivity (Zi) and among-module connectivity (Pi), which were calculated using the method described in [48,49]. Nodes in the network can be classified as network hubs (Zi > 2.5 and Pi > 0.62), module hubs (Zi > 2.5 and Pi < 0.62), connectors (Zi < 2.5 and Pi > 0.62), and peripherals (Zi < 2.5 and Pi < 0.62). Here, we defined the network hubs, module hubs, and connectors as keystone species.

To further evaluate the species network features, robustness was calculated based on the network natural connectivity, and the network stability was evaluated by removing edges randomly and repetitively to estimate how quickly the network robustness degraded [50,51]. Robustness analysis was shown as linear regression curves fitted by the natural connectivity and the proportion of removed edges, and the slopes of the curves were then compared by performing 1000 permutations using the "Simba" R package [52]. A greater absolute value of slope indicates a weaker network stability [53].

2.4.4. Community Assembly Process

To determine the relative importance of stochastic and deterministic processes for bacterial and fungal communities, phylogenetic normalized stochasticity ratio (pNST) analysis was applied, with pNST < 0.5 indicating a more deterministic assembly [54]. Differences in the pNST index between the domesticated and wild wheat rhizospheres were tested using the Wilcoxon test. A neutral community model (NCM) was used to further assess the potential importance of stochasticity in assembling for both bacterial and fungal communities, as described in Chen et al. [55]. In this model, the parameter "m" assesses the estimated migration rate, and "R^2" represents the overall fit to the neutral model. The ASVs were separated into three partitions depending on whether they occurred above, below, or within (neutral) the 95% confidence interval of the NCM predictions. All calculations were performed in R v4.1.0, as previously described Chen et al. [55].

3. Results

3.1. Microbial Alpha Diversity and Community Composition

We found no significant differences in alpha diversity between the rhizosphere microbiomes of the domesticated and wild wheat. Specifically, there were no significant differences in the richness, Chao1, Shannon or Simpson indices between the wild and domesticated wheat in both the bacterial and fungal communities (Supplementary Figure S1).

In both the wild and domesticated wheat, the bacterial community was dominated by Pseudomonadota, with an average relative abundance of 39.25% in the wild and 34.06% in the domesticated wheat rhizospheres, respectively. This was followed by Bacteroidota (29.23% and 20.71%, respectively), Acidobacteriota (11.03% and 11.55%, respectively), and

Actinomycetota (9.84% and 8.98%, respectively) (Supplementary Figure S2A). Pseudomonadota were significantly more abundant in the wild wheat rhizosphere, while Bacteroidota were more abundant in domesticated wheat. The relative abundances of other dominant bacterial phyla showed no significant differences between the two rhizospheres.

In the fungal community (Supplementary Figure S2B), Ascomycota was the most abundant phylum, with an average relative abundance of 57.68% in the domesticated and 49.81% in the wild wheat rhizosphere. This was followed by Basidiomycota (38.16% and 45.24%, respectively), Chytridiomycota (2.07% and 1.51%, respectively), Zygomycota (0.71% and 0.90%, respectively), and Glomeromycota (0.23% and 0.42%, respectively). No significant differences were observed in the overall fungal community composition between the domesticated and wild wheat rhizospheres. The NMDS plots (Figure 1) further illustrate the minor differences in the bacterial ($R^2 = 0.25$, $p < 0.01$) and fungal ($R^2 = 0.11$, $p > 0.05$) community structures between the rhizosphere biota of the domesticated and wild wheat at the ASV level.

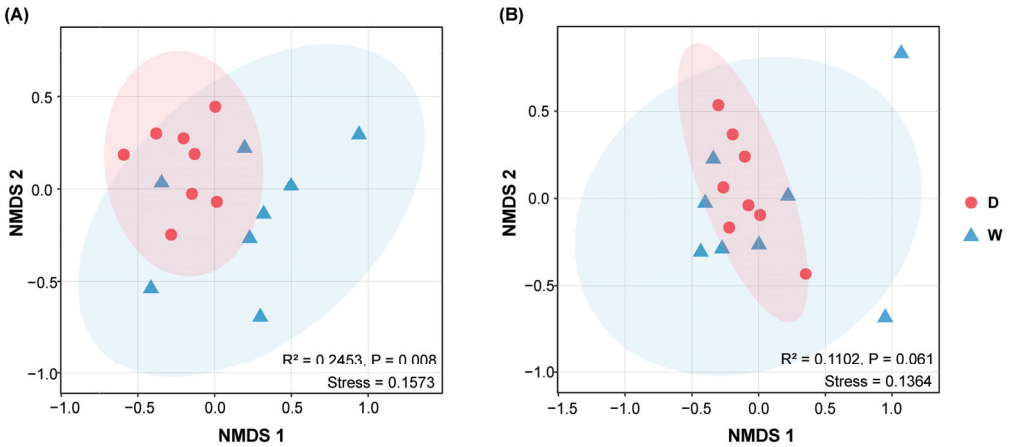


Figure 1. Non-metric multidimensional scaling (NMDS) plots comparing the (**A**) bacterial and (**B**) fungal communities in wild ("W") and domesticated ("D") wheat rhizosphere soils based on the pairwise Bray–Curtis distance.

3.2. Predicted Functions of the Microbial Communities

The potential function predicted by FAPROTAX analysis (Figure 2A) showed that in the bacterial community, chemoheterotrophy (especially aerobic chemoheterotrophy) was the most abundant, followed by ureolysis, aromatic compound degradation, and chitinolysis, whose average proportions were higher than 1%. Except for the function of chitinolysis, which accounted for a relatively higher proportion in the wild wheat rhizosphere, no significant difference was observed in other functions between the wild and domesticated wheats.

The FRI was applied to compare functional redundancy between the rhizosphere bacteria of the domesticated and wild wheat, revealing higher functional redundancy in the domesticated wheat than in the wild wheat (Figure 3A). Approximately 5909 functions from bacteria displayed higher functional redundancies in the domesticated rhizosphere samples, while only 1922 functions showed higher redundancy in the wild groups. The volcano plot indicated that wheat domestication significantly altered the functional genes in the rhizosphere soils (Figure 3B). For instance, the relative abundance of genes involved in the soil C cycle (e.g., K00171, K00172, K00169, and K10946) and N cycle (K01915) were enriched in the domesticated wheat soils.

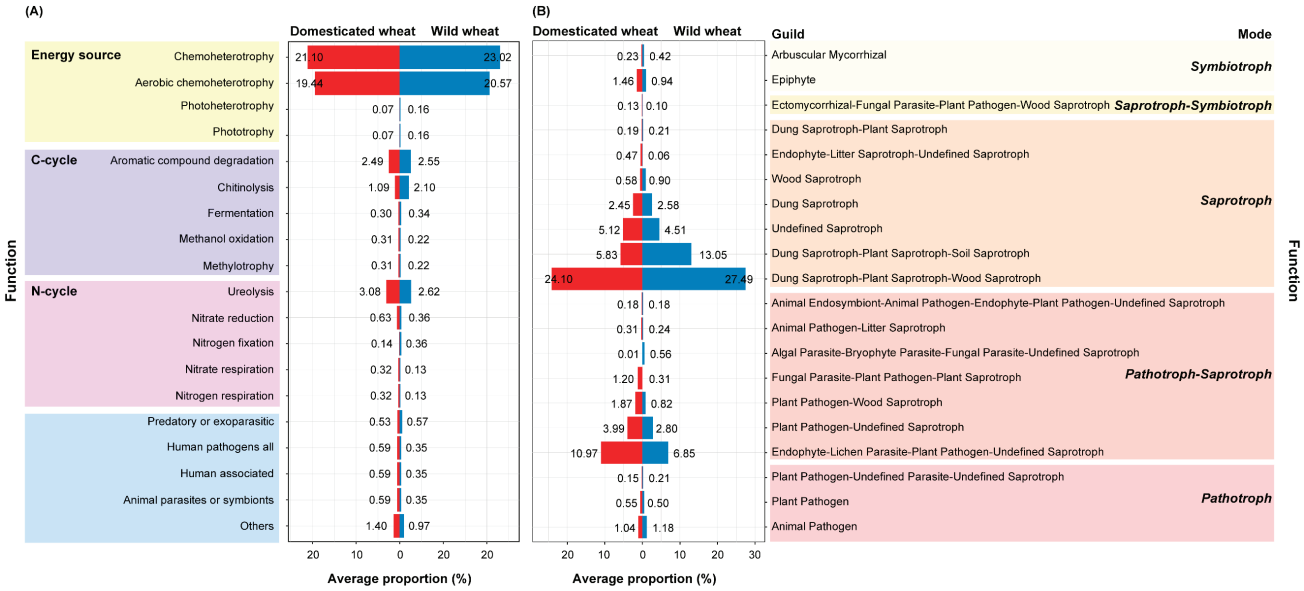


Figure 2. (**A**) Predicted functional profiles of the bacterial communities. Only the inferred functional groups with average proportions of ASVs greater than 0.1% are shown in the plot. (**B**) Predicted functional profiles of the fungal communities. Only the inferred functional groups with a high confidence (indicated as "highly probable" or "probable") and with average proportions of ASVs higher than 0.1% are shown in the plot.

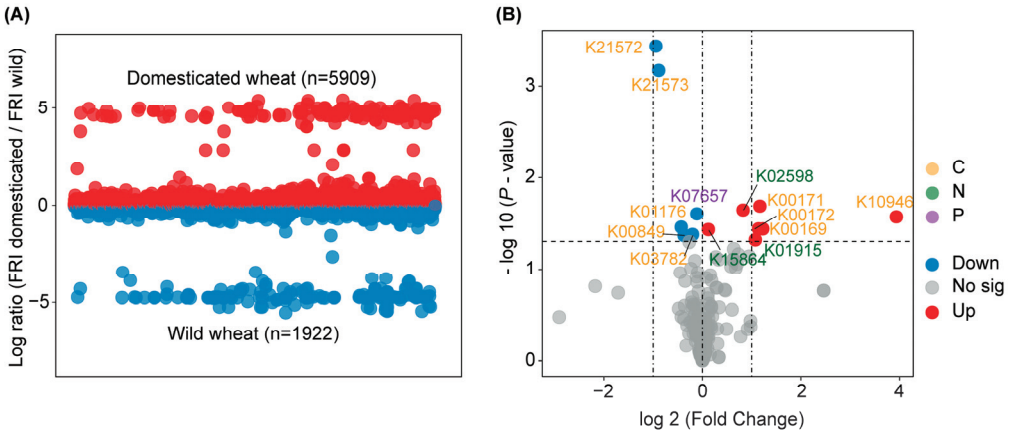


Figure 3. (**A**) Relative functional redundancy indices (FRI) in the rhizosphere of domesticated (red) and wild (blue) wheats, respectively. All predictions were implemented using a 97% similarity cut-off. A log ratio greater than 0 indicates that a function was more redundant in the domesticated wheat. (**B**) Volcano plot showing the difference in the relative abundance of functional genes involved in C, N, and P cycling between the rhizosphere of domesticated (red) and wild (blue) wheat.

For the fungal community, the results based on the FUNGuild database identified five trophic modes assigned to the samples (Figure 2B). The most abundant guild was Dung Saprotroph-Plant Saprotroph-Wood Saprotroph, followed by Dung Saprotroph-Plant Saprotroph-Soil Saprotroph and Endophyte-Lichen Parasite-Plant Pathogen-Undefined Saprotroph, for both wild and domesticated wheat. Among them, Endophyte-Lichen Parasite-Plant Pathogen-Undefined Saprotroph, Fungal Parasite Plant Pathogen Plant Saprotroph, Endophyte Litter Saprotroph Undefined Saprotroph, and Plant Pathogen-Wood Saprotroph accounted for a significantly higher proportion in the domesticated wheat than in the wild wheat ($p < 0.05$, tested by the Wilcoxon test).

3.3. Co-Occurrence Networks of Soil Microorganisms

In the bacteria–fungi networks, there were 591 nodes and 2056 edges in the domesticated wheat rhizosphere, compared to 591 nodes and 2204 edges in the wild wheat rhizosphere (Figure 4A). In the bacteria-bacteria networks, there were 284 nodes and 540 edges in the domesticated wheat rhizosphere, while the wild wheat rhizosphere had 287 nodes and 546 edges. The nodes in these networks were primarily affiliated with Pseudomonadota (Figure 4B). For the fungi-fungi networks, there were 275 nodes and 435 edges in the networks of the domesticated wheat rhizospheres, while there were 278 nodes and 493 edges in the wild wheat rhizospheres, with most of these nodes affiliated to Ascomycota (Figure 4C).

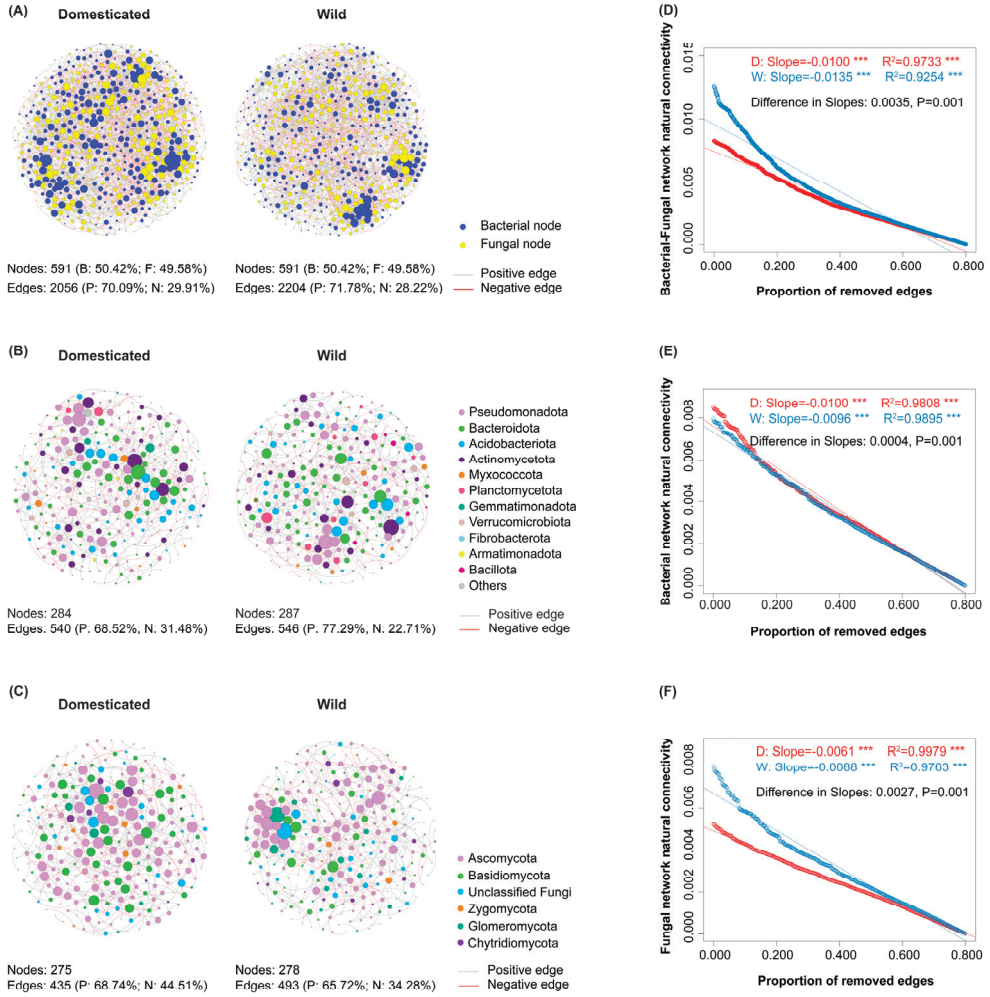


Figure 4. Networks and the stability of the network structures for microbial communities in rhizosphere soils of domesticated and wild wheat. (**A**) Bacteria–fungi networks based on top 300 abundant bacterial and fungal ASVs, (**B**) bacteria-bacteria network based on top 300 abundant bacterial ASVs, and (**C**) fungi-fungi network based on top 300 abundant fungal ASVs selected from rhizosphere soil of domesticated and wild wheat. A node represents a microbial ASV, with the size of each node being proportional to the degree and the color of each node representing bacterial or fungal phylum. An edge represents a strong ($|r| > 0.6$) and significant ($p < 0.01$) correlation between paired ASVs. (**D**) Stability for bacteria–fungi joint network, (**E**) bacteria-bacteria network, and (**F**) fungi-fungi networks. ***, $p < 0.001$ "W" represents wild and "D" represents domesticated wheat network.

Among all these networks, positive edges were more commonly observed than negative ones, indicating that positive cooperation predominantly characterized the connections

(Figure 4). Additionally, in the bacteria–fungi joint networks and the fungi-fungi networks, wild wheat rhizospheres had a significantly higher proportion of positive edges when compared to domesticated wheat rhizospheres (Supplementary Figure S3). However, except for the number of nodes and the proportions of negative/positive edges, there were no significant differences in the topological structure of the microbial networks for the bacterial and fungal communities in the domesticated and wild wheat rhizospheres.

We further tested the stability of the microbial networks by assessing the slopes of decreased natural connectivity with the removal of edges. This showed that the natural connectivity of both the joint and fungi-fungi networks decreased to a greater degree in the wild than in the domesticated wheat rhizospheres when the same proportion of edges were removed (Figure 4D–F), indicating greater network stability in the domesticated wheat, while the bacteria-bacteria networks were the opposite.

3.4. Keystone Species in Microbial Networks

For both the joint bacteria–fungi and fungi-only networks, there were more keystones present in the domesticated wheat rhizosphere (Supplementary Figure S4). In the bacteria–fungi networks, nearly half of the nodes were fungal ASVs (among 591 nodes in both the domesticated and wild wheat, a total of 293 nodes were fungal ASVs). However, only 8 and 13 fungal ASVs were keystones, with all of them functioning as connectors (Supplementary Table S2).

The role assumed by individual ASVs in the networks rarely overlapped between the domesticated and wild wheat rhizospheres. Only a few ASVs acted as keystones in the networks of both types of wheat. For example, in the joint bacteria–fungi networks, only two bacterial ASVs (B_ASV43 *Dyadobacter* and B_ASV55 unclassified *Comamonadaceae*) maintained their roles as connectors in both wheat types (Supplementary Table S2). Additionally, one bacterial module hub in the domesticated wheat rhizosphere (B_ASV17, unclassified *Chitinophagaceae*) transitioned to a connector role in the wild wheat rhizosphere. In the bacteria-only networks, the module hub B_ASV14 (*Altererythrobacter*) in the domesticated wheat rhizosphere shifted to being a connector in the wild wheat rhizosphere (Supplementary Table S3).

Only a small proportion of the keystone species in the community can be affiliated to any predicted ecological function (Supplementary Tables S2–S4). Among these keystone species, most of the bacteria were inferred to be related to aerobic chemoheterotrophy, while most of the fungi were saprotrophs (Supplementary Tables S2–S4). In addition, some bacteria (B_ASV110 and B_ASV41, for instance) involved in N cycling acted as connectors in the joint networks for the wild wheat rhizosphere.

3.5. Differences in the Microbial Assembly Processes in the Rhizosphere Soils of Wild and Domesticated Wheats

For the rhizosphere of both the wild and domesticated wheat, the pNST index revealed the dominance of a deterministic process in structuring both the bacterial and fungal communities (Figure 5A,B), with the median of the pNST value being less than 0.5, but there was no significant difference between the domesticated and wild wheats. The goodness-of-fit to the neutral model of the fungal communities was lower than that of the bacterial communities, and it was lower in the microbial communities of the wild wheat than of the domesticated wheat (Figure 5C–F).

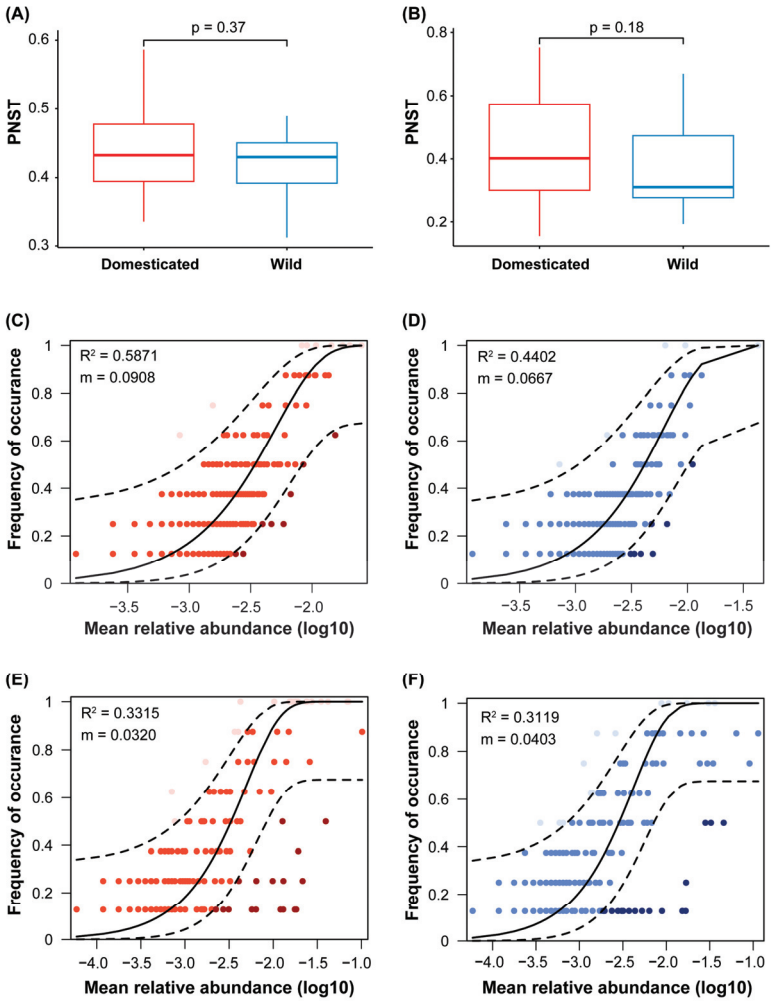


Figure 5. Phylogenetic normalized stochasticity ratio (pNST) for (**A**) bacterial and (**B**) fungal community in domesticated and wild wheat soils. The differences were compared using pairwise Wilcoxon tests. Neutral community model (NCM) plots for (**C**,**D**) bacterial and (**E**,**F**) fungal communities. Dashed lines indicate the 95% confidence intervals around all fitting statistics based on bootstrapping with 1000 bootstrap replicates. Points shown between the two dashed lines represent the operational taxonomic units (ASVs) with the frequency of occurrence within the 95% confidence intervals around the NCM prediction. ASVs that occurred more frequently than the value predicted by the model are shown in a lighter color, while those that occurred less frequently than predicted are shown in a darker color. R^2 represents the overall fit to the neutral model. The parameter "m" assesses the estimated migration rate.

4. Discussion

4.1. Similar Microbial Community Diversity of the Wild and Domesticated Wheat

We hypothesized that wheat domestication and subsequent breeding for commercial traits would have changed the microbiome composition, with the domesticated wheat ancestor harboring a less diverse rhizosphere microbiome. However, the comparison showed no significant difference in alpha diversity between the wild and domesticated wheat (Supplementary Figure S1). Furthermore, a significant difference was only observed in the bacterial community structure (Figure 1), while the relative abundance of fungal phyla did not differ significantly between the wild and domesticated wheat (Supplementary Figure S2B). The history of domestication in nutrient-enriched agricultural environments might be expected to have selected against heavy investment by the plant in AMF fungi.

For example, the ancient Glomeromycota families (e.g., Archaeosporaceae and Paraglomeraceae) were thought to be less beneficial for plant growth and nutrient uptake than more recent families (e.g., Glomeraceae) [56]. Here, there were no significant differences in either the relative abundance of Glomeromycota (Supplementary Figure S2B) or the symbiotroph guild predicted by FUNGuild (Figure 2B) between the wild and domesticated wheat. Similar results were also observed for some mutualistic bacterial groups, such as Rhizobium/Bradyrhizobium, further confirming the conserved nature of wheat microbiota despite the influence of domestication and hybridization.

The lack of differences in the rhizosphere microbial communities between the wild and domesticated species in this study may not only be due to differences in root secretions but also due to the growth stage of the plant, which can significantly impact the composition and diversity of the microbiome [16,57,58]. As shown by Gholizadeh et al. [58], the diversity and structure of the rhizosphere microbial community of wild and domesticated species differed more strikingly in early stages of growth than in later stages. The high-input field provided a favorable environment for microbial survival, enabling rapid colonization [59]. By the time of sampling, the C allocation would potentially have shifted from the belowground (i.e., roots/microbiome) to the developing wheat grains, resulting in the stabilization of the rhizosphere microbial community composition [16,58]. Furthermore, the presence of common microbiome members in the rhizosphere (e.g., Pseudomonadota, Bacteroidota, Actinomycetota, and Ascomycota) has been consistently observed in wheat and other crops, indicating the potential for the existence of a highly conserved, coevolved, and host-independent core microbial taxa that plays a role in facilitating microbial cooperation and maintaining crop fitness [60,61].

4.2. Functional Differences Between the Domesticated and Wild Wheat Rhizobiome

We hypothesized that the wild wheat would have a functionally integrated root microbiome in order to support a range of functions necessary for survival. The results showed that the predicted functions of the bacterial communities in the rhizosphere of the two wheats exhibited negligible compositional divergence (Figure 2A). However, the higher FRI values indicated that the domesticated rhizosphere bacteria had a greater number of redundant functions than the wild wheat (Figure 3A) [36]. High functional redundancy is crucial for maintaining ecological processes facing disturbance or species extinction, especially in maintaining ecosystem productivity, C sequestration, and nutrient cycling, which play an essential role in enhancing ecosystem resilience and stability [62,63]. Combining with the enriched C cycling genes in the domesticated wheat rhizosphere (Figure 3B), these results suggest that the bacterial members of the domesticated wheat rhizosphere soils underwent functional changes and adapted well to the microenvironment or substrate renewal in the habitat and to local agricultural practices [64].

Meanwhile, our results showed that domestication and associated agricultural practices may have reduced the ability of the domesticated wheat rhizosphere microbiota to naturally control fungal pathogens, since the relative abundance of inferred plant pathogenic fungi was higher among the fungal communities in the rhizosphere of the domesticated wheat than in the wild wheat (Figure 2B). Root exudates are important in shaping the rhizosphere the microbial community, with several compounds found in root exudates that may recruit beneficial bacteria or have an effect on the expression of bacterial antifungal biosynthetic genes, presumably as a plant systemic response to deal with pathogens [13]. According to Kapulnik and Kushnir [65] and Valente et al. [66], wild ancient wheat varieties were more capable of interacting with beneficial plant-growth-promoting rhizobacteria. The advancement of conventional agricultural techniques and alterations in plant phys-

iology and morphology throughout the process of domestication have also shaped the environmental guilds of the rhizosphere-associated fungal microbiome [67]. Protection by pesticides may make it unnecessary for the root systems of modern cultivars to continuously maintain this ability to recruit beneficial bacteria to resist pests and diseases, and frustratingly, it may have reduced crop resistance to potential biotic stresses [2]. As it is difficult to determine whether fungi are symbiotic or pathogenic merely based on taxonomy, these patterns need to be further investigated in future studies and inspire future breeding efforts to use rhizosphere microbial traits as indicators of crop development [20,39].

4.3. Similar Cooccurrence Network Pattern of Domesticated and Wild Wheat Rhizobiome

Despite its limitations, network analysis can help us understand the significance of rhizosphere microbes for plant growth [14]. We hypothesized that there would be greater network complexity and stability in the microbial community of the wild wheat rhizosphere compared to the domesticated wheat. However, our results showed that there was no significant difference in topological features except for fewer positive connections in the joint bacteria–fungi network and fungi-only network of the domesticated wheat than those of the wild wheat (Figure 4, Supplementary Figure S3). In addition, the joint bacteria–fungi network and fungi-only network of the domesticated wheat were more stable (Figure 4).

Despite the fact that some studies on soybean and rice [18,68] have previously found that wild ancestors of crop plants have more complex and tighter associations amongst the community of root-associated microorganisms, the extent to which rhizosphere microorganisms develop deleterious, beneficial, or neutral interactions with each other, and the density and complexity of the resulting interaction networks, depends on taxa richness, microbial abundance, and activity levels [11,69–71]. As mentioned above, the discrepancy in the diversity and composition of the rhizosphere microbes was negligible, and the microbial interaction network structures were inevitably similar.

One interesting difference, however, is the reduced proportion of positive connections in the joint bacteria–fungi network and the fungi-only network for the domesticated wheat (Supplementary Figure S3). Considering that crop domestication is a process driven by loss-of-function alleles and indels in plant genomes, domesticated wheat might have lost the genes responsible for mutualistic relationships with fungal species [72]. The ratio of negative associations to positive associations between taxa can be used as a property to predict the stability of co-occurrence networks, with positive relationships representing high niche overlap and negative relationships indicating divergent niches [73]. Positive interactions can destabilize microbial communities by creating positive feedback loops between taxa supporting each other's fitness [73]. Our results showing that the joint bacteria–fungi network and fungi-only network of the domesticated wheat with a smaller proportion of positive edges were more stable than those of the wild wheat also correspond to this viewpoint.

Our results showed that the domesticated wheat rhizo-biome harbored more keystone species than the networks of the wild wheat (Supplementary Figure S4). Keystone species are usually highly connected with other species within networks and potentially have a considerable influence on the entire microbial community [74,75]. Our results aligned with previous research suggesting that agricultural practice might affect the abundance of keystone taxa in rhizo-microbiome networks [75].

We also found that the representative ASVs for each keystone category in the domesticated and wild wheat networks were rarely the same. Each identifiable type of microorganism has multiple biogeochemical functions, and each function is often shared by different strains and species, leading to functional redundancy in microbial communities [76]. For

root-associated microorganisms, a variety of microorganisms may maintain biogeochemical processes by assuming various functional roles [77–79]. In addition, although taxonomic differences within individual functional groups do not appear to fluctuate significantly with soil and other environmental conditions, the functional potential of microbiota is thought to be closely related to environmental conditions (soil physico-chemical properties, plant genotype, and growth stage) [76,78,80]. Therefore, similar environments should have promoted similar microbial communities while allowing for taxonomic differences within individual functional groups.

4.4. Deterministic Processes Dominate Microbial Community Assembly for Both Domesticated and Wild Wheat Rhizosphere Soils

We had hypothesized that wild wheat would have a more functionally selected deterministic community structure in its rhizosphere. However, our analysis revealed that deterministic processes dominated community assemblies for both domesticated and wild wheat rhizobiomes (Figure 5), a finding which is consistent with studies on agricultural soils for domesticated wheat in northern [81] and eastern China [82,83].

It is important, however, to note that neither the wild nor the domesticated wheat in this study were growing in a soil that truly resembled the preagricultural state. It is known that rhizobiomes are influenced by interactions between plant genotype, soil, and environmental stresses [20,84], and in this study, the wild and domesticated plants were growing in a high-density wheat field in close proximity. In this wheat field setting, where they grew intermingled, both types of wheat would thus have experienced the same conditions, both abiotic and biotic, for example, enhanced water availability in deeper and well-conditioned soils, increased nutrient input from chemical fertilizer, and spraying with pesticides. According to the habitat and environmental filtering perspectives [81–83], a one-to-one match may exist between niche availability and community structure, which could explain the similarity in microbiomes between the domesticated and wild wheats. It is also important to note that the wild wheat population here has likely grown for many generations as a weed in a wheat field under high-intensity modern farming—a situation very different from those in which its own wild ancestors lived. The wild wheat population has been self-sowing and subject to essentially the same wheat field environment as domesticated wheat. In this sense, both the wild and domesticated wheats have likely experienced evolutionary selection under the high-nutrient and pesticide-protected conditions of modern intensive farming.

Nevertheless, despite the overall similarity, we did find a somewhat more prominent role of neutral processes in the assembly of the microbiota of domesticated wheat, and we propose that domestication may have relaxed selective processes in the assembly of the wheat microbiota. This finding suggests that, as expected, wild wheat does exert more selection and control on the composition of its rhizosphere microbiota [79]. In addition, future studies should examine the microbiomes of other plants (e.g., weeds) in the same field to gain a deeper insight into whether it is the plant type/genotype, soil characteristics, or other environmental stresses that drive the conserved microbiome structure.

5. Conclusions

Given the various studies demonstrating differences in root-associated microbiome between domesticated crops and their relatives, the findings from our comparison of two related wheats growing in the same field was surprising. In this context, the wheat rhizobiome appears to be highly conserved in community composition, despite the two lineages having been separate for around 10,000 years of breeding and selection by the

agricultural environment, as well as having incorporated other genomes (e.g., *Aegilops*) in hybridization events [85]. This lack of difference may be attributed to the fact that both the domesticated and the wild wheat grew in the same fields and were subject to similar selection pressures regarding their ability to support or suppress components of their microbiome. However, since the wild wheat itself is presumably well adapted to the crop field environment, its features may be more relevant to breeders. It remains possible that differences do exist at the root surface or within the root (the endosphere), but there are no strong indications of such differences in the rhizosphere. Meanwhile, our results revealed that the rhizosphere of domesticated wheat displayed higher functional redundancy, with a significant enrichment of genes involved in carbon and nitrogen cycling. Furthermore, a greater prevalence of inferred fungal pathogens was observed in the rhizosphere of domesticated wheat compared to that of wild wheat. This shift was likely due to hybridization and selective breeding during domestication, which may have raised a functional shift in the rhizosphere microbiome to help increase the crop's resource utilization efficiency while reducing the crop's native resistance to potential pathogens.

This study has deepened our understanding of the rhizosphere microorganisms on wheat by comparing domesticated wheat and its wild relative directly in a naturally agricultural field environment. It appears, from this study at least, that we should regard rhizosphere microbial traits as an indicator for the development of crops in future breeding work.

Supplementary Materials: The following supporting information can be downloaded at: https://www.mdpi.com/article/10.3390/jof11030168/s1. Figure S1: Alpha diversity including Chao 1, Richness, Simpson and Shannon indexes for bacterial (A) and fungal (B) communities; Figure S2: Boxplots comparing the relative abundances of most abundant bacterial (A) and fungal (B) phylum in rhizosphere soils of the wild wheat and domesticated wheat; Figure S3: Microbial network topologic feature comparison between domesticated and wild wheat; Figure S4: Keystone species in microbial networks. Table S1: Definitions of topological parameters; Table S2: Information of keystones in the bacteria-fungi joint networks in domesticated and wild wheat soils; Table S3: Information of keystones in the bacteria single networks in domesticated and wild wheat soils. Table S4: Information of keystones in the fungi single networks in domesticated and wild wheat soils.

Author Contributions: J.F.: formal analysis, methodology, visualization, writing—original draft, writing—review and editing. M.B.: investigation, resources, writing—original draft. A.D.: writing—review and editing. Z.L.: investigation, writing—review and editing. S.R.: conceptualization, supervision, writing—review and editing. B.S.: investigation. J.M.A.: conceptualization, funding acquisition, supervision, writing—review and editing. All authors have read and agreed to the published version of the manuscript.

Funding: This study was supported by the National Natural Science Foundation of China (32372058), Jiangsu Agricultural Biodiversity Cultivation and Utilization Research Center (0270756100ZX), and the Goldinger Trust—Jewish Federation of Delaware for promoting and expanding agricultural research for food and fiber and animal science in Israel.

Institutional Review Board Statement: Not applicable.

Informed Consent Statement: Not applicable.

Data Availability Statement: The obtained sequences were submitted to the NCBI Sequence Read Archive (SRA) with accession number PRJNA917337.

Conflicts of Interest: The authors have no relevant financial or non-financial interests to disclose.

References

1. Fragasso, M.; Iannucci, A.; Papa, R. Durum wheat and allelopathy: Toward wheat breeding for natural weed management. *Front. Plant Sci.* **2013**, *4*, 375. [CrossRef] [PubMed]
2. Abdullaeva, Y.; Ratering, S.; Rosado-Porto, D.; Ambika Manirajan, B.; Glatt, A.; Schnell, S.; Cardinale, M. Domestication caused taxonomical and functional shifts in the wheat rhizosphere microbiota, and weakened the natural bacterial biocontrol against fungal pathogens. *Microbiol. Res.* **2024**, *281*, 127601. [CrossRef]
3. Schmidhuber, J.; Tubiello, F.N. Global food security under climate change. *Proc. Natl. Acad. Sci. USA* **2007**, *104*, 19703–19708. [CrossRef]
4. Lobell, D.B.; Gourdji, S.M. The influence of climate change on global crop productivity. *Plant Physiol.* **2012**, *160*, 1686–1697. [CrossRef]
5. Shao, G.; Zhou, J.; Liu, B.; Alharbi, S.A.; Liu, E.; Kuzyakov, Y. Carbon footprint of maize-wheat cropping system after 40-year fertilization. *Sci. Total Environ.* **2024**, *926*, 172082. [CrossRef] [PubMed]
6. Abbo, S.; Pinhasi van-Oss, R.; Gopher, A.; Saranga, Y.; Ofner, I.; Peleg, Z. Plant domestication versus crop evolution: A conceptual framework for cereals and grain legumes. *Trends Plant Sci.* **2014**, *19*, 351–360. [CrossRef] [PubMed]
7. Purugganan, M.D. Evolutionary insights into the nature of plant domestication. *Curr. Biol.* **2019**, *29*, 705–714. [CrossRef]
8. Fitzpatrick, C.R.; Copeland, J.; Wang, P.W.; Guttman, D.S.; Kotanen, P.M.; Johnson, M.T. Assembly and ecological function of the root microbiome across angiosperm plant species. *Proc. Natl. Acad. Sci. USA* **2018**, *115*, 1157–1165. [CrossRef] [PubMed]
9. Sasse, J.; Martinoia, E.; Northen, T. Feed your friends: Do plant exudates shape the root microbiome? *Trends Plant. Sci.* **2018**, *23*, 25–41. [CrossRef] [PubMed]
10. Arif, I.; Batool, M.; Schenk, P.M. Plant microbiome engineering: Expected benefits for improved crop growth and resilience. *Trends Biotechnol.* **2020**, *38*, 1385–1396. [CrossRef] [PubMed]
11. Tkacz, A.; Pini, F.; Turner, T.R.; Bestion, E.; Simmonds, J.; Howell, P.; Greenland, A.; Cheema, J.; Emms, D.M.; Uauy, C. Agricultural selection of wheat has been shaped by plant-microbe interactions. *Front. Microbiol.* **2020**, *11*, 132. [CrossRef] [PubMed]
12. Preece, C.; Peñuelas, J. A return to the wild: Root exudates and food security. *Trends Plant Sci.* **2020**, *25*, 14–21. [CrossRef]
13. Pérez-Jaramillo, J.E.; Mendes, R.; Raaijmakers, J.M. Impact of plant domestication on rhizosphere microbiome assembly and functions. *Plant Mol. Biol.* **2016**, *90*, 635–644. [CrossRef] [PubMed]
14. Yue, H.; Yue, W.; Jiao, S.; Kim, H.; Lee, Y.-H.; Wei, G.; Song, W.; Shu, D. Plant domestication shapes rhizosphere microbiome assembly and metabolic functions. *Microbiome* **2023**, *11*, 70. [CrossRef] [PubMed]
15. Shenton, M.; Iwamoto, C.; Kurata, N.; Ikeo, K. Effect of wild and cultivated rice genotypes on rhizosphere bacterial community composition. *Rice* **2016**, *9*, 42. [CrossRef]
16. Pérez-Jaramillo, J.E.; Carrión, V.J.; Bosse, M.; Ferrão, L.F.; De Hollander, M.; Garcia, A.A.; Ramírez, C.A.; Mendes, R.; Raaijmakers, J.M. Linking rhizosphere microbiome composition of wild and domesticated Phaseolus vulgaris to genotypic and root phenotypic traits. *ISME J.* **2017**, *11*, 2244–2257. [CrossRef] [PubMed]
17. Pérez-Jaramillo, J.E.; de Hollander, M.; Ramírez, C.A.; Mendes, R.; Raaijmakers, J.M.; Carrión, V.J. Deciphering rhizosphere microbiome assembly of wild and modern common bean (*Phaseolus vulgaris*) in native and agricultural soils from Colombia. *Microbiome* **2019**, *7*, 114. [CrossRef] [PubMed]
18. Chang, J.; Sun, Y.; Tian, L.; Ji, L.; Luo, S.; Nasir, F.; Kuramae, E.E.; Tian, C. The structure of rhizosphere fungal communities of wild and domesticated rice: Changes in diversity and co-occurrence patterns. *Front. Microbiol.* **2021**, *12*, 610823. [CrossRef] [PubMed]
19. Bulgarelli, D.; Garrido-Oter, R.; Münch, P.C.; Weiman, A.; Dröge, J.; Pan, Y.; McHardy, A.C.; Schulze-Lefert, P. Structure and function of the bacterial root microbiota in wild and domesticated barley. *Cell Host Microbe* **2015**, *17*, 392–403. [CrossRef] [PubMed]
20. Leff, J.W.; Lynch, R.C.; Kane, N.C.; Fierer, N. Plant domestication and the assembly of bacterial and fungal communities associated with strains of the common sunflower, *Helianthus annuus*. *New Phytol.* **2017**, *214*, 412–423. [CrossRef] [PubMed]
21. Doebley, J.; Gaut, B.S.; Smith, B.D. The molecular genetics of crop domestication. *Cell* **2006**, *127*, 1309–1321. [CrossRef] [PubMed]
22. Purugganan, M.D.; Fuller, D.Q. The nature of selection during plant domestication. *Nature* **2009**, *457*, 843–848. [CrossRef]
23. Petersen, G.; Seberg, O.; Yde, M.; Berthelsen, K. Phylogenetic relationships of *Triticum* and *Aegilops* and evidence for the origin of the A, B, and D genomes of common wheat (*Triticum aestivum*). *Mol. Phylogenet. Evol.* **2006**, *39*, 70–82. [CrossRef]
24. Lev-Yadun, S.; Gopher, A.; Abbo, S. The Cradle of Agriculture. *Science* **2000**, *288*, 1602–1603. [CrossRef] [PubMed]
25. Gross, L. The Red Queen gets a new lease on life. *PLoS Biol.* **2006**, *4*, e285. [CrossRef] [PubMed]
26. Marcussen, T.; Sandve, S.R.; Heier, L.; Spannagl, M.; Pfeifer, M.; International Wheat Genome Sequencing Consortium; Jakobsen, K.S.; Wulff, B.B.; Steuernagel, B.; Mayer, K.F. Ancient hybridizations among the ancestral genomes of bread wheat. *Science* **2014**, *345*, 1250092. [CrossRef] [PubMed]
27. Quince, C.; Lanzen, A.; Davenport, R.J.; Turnbaugh, P.J. Removing noise from pyrosequenced amplicons. *BMC Bioinform.* **2011**, *12*, 38. [CrossRef]

28. Siddique, A.B.; Unterseher, M. A cost-effective and efficient strategy for Illumina sequencing of fungal communities: A case study of beech endophytes identified elevation as main explanatory factor for diversity and community composition. *Fungal Ecol.* **2016**, *20*, 175–185. [CrossRef]
29. Lundberg, D.S.; Yourstone, S.; Mieczkowski, P.; Jones, C.D.; Dangl, J.L. Practical innovations for high-throughput amplicon sequencing. *Nat. Methods* **2013**, *10*, 999–1002. [CrossRef]
30. Callahan, B.J.; McMurdie, P.J.; Rosen, M.J.; Han, A.W.; Johnson, A.J.; Holmes, S.P. DADA2: High-resolution sample inference from Illumina amplicon data. *Nat. Methods* **2016**, *13*, 581–583. [CrossRef] [PubMed]
31. Zhou, X.; Rahman, M.K.U.; Liu, J.; Wu, F. Soil acidification mediates changes in soil bacterial community assembly processes in response to agricultural intensification. *Environ. Microbiol.* **2021**, *23*, 4741–4755. [CrossRef] [PubMed]
32. Pedregosa, F.; Varoquaux, G.; Gramfort, A.; Michel, V.; Thirion, B.; Grisel, O.; Blondel, M.; Louppe, G.; Prettenhofer, P.; Weiss, R.; et al. Scikit-learn: Machine learning in Python. *arXiv* **2011**, arXiv:1201.0490.
33. Oksanen, J. *Vegan: An Introduction to Ordination*; University of Helsinki: Helsinki, Finland, 2008.
34. Anderson, M.J.; Walsh, D.C.I. PERMANOVA, ANOSIM, and the Mantel test in the face of heterogeneous dispersions: What null hypothesis are you testing? *Ecol. Monogr.* **2013**, *83*, 557–574. [CrossRef]
35. Louca, S.; Parfrey, L.W.; Doebeli, M. Decoupling function and taxonomy in the global ocean microbiome. *Science* **2016**, *353*, 1272–1277. [CrossRef]
36. Wemheuer, F.; Taylor, J.A.; Daniel, R.; Johnston, E.; Meinicke, P.; Thomas, T.; Wemheuer, B. Tax4Fun2: Prediction of habitat-specific functional profiles and functional redundancy based on 16S rRNA gene sequences. *Environ. Microbiome* **2020**, *15*, 11. [CrossRef]
37. Luo, W.; Wang, J.; Li, Y.; Wang, C.; Yang, S.; Jiao, S.; Wei, G.; Chen, W. Local domestication of soybean leads to strong root selection and diverse filtration of root-associated bacterial communities. *Plant Soil* **2022**, *480*, 439–455. [CrossRef]
38. Liu, L.; Gao, Y.; Gao, Z.; Zhu, L.; Yan, R.; Yang, W.; Yang, Y.; Liu, J. The core microbiota as a predictor of soil functional traits promotes soil nutrient cycling and wheat production in dryland farming. *Funct. Ecol.* **2023**, *37*, 2325–2337. [CrossRef]
39. Nguyen, N.H.; Song, Z.; Bates, S.T.; Branco, S.; Tedersoo, L.; Menke, J.; Schilling, J.S.; Kennedy, P.G. FUNGuild: An open annotation tool for parsing fungal community datasets by ecological guild. *Fungal Ecol.* **2016**, *20*, 241–248. [CrossRef]
40. Fan, K.; Delgado-Baquerizo, M.; Guo, X.; Wang, D.; Wu, Y.; Zhu, M.; Yu, W.; Yao, H.; Zhu, Y.G.; Chu, H. Suppressed N fixation and diazotrophs after four decades of fertilization. *Microbiome* **2019**, *7*, 143. [CrossRef]
41. Friedman, J.; Alm, E.J. Inferring correlation networks from genomic survey data. *PLoS Comput. Biol.* **2012**, *8*, e1002687. [CrossRef]
42. Jiao, S.; Xu, Y.; Zhang, J.; Hao, X.; Lu, Y. Core microbiota in agricultural soils and their potential associations with nutrient cycling. *mSystems* **2019**, *4*, e00313-18. [CrossRef]
43. Fruchterman, T. Graph drawing by force-directer placement. *Softw. Pract. Exp.* **1991**, *21*, 1129–1164. [CrossRef]
44. Csardi, G.; Nepusz, T. The igraph software package for complex network research. *Int. J. Complex Syst.* **2006**, *1695*, 1–9.
45. Deng, Y.; Jiang, Y.H.; Yang, Y.; He, Z.; Luo, F.; Zhou, J. Molecular ecological network analyses. *BMC Bioinform.* **2012**, *13*, 113. [CrossRef]
46. Ma, B.; Wang, H.Z.; Dsouza, M.; Lou, J.; He, Y.; Dai, Z.M.; Brookes, P.C.; Xu, J.M.; Gilbert, J.A. Geographic patterns of co-occurrence network topological features for soil microbiota at continental scale in eastern China. *ISME J.* **2016**, *10*, 1891–1901. [CrossRef] [PubMed]
47. Barberán, A.; Bates, S.T.; Casamayor, E.O.; Fierer, N. Using network analysis to explore co-occurrence patterns in soil microbial communities. *ISME J.* **2012**, *6*, 343–351. [CrossRef]
48. Banerjee, S.; Kirkby, C.A.; Schmutter, D.; Bissett, A.; Kirkegaard, J.A.; Richardson, A. Network analysis reveals functional redundancy and keystone taxa amongst bacterial and fungal communities during organic matter decomposition in an arable soil. *Soil Biol. Biochem.* **2016**, *97*, 188–198. [CrossRef]
49. Shi, Y.; Li, Y.; Yang, T.; Chu, H. Threshold effects of soil pH on microbial co-occurrence structure in acidic and alkaline arable lands. *Sci. Total Environ.* **2021**, *800*, 149592. [CrossRef] [PubMed]
50. Peng, G.S.; Wu, J. Optimal network topology for structural robustness based on natural connectivity. *Phys. A* **2016**, *443*, 212–220. [CrossRef]
51. Wu, M.H.; Chen, S.Y.; Chen, J.W.; Xue, K.; Chen, S.L.; Wang, X.M.; Chen, T.; Kang, S.C.; Rui, J.P.; Thies, J.E. Reduced microbial stability in the active layer is associated with carbon loss under alpine permafrost degradation. *Proc. Natl. Acad. Sci. USA* **2021**, *118*, e2025321118. [CrossRef]
52. Nekola, J.C.; White, P.S. The distance decay of similarity in biogeography and ecology. *J. Biogeogr.* **1999**, *26*, 867–878. [CrossRef]
53. Yuan, M.M.; Guo, X.; Wu, L.; Zhang, Y.; Xiao, N.; Ning, D.; Shi, Z.; Zhou, X.; Wu, L.; Yang, Y. Climate warming enhances microbial network complexity and stability. *Nat. Clim. Chang.* **2021**, *11*, 343–348. [CrossRef]
54. Ning, D.L.; Deng, Y.; Tiedje, J.M.; Zhou, J.Z. A general framework for quantitatively assessing ecological stochasticity. *Proc. Natl. Acad. Sci. USA* **2019**, *116*, 16892–16898. [CrossRef]

55. Chen, W.D.; Ren, K.X.; Isabwe, A.; Chen, H.H.; Liu, M.; Yang, J. Stochastic processes shape microeukaryotic community assembly in a subtropical river across wet and dry seasons. *Microbiome* **2019**, *7*, 148.
56. Säle, V.; Palenzuela, J.; Azcón-Aguilar, C.; Sánchez-Castro, I.; da Silva, G.A.; Seitz, B.; Sieverding, E.; van der Heijden, M.G.A.; Oehl, F. Ancient lineages of arbuscular mycorrhizal fungi provide little plant benefit. *Mycorrhiza* **2021**, *31*, 559–576. [CrossRef]
57. Iannucci, A.; Fragasso, M.; Beleggia, R.; Nigro, F.; Papa, R. Evolution of the crop rhizosphere: Impact of domestication on root exudates in tetraploid wheat (*Triticum turgidum* L.). *Front. Plant Sci.* **2017**, *8*, 2124. [CrossRef] [PubMed]
58. Gholizadeh, S.; Mohammadi, S.A.; Salekdeh, G.H. Changes in root microbiome during wheat evolution. *BMC Microbiol.* **2022**, *22*, 64. [CrossRef] [PubMed]
59. Edwards, J.; Johnson, C.; Santos-Medellín, C.; Lurie, E.; Podishetty, N.K.; Bhatnagar, S.; Eisen, J.A.; Sundaresan, V. Structure, variation, and assembly of the root-associated microbiomes of rice. *Proc. Natl. Acad. Sci. USA* **2015**, *112*, 911–920. [CrossRef] [PubMed]
60. Hassani, M.A.; Durán, P.; Hacquard, S. Microbial interactions within the plant holobiont. *Microbiome* **2018**, *6*, 58. [CrossRef] [PubMed]
61. Guo, J.; Ling, N.; Li, Y.; Li, K.; Ning, H.; Shen, Q.; Guo, S.; Vandenkoornhuyse, P. Seed-borne, endospheric and rhizospheric core microbiota as predictors of plant functional traits across rice cultivars are dominated by deterministic processes. *New Phytol.* **2021**, *230*, 2047–2060. [CrossRef] [PubMed]
62. Biggs, C.R.; Yeager, L.A.; Bolser, D.G.; Bonsell, C.; Dichiera, A.M.; Hou, Z.; Keyser, S.R.; Khursigara, A.J.; Lu, K.; Muth, A.F.; et al. Does functional redundancy affect ecological stability and resilience? a review and meta-analysis. *Ecosphere* **2020**, *11*, e03184. [CrossRef]
63. de Bello, F.; Lavorel, S.; Hallett, L.M.; Valencia, E.; Garnier, E.; Roscher, C.; Conti, L.; Galland, T.; Goberna, M.; Májeková, M.; et al. Functional trait effects on ecosystem stability: Assembling the jigsaw puzzle. *Trends Ecol. Evol.* **2021**, *36*, 822–836. [CrossRef]
64. Wang, Y.; Zou, Q. Deciphering microbial adaptation in the rhizosphere: Insights into niche preference, functional profiles, and cross-kingdom co-occurrences. *Microb. Ecol.* **2024**, *87*, 74. [CrossRef] [PubMed]
65. Kapulnik, Y.; Kushnir, U. Growth dependency of wild, primitive and modern cultivated wheat lines on vesicular-arbuscular mycorrhiza fungi. *Euphytica* **1991**, *56*, 27–36. [CrossRef]
66. Valente, J.; Gerin, F.; Le Gouis, J.; Moënne-Loccoz, Y.; Prigent-Combaret, C. Ancient wheat varieties have a higher ability to interact with plant growth-promoting rhizobacteria. *Plant Cell Environ.* **2020**, *43*, 246–260. [CrossRef]
67. Spor, A.; Roucou, A.; Mounier, A.; Bru, D.; Breuil, M.-C.; Fort, F.; Vile, D.; Roumet, P.; Philippot, L.; Violle, C. Domestication-driven changes in plant traits associated with changes in the assembly of the rhizosphere microbiota in tetraploid wheat. *Sci. Rep.* **2020**, *10*, 12234. [CrossRef] [PubMed]
68. Shi, S.; Chang, J.; Tian, L.; Nasir, F.; Ji, L.; Li, X.; Tian, C. Comparative analysis of the rhizomicrobiome of the wild versus cultivated crop: Insights from rice and soybean. *Arch. Microbiol.* **2019**, *201*, 879–888. [CrossRef]
69. Finlay, B.J.; Maberly, S.C.; Cooper, J.I. Microbial Diversity and Ecosystem Function. *Oikos* **1997**, *80*, 209–213. [CrossRef]
70. Fuhrman, J.A. Microbial community structure and its functional implications. *Nature* **2009**, *459*, 193–199. [CrossRef] [PubMed]
71. Gruet, C.; Muller, D.; Moënne-Loccoz, Y. Significance of the diversification of wheat species for the assembly and functioning of the root-associated microbiome. *Front. Microbiol.* **2021**, *12*, 782135. [CrossRef] [PubMed]
72. Meyer, R.S.; Purugganan, M.D. Evolution of crop species: Genetics of domestication and diversification. *Nat. Rev. Genet.* **2013**, *14*, 840–852. [CrossRef]
73. Hernandez, D.J.; David, A.S.; Menges, E.S.; Searcy, C.A.; Afkhami, M.E. Environmental stress destabilizes microbial networks. *ISME J.* **2021**, *15*, 1722–1734. [CrossRef] [PubMed]
74. Agler, M.T.; Ruhe, J.; Kroll, S.; Morhenn, C.; Kim, S.T.; Weigel, D.; Kemen, E.M. Microbial hub taxa link host and abiotic factors to plant microbiome variation. *PLoS Biol.* **2016**, *14*, e1002352. [CrossRef] [PubMed]
75. Banerjee, S.; Walder, F.; Büchi, L.; Meyer, M.; Held, A.Y.; Gattinger, A.; Keller, T.; Charles, R.; van der Heijden, M.G. Agricultural intensification reduces microbial network complexity and the abundance of keystone taxa in roots. *ISME J.* **2019**, *13*, 1722–1736. [CrossRef] [PubMed]
76. Louca, S.; Jacques, S.M.S.; Pires, A.P.F.; Leal, J.S.; Srivastava, D.S.; Parfrey, L.W.; Farjalla, V.F.; Doebeli, M. High taxonomic variability despite stable functional structure across microbial communities. *Nat. Ecol. Evol.* **2016**, *1*, 0015. [CrossRef] [PubMed]
77. Vandenkoornhuyse, P.; Quaiser, A.; Duhamel, M.; Le Van, A.; Dufresne, A. The importance of the microbiome of the plant holobiont. *New Phytol.* **2015**, *206*, 1196–1206. [CrossRef] [PubMed]
78. Lemanceau, P.; Blouin, M.; Muller, D.; Moënne-Loccoz, Y. Let the core microbiota be functional. *Trends Plant Sci.* **2017**, *22*, 583–595. [CrossRef] [PubMed]
79. Hassani, M.A.; Özkurt, E.; Franzenburg, S.; Stukenbrock, E.H. Ecological assembly processes of the bacterial and fungal microbiota of wild and domesticated wheat species. *Phytobiomes J.* **2020**, *4*, 217–224. [CrossRef]

80. Guo, X.; Zhou, X.; Hale, L.; Yuan, M.; Feng, J.; Ning, D.; Shi, Z.; Qin, Y.; Liu, F.; Wu, L.; et al. Taxonomic and functional responses of soil microbial communities to annual removal of aboveground plant biomass. *Front. Microbiol.* **2018**, *9*, 954. [CrossRef]
81. Shi, Y.; Li, Y.; Xiang, X.; Sun, R.; Yang, T.; He, D.; Zhang, K.; Ni, Y.; Zhu, Y.G.; Adams, J.M. Spatial scale affects the relative role of stochasticity versus determinism in soil bacterial communities in wheat fields across the North China Plain. *Microbiome* **2018**, *6*, 27. [CrossRef]
82. Feng, M.; Tripathi, B.M.; Shi, Y.; Adams, J.M.; Zhu, Y.G.; Chu, H. Interpreting distance-decay pattern of soil bacteria via quantifying the assembly processes at multiple spatial scales. *MicrobiologyOpen* **2019**, *8*, e00851. [CrossRef]
83. Jiao, S.; Lu, Y. Abundant fungi adapt to broader environmental gradients than rare fungi in agricultural fields. *Global Chang. Biol.* **2020**, *26*, 4506–4520. [CrossRef] [PubMed]
84. Tkacz, A.; Cheema, J.; Chandra, G.; Grant, A.; Poole, P.S. Stability and succession of the rhizosphere microbiota depends upon plant type and soil composition. *ISME J.* **2015**, *9*, 2349–2359. [CrossRef] [PubMed]
85. Zhang, Y.; Fan, C.; Chen, Y.; Wang, R.R.C.; Zhang, X.; Han, F.; Hu, Z. Genome evolution during bread wheat formation unveiled by the distribution dynamics of SSR sequences on chromosomes using FISH. *BMC Genom.* **2021**, *22*, 55. [CrossRef]

Disclaimer/Publisher's Note: The statements, opinions and data contained in all publications are solely those of the individual author(s) and contributor(s) and not of MDPI and/or the editor(s). MDPI and/or the editor(s) disclaim responsibility for any injury to people or property resulting from any ideas, methods, instructions or products referred to in the content.

Journal of *Fungi*

MDPI

Article

Distribution Pattern and Assembly Process of Fungal Communities Along Altitude Gradient in Sediments of the Yellow River Basin

Kang Fang [1], Guoce Xu [1,*], Xin Chen [1], Jing Li [1], Yuting Cheng [2] and Yifan Cheng [1]

[1] State Key Laboratory of Water Engineering Ecology and Environment in Arid Area, Xi'an University of Technology, Xi'an 710048, China; kangjie5065@163.com (K.F.); cx852329@163.com (X.C.); lijing8615@163.com (J.L.); 15369869675@163.com (Y.C.)
[2] Geology and Environment, Xi'an University of Science and Technology, Xi'an 710048, China; chengyutingstar@163.com
* Correspondence: xuguoce_x@163.com

Abstract: Microorganisms have a profound impact on the stability and ecological health of aquatic environments. Fungi, as important components of river ecosystems, play critical roles as decomposers and symbionts. A comprehensive understanding of the mechanisms underlying fungal community assembly is essential for the effective conservation and management of river ecosystems. However, the distribution patterns and assembly process of fungal communities along elevation gradients in river sediments remain poorly understood. In this study, ITS amplicon sequencing, a neutral community model, and a null model were employed to analyze the distribution patterns and assembly processes of fungal communities in sediments along the altitudinal gradient of the Yellow River. The results indicated that Ascomycota (47.79%) and Basidiomycota (15.68%) were identified as the dominant phyla in the sediments, collectively accounting for 63.47% of the total relative abundance of the community. In the three different altitudinal gradients, the fungal community diversity (Shannon) showed a gradually decreasing trend with increasing altitude. The co-line networks of fungal communities exhibited positive interactions and had more complex and compact networks in the sediments of the Tibetan Plateau area (YRA). Environmental factors in the sediments played an important role in shaping the structure of fungal communities, with lead (Pb), total nitrogen (TN), silt, and total organic carbon (TOC) being the main factors driving changes in community structure, contributing 15.5%, 12.3%, 10.7%, and 10.2%, respectively. In the community assembly process, deterministic processes were found to dominate, with homogenizing selection contributing the most (69.66%). These research results help us understand the distribution patterns of fungal communities along altitudinal gradients and the mechanisms of community assembly, and also provide a scientific basis for biodiversity conservation and the rational use of biological resources.

Keywords: altitudinal gradient; fungal community; distribution pattern; assembly process; Yellow River basin

1. Introduction

Rivers are key components of the hydrological cycle, providing indispensable water resources for industrial and agricultural activities [1]. However, aquatic ecosystems have

been severely impacted by the intensification of human activities and the disruptions caused by global environmental changes [2,3]. Microorganisms serve as decomposers in aquatic ecosystems, playing a crucial role in maintaining structural and functional stability [3,4]. Fungi represent a significant component of microbial communities, comprising more than 140,000 species, and exhibit the highest diversity within the eukaryotic domain [5]. Fungal communities are widely distributed across diverse habitats, including freshwater, marine, and terrestrial environments [4,6,7]. Fungal communities can act as decomposers and facilitators in the cycling of organic matter, functioning both as parasites/pathogens and as symbionts with higher trophic organisms to participate in material cycling [8–10]. As fungal communities participate in diverse ecological processes, variations in their composition can provide valuable insights for assessing river water quality and ecosystem health [11,12].

In order to adapt to the stresses brought about by environmental change, microorganisms often develop unique community structures under the influence of a variety of factors [13]. The community assembly process of microorganisms refers to the process in which microorganisms interact through different ecological and evolutionary processes under specific environmental conditions to ultimately form a stable community [14]. The community assembly process has been extensively applied in microbial research [1,15–19]. Community assembly process research seeks to distinguish and quantify ecological processes, using statistical analysis, model inference, and network analysis methods to explain microbial community responses to disturbances, which helps us to understand the mechanisms maintaining microbial community stability [20]. Deterministic and stochastic processes are two important theories to explain species coexistence. Both of them jointly affect the assembly process of microbial communities [16,21,22], but the relative importance of these two mechanisms in the community assembly process varies among different ecosystems. The assembly mechanisms of fungal communities involve multiple ecological processes, including selection, dispersal, speciation, and drift [23]. In recent years, driven by advancements in high-throughput sequencing technologies and bioinformatics, significant progress has been made in the study of fungal community assembly mechanisms. It is not clear whether the community distribution pattern and community building mechanism of fungal communities in sediments of the Yellow River Basin differ from those of other rivers under differences in elevation gradients.

The Yellow River is the second longest river in China, and for thousands of years it has been the fulcrum of the development and progress of Chinese civilization. The Yellow River is famous for its high sediment content, and with severe sedimentation and unpredictable channel changes, the ecological environment within the basin is highly sensitive and fragile [24,25]. The Yellow River Basin is excellent to study microbial communities due to its complex geomorphology and diverse sedimentary environments. Some studies have been conducted on the Yellow River Basin, showing that there are differences in bacteria and fungi in the sediments of the Yellow River oxbow lakes at three successional stages [24]; the dominant bacterial phyla in the sediments of the Yellow River are Proteobacteria, Firmicutes, and Bacteroidetes [26]; water temperature (WT), electrical conductivity (EC) and NH_4^+-N are factors contributing to the differences in microbial structure in Yellow River water and the sediment column in the Jinan section [27]. Although several studies on microbial communities in the Yellow River Basin have been conducted, most have focused on specific sections or tributaries, covering a relatively limited scope. There are few reports on the distribution patterns and assembly mechanisms of fungal communities in sediments across the entire basin.

In this study, ITS high-throughput sequencing was employed to investigate fungal community distribution patterns and assembly mechanisms in sediments across elevational

gradients within the Yellow River Basin. The study aims to determine the following: (1) the characteristics of fungal communities in sediments at different altitudinal gradients; (2) distribution patterns of fungal communities in sediments along elevational gradients; and (3) assembly processes of fungal communities in sediments.

2. Materials and Methods

2.1. Study Area

The Yellow River is China's second-longest watercourse (5464 km), originating from the Yoguzonglei Basin in the northern foothills of the Ba Yan Ka La Mountains on the Qinghai–Tibet Plateau, and crossing the three terraces from west to east, it flows through a number of geomorphologic units before being injected into the Bohai Sea in Kenli County, Shandong Province. The basin area is 795,000 km^2 (32°10′~41°50′ N, 95°53′~119°05′ E), and belongs to a typical transition zone between a monsoon and continental climate [28], with an annual average temperature ranging from −4 to 14 °C. Precipitation in the basin is unevenly distributed in time and space, mainly concentrated in July and August, with amounts ranging from 140 mm per year in the northern part of the basin to 1100 mm per year in the eastern part and an average annual precipitation of 495.6 mm [29]. Forty-four sampling sites were arranged in the Yellow River Basin (Figure 1), and the sampling sites were categorized according to the elevation gradient: the YRA group (1600–4500 m, Qinghai–Tibetan Plateau area), YRB group (150–1600 m, Loess Plateau area), and YRC group (<150 m, Yellow-Huai-Hai Plain area).

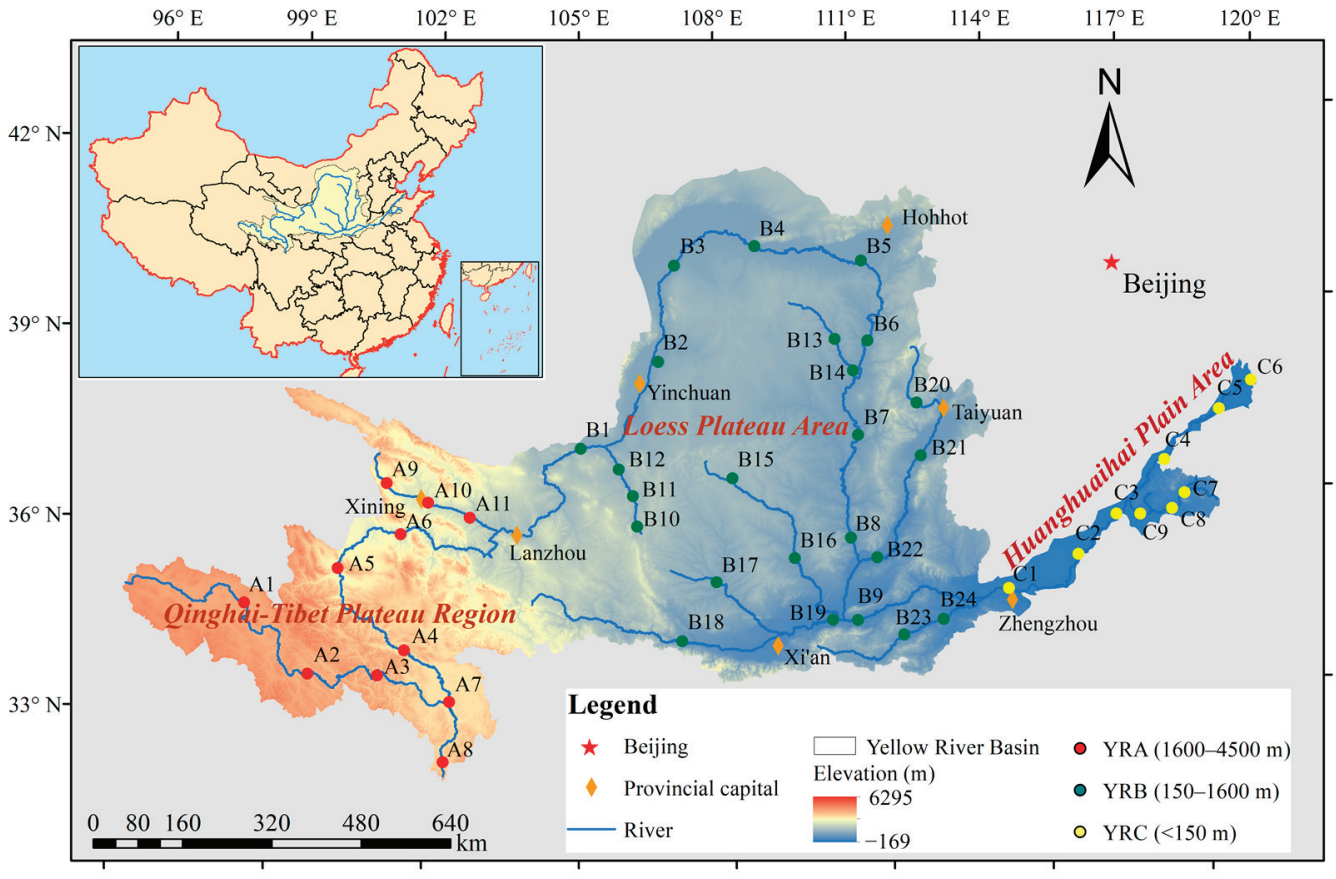


Figure 1. Schematic diagram of the Yellow River Basin and sampling points.

2.2. Sample Collection and Analysis

Surface sediment samples (500 g) were collected from the main stem and major tributaries of the Yellow River Basin during July and August 2022 using a grab sediment sampler. Following collection, a portion of the samples was transferred into 10 mL sterile centrifuge tubes for fungal community composition analysis, while the remainder was preserved in sterile sampling bags for subsequent physicochemical characterization. The coordinates and elevation of the sampling sites were recorded using a GPS locator. A fully automated intermittent chemistry analyzer (SmartChem 200, AMS Allinace, Rome, Italy) was used for the determination of total nitrogen (TN), ammonia nitrogen (NH_4^+-N), nitrate nitrogen (NO_3^--N), and total phosphorus (TP) in sediments. A Malvern laser particle sizer (Malvern Instruments, Malvern, UK) was used to determine sediment particle size. An organic carbon analyzer (multi N/C® 3100, Jena, Germany) was used to determine the total organic carbon (TOC) content in sediments. Following acid digestion, the concentrations of heavy metals (Cr, Ni, Cu, Zn, As, Cd, Pb) were measured by inductively coupled plasma mass spectrometry (iCAP Q, Thermo Fisher Scientific, Waltham, MA, USA).

2.3. High-Throughput Sequencing

DNA from the samples was extracted following the guidelines provided by the Soil DNA Rapid Extraction Kit (MP Biomedicals, Santa Ana, CA, USA), followed by qualitative assessment through 1% agarose gel electrophoresis. The amplification of the fungal ITS region was performed using the universal primers ITS1F_ITS2R [9,25]. The resulting PCR products were then recovered from 2% agarose gel and purified with a DNA gel extraction kit [25,30]. Additional methodological details are available in the Supplementary Materials. DNA extraction and sequencing were entrusted to Shenzhen Microman Technology Group Co. (Shenzhen, China) (www.bioincloud.tech).

2.4. Data Statistics and Microbial Analysis

Statistical analyses were conducted using SPSS 23.0 (IBM Corp.) and Microsoft Excel 2010, with significance determined through one-way analysis of variance (ANOVA) followed by Tukey's post hoc tests ($p < 0.05$). Community alpha-diversity indices (Shannon and Simpson) were calculated alongside non-metric multidimensional scaling (NMDS) and analysis of similarity (ANOSIM) using the Vegan package (v2.6-4) in R (v4.2.1). Distance–decay relationships were quantified through geospatial analysis implemented with the vegan (v2.6-4) and geosphere (v1.5-18) packages. β-diversity patterns were assessed based on Bray–Curtis dissimilarity matrices using the NST package (v1.2.1). Neutral community modeling was performed using the "Hmisc" package. Redundancy analysis was performed using Canoco.5 to explore the effect of environmental factors on fungal communities. Visualization of co-occurrence networks was implemented in Gephi (0.10.1). The location map of the study area and the sampling site diagram were drawn using ArcMap 10.2.

3. Results

3.1. Species Composition and Diversity of Fungal Communities

High-throughput ITS sequencing was conducted on fungal communities in sedimentary samples, with the relative abundance distributions of the top ten phyla and genera presented in Figure 2. Through taxonomic abundance analysis, 23 phyla and 674 genera were identified through species abundance analysis and annotation. In the taxonomic hierarchy, microbial groups with lower abundance rankings were classified as "other". The results showed that 0.28% and 28.23% of fungi were classified as "other" at the phylum and genus levels, respectively. In addition, the number of ASVs (Amplicon Sequence

Variants) unique to fungal communities in YRA, YRB, and YRC were 2930, 5991, and 1670, respectively, with 280 ASVs shared among the three altitudinal regions (Figure S3).

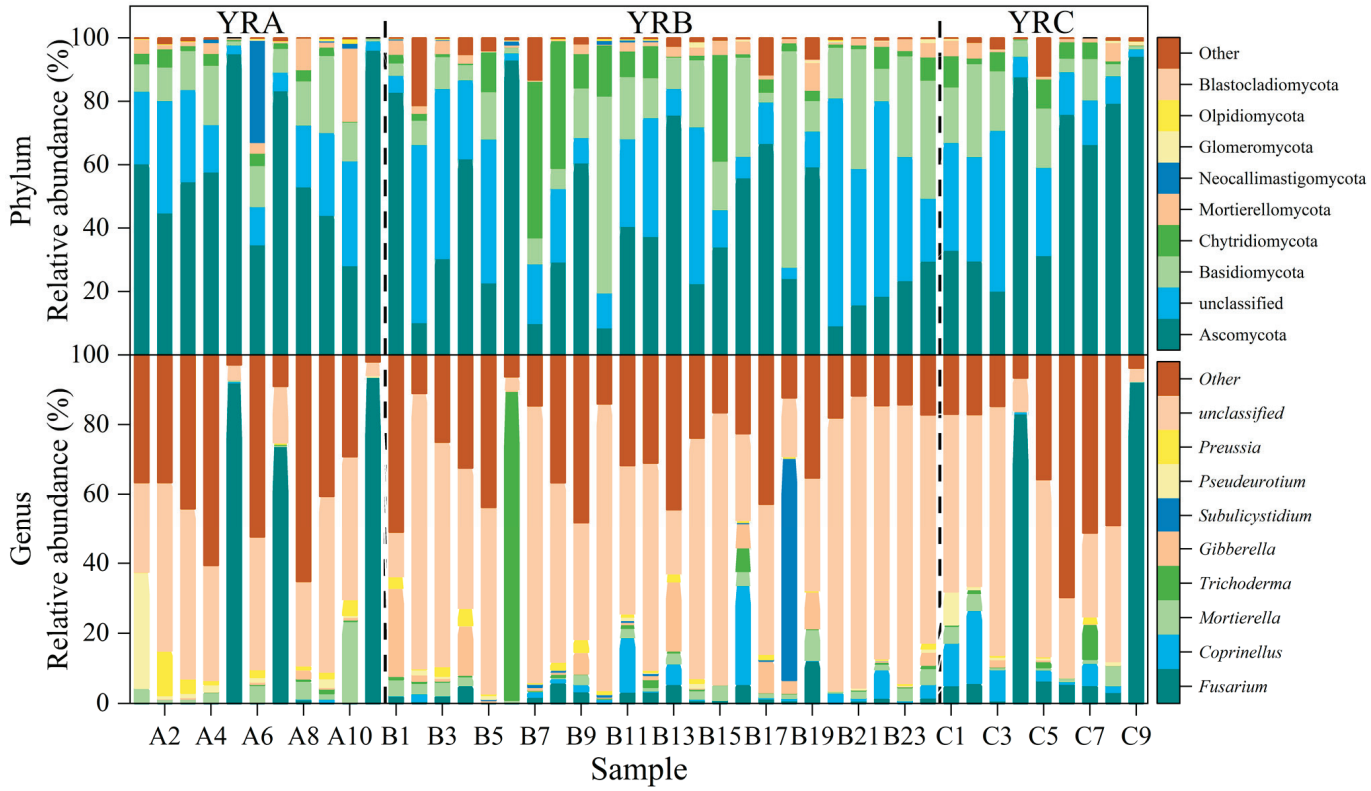


Figure 2. Characterization of fungal communities in Yellow River sediments.

The fungal communities were composed of Ascomycota (47.79%), unclassified (23.54%), Basidiomycota (15.68%), Chytridiomycota (6.47%), Mortierellomycota (2.68%), and Neocallimastigomycota (1.24%) (Figure 2). Ascomycota and Basidiomycota were the first and second dominant phyla in sediments, respectively, with Ascomycota having abundances of 58.53%, 38.64%, and 57.61% in YRA, YRB, and YRC, respectively; Basidiomycota had abundances of 18.25%, 26.89%, and 21.08% in YRA, YRB, and YRC, respectively. In addition, the abundance of Chytridiomycota in B7, B8, and B15 of the YRB group was significantly higher than in other sampling sites, with abundances of 53.99%, 39.17%, and 33.93%, respectively; in the YRA group, the abundance of Neocallimastigomycota was significantly higher than in other sampling sites, with an abundance as high as 47.47%.

Fungal community composition at the genus level was characterized by unclassified taxa (43.65%), *Fusarium* (12.10%), *Coprinellus* (2.98%), *Mortierella* (2.81%), *Trichoderma* (2.79%), and *Gibberella* (2.62%) in descending order of relative abundance. *Fusarium* was the dominant genus in the fungal community, with abundances of 23.88%, 2.56%, and 23.13% in YRA, YRB, and YRC, respectively; the abundance in YRA and YRC was significantly higher than that in YRB ($p < 0.05$). In addition, the relative abundance of *Fusarium* was higher in A5, A7, A11, C4, and C9 than in other sample sites ($p < 0.05$), whereas the abundance of *Trichoderma* was the highest in sample site B6, with an abundance of 88.69%.

A gradual decline in the Shannon diversity index was observed with increasing altitude (Figure 3), whereas the Simpson diversity index demonstrated an inverse pattern in its correlation with elevation. The Shannon diversity index was recorded at 5.38 in YRA. In comparison to YRA, elevations YRB and YRC exhibited increases of 3.35% and 21.56%, respectively.

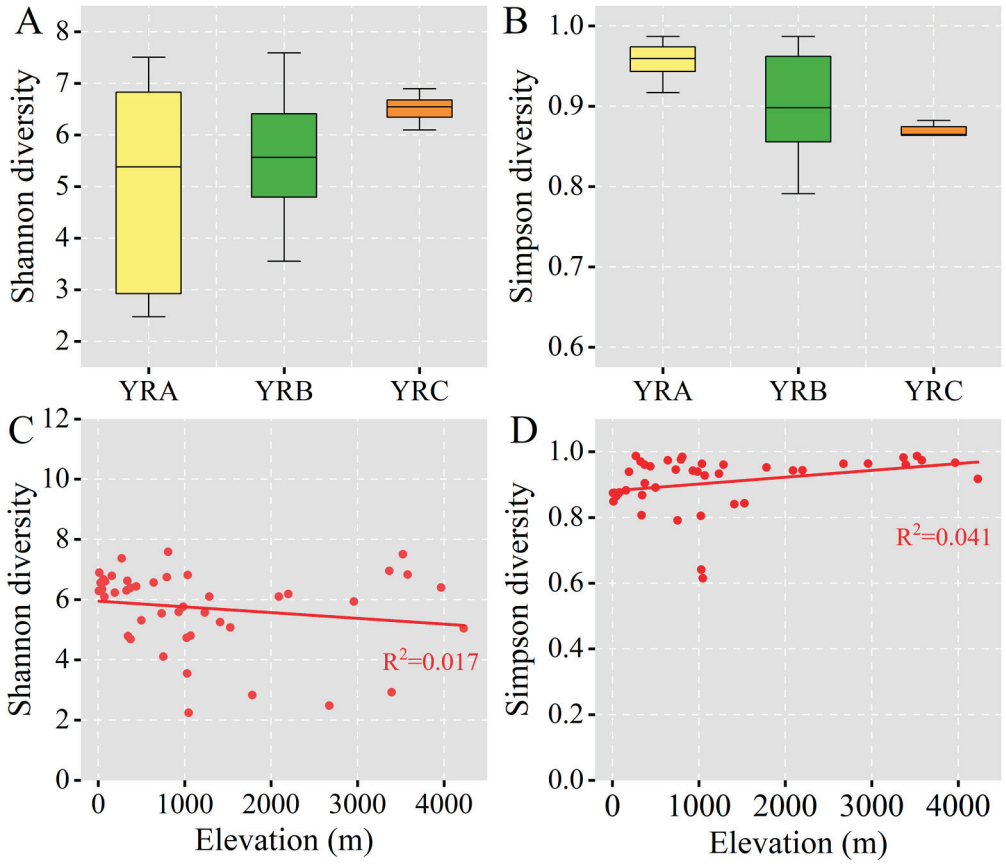


Figure 3. α-diversity of fungal community. (**A**) Distribution characteristics of fungal community Shannon diversity along the altitudinal gradient. (**B**) Distribution characteristics of fungal community Simpson diversity along the altitudinal gradient. (**C**) Variation characteristics of fungal community Shannon diversity with altitude. (**D**) Variation characteristics of fungal community Simpson diversity with altitude.

3.2. Biogeographical Analysis of Fungal Communities

Differences in fungal community structure in sediments from different elevation gradients are shown in Figure 4, with Bray–Curtis dissimilarity of 0.96, 0.95, and 0.93 for YRA, YRB, and YRC, respectively. To explore the potential driving factors of fungal community variation, we conducted biogeographical analysis. The distance–decay relationship is a well-known biogeographical model that explores the relationship between regional geographical distance (stochastic process) and local environmental distance (deterministic process) and community differences [31]. Among all sampling sites, the differences in fungal communities significantly increased with increasing geographical distance ($p < 0.01$) (Figure 4C). Across altitudinal gradients, differences in fungal communities in the YRA group had the strongest attenuation effect with geographic distance across the altitudinal gradient compared to YRB and YRC. In addition, the environmental distance attenuation effect of fungal communities in sediments at the three altitudinal gradients was stronger than the geographical distance (Figure 3C,D), indicating that the distribution pattern of fungal communities in sediments of the Yellow River Basin was more influenced by environmental factors.

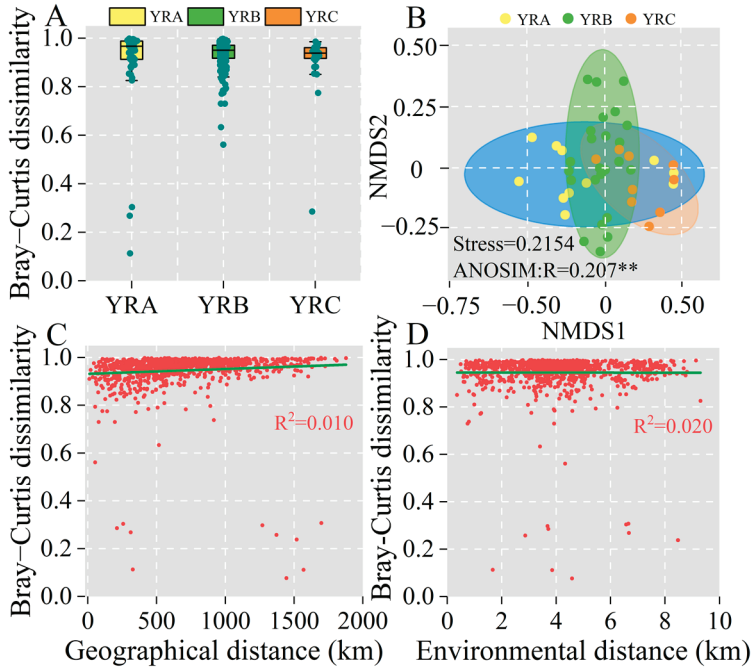


Figure 4. β-diversity of fungal community. (**A**) Spatial characterization of Bray–Curtis differences in fungal communities. (**B**) Non-metric multidimensional scaling analysis (NMDS) of elevation gradients in fungal communities. (**C**) The variation characteristics of fungal community Bray–Curtis dissimilarity with increasing geographical distance. (**D**) The variation characteristics of fungal community Bray–Curtis dissimilarity with increasing environmental distance. Note: ** indicates $p < 0.01$.

3.3. Characteristics of Fungal Community Co-Occurrence Networks

A co-occurrence network analysis was conducted to examine fungal communities in sediments of the Yellow River Basin across three distinct altitudinal gradients (Figure 5). The results demonstrated that interspecific connectivity within fungal communities was predominantly characterized by positive correlations across all altitudinal gradients, indicating that synergistic interactions prevailed over competitive relationships. Higher values of nodes (61) and average degree (10.75), combined with a lower average path length (2.27), were observed in YRA (Table 1). The number of edges in the co-occurrence network of fungal communities in YRA sediments was 327, significantly higher than that in YRB (54) and YRC (66). This suggests that fungal communities in YRA sediments exhibit greater network complexity and connectivity and are more concentrated than YRB and YRC.

Table 1. Statistical characteristics of fungal community nodes and topological parameters.

Basin	Node	Edge	Average Degree	Average Path Length	Network Diameter	Clustering Coefficient	Density	Heterogeneity	Centralization
YRA	61	328	10.75	2.27	3	0.52	0.18	0.51	0.24
YRB	51	54	2.12	3.13	5	0.21	0.04	0.68	0.08
YRC	45	66	2.93	3.61	5	0.27	0.07	0.63	0.09

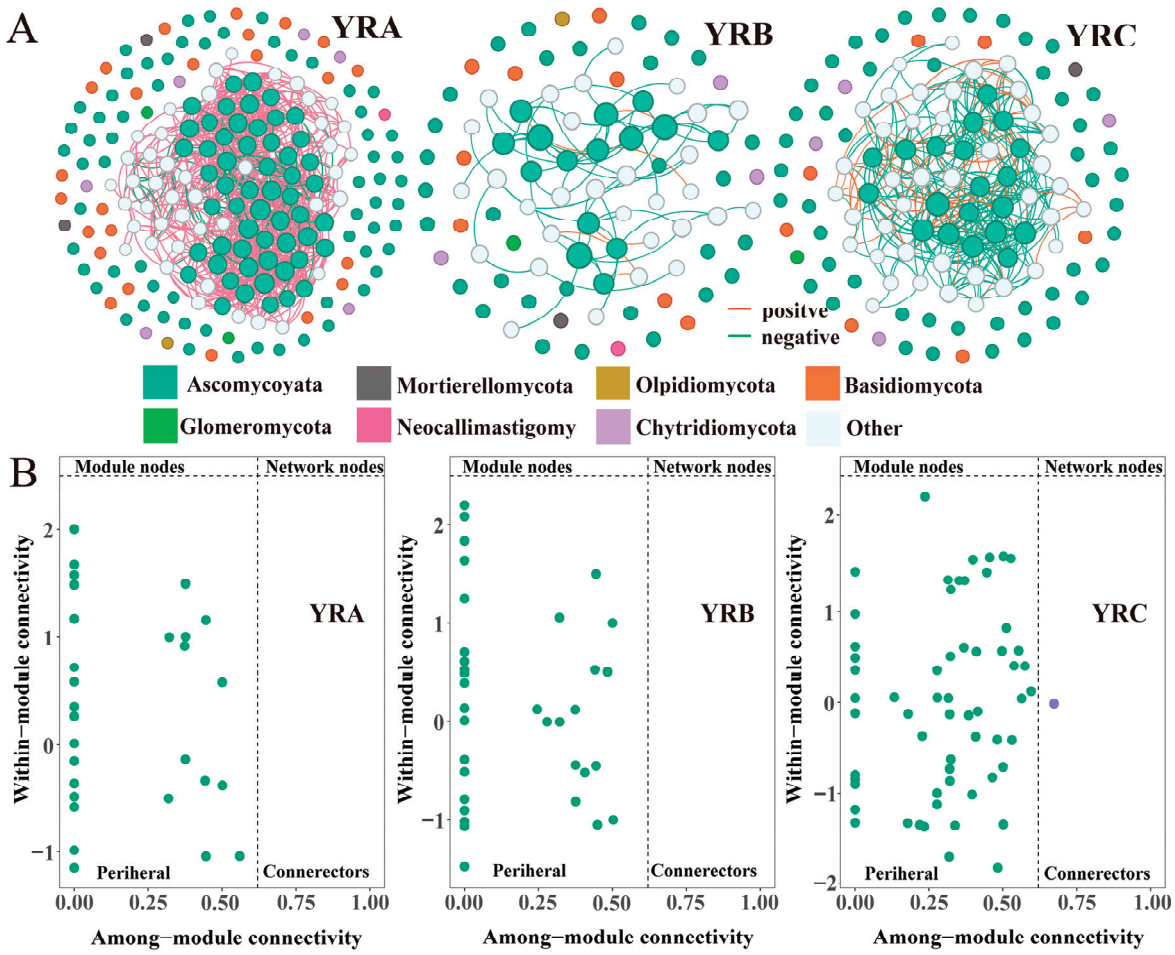


Figure 5. Co-linear network analysis of fungal communities. (**A**) Co-linear network of fungal communities in sediments at different elevation gradients. (**B**) Key species analysis.

Generally, network nodes, module nodes, and connectors are considered keystone species in building communities and may play important roles in maintaining community structure [15]. If these taxa are removed, modules and networks may collapse. In our study, fungal communities in sediments at different altitudinal gradients in the Yellow River Basin did not have module nodes and network nodes, with only one connector present in YRC (Figure 5B).

3.4. Analysis of Fungal Community Assembly Processes

To further quantify the relative contributions of stochastic versus deterministic processes in microbial community assembly, the phylogenetic normalized stochasticity ratio (pNST) was determined through null model analysis (Figure 6). The βNTI results indicated that deterministic processes played a dominant role in the assembly of fungal communities, accounting for 88.56%. During the assembly process, homogenizing selection accounted for the highest proportion (69.66%) in the assembly of fungal communities. In addition, homogenizing dispersal also made a significant contribution to the assembly of fungal communities, accounting for 17.55%. The migration rate (Nm) estimated by the neutral model reflects the dispersal ability of the species, with higher values of Nm resulting in higher migration rates [32]. The Nm value in YRA sediments was the highest (Figure 6D), indicating that the fungal communities in YRA had a higher migration rate.

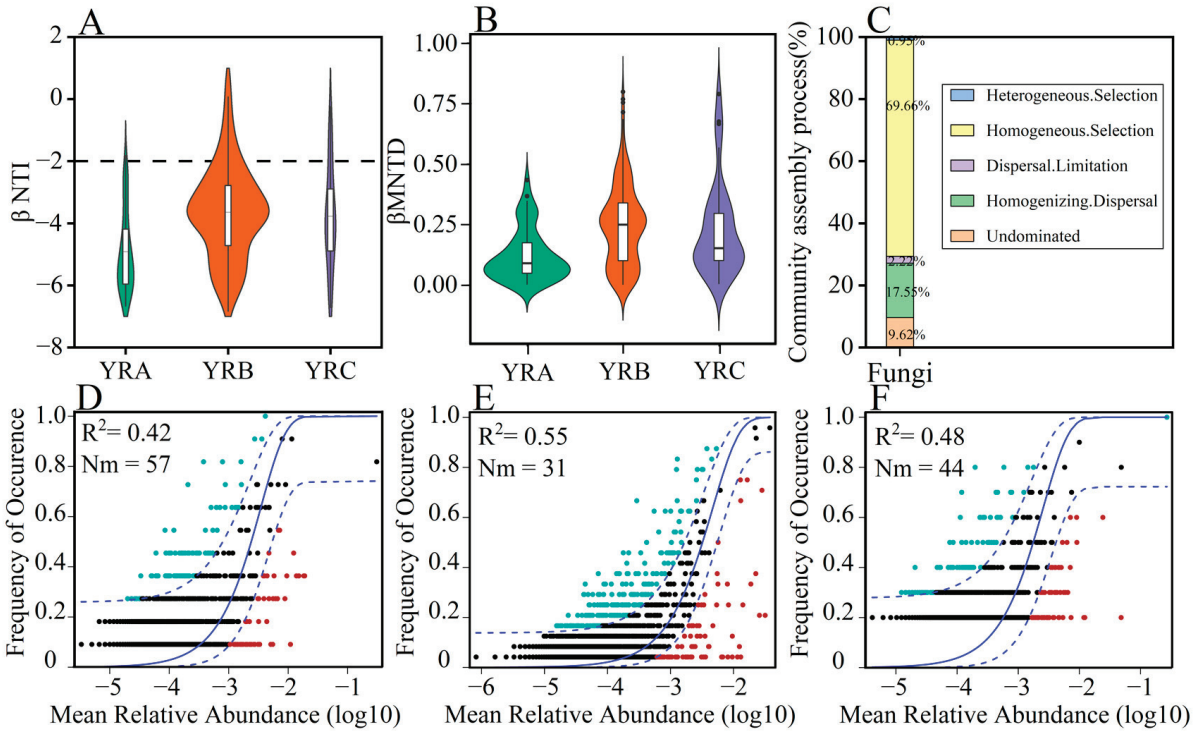


Figure 6. Fungal community assembly processes. (**A**) Changes in fungal community βNTI with altitudinal gradient. (**B**) Changes in fungal community βMNTD with altitudinal gradient. (**C**) The role of different ecological processes in assembling fungal communities. (**D**) Neutral community model fitting of fungal communities in YRA. (**E**) Neutral community model fitting of fungal communities in YRB. (**F**) Neutral community model fitting of fungal communities in YRC. Note: Green and red dots represent those ASVs that occur more frequently and less frequently than predicted by the model, respectively. The solid blue line shows the best-fit result of the neutral community model, while the dashed blue line marks the 95% confidence interval. Nm indicates the estimated migration rate, while R^2 reflects the degree of model fit.

3.5. Analysis of Factors Influencing Fungal Community Differences

The physicochemical properties of the sediment were measured, and the results are presented in Figures S1 and S2. Redundancy analysis (RDA) was performed to assess the influence of sediment environmental factors on fungal community variations (Figure 7 and Table 2). The first RDA axis accounted for the majority of fungal community variation, capturing 41% of the total explained variance. Significant explained quantities in the YRA group were Pb (19.4%), Ni (24.0%), TN (17.4%), and silt (11.6%); significant explained quantities in the YRB group were Ni (13.9%), sand (14.4%), and TN (10.4%); significant explained quantities in the YRC group were TP (27.9%), Consimd (24.0%), As (12%), and NO_3^--N (11.6%); significant explained quantities in the Yellow River Basin group were TOC (10.2%), Pb (15.5%), silt (10.7%), and TN (12.3%). Therefore, carbon, nitrogen, sediment particle composition, and heavy metal content are the primary factors influencing the differences in fungal communities within the sediments of the Yellow River Basin.

Significant negative correlations between Pb and Ascomycota were observed ($p < 0.05$), with spatial heterogeneity across altitudinal gradients: a negative association in YRA ($p < 0.05$), a positive correlation in YRB ($p < 0.05$), and a non-significant relationship in YRC. Total organic carbon (TOC) exhibited basin-scale positive correlations with Ascomycota ($p < 0.05$), though gradient-specific variations emerged: non-significant in YRA, negative in YRB ($p < 0.05$), and positive in YRC ($p < 0.05$). Silt content demonstrated basin-wide negative correlations with Ascomycota ($p < 0.05$), showing consistent negativity in YRA/YRB

($p < 0.05$) but positivity in YRC ($p < 0.05$). Regarding Basidiomycota, abundance was positively associated with Pb at the basin scale ($p < 0.05$), showing significant correlations in YRA/YRB ($p < 0.05$) but no significance in YRC. Notably, TOC and silt content showed contrasting spatial patterns with Basidiomycota: basin-scale positive correlations ($p < 0.05$) existed alongside non-significant (YRA), positive (YRB), and negative (YRC) regional associations ($p < 0.05$).

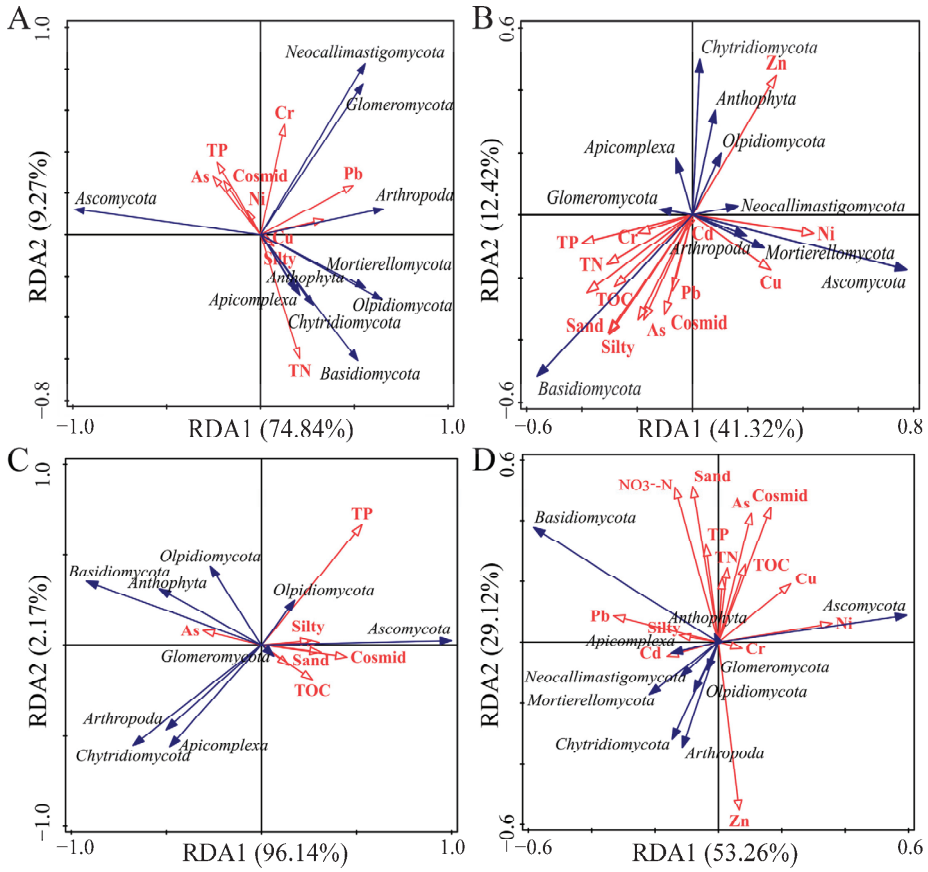


Figure 7. Redundancy analysis of fungal communities in sediments and environmental factors. (**A**) YRA group. (**B**) YRB group. (**C**) YRC group. (**D**) Entire basin.

Table 2. The contributions of sediment factors to changes in fungal communities according to the results of redundancy analysis (RDA).

Basin	Explained Variation (%)			Explanatory Variables (Contribution %)
	Axls 1	Axls 2	All Axes	
YRA	74.84	19.27	94.11	Pb (19.4), Ni (24), TN (17.4), Silty (11.6)
YRB	41.32	12.42	53.74	Ni(13.9), Sand(14.4), TN(10.4)
YRC	96.14	2.17	98.31	TP (27.9), Consimd (24), As (12), NO_3^--N (11.6)
Yellow River Basin	53.26	29.12	82.38	TOC (10.2), Pb (15.5), Silty (10.7), TN (12.3)

4. Discussion

4.1. Fungal Community Structure and Diversity at Different Altitudinal Gradients

The characteristics of river microbial communities are one of the key bases for evaluating the health of ecological environments, and the distribution patterns and diversity of microbial communities directly affect the stability of the structure and function of river ecosystems [1,33]. In this study, we found that fungal community diversity decreased with

increasing altitude. It has been found that microbial diversity at high altitude is negatively correlated with altitude [15], and our results are consistent with this finding. This may be due to the differences in sedimentary environmental conditions at different altitudinal gradients leading to differences in fungal community composition and diversity. Secondly, the high content of heavy metals in the sediments of the YRA area led to a decrease in fungal community diversity.

Similarly to previous studies, Ascomycota and Basidiomycota are the dominant phyla of fungal communities in the sediments of the Yellow River Basin [34]. We used Stamp analysis to explore the significantly different taxa in sediments at different altitudinal gradients (Figure 8), which are often closely related to river environmental factors. The Yellow River is a typical high-silt river, and its microbial community structure is highly complex and variable due to human activities and climate change. While existing research has predominantly examined microbial community structure and diversity in the Yellow River ecosystem, there remains a paucity of investigations specifically addressing spatial distribution patterns and assembly mechanisms of sedimentary fungal communities.

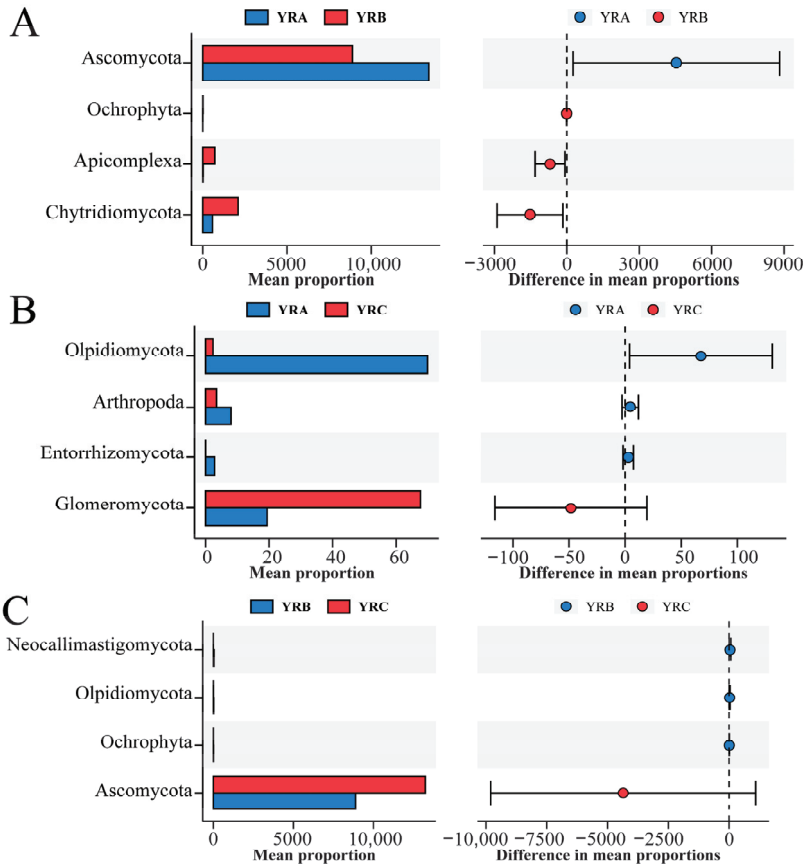


Figure 8. Differences in fungal community composition in sediments from the Yellow River Basin. (**A**) Differences in YRA and YRB communities. (**B**) Differences between YRA and YRC communities. (**C**) Difference between YRB and YRC communities.

Analytical results reveal that Ascomycota and Basidiomycota constitute the predominant phyla within fungal communities in the sedimentary environments of the Yellow River Basin. Ascomycota was observed to dominate with a relative abundance of 47.79%, followed by Basidiomycota at 15.68%. These observations align with previous findings from the Wuding River ecosystem, where Ascomycota has been reported as the dominant phylum in benthic fungal communities, exhibiting relative abundances of 38.72% and

19.47% during non-flood and flood seasons, respectively [35]. In contrast, Chytridiomycota has been documented as the predominant group during dry seasons in the Mekong River, whereas Ascomycota and Basidiomycota prevail in rainy seasons [9]. Similarly, Ascomycota (60%) and Basidiomycota (32%) have been identified as the dominant components of fungal assemblages in central Finnish lotic systems [36]. The abundance of Ascomycota was significantly higher in the YRA and YRC regions than in the YRB region. This is mainly because the high concentration of nutrients in the YRA region promotes the reproduction of Ascomycota, while the low-flow aquatic environment in the YRC region is conducive to the colonization and growth of Ascomycota in sediments. Basidiomycota are important decomposers that can break down organic matter in river sediments, such as plant residues and lignocellulose, converting complex organic compounds into simpler inorganic substances, thereby promoting the cycling of carbon and nitrogen [37]. The abundance of Chytridiomycota in B7, B8, and B15 of the YRB group was significantly higher than that of other sample sites, with its abundance being 53.99%, 39.17%, and 33.93%, respectively, which may be due to the entry of residual straw from the crops into the riverine environment in these sample sites.

In addition, 6.47%, 2.68%, and 1.24% of the fungal communities were identified as Chytridiomycota, Mortierellomycota, and Neocallimastigomycota, respectively. However, the relative abundance of these fungi varied among all samples, and some were not detected at certain sampling sites; these low-frequency fungi may play specific ecological roles in the sediments of the Yellow River Basin [38]. At the genus level, dominant taxa were identified as *Fusarium*, *Coprinellus*, *Mortierella*, *Trichoderma*, *Gibberella*, and *Subulicystidium*. Interestingly, these genera are predominantly associated with terrestrial ecosystems, particularly inhabiting soil matrices and decomposing plant detritus. These fungi are usually widely distributed in terrestrial ecosystems, especially in soil and plant residues. Their high abundance in the sediments of the Yellow River is related to the serious soil erosion in the Yellow River Basin. The Yellow River Basin is one of the most severely soil-eroded areas in the world, with the sediment discharge of the Yellow River reaching 1.59×10^8 t/yr [39]. During the process of soil erosion, fungal communities from soil and plant residues enter the river environment and colonize the sediments. Although these fungi are not typical aquatic fungi, their presence has certain ecological significance for the aquatic ecosystem.

4.2. Assembly Processes of Fungal Communities in Sediments

The mechanisms underlying biodiversity formation and maintenance, specifically the process of community assembly, have long constituted a central focus in ecological research. Furthermore, investigations into microbial community assembly processes currently represent a prominent research frontier in microbial ecology [40,41]. Neutral models and standardized stochastic rates have been recognized as critical analytical tools in ecological research, enabling effective quantification of the relative contributions made by deterministic and stochastic factors during community assembly processes [42,43]. The mechanism of riverine microbial community formation may be influenced by a variety of factors, among which changes in environmental factors are an important driver, considering that differences in birth, apoptosis, community evolution, and species formation in the aquatic environment shape different types of microbial communities [44–46]. The assembly of microbial communities involves both deterministic and stochastic processes [22,47,48], and these two mechanisms complement each other, but at the same time there are interactions and constraints.

This study showed that homogenizing selection accounted for the highest proportion (69.66%) in the assembly of fungal communities in sediments. Homogenizing selection

is the environmental selection effect formed by the interaction between similar abiotic environments in space and time and biota, which may lead to convergence in microbial community composition [49–51]. Our study found that deterministic processes (especially homogenizing selection) play a dominant role in the assembly of riverine fungal communities. This finding is consistent with some similar studies, but also has differences. For example, in the study of the Three Gorges Reservoir, homogenizing selection was also considered as the main driving force for microbial community assembly [52]. However, in the study of the Shenzhen River estuary continuum, the assembly of bacterial communities was mainly affected by homogeneous selection and dispersal limitation [53]. Dispersal limitation is a key ecological process in the assembly of fungal communities. In mining-affected rivers, the proportion of fungal community assembly attributed to dispersal limitation was 73.4%, indicating that dispersal limitation plays an important role in fungal community assembly [54]. These differences may be related to the specific environmental conditions of the study area. In river and sediment ecosystems, environmental factors (such as pH, temperature, dissolved oxygen, and organic matter content) have a significant impact on the assembly of fungal communities.

4.3. Co-Occurrence Network Analysis of Fungal Communities

In addition to the abiotic factors of environmental filtering and dispersal limitation, interspecific interactions are also considered important factors affecting microbial community assembly processes. Network structure can reflect the complexity and stability of communities [55]. Analysis of sedimentary fungal communities across three distinct altitudinal gradients revealed a predominance of positive interspecific associations. This is likely because sediments accepted nutrients that settled from the water, providing conditions for material transfer among fungal community species and facilitating species growth and reproduction through symbiotic or mutualistic relationships [56].

In extreme environments, competition among community species is weakened, and they rely more on mutual cooperation to maintain the river's ecological network [57]. The average degree and average clustering coefficient were higher in YRA, while the average path length was lower. Moreover, the co-occurrence network of fungal communities in YRA sediments had the most edges, indicating that fungal communities in YRA exhibited more correlations. Thus, the co-occurrence network in YRA was more closely connected, with greater network complexity and connectivity. This phenomenon may be related to the environmental characteristics of high-altitude areas. High-altitude ecosystems impose stringent environmental filters, resulting in selective retention of microbial taxa exhibiting adaptive traits for extremophilic survival and reproductive success. This filtering mechanism drives community homogenization, consequently amplifying interaction frequencies through niche overlap optimization [57].

Network analysis further demonstrated that a more stable network structure was observed in fungal communities at high-altitude areas, which may be attributed to the enhanced adaptive capabilities and stress tolerance exhibited by these fungal species. This stable network structure helps microbial communities better cope with environmental changes and maintain ecosystem functions. For example, certain microbes may enhance the stability and function of the entire community through symbiotic relationships or metabolic complementarity [57,58]. In addition, fungal networks in high-altitude areas have more network nodes, indicating the presence of multiple closely connected subgroups within fungal communities. This structure may reflect the differentiation and synergistic action of fungi in different ecological niches, contributing to the enhancement of the entire ecosystem's diversity and stability [59].

4.4. Main Factors Influencing Fungal Community Changes in Sediments of the Yellow River Basin

As pollutants from the river's surroundings continue to enter the river environment, they accumulate in the river's surface sediments, which in turn have a serious impact on the fungal community. In this study, we used redundancy analysis to explore the main environmental factors affecting microbial community differences (Figure 7); Pb, TN, TOC, and silt were the main factors affecting microbial community differences. The impact of environmental factors on microbial community composition may also extend to the transformation of chemical cycling and redox processes; disturbances to microbial community structure often lead to shifts in community function [60]. TOC can affect related microbial community structures, and differences in TOC content can affect microbial community structure, function, diversity, and abundance [61]. Studies have shown that nitrogen addition generally has a positive impact on Ascomycota [62], but the combined addition of nitrogen and phosphorus has a negative impact on Ascomycota [63]. The type and concentration of carbon sources can limit the growth and reproduction of certain fungal groups through environmental filtering. For example, in the study of the middle and lower reaches of the Jialing River, fungal communities at sections with less exogenous material input (such as undisturbed and sand mining disturbed sections) had higher diversity, while those at sections with more exogenous material input (such as tributary-disturbed and engineering-disturbed sections) had lower diversity [64]. Nitrogen addition can limit the growth and reproduction of certain fungal groups through environmental filtering. For example, in the study of the upper reaches of the Yellow River, agricultural land use led to an increase in total nitrogen concentration in the water, and the diversity of fungal communities was significantly reduced [65]. Rivers are open systems, with various substances entering the river environment from the surrounding areas, thereby affecting fungal communities in sediments.

Sediment physicochemical characteristics have been demonstrated to exert profound influences on microbial assemblages [66], with fungal communities exhibiting greater sensitivity to anthropogenic disturbances relative to bacterial counterparts [67], while simultaneously serving as bioindicators of pollution intensity [68]. The impact of particle size characteristics has been shown to significantly influence both microbial abundance and structural diversity within communities [69]. In sedimentary environments, fine silt particles usually have a higher content of mineral salts and can bring microorganisms closer together, allowing them to easily obtain nutrients [70]. Particle size characteristics not only affect microorganisms through chemical properties, but also directly affect microbial life processes through changes in attachable surface area and hydraulic properties [21,71]. In this study, the sediment grain size characteristics of the Yellow River Basin had significant differences. The grain size in the YRA area was mainly silty, while the YRB area was dominated by Cosmid, and the sediment grain size distribution in the YRC area was relatively uniform; this may be due to the topography and hydrodynamic conditions within the basin.

The toxic effects of high heavy metal concentrations are exerted on nearly all microorganisms through the disruption of metabolic functions including protein synthesis [72]. The coexistence of multiple heavy metals has been found to diminish microbial community tolerance, with particularly exacerbated toxicity observed under Cu-Zn co-occurrence conditions [73]. Previous research has demonstrated that niche differentiation and symbiotic network stability constitute key response mechanisms employed by fungal communities in heavy metal-polluted environments [74]. Under heavy metal pollution, niche differentiation is observed in fungal communities, resulting in metal-tolerant fungi emerging as dominant taxa [75]. For example, in mining-affected rivers, fungal communities exhibit

higher niche breadth and more stable symbiotic networks, enabling them to better adapt to highly heavy metal-polluted environments [54]. In addition, Pb and Zn are the main factors affecting fungal community structure [72], and our results are similar. Elevated concentrations of copper (Cu) and zinc (Zn) were detected in the YRA area relative to YRB and YRC sampling sites. Furthermore, chromium (Cr), nickel (Ni), and cadmium (Cd) concentrations were consistently elevated in YRA samples. The reduced microbial diversity in YRA is attributed to the cumulative toxicity effects of heavy metal exposure. This also explains why, despite higher contents of carbon, nitrogen, and phosphorus in the YRA area compared to YRB and YRC, the diversity was the lowest. Sediment environmental factors are to some extent drivers of changes in fungal community composition and structure. The unique geographical environment constructs specific habitat patterns of microbial community structure, which provides a theoretical basis for the ecological assessment of microorganisms in the Yellow River Basin and for future research on microbial distribution patterns and community assembly mechanisms.

5. Conclusions

A comprehensive analysis of sedimentary fungal communities was conducted in the Yellow River Basin (YRB) aimed at elucidating altitudinal distribution patterns and community assembly mechanisms along the elevation gradient. The fungal communities in the sediments of the Yellow River Basin were mainly composed of Ascomycota, Basidiomycota, Chytridiomycota, Mortierellomycota, and Apicomplexa, with Ascomycota and Basidiomycota being the dominant groups. The diversity (Shannon) of fungal communities decreased gradually with increasing altitude. The distance–decay analysis showed that the environmental distance attenuation effect of fungal communities in sediments at the three altitudinal gradients was stronger than the geographical distance. Environmental factors in sediments play an important role in shaping fungal community structure; TOC, Pb, silt, and TN are the main factors causing differences in fungal community structure. During the assembly of fungal communities, deterministic processes dominate, with the highest contribution from homogeneous selection (69.66%). These findings provide enhanced insights into microbial community assembly mechanisms in aquatic ecosystems, offering critical foundations for developing targeted ecological conservation strategies and sustainable water resource management protocols in the Yellow River Basin.

Supplementary Materials: The following supporting information can be downloaded at https://www.mdpi.com/article/10.3390/jof11030214/s1: Figure S1: Characteristics of sediment carbon, nitrogen, phosphorus, and heavy metal content; Figure S2: Characteristics of sediment grain size distribution; Figure S3: Characteristics of fungal community structure in sediments. Note: The numbers in the figure represent the number of ASVs; Figure S4: Analysis of microbial distance decay in sediments. (A) Relationship between Bray-Curtis dissimilarity and geographical distance in the YRA area. (B) Relationship between Bray-Curtis dissimilarity and geographical distance in the YRB area. (C) Relationship between Bray-Curtis dissimilarity and geographical distance in the YRC area. (D) Relationship between Bray-Curtis dissimilarity and environmental distance in the YRA area. (E) Relationship between Bray-Curtis dissimilarity and environmental distance in the YRB area. (F) Relationship between Bray-Curtis dissimilarity and environmental distance in the YRC area; Table S1: Fungal communities at the phylum level in sediments; Table S2: The top ten non-aquatic fungal communities at the genus level in sediments.

Author Contributions: Conceptualization, K.F. and G.X.; methodology, K.F., G.X. and X.C.; software, G.X.; validation, K.F., J.L. and G.X.; formal analysis, K.F. and Y.C. (Yifan Cheng); investigation, K.F.; resources, G.X.; data curation, Y.C. (Yifan Cheng); writing—original draft preparation, K.F.;

writing—review and editing, K.F. and X.C.; visualization, J.L. and Y.C. (Yuting Cheng); supervision, G.X. and Y.C. (Yuting Cheng); project administration, G.X.; funding acquisition, G.X. and Y.C. (Yuting Cheng). All authors have read and agreed to the published version of the manuscript.

Funding: This research was supported by the National Natural Science Foundation of China (No. 42377344), and the Scientific Research Program of Shaanxi Provincial Education Department (Youth Innovation Team project) (Grant No. 2024-149).

Institutional Review Board Statement: Not applicable.

Informed Consent Statement: Not applicable.

Data Availability Statement: The raw data supporting the conclusions of this article will be made available by the authors on request.

Conflicts of Interest: The authors declare that they have no known competing financial interests or personal relationships that could have appeared to influence the work reported in this paper.

References

1. Liu, X.; Zhang, L.; Wang, Y.C.; Hu, S.; Zhang, J.; Huang, X.L.; Li, R.W.; Hu, Y.X.; Yao, H.Y.; Wang, Z. Microbiome analysis in Asia's largest watershed reveals inconsistent biogeographic pattern and microbial assembly mechanisms in river and lake systems. *iScience* **2024**, *27*, 110053. [CrossRef]
2. Kraemer, S.A.; Barbosa da Costa, N.; Shapiro, B.J.; Fradette, M.; Huot, Y.; Walsh, D.A. A large-scale assessment of lakes reveals a pervasive signal of land use on bacterial communities. *ISME J.* **2020**, *14*, 3011–3023. [CrossRef]
3. Hu, A.Y.; Yang, X.Y.; Chen, N.W.; Hou, L.Y.; Ma, Y.; Yu, C.P. Response of bacterial communities to environmental changes in a mesoscale subtropical watershed, Southeast China. *Sci. Total Environ.* **2014**, *472*, 746–756. [CrossRef] [PubMed]
4. Liao, H.; Yen, J.Y.; Guan, Y.; Ke, D.; Liu, C. Differential responses of stream water and bed sediment microbial communities to watershed degradation. *Environ. Int.* **2020**, *134*, 105198. [CrossRef]
5. Li, X.L.; Li, Y.J.; Wang, Y.Y.; Liu, Y.Y.; Riaz, L.; Wang, Q.Q.; Zeng, X.P.; Qin, Z.; Irfan, M.; Yang, Q.X. Methodology comparison of environmental sediment fungal community analysis. *Environ. Res.* **2024**, *263*, 120260. [CrossRef] [PubMed]
6. Lücking, R.; Aime, M.C.; Robbertse, B.; Miller, A.N.; Ariyawansa, H.A.; Aoki, T.; Cardinali, G.; Crous, P.W.; Druzhinina, I.S.; Geiser, D.M.; et al. Unambiguous identification of fungi: Where do we stand and how accurate and precise is fungal DNA barcoding? *IMA Fungus* **2020**, *11*, 14. [CrossRef] [PubMed]
7. Hyde, K.D.; Fryar, S.; Tian, Q.; Bahkali, A.H.; Xu, J.C. Lignicolous freshwater fungi along a north–south latitudinal gradient in the Asian/Australian region; can we predict the impact of global warming on biodiversity and function? *Fungal Ecol.* **2016**, *19*, 190–200. [CrossRef]
8. Bai, Y.H.; Wang, Q.J.; Liao, K.L.L.; Jian, Z.Y.; Zhao, C.; Qu, J.H. Fungal Community as a Bioindicator to Reflect Anthropogenic Activities in a River Ecosystem. *Front. Microbiol.* **2018**, *9*, 3152. [CrossRef]
9. Siriarchawatana, P.; Harnpicharnchai, P.; Phithakrotchanakoon, C.; Kitikhun, S.; Mayteeworakoon, S.; Chunhametha, S.; Huong, V.T.L.; Eurwilaichitr, L.; Jiang, C.Y.; Cai, L.; et al. Fungal communities as dual indicators of river biodiversity and water quality assessment. *Water Res.* **2024**, *253*, 121252. [CrossRef]
10. Kim, S.; Alizamir, M.; Seo, Y.; Heddam, S.; Chung, I.M.; Kim, Y.O.; Kisi, O.; Singh, V.P. Estimating the incubated river water quality indicator based on machine learning and deep learning paradigms: BOD5 Prediction. *Math. Biosci. Eng.* **2022**, *19*, 12744–12773. [CrossRef]
11. Calabon, M.S.; Hyde, K.D.; Jones, E.B.G.; Luo, Z.L.; Dong, W.; Hurdeal, V.G.; Gentekaki, E.; Rossi, W.; Leonardi, M.; Thiyagaraja, V.; et al. Freshwater fungal numbers. *Fungal Divers.* **2022**, *114*, 3–235.
12. Warnasuriya, S.D.; Udayanga, D.; Manamgoda, D.S.; Biles, C. Fungi as environmental bioindicators. *Sci. Total Environ.* **2023**, *892*, 164583. [CrossRef]
13. Tamminen, M.; Spaak, J.; Tlili, A.; Eggen, R.; Stamm, C.; Räsänen, K. Wastewater constituents impact biofilm microbial community in receiving streams. *Sci. Total Environ.* **2022**, *857*, 151080. [CrossRef]
14. Diamond, J.M. Assembly of species communities. In *Ecology and Evolution of Communities*; Harvard University Press: Boston, MA, USA, 1975; pp. 342–444.
15. Yang, Q.; Zhang, P.; Li, X.D.; Yang, S.X.; Chao, X.; Liu, H.Q.; Ba, S. Distribution patterns and community assembly processes of eukaryotic microorganisms along an altitudinal gradient in the middle reaches of the Yarlung Zangbo River. *Water Res.* **2023**, *239*, 120047. [CrossRef]

16. Dini-Andreote, F.; Stegen, J.C.; Van-Elsas, J.D.; Salles, J.F. Disentangling mechanisms that mediate the balance between stochastic and deterministic processes in microbial succession. *Proc. Natl. Acad. Sci. USA* **2015**, *112*, E1326–E1332. [CrossRef]
17. Sun, H.Y.; Sun, F.; Deng, X.L.; Storn, N. Soil carbon fractions drive microbial community assembly processes during forest succession. *J. Environ. Manag.* **2025**, *373*, 123638. [CrossRef] [PubMed]
18. Smith, S.K.; De Los Reyes, F.L. Quantifying patterns of microbial community assembly processes in bioreactors using different approaches leads to variable results. *Water Res.* **2025**, *272*, 122903. [CrossRef]
19. Soto, D.F.; Franzetti, A.; Gómez, I.; Huovinen, P. Functional filtering and random processes affect the assembly of microbial communities of snow algae blooms at Maritime Antarctic. *Sci. Total Environ.* **2022**, *805*, 150305. [CrossRef] [PubMed]
20. Zhou, J.Z.; Ning, D.L. Stochastic community assembly–Does it matter in microbial ecology? *Microbiol. Mol. Biol. Rev.* **2017**, *81*, e00002-17. [CrossRef]
21. Li, Y.; Zhu, J.X.; Wang, L.F.; Gao, Y.; Zhang, W.L.; Zhang, H.J.; Niu, L.H. Grain size tunes microbial community assembly and nitrogen transformation activity under frequent hyporheic exchange: A column experiment. *Water Res.* **2020**, *182*, 116040. [CrossRef]
22. Stegen, J.C.; Lin, X.J.; Fredrickson, J.K.; Chen, X.Y.; Kennedy, D.W.; Murray, C.J.; Rockhold, M.L.; Konopka, A. Quantifying community assembly processes and identifying features that impose them. *ISME J.* **2013**, *7*, 2069–2079. [CrossRef] [PubMed]
23. Li, J.; Li, X.C.; Guo, L.D. Research progress on community assembly mechanisms of fungi. *Mycosystema* **2023**, *42*, 13–25. (In Chinese)
24. Ding, Y.T.; Li, M.; Pan, B.Z.; Zhao, G.N.; Gao, L. Disentangling the drivers of phytoplankton community composition in a heavily sediment-laden transcontinental river. *J. Environ. Manag.* **2022**, *302*, 113939. [CrossRef] [PubMed]
25. Li, H.A.; Tian, S.M.; Shang, F.D.; Shi, X.Y.; Zhang, Y.; Cao, Y.T. Impacts of oxbow lake evolution on sediment microbial community structure in the Yellow River source region. *Environ. Res.* **2024**, *252*, 119042. [CrossRef]
26. Ren, Z.H.; Jiang, W.L.; Sun, N.; Shi, J.F.; Zhang, D.P.; Zhang, J.J.; Wang, Z.K.; Yang, J.S.; Yu, J.B.; Lv, Z.B. Responses of the structure and function of microbes in Yellow River Estuary sediments to different levels of mercury. *Mar. Environ. Res.* **2023**, *190*, 106097. [CrossRef]
27. Gao, Y.X.; Jiang, X.; Liu, Y.Y.; Wei, K.X.; Zhang, L.X.; Wang, X.; Wang, F.Q.; Liu, J.; Cheng, S.C. Structural changes and assembly mechanisms of microbial communities during rapid sedimentation of Yellow River sediments. *Environ. Technol. Innov.* **2024**, *35*, 103702. [CrossRef]
28. Tian, F.; Liu, L.Z.; Yang, J.H.; Wu, J.J. Vegetation greening in more than 94% of the Yellow River Basin (YRB) region in China during the 21st century caused jointly by warming and anthropogenic activities. *Ecol. Indic.* **2021**, *125*, 107479. [CrossRef]
29. Chen, X.G.; Lou, Y.; Hong, S.Z.; Zhang, X.X.; Huang, Q.Z.; Huang, G.H. Assessment of meteorological factors and human activities impact on wheat and maize water requirements in the Yellow River Basin. *Sci. Total Environ.* **2024**, *955*, 177056. [CrossRef]
30. Li, W.Z.; Liu, N.; Li, J.F.; Wang, B.L.; Shi, X.J.; Liang, X.; Yang, M.L.; Xu, S.; Liu, C.Q. Chemodiversity of Dissolved Organic Matter Is Governed by Microbial Biogeography in Inland Waters. *Environ. Sci. Technol.* **2023**, *57*, 7753–7763. [CrossRef]
31. Yi, M.L.; Li, L.Q.; Li, H.R.; Liu, C.; Deng, Y.; Wu, Z.; Li, Y. Spatiotemporal variations of plankton communities in different water bodies of the Yellow River: Structural characteristics, biogeographic patterns, environmental responses, and community assembly. *J. Hydrol.* **2024**, *640*, 131702. [CrossRef]
32. Chao, X.; Yang, S.X.; Liu, H.Q.; Yan, B.J.; Wei, P.P.; Wu, X.J.; Ba, S. Mechanism and driving factors of phytoplankton community construction in the lower reaches of Yarlung Zangbo River. *J. Lake Sci.* **2025**, *37*, 215–229. (In Chinese)
33. Chang, C.; Hu, E.; Shi, Y.F.; Pan, B.Z.; Li, M. Linking microbial community coalescence to ecological diversity, community assembly and species coexistence in a typical subhumid river catchment in northern China. *Sci. Total Environ.* **2024**, *938*, 173367. [CrossRef]
34. Qi, H.Y.; Huang, D.; Wang, F.H.; Ye, M.; Jiang, X. Spatial dynamics of prokaryotic microbial communities in sediments of the Yellow Sea: Assembly process, co-occurrence relationships, and environmental implications. *J. Environ. Manag.* **2022**, *319*, 115645. [CrossRef] [PubMed]
35. Xu, G.C.; Zhi, Z.X.; Li, Z.B.; Zhuang, J.; Guo, M.J.; Fang, K.; Yi, J.; Ren, Z.P.; Gao, H.D.; Jia, L. Attribution of sediment changes and influencing factors of microbial communities in sediment in the Wuding River basin of the Yellow River. *Catena* **2025**, *249*, 108626. [CrossRef]
36. Jyväsjärvi, J.; Lehosmaa, K.; Aroviita, J.; Turunen, J.; Rajakallio, M.; Marttila, H.; Tolkkinen, M.; Mykrä, H.; Muotka, T. Fungal assemblages in predictive stream bioassessment: A cross-taxon comparison along multiple stressor gradients. *Ecol. Indic.* **2021**, *121*, 106986. [CrossRef]
37. Ghobad-Nejhad, M.; Dima, B.; Cui, B.K.; Si, J. Basidiomycete fungi: From biosystematics and biodiversity to biotechnology. *Front. Microbiol.* **2023**, *14*, 1128319. [CrossRef] [PubMed]

38. Gao, M.H.; Liu, B.H.; Li, J.M.; Deng, Y.Y.; Zhang, Y.L.; Zhang, N.; Li, F.; Li, C.L.; Huang, X.H.; Hu, Z.X. Diversity and Distribution of Fungi in the Marine Sediments of Zhanjiang Bay, China. *J. Fungi* **2025**, *10*, 867. [CrossRef]
39. Ma, Y.H.; Nong, X.Z.; Chen, L.H.; Wei, J.H.; Li, R.H. Spatiotemporal variation characteristics and environmental relationships of sediment loadings in large rivers of China: National perspective from 2002 to 2022. *Ecol. Indic.* **2024**, *166*, 112380. [CrossRef]
40. Chen, J.; Wang, P.F.; Wang, C.; Wang, X.; Miao, L.Z.; Liu, S.; Yuan, Q.S. Dam construction alters function community composition of diazotrophs in riparian and soils across an environmental gradient. *Soil Biol. Biochem.* **2019**, *132*, 14–23. [CrossRef]
41. Li, M.Y.; Mi, T.Z.; He, H.; Chen, Y.; Zhen, Y.; Yu, Z.G. Active bacterial and archaeal communities in coastal sediments: Biogeography pattern, assembly process and co-occurrence relationship. *Sci. Total Environ.* **2021**, *750*, 142252. [CrossRef]
42. Yang, S.X.; Yang, Q.; Li, X.D.; Chao, X.; Liu, H.Q.; Wei, L.R.X.; Ba, S. Deterministic processes dominate the geographic distribution pattern and community assembly of phytoplankton in typical plateau rivers. *Biodivers. Sci.* **2023**, *31*, 43–57. (In Chinese) [CrossRef]
43. Luo, Z.M.; Liu, J.X.; Zhao, P.Y.; Jia, T.; Li, C.; Chai, B.F. Biogeographic patterns and assembly mechanisms of bacterial communities differ between habitat generalists and specialists across elevational gradients. *Front. Microbiol.* **2019**, *10*, 169. [CrossRef]
44. Southwell, R.V.; Hilton, S.L.; Pearson, J.M.; Hand, L.H.; Bending, G.D. Inclusion of seasonal variation in river system microbial communities and phototroph activity increases environmental relevance of laboratory chemical persistence tests. *Sci. Total Environ.* **2020**, *733*, 139070. [CrossRef] [PubMed]
45. Nishihama, S.; Haraguchi, A.; Kawano, T.; Michiki, K.; Nakazawa, K.; Suzuki, T.; Uezu, K.; Yoshizuka, K. Seasonal changes in the microbial population of the water column and sediments of the Ongagawa River, northern Kyushu, Japan. *Limnology* **2008**, *9*, 35–45. [CrossRef]
46. Xu, M.; Xu, R.Z.; Shen, X.X.; Gao, P.; Xue, Z.X.; Huang, D.C.; Jin, G.Q.; Li, C.; Cao, J.S. The response of sediment microbial communities to temporal and site-specific variations of pollution in interconnected aquaculture pond and ditch systems. *Sci. Total Environ.* **2022**, *806*, 150498. [CrossRef] [PubMed]
47. Bahram, M.; Kohout, P.; Anslan, S.; Harend, H.; Abarenkov, K.; Tedersoo, L. Stochastic distribution of small soil eukaryotes resulting from high dispersal and drift in a local environment. *ISME J.* **2016**, *10*, 885–896. [CrossRef]
48. Stegen, J.C.; Lin, X.J.; Konopka, A.E.; Fredrickson, J.K. Stochastic and deterministic assembly processes in subsurface microbial communities. *ISME J.* **2012**, *6*, 1653–1664. [CrossRef]
49. Stegen, J.C.; Lin, X.J.; Fredrickson, J.K.; Konopka, A.E. Estimating and mapping ecological processes influencing microbial community assembly. *Front. Microbiol.* **2015**, *6*, 370. [CrossRef]
50. Fodelianakis, S.; Washburne, A.D.; Bourquin, M.; Pramateftaki, P.; Kohler, T.J.; Styllas, M.; Tolosano, M.; De Staercke, V.; Schön, M.; Busi, S.B.; et al. Microdiversity characterizes prevalent phylogenetic clades in the glacier-fed stream microbiome. *ISME J.* **2022**, *16*, 666–675. [CrossRef]
51. Prussin, A.J.; Belser, J.A.; Bischoff, W.; Kelley, S.T.; Lin, K.; Lindsley, W.G.; Nshimyimana, J.P.; Schuit, M.; Wu, Z.; Bibby, K.; et al. Viruses in the Built Environment (VIBE) meeting report. *Microbiome* **2020**, *8*, 1. [CrossRef]
52. Gao, Y.; Zhang, W.L.; Li, Y. Microbial community coalescence: Does it matter in the Three Gorges Reservoir? *Water Res.* **2021**, *205*, 117638. [CrossRef] [PubMed]
53. Liang, H.B.; Huang, J.; Xia, Y.; Yang, Y.; Yu, Y.; Zhou, K.; Lin, L.; Li, X.Y.; Li, B. Spatial distribution and assembly processes of bacterial communities in riverine and coastal ecosystems of a rapidly urbanizing megacity in China. *Sci. Total Environ.* **2024**, *934*, 173298. [CrossRef] [PubMed]
54. Li, C.Y.; Zhong, M.; Guo, E.D.; Xu, H.S.; Wen, C.; Zhu, S.Q.; Li, Q.; Zhu, D.; Luo, X. Response of bacterial and fungal communities in natural biofilms to bioavailable heavy metals in a mining-affected river. *Water Res.* **2024**, *267*, 122470. [CrossRef]
55. Konopka, A.; Lindemann, S.; Fredrickson, J. Dynamics in microbial communities: Unraveling mechanisms to identify principles. *ISME J.* **2015**, *9*, 1488–1495. [CrossRef] [PubMed]
56. Chen, J.; Sun, S.H.; Wang, P.F.; Wang, C.; Wang, X.; Gao, H.; Miao, L.Z.; Liu, S.; Yuan, Q.S. Sedimentary microeukaryotes reveal more dispersal limitation and form networks with less connectivity than planktonic microeukaryotes in a highly regulated river. *Freshw. Biol.* **2021**, *66*, 826–841. [CrossRef]
57. Barberán, A.; Bates, S.T.; Casamayor, E.O.; Fierer, N. Using network analysis to explore co-occurrence patterns in soil microbial communities. *ISME J.* **2014**, *8*, 952. [CrossRef]
58. Liu, C.; Li, C.A.; Jiang, Y.Q.; Zeng, R.J.; Yao, M.J.; Li, X.Z. A guide for comparing microbial co-occurrence networks. *IMETA* **2024**, *2*, e71. [CrossRef]
59. Tong, Z.M.; Zhang, Z.Y.; Lu, Y.C.; Liu, Y.L.; An, R.; Luo, X.; Liu, S.; Zhang, B. Optimization of ecological network function and structure by coupling spatial operators and biomimetic intelligent algorithm. *J. Clean. Prod.* **2024**, *465*, 142794. [CrossRef]
60. Shade, A.; Peter, H.; Allison, S.D.; Baho, D.L.; Berga, M.; Bürgmann, H.; Huber, D.H.; Langenheder, S.; Lennon, J.T.; Martiny, J.B.H.; et al. Fundamentals of microbial community resistance and resilience. *Front. Microbiol.* **2012**, *3*, 417. [CrossRef]

61. Wang, K.; Bi, Y.L.; Cao, Y.; Peng, S.P.; Christie, P.; Ma, S.P.; Zhang, J.Y.; Xie, L.L. Shifts in composition and function of soil fungal communities and edaphic properties during the reclamation chronosequence of an open-cast coal mining dump. *Sci. Total Environ.* **2021**, *767*, 144465. [CrossRef]
62. Song, B.; Li, Y.; Yang, L.Y.; Shi, H.Q.; Li, L.H.; Bai, W.M.; Zhao, Y. Soil acidification under long-term N addition decreases the diversity of soil bacteria and fungi and changes their community composition in a semiarid grassland. *Microb. Ecol.* **2023**, *85*, 221–231. [CrossRef]
63. Ma, X.Y.; Song, Y.Y.; Song, C.C.; Wang, X.W.; Wang, N.N.; Gao, S.Q.; Cheng, X.F.; Liu, Z.D.; Gao, J.L.; Du, Y. Effect of nitrogen addition on soil microbial functional gene abundance and community diversity in Permafrost Peatland. *Microorganisms* **2021**, *9*, 2498. [CrossRef] [PubMed]
64. Wang, Y.; Xu, F.; Zhu, L.P.; Zhang, T.; Liu, S.Y.; Jian, L.; Lu, S.C. Structure and Function of Fungal Community in Channel Sediments of Different Sections of Jialing River. *Environ. Sci.* **2024**, *45*, 4006–4013.
65. Ye, L.; Huang, J.J.; Yin, Q.L.; Xie, L.; Bai, X.; Pang, Q.Q.; Zhao, J.; Yang, W.G.; Peng, F.u.Q.; Zhu, X.; et al. The effects of land use patterns on carbon and nitrogen cycling microbe in a river of the upper reaches of the Yellow River. *China Environ. Sci.* **2024**, *44*, 6846–6857. (In Chinese)
66. Obi, C.C.; Adebusoye, S.A.; Ugoji, E.O.; Ilori, M.O.; Amund, O.O.; Hickey, W.J. Microbial communities in sediments of Lagos Lagoon, Nigeria: Elucidation of community structure and potential impacts of contamination by municipal and industrial wastes. *Front. Microbiol.* **2016**, *7*, 1213. [CrossRef]
67. Wang, W.J.; Yi, Y.J.; Yang, Y.F.; Zhou, Y.; Zhang, S.H.; Wang, X.; Yang, Z.F. Impact of anthropogenic activities on the sediment microbial communities of Baiyangdian shallow lake. *Int. J. Sediment Res.* **2020**, *35*, 180–192. [CrossRef]
68. Liu, J.; Wang, J.N.; Gao, G.H.; Bartlam, M.G.; Wang, Y.Y. Distribution and diversity of fungi in freshwater sediments on a river catchment scale. *Front. Microbiol.* **2015**, *6*, 329.
69. Zhang, P.J.; Zheng, J.F.; Pan, G.X.; Zhang, X.H.; Li, L.Q.; Tippkotter, R. Changes in microbial community structure and function within particle size fractions of a paddy soil under different long-term fertilization treatments from the Tai Lake region, China. *Colloids Surf. B Biointerfaces* **2007**, *58*, 264–270. [CrossRef]
70. Lin, J.; Zhou, X.T.; Lu, X.; Xu, Y.F.; Wei, Z.P.; Ruan, A.D. Grain size distribution drives microbial communities vertically assemble in nascent lake sediments. *Environ. Res.* **2023**, *227*, 115828. [CrossRef]
71. Nogaro, G.; Datry, T.; Mermillod-Blondin, F.; Foulquier, A.; Montuelle, B. Influence of hyporheic zone characteristics on the structure and activity of microbial assemblages. *Freshw. Biol.* **2013**, *58*, 2567–2583. [CrossRef]
72. Pan, X.M.; Zhang, S.R.; Zhong, Q.M.; Gong, G.S.; Wang, G.Y.; Guo, X.; Xu, X.X. Effects of soil chemical properties and fractions of Pb, Cd, and Zn on bacterial and fungal communities. *Sci. Total Environ.* **2020**, *715*, 136904. [CrossRef] [PubMed]
73. Zhang, F.; Xie, Y.H.; Peng, R.; Ji, X.H.; Bai, L.Y. Heavy metals and nutrients mediate the distribution of soil microbial community in a typical contaminated farmland of South China. *Sci. Total Environ.* **2024**, *947*, 174322. [CrossRef] [PubMed]
74. Rose, R.K.; Devi, R. Heavy metal tolerance and adaptability assessment of indigenous filamentous fungi isolated from industrial wastewater and sludge samples. *Beni-Suef Univ. J. Basic Appl. Sci.* **2018**, *7*, 688–694. [CrossRef]
75. Du, Q.L.; Jiang, J.M.; Li, X.Y.; Xie, X. Study on the Mechanism of Heavy Metal Enrichment of Macrofungi. *J. Mt. Agric. Biol.* **2021**, *40*, 36–41. (In Chinese)

Disclaimer/Publisher's Note: The statements, opinions and data contained in all publications are solely those of the individual author(s) and contributor(s) and not of MDPI and/or the editor(s). MDPI and/or the editor(s) disclaim responsibility for any injury to people or property resulting from any ideas, methods, instructions or products referred to in the content.

Journal of *Fungi*

MDPI

Article

Variation of Arbuscular Mycorrhizal Fungi Communities Between Root and Rhizosphere Soil of Endangered Plant *Heptacodium miconioides* Along Elevation Gradient

Yueling Li [1,2], Guangyu Luo [1,2], Shijie Wu [1,2], Dang Yang [1,2], Pengpeng Lv [1,2], Zexin Jin [1,2,*] and Junmin Li [1,2,*]

[1] Zhejiang Key Laboratory for Restoration of Damaged Coastal Ecosystems, School of Life Sciences, Taizhou University, Taizhou 318000, China; liyl@tzc.edu.cn (Y.L.); luogy@tzc.edu.cn (G.L.); wushijietzc@163.com (S.W.); yangdangyd@163.com (D.Y.); lvpeng0903@163.com (P.L.)
[2] Institute of Ecology, School of Life Sciences, Taizhou University, Taizhou 318000, China
* Correspondence: jzx@tzc.edu.cn (Z.J.); lijm@tzc.edu.cn (J.L.)

Abstract: Arbuscular mycorrhizal fungi (AMF) are considered crucial for the survival of many endangered plant species. However, the dynamics of AMF communities in the roots and rhizosphere soil of *Heptacodium miconioides*, particularly along elevation gradients, remain underexplored. This study investigates AMF colonization, spore density, and community structure in the root and rhizosphere soil of *H. miconioides* across an elevation range from 306 to 1028 m a.s.l., employing high-throughput sequencing. Our results show that AMF colonization and spore density in *H. miconioides* increased with elevation. *Glomus* was the dominant genus in both root and rhizosphere samples. Elevation significantly influenced the AMF community structure and diversity in the root, with alpha diversity decreasing linearly with elevation. In contrast, no significant elevation-related changes were observed in the rhizosphere soil alpha diversity. The difference in AMF beta diversity between the root and rhizosphere soil was lowest at the highest elevation. Compared to the rhizosphere soil, the degree and degree centralization of AMF community co-occurrence networks in the root showed a significant increase at higher elevations. Variations in soil properties, particularly soil pH, available phosphorus, and total nitrogen levels strongly influenced AMF communities in rhizosphere soil, while nitrate nitrogen, available potassium, and acid phosphatase were correlated with AMF communities in the root. These findings highlight the impact of elevation on AMF communities in both root and rhizosphere soil, providing valuable insights for the habitat restoration and conservation efforts for this species.

Keywords: arbuscular mycorrhizal fungi; endangered plant; elevation gradient; diversity; root and rhizosphere soil

1. Introduction

Endangered plant species are vital components of natural ecosystems and global biodiversity [1]. However, these species are increasingly threatened by factors such as over-exploitation, habitat loss, invasive species, and environmental changes, including global warming and acid rain [2]. As a result, protecting endangered plants and enhancing the viability of their populations has become a critical conservation priority. Soil microorganisms are required to maintain the stability of an ecosystem [3], with arbuscular

mycorrhizal fungi (AMF) being key symbionts for over 80% of terrestrial plants. AMF serve as a crucial link between aboveground and belowground ecosystems [4]. These fungi enhance mineral nutrient uptake, improve soil stability, and increase plant resilience to environmental stressors [5], while also influencing plant fitness and reproduction [6]. Recently, AMF's role in the conservation of endangered plants has gained increasing attention. Numerous studies have demonstrated that rare and endangered plant species exhibit improved performance and greater mycorrhizal dependence in the presence of AMF [7,8]. For example, inoculating the endangered species *Pterocarpus santalinus* with AMF symbionts promoted seedling growth and facilitated successful field establishment [9]. Likewise, Wang et al. [10] found that AMF inoculation helped protect *Zelkova serrata* from acid rain stress by enhancing photosynthetic capacity, osmolyte regulation, and activating antioxidant enzymes. These findings underscore the potential of AMF to support the survival and environmental resilience of endangered plants, thereby offering a promising approach to their conservation.

Mountain elevation gradients, with their varying environmental conditions, provide a useful model for studying soil microbial patterns, including AMF [11]. Elevation induces distinct changes in climate, seasonality, vegetation, and soil properties, all of which influence microbial communities [12]. While the relationship between AMF abundance and diversity along elevation gradients has been widely studied, the results remain inconclusive. For instance, some studies have reported a negative correlation between AMF colonization, spore density, and community diversity with elevation in Tibetan alpine grasslands [13,14]. In contrast, Vieira et al. [15] observed a higher Shannon diversity of AMF species at mid-to-high elevations in tropical mountains. Furthermore, Yu et al. [16] found that elevation positively correlated with the relative abundances of *Ambispora* and *Glomus* in the rhizosphere of *Siraitia grosvenorii*, significantly shaping AMF community composition. Other studies, such as Zhang et al. [17], suggested a bimodal pattern of AMF diversity with increasing elevation in Mt. Taibai, Qinling Mountains. These disparate findings highlight the need for further research to establish a comprehensive understanding of how AMF diversity responds to elevation in natural ecosystems.

AMF in both the root and rhizosphere soil play distinct yet complementary roles in supporting plant growth and health. Previous studies have shown that functional groups of AMF in these two environments differ significantly in terms of biomass allocation [18]. For example, *Rhizophagus* species tend to allocate more biomass to the root, while *Acaulospora* species are more likely to allocate biomass to the rhizosphere soil. This differentiation suggests that AMF in the roots are specialized for nutrient exchange and stress tolerance, whereas AMF in the rhizosphere soil are more diverse, contributing to nutrient acquisition, soil structure, and microbial interactions [19,20]. Stevens et al. [21] demonstrated that the soil AMF community structure is primarily influenced by environmental factors, while root AMF communities are more strongly impacted by disturbances and host–plant interactions. Forest management practices, such as the mixed forest management of *Juglans mandshurica*, were reported to alter the AMF composition in the soil but had minimal effect on the root AMF community [22]. These findings suggest that the AMF species in roots are different from those in the rhizosphere soil. However, most studies to date were mainly carried out on farmland [23] and grassland ecosystems [24], with limited research on AMF diversity changes in both root and rhizosphere soils in mountainous ecosystems. Studying AMF distribution patterns along elevation gradients can provide valuable insights into the factors driving elevation-related changes in diversity.

Heptacodium miconioides Rehd., a member of the monotypic genus *Heptacodium* in the Caprifoliaceae family, is an endemic and endangered deciduous tree. As a perennial species,

H. miconioides occupies a unique position in the evolutionary history of Caprifoliaceae and holds significant scientific and ornamental value [25]. However, due to habitat fragmentation, low reproductive rates, poor environmental conditions, and human activities the natural populations of *H. miconioides* have been severely threatened [26]. It is classified as a second-class national protected plant in China and is listed as a vulnerable species on the IUCN Red List [27,28]. Previous studies have shown that *H. miconioides* forms a beneficial symbiotic relationship with AMF [29]. For instance, inoculation with *Rhizophagus intraradices* has been shown to enhance drought tolerance and promote seedling growth in *H. miconioides* [28]. Here, we used root and rhizosphere soil samples from *H. miconioides* across five elevation gradients in Dongbai Mountain to perform Illumina Miseq sequencing and analyze AMF diversity changes and community composition. The objective of this work was to achieve a deeper understanding of the diversity and structure of AMF communities in the root and rhizosphere soil associated with *H. miconioides* along elevation gradients. We aimed to: (1) compare the AMF community composition between the root and rhizosphere soil; (2) evaluate the response of AMF community diversity and distribution patterns to elevation gradients; and (3) assess the influence of edaphic factors and soil enzyme activity on AMF community structure in both the root and rhizosphere soils. Our results could provide insights into the role of AMF in the conservation, growth, and habitat restoration of *H. miconioides* and other endangered plant species.

2. Materials and Methods

2.1. Study Area

The study was conducted in Dongbai Mountain (29°30′42.11″ N, 120°26′12.57″ E), located in Zhuji City, Zhejiang Province, China (Figure 1). The region has a subtropical monsoon climate, characterized by an average annual temperature of 11 °C, annual rainfall exceeding 1500 mm, with extreme temperatures ranging from −10.7 °C to 32 °C. The frost-free period lasts approximately 180 days. The highest elevation on Dongbai Mountain is 1194.6 m, which is one of the primary habitats for *H. miconioides*. The dominant soil type is hilly mountain red loam.

2.2. Root and Rhizosphere Soil Sampling

In mid-July 2019, five elevation gradients (306, 518, 644, 840, and 1028 m) were selected for sampling along the mountain from its base to summit. At each elevation, four independent replicate plots (5 m × 5 m) were randomly established, with two healthy *H. miconioides* individuals selected per plot, ensuring a minimum distance of 3.5 m between adjacent plots. Fine roots (<2 mm diameter) were collected from the 0–10 cm depth, and rhizosphere soil was gently brushed off using a soft-bristled paintbrush. Root and rhizosphere soil from two trees within each plot were combined into a single sample, yielding a total of 20 samples. Rhizosphere soil was passed through a 5 mm sieve to remove root debris and small stones. The root and rhizosphere samples were processed as follows: one portion of the root was preserved in FAA solution for AMF colonization analysis; a second portion of the rhizosphere soil was air-dried for physicochemical properties and enzyme activity assays; and the remaining root and rhizosphere soil was stored in ice boxes and subsequently kept at −80 °C for DNA extraction.

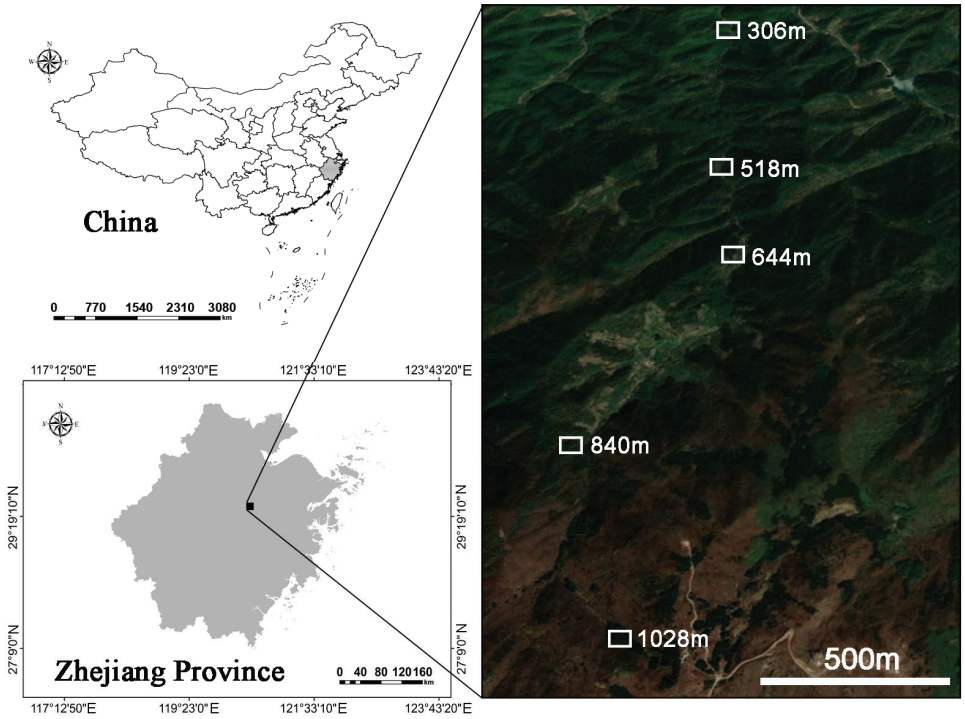


Figure 1. The location of the study area of the Heptacodium miconioides population on Dongbai Mountain, Zhuji City, Zhejiang Province, China.

2.3. Soil Properties and Analysis

The pH of soil (soil–water = 1:2.5 *w/v*) was measured with a calibrated pH meter. The contents of soil water (WC) and soil organic matter (OM) were determined via the drying method and the $K_2Cr_2O_7/FeSO_4$ method, respectively [30]. Total nitrogen (TN) and total phosphorus (TP) were measured using a continuous flow analyzer (AA3, Germany) as previously described [31]. Ammonium nitrogen (NH_4^+-N) and nitrate nitrogen (NO_3^--N) were extracted with KCl solution and analyzed using the AA3 continuous flow analyzer. Available phosphorus (AP) was extracted with $NaHCO_3$ solution and measured with the same analyzer, while available potassium (AK) was measured using inductively coupled plasma optical emission spectrometry (ICP/OES, Optima 2100DV, Shelton, CT, USA). Soil enzyme activities were measured as follows: sucrase activity was determined by the 3,5-dinitrosalicylic acid colorimetric method, and catalase and acid phosphatase activities were measured according to the published report [32].

2.4. AMF Colonization and Spore Density

AMF colonization was assessed by collecting fine roots (<1 mm diameter) of *H. miconioides* and preserving them in FAA solution (formalin: glacial acetic acid: 50% ethanol = 5:5:90) at 4 °C. AMF colonization rates for hyphae, vesicles, and arbuscules in the roots were determined using acid fuchsin staining [33], with data extracted via an Axio Scope A1 light microscopy (Zeiss, Jena, Germany). For each biological replicate, 30 root segments of approximately 1 cm in length were randomly selected and loaded onto glass slides, and then fixed with a lactic acid/glycerol mixture (*v*/*v* = 1:1). Colonization rates were quantified by the gridline intersect method [34]. AMF spores were extracted from 10 g of air-dried soil samples after 20-, 100-, and 300-mesh wet sieving and 60% sucrose centrifugation [35]. Spore density was counted under a binocular stereomicroscope with gridline method.

2.5. DNA Extraction, MiSeq Sequencing, and Bioinformatic Analysis

Total microbial genomic DNA was extracted and purified from all rhizosphere soil and root samples using an E.Z.N.A.® Soil DNA Kit (Omega, Auburn, WA, USA). DNA quality was checked in 1% agarose gel electrophoresis and its concentration was assessed using a NanoDrop2000 system (Thermo Scientific, Waltham, MA, USA). The fungal 18S rRNA gene was amplified with the primers AMV4.5NF (5′-AAGCTCGTAGTTGAATTTCG-3′) and AMDGR (5′-CCCAACTATCCCTATTAATCAT-3′) [36]. The PCR procedure and conditions were carried out according to the method of Ji et al. [22]. The PCR products were separated by 2% agarose gels, stained with ethidium bromide, and visualized under a UV transilluminator apparatus (Bio-Rad, Hercules, CA, USA). The extracted PCR products were then purified using a PCR Clean-Up Kit (YuHua, Shanghai, China), and quantified using Qubit 4.0 (Thermo Fisher, Waltham, MA, USA). Purified amplicons were pooled in equimolar amounts and sequenced in paired-end mode on an Illumina Nextseq2000 platform (Illumina, San Diego, CA, USA).

Raw sequencing reads were de-multiplexed using an in-house Perl script, quality-filtered with fastp (v0.19.6) [37], and merged with FLASH (v1.2.7) [38]. The resulting optimized sequences were clustered into operational taxonomic units (OTUs) at a 97% sequence similarity threshold using UPARSE 7.1 [39]. Taxonomic assignments for each OTU representative sequence were performed using the RDP Classifier (v2.2) against the maarjam20220506/AM species database with a confidence threshold of 0.7 [40].

2.6. Statistical Analysis

The effects of elevation on soil characteristics were evaluated using one-way ANOVA, followed by post hoc comparisons with either LSD or Dunnett's T3 tests at a 5% significance level, conducted using SPSS software (IBM, Armonk, NY, USA, v22.0). Linear regression analysis was performed to assess the relationship between AMF colonization rates, spore density, and AMF community alpha diversity in the root and rhizosphere soils of *H. miconioides* across the elevation gradient.

For the Illumina MiSeq sequencing data, rarefaction curves and alpha diversity indices, including the number of observed OTUs, Chao1, and Shannon indexes, were generated using Mothur v1.30.1 [41]. The common and unique OTUs across different samples were identified using Venn diagrams, generated with R software (v3.3.1). To visualize the composition of the AMF community at the genus level, a community bar plot was created using R (v3.3.1). Differences in alpha diversity, including Chao1 and Shannon indices, between the root and rhizosphere soils were analyzed using Student's *t*-tests at the 5% significance level.

The similarity of AMF communities across different samples was evaluated using non-metric multidimensional scaling (NMDS), based on Bray–Curtis dissimilarity, in R (v2.5-3). Differences in AMF alpha diversity (Shannon index and Chao1 index) and beta diversity (NMDS1 and NMDS2) across the elevation gradient were calculated according to the formula described by Zhao et al. [42]. Statistical significance was assessed using the Adonis test.

The co-occurrence networks were constructed to explore the internal AMF community relationships across the samples at different elevations. A correlation between two nodes was considered to be statistically robust (Spearman's correlation coefficient over 0.7 or less than -0.7) and significantly correlated (p-value less than 0.01). Network topology parameters (degree and degree centralization) were calculated, and the networks were visualized using Networkx (v.1.11).

Canonical correlation analysis (CCA) was conducted to examine the relationship between environmental factors and the AMF community using R (v2.4.3). The Mantel test, with a Monte Carlo simulation (999 randomizations), was employed to assess the correlation between the Euclidean distances of environmental variables and the AMF community. Pearson correlation analysis was used to explore the relationships between soil properties and AMF colonization rate, spore density, Shannon and Chao1 diversity indices, and the AMF community composition (genus level) in both the root and rhizosphere soils.

3. Results

3.1. Soil Characteristics Along the Elevation Gradient

The variations in soil environmental factors and enzyme activities along the elevation gradient are summarized in Table 1. As elevation increased, there were significant positive correlations with soil AK (R^2 = 0.31, p = 0.006), OM (R^2 = 0.85, p < 0.001), WC (R^2 = 0.44, p < 0.001), catalase (R^2 = 0.27, p = 0.012), and acid phosphatase (R^2 = 0.32, p = 0.006), while soil pH significantly decreased (R^2 = 0.63, p < 0.001). The NO_3^--N content (R^2 = 0.57, p < 0.001) initially decreased and then increased with elevation. However, no significant differences were observed in the AP, TP, TN, NH_4^+-N, or sucrase levels across elevations.

Table 1. Soil physicochemical properties and enzyme activities of *H. miconioides* under different elevation gradients.

Soil Properties	Elevation					Regression
	306 m	518 m	644 m	840 m	1028 m	R^2
NH_4^+-N	49.14 ± 7.80 ^{ab}	31.37 ± 3.19 ^{c}	57.36 ± 15.76 ^{a}	36.36 ± 9.31 ^{bc}	54.92 ± 5.61 ^{a}	0.09
NO_3^--N	38.77 ± 3.42 ^{b}	5.70 ± 2.73 ^{d}	31.34 ± 5.61 ^{bc}	24.37 ± 3.94 ^{c}	51.29 ± 5.41 ^{a}	0.57 **
AK	0.76 ± 0.19 ^{c}	0.86 ± 0.14 ^{bc}	0.88 ± 0.13 ^{bc}	1.31 ± 0.33 ^{a}	1.24 ± 0.29 ^{ab}	0.31 **
pH	5.52 ± 0.05 ^{a}	5.19 ± 0.13 ^{b}	5.37 ± 0.10 ^{ab}	4.86 ± 0.10 ^{c}	4.91 ± 0.13 ^{c}	0.63 **
OM	82.21 ± 12.1 ^{c}	100.22 ± 25.92 ^{c}	89.34 ± 16.24 ^{c}	137.65 ± 7.83 ^{b}	206.55 ± 13.31 ^{a}	0.85 **
WC	8.96 ± 3.47 ^{c}	17.93 ± 1.82 ^{bc}	28.58 ± 9.07 ^{ab}	24.17 ± 7.88 ^{ab}	33.85 ± 10.34 ^{a}	0.44 **
AP	11.83 ± 0.37 ^{a}	9.29 ± 0.83 ^{a}	10.85 ± 4.60 ^{a}	9.52 ± 1.80 ^{a}	12.25 ± 2.01 ^{a}	0.02
TN	1.22 ± 0.07 ^{b}	1.61 ± 0.49 ^{b}	2.52 ± 0.56 ^{a}	1.61 ± 0.57 ^{b}	2.02 ± 0.45 ^{ab}	0.12
TP	0.25 ± 0.03 ^{b}	0.32 ± 0.02 ^{ab}	0.27 ± 0.09 ^{ab}	0.36 ± 0.07 ^{a}	0.28 ± 0.04 ^{ab}	0.01
Catalase	14.68 ± 1.96 ^{bc}	14.57 ± 2.77 ^{c}	17.94 ± 1.80 ^{ab}	16.88 ± 0.70 ^{ac}	18.57 ± 1.5 ^{a}	0.27 *
Acid phosphatase	0.03 ± 0.02 ^{b}	0.03 ± 0.02 ^{b}	0.11 ± 0.06 ^{a}	0.08 ± 0.02 ^{ab}	0.13 ± 0.06 ^{a}	0.32 **
Sucrase	2.64 ± 0.62 ^{a}	1.32 ± 0.31 ^{b}	3.48 ± 0.87 ^{a}	2.41 ± 0.47 ^{ab}	3.15 ± 0.89 ^{a}	0.04

NH_4^+-N: ammonium nitrogen; NO_3^--N: nitrate nitrogen; AK: available potassium; pH: pH value; OM: organic matter; WC: water content; AP: available phosphorus; TN: total nitrogen; and TP: total phosphorus. Significant differences in same column are denoted by lowercase letters (p < 0.05). R^2 values indicate proportion of variance explained in regression analysis. Data are presented as mean ± SD (n = 4). * p < 0.05, ** p < 0.01.

3.2. AMF Colonization and Spore Density Along the Elevation Gradient

The roots of *H. miconioides* exhibited robust AMF colonization, with colonization rates ranging from 58.33% to 93.44% (Figure 2). Both the AMF colonization rate (R^2 = 0.38, p < 0.001) and spore density (R^2 = 0.49, p < 0.001) showed significant positive correlations with elevation. The Pearson correlation analysis revealed that AMF colonization was positively correlated with WC and catalase but negatively correlated with pH (Table S1). Spore density was positively correlated with WC, TN, catalase, and acid phosphatase, and negatively correlated with pH.

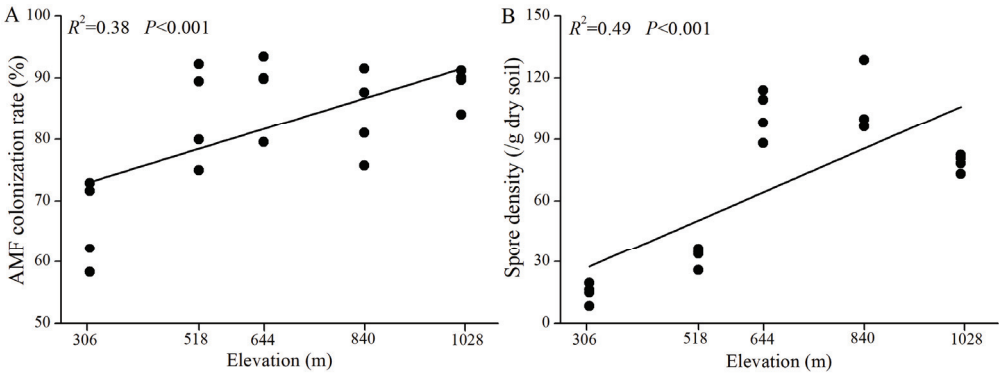


Figure 2. Linear correlations between elevation and AMF colonization rate (**A**) and spore density (**B**) of *H. miconioides*.

3.3. Overall Sequencing and Taxonomic Assignments in Root and Rhizosphere Soil

The sequencing generated a total of 476,816 reads (range: 22,985–24,634) from the root samples and 458,501 reads (range: 14,888–24,656) from the rhizosphere soil samples (Table S2). Based on the maarjam20220506/AM species database, 476,816 reads were classified into one phylum, four classes, six orders, twelve families, thirteen genera, and eighty-eight species in the root samples. In the rhizosphere soil, the data revealed one phylum, four classes, six orders, eleven families, thirteen genera, and seventy-six species. These sequences were grouped into 266 and 255 AMF OTUs in the root and rhizosphere samples, respectively, based on 97% sequence similarity, with 164 OTUs shared between the two environments (Figure 3A,B). Rarefaction curves for alpha diversity (Figure S1) showed a leveling off, indicating an adequate sequencing depth and suggesting that AMF diversity in the roots was higher than that in the rhizosphere soil.

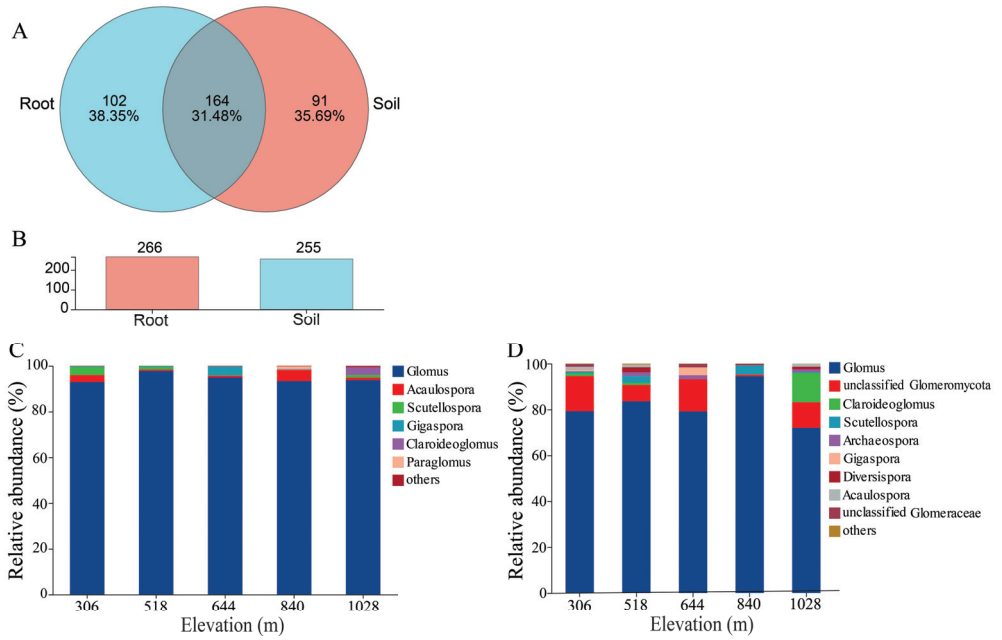


Figure 3. Relative abundance of AMF community composition in root and rhizosphere soil of *H. miconioides* along elevation gradients. (**A**) Venn diagram showing number of common and unique OTUs between root and rhizosphere soil. (**B**) Bar graphs representing total number of OTUs between root and rhizosphere soil. Relative abundance of AMF community composition at genus level in root (**C**) and rhizosphere soil (**D**).

At the genus level (Figure 3C,D), five genera were identified in the roots, including *Glomus*, *Scutellospora*, *Acaulospora*, *Gigaspora*, and *Claroideoglomus*. *Glomus* (94.57%) was the most abundant genus across all elevation gradients, followed by *Acaulospora* (2.08%). The genus-level analysis revealed that *Glomus*, *Scutellospora*, and *Acaulospora* were consistently present at all elevations, indicating their widespread distribution in Dongbai Mountain. In contrast, *Paraglomus* and *Claroideoglomus* were exclusively found in high-elevation root samples. In the rhizosphere soil, nine genera were detected, including *Glomus* (81.74%), unclassified *Glomeromycota* (9.68%), *Claroideoglomus* (2.98%), *Scutellospora* (1.61%), *Archaeospora* (0.98%), *Diversispora* (0.85%), *Gigaspora* (0.83%), *Acaulospora* (0.72%), and unclassified *Glomeraceae* (0.55%). Notably, *Claroideoglomus* exhibited significant differences ($p = 0.043$) across rhizosphere samples (Figure 3C,D, Table S3). A more detailed analysis at 1028 m elevation revealed the significant dominance of *Glomus* in both the root and rhizosphere soils (Figure S3). While *Scutellospora*, *Acaulospora*, *Gigaspora*, and *Claroideoglomus* were detected in samples of both the root and rhizosphere, unclassified *Glomeromycota*, *Archaeospora*, *Diversispora*, and unclassified *Glomeraceae* were exclusive to the rhizosphere soil.

3.4. Alpha Diversity of AMF in Root and Rhizosphere Soil

Alpha diversity indices (Shannon and Chao1) were used to assess the diversity of AMF communities in the root and rhizosphere soil of *H. miconioides* (Figure 4). The Shannon index for the root AMF communities significantly declined with elevation ($R^2 = 0.16$, $p = 0.046$), whereas the Chao1 index showed no significant correlation with elevation. Nevertheless, the Chao1 index in the roots was significantly higher than in the rhizosphere soil ($p = 0.022$; Figure S2). In the rhizosphere soil, neither the Shannon nor Chao1 indices exhibited significant changes along the elevation gradient. Additionally, no significant differences in AMF alpha diversity between the root and rhizosphere soil were observed across elevation gradients (Figure 4C,F).

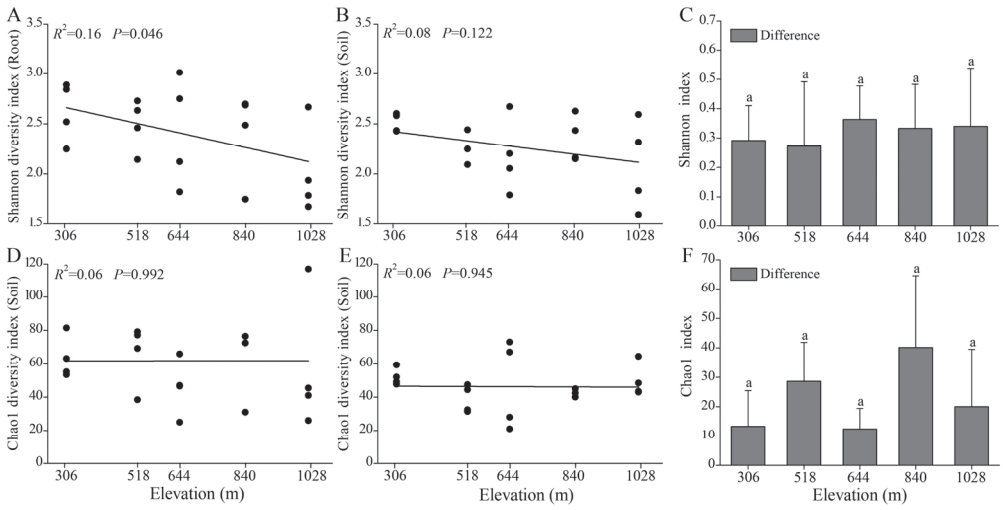


Figure 4. Linear correlations between elevation and alpha diversity indices (Shannon and Chao1) in root (**A**,**D**), rhizosphere soil (**B**,**E**), and their differences (**C**,**F**) in *H. miconioides*. Data are presented as means ± SD. Significant differences are denoted by lowercase letters ($p < 0.05$).

3.5. Beta Diversity of AMF in Root and Rhizosphere Soil

The NMDS analysis based on Bray–Curtis distances and Adonis tests at the OTU level revealed significant differences in the AMF community structure along elevation gradients in both the root ($R^2 = 0.32$; $p = 0.015$) and rhizosphere soil samples ($R^2 = 0.26$; $p = 0.044$) (Figure 5A,B). The AMF communities at the 1028 m elevation were distinctly separated

from those at 840 m and 518 m. In the root samples, significant species differences were also observed between 840 m and 306 m elevations. In the rhizosphere soil, the 1028 m elevation community significantly differed from the 306 m elevation community. Interestingly, differences in AMF beta diversity between the root and rhizosphere soil initially increased and then decreased with elevation (Figure 5C). These results clearly distinguish between AMF communities in higher and lower elevations.

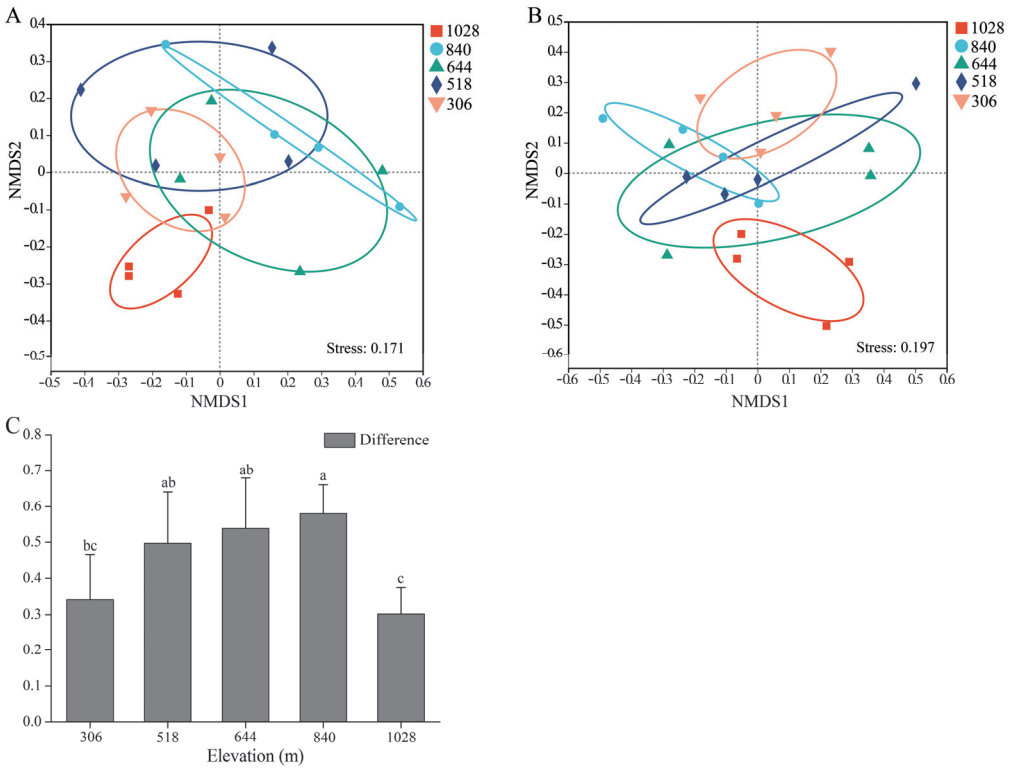


Figure 5. Nonmetric multidimensional scaling (NMDS) ordinations of AMF community compositions (Bray–Curtis) in root (**A**), rhizosphere soil (**B**), and their differences (**C**) based on OTU abundance along elevation gradients. Data are presented as means ± SD. Significant differences are denoted by lowercase letters ($p < 0.05$).

3.6. Co-Occurrence Network Analysis of AMF Community in Root and Rhizosphere Soil

We constructed correlation networks of the AMF communities in the root and rhizosphere soil along elevation gradients (Figure 6A–J). The networks generated a total of 217 nodes (range: 40–45) connected by 424 edges (range: 51–114) from the root samples and 210 nodes (range: 38–46) connected by 657 edges (range: 69–184) from the rhizosphere soil samples (Table S4). The rhizosphere soil contained more edges than the root. In the root and rhizosphere soil co-occurrence networks, the average proportion of positive edges was 0.91 (range: 0.80–0.97) and 0.97 (range: 0.92–1), respectively (Table S4). The number of nodes and edges of the root AMF community co-occurrence networks generally increased with increasing elevation, but not with the rhizosphere soil AMF community co-occurrence network. Furthermore, correlation analysis showed that the degree and degree centralization in the root AMF community co-occurrence network significantly increased with increasing elevation gradient (Figure 6K,L). However, no significant correlations between these topological parameters and the elevation gradient were observed in the rhizosphere soil AMF community co-occurrence network (Figure 6M,N). These results suggest that elevation gradients play more important roles in shaping the AMF community co-occurrence network structure of the root than the rhizosphere soil.

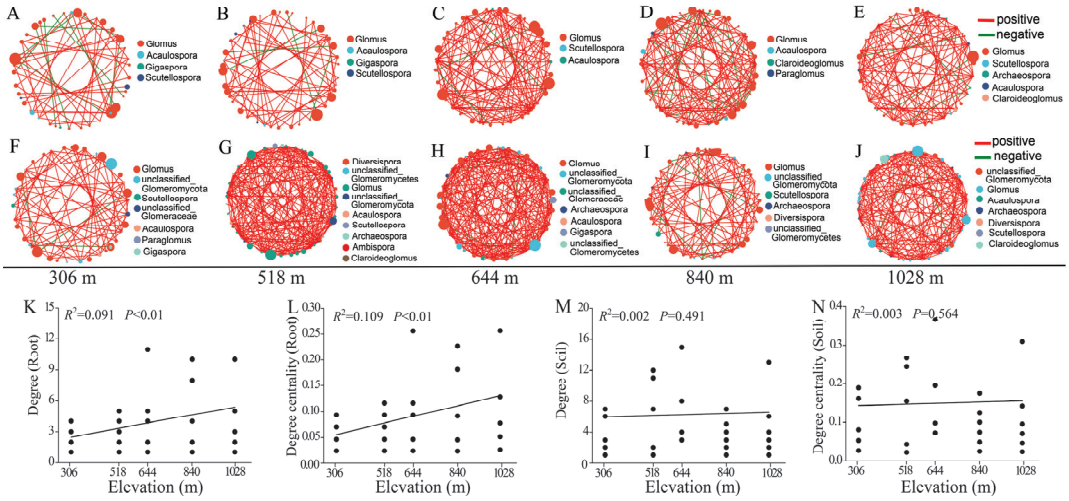


Figure 6. The co-occurrence networks analysis of AMF community along elevation gradients. The changes in the AMF community co-occurrence networks in the root at 306 m (**A**), 518 m (**B**), 644 m (**C**), 840 m (**D**), and 1028 m (**E**) elevation. The changes in the AMF community co-occurrence networks in the rhizosphere soil at 306 m (**F**), 518 m (**G**), 644 m (**H**), 840 m (**I**), and 1028 m (**J**) elevation. Linear correlations between elevation and topological parameters of the AMF community co-occurrence networks in the root (**K**,**L**) and rhizosphere soil (**M**,**N**) of *H. miconioides*. The positive and negative correlations are indicated by red and blue lines, respectively.

3.7. Relationships Between Soil Characteristics and AMF Community

CCA and permutest analyses identified NO_3^--N, AK, OM, acid phosphatase, and elevation as significant factors influencing AMF community structure in the roots (Figure 7A). In the rhizosphere soil, pH, AP, TN, and NH_4^+-N significantly affected the AMF community composition (Figure 7B). The Mantel test results indicated that the root AMF community structure was significantly correlated with AP and TN contents, while the rhizosphere soil community was correlated with TN content (Table 2). Pearson's correlation analysis further showed that the Shannon and Chao1 indices for AMF in the rhizosphere soil were not significantly associated with soil properties (Table S5). However, in the roots AP, TN, and catalase activity were significantly correlated with the Shannon index (Table S5).

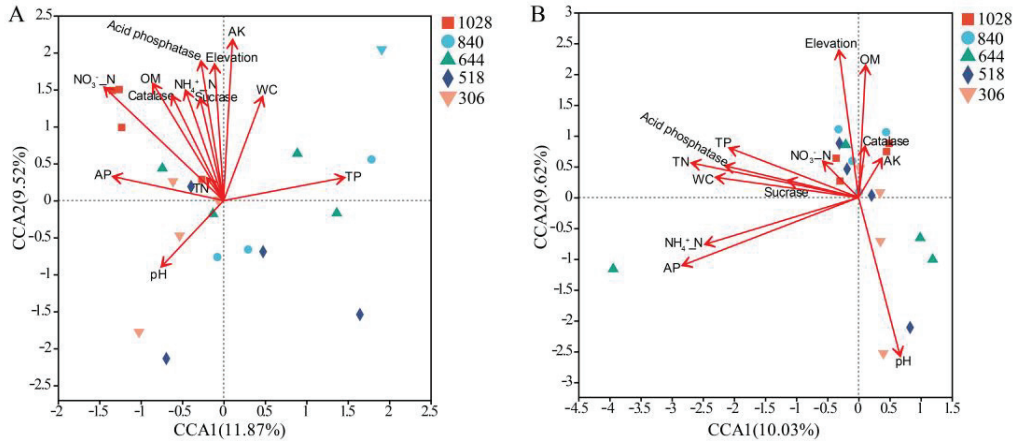


Figure 7. Canonical correspondence analysis (CCA) plots of AMF community compositions and soil properties in root (**A**) and rhizosphere soil (**B**) based on OTU abundance along elevation gradients.

Table 2. Mantel analysis of relationship between OTU relative abundance and soil parameters.

Soil Properties	Rhizosphere Soil		Root	
	R^2	p	R^2	p
NH_4^+-N	0.020	0.424	0.123	0.138
NO_3^--N	0.056	0.306	0.147	0.058
AK	−0.015	0.513	0.041	0.342
pH	−0.003	0.497	−0.081	0.861
OM	0.114	0.164	0.138	0.092
WC	−0.066	0.689	−0.084	0.785
AP	0.038	0.369	0.238	0.021
TN	0.233	0.029	0.177	0.036
TP	−0.090	0.775	0.001	0.497
Catalase	0.164	0.072	0.050	0.296
Acid phosphatase	0.071	0.271	0.035	0.664
Sucrase	0.132	0.150	−0.051	−0.27
Elevation	0.104	0.122	−0.009	0.534

R^2 values indicate proportion of variance explained in regression analysis. p values indicate significance level ($p < 0.05$).

Pearson's correlation analysis was performed to investigate the relationships between the soil properties and AMF diversity at the genus level (Figure 8). In the root samples, OM content was positively correlated with *Claroideoglomus*, while AK content showed a positive correlation with *Paraglomus* (Figure 8A). TP content exhibited a positive correlation with *Glomus* and a negative correlation with *Gigaspora*. In the rhizosphere soil, AP and NH_4^+-N were negatively correlated with *Glomus* but positively associated with unclassified *Glomeromycota*. TN, AP, NH_4^+-N, and acid phosphatase were positively correlated with *Gigaspora* (Figure 8B). Furthermore, AK and TP exhibited positive correlations with *Scutellospora*.

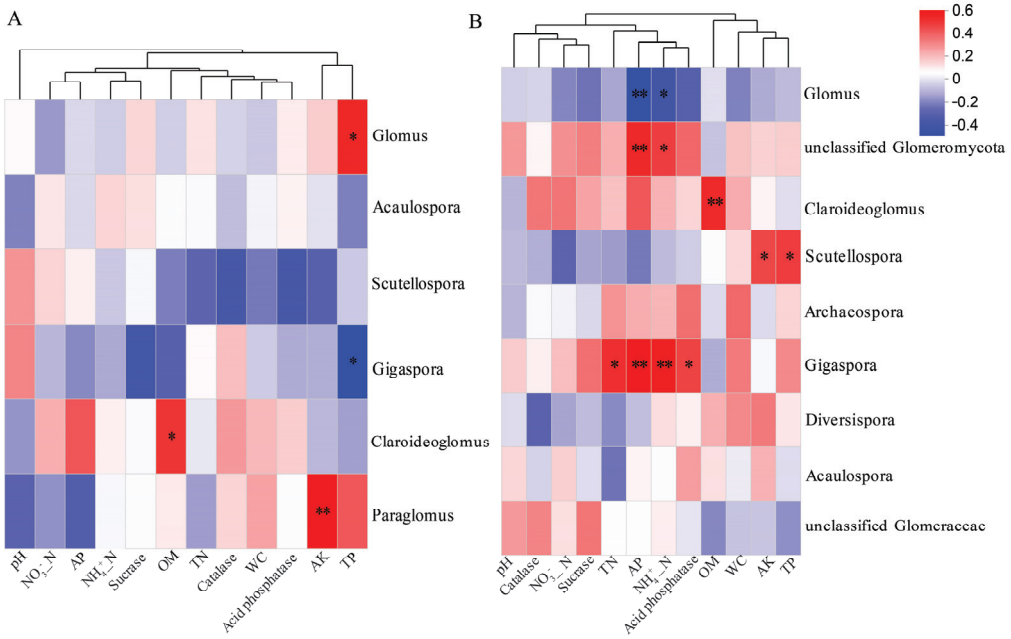


Figure 8. Pearson correlations between AMF communities at genus level in root (**A**) and rhizosphere soil (**B**) along elevation gradients. * $p < 0.05$; ** $p < 0.01$.

4. Discussion

AMF play a crucial role in ecosystem stability and ecological restoration [4,5]. Many endangered plants form symbiotic relationships with AMF, often thriving in specialized habitats that harbor unique AMF species [43]. This study investigated the colonization and

diversity of AMF in the root and rhizosphere soil of endangered *H. miconioides* across elevation gradients, identifying key environmental factors that shape AMF community structure.

4.1. Changes in AMF Colonization and Spore Density of H. miconioides Along Elevation Gradients

AMF colonization and spore density are critical indicators of AMF growth and their symbiotic relationships with host plants [34]. Our previous research demonstrated that AMF inoculation successfully formed a robust symbiosis with *H. miconioides* roots under greenhouse conditions, achieving a colonization rate exceeding 80% [28]. In the current study, AMF colonization and spore density increased linearly with elevation, indicating a strengthening symbiotic relationship at higher elevations. This trend aligns with the natural distribution of *H. miconioides*, which is more abundant at higher elevations. The increased AMF colonization and spore density at higher elevations likely reflect AMF's role in enhancing soil nutrient availability and promoting plant growth. However, these findings contrast with previous studies reporting either negative correlations between AMF colonization and elevation [13,44] or non-linear trends [45]. The discrepancy may be attributed to differences in elevation ranges, as previous studies examined gradients up to 1000 m, whereas this study focused on gradients of approximately 700 m. Variations in host plant species and the harsh environmental conditions of high-altitude ecosystems may also contribute to these differences [46,47]. Additionally, spore density in the rhizosphere soil also increased linearly with elevation, corroborating the findings of Coutinho et al. [48], who reported the highest spore density at 1100 m. However, other research on *Chamaecyparis formosensis* at elevations ranging from 1200 to 2500 m found no significant elevation effect on spore density [49]. Factors such as soil nutrient availability, host dependency, natural habitat, and spore ecological adaptations likely influence AMF spore distribution patterns [14,49,50]. Pearson's correlation analysis revealed significant positive correlations between AMF spore density and WC, TN, catalase, and acid phosphatase levels, while a negative correlation was observed with pH. AMF spore density may be linked to acidic soils, which produce higher AMF spore counts but lower taxonomic diversity compared to slightly acidic soils [51]. Our results suggest that soil moisture, TN, and enzyme activities may play important roles in enhancing soil microbial reproduction, resulting in increased mycorrhizal sporulation [52–54]. These findings underscore the critical influence of soil properties on the rhizosphere spore density of *H. miconioides* along elevation gradients.

4.2. Comparison of AMF Communities in Root and Rhizosphere Soil of H. miconioides Along Elevation Gradients

AMF occupy dual niches within the host roots and surrounding soil, playing a critical role in maintaining plant populations [43,55]. At the genus level, *Glomus* was more abundant in *H. miconioides* roots than in rhizosphere soil and consistently dominated AMF communities at all elevations. A similar dominance by *Glomus* or members of Glomeraceae has been observed in other endangered plants, including *Ulmus chenmoui* [52], *Toona ciliata* [56], and *Tetraena mongolica* [57]. The extensive colonization of *Glomus* within roots across diverse habitats enhances plant resistance and adaptability to environmental stress [58]. Nevertheless, other studies have identified Acaulosporaceae and Gigasporaceae as dominant AMF in the roots of endangered plants [59], suggesting that AMF dominance may depend on host specificity. Moreover, elevational differences also influenced the relative abundance of other AMF genera. *Paraglomus* and *Claroideoglomus* were predominantly detected at higher elevations, while *Gigaspora* was more common at lower elevations. Variations in water and nutrient availability likely shaped these distribution patterns. For instance, Gigasporaceae, known for producing extensive external hyphae, is well suited for

nutrient acquisition in nutrient-poor soils [58]. The poor soil conditions at lower elevations in this study likely favored *Gigaspora*, whose well-developed external hyphae network supports nutrient absorption for host plants.

Our study also found that the AMF community compositions in roots and rhizosphere soil differed significantly, consistent with previous findings from forest ecosystems [22]. Bonfim et al. [60] reported high AMF diversity in rhizosphere soil in a Brazilian Atlantic forest, with only Glomeraceae detected within roots. These compositional differences may be due to the selective preferences of plant root systems and the varying responses of AMF taxa to root and rhizosphere environments [22]. Root-associated AMF communities are primarily shaped by plant characteristics, whereas those in rhizosphere soil are influenced by external environmental factors. Moreover, the differences in beta diversity between root and rhizosphere AMF communities initially increased along elevation gradients but decreased at the highest elevation (1028 m), resembling trends observed in Taibai Mountain alpine meadows [42]. The shift from dispersion at medium elevations (low-nutrient conditions) to aggregation at high elevations (high-nutrient conditions) indicates that abiotic factors significantly influence AMF community structure. The reduced beta diversity differences at the highest elevation suggest that environmental conditions at high elevations foster more uniform AMF community assemblies between the roots and rhizosphere soil in *H. miconioides*. Furthermore, previous studies have shown that topological parameters in co-occurrence networks, such as clustering coefficient, average degree, and degree centralization, can reflect the interaction intensity between species [61,62]. In this study, the degree and degree centralization of the root AMF community co-occurrence networks significantly increased with the increasing elevation, while no significant difference in the rhizosphere soil was observed. These findings further suggest that the interaction intensities of the AMF community within *H. miconioides* roots are more pronounced at higher elevations compared to those at lower elevations.

In addition to differences composition and distribution, alpha diversity patterns also varied between root and rhizosphere AMF communities along elevation gradients. Root AMF diversity significantly decreased with increasing elevation, aligning with previous studies reporting negative correlations between AMF diversity and elevation [13,14]. However, contrasting results from Brazilian forests, where AMF diversity increased at higher elevations [60], highlight the influence of regional environmental factors and soil characteristics. Despite the decline in root AMF diversity, no significant changes were observed in rhizosphere AMF diversity along elevation gradients. This discrepancy suggests that the reduced AMF-root symbiotic associations at high elevations are not due to the absence of symbiotic AMF in the rhizosphere but rather host plant selection against diverse fungal communities [63]. Interestingly, the Chao1 richness index for AMF communities remained stable in both root and rhizosphere samples across elevations. These findings indicate that neither the availability of AMF in rhizosphere soil nor the capacity of *H. miconioides* to establish and maintain mycorrhizal associations were significantly influenced by elevation gradients.

4.3. Relationship Between Environmental Factors and AMF Communities in Root and Rhizosphere Soil of H. miconioides

The structure of the AMF community in the roots and rhizosphere soil of *H. miconioides* shows distinct relationships with environmental factors. Previous studies have demonstrated that soil properties, elevation, and environmental filtering significantly influence AMF diversity, leading to spatial variations in AMF communities at local scales [55,64]. Our findings indicate that the composition of rhizosphere soil AMF communities in *H.*

miconioides is strongly associated with soil pH, AP, and TN levels. Soil pH plays a crucial role in shaping AMF community structure [65], likely affecting spore formation and development [56], nutrient availability [66], and the distribution of AMF genera [67]. In this study, while pH did not significantly influence root-associated AMF communities, it had a pronounced effect on the AMF composition in rhizosphere soil, suggesting that AMF communities in the rhizosphere are more sensitive to pH changes. Additionally, AP and TN levels were significantly correlated with AMF diversity in the rhizosphere soil, aligning with previous findings [57]. Changes in AP and TN likely influence AMF spore germination, mycelial growth, and the efficiency of mycorrhizal symbiosis [68]. The Mantel test further confirmed the significant impact of TN content on AMF community structure, supporting this viewpoint.

In contrast, the root-associated AMF composition was significantly correlated with NO_3^--N, AK, OM, acid phosphatase, and elevation. Correlation analysis revealed that OM content was positively associated with *Claroideoglomus*, while AK content correlated positively with *Paraglomus*. Nutrient enrichment, particularly increased OM levels, may enhance AMF reproduction, influencing community abundance and diversity [69]. AK is also known to support AMF colonization and the establishment of effective symbioses in certain plant species [70]. Acid phosphatase may have direct or indirect roles in soil and microbial-mediated phosphorus cycling, further influencing AMF abundance. Collectively, these findings suggest that variations in soil properties (pH, AP, TN, NO_3^--N, AK, OM, and acid phosphatase) along elevation gradients significantly affect AMF genera, driving differences in the AMF composition between roots and rhizosphere soil. Our study underscores the ecological preferences of symbiotic AMF in response to elevation-related environmental changes within the natural distribution area of *H. miconioides*. Future research examining the influence of additional environmental factors, such as climate variables and vegetation types, could provide deeper insights into the mechanisms governing AMF community assembly and diversity along elevational gradients.

5. Conclusions

Our field investigation revealed a significant increase in AMF colonization rates and spore density in *H. miconioides* natural populations with the increase in the elevation gradient. The dominant AMF genera in both the root and rhizosphere soil included *Glomus*, *Claroideoglomus*, unclassified *Glomeromycota*, *Scutellospora*, *Gigaspora*, and *Acaulospora*, though their relative proportions varied with elevation. The root-associated AMF alpha diversity decreased linearly with increasing elevation, whereas the rhizosphere soil diversity remained largely unchanged. Beta diversity differences between the root and rhizosphere soil initially increased and then declined with elevation. Rhizosphere AMF communities were closely associated with soil pH, AP, and TN, while root-associated communities were significantly correlated with NO_3^--N, AK, OM, acid phosphatase, and elevation. These findings provide valuable insights into the diversity and ecological preferences of the AMF species associated with *H. miconioides*. The characterization and identification of AMF species in the natural habitat of *H. miconioides* hold the potential for isolating highly effective AMF strains that have co-evolved with the species. Such strains could be harnessed as AMF inoculants to support *H. miconioides* conservation and habitat restoration efforts. These insights also offer a novel perspective for enhancing the conservation of other endangered plant species capable of forming AMF associations.

Supplementary Materials: The following supporting information can be downloaded at https://www.mdpi.com/article/10.3390/jof11030222/s1, Table S1. Pearson correlation analysis of soil

properties with AMF colonization rate and spore density; Table S2. AMF sequences and mean length of sequences in each rhizosphere soil and root samples at different elevations; Table S3. Relative abundance of AMF in the *H. miconioides* rhizosphere soil and root along elevation gradient; Table S4. The topological parameters of the AMF community co-occurrence networks in rhizosphere soil and root; Table S5. Pearson correlation analysis of soil properties with Shannon and Chao1 diversity in rhizosphere soil and root; Figure S1. AMF community dilution curves for soil at different elevations; Figure S2. Alpha diversity indices of AMF communities were compared between root (n = 20) and rhizosphere soil (n = 20) samples; Figure S3. The relative abundances of *Glomus* in the root and soil samples. Values in the bar plot are expressed as mean ± standard deviation. Asterisks indicate significant difference between treatments based on Student's t-test ($p < 0.05$).

Author Contributions: Y.L. and G.L. conducted most of the experiments. G.L. and D.Y. worked with Y.L. on the field sample collection. S.W. and P.L. worked with Y.L. on data analysis. J.L. and Z.J. conceived the experiments and revised the draft manuscript. All authors have read and agreed to the published version of the manuscript.

Funding: This study was supported by the Zhejiang Provincial Natural Science Foundation of China (LTY22C030002; LQ19C030001) and the National Natural Science Foundation of China (32001113).

Institutional Review Board Statement: Not applicable.

Informed Consent Statement: Not applicable.

Data Availability Statement: The dataset was deposited in the NCBI under accession numbers PRJNA1230584 (rhizosphere soil) and PRJNA1230586 (root).

Conflicts of Interest: The authors claim to have no conflicts of interest.

References

1. Boonman, C.C.F.; Serra-Diaz, J.M.; Hoeks, S.; Guo, W.Y.; Enquist, B.J.; Maitner, B.; Malhi, Y.; Merow, C.; Buitenwerf, R.; Svenning, J. More than 17,000 tree species are at risk from rapid global change. *Nat. Commun.* **2024**, *15*, 166. [CrossRef] [PubMed]
2. Thomas, C.D.; Cameron, A.; Green, R.E.; Bakkenes, M.; Beaumont, L.J.; Collingham, Y.C.; Erasmus, B.F.N.; de Siqueira, M.F.; Grainger, A.; Hannah, L.; et al. Extinction risk from climate change. *Nature* **2004**, *427*, 145–148. [CrossRef]
3. de Vries, F.; Lau, J.; Hawkes, C.; Semchenko, M. Plant-soil feedback under drought: Does history shape the future? *Trends Ecol. Evol.* **2023**, *8*, 708–718. [CrossRef]
4. Willing, C.E.; Wan, J.; Yeam, J.J.; Cessna, A.M.; Peay, K.G. Arbuscular mycorrhizal fungi equalize differences in plant fitness and facilitate plant species coexistence through niche differentiation. *Nat. Ecol. Evol.* **2024**, *8*, 2058–2071. [CrossRef]
5. Smith, S.; Facelli, E.; Pope, S.; Andrew Smith, F. Plant performance in stressful environments: Interpreting new and established knowledge of the roles of arbuscular mycorrhizas. *Plant Soil* **2010**, *326*, 3–20. [CrossRef]
6. Nuortila, C.; Kytöviita, M.; Tuomi, J. Mycorrhizal symbiosis has contrasting effects on fitness components in Campanula rotundifolia. *New Phytol.* **2004**, *164*, 543–553. [CrossRef]
7. Zubek, S.; Turnau, K.; Tsimilli-Michael, M.; Strasser, R.J. Response of endangered plant species to inoculation with arbuscular mycorrhizal fungi and soil bacteria. *Mycorrhiza* **2009**, *19*, 113–123. [CrossRef] [PubMed]
8. Rigg, J.L.; Offord, C.A.; Singh, B.K.; Anderso, I.; Clarke, S.; Powell, J.R. Soil microbial communities influence seedling growth of a rare conifer independent of plant–soil feedback. *Ecology* **2016**, *97*, 3346–3358. [CrossRef]
9. Karthikeyan, A.; Arunprasad, T. Growth response of *Pterocarpus santalinus* seedlings to native microbial symbionts (arbuscular mycorrhizal fungi and Rhizobium aegyptiacum) under nursery conditions. *J. For. Res.* **2021**, *32*, 225–231. [CrossRef]
10. Wang, Y.H.; Shao, C.L.; Qiu, Y.J.; Yu, S.Q.; Xia, L.; He, X.B.; Wu, A.P.; Zhang, N.L. Arbuscular mycorrhizal fungi protect a subtropical tree species exposed to simulated acid rain by accelerating photosynthetic ability, antioxidant enzymes and osmolyte accumulation. *J. Plant Ecol.* **2022**, *15*, 1036–1048. [CrossRef]
11. Nottingham, A.T.; Bååth, E.; Reischke, S.; Salinas, N.; Meir, P. Adaptation of soil microbial growth to temperature: Using a tropical elevation gradient to predict future changes. *Global Change Biol.* **2019**, *25*, 827–838. [CrossRef] [PubMed]
12. Körner, C. The use of 'altitude' in ecological research. *Trends Ecol. Evol.* **2007**, *22*, 569–574. [CrossRef] [PubMed]
13. Gai, J.P.; Tian, H.; Yang, F.Y.; Christie, P.; Li, X.L.; Klironomos, J.N. Arbuscular mycorrhizal fungal diversity along a Tibetan elevation gradient. *Pedobiologia* **2012**, *55*, 145–151. [CrossRef]

14. Liu, L.; Hart, M.M.; Zhang, J.; Cai, X.; Gai, J.; Christie, P.; Li, X.; Klironomos, J.N. Altitudinal distribution patterns of Am fungal assemblages in a Tibetan alpine grassland. *FEMS Microbiol. Ecol.* **2015**, *91*, fiv078. [CrossRef] [PubMed]
15. Vieira, L.C.; da Silva, D.K.A.; de Melo, M.A.C.; Escobar, I.E.C.; Oehl, F.; da Silva, G.A. Edaphic factors influence the distribution of arbuscular mycorrhizal fungi along an altitudinal gradient of a Tropical Mountain. *Microb. Ecol.* **2019**, *78*, 904–913. [CrossRef]
16. Yu, L.; Zhang, Z.; Zhou, L.; Huang, K. Effects of Altitude and Continuous Cropping on Arbuscular Mycorrhizal Fungi Community in *Siraitia grosvenorii* Rhizosphere. *Agriculture* **2023**, *13*, 1548. [CrossRef]
17. Zhang, M.; Shi, Z.; Yang, M.; Lu, S.; Cao, L.; Wang, X. Molecular Diversity and Distribution of Arbuscular Mycorrhizal Fungi at Different Elevations in Mt. Taibai of Qinling Mountain. *Front. Microbiol.* **2021**, *12*, 609386. [CrossRef]
18. Maherali, H.; Klironomos, J.N. Influence of Phylogeny on Fungal Community Assembly and Ecosystem Functioning. *Science* **2007**, *316*, 1746–1748. [CrossRef]
19. Chagnon, P.L.; Bradley, R.L.; Maherali, H.; Klironomos, J.N. A trait-based framework to understand life history of mycorrhizal fungi. *Trends Plant Sci.* **2013**, *18*, 484–491. [CrossRef]
20. Pascual, J.; Blanco, S.; Ramos, J.L.; van Dillewijn, P. Responses of bulk and rhizosphere soil microbial communities to thermoclimatic changes in a Mediterranean ecosystem. *Soil Biol. Biochem.* **2018**, *118*, 130–144. [CrossRef]
21. Stevens, B.M.; Propster, J.R.; Öpik, M.; Wilson, G.W.; Alloway, S.L.; Mayemba, E.; Johnson, N.C. Arbuscular mycorrhizal fungi in roots and soil respond differently to biotic and abiotic factors in the Serengeti. *Mycorrhiza* **2020**, *30*, 79–95. [CrossRef] [PubMed]
22. Ji, L.; Zhang, Y.; Yang, Y.C.; Yang, L.X.; Yang, N.; Zhang, D.P. Long-term effects of mixed planting on arbuscular mycorrhizal fungal communities in the roots and soils of *Juglans mandshurica* plantations. *BMC Microbiol.* **2020**, *20*, 304. [CrossRef]
23. Mirás-Avalos, J.M.; Antunes, P.M.; Koch, A.; Khosla, K.; Klironomos, J.N.; Dunfield, K.E. The influence of tillage on the structure of rhizosphere and root-associated arbuscular mycorrhizal fungal communities. *Pedobiologia* **2011**, *54*, 235–241. [CrossRef]
24. Hempel, S.; Renker, C.; Buscot, F. Differences in the species composition of arbuscular mycorrhizal fungi in spore, root and soil communities in a grassland ecosystem. *Environ. Microbiol.* **2007**, *9*, 1930–1938. [CrossRef] [PubMed]
25. Li, Y.L.; Sun, Z.S.; Jin, Z.X.; Li, J.M. Genome sequencing provides insights into Caprifoliaceae genome evolution and the mechanism underlying second blooming phenomenon in *Heptacodium miconioides*. *Hortic. Plant J.* **2024**, *10*, 897–910. [CrossRef]
26. Zhang, Y.F.; Chen, C.; Jin, Z.X.; Yang, Z.N.; Li, Y.L. Leaf anatomy, photosynthesis, and chloroplast ultrastructure of *Heptacodium miconioides* seedlings reveal adaptation to light environment. *Environ. Exp. Bot.* **2022**, *195*, 104780. [CrossRef]
27. Christenhusz, M.J.M.; Mian, S.; Lambkin, D. 1057. Heptacodium miconioides Rehder. *Curtis's Bot. Mag.* **2023**, *40*, 65–73. [CrossRef]
28. Li, Y.L.; Wang, X.Y.; Chen, X.Y.; Lu, J.Y.; Jin, Z.X.; Li, J.M. Functions of arbuscular mycorrhizal fungi in regulating endangered species *Heptacodium miconioides* growth and drought stress tolerance. *Plant Cell Rep.* **2023**, *42*, 1967–1986. [CrossRef]
29. Li, Y.L.; Jin, Z.X.; Luo, G.Y.; Chen, C.; Sun, Z.S.; Wang, X.Y. Effects of arbuscular mycorrhizal fungi inoculation on non-structural carbohydrate contents and C:N:P stoichiometry of *Heptacodium miconioides* under drought stress. *Chin. J. Appl. Ecol.* **2022**, *33*, 963–971.
30. Mebius, L. A rapid method for the determination of organic carbon in soil. *Anal. Chim. Acta* **1960**, *22*, 120–124. [CrossRef]
31. Liu, G.; Liu, R.L.; Zhang, W.G.; Yang, B.; Bi, X.Q.; Li, M.Z.; Chen, X.Y.; Nie, H.; Zhu, Z.H. Arbuscular mycorrhizal colonization rate of an exotic plant, *Galinsoga quadriradiata*, in mountain ranges changes with altitude. *Mycorrhiza* **2021**, *31*, 161–171. [CrossRef] [PubMed]
32. Zhen, Z.; Wang, S.B.; Luo, S.W.; Ren, L.; Liang, Y.Q.; Yang, R.C.; Li, Y.T.; Zhang, Y.Q.; Deng, S.Q.; Zou, L.N. Significant impacts of both total amount and availability of heavy metals on the functions and assembly of soil microbial communities in different land use patterns. *Front. Microbiol.* **2019**, *10*, 2293. [CrossRef]
33. Phillips, J.M.; Hayman, D.S. Improved procedures for clearing roots and staining parasitic and vesicular-arbuscular mycorrhizal fungi for rapid assessment of infection. *Brit. Mycol. Soc.* **1970**, *55*, 158–161. [CrossRef]
34. Giovannetti, M.; Mosse, B. An evaluation of techniques for measuring vesicular arbuscular mycorrhizal infection in roots. *New Phytol.* **1980**, *84*, 489–500. [CrossRef]
35. Brundrett, M.; Melville, L.; Peterson, L. *Practical Methods in Mycorrhiza Research: Based on a Workshop Organized in Conjunction with the Ninth North American Conference on Mycorrhizae*; University of Guelph, Canada, Mycologue Publication: Guelph, ON, Canada, 1994.
36. Lumini, E.; Orgiazzi, A.; Borriello, R.; Bonfante, P.; Bianciotto, V. Disclosing arbuscular mycorrhizal fungal biodiversity in soil through a land-use gradient using a Pyrosequencing approach. *Environ. Microbiol.* **2010**, *12*, 2165–2179. [CrossRef] [PubMed]
37. Chen, S.F.; Zhou, Y.Q.; Chen, Y.R.; Gu, J. fastp: An ultra-fast all-in-one FASTQ preprocessor. *Bioinformatics* **2018**, *34*, i884–i890. [CrossRef]
38. Magoč, T.; Salzberg, S.L. FLASH: Fast length adjustment of short reads to improve genome assemblies. *Bioinformatics* **2011**, *27*, 2957–2963. [CrossRef]
39. Edgar, R.C. UPARSE: Highly accurate OTU sequences from microbial amplicon reads. *Nat. Methods* **2013**, *10*, 996–998. [CrossRef]

40. Wang, Q.; Garrity, G.M.; Tiedje, J.M.; Cole, J.R. Naive Bayesian classifier for rapid assignment of rRNA sequences into the new bacterial taxonomy. *Appl. Environ. Microbiol.* **2007**, *73*, 5261–5267. [CrossRef]
41. Schloss, P.D.; Westcott, S.L.; Ryabin, T.; Hall, J.R.; Hartmann, M.; Hollister, E.B.; Lesniewski, R.A.; Oakley, B.B.; Parks, D.H.; Robinson, C.J.; et al. Introducing mothur: Open-Source, Platform-Independent, Community-Supported Software for Describing and Comparing Microbial Communities. *Appl. Environ. Microb.* **2009**, *75*, 7537. [CrossRef]
42. Zhao, F.Z.; Feng, X.X.; Guo, Y.X.; Ren, C.J.; Wang, J.; Doughty, R. Elevation gradients affect the differences of arbuscular mycorrhizal fungi diversity between root and rhizosphere soil. *Agric. For. Meteorol.* **2020**, *284*, 107894. [CrossRef]
43. Bothe, H.; Turnau, K.; Regvar, M. The potential role of arbuscular mycorrhizal fungi in protecting endangered plants and habitats. *Mycorrhiza* **2010**, *20*, 445–457. [CrossRef]
44. Kotilinek, M.; Hiiesalu, I.; Košnar, J.; Šmilauerová, M.; Šmilauer, P.; Altman, J.; Dvorský, M.; Kopecký, M.; Doležal, J. Fungal root symbionts of high-altitude vascular plants in the Himalayas. *Sci. Rep.* **2017**, *7*, 6562. [CrossRef]
45. Zhang, M.; Yang, M.; Shi, Z.; Gao, J.; Wang, X. Biodiversity and Variations of Arbuscular Mycorrhizal Fungi Associated with Roots along Elevations in Mt. Taibai of China. *Diversity* **2022**, *14*, 626. [CrossRef]
46. Wahl, A.L.; Spiegelberger, T. Arbuscular mycorrhizal fungi in changing mountain grassland ecosystems: A challenge for research. *Botany* **2016**, *94*, 435–458. [CrossRef]
47. Yang, Y.; Zhang, H.B.; Chai, Y.B.; Xie, H.J.; Mi, N.N.; Li, X.L.; Jin, Z.B.; Gai, J.P. Elevational distribution and occurrence of arbuscular mycorrhizal fungi in non-host *Carex capillacea*. *Mycorrhiza* **2021**, *31*, 713–722. [CrossRef] [PubMed]
48. Coutinho, E.S.; Fernandes, G.W.; Berbara, R.L.L.; Valério, H.M.; Goto, B.T. Variation of arbuscular mycorrhizal fungal communities along an altitudinal gradient in rupestrian grasslands in Brazil. *Mycorrhiza* **2015**, *25*, 627–638. [CrossRef] [PubMed]
49. Lin, T.C.; Lin, W.R.; Lin, L.C.; Wang, P.H. Arbuscular mycorrhizal fungal diversity associated with an endangered species, *Chamaecyparis formosensis*, in the nature habitat. *Trop. Ecol.* **2024**, *65*, 271–277. [CrossRef]
50. Lisboa, F.J.G.; Chaer, G.; Fernandes, M.F.; Berbara, R.L.L.; Madari, B. The match between microbial community structure and soil properties is modulated by land use types and sample origin within an integrated agroecosystem. *Soil Biol. Biochem.* **2014**, *78*, 97–118. [CrossRef]
51. Coughlan, A.P.; Dalpé, Y.; Lapointe, L.; Piché, Y. Soil pH-induced changes in root colonization, diversity, and reproduction of symbiotic arbuscular mycorrhizal fungi from healthy and declining maple forests. *Can. J. Forest Res.* **2000**, *30*, 1543–1554. [CrossRef]
52. Song, J.; Chen, L.; Chen, F.M.; Ye, J.R. Edaphic and host plant factors are linked to the composition of arbuscular mycorrhizal fungal communities in the root zone of endangered *Ulmus chenmoui* Cheng in China. *Ecol. Evol.* **2019**, *9*, 8900–8910. [CrossRef] [PubMed]
53. Shukla, A.; Vyas, D.; Jha, A. Soil depth: An overriding factor for distribution of arbuscular mycorrhizal fungi. *J. Soil Sci. Plant Nutr.* **2013**, *13*, 23–33. [CrossRef]
54. Bowles, T.M.; Acosta-Martínez, V.; Calderón, F.; Jackson, L.E. Soil enzyme activities, microbial communities, and carbon and nitrogen availability in organic agroecosystems across an intensively-managed agricultural landscape. *Soil Biol. Biochem.* **2014**, *68*, 252–262. [CrossRef]
55. Vályi, K.; Mardhiah, U.; Rillig, M.C.; Hempel, S. Community assembly and coexistence in communities of arbuscular mycorrhizal fungi. *ISME J.* **2016**, *10*, 2341–2351. [CrossRef] [PubMed]
56. Pan, J.F.; Wang, Q.; Guo, X.Y.; Jiang, X.R.; Cheng, Q.Q.; Fu, L.; Liu, W.; Zhang, L. Local patterns of arbuscular mycorrhizal fungal diversity and community structure in a natural *Toona ciliata* var. pubescens forest in South Central China. *PeerJ* **2021**, *9*, e11331. [CrossRef] [PubMed]
57. Xu, D.; Yu, X.; Chen, J.; Liu, H.; Zheng, Y.; Qu, H.; Bao, Y. Arbuscular Mycorrhizae Fungi Diversity in the Root–Rhizosphere–Soil of *Tetraena mongolica*, *Sarcozygium xanthoxylon*, and *Nitraria tangutorum* Bobr in Western Ordos, China. *Agronomy* **2023**, *13*, 1485. [CrossRef]
58. Weber, S.E.; Diez, J.M.; Andrews, L.V.; Goulden, M.L.; Aronson, E.L.; Allen, M.F. Responses of arbuscular mycorrhizal fungi to multiple coinciding global change drivers. *Fungal Ecol.* **2019**, *40*, 62–71. [CrossRef]
59. Soteras, F.; Moreira, B.C.; Grilli, G.; Pastor, N.; Mendes, F.C.; Mendes, D.R.; Renison, D.; Kasuya, M.C.M.; de Souza, F.A.; Becerra, A. Arbuscular mycorrhizal fungal diversity in rhizosphere spores versus roots of an endangered endemic tree from Argentina: Is fungal diversity similar among forest disturbance types? *Appl. Soil Ecol.* **2016**, *98*, 272–277. [CrossRef]
60. Bonfim, J.A.; Vasconcellos, R.L.F.; Gumiere, T.; Mescolotti, D.D.L.C.; Oehl, F.; Cardoso, E.J.B.N. Diversity of arbuscular mycorrhizal fungi in a Brazilian atlantic forest toposequence. *Microb. Ecol.* **2016**, *71*, 164–177. [CrossRef]
61. Ma, B.; Wang, H.Z.; Dsouza, M.; Lou, J.; He, Y.; Dai, Z.M.; Brookes, P.C.; Xu, J.M.; Gilbert, J.A. Geographic patterns of co-occurrence network topological features for soil microbiota at continental scale in eastern China. *ISME J.* **2016**, *10*, 1891–1901. [CrossRef]

62. de Vries, F.T.; Griffiths, R.I.; Bailey, M.; Craig, H.; Girlanda, M.; Gweon, H.S.; Hallin, S.; Kaisermann, A.; Keith, A.M.; Kretzschmar, M.; et al. Soil bacterial networks are less stable under drought than fungal networks. *Nat. Commun.* **2018**, *9*, 3033. [CrossRef]
63. Carvalho, F.; Souza, F.A.; Carrenho, R.; Moreira, F.M.S.; Jesus, E.C.; Fernandes, G.W. The mosaic of habitats in the high-altitude Brazilian rupestrian fields is a hotspot for arbuscular mycorrhizal fungi. *Appl. Soil Ecol.* **2012**, *52*, 9–19. [CrossRef]
64. Camenzind, T.; Hempel, S.; Homeier, J.; Horn, S.; Velescu, A.; Wilcke, W.; Rillig, M.C. Nitrogen and phosphorus additions impact arbuscular mycorrhizal abundance and molecular diversity in a tropical montane forest. *Glob. Change Biol.* **2014**, *20*, 3646–3659. [CrossRef] [PubMed]
65. Van Geel, M.; Jacquemyn, H.; Plue, J.; Saar, L.; Kasari, L.; Peeters, G.; van Acker, K.; Honnay, O.; Ceulemans, T. Abiotic rather than biotic filtering shapes the arbuscular mycorrhizal fungal communities of European seminatural grasslands. *New Phytol.* **2018**, *220*, 1262–1272. [CrossRef] [PubMed]
66. Helgason, T.; Fitter, A.H. Natural selection and the evolutionary ecology of the arbuscular mycorrhizal fungi (phylum Glomeromycota). *J. Exp. Bot.* **2009**, *60*, 2465–2480. [CrossRef]
67. Gai, J.; Liu, R. Effects of soil factors on arbuscular mycorrhizae (AM) fungi around roots of wild plants. *Chin. J. Appl. Ecol.* **2003**, *14*, 470.
68. Johnson, N.C.; Wilson, G.W.T.; Wilson, J.A.; Miller, R.M.; Bowker, M.A. Mycorrhizal phenotypes and the law of the minimum. *New Phytol.* **2015**, *205*, 1473–1484. [CrossRef]
69. Zhao, L.L.; Zhang, K.X.; Sun, X.; He, X.L. Dynamics of arbuscular mycorrhizal fungi and glomalin in the rhizosphere of Gymnocarpos przewalskii in Northwest Desert China. *Appl. Soil Ecol.* **2022**, *170*, 104251. [CrossRef]
70. Ouimet, R.; Camiré, C.; Furlan, V. Effect of soil K, Ca and Mg saturation andendo mycorrhization on growth and nutrient uptake of sugar maple seedlings. *Plant Soil* **1996**, *179*, 207–216. [CrossRef]

Disclaimer/Publisher's Note: The statements, opinions and data contained in all publications are solely those of the individual author(s) and contributor(s) and not of MDPI and/or the editor(s). MDPI and/or the editor(s) disclaim responsibility for any injury to people or property resulting from any ideas, methods, instructions or products referred to in the content.

Journal of *Fungi*

MDPI

Article

Pomegranate Woody Mycobiota Associated with Wood Decay

Valentino Bergamaschi [1,*], Maria Teresa Valente [1] and Rosario Muleo [2]

[1] Research Centre for Plant Protection and Certification (CREA-DC), Council for Agricultural Research and Economics (CREA), 00156 Rome, Italy; mariateresa.valente@crea.gov.it
[2] Department of Agriculture and Forest Sciences (DAFNE), University of Tuscia, 01100 Viterbo, Italy; muleo@unitus.it
* Correspondence: valentino.bergamaschi@crea.gov.it

Abstract: The rapid expansion of pomegranate (*Punica granatum* L.) cultivation in central and southern Italy has revealed emerging phytosanitary challenges, including "pomegranate wood decay syndrome", characterised by cortical cankers, wood browning, and progressive plant decline. This study investigates the fungal microbiota associated with symptomatic pomegranate wood using a combined approach of traditional fungal isolation and ITS2 metabarcoding analysis. Samples from two orchards in Lazio were examined, revealing a complex fungal community with a high prevalence of *Neofusicoccum parvum* (putative) and species belonging to the genus *Diaporthe*. Pathogenicity tests confirmed the role of *N. parvum* in causing significant wood browning, while other isolates showed variable virulence. Statistical analyses validated the pathogenicity of select isolates, with the putative *Diaporthe eres* (Nitschke) consistently demonstrating potential pathogenic activity across all trials. Metabarcoding identified 289 taxa, highlighting a richer fungal diversity in the symptomatic wood compared to the asymptomatic sections. Notably, *Coniella granati*, previously implicated in pomegranate decline, was absent in the studied orchards. The findings reveal that pomegranate wood decay is a complex syndrome driven by fungal pathogens and environmental stressors, such as low temperatures. This study highlights the value of integrative approaches for understanding and managing fungal-associated wood diseases in pomegranate orchards.

Keywords: wood decay; *Diaporthe*; pathogenicity test; metabarcoding; ITS 2

1. Introduction

The interest in the cultivation of pomegranates (*Punica granatum* L.) in Italy has led to research to increase the knowledge about this crop, whose fruit is considered a functional product of great benefit from the organoleptic and nutraceutical points of view, as well as for the possibility of pharmaceutical applications, given the content of active molecules that reduce the risk of vascular diseases, coronary artery problems, and cancer mortality [1,2]. Among the bioactive compounds present in pomegranate juice, there are phenols and tannins such as punicalin, punicalagin, and ellagic acid; moreover, varieties with red arils contain a large number of anthocyanins, including cyanidin, delphinidin, and pelargonidin, and related glycosides with strong antioxidant capacities [3–5].

In some of the main pomegranate cultivation areas of Italy, including the central and southern regions as well as the islands, young plants have experienced phytosanitary problems that, in some cases, have led to the loss of both fruit production and entire plants [6]. This disease, called "Pomegranate canker" or, more generically, "Pomegranate

decay", shows progressively worsening conditions of the plant: the first symptom is leaf chlorosis, and later, the plant shows the formation of cankers on the stem and branches with wood browning below the symptoms [6]. The main fungi isolated from the symptomatic portions of pomegranate wood were *Coniella granati*, previously reported in Italy, Iran, Israel, Turkey, Greece, and Spain [6–11], and *Neofusicoccum parvum* (Pennycook and Samuels) Crous, Slippers, and Phillips, previously reported in Greece [12], in Florida [13], and recently in an orchard in Lazio, Italy [14]. *Neofusicoccum parvum* was also reported on other plants of agricultural interest, including the grapevine, kiwifruit, and avocado [15–17]. This fungus enters through wounds (e.g., pruning cuts or mechanical damage due to abiotic agents such as frost or hail). The infection causes the browning of the bark on the trunk and branches and the discolouration of the wood underlying the affected areas, resulting in the general decay of the plant and subsequent die-off of the shoots. The fungus often causes significant cankers that can affect the whole plant [14].

Wood decay often represents a disease complex, due to the characteristic mixed infections [18], and the simultaneous presence of several fungal species complicates the diagnosis. The traditional phytosanitary approach requires an initial culturing step, which excludes the detection of biotrophic, endophytic species and may limit the detection of slow-growing fungi. As trunk pathogens cause mixed infections, it is important to characterise the composition of the species complex. In recent years, due to the growing power and reduced cost of next-generation sequencing technologies, DNA metabarcoding analysis has been used extensively for the characterisation of microbial communities [19–23]. The internal transcribed spacer (ITS) regions of ribosomal DNA (rDNA) are the most predominant DNA barcode sequences used for fungal metabarcoding, since they can be easily amplified and sequenced and they are highly represented in GenBank and other databases [24,25]. The Illumina MiSeq NGS technology is the most used in metabarcoding studies [26], due to its high diversity coverage, high accuracy, low cost, and availability of several consolidated data processing pipelines; however, due to the limited sequence lengths, it allows for the sequencing of only one of the ITS subregions. The choice of using either ITS1 or ITS2 for the best taxonomic resolution is still debated [27,28]. ITS2 shows some advantageous features: it is less variable in length, has no intron regions, is better represented in public databases, and has a longer portion of the sequence providing taxonomic information [29].

This work aims to study and characterise the fungal flora present in diseased pomegranate wood through a traditional phytosanitary analysis combined with an ITS metabarcoding analysis, and to verify the disease involvement of the more frequently isolated fungi through a pathogenicity test. To the best of our knowledge, this is the first study combining culturing and DNA metabarcoding approaches to assess the fungal pathogen diversity associated with pomegranate wood decay.

2. Materials and Methods

2.1. Collection of Samples

Two pomegranate Italian orchards, both in the Lazio region, were selected: Sermoneta (41.556459, 12.979830) and Pavona (41.742874, 12.603806). In both orchards, the pomegranate plants belong to the cultivar 'Wonderful'. In Pavona, the soils are of volcanic origin, very deep, sub-acidic, non-calcareous, and characterised by a medium to fine texture, with good organic matter content. On the other hand, in Sermoneta, the substrate consists of alluvial sediments with a fine texture, featuring a surface mineral horizon highly enriched in organic matter and affected by limited oxygen availability. Overall, both soils show good organic matter contents [30], and according to the soil analysis provided by the owner, no deficiencies in macro- or micronutrients were detected. The soils of the

Sermoneta orchard were classified predominantly as Haplic Luvisols (>75%) with Luvic Phaeozems (10–25%), while the Pavona orchard soils were classified as Haplic Phaeozems (25–50%), Luvic Phaeozems (10–25%), and Cambic Endoleptic Phaeozems (<10%) [30]. Furthermore, the Lazio region experiences colder winter climatic conditions than in southern Italy, where pomegranate cultivation is more successful [31]. Fifteen symptomatic plants obtained from both of the orchards from 2017 to 2019 were transferred to the laboratory of the Research Centre for Plant Protection and Certification (CREA-DC, Roma) and analysed by the isolation and morphological and molecular identification of the fungal flora. Two plants showing the symptoms of pomegranate decay (identified as Plant 1 and Plant 2, Figure 1) from the Pavona site (2018) were analysed by the conventional method (isolation and identification) and by the metabarcoding approach. Plant 1 presented some cankers on the stem and some branches, subcortical browning of the wood, and yellowing; Plant 2 showed an extended canker on the whole trunk, with extended subcortical browning (Figure 1).

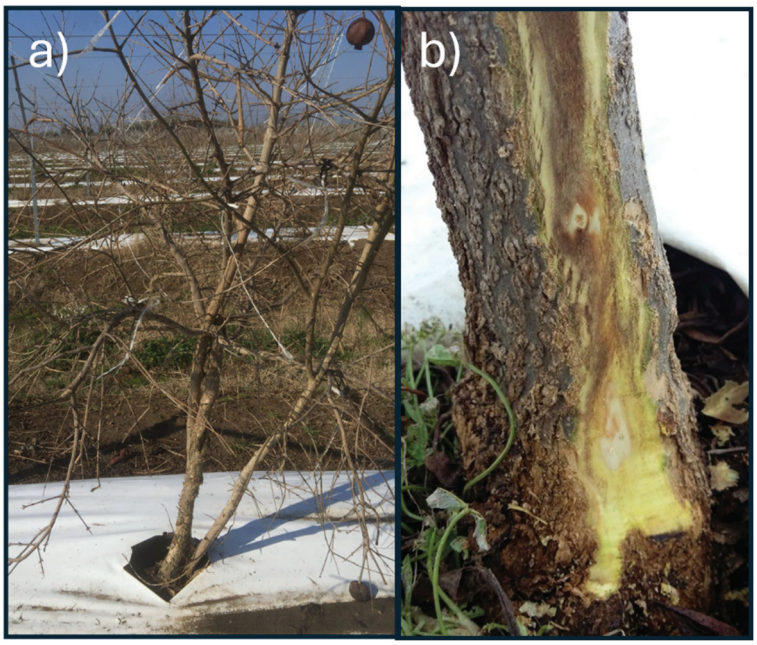


Figure 1. Symptomatic Plant 1 showing a large canker on the trunk (**a**) and subcortical browning on Plant 2 (**b**), both sampled for the metabarcoding analysis in Pavona (RM).

The plants (stem and branches) were divided into sections (Figure 2) representative of the different asymptomatic and symptomatic wood tissues from the trunks and the branches.

2.2. Fungal Isolation and Identification

Longitudinal sections of the tissues sampled as described above were obtained aseptically; small portions between the healthy and symptomatic tissues were explanted from the browned wood and placed on a Potato Dextrose Agar (PDA) culture medium, amended with 100 μg/mL of streptomycin and ampicillin sodium salt antibiotics, and incubated at 22 °C until the development of fungal colonies. The colonies were then transferred onto fresh PDA plates and incubated at 22 °C under near-ultraviolet (NUV) light with a 12 h light/12 h dark photoperiod to promote fungal growth and sporulation. The fungal identification was carried out based on the morphological features of the colonies, including macroscopic characteristics such as colony colour, texture, and growth pattern, as well as

microscopic observations of the fruiting structures, including pycnidia and conidiomata produced in the culture. The morphological identification was confirmed by the sequencing of the ITS region amplified with ITS4/ITS5 primers [32] performed at the BioFab Research laboratory (Rome, Italy). Since only the ITS region was used for molecular identification, isolates were classified as putative species based on the most abundant species showing 100% identity in the NCBI database. The sequences were blasted in the GenBank database by using the nBLAST search. The isolated and identified species were preserved in the fungal collection of the CREA-DC (Rome, Italy).

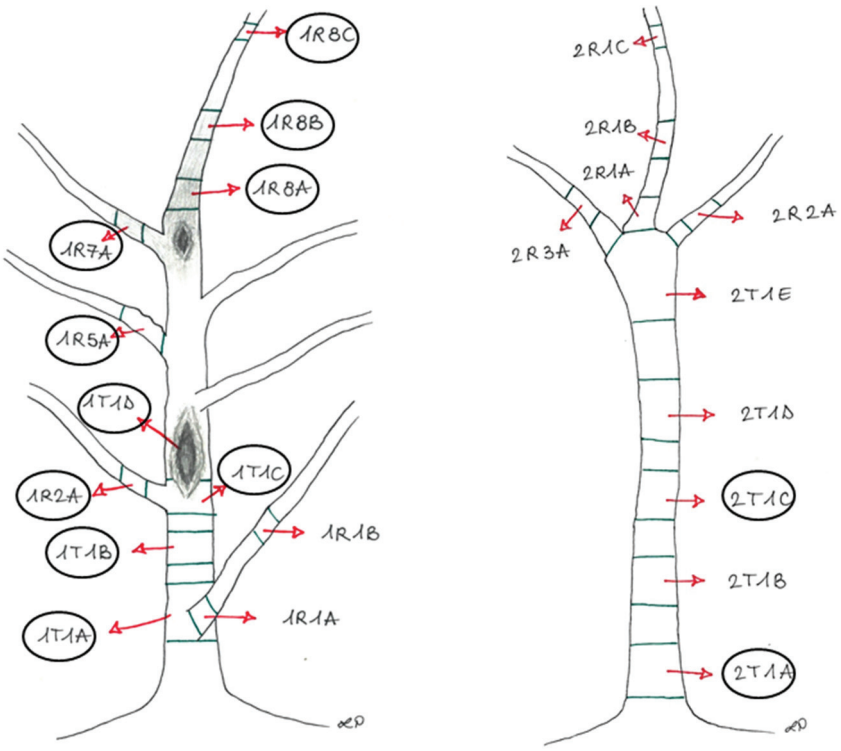


Figure 2. The sampling points of Plant1 (**left**) and Plant2 (**right**), showing the cankers and browning wood, with the identification legend of each sampled section, later described in Table 1. The circled sections were used for the metabarcoding analysis.

Table 1. A description of the experimental units is reported in Figure 2.

Experimental Units	Section	Phenotypic Features
1	1R8A + 1R8B	Brown tissues above the canker from the apical portion (Plant 1)
2	1R7A	Brown tissues from the lateral branch close to the canker (Plant 1)
3	1R2A + 1R8C	Asymptomatic tissues from the branches (Plant 1)
4	1R5A	Asymptomatic tissues (showing bark roughness) from the lateral branch (Plant 1)
5	1T1A	Brown tissues from the basal area of the trunk, corresponding to the collar (Plant 1)
6	1T1B	Brown tissues below the canker from the trunk (Plant 1)
7	1T1C + 1T1D	Brown tissues into the canker area (Plant 1)
8	2T1A + 2T1C	Brown tissues from the trunk (Plant 2)

2.3. DNA Extraction

The DNA from the fungal mycelium was extracted with the rapid protocol of Cenis [33], starting from 100 mg of mycelium modified for the plate-grown mycelium [34]. The pomegranate wood was ground in liquid nitrogen; an aliquot of ground wood (about

100 mg) was used for DNA extraction, performed with the DNeasy Plant Mini Kit (QIAGEN, Hilden, Germany) according to the manufacturer's instructions. The quantity and quality of the purified DNA extracts were determined using a Qubit 2.0 fluorometer (Life Technologies, Carlsbad, CA, USA) and a DS-11 FX spectrophotometer (DeNovix Inc., Wilmington, DE, USA), respectively.

2.4. Metabarcoding Analysis

A metabarcoding analysis was carried out on Plant 1 and Plant 2 from the Pavona pomegranate orchard to confirm the data derived from the isolation and identification of the fungal flora, and to obtain more information about the fungal communities in the asymptomatic and symptomatic wood tissues. The different samples were combined into 8 experimental units (Table 1), 7 from Plant 1 and 1 from Plant 2.

The DNA samples were amplified by PCR targeting the ITS2 region of the fungal rDNA using ITS3 and ITS4 primers [32]. These primers were modified by the 5′-end Illumina overhang adapter sequences (34 and 35 nucleotides) and by the different 5′-end identifier (index) sequences of 6 nucleotides, generating 8 oligo pairs of unique tags (Table S1). PCRs were conducted for the 8 samples with each of the 8 newly designed primer pairs to test for variability in the amplification success. Each sample was assigned a different forward/reverse index combination for sample-specific labelling.

The amplification reaction was performed following the protocol proposed by Miller et al. [35]. The reaction mix contained 10 ng of template DNA, 1× BioTaq PCR NH_4-based reaction buffer, 4 mM of $MgCl_2$, 0.8 mM of dNTP mix (Bioline, London, UK), 0.8 mg/mL of bovine serum albumin (BSA, Invitrogen, Carlsbad, CA, USA), 2.5 U of BioTaqTM DNA polymerase (Bioline, London, UK), and 0.5 µM of each forward and reverse primer in a 25 µL reaction volume. For each sample, three PCRs were carried out at three different annealing temperatures; combining PCR products using a range of annealing temperatures reduces the primer bond distortion and decreases the stochasticity of the individual PCRs [19]. The following cycling conditions were used for the amplification: an initial denaturation at 94 °C for 30 s, followed by 30 cycles of denaturation at 94 °C for 1 min, annealing at 50/53/56 °C for 1 min, extension at 72 °C for 30 s, and a final extension at 72 °C for 2 min. The PCR products were visualised in 1% agarose gel electrophoresis using GelRed™ dye (Biotium, Hayward, CA, USA). Purification of the amplicons was performed using the Isolate II PCR and Gel Kit (Bioline, London, UK). The cleaned PCR products were then quantified using a Qubit 2.0 Fluorometer (Life Technologies, Carlsbad, CA, USA) and mixed in equimolar amounts (75 ng for each sample). A single sample consisting of the pooled amplification products was sent to the BioFab Research laboratory (Rome, Italy). The sequencing was performed on the Illumina MiSeq platform (Illumina, San Diego, CA, USA) with a 2 × 300 paired-end run and a reading depth of 100,000 reads. The reads forward and reverse were merged and filtered by quality (Q > 30). Subsequently, a demultiplexing of the sequenced sample was carried out, obtaining the results of the 8 separate experimental units. Bioinformatic processing of the sequences was conducted using the USEARCH pipeline and the UPARSE-OTU algorithm [36].

The paired-end (PE) sequences were merged using the -fastq_mergepairs command. Next, the PE reads were quality-filtered (maximum e-value: 1.0), trimmed to 340 bp, dereplicated, and sorted by abundance (singletons removed). Chimaera detection and operational taxonomic unit (OTU) clustering at 97% sequence identity followed. The original sequences were then mapped to OTUs at the 97% identity threshold, generating separate OTU tables for the prokaryotic and fungal communities.

The taxonomic affiliation of each OTU was assigned using the -syntax algorithm against the UNITE_all_eukaria database [37] with an 80% confidence threshold. The sequencing depth was normalised across the libraries, and the resulting OTU tables were used for downstream analyses.

2.5. Pathogenicity Test

Artificial inoculations were performed using the 5 fungal species isolated with a higher incidence and belonging to the most represented *Genus* in the metabarcoding analysis (*Neofusicoccum parvum*, isolate ER 2123; *Diaporthe eres* (Nitschke), isolate ER 2111; *D. phaseolorum* (Cooke & Ellis) Sacc., isolate ER 2126; *D. rudis* (Sacc.) Sacc., isolate ER 2127; *D. foeniculina* (Sacc.) Udayanga & Castl., isolates ER 2125 and ER 2128). *Neofusicoccum parvum* ER 2123 was used as a positive control, since it is reported as a pathogen of pomegranate wood [14].

The pathogenicity was evaluated through a test carried out on the cut twigs and plants. The twigs were prepared in sections approximately 20 cm long and harbouring at least two buds, between which were performed the inoculation. The inoculation area was previously surface sterilised with denatured ethyl alcohol.

Three inoculation procedures were performed.

First procedure: Detached pomegranate twigs at least one year old, as described by Palavouzis et al. [12]. The test was carried out with 5 mm diameter mycelium plugs taken from the margins of the fungal colonies, about one week old, grown in purity on the PDA medium. A 5 mm diameter disc of the bark was previously removed from the twigs with a cork borer to expose the cambium to the mycelium applied with a PDA plug. Then, the twigs were placed in the dark in a humid chamber at room temperature to promote the infection (Figure 3). After 3 days, when presumably the mycelium had colonised the wood, the humid chambers were opened. The test was completed at 7 days post inoculation (DPI).



Figure 3. Pomegranate twigs inoculated and placed in humid chamber.

Second procedure: Detached twigs of at least four years old, placed in water, were inoculated, wounding the bark with a razor blade in a basipetal orientation and exposing the youngest wood; then, the strip of tissue was pulled back to place the PDA with the mycelium on the exposed xylem. The inoculation area was covered with a cotton disc soaked with 3 mL of sterile tap water, wrapped with tinfoil strips, and stuck with paper tape, as shown in Figure 4 [38]. The twigs were placed in water at 25 °C with a photoperiod

of 13 h of light (13/11), and were checked weekly to change the water. After seven days, the tinfoil strips were removed. The test was completed at 90 DPI.



Figure 4. Pomegranate twigs (4 years old) inoculated and placed in water.

Third procedure. In vivo plants were inoculated as described in the second procedure and placed outdoors in the nursery. After 30 days, when presumably the mycelium had colonised the wood, the tinfoil strips and the paper tape were removed; the test was completed in 90 days.

At the end of these tests, the first layers of the bark were removed with a razor blade to show and measure the length of the browned area in the longitudinal direction of the twig (Figure 5).

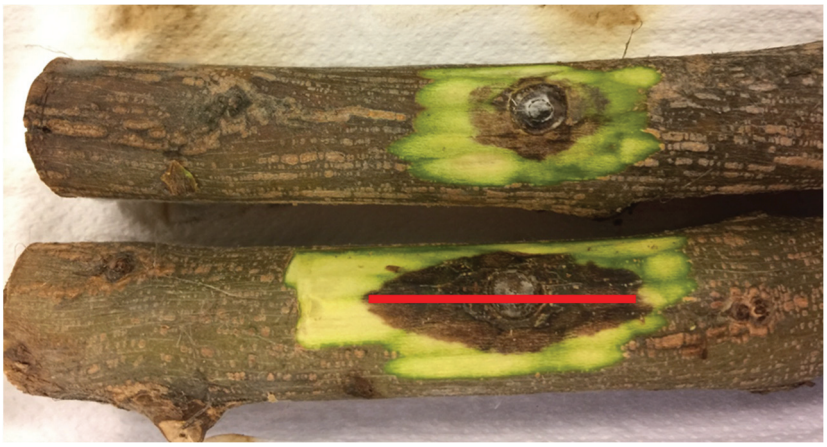


Figure 5. Pomegranate branches with the first layers of the bark removed to discover the browned area and measure its length in the longitudinal direction (highlighted in red).

The tests were conducted in randomised blocks, with four repetitions for procedures 1 and 2 and five repetitions for procedure 3. This was applied to each fungal isolate, as well as to the negative control (sterile PDA plugs) and the positive control (ER 2123).

Moreover, control isolations were carried out from the symptomatic areas to verify the Kock's postulates.

2.6. Statistical Analysis

The data from the pathogenicity test were analysed using R software version 4.2.1 to perform a One-Way ANOVA, assessing the significant differences in browning length (cm) among the treatments to evaluate the virulence of the fungus compared to the negative controls.

Before the ANOVA, the normality was checked using the shapiro.test function, while the homoscedasticity and non-additivity were verified with the bartlett.test and leveneTest functions, respectively, considering $p > 0.05$ as the threshold for homogeneity. The ANOVA was performed using the aov function, followed by Tukey's HSD post hoc test with the Tukey HSD function, to identify the significant differences between the treatment groups ($p = 0.05$). The ANOVA results were considered significant at $p < 0.05$ and highly significant at $p < 0.01$.

3. Results

3.1. Phytosanitary Analysis of Pomegranate Plants Affected by Decay

Plants exhibiting wood decay symptoms, including reduced growth, leaf yellowing, and reddening, were sampled. Their trunks and twigs displayed cortical cankers, with some located above the collar and others extending along the entire trunk. In the early stages of the disease, before the canker formation, the bark appeared darker, and the underlying cambium showed distinct darkening and damage.

Laboratory dissections revealed browned wood, particularly beneath the cankers, with necrosis spreading in both the basipetal and acropetal directions. In cases of multiple cankers, the browning could extend throughout the entire trunk.

The fungal isolations from 325 symptomatic tissues yielded 188 colonies. The morphological and DNA sequence analyses identified 11 distinct species (Table 2). *Neofusicoccum parvum* was detected at both the Pavona and Sermoneta sites, but only in early autumn. *Diaporthe* spp. and *Gliocladium* spp. were more frequently isolated and exhibited a high incidence.

Table 2. List of fungal species (putative) isolated from symptomatic pomegranate wood in two sampling sites, with sampling times, representative strains, and GenBank numbers. * Samples used for metabarcoding analysis, from all 8 experimental units.

Strain CREA-DC Collection Code	Species	Isolation Incidence (% of the Total Fungal Colonies)	Pavona			Sermoneta		GenBank Accession Number
			July 2017	October 2017	March 2018 *	September 2018	February 2019	
ER2123	*N. parvum*	27.6	Absent	Present	Absent	Present	Absent	MW020287
ER2111	*D. eres*	20.7	Present	Absent	Present	Absent	Absent	MW020285
ER2125, ER2128	*D. foeniculina*	17.2	Absent	Present	Present	Absent	Absent	MW020288, MW032268
ER2126	*D. phaseolorum*	3.4	Absent	Present	Absent	Absent	Absent	MW020289
ER2127	*D. rudis*	3.4	Absent	Present	Present	Absent	Absent	MW032267
ER2145	*Cytospora acaciae*	3.4	Absent	Absent	Absent	Present	Absent	/
/	*Eutypa lata*	0.5	Absent	Absent	Present	Absent	Absent	/
ER2130	*Gliocladium* spp.	24.1	Absent	Present	Present	Present	Present	/
/	*Phoma glomerata*	5.3	Absent	Absent	Present	Absent	Present	/
/	*Neopestalotiopsis clavispora*	1	Absent	Absent	Present	Absent	Absent	/
/	*Fusarium* spp.	18.6	Absent	Absent	Present	Absent	Absent	/

3.2. Metabarcoding Analysis

A fragment of the expected size (340 bp) was obtained from the ITS2 amplification in all of the samples investigated.

The dataset comprises 114,486 reads distributed across the eight samples, with a total of 41 operational taxonomic units (OTUs) identified. Notably, all OTUs and samples contain nonzero counts, with no missing data or singleton OTUs.

In terms of OTU abundance and distribution, none of the OTUs have a total count of one, meaning that all identified taxa are represented by multiple reads across the samples. A total of 328 counts were recorded, with 44.5% (146 counts) being zero and 55.5% (182 counts) showing at least ten occurrences. This suggests a relatively balanced distribution of the microbial taxa, although a portion of the OTUs remain rare across the samples.

Regarding the core microbiomes and ubiquity of the OTUs, 13 OTUs (31.7%) are present in all samples, defining a core microbiome that is consistently detected across the dataset; 23 OTUs (56.1%) are detected in at least 50% of the samples, indicating a moderate level of species turnover across the different sampling points.

The sample sizes and sequencing depths vary, with the smallest sample containing 3749 reads and the largest 19,253 reads. The median sample size is 15,599 reads, while the mean is 14,310 reads, suggesting an overall well-balanced sequencing depth across the samples. The lower quartile (14,171 reads) and upper quartile (19,157 reads) indicate that most samples fall within a reasonable range, minimising the risk of uneven sequencing depth affecting the downstream analyses.

The NGS analysis of the ITS2 region revealed a wide diversity (Figures 6–8).

Genus	1	2	3	4	5	6	7	8
Unassigned	7.74	7.36	20.70	3.44	18.40	20.00	32.00	28.50
Diaporthe	86.60	86.20	17.10	4.29	60.80	69.30	41.80	49.40
Trebouxia	0.00	0.00	0.00	0.00	0.32	0.00	0.00	0.00
Vishniacozyma	0.05	0.19	0.93	0.00	0.16	0.19	0.11	0.05
Phaeoacremonium	0.93	1.28	0.91	0.29	1.15	1.52	10.70	1.12
Neosetophoma	0.00	0.00	0.00	0.00	0.05	0.00	0.00	0.00
Paecilomyces	0.00	0.00	0.35	0.00	0.19	0.05	0.24	0.00
Sporocadus	0.00	0.00	0.00	0.00	0.37	0.00	0.00	0.00
Clonostachys	0.40	0.56	0.00	0.11	0.67	0.56	4.03	0.83
Elsinoe	0.00	0.00	0.00	0.13	0.00	0.00	0.00	0.00
Cystobasidium	0.00	0.00	0.00	0.00	0.08	0.00	0.00	0.00
Alternaria	0.00	0.00	0.35	0.00	0.00	0.00	0.00	0.00
Aureobasidium	0.05	0.13	4.37	0.29	0.56	0.21	0.19	0.16
Fusarium	0.83	0.99	0.45	0.16	0.91	2.88	5.44	0.64
Libertasomyces	0.00	0.00	0.00	0.00	0.29	0.13	0.00	0.00
Eutypa	0.08	0.05	0.00	0.00	0.13	0.00	0.16	0.91
Punica	3.23	3.28	54.50	91.30	15.80	5.09	5.33	18.40

Figure 6. The fungal relative abundance at the genus level in the different sections of the 8 experimental units. Blue bar length within each cell graphically indicates the relative abundance. A description of each sample is provided in Table 1.

Based on Figure 6, the most frequently occurring taxon across the samples was *Diaporthe*, which shows a consistently high relative abundance, ranging from 17.10% to 86.60%. This genus dominates several samples, particularly samples 1, 2, 5, and 6, where its relative abundance exceeds 60%.

Another notable taxon is *Punica*, which exhibits the highest relative abundance in sample 4 (91.30%) and sample 3 (54.50%), which were asymptomatic sections. In contrast, taxa such as *Vishniacozyma*, *Phaeoacremonium*, and *Fusarium* are present in lower proportions, but show some variability across the samples, with *Phaeoacremonium* reaching 10.70% in sample 7.

Regarding the species richness, sample 7 (symptomatic section) appears to have the highest diversity, as it contains multiple taxa with substantial relative abundances,

including *Diaporthe* (41.80%), *Phaeoacremonium* (10.70%), *Fusarium* (5.44%), and *Clonostachys* (4.03%). This indicates a more heterogeneous microbial community in this sample.

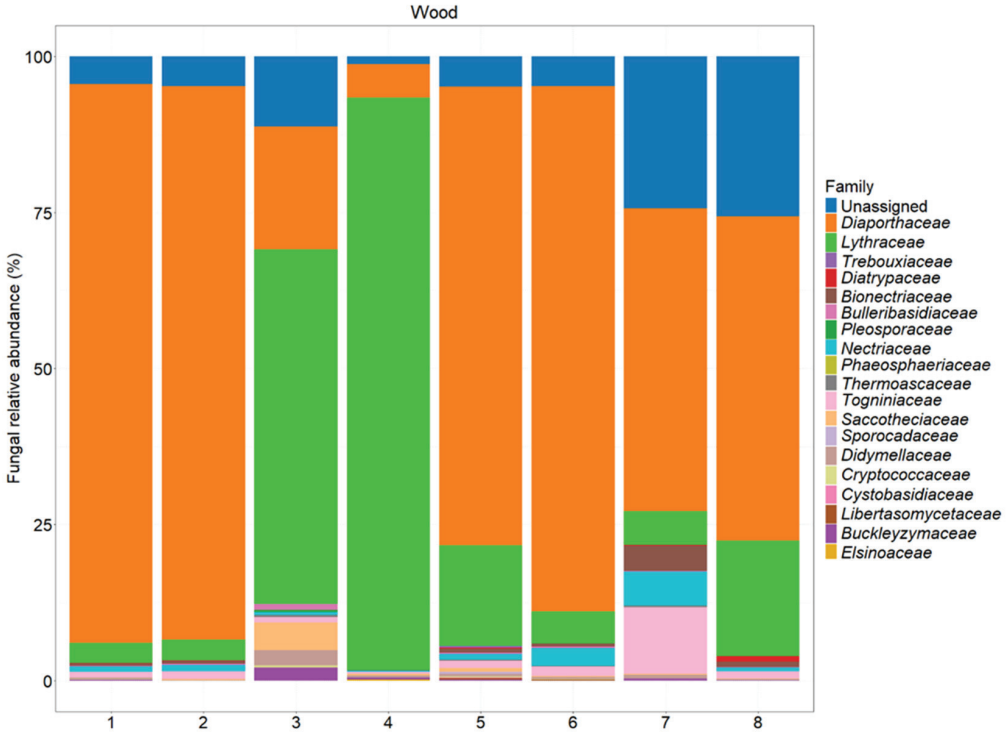


Figure 7. The fungal abundance at the family level in different sections of the tested plants. A description of each sample is provided in Table 1.

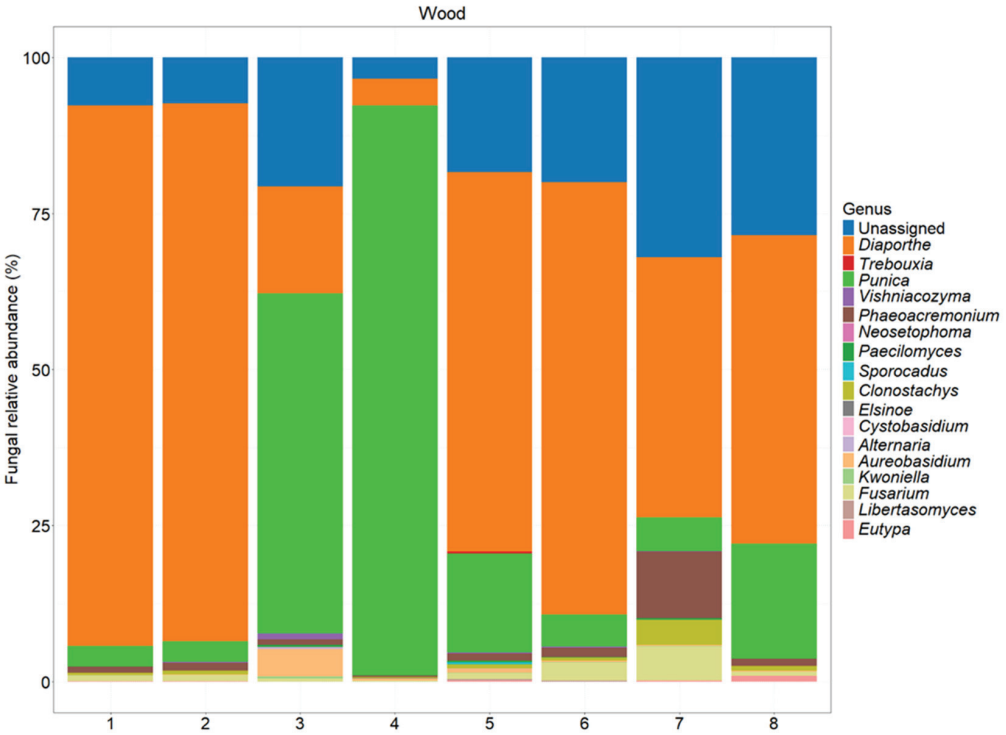


Figure 8. The fungal abundance at the genus level in different sections of the tested plants. A description of each sample is provided in Table 1.

Conversely, samples 3 and 4 (asymptomatic sections) exhibited the lowest species richness, as they are overwhelmingly dominated by *Punica* (54.50% and 91.30%, respectively) and *Diaporthe* (17.10% and 4.29%, respectively), with the other taxa either absent or present in very low amounts.

Overall, the results highlight a strong predominance of *Diaporthe*, variations in the microbial community structure across the samples, and a marked difference in the species richness, with sample 7 exhibiting the highest diversity and sample 4 the lowest.

The results confirmed the correlation between isolated fungal and fungal genera detected with metabarcoding analysis.

3.3. Pathogenicity Test

The artificial inoculation tests on the twigs were able to reproduce the symptom of browning of the wood by all tested fungi, which had been obtained from the diseased wood of pomegranate plants affected by decay, and to highlight their greater or lesser aggressiveness. The positive control *N. parvum* (ER 2123 tube) caused the expected symptoms in the three tests, confirming that the inoculation method worked properly (Tables S2–S4, Figure S1). The ANOVA results highlighted highly significant differences in terms of the length of browning between the treatments in all three tests (Tables 3–5).

Table 3. ANOVA results conducted on length (cm) of browning caused by inoculated fungi on pomegranate-detached twigs in humid chamber in 2019.

EFFECT	SS	DF	MS	F	ProbF
Isolate	1.49215	5	0.29843	13.64701997	3.93174×10^{-5}
Residual	0.328016667	15	0.021867778		
Total	1.94685	23	0.084645652		

Table 4. ANOVA results conducted on length (cm) of browning caused by inoculated fungi on pomegranate-detached twigs in water in 2019.

EFFECT	SS	DF	MS	F	ProbF
Isolate	8.419153439	5	1.683831	14.04785	4.26×10^{-6}
Residual	2.517142857	21	0.119864		
Total	10.9362963	26	0.420627		

Table 5. ANOVA results conducted on length (cm) of browning caused by inoculated fungi on pomegranate plants in 2020.

EFFECT	SS	DF	MS	F	ProbF
Isolate	16.79066667	5	3.358133	9.631358	3.84×10^{-5}
Residual	8.368	24	0.348667		
Total	25.15866667	29	0.86754		

Diaporthe eres (ER 2111 tube) was the only isolate that showed a constant pathogenicity in the three analyses (Figure 9). The other isolates, *D. phaseolorum* (ER 2126 tube), *D. foeniculina* (ER 2128 and ER 2125 tubes), and *D. rudis* (ER 2127 tube), were less aggressive and showed no statistically significant differences compared to the control. Despite this, their presence on the symptomatic wood was not completely negligible, and although with less aggression, the mycelium managed to develop through the tissues of the pomegranate wood.

Figures 10–12 show the average lengths (cm) of browning caused by the five inoculated isolates.

In the detached twig assay conducted under humid chamber conditions, significant differences in browning length were observed among the tested *Diaporthe* species (Figure 10).

The control (PDA) treatment resulted in minimal browning, confirming the absence of natural infection. Among the isolates, *Diaporthe phaseolorum* (ER 2126) induced the most severe symptoms, causing significantly greater browning compared to the control and all other species. *Diaporthe eres* (ER 2111), *D. foeniculina* (ER 2125 and ER 2128), and *D. rudis* (ER 2127) caused intermediate levels of browning, with overlapping statistical groupings.



Figure 9. On the left (4 branches) are the results of the inoculation of *D. foeniculina* (ER 2128 tube); on the right (4 branches) are the results of the inoculation of *D. eres* (ER 2111 tube), using procedure 1.

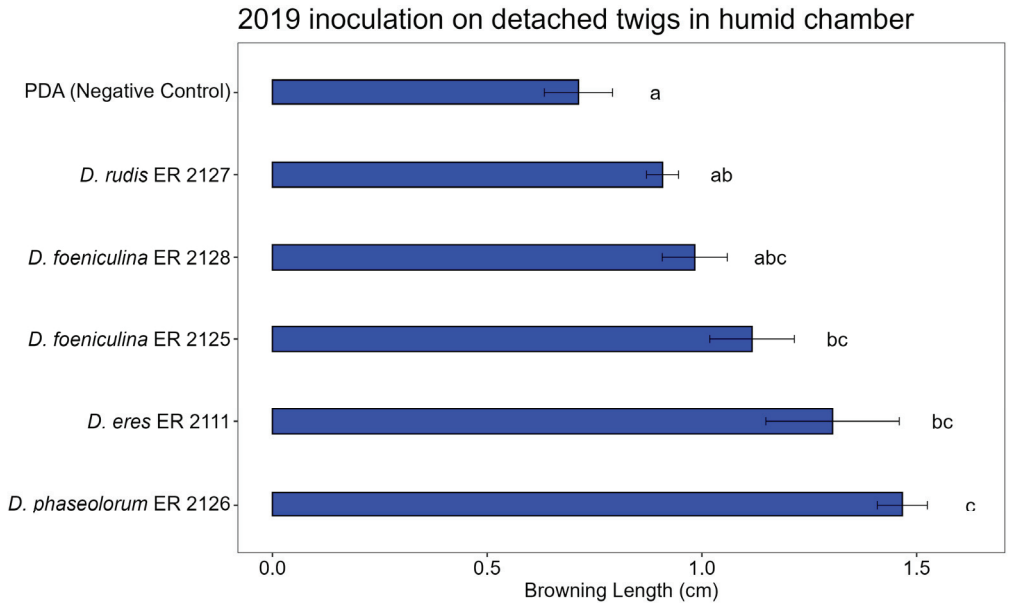


Figure 10. Bar plot showing average lengths (cm) of browning caused by inoculations on detached twigs placed in humid chamber is reported. Letters above bars indicate significant statistical differences between treatments (Tukey's HSD, $p < 0.05$). Different letters indicate significant differences based on One-Way ANOVA results at $p < 0.05$. Error bars represent standard error of mean (4 replicates).

In the 2019 twig inoculation assay with an incision and incubation in water, significant differences in browning length were observed among the *Diaporthe* species tested, confirmed by Tukey's HSD test (Figure 11). The control (PDA) exhibited minimal browning,

confirming the effectiveness of the wounding method without fungal inoculation. *Diaporthe eres* (ER 2111) caused the most severe symptoms, producing significantly longer browning compared to all other treatments. *Diaporthe foeniculina* (ER 2125) also induced substantial browning, although less than *D. eres*, while *D. rudis* (ER 2127), *D. phaseolorum* ER 2126, and *D. foeniculina* ER 2128 showed intermediate levels of browning, with no significant differences compared to the control.

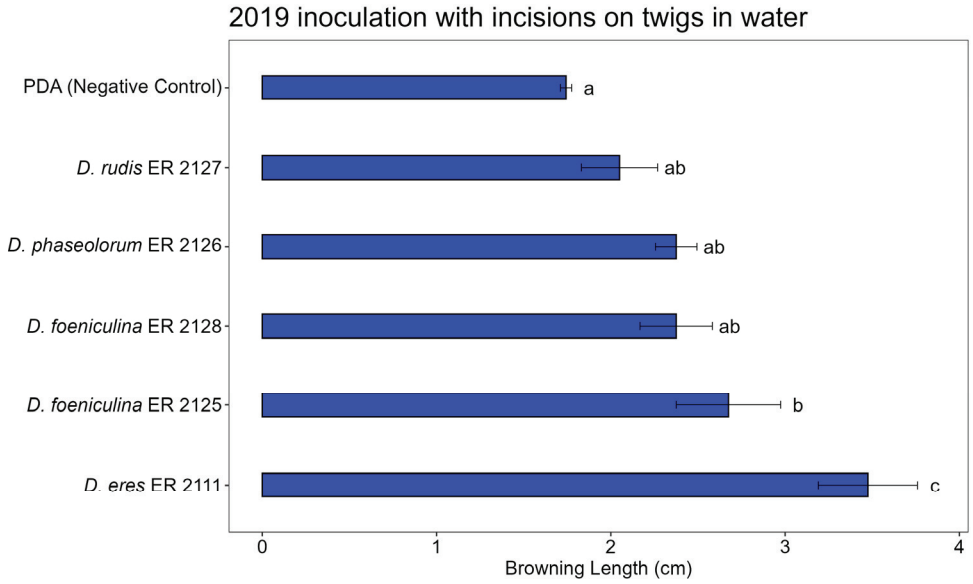


Figure 11. Bar plot showing average lengths (cm) of browning caused by inoculations on detached twigs in water is reported. Letters above bars indicate significant statistical differences between treatments (Tukey's HSD, $p < 0.05$). Different letters indicate significant differences based on One-Way ANOVA results at $p < 0.05$. Error bars represent standard error of mean (4 replicates).

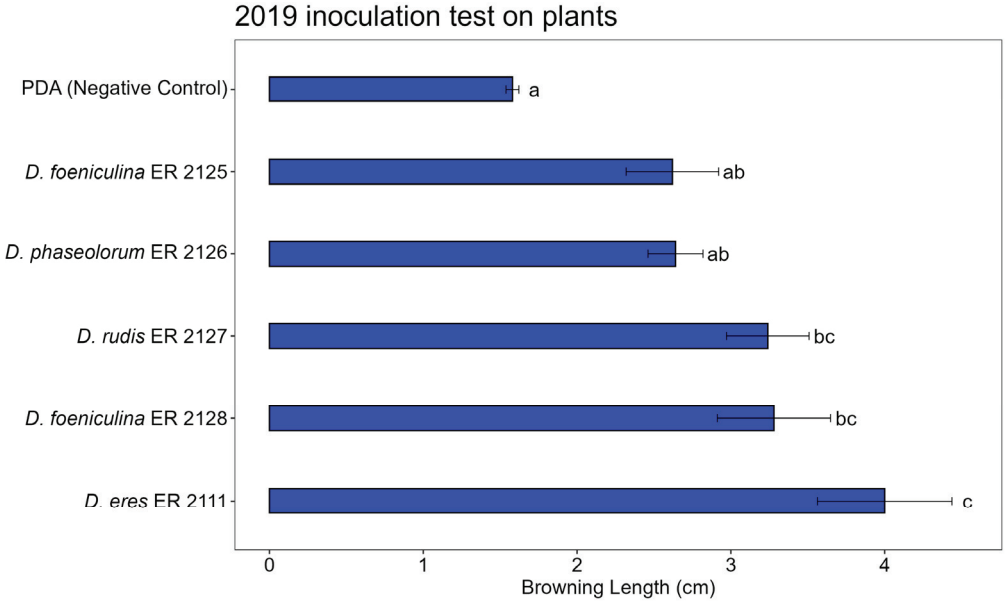


Figure 12. Bar plot showing average browning lengths (cm) caused by inoculations on pomegranate plants in 2020. Letters above bars indicate significant statistical differences between treatments (Tukey's HSD, $p < 0.05$). Different letters indicate significant differences based on One-Way ANOVA results at $p < 0.05$. Error bars represent standard error of mean (4 replicates).

In the 2020 inoculation test on pomegranate plants (Figure 13a), significant differences in browning length were observed among the *Diaporthe* isolates (Figures 12 and 13b). The control (PDA) treatment caused minimal browning (Figure 13c), confirming the absence of natural infection. Among the tested isolates, *Diaporthe eres* (ER 2111) induced the most severe symptoms, with significantly greater browning compared to all other treatments, according to Tukey's HSD test. *Diaporthe rudis* (ER 2127) and *D. foeniculina* (ER 2128) caused intermediate browning lengths, statistically grouped together. *Diaporthe foeniculina* (ER 2125) and *D. phaseolorum* (ER 2126) showed lower levels of browning, not significantly different compared to the control. These results further confirm the high pathogenic potential of *D. eres* (ER 2111) and highlight the variability in aggressiveness among the *Diaporthe* species under field-like conditions.



Figure 13. (**a**) Pomegranate plants immediately after inoculation. (**b**) A pomegranate trunk with the outer bark layers removed, revealing a browned area at the end of the trial with *D. eres*. (**c**) Negative control: a pomegranate trunk with the outer bark layers removed, inoculated with sterile PDA, showing healthy tissues.

4. Discussion

The rapid expansion of pomegranate cultivation in central and southern Italy, primarily using foreign varieties, has revealed unexpected phytosanitary issues. This is notable for a plant traditionally considered hardy and relatively free from phytosanitary concerns, apart from well-documented issues affecting the fruit. Over the past three years, the first cases of plant decline and mortality have been reported, with the losses reaching 30–40% in 2015 and escalating to 90% in subsequent years. In Puglia, in 2016, Pollastro et al. [6] identified *Coniella granati*, a pathogen already known in various pomegranate-growing regions worldwide, as the causative agent of fruit rot. However, in China, Iran, and Spain, *C. granati* has also been associated with cankers and pomegranate tree mortality, while in Greece and Turkey, it has been reported as a cause of stem cankers [39].

In central Italy, particularly in Lazio, this issue was initially unknown at the start of our investigation. However, following the reports and subsequent inspections and analyses described in this study, two potential fungal pathogens were identified: *N. parvum* (putative) and *Diaporthe* spp., which are likely to act synergistically. Initially, *N. parvum* was considered the only causal agent [14], and was therefore the primary focus of further investigations. The pathogenicity tests confirmed that the *Diaporthe* species are less aggressive than *N. parvum*, and likely play a minor role in symptom development. However, *Diaporthe* spp. were consistently isolated from the symptomatic wood and detected through the metabarcoding analysis, suggesting their constant presence in the affected tissues. The

combined presence of *N. parvum* and *Diaporthe* spp. may contribute to symptom expression comparable to that caused by *C. granati*.

The metabarcoding analysis had limitations due to the availability of ITS2 sequences in the UNITE database, which, at present, does not allow for a taxonomic resolution sufficient to classify all DNA in the sample at the species level. As a result, a proportion of the fungal DNA could only be identified at the division or, at best, genus levels. Additionally, a significant proportion of the DNA (on average 29.3%) remained unassigned, potentially concealing other pathogenic fungi. The metabarcoding analysis, even within its limits, allowed us to highlight in the two plants analysed that *N. parvum* and *C. granati* were not present in the diseased wood, where it was not isolated, nor even in the healthy wood, excluding the possibility that it was present as an endophyte.

This result was significant, as it validated the test performed, confirming the presence of a substantially richer fungal community in the symptomatic tissue, which exhibited clear signs such as cankers and wood browning. In contrast, the fungal DNA detected in the asymptomatic samples was likely associated with the endophytic fungal flora naturally present in pomegranate wood.

Different diseases are already known as the Esca of Grapevine [40] and Esca-like symptoms of *Actinidia* [41] caused by fungi complexes. Today, there are other diseases, such as "Kiwifruit Vine Decline Syndrome" (KVDS), caused by different microorganisms and abiotic disorders. The causes of decline are still discussed; currently, pathogenic species such as *Phytopythium vexans* [42,43], *Phytophthora* spp. [44], *Cylindrocarpon* [45], and the anaerobic bacteria *Clostridium* are involved and reported [46].

Similarly to other complex syndromes, abiotic stress could represent a trigger factor for the disease. The pomegranate, mainly the 'Wonderful' cultivar, is widely cultivated in warm climates and originates from regions such as Iran and the surrounding regions, from where it spread to other parts of the world [47], where the temperature conditions are more similar to those of southern Italy rather than central regions like Lazio. This difference is attributed to the latitudinal gradient, as well as variations in altitude and proximity to the sea, which influence the mean winter temperatures [31] For this reason, climatic conditions play a central role as a trigger for wood decay.

Few studies have dealt with the taxonomic resolution obtained using both the ITS1 and the ITS2 barcodes on the same dataset [27,48–51]. They have been carried out on both *Ascomycota* [52,53] and *Basidiomycota* [54]. The choice of primers can introduce taxonomic bias, as they may produce a higher number of mismatches in certain taxa [53,55,56]. Some studies also reported that the two spacers are prone to preferential amplification at different levels [48–50,52,53]. Basidiomycetous taxa have, on average, longer amplicon sequences for ITS2, and since the shorter sequences are preferentially sequenced with high-throughput sequencing (HTS), the use of ITS2 would favour the detection of ascomycetes [53]. On the other hand, ITS1 often contains an intron that extends its sequence at the 5′-end [57], thereby promoting an over-representation of those sequences that lack the intron [49]. Because ITS2 is more frequently represented in public databases, has a higher number of available sequences, and offers a better taxonomic resolution, it has been proposed as the better choice for parallel sequencing [52]. In some cases, however, no substantial differences between ITS1 and ITS2 were recovered [27,54]. Finally, there are numerous studies that consider a single spacer, either ITS1 or ITS2 [35,53,58,59].

As fungal metabarcoding studies have used different HTS platforms [60], different bioinformatic pipelines have been proposed [61,62]. These have been developed based on the experience gained from the data analyses of prokaryote datasets [63]. However, no standard procedure has been established so far for fungal sequence data. The analyses

seem strongly dependent on the working hypotheses of each study and on the type of sequence at hand. As the majority of the studies target fungal communities to uncover unknown diversity, an important and ongoing problem is the definition of those sequences lacking an assigned taxonomy [52]. For this reason, many sequences remain identified as "unassigned". In addition, many fungi have not yet been sequenced and cannot offer reference sequences for ongoing studies [63].

The molecular markers used in this investigation have a broad level of fungal species identification, so the failure to detect *Coniella granati* among the identified species allows us to speculate that other species are implicated in pomegranate wood decay syndrome. In fact, the metabarcoding results suggested a relatively stable microbial community, with a substantial proportion of OTUs present in multiple samples. For *C. granati*, in the two plant objects of our study, it can be said with certainty that it was not present and, therefore, was not involved with the cankers and deaths found in Pavona and Sermoneta. This is confirmed both by the isolations carried out on the diseased plants and by the metagenomic analysis, where the presence of *Schizoparmaceae* was not found.

The presence of a well-defined core microbiome (31.7% of OTUs in all samples) indicates a consistent microbial signature across different conditions. The data also suggest a good sequencing depth, with minimal bias from zero- or low-count OTUs.

5. Conclusions

To conclude, pomegranate wood decay syndrome is probably a complex syndrome, where the triggering factor could be climatic conditions such as low temperature stress, from which plants become susceptible to various wood pathogens including *N. parvum* and other fungi of the *Diaporthe* complex. The wood deterioration caused by *C. granati* may represent a disease with its own epidemiology and progression, capable of damaging pomegranate plants even in the absence of abiotic stress.

Supplementary Materials: The following supporting information can be downloaded at https://www.mdpi.com/article/10.3390/jof11040254/s1. Figure S1: Bar plot showing average browning lengths (cm) caused by inoculations with positive control Neofusicoccum parvum (ER 2123) across three inoculation methods. Letters above bars indicate significant statistical differences between treatments (Tukey's HSD, $p < 0.05$). Different letters indicate significant differences based on One-Way ANOVA results at $p < 0.05$. Error bars represent standard error of mean (4 replicates); Table S1: The sequences of primer pairs used for the 8 experimental units (sample), showing, separately, the adapter sequences for the Illumina system, the indexed tags, and the sequences of the universal ITS3 and ITS4 (original primers); Table S2: ANOVA results conducted on length (cm) of browning caused by positive control, *N. parvum* (ER 2123), inoculated on pomegranate-detached twigs in humid chamber in 2019; Table S3: ANOVA results conducted on length (cm) of browning caused by positive control, *N. parvum* (ER 2123), inoculated on pomegranate-detached twigs in water in 2019; Table S4: ANOVA results conducted on length (cm) of browning caused by positive control, *N. parvum* (ER 2123), inoculated on pomegranate plants in 2020.

Author Contributions: Conceptualisation, V.B., M.T.V. and R.M.; methodology, V.B., M.T.V. and R.M.; formal analysis, V.B., M.T.V. and R.M.; investigation, V.B., M.T.V. and R.M.; resources, V.B., M.T.V. and R.M.; data curation, V.B., M.T.V. and R.M.; writing—original draft preparation, V.B., M.T.V. and R.M.; writing—review and editing, V.B., M.T.V. and R.M.; visualisation, V.B., M.T.V. and R.M.; supervision, V.B., M.T.V. and R.M. All authors have read and agreed to the published version of the manuscript.

Funding: This research was partially carried out within the framework of The Ministry of University and Research (MUR) initiative "Department of Excellence" (Law 232/2016) and DAFNE Project

2023-27 "Digital, Intelligent, Green, and Sustainable" (acronym: D.I.Ver.So), https://www.unitus.it/ricerca/dipartimenti-di-eccellenza/ (accessed on 14 March 2025).

Data Availability Statement: The original contributions presented in this study are included in the article/Supplementary Materials. Further inquiries can be directed to the corresponding author.

Acknowledgments: This study is dedicated to our friend, Luca Riccioni, for his contributions and memory. We are grateful to him for making this work possible.

Conflicts of Interest: The authors declare no conflicts of interest.

References

1. Cristofori, V.; Caruso, D.; Latini, G.; Dell'Agli, M.; Cammilli, C.; Rugini, E.; Bignami, C.; Muleo, R. Fruit quality of italian pomegranate (*Punica granatum* L.) autochthonous varieties. *Eur. Food Res. Technol.* **2011**, *232*, 397–403.
2. Hajleh, M.N.A.; Al-Dujaili, E.A.S. Anti-cancer activity of pomegranate and its biophenols; general review. *EC Nutr.* **2016**, *6*, 28–52.
3. Fanali, C.; Belluomo, M.G.; Cirilli, M.; Cristofori, V.; Zecchini, M.; Cacciola, F.; Russo, M.; Muleo, R.; Dugo, L. Antioxidant activity evaluation and HPLC-photodiode array/MS polyphenols analysis of pomegranate juice from selected Italian cultivars: A comparative study. *Electrophoresis* **2016**, *37*, 1947–1955. [PubMed]
4. Reddy, M.K.; Gupta, S.K.; Jacob, M.R.; Khan, S.I.; Ferreira, D. Antioxidant, antimalarial and antimicrobial activities of tannin-rich fractions, ellagitannins and phenolic acids from *Punica granatum* L. *Planta Medica* **2007**, *73*, 461–467.
5. Giménez-Bastida, J.A.; Ávila-Gálvez, M.Á.; Espín, J.C.; González-Sarrías, A. Evidence for health properties of pomegranate juices and extracts beyond nutrition: A critical systematic review of human studies. *Trends Food Sci. Technol.* **2021**, *114*, 410–423.
6. Pollastro, S.; Dongiovanni, C.; Gerin, D.; Pollastro, P.; Fumarola, G.; De Miccolis Angelini, R.M.; Faretra, F. First report of *Coniella granati* as a causal agent of pomegranate crown rot in southern Italy. *Plant Dis.* **2016**, *100*, 1498. [CrossRef]
7. Mirabolfathy, M.; Groenewald, J.Z.; Crous, P.W. First report of *Pilidiella granati* causing dieback and fruit rot of pomegranate (*Punica granatum*) in Iran. *Plant Dis.* **2012**, *96*, 461.
8. Levy, E.; Elkind, G.; Ben-Arie, R.; Ben-Ze'ev, I.S. First report of *Coniella granati* causing pomegranate fruit rot in Israel. *Phytoparasitica* **2011**, *39*, 403–405.
9. Çeliker, N.M.; Uysal, A.; Çetinel, B.; Poyraz, D. Crown rot on pomegranate caused by *Coniella granati* in Turkey. *Australas. Plant Dis. Notes* **2012**, *7*, 161–162.
10. Tziros, G.T.; Tzavella-Klonari, K. Pomegranate fruit rot caused by *Coniella granati* confirmed in Greece. *Plant Pathol.* **2008**, *57*, 783.
11. Palou, L.; Guardado, A.; Montesinos-Herrero, C. First report of *Penicillium* spp. and *Pilidiella granati* causing postharvest fruit rot of pomegranate in Spain. *New Dis. Rep.* **2010**, *22*, 21. [CrossRef]
12. Palavouzis, S.C.; Tzamos, S.; Paplomatas, E.; Thomidis, T. First report of *Neofusicoccum parvum* causing shoot blight of pomegranate in northern Greece. *New Dis. Rep.* **2015**, *32*, 10.
13. KC, A.N.; Vallad, G.E. First report of *Neofusicoccum parvum* causing shoot blight and stem cankers on pomegranate in Florida. *Plant Dis.* **2016**, *100*, 1783.
14. Riccioni, L.; Valente, M.T.; Giambattista, G.d. First report of *Neofusicoccum parvum* causing shoot blight and plant decay on pomegranate in Tarquinia, Italy. *J. Plant Pathol.* **2017**, *99*, 294.
15. Molina-Gayosso, E.; Silva-Rojas, H.V.; García-Morales, S.; Avila-Quezada, G. First report of black spots on avocado fruit caused by *Neofusicoccum parvum* in Mexico. *Plant Dis.* **2012**, *96*, 287.
16. Phillips, A.J.L.; Alves, A.; Abdollahzadeh, J.; Slippers, B.; Wingfield, M.J.; Groenewald, J.Z.; Crous, P.W. The *Botryosphaeriaceae*: Genera and species known from culture. *Stud. Mycol.* **2013**, *76*, 51–167.
17. Úrbez-Torres, J.R.; Gubler, W.D. Susceptibility of grapevine pruning wounds to infection by *Lasiodiplodia theobromae* and *Neofusicoccum parvum*. *Plant Pathol.* **2011**, *60*, 261–270.
18. Lamichhane, J.R.; Venturi, V. Synergisms between microbial pathogens in plant disease complexes: A growing trend. *Front. Plant Sci.* **2015**, *6*, 385.
19. Schmidt, P.-A.; Bálint, M.; Greshake, B.; Bandow, C.; Römbke, J.; Schmitt, I. Illumina metabarcoding of a soil fungal community. *Soil Biol. Biochem.* **2013**, *65*, 128–132.
20. Abdelfattah, A.; Li Destri Nicosia, M.G.; Cacciola, S.O.; Droby, S.; Schena, L. Metabarcoding analysis of fungal diversity in the phyllosphere and carposphere of Olive (*Olea europaea*). *PLoS ONE* **2015**, *10*, e0131069.
21. Abdelfattah, A.; Cacciola, S.O.; Mosca, S.; Zappia, R.; Schena, L. Analysis of the fungal diversity in citrus leaves with greasy spot disease symptoms. *Microb. Ecol.* **2017**, *73*, 739–749. [PubMed]
22. Morales-Cruz, A.; Figueroa-Balderas, R.; García, J.F.; Tran, E.; Rolshausen, P.E.; Baumgartner, K.; Cantu, D. Profiling grapevine trunk pathogens in planta: A case for community-targeted DNA metabarcoding. *BMC Microbiol.* **2018**, *18*, 214.

23. Del Frari, G.; Gobbi, A.; Aggerbeck, M.R.; Oliveira, H.; Hansen, L.H.; Ferreira, R.B. Characterization of the wood mycobiome of *Vitis vinifera* in a vineyard affected by Esca. Spatial distribution of fungal communities and their putative relation with leaf symptoms. *Front. Plant Sci.* **2019**, *10*, 910. [CrossRef] [PubMed]
24. Kõljalg, U.; Larsson, K.-H.; Abarenkov, K.; Nilsson, R.H.; Alexander, I.J.; Eberhardt, U.; Erland, S.; Høiland, K.; Kjøller, R.; Larsson, E.; et al. Unite: A database providing web-based methods for the molecular identification of ectomycorrhizal fungi. *New Phytol.* **2005**, *166*, 1063–1068. [CrossRef]
25. Meiklejohn, K.A.; Damaso, N.; Robertson, J.M. Assessment of BOLD and genbank–their accuracy and reliability for the identification of biological materials. *PLoS ONE* **2019**, *14*, e0217084.
26. van der Loos, L.M.; Nijland, R. Biases in bulk: DNA metabarcoding of marine communities and the methodology involved. *Mol. Ecol.* **2021**, *30*, 3270–3288.
27. Blaalid, R.; Kumar, S.; Nilsson, R.H.; Abarenkov, K.; Kirk, P.M.; Kauserud, H. ITS1 versus ITS2 as DNA metabarcodes for fungi. *Mol. Ecol. Resour.* **2013**, *13*, 218–224.
28. Mbareche, H.; Veillette, M.; Bilodeau, G.; Duchaine, C. Comparison of the performance of ITS1 and ITS2 as barcodes in amplicon-based sequencing of bioaerosols. *PeerJ* **2020**, *8*, e8523.
29. Yang, R.-H.; Su, J.-H.; Shang, J.-J.; Wu, Y.-Y.; Li, Y.; Bao, D.-P.; Yao, Y.-J. Evaluation of the ribosomal DNA internal transcribed spacer (its), specifically ITS1 and ITS2, for the analysis of fungal diversity by deep sequencing. *PLoS ONE* **2018**, *13*, e0206428.
30. Napoli, R.; Paolanti, M.; Di Ferdinando, S. *Atlante dei suoli del lazio*; ARSIAL Regione Lazio: Rome, Italy, 2019; ISBN 978-88-904841-2-4.
31. Fratianni, S.; Acquaotta, F. The climate of italy. In *Landscapes and Landforms of Italy*; Soldati, M., Marchetti, M., Eds.; Springer International Publishing: Cham, Switzerland, 2017; pp. 29–38.
32. White, T.J.; Bruns, T.; Lee, S.; Taylor, J. 38-amplification and direct sequencing of fungal ribosomal RNA genes for phylogenetics. In *PCR Protocols*; Innis, M.A., Gelfand, D.H., Sninsky, J.J., White, T.J., Eds.; Academic Press: San Diego, CA, USA, 1990; pp. 315–322.
33. Cenis, J.L. Rapid extraction of fungal DNA for PCR amplification. *Nucleic Acids Res.* **1992**, *20*, 2380.
34. Aragona, M.; Minio, A.; Ferrarini, A.; Valente, M.T.; Bagnaresi, P.; Orrù, L.; Tononi, P.; Zamperin, G.; Infantino, A.; Valè, G.; et al. De novo genome assembly of the soil-borne fungus and tomato pathogen *Pyrenochaeta lycopersici*. *BMC Genom.* **2014**, *15*, 313.
35. Miller, K.E.; Hopkins, K.; Inward, D.J.G.; Vogler, A.P. Metabarcoding of fungal communities associated with bark beetles. *Ecol. Evol.* **2016**, *6*, 1590–1600.
36. Edgar, R.C. Uparse: Highly accurate OTU sequences from microbial amplicon reads. *Nat. Methods* **2013**, *10*, 996–998. [PubMed]
37. Abarenkov, K.Z.A.; Timo, P.; Raivo, P.; Filipp, I.; Henrik, N.R.; Urmas, K. *Unite Usearch/Utax Release for Eukaryotes*; Version 04.04.2024; UNITE Community: London, UK, 2024.
38. Manetti, G.; Brunetti, A.; Lumia, V.; Sciarroni, L.; Marangi, P.; Cristella, N.; Faggioli, F.; Reverberi, M.; Scortichini, M.; Pilotti, M. Identification and characterization of *Neofusicoccum stellenboschiana* in branch and twig dieback-affected olive trees in Italy and comparative pathogenicity with *N. mediterraneum*. *J. Fungi* **2023**, *9*, 292. [CrossRef] [PubMed]
39. Moncini, L.; Pachetti, G.; Pollastro, S. Il cancro del fusto minaccia il melograno italiano. *L'informatore Agrario* **2017**, *27*, 54–56.
40. Graniti, A.; Surico, G.; Mugnai, L. Esca of grapevine: A disease complex or a complex of diseases? *Phytopathologia Mediterranea* **2000**, *39*, 16–20.
41. Hennion, B.; Lecomte, P.; Larignon, P.; Baudry, A.; Durpaire, M.P.; Mouillon, M.; Tailleur, J.L.; Dupuy, O. First observations of a wood decay (Esca-loke disease) on kiwifruit in France. *Acta Hortic.* **2003**, *610*, 409–413.
42. Savian, F.; Ginaldi, F.; Musetti, R.; Sandrin, N.; Tarquini, G.; Pagliari, L.; Firrao, G.; Martini, M.; Ermacora, P. Studies on the aetiology of kiwifruit decline: Interaction between soil-borne pathogens and waterlogging. *Plant Soil* **2020**, *456*, 113–128.
43. Prencipe, S.; Savian, F.; Nari, L.; Ermacora, P.; Spadaro, D.; Martini, M. First report of *Phytopythium vexans* causing decline syndrome of *Actinidia deliciosa* 'hayward' in Italy. *Plant Dis.* **2020**, *104*, 2032.
44. Donati, I.; Cellini, A.; Sangiorgio, D.; Caldera, E.; Sorrenti, G.; Spinelli, F. Pathogens associated to kiwifruit vine decline in italy. *Agriculture* **2020**, *10*, 119. [CrossRef]
45. Tacconi, G.; Paltrinieri, S.; Mejia, J.F.; Fuentealba, S.P.; Bertaccini, A.; Tosi, L.; Giacopini, A.; Mazzucchi, U.; Favaron, F.; Sella, L.; et al. Vine decline in kiwifruit: Climate change and effect on waterlogging and *Phytophthora* in north Italy. *VIII Int. Symp. Kiwifruit* **2015**, *1096*, 93–97.
46. Spigaglia, P.; Barbanti, F.; Marocchi, F.; Mastroleo, M.; Baretta, M.; Ferrante, P.; Caboni, E.; Lucioli, S.; Scortichini, M. *Clostridium bifermentans* and *C. subterminale* are associated with kiwifruit vine decline, known as *moria*, in Italy. *Plant Pathol.* **2020**, *69*, 765–774.
47. Chandra, R.; Babu, K.D.; Jadhav, V.T.; Silva, J.T.d. Origin, history and domestication of pomegranate. *Fruit Veg. Cereal Sci. Biotechnol.* **2010**, *2*, 1–6.
48. Mello, A.; Lumini, E.; Napoli, C.; Bianciotto, V.; Bonfante, P. Arbuscular mycorrhizal fungal diversity in the *Tuber melanosporum* brûlé. *Fungal Biol.* **2015**, *119*, 518–527. [PubMed]

49. Bazzicalupo, A.L.; Bálint, M.; Schmitt, I. Comparison of ITS1 and ITS2 rDNA in 454 sequencing of hyperdiverse fungal communities. *Fungal Ecol.* **2013**, *6*, 102–109.
50. Monard, C.; Gantner, S.; Stenlid, J. Utilizing ITS1 and ITS2 to study environmental fungal diversity using pyrosequencing. *FEMS Microbiol. Ecol.* **2013**, *84*, 165–175.
51. Orgiazzi, A.; Bianciotto, V.; Bonfante, P.; Daghino, S.; Ghignone, S.; Lazzari, A.; Lumini, E.; Mello, A.; Napoli, C.; Perotto, S.; et al. 454 pyrosequencing analysis of fungal assemblages from geographically distant, disparate soils reveals spatial patterning and a core mycobiome. *Diversity* **2013**, *5*, 73–98. [CrossRef]
52. Nilsson, R.H.; Ryberg, M.; Abarenkov, K.; Sjökvist, E.; Kristiansson, E. The its region as a target for characterization of fungal communities using emerging sequencing technologies. *FEMS Microbiol. Lett.* **2009**, *296*, 97–101.
53. Bellemain, E.; Davey, M.L.; Kauserud, H.; Epp, L.S.; Boessenkool, S.; Coissac, E.; Geml, J.; Edwards, M.; Willerslev, E.; Gussarova, G.; et al. Fungal palaeodiversity revealed using high-throughput metabarcoding of ancient DNA from arctic permafrost. *Environ. Microbiol.* **2013**, *15*, 1176–1189.
54. Badotti, F.; de Oliveira, F.S.; Garcia, C.F.; Vaz, A.B.M.; Fonseca, P.L.C.; Nahum, L.A.; Oliveira, G.; Góes-Neto, A. Effectiveness of its and sub-regions as DNA barcode markers for the identification of basidiomycota (fungi). *BMC Microbiol.* **2017**, *17*, 42.
55. Tedersoo, L.; Anslan, S.; Bahram, M.; Põlme, S.; Riit, T.; Liiv, I.; Kõljalg, U.; Kisand, V.; Nilsson, H.; Hildebrand, F.; et al. Shotgun metagenomes and multiple primer pair-barcode combinations of amplicons reveal biases in metabarcoding analyses of fungi. *MycoKeys* **2015**, *10*, 1–43.
56. Tedersoo, L.; Lindahl, B. Fungal identification biases in microbiome projects. *Environ. Microbiol. Rep.* **2016**, *8*, 774–779. [PubMed]
57. Martin, K.J.; Rygiewicz, P.T. Fungal-specific PCR primers developed for analysis of the ITS region of environmental DNA extracts. *BMC Microbiol.* **2005**, *5*, 28.
58. Langarica-Fuentes, A.; Zafar, U.; Heyworth, A.; Brown, T.; Fox, G.; Robson, G.D. Fungal succession in an in-vessel composting system characterized using 454 pyrosequencing. *FEMS Microbiol. Ecol.* **2014**, *88*, 296–308. [PubMed]
59. U'Ren, J.M.; Riddle, J.M.; Monacell, J.T.; Carbone, I.; Miadlikowska, J.; Arnold, A.E. Tissue storage and primer selection influence pyrosequencing-based inferences of diversity and community composition of endolichenic and endophytic fungi. *Mol. Ecol. Resour.* **2014**, *14*, 1032–1048.
60. Cuadros-Orellana, S.; Leite, L.R.; Smith, A.; Medeiros, J.D.; Badotti, F.; Fonseca, P.L.; Vaz, A.B.; Oliveira, G.; Góes-Neto, A. Assessment of fungal diversity in the environment using metagenomics: A decade in review. *Fungal Genom. Biol.* **2013**, *3*, 1.
61. Bálint, M.; Schmidt, P.-A.; Sharma, R.; Thines, M.; Schmitt, I. An illumina metabarcoding pipeline for fungi. *Ecol. Evol.* **2014**, *4*, 2642–2653.
62. Gweon, H.S.; Oliver, A.; Taylor, J.; Booth, T.; Gibbs, M.; Read, D.S.; Griffiths, R.I.; Schonrogge, K. Pipits: An automated pipeline for analyses of fungal internal transcribed spacer sequences from the illumina sequencing platform. *Methods Ecol. Evol.* **2015**, *6*, 973–980.
63. Hibbett, D.; Abarenkov, K.; Kõljalg, U.; Öpik, M.; Chai, B.; Cole, J.; Wang, Q.; Crous, P.; Robert, V.; Helgason, T.; et al. Sequence-based classification and identification of fungi. *Mycologia* **2016**, *108*, 1049–1068.

Disclaimer/Publisher's Note: The statements, opinions and data contained in all publications are solely those of the individual author(s) and contributor(s) and not of MDPI and/or the editor(s). MDPI and/or the editor(s) disclaim responsibility for any injury to people or property resulting from any ideas, methods, instructions or products referred to in the content.

Journal of *Fungi*

MDPI

Article

Fungal Community Complexity and Stability in Clay Loam and Sandy Soils in Mangrove Ecosystems

Shengyao Zhou [1], Xiaojie Deng [1], Rajapakshalage Thashikala Nethmini [1], Huaxian Zhao [2], Qing He [1], Gonglingxia Jiang [1], Qinghua Hou [1], Qingxiang Chen [1], Xiaolei Li [1], Ke Dong [3] and Nan Li [1,*]

[1] Tropical Ocean Environment in Western Coastal Waters Observation and Research Station of Guangdong Province, Key Laboratory of Climate, Resources and Environment in Continental Shelf Sea and Deep Sea of Department of Education of Guangdong Province, Department of Oceanography, Key Laboratory for Coastal Ocean Variation and Disaster Prediction, College of Ocean and Meteorology, Guangdong Ocean University, Zhanjiang 524088, China; syzhou001009@163.com (S.Z.); 15270735195@163.com (X.D.); nethmini1207@gmail.com (R.T.N.); 13531051195@163.com (Q.H.); stonecold_nan@163.com (G.J.); huaqingh@163.com (Q.H.); chenqxocean@163.com (Q.C.); xli@gdou.edu.cn (X.L.)

[2] Key Laboratory of Ministry of Education for Environment Change and Resources Use in Beibu Gulf, Guangxi Key Laboratory of Earth Surface Processes and Intelligent Simulation, Nanning Normal University, Nanning 530001, China; zhx343@gmail.com

[3] Department of Biological Sciences, Kyonggi University, 154-42, Gwanggyosan-ro, Yeongtong-gu, Suwon-si 16227, Gyeonggi-do, Republic of Korea; dongke-007@163.com

* Correspondence: nli0417@163.com

Abstract: Soil fungi in mangroves are diverse and crucial for organic matter decomposition and element cycling. However, the drivers influencing network complexity and the stability of fungal communities across different mangrove soil habitats remain unclear. This study investigated the main factors driving the composition, diversity, complexity, and stability of fungal communities in clay loam and sandy soils in mangrove ecosystems. Results showed that *Dothideomycetes* and *Sordariomycetes* dominated in clay loam and sandy soils, respectively. Sandy soils exhibited higher alpha diversity than clay loam. Beta diversity analysis revealed significant differences in the fungal community structure between the two soil types. Network analysis demonstrated higher complexity and stability of fungal communities in clay loam than in sandy soil. Spearman's correlation analysis revealed that NH_4^+-N and total nitrogen were the main factors affecting complexity and stability in clay loam, respectively. Partial least squares path modeling demonstrated that alpha diversity and soil properties were closely linked to the complexity and stability of fungal communities in clay loam, whereas beta diversity was the primary driver in sandy soil. Our study enhances the understanding of the mechanisms that maintain fungal diversity and community stability in mangrove ecosystems, with important implications for restoring vegetation in degraded areas.

Keywords: fungi; mangrove ecosystems; co-occurrence network; complexity; stability; clay loam; sandy soil

1. Introduction

The fungal community in soil is rich and diverse, playing significant ecological roles as a key component of microbial communities, particularly in promoting plant nutrition, carbon cycling, and pathology [1,2]. In ecology, ecosystem complexity typically refers to the abundance of species and their interrelationships within the system, whereas stability

refers to the ability of a system to maintain its function and structure despite external disturbances [3]. Human disturbances and ecological drivers inevitably impact biodiversity and fungal communities in various soil ecosystems. For example, S Luo et al. [4] found that increased grassland degradation caused by human disturbance on the Qinghai–Tibet Plateau led to a less complex and stable soil fungal community structure, highlighting the need to restore and protect the degradation-induced simplification of fungal communities. P Zhao et al. [5] identified soil nutrients as the determining factors of fungal network complexity and stability in Mongolian pine plantations, followed by climate conditions, which is helpful for understanding the interactions between plants and soil fungi. However, factors influencing fungal complexity and stability in saline soils remain poorly understood.

Mangrove forests hold significant ecological and economic values owing to their unique ecological environment. Mangroves provide ideal habitats for birds, insects, fish, and mammals [6] and protect coastlines by serving as natural barriers against tropical storms and waves [7]. The community structure and diversity of mangrove soil fungi are influenced by pH, salinity, and organic matter content [8–10]. In many cases, nutrient levels in mangrove soils are key ecological drivers of the fungal community structure [11,12]. For example, P Wei et al. [13] showed that phosphorus is important for fungal communities in mangrove ecosystems. Additionally, environments with abundant organic matter and appropriate pH levels promote greater fungal diversity in mangrove sediments [14].

Recent studies have highlighted the significant role of soil types in shaping fungal communities and their composition across various ecosystems. Different soil types create distinct ecological environments, which affect fungal diversity. For example, in forest soils, pH and carbon concentrations have strong indirect effects on fungal community composition [15]. Moreover, soil pH and available nutrients (such as nitrogen and phosphorus) are major drivers of fungal community shifts and diversity in desert grasslands [16]. However, fungal community composition and the key environmental factors driving its complexity and stability in various mangrove soil habitats remain poorly understood.

This study aimed to clarify the impact of different soil types on fungal community structures in mangrove soils in different habitats. Therefore, we collected clay loam and sandy soil samples from mangroves in Zhangjiang, Beihai, and Fangchenggang in southern China. The main objectives of this study were to (a) identify the species composition and diversity of fungal communities in clay loam and sandy mangrove soils, (b) evaluate the complexity and stability of fungal communities in these soils, and (c) clarify the key drivers determining the complexity and stability of fungal communities in clay loam and sandy mangrove soils. Overall, this study enhances our understanding of how different soil types influence fungal diversity maintenance mechanisms in mangrove ecosystems and provides valuable insights for the restoration and conservation of mangrove forests.

2. Materials and Methods

2.1. Study Area and Field Sampling

The sampling sites were located in coastal mangrove nature reserves in Zhenzhu Bay (ZZ), Shankou (SK), and Leizhou (LZ) in southern China (Figure 1). In July 2019, we collected 75 individual samples from the three accessible mangrove sites. Five plots (5×5 m^2) were established in each region for sampling. Sediment samples were collected from the surface layer (1–2 cm) and divided into three categories based on sand content: 0–10% (muddy or clay soil), 10–60% (mud–sand mixed soil or clay loam), and 60–100% (sandy soil) [17]. The LZ sample consisted of clay loam. Samples SK and ZZ were categorized as sandy soil. The salinity of the LZ sample is higher than that of the SK and ZZ samples. The content of clay

and silt in the LZ sample is significantly higher than that in the SK and ZZ samples. The content of sand in the LZ sample is lower than that in the SK and ZZ samples.

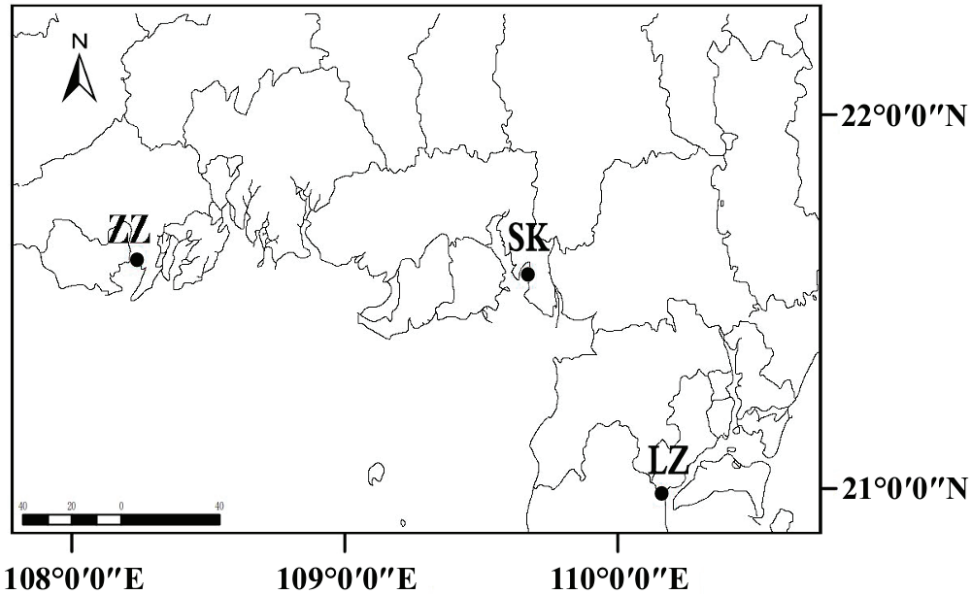


Figure 1. Distribution of the three mangrove sampling sites in southern China. ZZ: Zhenzhuwan mangrove site, sandy soil; SK: Shankou mangrove site, sandy soil; LZ: Leizhou mangrove site, clay loam. Two sites, SK and ZZ, are located in Guangxi province, while LZ is located in Guangdong province.

All individual collections were stored at −80 °C in case of DNA extraction for sequencing analysis.

2.2. Biochemical Factor Analyses

Biochemical parameters such as temperature, salinity, pH, and dissolved oxygen (DO) were measured in each region using a portable meter (556 MPS, YSI, Yellow Springs, OH, USA) for mangrove sediment samples. A Malvern Mastersizer 2000 (Malvern, UK) was used to determine the soil texture (sand, silt, and clay). Measurements were taken for total organic carbon (TOC), total carbon (TC), total sulfur (TS), total nitrogen (TN), total phosphorus (TP), total inorganic carbon (TIC), PO_4^{3-}, SO_4^{2-}, and inorganic nitrogen (NO_2^--N, NO_3^--N, and NH_4^+-N) in the laboratory.

2.3. DNA Extraction and PCR Amplification

The DNeasy PowerOil Pro kit (QIAGEN, Hilden, Germany) was used to extract DNA from 75 frozen mangrove sediment samples (0.25 g), following the manufacturer's protocols of the reagent kit. DNA integrity and purity were evaluated using a Nanodrop-2000 spectrophotometer (Thermo Fisher Scientific, Waltham, MA, USA). The DNA samples were stored at −80 °C. For fungal DNA amplification of the ITS1 region, primers ITS1F (5′-ACTTGGTCATTTAGAGGAAGTAA-3′) and ITS2 (5′-BGCTGCGTTCTT-CATCGATGC-3′) were used. The amplification process was carried out with the following cycling conditions: 95 °C for 5 min, followed by 30 cycles of 94 °C for 30 s, 50 °C for 45 s, 72 °C for 2 min, and a final extension at 72 °C for 10 min. The quality of PCR products was tested using 2% agarose gel electrophoresis and a Nanodrop 2000 spectrophotometer (Thermo Scientific, Wilmington, DE, USA). Sequencing samples were prepared using a TruSeq DNA kit (Illumina, San Diego, CA, USA) following the manufacturer's guidelines and sequenced using the Illumina MiSeq platform (San Diego, CA, USA) with a 2 × 250 bp Reagent Kit v2.

2.4. Bioinformatics Analysis

Primer mismatches or lengths of <275 bp, low-quality reads (quality scores < 30), and barcode sequences were removed using the DADA2 denoising method in QIIME 2. Amplicon sequence variants generated from the Illumina Scale amplicon data were used for further analysis. Taxonomic classification was conducted using the Ribosomal Database Project (RDP) classifier with a confidence threshold set at 80%. To reduce bias, the original sequence data were deposited in GenBank under BioProject Accession PRJNA771484.

2.5. Statistical Analyses

Statistical analyses were performed using the R software (version 4.3.2) (http://www.r-project.org/ accessed on 18 January 2019). The indices of Shannon was calculated using the "vegan" package (version 2.6-10). The Shannon index was used to represent alpha diversity. Principal coordinate analysis (PcoA) and analysis of similarity (ANOSIM) were performed to evaluate the differences in community structures among different samples based on the Bray–Curtis distance using the "vegan" package and visualized using the "ggplot2" package (version 3.5.1). Network analysis was performed using the "Hmisc" package (version 5.2-3) and visualized using the Gephi 0.9.2 software. Average degree measured the average interaction strength of microorganisms in the network. Density was calculated based on the tightness and complexity of the network. Modularity quantified the degree to which a network is compartmentalized into different modules. To determine the complexity and stability of the samples, total cohesion was calculated to reflect complexity. Positive cohesion, resulting from positive pairwise correlations, may represent the extent of cooperative behaviors within a sample, while negative cohesion could suggest the level of competitive interactions among community members [18]. Robustness was considered as an indicator of stability. Network robustness was quantified as the proportion of the remaining species in this network after random or targeted node removal. We measured the robustness when 50% of random nodes or five module hubs were removed [18]. As described in [18,19], Average Degree $= \frac{1}{n}\sum_{i=1}^{n} k_i$, where k_i is the degree of node i and n is the number of nodes; Density $= \frac{l}{l_{exp}} = \frac{2l}{n(n-1)}$, where l is the sum of total links and l_{exp} is the number of possible links; Cohesion $= \sum_{i=1}^{m} abundance_i \times connectedness_i$, where m is the total number of taxa in a community; Robustness $= \frac{\sum_{j \neq i} b_j s_{ij}}{\sum_{j \neq i} b_j}$, where b_j is the relative abundance of species j and s_{ij} is the association strength between species i and j, which is calculated using Pearson's correlation coefficient. Geographical distance matrices were computed using the distGeo function from the "geosphere" package (version 1.5-20) in R, based on the WGS84 ellipsoid model. Correlations were calculated using Spearman's rank method. Mantel test analysis was conducted to identify environmental factors that affect the structure of sediment fungal communities using the "vegan" package. Spearman heatmaps were generated using the "pheatmap" package (version 1.0.12) to display the relationship among environmental factors, complexity, and stability. Linear regression analysis was performed using the "ggplot2" (version 3.5.1) and "ggpmisc" packages (version 0.6.1). Partial least squares path modeling (PLS-PM) was conducted to determine the direct and indirect contributions of driving factors on complexity and stability using the "plspm" package (version 0.5.1).

3. Results

3.1. Composition and Diversity of Fungal Communities in Mangrove Clay Loam and Sandy Soil

In this study, 75 mangrove sediment samples were collected from the clay loam and sandy soil sites. Ultimately, 399 and 150 high-quality sequences were obtained. In the

clay loam samples, *Dothideomycetes* (64%) was the most dominant class, followed by *Sordariomycetes* (19%) and *Eurotiomycetes* (8%). In contrast, in the sandy soil samples, the abundances of *Sordariomycetes* (25%) and *Eurotiomycetes* (23%) ranked first and second, respectively. The sandy soil samples were obtained from the ZZ and SK sites. At the ZZ site, *Tremellomycetes* was the dominant class (25%), followed by *Sordariomycetes* (20%) and *Saccharomycetes* (17%). At the SK site, the community was mainly composed of *Eurotiomycetes* (32%), followed by *Sordariomycetes* (30%) and *Agaricomycetes* (11%) (Figure 2). These results indicate that environmental heterogeneity influences the composition of the mangrove fungal community.

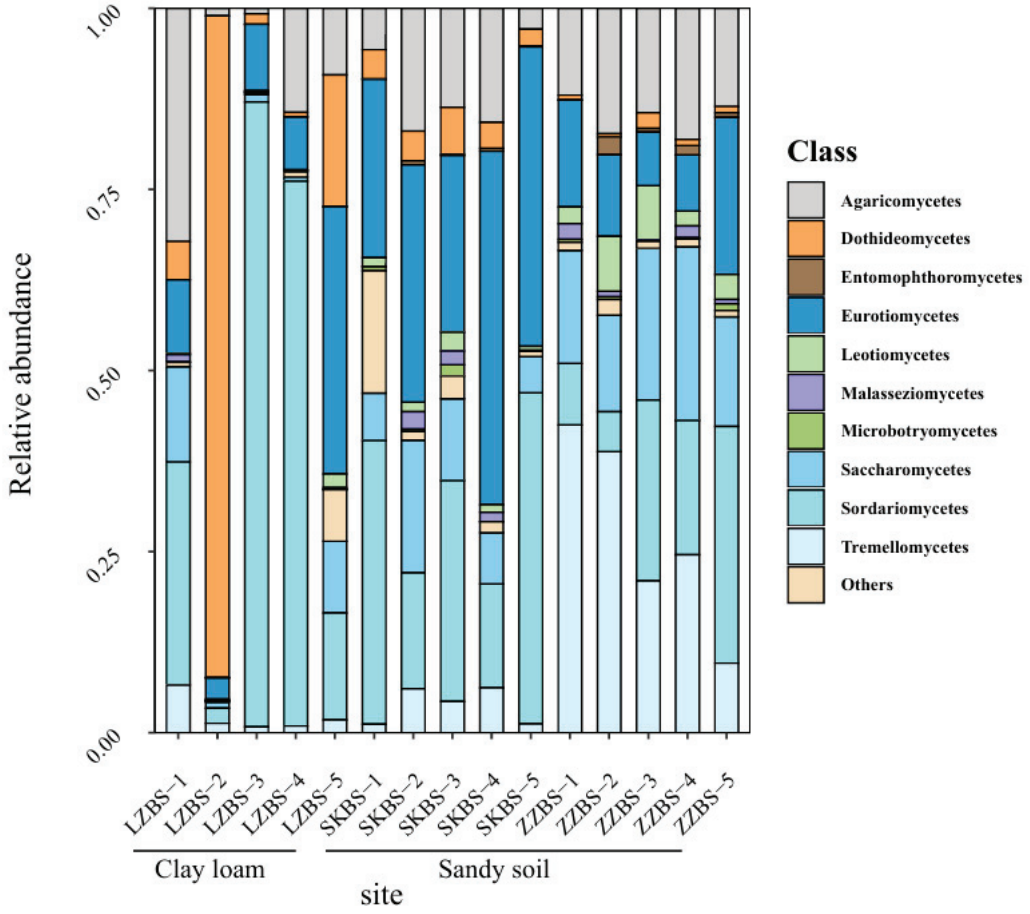


Figure 2. Relative abundance of fungi in mangrove clay loam and sandy soil (class level). BS: bulk sample; 1–5: site name.

Alpha diversity analysis demonstrated that the Shannon index of the sandy soil sample was higher than that of the clay loam. Additionally, fungi from the sandy soil at site ZZ exhibited significantly greater alpha diversity than those in the samples from other sites. The Shannon index of the sandy soil ZZ site was the highest, whereas that of the clay loam LZ site was the lowest. Intergroup differences were observed between the clay loam LZ and SK sites, but no intergroup differences were observed when compared to the sandy soil ZZ site (Figure 3a). PCoA of beta diversity (Bray–Curtis distance) revealed differences in fungal community structures between mangrove soils at different locations, clay loam, and sandy soils (Figure 3b,c). The first ordination axis (PCo1) and second ordination axis (PCo2) explained 20.44% and 19.47% of the community variation, respectively. The ANOSIM

test confirmed significant differences in the fungal community structure among mangrove sediments from different sites (R = 0.546, $p < 0.001$) (Figure 3b).

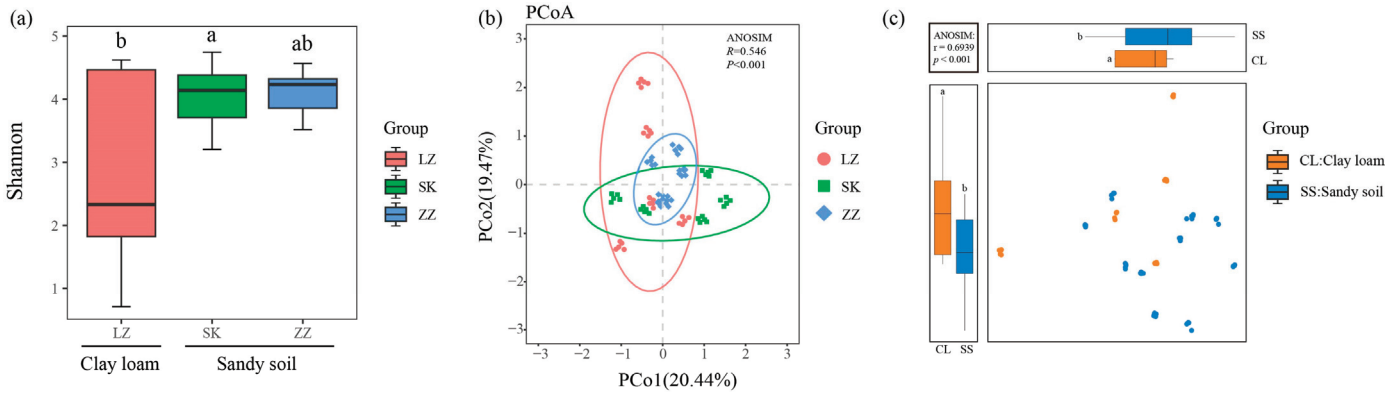


Figure 3. (**a**) Alpha diversity (Shannon index) presented by boxplots. In the boxplots, the upper whisker represents the maximum value; the upper line of the box represents upper quartile; the center line inside the box represents the median; the lower line of the box represents the lower quartile, and the lower whisker represents the minimum value. Different lowercase letters represent significant differences ($p < 0.05$), while the same lowercase letters indicate no significant differences ($p > 0.05$). (**b**) Differences in fungal community structures across different sites (PCoA). (**c**) Differences in fungal community structures between clay loam and sandy soils. "a" and "b" are commonly used to denote statistically significant differences between groups.

3.2. Topological Analysis of Fungal Community Structures in Mangrove Sediments

The degree of community complexity was quantified using the cohesion index [18]. The total cohesion index of the clay loam (0.790) was greater than that of the sandy soil (0.755) (Figure 4a), indicating that the complexity of fungal communities in mangrove clay loam was higher than that in the sandy soil. Moreover, the concentration of community stability was quantified using robustness. The robustness of the clay loam (0.286) was higher than that of the sandy soil (0.284) (Figure 4b), indicating that the stability of fungal communities in mangrove clay loam was greater than that in sandy soil. The clay loam LZ network exhibited the greatest average degree (35.286) and density (0.195), followed by the sandy soil SK network (average degree = 31.05; density = 0.172). These results revealed that OTUs in the clay loam LZ had a relatively greater number of relationships with the other OTUs in the network. While all networks showed the same modules (Modules = 1), the sandy soil ZZ had a greater modularity index (0.575) than LZ (0.518) and SK (0.51) (Table S1). These results indicated that the sandy soil ZZ had stronger anti-interference ability than the clay loam LZ and sandy soil SK (Figure 5).

3.3. Environmental Drivers of Fungal Diversity, Complexity, and Stability in Mangrove Sediments

In clay loam samples, Spearman's correlation analysis revealed that NO_2^--N was the most significant factors influencing the Shannon index ($p < 0.001$) (Table S2). TC was the predominant factor in the clay loam samples ($p < 0.001$) (Table S2). In contrast, C:N, salinity, and PO_4^{3-} were the most influential drivers in the sandy soil samples ($p < 0.001$) (Table S2).

In the clay loam samples, significant correlations were observed between the variables and the Mantel test, with temperature, C:P, and ORP showing the strongest correlation ($p < 0.001$) (Table S3). In contrast, in the sandy soil samples, pH, TS, and SO_4^{2-} were the most influential drivers, also displaying significant correlations ($p < 0.001$) (Table S3).

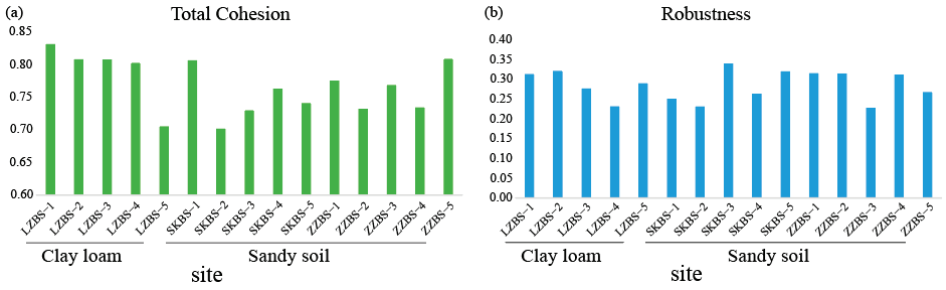


Figure 4. Total cohesion and robustness of fungi in the clay loam and sandy soil in mangrove soils. (**a**): total cohesion; (**b**): robustness.

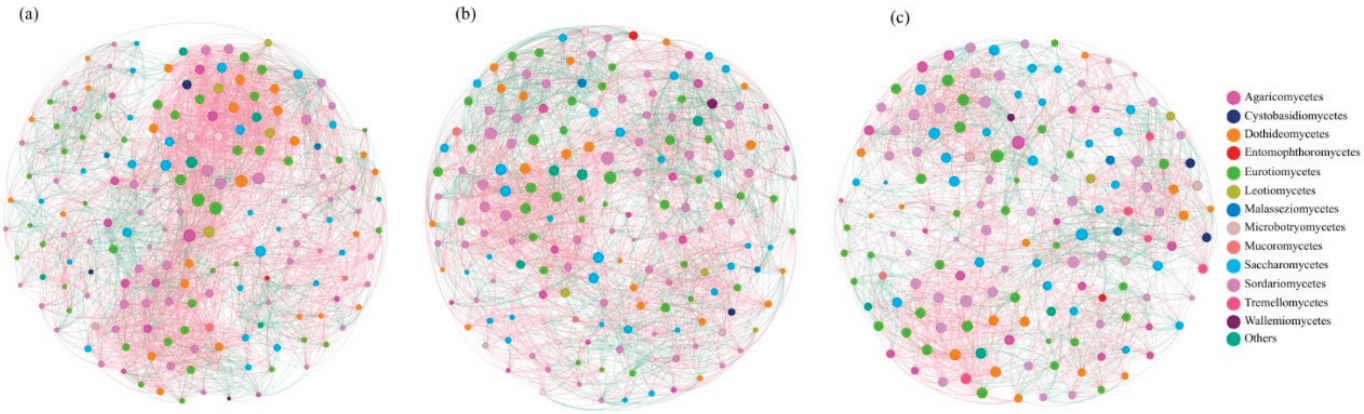


Figure 5. Co-occurrence network of the three groups. (**a**) LZ: Leizhou mangrove site, clay loam; (**b**) SK: Shankou mangrove site, sandy soil; (**c**) ZZ: Zhenzhuwan mangrove site, sandy soil. The color of nodes indicates species from the same module in each network. The line color indicates positive (pink) and negative (green) correlation coefficients.

According to Spearman's rank correlation analysis and the heatmap, in the clay loam samples, NH_4^+-N had the strongest impact on complexity, followed by salinity. Total nitrogen was the primary environmental factor affecting stability (Table S4). In contrast, in the sandy soil samples, no environmental factors were significantly correlated (Table S4). However, compared to other environmental drivers, TOC and TP exhibited stronger correlations with complexity and stability, respectively.

PLS-PM was constructed to analyze the relationships among complexity, stability, and diversity, as well as soil properties, nutrients, and geographic distance, in different soil types. In clay loam samples, alpha diversity (path coefficients = −0.28, $p < 0.001$) and beta diversity (path coefficients = 0.08, $p < 0.001$) jointly affected the stability of the fungal community structure, with alpha diversity showing a direct and total negative effect, while beta diversity exhibited a direct and total positive effect (Figure 6a,c). Additionally, geographic distance (path coefficients = −0.27, $p < 0.001$) had a greater negative direct effect on the stability, whereas nutrients (path coefficients = 0.21, $p < 0.05$) had a positive direct effect on the stability (Figure 6a,c). For the complexity of fungal community structures in clay loam, alpha diversity (path coefficients = 0.24, $p < 0.001$) showed a direct and total positive effect, whereas beta diversity (path coefficients = 0.05, $p > 0.05$) showed no effect (Figure 6a,b). Moreover, geographic distance (path coefficients = 0.68, $p < 0.001$) had a stronger positive direct effect on the complexity, whereas nutrients (path coefficients = −0.24, $p < 0.05$) and soil properties (path coefficients = −0.24, $p < 0.05$) showed negative effects on the complexity (Figure 6a,b). In the sandy soil samples, alpha diversity (path coefficients = −0.26, $p < 0.001$) and beta diversity (path coefficients = 0.14, $p < 0.001$)

were also significantly related to complexity, with alpha diversity showing a direct and total negative effect, whereas beta diversity showed a direct and total positive effect. Nutrients (path coefficients = −0.14, $p < 0.001$) and geographic distance (path coefficients = −0.17, $p < 0.001$) were significantly negatively correlated with complexity, whereas soil properties (path coefficient = 0.08, $p < 0.05$) showed a positive correlation (Figure 7a,b). For stability in sandy soil, beta diversity (path coefficients = 0.48, $p < 0.001$) exhibited a significantly positive direct and total effect, whereas alpha diversity (path coefficient = −0.04, $p > 0.05$) had no effect on stability. Additionally, only geographic distance (path coefficients = −0.14, $p < 0.001$) exerted a stronger negative effect (Figure 7a,c). From the above results, we concluded that alpha diversity emerged as the most influential factor in the complexity and stability of the fungal community structure in the clay loam samples compared to beta diversity, whereas nutrients and geographic distance were identified as the most vital factors for complexity and stability (Figure 6a–d). In contrast, in the sandy soil samples, beta diversity emerged as the most influential factor, affecting both complexity and stability (Figure 7a–d).

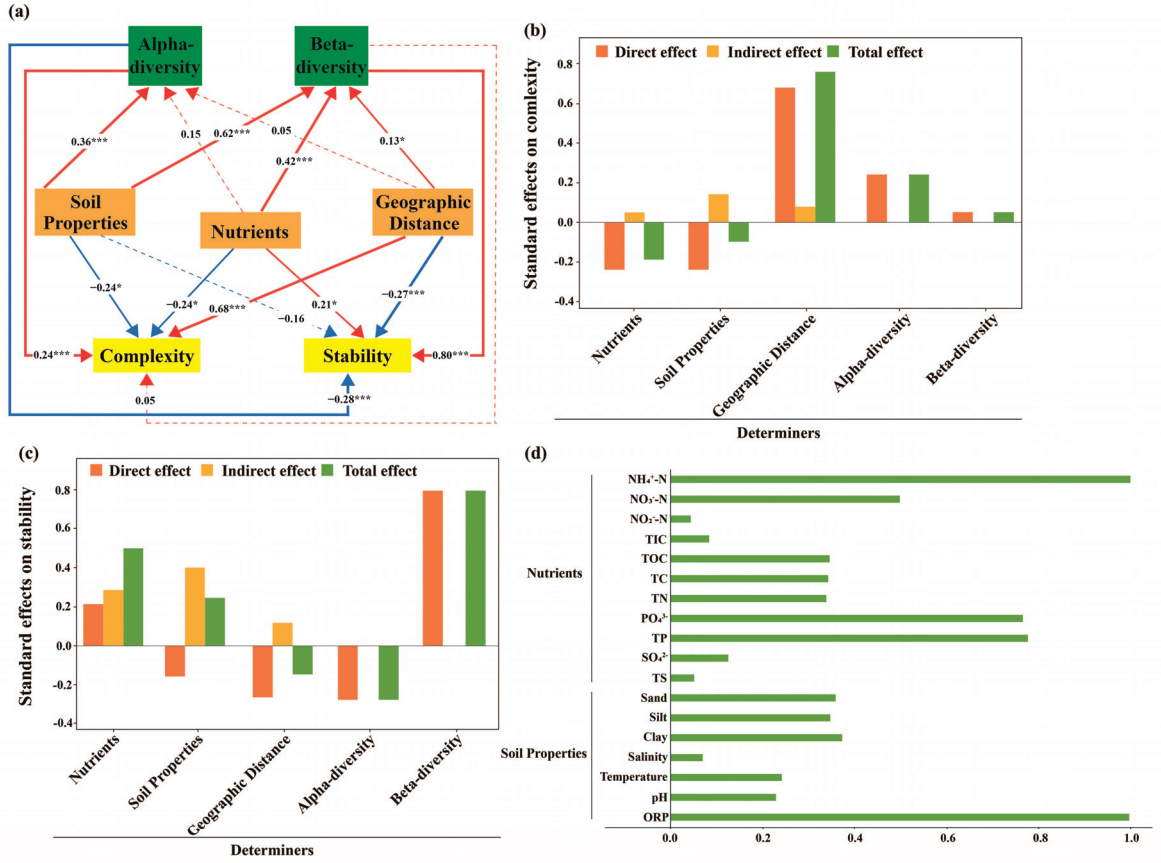


Figure 6. Path analysis representing the relationship between complexity, stability, soil properties, nutrients, alpha diversity, and beta diversity in the clay loam samples. (**a**) Solid and dashed arrows represent significance and insignificance at $p < 0.05$, respectively. Red and blue arrows indicate positive and negative effects, respectively. Significance levels, *: $p < 0.05$; ***: $p < 0.001$, are indicated using different widths of the solid line arrows; the numbers are path coefficients. (**b**) The direct, indirect, and total effects of different factors on the complexity. (**c**) The direct, indirect, and total effects of different factors on the stability. (**d**) The individual factor's contribution to the module. ORP, pH, temperature, salinity, and soil texture (clay, silt, and sand) are summarized as soil properties. NH_4^+-N, NO_2^--N, NO_3^--N, TIC, TOC, TC, TN, PO_4^{3-}, TP, SO_4^{2-}, and TS are summarized as nutrients.

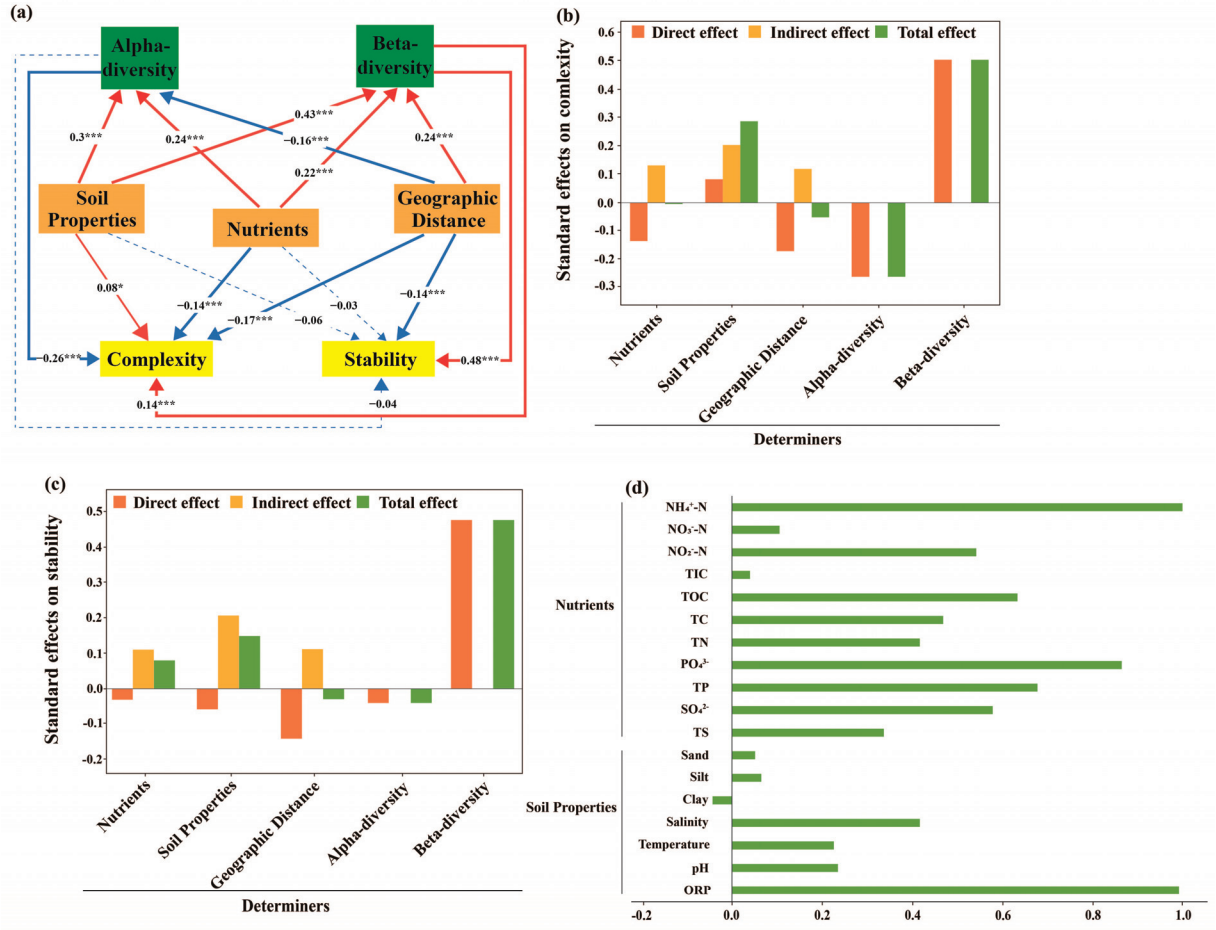


Figure 7. Path analysis representing the relationship between complexity, stability, soil properties, nutrients, alpha diversity, and beta diversity in the sandy soil samples. (**a**) Solid and dashed arrows represent significance and insignificance at $p < 0.05$, respectively. Red and blue arrows indicate positive and negative effects, respectively. Significance levels, *: $p < 0.05$; ***: $p < 0.001$, are indicated using different widths of the solid line arrows; the numbers are path coefficients. (**b**) The direct, indirect, and total effects of different factors on the complexity. (**c**) The direct, indirect, and total effects of different factors on the stability. (**d**) The individual factor's contribution to the module. ORP, pH, temperature, salinity, and soil texture (clay, silt, and sand) are summarized as soil properties. NH_4^+-N, NO_2^--N, NO_3^--N, TIC, TOC, TC, TN, PO_4^{3-}, TP, SO_4^{2-}, and TS are summarized as nutrients.

4. Discussion

4.1. Soil Types and Nutrient Availability Influencing Fungal Community Composition and Diversity in Mangrove Sediments

Nutrient availability and soil types significantly affected the composition of fungal communities in mangrove sediments. In the present study, the clay loam and sandy soil samples exhibited different dominant fungal classes. *Sordariomycetes* and *Eurotiomycetes* were commonly found in mangrove sediments, with a high relative abundance in the sandy soil. *Sordariomycetes* and *Eurotiomycetes* are prevalent in coastal ecosystems because of their adaptability to environments with abundant organic material and stress factors such as salt and water temperature [20]. These fungal classes, particularly in mangroves and coastal wetlands, play key roles in the decomposition of organic materials such as plant residues, wood, and cellulose which are prevalent in these ecosystems [21,22]. Their ability to degrade complex organic compounds, such as lignin and cellulose, is especially

important in areas rich in organic matter, such as mangrove sediments [23,24]. It is crucial to maintain soil fertility and ecosystem health [25,26]. Sandy soils typically have high aeration and low water retention capacity, which allow certain fungal groups to thrive and grow better in humid, organic-rich environments [27].

In our study, the sandy soil samples exhibited higher alpha diversity, whereas the clay loam samples showed the lowest alpha diversity (Figure 3a). This suggested more ecological niches and greater environmental adaptability in the sandy soil. This may be attributed to the favorable ecological conditions, environmental factors, and soil properties in that area. For example, K Palit et al. [28] and J Lai et al. [29] found that environmental factors like salinity, pH levels, and organic matter content can affect microbial diversity, which aligns with our observations. In contrast, the low diversity in the clay loam samples may reflect the extreme environmental conditions in this region, such as high salinity or low organic matter content, which may constrain the ability of certain fungal communities to thrive, leading to a more homogeneous fungal community in clay loam soils [30]. The results of PCoA and ANOSIM analyses further confirmed that fungal community structures in mangrove sediments exhibited significant differences (Figure 3b,c). These differences can be attributed to the unique properties of mangrove ecosystems and sediments, including variable salinity, organic matter content, and tidal dynamics, which collectively influence fungal community diversity in mangrove soils. These findings showed that fungal communities in mangrove ecosystems are highly dynamic and responsive to soil types and environmental conditions, including hydrodynamic factors, salinity conditions, and spatial distribution [31,32]. Our results suggest that fungal communities display distinct characteristics and variations in response to environmental changes in clay loam and sandy mangrove soils.

4.2. Higher Complexity and Stability of Fungal Communities in Clay Loam Compared to Sandy Soil in Mangrove Ecosystems

Cohesion is regarded as an index that reflects the complexity of the fungal community structure, indicating the degree of interaction between the fungal community structures. The cohesion index of clay loam (total cohesion = 0.790) was higher than that of sandy soil (total cohesion = 0.755), suggesting that the complexity of the fungal community structure in clay loam is greater than that in sandy soil. Robustness is also considered an indicator of the stability of the fungal community structure. Our results indicate that the robustness index for clay loam (robustness = 0.286) was greater than that for sandy soil (robustness = 0.284), implying that the fungal community structure in clay loam was more stable than that in sandy soil. These results suggest that the fungal communities in clay loam mangrove soils exhibit more species interactions and a greater ability to adapt to environmental changes [33]. However, K Zhang et al. [34] found that the biodiversity and interactions within microbial communities are crucial determinants of their resistance to and resilience following disturbances. In our research, the sandy soil samples exhibited higher alpha diversity compared to the clay loam. Clay loam has a stronger water retention capacity and lower erosivity, which helps reduce environmental disturbance and provides a more stable habitat under dynamic environmental conditions [35]. Due to the poor nutrient retention capacity of sandy soil [36], fungi may quickly adapt to rapidly changing nutrient environments, which may lead to an increase in the number of certain fungal species, thereby increasing the alpha diversity of the community. In comparison with the sandy soil samples (nodes = 181 and 157; edges = 2810 and 2119), nodes and edges were higher in the clay loam samples (nodes = 182; edges = 3211), which may imply that the soil type, to some extent, determined the ecological structure of mangrove fungal communities. In

addition, fungal relationships tend to be more positive and cooperative in clay loams [37]. Therefore, understanding the complexity and stability of fungal communities is crucial for recovering from disturbances and preventing the degradation of mangrove forests.

4.3. Main Driving Factors Influencing Complexity and Stability in Clay Loam and Sandy Soil in Mangrove Ecosystems

Our findings revealed a complex interplay between driving factors and fungal community dynamics across soil types in mangrove ecosystems. C Wang et al. [38] suggested that in various interactions, competition for resources is the main factor determining the adaptation and niche differentiation of soil fungal communities. The observed negative correlation between carbon or nitrogen availability (TC, NO_2^--N, and TOC) and fungal diversity (Shannon index) in the clay loam samples aligns with competition for soil resources in ecology. Our study also found that pH was significantly positively correlated with the Shannon index (Table S2), revealing that fungal community diversity was higher in soils with higher pH. Mantel test results demonstrated that temperature, the C:P ratio, and the C:N ratio were crucial environmental driving factors of fungal community composition in mangrove sediments (Table S3). Consistently, H Craig et al. [39] documented that nitrogen addition can alter the composition and diversity of microbial communities in mangrove soils. Z-F Zhang et al. [10] found that carbon cycling supports a variety of adapted microorganisms in terms of abundance and diversity. This may be because higher concentrations of carbon and nitrogen compounds increase resource competition. Our previous results revealed that there is more competition than cooperation among fungi in mangrove soils. J Rousk et al. [40] found that fungi in soil proliferate in acidic environments. However, we observed that in soils with higher pH values, fungal community diversity was higher. This may be due to the stimulation of certain enzymes by neutral (pH = 7) and alkaline (pH = 9) conditions [41], which promoted fungal growth and metabolism. This result may explain why *Eurotiomycetes* and *Sordariomycetes* are dominant in mangrove soils.

In contrast, the Shannon index was significantly positively correlated with salinity and the C:N ratio in the sandy soil samples, demonstrating that higher salinity and C:N ratios might promote fungal diversity (Table S2). In addition, our research revealed that PO_4^{3-} was significantly negatively correlated with the Shannon index, indicating that the higher the phosphate concentration, the lower the fungal community diversity in mangrove sediments (Table S2). The Mantel test showed that SO_4^{2-}, TC, and TS were important environmental factors driving fungal community composition (Table S3). Similarly, microorganisms play a crucial role in sulfur transformation in mangrove ecosystems [42]. Mangrove plants may absorb sulfate through their root systems [43], influencing the availability of sulfur in the soil, which in turn affects the distribution of fungi. Finally, it alters the composition of the fungal communities. Sulfur may synergize with carbon and nitrogen cycling to shape fungal distribution in mangrove ecosystems. The content of sulfur, carbon, and nitrogen may serve as the comprehensive indicators of the health of mangrove ecosystems.

Soil types emerge as a critical mediator for regulating the complexity and stability of fungal communities in response to environmental drivers. High water retention of clay loam facilitated nitrogen accumulation, especially NH_4^+-N and total nitrogen (Table S4), driving intricate fungal networks through competitions for resources [27]. Similar to our findings, H Yang et al. [44] found that nitrogen addition could disrupt the complexity and stability of fungal networks. In contrast, no clear environmental factors influenced the network in sandy soil samples (Table S4). These findings may have been caused by high permeability, leading to rapid nutrient loss and lower nitrogen content. This may

be because fungi in mangrove sediments compete for limited resources and exhibit less cooperative behavior. These findings highlight the complex interactions between soil types and fungal network dynamics in mangrove sediments, which are crucial for understanding the ecological functions of mangrove ecosystems, and have significant implications for the restoration, planting, and conservation of mangroves.

PLS–PM analysis revealed that while alpha diversity directly enhanced the complexity of fungal complexity in the clay loam, it weakened the stability of the fungal communities. Fungi can extend their spatial niches to acquire carbon and nutrient resources through the formation of hyphae and mycelia [38], which leads to niche overlap, reduces the efficiency of effective resource allocation, and intensifies competition among species, resulting in an unstable community structure [45]. Beta diversity had a stronger correlation with complexity and stability than alpha diversity in the sandy soil. The impact of beta diversity may enhance community stability by increasing heterogeneity between fungal communities. In conclusion, this study emphasized the main factors driving the complexity and stability of fungal communities, thereby providing theoretical guidance for the biodiversity and protection of mangrove ecosystems.

5. Conclusions

In this study, we investigated the fungal community composition and diversity in clay loam and sandy soils in mangrove ecosystems. The alpha and beta diversities exhibited significant divergence between clay loam and sandy mangrove soil samples. Additionally, fungal communities in the clay loam of mangrove soils were more complex and stable than those in sandy soils. NH_4^+-N and TN were the main environmental drivers that affected the complexity and stability in the clay loam, respectively. TOC and TP had the greatest correlation ($p > 0.05$) with complexity and stability, respectively, in the sandy soil. PLS-PM analysis demonstrated that alpha diversity limited the complexity and stability of the fungal community and was regulated by soil properties in clay loam. However, the principal limitation on fungal community complexity and stability in the sandy soil was beta diversity. Overall, our research promotes the understanding of how soil types and nutrient dynamics influence fungal community complexity and stability in mangrove ecosystems.

Supplementary Materials: The following supporting information can be downloaded at https://www.mdpi.com/article/10.3390/jof11040262/s1, Table S1. Topological parameters of the fungal co-occurrence network for the three groups; Table S2. Spearman's correlation test between the alpha diversity index and environmental factors; Table S3. The Mantel test for correlations between the beta diversity index and environmental factors; Table S4: Correlation among complexity, stability, and environmental factors.

Author Contributions: Writing—original draft preparation, S.Z.; software, X.D.; validation, R.T.N., Q.H. (Qing He) and G.J.; visualization, Q.H. (Qinghua Hou) and H.Z.; supervision, Q.C., X.L. and K.D.; writing—review and editing, N.L. All authors have read and agreed to the published version of the manuscript.

Funding: This research was jointly funded by the Guangdong Ocean University Innovative Team (Early-warning of marine disasters) (Grant number 2023KCXTD015); Guangxi Key Research and Development Program (Grant number AB24010109), the Scientific Research Start Funds of Guangdong Ocean University; the National Research Foundation of Korea (NRF) grant funded by the Korea government (MSIT) (RS-2022-NR073058).

Institutional Review Board Statement: Not applicable.

Informed Consent Statement: Not applicable.

Data Availability Statement: The original sequence data were deposited in GenBank under BioProject Accession PRJNA771484.

Acknowledgments: We would like to thank Qun Xie at Analytical and Testing Center of Guang dong Ocean University for their assistance with nutrient analysis. Additional technical support for field material was equally provided by Guangdong Provincial Observation and Research Station for Tropical Ocean Environment in Western Coastal Waters (GSTOEW) and Construction of Key Disciplines in Ocean Science at High-level Universities (231420003 and 080503032101).

Conflicts of Interest: The authors declare no conflicts of interest.

Abbreviations

The following abbreviations are used in this manuscript:

DO	Dissolved oxygen
TC	Total carbon
TOC	Total organic carbon
TP	Total phosphorus
TS	Total sulfur
TN	Total nitrogen
TIC	Total inorganic carbon
ORP	Oxidation-reduction potential
PCoA	Principal coordinate analysis
ANOSIM	Analysis of Similarity

References

1. Tedersoo, L.; Bahram, M.; Põlme, S.; Kõljalg, U.; Yorou, N.S.; Wijesundera, R.; Ruiz, L.V.; Vasco-Palacios, A.M.; Thu, P.Q.; Suija, A.; et al. Global diversity and geography of soil fungi. *Science* **2014**, *346*, 1256688. [PubMed]
2. Kuske, C.R.; Hesse, C.N.; Challacombe, J.F.; Cullen, D.; Herr, J.R.; Mueller, R.C.; Tsang, A.; Vilgalys, R. Prospects and challenges for fungal metatranscriptomics of complex communities. *Fungal Ecol.* **2015**, *14*, 133–137.
3. Pettersson, S. *Stability and Complexity of Ecosystems-Global Interaction Constraints, Landscape and Extinctions*; Chalmers Tekniska Hogskola: Göteborg, Sweden, 2023.
4. Luo, S.; Png, G.K.; Ostle, N.J.; Zhou, H.; Hou, X.; Luo, C.; Quinton, J.N.; Schaffner, U.; Sweeney, C.; Wang, D. Grassland degradation-induced declines in soil fungal complexity reduce fungal community stability and ecosystem multifunctionality. *Soil Biol. Biochem.* **2023**, *176*, 108865.
5. Zhao, P.; Gao, G.; Ding, G.; Zhang, Y.; Ren, Y. Fungal complexity and stability across afforestation areas in changing desert environments. *Sci. Total Environ.* **2024**, *912*, 169398. [CrossRef]
6. Nagelkerken, I.; Blaber, S.; Bouillon, S.; Green, P.; Haywood, M.; Kirton, L.; Meynecke, J.-O.; Pawlik, J.; Penrose, H.; Sasekumar, A. The habitat function of mangroves for terrestrial and marine fauna: A review. *Aquat. Bot.* **2008**, *89*, 155–185.
7. Jia, S.-L.; Chi, Z.; Liu, G.-L.; Hu, Z.; Chi, Z.-M. Fungi in mangrove ecosystems and their potential applications. *Crit. Rev. Biotechnol.* **2020**, *40*, 852–864.
8. Barbi, F.; Prudent, E.; Vallon, L.; Buée, M.; Dubost, A.; Legout, A.; Marmeisse, R.; Fraissinet-Tachet, L.; Luis, P. Tree species select diverse soil fungal communities expressing different sets of lignocellulolytic enzyme-encoding genes. *Soil Biol. Biochem.* **2016**, *100*, 149–159. [CrossRef]
9. Luis, P.; Saint-Genis, G.; Vallon, L.; Bourgeois, C.; Bruto, M.; Marchand, C.; Record, E.; Hugoni, M. Contrasted ecological niches shape fungal and prokaryotic community structure in mangroves sediments. *Environ. Microbiol.* **2019**, *21*, 1407–1424. [CrossRef]
10. Zhang, Z.-F.; Pan, Y.-P.; Liu, Y.; Li, M. High-level diversity of basal fungal lineages and the control of fungal community assembly by stochastic processes in mangrove sediments. *Appl. Environ. Microbiol.* **2021**, *87*, e00928-21.
11. Yu, H.; Liu, X.; Yang, C.; Peng, Y.; Yu, X.; Gu, H.; Zheng, X.; Wang, C.; Xiao, F.; Shu, L. Co-symbiosis of arbuscular mycorrhizal fungi (AMF) and diazotrophs promote biological nitrogen fixation in mangrove ecosystems. *Soil Biol. Biochem.* **2021**, *161*, 108382.
12. Behera, B.; Singdevsachan, S.K.; Mishra, R.; Dutta, S.; Thatoi, H. Diversity, mechanism and biotechnology of phosphate solubilising microorganism in mangrove—A review. *Biocatal. Agric. Biotechnol.* **2014**, *3*, 97–110. [CrossRef]

13. Wei, P.; Lei, A.; Zhou, H.; Hu, Z.; Wong, Y.; Tam, N.F.; Lu, Q. Comparison of microbial community structure and function in sediment between natural regenerated and original mangrove forests in a National Nature Mangrove Reserve, South China. *Mar. Pollut. Bull.* **2021**, *163*, 111955. [PubMed]
14. Ghizelini, A.M.; Mendonça-Hagler, L.C.S.; Macrae, A. Microbial diversity in Brazilian mangrove sediments: A mini review. *Braz. J. Microbiol.* **2012**, *43*, 1242–1254. [CrossRef]
15. Nagati, M.; Roy, M.; Manzi, S.; Richard, F.; Desrochers, A.; Gardes, M.; Bergeron, Y. Impact of local forest composition on soil fungal communities in a mixed boreal forest. *Plant Soil* **2018**, *432*, 345–357. [CrossRef]
16. Kang, P.; Hu, J.; Pan, Y.; Qu, X.; Ran, Y.; Yang, C.; Liu, B. Response of soil fungal-community structure and function to land conversion to agriculture in desert grassland. *Front. Microbiol.* **2024**, *15*, 1413973.
17. Wang, Q.; Wen, Y.; Zhao, B.; Hong, H.; Liao, R.; Li, J.; Liu, J.; Lu, H.; Yan, C. Coastal soil texture controls soil organic carbon distribution and storage of mangroves in China. *Catena* **2021**, *207*, 105709. [CrossRef]
18. Yuan, M.M.; Guo, X.; Wu, L.; Zhang, Y.; Xiao, N.; Ning, D.; Shi, Z.; Zhou, X.; Wu, L.; Yang, Y. Climate warming enhances microbial network complexity and stability. *Nat. Clim. Change* **2021**, *11*, 343–348. [CrossRef]
19. Deng, Y.; Jiang, Y.-H.; Yang, Y.; He, Z.; Luo, F.; Zhou, J. Molecular ecological network analyses. *BMC Bioinform.* **2012**, *13*, 113.
20. Wijayawardene, N.N.; Dai, D.-Q.; Jayasinghe, P.K.; Gunasekara, S.S.; Nagano, Y.; Tibpromma, S.; Suwannarach, N.; Boonyuen, N. Ecological and oceanographic perspectives in future marine fungal taxonomy. *J. Fungi* **2022**, *8*, 1141. [CrossRef]
21. Sánchez, C. Lignocellulosic residues: Biodegradation and bioconversion by fungi. *Biotechnol. Adv.* **2009**, *27*, 185–194. [CrossRef]
22. Cohen, R.; Hadar, Y. The roles of fungi in agricultural waste conversion. *Fungi Bioremediat.* **2001**, *23*, 305–334.
23. Onlamun, T.; Boonthavee, A.; Brooks, S. Diversity and Advantages of Culturable Endophytic Fungi from Tea (*Camellia sinensis*). *J. Fungi* **2023**, *9*, 1191. [CrossRef] [PubMed]
24. Yang, W.; Diao, L.; Wang, Y.; Yang, X.; Zhang, H.; Wang, J.; Luo, Y.; An, S.; Cheng, X. Responses of soil fungal communities and functional guilds to ~160 years of natural revegetation in the Loess Plateau of China. *Front. Microbiol.* **2022**, *13*, 967565. [CrossRef] [PubMed]
25. Tiessen, H.; Cuevas, E.; Chacon, P. The role of soil organic matter in sustaining soil fertility. *Nature* **1994**, *371*, 783–785. [CrossRef]
26. Deininger, A.; Frigstad, H. Reevaluating the role of organic matter sources for coastal eutrophication, oligotrophication, and ecosystem health. *Front. Mar. Sci.* **2019**, *6*, 210. [CrossRef]
27. Musei, S.K.; Kuyah, S.; Nyawira, S.; Ng'ang'a, S.K.; Karugu, W.N.; Smucker, A.; Nkurunziza, L. Sandy soil reclamation technologies to improve crop productivity and soil health: A review. *Front. Soil Sci.* **2024**, *4*, 1345895. [CrossRef]
28. Palit, K.; Rath, S.; Chatterjee, S.; Das, S. Microbial diversity and ecological interactions of microorganisms in the mangrove ecosystem: Threats, vulnerability, and adaptations. *Environ. Sci. Pollut. Res.* **2022**, *29*, 32467–32512. [CrossRef]
29. Lai, J.; Cheah, W.; Palaniveloo, K.; Suwa, R.; Sharma, S. A systematic review of the physicochemical and microbial diversity of well-preserved, restored, and disturbed mangrove forests: What is known and what is the way forward? *Forests* **2022**, *13*, 2160. [CrossRef]
30. Jiménez-Gómez, I.; Valdés-Muñoz, G.; Moreno-Perlin, T.; Mouriño-Pérez, R.R.; Sánchez-Carbente, M.d.R.; Folch-Mallol, J.L.; Pérez-Llano, Y.; Gunde-Cimerman, N.; Sánchez, N.d.C.; Batista-García, R.A. Haloadaptative responses of Aspergillus sydowii to extreme water deprivation: Morphology, compatible solutes, and oxidative stress at NaCl saturation. *J. Fungi* **2020**, *6*, 316. [CrossRef]
31. Adame, M.F.; Neil, D.; Wright, S.F.; Lovelock, C.E. Sedimentation within and among mangrove forests along a gradient of geomorphological settings. *Estuar. Coast. Shelf Sci.* **2010**, *86*, 21–30. [CrossRef]
32. Woodroffe, C.D.; Rogers, K.; McKee, K.L.; Lovelock, C.E.; Mendelssohn, I.; Saintilan, N. Mangrove sedimentation and response to relative sea-level rise. *Annu. Rev. Mar. Sci.* **2016**, *8*, 243–266.
33. Vanegas, J.; Muñoz-García, A.; Pérez-Parra, K.A.; Figueroa-Galvis, I.; Mestanza, O.; Polanía, J. Effect of salinity on fungal diversity in the rhizosphere of the halophyte *Avicennia germinans* from a semi-arid mangrove. *Fungal Ecol.* **2019**, *42*, 100855. [CrossRef]
34. Zhang, K.; Chen, C.; Long, D.; Wang, S.; Li, J.; Lin, X. Unveiling sedimentary microbial communities: Restored mangrove wetlands show higher heterogeneity and network stability than natural ones. *Ecol. Indic.* **2024**, *166*, 112274.
35. Bordoloi, R.; Das, B.; Yam, G.; Pandey, P.K.; Tripathi, O.P. Modeling of water holding capacity using readily available soil characteristics. *Agric. Res.* **2019**, *8*, 347–355. [CrossRef]
36. Kheoruenromne, I.; Suddhiprakarn, A.; Kanghae, P. Properties, environment and fertility capability of sandy soils in Northeast Plateau, Thailand. *Agric. Nat. Resour.* **1998**, *32*, 355–373.
37. Yang, T.; Tedersoo, L.; Liu, X.; Gao, G.F.; Dong, K.; Adams, J.M.; Chu, H. Fungi stabilize multi-kingdom community in a high elevation timberline ecosystem. *Imeta* **2022**, *1*, e49.
38. Wang, C.; Kuzyakov, Y. Mechanisms and implications of bacterial–fungal competition for soil resources. *ISME J.* **2024**, *18*, wrae073.

39. Craig, H.; Antwis, R.E.; Cordero, I.; Ashworth, D.; Robinson, C.H.; Osborne, T.Z.; Bardgett, R.D.; Rowntree, J.K.; Simpson, L.T. Nitrogen addition alters composition, diversity, and functioning of microbial communities in mangrove soils: An incubation experiment. *Soil Biol. Biochem.* **2021**, *153*, 108076.
40. Rousk, J.; Brookes, P.C.; Bååth, E. Investigating the mechanisms for the opposing pH relationships of fungal and bacterial growth in soil. *Soil Biol. Biochem.* **2010**, *42*, 926–934. [CrossRef]
41. Maria, G.; Sridhar, K.; Raviraja, N. Antimicrobial and enzyme activity of mangrove endophytic fungi of southwest coast of India. *J. Agric. Technol.* **2005**, *1*, 67–80.
42. Thatoi, H.; Behera, B.C.; Mishra, R.R.; Dutta, S.K. Biodiversity and biotechnological potential of microorganisms from mangrove ecosystems: A review. *Ann. Microbiol.* **2013**, *63*, 1–19. [CrossRef]
43. Ferreira, T.; Otero, X.; Vidal-Torrado, P.; Macías, F. Effects of bioturbation by root and crab activity on iron and sulfur biogeochemistry in mangrove substrate. *Geoderma* **2007**, *142*, 36–46. [CrossRef]
44. Yang, H.; Cheng, L.; Che, L.; Su, Y.; Li, Y. Nutrients addition decreases soil fungal diversity and alters fungal guilds and co-occurrence networks in a semi-arid grassland in northern China. *Sci. Total Environ.* **2024**, *926*, 172100. [CrossRef]
45. Dou, X.; Wang, R.; Li, C.; Zheng, C.; Zhou, X. Spatial distribution of soil water, plant roots, and water use pattern under different drip fertigation regimes in an apple-soybean intercropping system on the Loess Plateau, China. *Agric. Water Manag.* **2022**, *269*, 107718. [CrossRef]

Disclaimer/Publisher's Note: The statements, opinions and data contained in all publications are solely those of the individual author(s) and contributor(s) and not of MDPI and/or the editor(s). MDPI and/or the editor(s) disclaim responsibility for any injury to people or property resulting from any ideas, methods, instructions or products referred to in the content.

Journal of *Fungi*

MDPI

Article

Distribution Patterns of Wood-Decay Macrofungi (Agaricomycetes) in Floodplain Forest Islands of the Eastern Amazon

Vitória Pinto Farias [1], Maria do Perpétuo Socorro Progene Vilhena [1], Antonio Walison Gondim-Vieira [1,2], Richard Bruno Mendes-Freire [1,2], Renan Domingues Pacheco [3], Braian Saimon Frota da Silva [4] and Adriene Mayra da Silva Soares [2,5,*]

[1] Programa de Pós-Graduação em Ciências Biológicas, Universidade Federal Rural da Amazônia, Avenida Presidente Tancredo Neves, 2501, Terra Firme, Belém 66077-830, PA, Brazil; vitoriapintofarias@gmail.com (V.P.F.); sprogene@ufra.edu.br (M.d.P.S.P.V.); gondimwalison@gmail.com (A.W.G.-V.); richard.b.m.freire@gmail.com (R.B.M.-F.)
[2] Coordenação de Botânica, Museu Paraense Emílio Goeldi, Avenida Perimetral, 1901, Terra Firme, Belém 66077-830, PA, Brazil
[3] Programa de Pós-Graduação em Ecologia, Universidade Federal do Pará, Rua Augusto Corrêa, Guamá, Belém 66075-110, PA, Brazil; renandomingues013@gmail.com
[4] Instituto de Ciências Exatas e Naturais, Federal do Pará, Rua Augusto Corrêa, 01, Guamá, Belém 66075-110, PA, Brazil; braiansaimon@yahoo.com.br
[5] Laboratório de Botânica e Micologia, Universidade Federal Rural da Amazônia, Rodovia PA-451, Km-03, Açaizal, Tomé-Açu 68680-000, PA, Brazil
* Correspondence: adriene.soares@ufra.edu.br

Abstract: Macrofungi are key decomposers of organic matter and play an active role in biogeochemical cycles, thereby contributing to carbon sequestration in forest ecosystems. Floodplain forests (várzeas) are characterized by the dynamics of rising and receding waters, which are rich in suspended material and influence species variation and adaptation. The knowledge about the distribution of macrofungi in várzea environments in the Brazilian Amazon is limited. This study aims to evaluate the diversity and composition of macrofungi on three várzea forest islands, while also examining differences in species richness and abundance between seasonal periods. A total of 88 macrofungal species that belong to the phylum Basidiomycota were identified. The findings revealed significant variations in species composition, yet no notable differences in species richness or abundance were observed between the seasonal periods. The environmental conditions and resources available to macrofungi appear to be consistent among the islands, which leads to a balanced diversity. However, additional research is essential to uncover the true distribution patterns of macrofungi in the várzeas of the Brazilian Amazon, an area under significant threat to its biodiversity.

Keywords: amazonian ecosystems; conservation; seasonal dynamics; wood-decay fungal communities

1. Introduction

The Amazon is represented by different ecosystems that are characterized according to the type of predominant vegetation and the influence of seasonal regimes of rivers. In addition to ombrophilous forests, igapó and floodplain forests show a peculiarity: they are constantly fertilized by the rising and falling waters of the rivers, which determines the

variation and adaptation of the species present [1]. Just as the level of the rivers interferes with the dynamics of organisms, the composition of their waters also plays an important role in the contribution of organic matter. While blackwater rivers, common in the igapó areas, have low levels of sediment and nutrients, whitewater rivers, rich in suspended material, fertilize the floodplain areas, which constitute the second largest plant formation in the Amazon [2–4].

Floodplain forests are ecosystems that store a large amount of carbon in the soil and actively participate in river dynamics and regulating biogeochemical cycles, thus making them a unique habitat for adapted species of animals, plants, and fungi [4]. Some species are strongly adapted and have a preference for certain flooded habitats and, in view of this, their unique ecological functions can be sensitive to climate and environmental changes [5]. Studies show that some species either tolerate or are resistant to disturbances such as severe floods or droughts, while others may be impacted or even lost [6,7].

In addition, due to the seasonal flow of rich nutrients from the sediments, the substrates of floodplain areas are highly fertile and become widely used by local communities in the Amazon in the cultivation, mainly of açaí palms (*Euterpe oleraceae* Mart.), cassava (*Manihot esculenta* Crantz), and cocoa (*Theobroma cacao* L.) [8]. Due to this dynamic ecosystem, these floodplain forests are subject to anthropogenic impacts caused by both agriculture and logging, which can cause losses in floodplain biodiversity [9]. Therefore, the floodplain is a naturally sensitive region, both in relation to temperature variations and rainfall levels and to human-induced impacts [10,11].

Macrofungi are members of the phyla Ascomycota and Basidiomycota and are part of the community of organisms present in floodplain ecosystems. The vast majority of these macrofungi belong to the class Agaricomycetes (Basidiomycota) and are known as mushrooms and wood ears (due to the characteristic shape of their basidiomes). The species can be parasitic, symbiotic, and/or saprophytic and are among nature's main decomposers of organic matter [12]. Among the parasitic species, *Moniliophthora perniciosa* (Stahel) Aime and Phillips-Mora has a wide spectrum of hosts, including plants of economic importance such as cocoa, which causes serious economic and social impacts in areas that include floodplain plantations in the Amazon [13]. On the other hand, ectomycorrhizas establish symbiotic associations with plant roots and are essential for growth, protection, and tolerance in contaminated soils [14,15].

However, the vast majority of species act as saprophytes and actively participate in the cycling of elements. The conversion of the substrate and consequent release of carbon and nitrogen to the environment occurs in different ways, depending on the enzymatic arsenal of the fungus. In this way, organisms can be classified into different categories; for example, those that cause white rot are able to degrade lignin, cellulose, and hemicellulose, the three main polymers of wood. The species that cause brown rot, on the other hand, degrade only cellulose and hemicellulose, and those that cause soft rot secrete cellulase enzymes that cause a characteristic pattern of decomposition [16].

In addition to playing a fundamental ecological role in nature, research has shown that macrofungi, as well as plants, also present a wide variety of bioactive compounds with some type of action and/or health benefit. In fact, the demand for macrofungi has been increasing globally among consumers due to their outstanding taste and nutritional capacity as a result of the presence of polysaccharides, vitamins, flavones, and unsaturated fatty acids. In turn, the therapeutic capacities are associated with the immunomodulatory, antimicrobial, and antioxidant abilities of these bioactive substances, which have an important effect in the fight against cancer, diabetes, obesity, and hypertension, for example [17]. Depending on how they act in the ecosystem, biotic and abiotic factors

exert selective pressures that interfere with the frequency and distribution of species. As important as temperature, seasonal variations in river levels and the contribution of organic matter, and the construction of housing and land use by riverine populations (mainly in monocultures) demand even more from the adaptive processes of fungi in the floodplain environment. Most studies in floodplain forests are related to floristic inventories, diversity, and composition [18–21], as well as effects of the flood pulse and soil organic matter on vegetation [22,23]. However, knowledge about macrofungi in these areas is still scarce. Since knowledge on the dynamics of the macrofungi species from the class Agaricomycetes in these flooded areas is scarce, this study aims to verify the diversity and composition of macrofungi in three floodplain forest islands, as well as the differences in richness and abundance between seasonal periods.

2. Materials and Methods

2.1. Study Area

This study was conducted in the state of Pará, in the municipality of Mocajuba, located in the mesoregion of northeastern Pará and in the microregion of Cametá (02°35′31″ S, 49°28′60″ W). The predominant ecosystems are those of terra-firme—with the islands presenting a dense alluvial ombrophilous forest type vegetation—and the floodplain areas, managed and exploited by the riverine population in the form of monocultures and for agroforestry based on cocoa plantations [24,25].

The patterns related to humidity, rainfall, and temperature in the municipality change according to the months of the year. The average temperatures range between 25 °C and 34 °C; when the temperature indices begin to increase in July, humidity and precipitation decrease, as do the water levels on the islands, determining the arrival of the dry season [26] and making it possible to access the trails on the islands (Figure 1). Three islands were selected as study areas: Tauaré, Santaninha, and Costa Santana. The selected areas are marked by native cocoa plantations and the predominance of vegetation is mainly characterized by *Hevea brasiliensis* (Willd. ex A. Juss.) Müll.Arg., *Euterpe oleracea*, *Virola surinamensis* (Rol. ex Rottb.) Warb., *Pterocarpus santalinoides* L'Hér. ex DC., and *Carapa guianensis* Aubl. (Table 1).

Table 1. Description of researched areas.

Islands/ Coordinates	Cocoa Plantation Age	Soil	Predominant Vegetation	Distance between Islands
Tauaré (02°35′56.3″ S, 49°30′46.7″ O)	15 years	Silty sand	*Hevea brasiliensis, Virola surinamensis, Pterocarpus santalinoides, Theobroma cacao, Euterpe oleracea, Carapa guianensis, Hydrochorea corymbosa, Genipa americana, Campsiandra laurifólia e Vatairea guianensis.*	8.76 km (Tauaré to Santaninha)
Santaninha (02°31′13″ S, 49°31′52″ O)	50 years	Silty sand	*Euterpe oleracea, Hevea brasiliensis, Virola surinamensis, Carapa guianensis, Pterocarpus santalinoides, Cecropia distachya, Crudia oblanga, Genipa americana, Pseudobombax munguba e Mauritia flexuosa.*	6.46 km (Santaninha to Costa Santana)
Costa Santana (02°34′37.2″ S, 49°32′20.1″ O)	50 years	Silty clay	*Theobroma cacao, Euterpe oleracea, Hevea brasiliensis, Virola surinamensis, Carapa guianensis, Pterocarpus santalinoides, Hydrochorea corymbosa, Genipa americana, Campsiandra laurifólia e Pachira aquática*	3.73 km (Costa Santana to Tauaré)

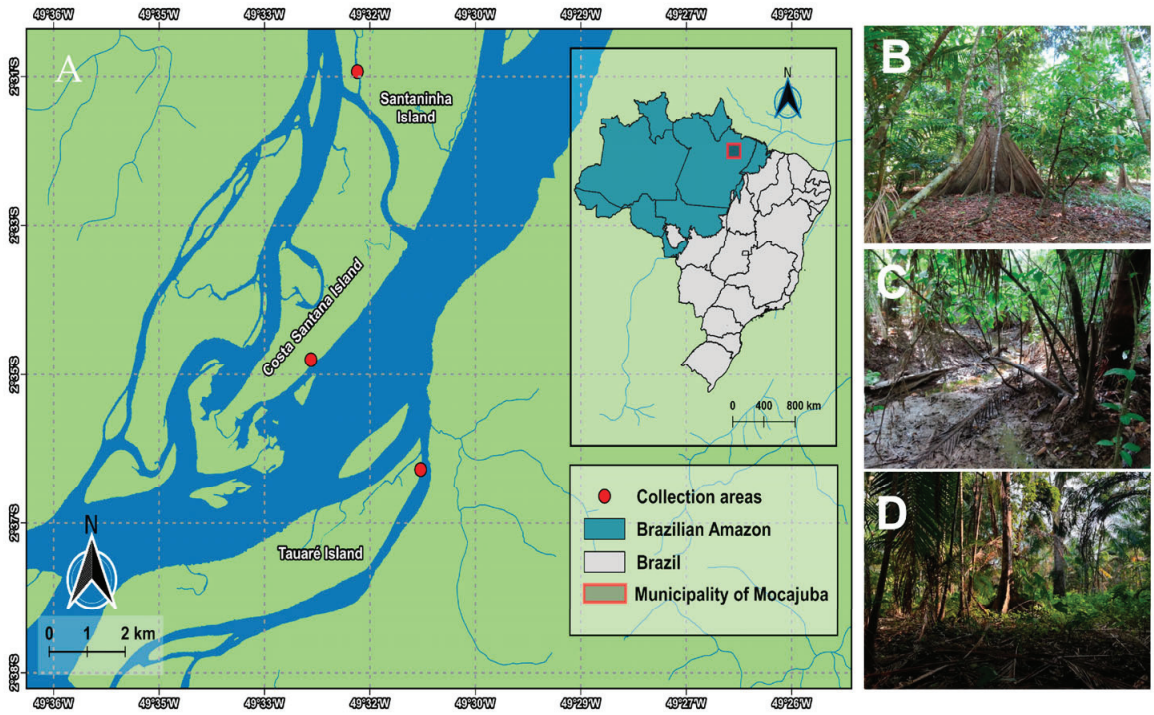


Figure 1. (**A**) Map of the studied region of the municipality of Mocajuba. (**B**) Costa Santana Island; (**C**) Santaninha Island; (**D**) Tauré Island.

2.2. Collection, Processing, and Identification

The collections were carried out in June and November of 2022 and 2023. The seasons chosen for the field trips mark the end of the rainy and dry periods, respectively, when the levels related to precipitation, humidity, and temperature vary significantly. In the selected floodplain areas, plots of two hectares were demarcated with the help of GPS, which could be covered in a period of two hours. The stages of collection, preservation, and herborization were based on the methodology of Fidalgo and Bononi [27] and Neves et al. [28]. Photographic records of the specimens were made, as well as the description of the substrate and notes on the main characteristics of the basidiomes (size, color, and consistency). The specimens were dehydrated in an electric oven.

Microscopic analyses were performed from freehand sections of the hymenial surface, the context, and the abhymenial surface with the help of steel blades. The fragments were placed on a slide with an aqueous solution of 3–5% potassium hydroxide and 1% phloxin. For cyanophilic observations, Amann's Blue was used, which stains the walls of hyphae, basidiospores, and cystidia blue. Melzer's reagent was used in the observation of amyloid (grayish, bluish, or purplish) or dextrinoid (reddish-brown) reactions of the walls of the basidiospores, hyphae, and other microstructures. The observation of the hyphalic system, shape, and size of fertile and sterile followed Teixeira [29]. The slides were observed under an optical microscope for the analysis and measurement of microscopic structures. For the identification, the works of Ryvarden [30–34], Zabin et al. [35], and Gomes-Silva et al. [36] and the specific literature for each taxonomic group were used.

2.3. Statistical Analysis

Species diversity was verified by means of relative frequency measurements between the different floodplain areas selected in this study, in addition to the estimation of richness indices. For the diversity analysis, the Shannon–Wiener index (represented by *H'*) was chosen, which was calculated based on the number of individuals of each species and

the total number of specimens sampled. The higher the Shannon–Wiener index, the greater the diversity of the sample [37]. The relative frequency of the species was based on the number of specimens and determined by the following equation, $F = n/N \times 100$, where n is the number of specimens of a species and N is the total number of individuals found [38]. The following frequency classes were considered regarding the occurrence of the species: $0.5 < F \leq 1.5\%$ = rare; $1.5 < F \leq 5\%$ = occasional; $5 < F \leq 10\%$ = frequent; $F > 10\%$ = abundant; while relative abundance used the equation [number of individuals of a species ($N_{specimens}$)/total number of individuals on the island (N_{total}) times 100] [39].

$$\text{Relative Abundance}(\%) = \frac{N_{\{specimens\}}}{N_{\{total\}}} \times 100$$

Analyses involving species richness and composition between islands were based on the Jaccard index, which measures similarity between finite sample sets through the relationship between the intersection and the size of the union of these same sets. The hypothesis of heterogeneity between the three islands was investigated with the aid of PERMDISP (permutational analysis of multivariate dispersions) and PERMANOVA (permutational multivariate analysis of variance) tests. In addition, the species accumulation curve demonstrated the relationship between sampling effort and observed richness, while the bootstrap method was used to calculate the estimates of richness accompanied by a confidence interval, thus increasing the reliability of the results. All the statistical analyses were performed in R 3.5.2 [40].

To verify the influence of seasonality (dry and rainy periods) on the abundance of macrofungi (n = 88) on the three islands, we used the analysis of variance (ANOVA). This method was selected for its effectiveness in comparing means between groups and identifying possible significant differences related to seasonal conditions. To complement the analysis, the Tukey post hoc and Fisher tests were applied, which allowed for us to detail the differences between the groups, providing different levels of confidence in the results. The box plot graphs were generated using MINITAB software version 14.13 (OSB Software, Bela Vista, SP, Brazil).

3. Results

3.1. Macrofungal Diversity, Richness and Composition Among the Islands

In all, 223 specimens of fungi were identified, representing 88 species belonging to 18 families from the class Agaricomycetes, of the phylum Basidiomycota (Figure 2; Table 2). The order Polyporales presented eleven families, while Agaricales and Hymenochaetales presented three families each, and Russulalles only one. Of the 17 families of Agaricomycetes identified in morphological analyses, Polyporaceae had the highest number of species collected in the floodplain islands (38), followed by Meripilaceae and Hymenochaetaceae with 12 and 8, respectively. Regarding the genera, *Rigidoporus*, *Lentinus*, and *Trametes* were the most diverse, with 12, 10, and 9 species, respectively, while 24 genera presented only a single species. When the absolute number of species and specimens was compared among the islands, Costa Santana presented the highest number of identified species (50) and the highest number of specimens collected (90). Santaninha island occupied the second place, with 37 species and 66 specimens, which was closely followed by Tauaré, with 36 species and 67 specimens.



Figure 2. Macrofungi from the flood forests studied in Brazilian Amazon: (**A**) *Ganoderma stipitatum*, (**B**) *Trametes elegans*, (**C**) *Rigidoporus ulmarium*, (**D**) *Earliella scabrosa*, (**E**) *Flaviporus liebmannii*, (**F**) *Cerrena caperata*, (**G**) *Foraminispora rugosa*, (**H**) *Amauroderma exile*, (**I**) *Lentinus swartzii*, (**J**) *Lentinus* sp., (**K**) *Lentinus concavus*, (**L**) *Favolus trigonus*, (**M**) *Favolus tenuiculus*, (**N**) *Pleurotus djamor*, (**O**) *Truncospora tephropora*.

Table 2. List of species collected in Mocajuba. Quantity of specimens and the relative abundance (%) based on the number of specimens. Relative frequency [%] classified as follows: R = rare, O = occasional, F = frequent, and A = abundant.

Order/Family/Species	Sampled Islands			Frequency
Agaricales Underw	**Santaninha**	**Tauaré**	**Costa Santana**	
Omphalotaceae Bresinsky	**Specimens and Relative Abundance**			
Lentinula raphanica (Murrill) Mata and R.H. Petersen	-	2 (2.99)	2 (2.22)	O
Pleurotaceae Kühner				
Pleurotus djamor (Rumph. ex Fr.) Boedijn	-	-	1 (1.11)	R
Schizophyllaceae Quél.				
Schizophyllum commune Fr.	-	1 (1.49)	-	R
Hymenochaetales Oberw.				
Hirschioporaceae Y.C. Dai, Yuan Yuan, and Meng Zhou				
Nigrohirschioporus sector (Ehrenb.) Y. C. Dai, Yuan Yuan, and Meng Zhou	-	1 (1.49)	-	R
Hymenochaetaceae Donk				
Fomitiporia murrillii Alves-Silva, R.M. Silveira, and Drechsler-Santos	1 (1.52)	-	-	R
Fomitiporia conyana Alves-Silva and Drechsler-Santos	1 (1.52)	-	-	R
Fomitiporia subtilissima Alves-Silva, Reck, and Drechsler-Santos	-	1 (1.49)	-	R
Fulvifomes kawakamii (M.J. Larsen, Lombard, and Hodges) T. Wagner and M. Fisch.	1 (1.52)	-	-	R
Fuscoporia licnoides (Mont.) Oliveira-Filho and Gibertoni	-	1 (1.49)	1 (1.11)	R
Fuscoporia scruposa (Fr.) Gibertoni and Oliveira-Filho	1 (1.52)	-	-	R
Hymenochaete sp.	1 (1.52)	-	-	R
Tropicoporus extensus (Lév.) Y.C. Dai and F. Wu	1 (1.52)	-	-	R
Schizoporaceae Jülich				
Xylodon flaviporus (Berk. and M.A. Curtis ex Cooke) Riebesehl and Langer	-	1 (1.49)	-	R
Polyporales Gäum.				
Cerrenaceae Miettinen, Justo, and Hibbett				
Cerrena caperata (Berk.) Zmitr.	-	-	1 (1.11)	R
Cerrena hydnoides (Sw.) Zmitr.	-	1 (1.49)	4 (4.44)	O
Fomitopsidaceae Jülich				
Antrodia albida (Fr.) Donk	-	-	1 (1.11)	R
Fomitopsis nivosa (Berk.) Gilb. and Ryvarden	-	2 (2.99)	-	R
Fomitopsis roseoalba A.M.S. Soares, Ryvarden, and Gibertoni	-	-	2 (2.22)	R
Fomitopsis sp.	-	1 (1.49)	-	R
Ganodermataceae Donk				
Amauroderma exile (Berk.) Torrend	-	-	2 (2.22)	R
Ganoderma australe (Fr.) Pat.	-	1 (1.49)	1 (1.11)	R
Ganoderma stipitatum (Murrill) Murrill	-	-	1 (1.11)	R
Irpicaceae Spirin and Zmitr.				
Ceriporia sp.	-	-	1 (1.11)	R
Laetiporaceae Jülich				
Berkcurtia persicina (Berk. and M.A. Curtis) Robledo and Campi	-	1 (1.49)	-	R
Meripilaceae Jülich				
Rigidoporus crocatus (Pat.) Ryvarden	-	1 (1.49)	1 (1.11)	R
Rigidoporus lineatus (Pers.) Ryvarden	8 (12.1)	-	4 (4.44)	F
Rigidoporus mariae Gibertoni, Gomes-Silva and Ryvarden	1(1.52)	-	-	R
Rigidoporus microporus (Sw.) Overeem	-	2 (2.99)	1 (1.11)	R

Table 2. *Cont.*

Order/Family/Species	Sampled Islands			Frequency
Rigidoporus ulmarius (Sowerby) Imazeki	-	-	3 (3.33)	R
Rigidoporus undatus (Pers.) Donk	1 (1.52)	-	1 (1.11)	R
Rigidoporus vinctus (Berk.) Ryvarden	2 (3.03)	1 (1.49)	1 (1.11)	O
Rigidoporus sp. 1	-	-	1 (1.11)	R
Rigidoporus sp. 2	-	-	1 (1.11)	R
Rigidoporus sp. 3	-	-	1 (1.11)	R
Rigidoporus sp. 4	-	-	1 (1.11)	R
Rigidoporus sp. 5	-	-	1 (1.11)	R
Panaceae Miettinen, Justo, and Hibbett				
Cymatoderma caperatum (Berk. and Mont.) D.A. Reid	2 (3.03)	-	2 (2.22)	O
Panus aff. fasciatus (Berk.) Singer	-	1 (1.49)	-	R
Panus neostrigosus Drechsler-Santos and Wartchow	-	2 (2.99)	-	R
Panus strigellus (Berk.) Chardón and Toro	-	-	1 (1.11)	R
Phanerochaetaceae Jülich				
Antrodiella angulatopora Ryvarden	-	-	1 (1.11)	R
Podoscyphaceae D.A. Reid				
Podoscypha aculeata (Berk. and M.A. Curtis) Boidin	-	7(10.4)	1 (1.11)	O
Podoscypha bubalina D.A. Reid	-	1 (1.49)	1 (1.11)	R
Polyporaceae Fr. ex Corda				
Cubamyces lactineus (Berk.) Lücking	1 (1.52)	-	2 (2.22)	R
Cubamyces menziesii (Berk.) Lücking	-	2 (2.99)	-	R
Cyanoporus fuligo (Berk. and Broome) Y.C. Dai, W.L. Mao, and Yuan Yuan	-	1 (1.49)	-	R
Earliella scabrosa (Pers.) Gilb. and Ryvarden	1 (1.52)	10 (14.9)	12 (13.3)	A
Fabisporus sanguineus (L.) Zmitr	-	-	1 (1.11)	R
Favolus trigonus Lloyd	1 (1.52)	-	1 (1.11)	R
Favolus tenuiculus P. Beauv.	1 (1.52)	-	1 (1.11)	R
Favolus pseudoprinceps (Murrill) Sacc. and Trotter	-	1 (1.49)	-	R
Fomes fasciatus (Sw.) Cooke	2 (3.03)	-	-	R
Foraminispora rugosa (Berk.) Costa-Rez., Drechsler-Santos, and Robledo	-	1 (1.49)	-	R
Grammothele lineata Berk. and M.A. Curtis	1 (1.52)	-	-	R
Lentinus atrobrunneus Pegler	1 (1.52)	-	-	R
Lentinus berteroi (Fr.) Fr.	4 (6.06)	7 (10.4)	1 (1.11)	F
Lentinus concavus (Berk.) Corner	2 (3.03)	-	-	R
Lentinus crinitus (L.) Fr.	2 (3.03)	4 (5.97)	3 (3.33)	O
Lentinus nigro-osseus Pilát	1 (1.52)	-	1 (1.11)	R
Lentinus scleropus (Pers.) Fr.	1 (1.52)	-	-	R
Lentinus sp.1	-	1 (1.49)	-	R
Lentinus sp.2	1 (1.52)	-	-	R
Lentinus swartzii Berk.	1 (1.52)	1 (1.49)	-	R
Lentinus tricholoma (Mont.) Zmitr.	2 (3.03)	1 (1.49)	1 (1.11)	O
Megasporia sp.	1 (1.52)	-	-	R
Megasporia cavernulosa (Berk.) C.R.S. Lira and T.B. Gibertoni	-	1 (1.49)	-	R
Microporellus dealbatus (Berk. and M.A. Curtis) Murrill	-	1 (1.49)	-	R
Perenniporia martia (Berk.) Ryvarden	-	-	1 (1.11)	R
Perenniporia minutopora Ryvarden and Decock	-	-	1 (1.11)	R
Polyporus guianensis Mont.	4 (6.06)	-	1 (1.11)	O
Polyporus leprieurii Mont.	1 (1.52)	-	-	R
Porogramme subargentea (Speg.) Y.C. Dai, W.L. Mao, and Yuan Yuan	1 (1.52)	-	1 (1.11)	R
Tinctoporellus isabellinus Ryvarden and Iturriaga	1 (1.52)	-	3 (3.33)	O
Trametes cotonea (Pat. and Har.) Ryvarden	1 (1.52)	-	-	R

Table 2. *Cont.*

Order/Family/Species	Sampled Islands			Frequency
Trametes elegans (Spreng.) Fr.	9 (13.6)	1 (1.49)	9 (10)	F
Trametes maxima (Mont.) A. David and Rajchenb	2 (3.03)	1 (1.49)	5 (5.56)	O
Trametes membranacea (Sw.) Kreisel	-	-	1 (1.11)	R
Trametes pavonia (Hook.) Ryvarden	-	-	1 (1.11)	R
Trametes supermodesta Ryvarden and Iturr.	-	1 (1.49)	-	R
Truncospora tephropora (Mont.) Zmitr.	-	1 (1.49)	-	R
Steccherinaceae Parmasto				
Flaviporus liebmannii (Fr.) Ginns	-	2 (2.99)	-	R
Junghuhnia chlamydospora Ryvarden	-	-	1 (1.11)	R
Nigroporus rigidus Ryvarden	2 (3.03)	-	-	R
Steccherinum meridionale (Rajchenb.) Westph., Tomšovský, and Rajchenb.	-	-	1 (1.11)	R
Russulales Kreisel ex P.M. Kirk, P.F. Cannon, and J.C. David				
Echinodontiaceae Donk				
Larssoniporia tropicalis (Cooke) Y.C. Dai, Jia J. Chen, and B.K. Cui	1(1.52)	-	-	R
Incertae sedis				
Trichaptum byssogenum (Jungh.) Ryvarden	-	2 (2.99)	1 (1.11)	R
Trichaptum deviatum Ryvarden	-	-	1 (1.11)	R
Trichaptum griseofuscum (Mont.) Ryvarden and Iturr	1(1.52)	-	1 (1.11)	R

Trametes elegans (Spreng.) Fr. (19 specimens) and *Lentinus berteroi* (Fr.) Fr. *Rigidoporus lineatus* (Pers.) *Ryvarden* (12 specimens) were considered to be frequent, while *Earliella scabrosa* (Pers.) Gilb. and Ryvarden was noted as being abundant (23 specimens). Each island analyzed in isolation showed at least one of these macrofungi in its list of abundant species.

Earliella scabrosa (12 specimens) was the most abundant species, while *Trametes elegans* (9 specimens) and *Trametes maxima* (Mont. A. David and Rajchenb (5 specimens) were the most frequent species in Costa Santana according to frequency classes. *Rigidoporus lineatus*, unlike on the other two islands, was one of the most representative species in Santaninha (with 8 specimens), with *Trametes elegans* (9) and *Polyporus guianensis* Mont. (4 specimens) occupying second place. As in Costa Santana, the most abundant species in Tauaré was *Earliella scabrosa* (10), followed by *Podoscypha aculeata* (Berk. and M. A. Curtis) Boidin (7) and *Lentinus berteroi* (7) (Table 2).

Analysis of the totality of the data provided a Shannon–Wiener index equivalent to 3.91 for the three islands. As evidenced by the absolute number of species and specimens collected, Costa Santana presented the greatest diversity among the three islands (3.54) (indicated by the respective Shannon–Wiener index), followed by Santaninha (3.30) and Tauaré (2.99).

According to the composition of the species recorded on the islands, 23 were exclusively observed in Costa Santana, 18 in Santaninha, and 19 species in Tauaré. In turn, the three islands share seven species between them. The number of species shared between Costa Santana/Santaninha was equal to 11 and Costa Santana/Tauaré was equal to 9. Interestingly, Santaninha presented only one species associated with Tauaré, but shared nine of them with Costa Santana (Figure 3).

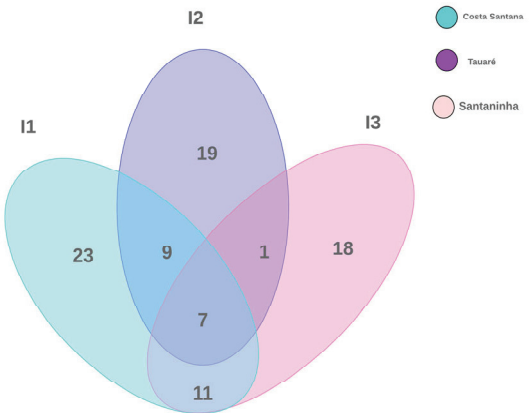


Figure 3. Venn diagram showing the total number of macrofungal species in floodplain forests investigated on three islands in the Brazilian Amazon.

Regarding species composition, the PERMANOVA showed a significant difference in fungal species composition among the islands ($F = 5.678$, $p = 0.045$). With a value of $p < 0.05$, we can infer that the mean composition of fungal species varies statistically among the islands, indicating that each island has a distinct set of species, which suggests specific ecological or environmental factors may be shaping these communities differently. The total variation in species composition ($R^2 = 0.45$) indicates that approximately 45% can be explained by the differences among the islands.

In contrast, the PERMDISP indicates that the dispersion of species compositions relative to their centroids (the mean or central point of species composition for each island) does not differ significantly between islands ($F = 1.234$, $p = 0.561$). This result suggests that although the islands have distinct mean species compositions, the variability or heterogeneity within each island (i.e., how species are distributed relative to the center of their mean composition) is similar. The dispersion of species compositions on each island is homogeneous.

The PCoA graph (Figure 4) illustrates these results visually. The dots represent individual samples, grouped by island, with different colors. The shaded areas reflect the dispersal of species compositions on each island. The separation of the groups indicates differences in the mean composition between the islands (confirmed by PERMANOVA), while the similar size and shape of the shaded areas suggest that the internal dispersion of the species within each island is homogeneous (corroborated by PERMDISP).

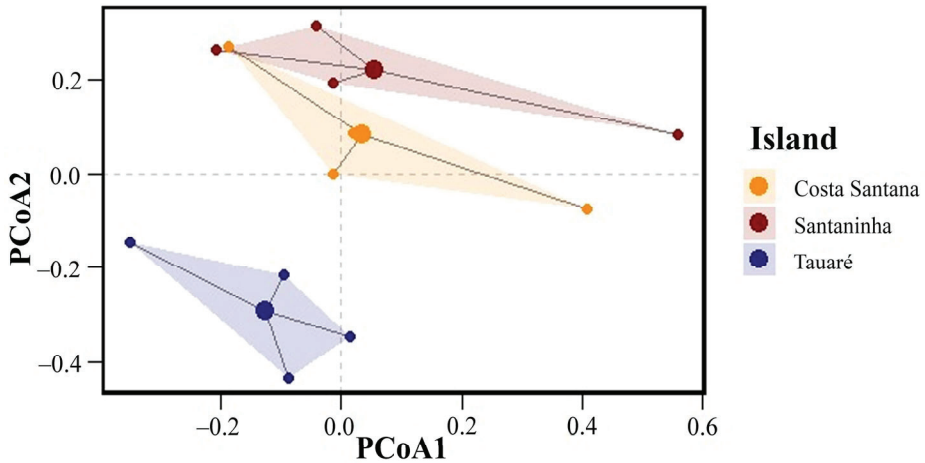


Figure 4. Principal coordinate analyses (PCoAs) of macrofungi composition on the three islands.

Regarding species richness, the rarefaction curve, obtained by the method of the collector, revealed that the estimated species richness increased rapidly at the beginning and later stabilized around 80 species after the collection of 10 samples. Bootstrap analysis complemented this assessment by providing robust estimates of richness, averaging approximately 83.46 species. The 95% confidence interval for the bootstrap richness estimate ranged from approximately 75.04 to 90.76 species, confirming the accuracy and robustness of the estimates and indicating a reliable species richness within this range of variation.

Combined analysis of the three islands over the twelve collections reveals an accumulation curve that indicates a rapid initial increase in species richness as more samples are collected. However, as sampling progresses, the curve shows signs of stabilization, suggesting that most of the species present on the three islands were identified during the collection period. This accumulation dynamic provides valuable information about biological diversity on the islands, demonstrating that the discovery of new species tends to decline as sampling progresses (Figure 5).

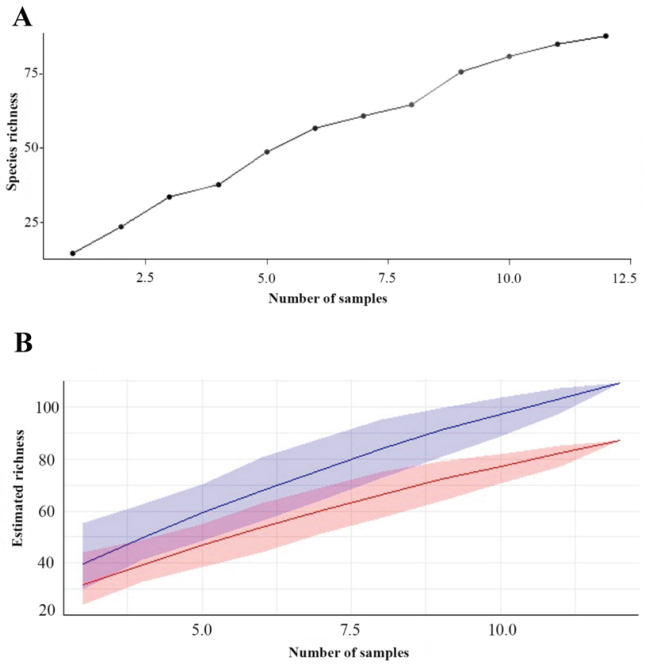


Figure 5. Dynamic accumulation: (**A**) Species accumulation curve in the three islands of floodplain forest. (**B**) Bootstrap chart. The red line represents the richness estimate calculated using bootstrap, while the blue line represents the observed or estimated richness directly from the data. The shaded area indicates the confidence interval.

3.2. Seasonal Diversity on the Three Islands

In relation to the differences between the dry and rainy periods, 41 species were recorded in the rainy period, 25 in the dry period, and 22 in both. In the rainy season, the highest number of species was recorded on Costa Santana with 34 species, and both Tauaré and Santaninha presented 25 species each. In the dry period, the largest number of species was recorded on Costa Santana (32 species), while Tauaré presented 22 and Santaninha 18 species.

There was no significant difference between the rainy season (June 2022 and 2023) and dry season (November 2022 and 2023) in relation to species richness ($F = 1.032$; $p = 0.367$). Although the means indicate that wealth is higher in the rainy season (mean = 27.7, standard deviation (SD) = 5.69) compared to the dry season (mean = 23.0, standard devia-

tion (SD) = 5.57), the ANOVA indicated that this difference is not statistically significant (Figure 6).

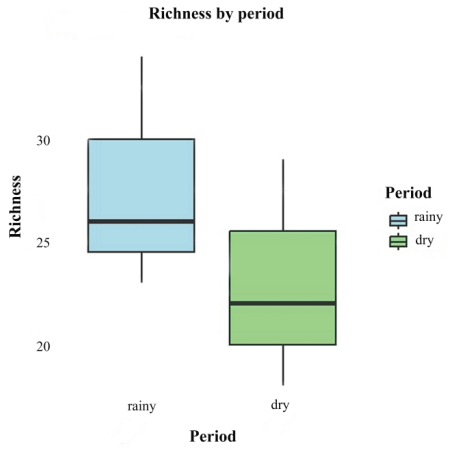


Figure 6. Box plots comparing the richness of fungi in different periods (rainy and dry).

An ANOVA was also applied to evaluate species abundance (n = 88) in relation to seasonality and there were no significant differences in the quantity of specimens of macrofungi on the islands ($p < 0.001$) (Figure 7). Nonetheless, the abundance is noticeable within each group reported via the outliers.

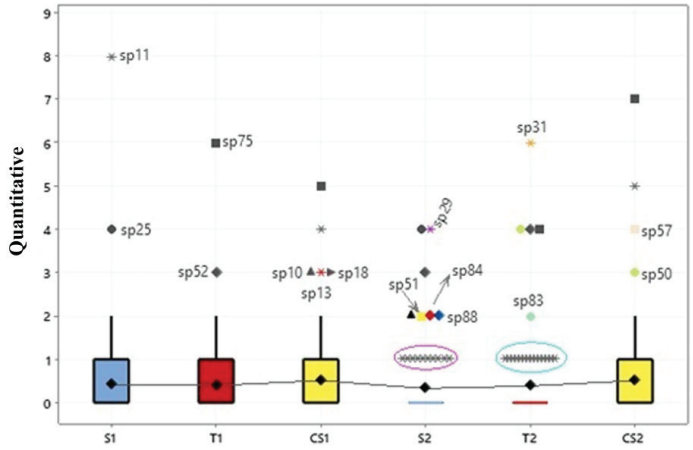


Figure 7. Box plots comparing the abundance of fungi on the three floodplain islands, in relation to seasonality. S = Santaninha; T = Tauaré; CS = Costa Santana; 1 = rainy season; 2 = dry season. Symbols represent the species, for example: * sp11= *Rigidoporus lineatus*.

In Figure 7, the outliers detected in the model demonstrated the most abundant groups of macrofungi in the different seasons. In the rainy season, on Santaninha island (S1), there was the highest occurrence of the species *Trametes elegans* (sp. 25) with eight specimens and *Rigidoporus lineatus* (sp. 11) with four specimens. On the island of Tauaré (T1), the species *Earliella scabrosa* (sp. 75) and *Lentinus berteroi* (sp. 52) were the most abundant, with seven and three specimens, respectively. Finally, on the island of Costa Santana (CS1), in addition to *E. scabrosa* (five specimens) and *T. elegans* (four specimens), already recorded in S1 and T1, *Trametes maxima* (sp. 10), *Tinctoporellus isabellinus* (sp. 13), and *R. ulmarius* (sp. 18) were also the most common.

In contrast, in the dry season, the variability of these macrofungi was intensified. In Santaninha (S2), there was an increase in *Polyporus guianensis* (sp.29), *L. berteroi*, *L. concavus*

(sp. 51), *T. maxima*, *Cymatoderma caperatum* (sp. 84), and *Fomes fasciatus* (sp. 88). On the island of Tauaré (T2), the most predominant macrofungi were the species *Podoscypha aculeata* (sp. 31), *L. crinitus* (sp. 50), *L. berteroi*, *E. scabrosa*, and *Lentinula raphanica* (sp. 83). On Costa Santana (CS2), the most frequent were *E. scabrosa*, *T. elegans*, *Cerrena hydnoides* (sp. 50), and *L. crinitus*.

The results of the Tukey and Fisher tests indicate a homogeneous distribution of these organisms, with certain highlights. This implies that the environmental conditions and resources available to macrofungi are similar among the islands and this reflects a balanced diversity.

4. Discussion

4.1. Composition and Richness Among the Islands

Geographical and edaphic attributes may explain the difference found in the diversity indices of the islands. The soil of Costa Santana presents high fertility in all its layers, which is fundamental for the development of plant species [41]. It has been a managed area for more than 50 years and is formed by native palms and tree species such as rubber trees, açaí palms, cocoa, and andiroba (*Carapa guianensis* Aubl.) trees and was the only one that presented the samaúma species [*Ceiba pentandra* (L.) Gaertn.—Malvaceae], a plant that is native to the Amazon. On the other hand, unlike Costa Santana, there are streams along the plantations of the Tauaré and Santaninha, characterizing a typically alluvial forest. In addition to the action of the water in the high-water period, it probably ends up selecting the plant and fungal species most adapted to the seasonal variations of the ecosystem. In fact, the specialization assumed by organisms along the floodplains causes the richness and diversity to be lower compared to the dry-land ecosystem [11,42].

In fact, the value related to species richness of macrofungi in the floodplain islands of this study was lower compared to that presented in regions of dry land in the Brazilian Amazon. Collections carried out in the Caxiuanã National Forest, located in the northwest of the state of Pará, showed indices of up to 130 species of Agaricomycetes against 88 on the floodplain islands [43,44]. Significant numbers of species were also found in Serra do Navio (100), and in Amapá National Forest (97), in the state of Amapá [45,46], as well as in a fragment of dense ombrophilous forest in the surroundings of HPP Silvio Braga, located in western Pará (91 species) [47]. However, a standardized comparative study is needed to confirm this hypothesis.

López-Quintero et al. [48] analyzed the diversity of macrofungi in two areas of the Colombian Amazon, one area being terra-firme and the other floodplains. The exclusive richness in each area was similar (n = 128), but the abundance was higher in the floodplain areas (804 sporocarps) than on dry land (741 sporocarps). The authors attributed this result to the nutrient-rich alluvial soils of the floodplains, which are due to the regular deposition of detritus in floodplain areas, and nutrients and organic matter during high/rising water, which occur on average twice a year. The authors stated that, despite the significant number of species, the rarefaction curve did not reach the asymptote, i.e., it did not saturate. This is different from the results found in this study, in which the accumulation curve stabilized from 80 species onwards.

Even if decomposing organisms are favored by organic matter and woody residues brought by river waters, it is necessary to check the richness in an area of floodplain primary forest for a more accurate assessment. Amazonian studies involving fungi associated with the floodplain ecosystem in the Brazilian Amazon, in addition to conidial microfungi [49], are scarce, especially when they report the richness and diversity of macrofungi. The data collected in this study are pioneering and fundamental for the increase in knowledge and

understanding of the diversity of Agaricomycetes in floodplain forest areas, where the lack of studies involving the taxonomy of macroscopic fungi does not reflect the ecological importance of this ecosystem.

4.2. Seasonal Diversity

Since the field trips took place in two different periods of the year, climatological aspects probably interfered with the numbers of specimens observed in the floodplain ecosystem. In June 2022, 70 specimens of macrofungi of the class Agaricomycetes were collected, a value 25% higher when compared to November of the same year, which totaled 56. Traditionally, June presents a higher index of precipitation and humidity in the northern region in contrast to the month of November (174.4 mm/78.9%) [26]. Although there are differences in absolute numbers, statistically, this difference was not significant, as demonstrated in the ANOVA. This is different from the findings of Putra et al. [50], who evaluated the seasonal distribution of macrofungi in three forest communities in Indonesia and found significant differences. For example, of the 130 species recorded by the authors, 81 occurred in the rainy season, 25 in the dry season, and 22 in both periods. In this study, the species that were common in both periods were mainly from the Polyporaceae family (*E. scabrosa*, *L. berteroi*, *T. elegans*). Such species have a leathery and resistant basidiome and are often observed on decaying wood in open areas and/or those with intense sunlight.

Despite this, factors unrelated to climate have the potential to alter the richness and diversity of organisms in a given area. In June 2023, there was a decrease of approximately 49% in the number of specimens compared to the same period of the previous year, with 47 individuals collected. The Tauaré islands suffered the impact of the felling of its native vegetation and removal of woody material in the clearing of the land, thus reducing the supply of substrate for the growth of macrofungi. Combined with abiotic aspects, the availability of organic matter is in a relationship that is directly proportional to the number of fungi observed in the ecosystem. In other words, the greater the quantity and quality of the substrate, the greater the quantity and diversity of the fungal community [51].

Rustøen et al. [52] investigated the affinity of wood decomposing fungi in relation to the substrate of angiosperms and conifers in the United Kingdom and the effects of climate on a 40-year time scale to ascertain whether there would be compositional changes related to temporal changes and identified that the composition of wood fungi was mainly structured by the properties of the substrate, and that climatic effects were the least significant.

Although the values obtained in the diversity and richness analyses were practically the same for the three islands of Mocajuba, Costa Santana showed itself to have the highest indices, followed by Santaninha and Tauaré.

4.3. Future Research Directions

Floodplain forests are huge, and seasonal flood regimes, those that reach the maximum level in the wettest months, such as those that occur in the Tocantins River, limit research in these areas [53]. Although the research was not carried out in a primary floodplain area, it was carried out in an agroforestry system, which is an economic model of sustainability for preserving tree species [54]. Such preserved tree species provide ecological conditions for the maintenance of macrofungal species and, since they play a fundamental role in nutrient cycling, it is important to understand and identify diversity for the conservation and management of species for ecosystem health.

Li et al. [55] compared the diversity of macrofungi in native forests and managed plantation areas in China and noticed that the diversity was significantly higher in native forests. However, the composition of the fungal community was different between the areas. The

authors point out that although diversity was the highest in native forests, the two management systems harbor distinct groups of macrofungi, suggesting that the two management methods together could provide a complementary range of macrofungi habitats.

Nonetheless, it is still necessary to compare areas of primary forests in order to discover the real distribution patterns of the species. This is a challenge in floodplain areas since they are forests that suffer from many types of anthropogenic pressures, by logging, livestock rearing and agriculture involving plants of economic interest, both for human survival and for commercialization [56]. In addition, few areas are under environmental protection, which makes it difficult to separate the effects of the impacts on populations of species.

5. Conclusions

Amazonian floodplain forests are rich and unique ecosystems, but they remain poorly explored regarding macrofungal diversity. Costa Santana island exhibited the highest diversity, likely associated with edaphic factors. In this study, significant differences in species composition were observed among the islands. However, no significant differences were found in the richness and abundance of the macrofungal species in relation to seasonality. Nevertheless, further investigation is needed to understand the true distribution patterns of species in the Amazon, a region severely threatened by loss of biodiversity.

Author Contributions: Conceptualization, V.P.F., M.d.P.S.P.V., A.W.G.-V., R.B.M.-F. and A.M.d.S.S.; methodology—formal analysis, R.D.P. and B.S.F.d.S.; data curation and review, A.W.G.-V., R.B.M.-F. and A.M.d.S.S.; funding acquisition, M.d.P.S.P.V.; writing—original draft preparation, V.P.F.; writing—review and editing, A.M.d.S.S. All authors have read and agreed to the published version of the manuscript.

Funding: This work was supported by "Fundação Amazônia de Amparo a Estudos e Pesquisas, grant number FAPESPA, No. 016/2021" and Coordination for the Improvement of Higher Education Personnel—Brazil (CAPES)—finance Code 001.

Institutional Review Board Statement: Not applicable.

Informed Consent Statement: Not applicable.

Data Availability Statement: The original contributions presented in this study are included in the article. Further inquiries can be directed to the corresponding author.

Acknowledgments: The authors thank the Museu Paraense Emílio Goeldi (MPEG), Universidade Federal Rural da Amazônia (UFRA) for the support and availability of the infrastructure to carry out this research and research project "Beneficiamento primário, propriedades físicas e químicas das amêndoas de cacau nativo (*Theobroma cacao*) e sistema informativo geográfico das ilhas de várzea".

Conflicts of Interest: The authors declare no conflict of interest.

References

1. Zappi, D.C. Tipos de Vegetação da Amazônia com ênfase no Pará. In *Abelhas Sem Ferrão do Pará: A Partir das Expedições Científicas de João M. F. Camargo*; Imperatriz-Fonseca, V.L., Alves, D.A., Eds.; Instituto Tecnológico Vale: Belém, Brazil, 2020; pp. 17–31.
2. Prance, G.T. Notes on the Vegetation of Amazonia III. The Terminology of Amazonian Forest Types Subject to Inundation. *Brittonia* **1979**, *31*, 26. [CrossRef]
3. Maués, B.A.R.; Jardim, M.A.G.; Batista, F.d.J.; Medeiros, T.D.S.; Quaresma, A.C. Composição florística e estrutura do estrato inferior da Floresta de Várzea na Área de Proteção Ambiental Ilha do Combu, município de Belém, Estado do Pará. *Rev. Árvore* **2011**, *35*, 669–677. [CrossRef]
4. Wittmann, F.; Householder, J.E.; Piedade, M.T.F.; Schöngart, J.; Demarchi, L.O.; Quaresma, A.C.; Junk, W.J. A Review of the Ecological and Biogeographic Differences of Amazonian Floodplain Forests. *Water* **2022**, *14*, 3360. [CrossRef]

5. Householder, J.E.; Wittmann, F.; Schöngart, J.; Piedade, M.T.F.; Junk, W.J.; Latrubesse, E.M.; Quaresma, A.C.; Demarchi, L.O.; de S. Lobo, G.; Aguiar, D.P.P.; et al. Author Correction: One Sixth of Amazonian Tree Diversity Is Dependent on River Floodplains. *Nat. Ecol. Evol.* **2024**, *8*, 1046–1047. [CrossRef] [PubMed]
6. Guimarães, D.F.d.S.; Silva, S.C.P.; Vasconcelos, M.A.; Mendes, G.S.; Pereira, H.S. A Morte Catastrófica de Árvores Por Inundação Na Ilha Do Careiro Da Várzea-AM. *Terceira Margem Amaz.* **2019**, *5*, 13. [CrossRef]
7. Ávila, J.V.C.; Ticktin, T.; Steward, A.M.; Giehl, E.L.H.; Cantor, M.; Clement, C.R. Recovery of Local Agrobiodiversity after an Extreme Flood in Amazon Floodplains. *Biol. Conserv.* **2024**, *292*, 110536. [CrossRef]
8. Freitas, M.A.B.; Vieira, I.C.G.; Albernaz, A.L.K.M.; Magalhães, J.L.L.; Lees, A.C. Floristic Impoverishment of Amazonian Floodplain Forests Managed for Açaí Fruit Production. *For. Ecol. Manag.* **2015**, *351*, 20–27. [CrossRef]
9. Junk, W.J.; Piedade, M.T.F. An Introduction to South American Wetland Forests: Distribution, Definitions and General Characterization. In *Amazonian Floodplain Forests: Ecophysiology, Biodiversity and Sustainable Management*; Springer: Berlin/Heidelberg, Germany, 2010; p. 210.
10. Choueri, R.B.; Azevedo, J.A.R. Biodiversidade e Impacto de Grandes Empreendimentos Hidrelétricos na Bacia Tocantins-Araguaia: Uma Análise Sistêmica. *Soc. Nat.* **2017**, *29*, 439–453. [CrossRef]
11. Kowalska, N.; Šigut, L.; Stojanović, M.; Fischer, M.; Kyselova, I.; Pavelka, M. Analysis of Floodplain Forest Sensitivity to Drought. *Philos. Trans. R. Soc. B Biol. Sci.* **2020**, *375*, 20190518. [CrossRef]
12. Niego, A.G.T.; Lambert, C.; Mortimer, P.; Thongklang, N.; Rapior, S.; Grosse, M.; Schrey, H.; Charria-Girón, E.; Walker, A.; Hyde, K.D.; et al. The Contribution of Fungi to the Global Economy. *Fungal Divers.* **2023**, *121*, 95–137. [CrossRef]
13. Lisboa, D.O.; Evans, H.C.; Araújo, J.P.M.; Elias, S.G.; Barreto, R.W. *Moniliophthora perniciosa*, the Mushroom Causing Witches' Broom Disease of Cacao: Insights into Its Taxonomy, Ecology and Host Range in Brazil. *Fungal Biol.* **2020**, *124*, 983–1003. [CrossRef] [PubMed]
14. Li, Y.; Zhang, T.; Zhou, Y.; Zou, X.; Yin, Y.; Li, H.; Liu, L.; Zhang, S. Ectomycorrhizal Symbioses Increase Soil Calcium Availability and Water Use Efficiency of Quercus Acutissima Seedlings under Drought Stress. *Eur. J. For. Res.* **2021**, *140*, 1039–1048. [CrossRef]
15. Chot, E.; Reddy, M.S. Role of Ectomycorrhizal Symbiosis Behind the Host Plants Ameliorated Tolerance Against Heavy Metal Stress. *Front. Microbiol.* **2022**, *13*, 855473. [CrossRef] [PubMed]
16. Goodell, B.; Qian, Y.; Jellison, J. Fungal Decay of Wood: Soft Rot-Brown Rot-White Rot. In *ACS Symposium Series*; Schultz, T.P., Militz, H., Freeman, M.H., Goodell, B., Nicholas, D.D., Eds.; ACS Publications: Aurora, IL, USA, 2008; Volume 982, pp. 9–31. ISBN 9780841239517.
17. Mazumder, M.; Roy, S.; Sarkar, A.K. Pharmacological and Therapeutic Value of Bamboo Mushroom *Phallus Indusiatus* (Agaricomycetes). *Ital. J. Mycol.* **2022**, *51*, 47–57.
18. Cattanio, J.H.; Anderson, A.B.; Carvalho, M.S. Floristic Composition and Topographic Variation in a Tidal Floodplain Forest in the Amazon Estuary. *Rev. Bras. Botânica* **2002**, *25*, 419–430. [CrossRef]
19. Almeida, S.S.; Amaral, D.D.; Silva, A.S.L. da Análise Florística e Estrutura de Florestas de Várzea No Estuário Amazônico. *Acta Amaz.* **2004**, *34*, 513–524. [CrossRef]
20. Assis, R.L.; Wittmann, F. Forest Structure and Tree Species Composition of the Understory of Two Central Amazonian Várzea Forests of Contrasting Flood Heights. *Flora-Morphol. Distrib. Funct. Ecol. Plants* **2011**, *206*, 251–260. [CrossRef]
21. Assis, R.L.; Wittmann, F.; Piedade, M.T.F.; Haugaasen, T. Effects of Hydroperiod and Substrate Properties on Tree Alpha Diversity and Composition in Amazonian Floodplain Forests. *Plant Ecol.* **2015**, *216*, 41–54. [CrossRef]
22. Assis, R.L.; Wittmann, F.; Bredin, Y.K.; Schöngart, J.; Nobre Quesada, C.A.; Piedade, M.T.F.; Haugaasen, T. Above-Ground Woody Biomass Distribution in Amazonian Floodplain Forests: Effects of Hydroperiod and Substrate Properties. *For. Ecol. Manag.* **2019**, *432*, 365–375. [CrossRef]
23. Zocatelli, R.; Moreira-Turcq, P.; Bernardes, M.; Turcq, B.; Cordeiro, R.C.; Gogo, S.; Disnar, J.R.; Boussafir, M. Sedimentary Evidence of Soil Organic Matter Input to the Curuai Amazonian Floodplain. *Org. Geochem.* **2013**, *63*, 40–47. [CrossRef]
24. Nogueira, K.N.S.; Costa, F.D.A.; Adami, M. Território e Trabalho: Análise Geoeconômica com base em Trajetórias Camponesas. *Novos Cad. NAEA* **2018**, *21*, 1. [CrossRef]
25. Barros, D.J.; Carvalho, G.A.; Chaves, M.G.; Vanzela, L.S.; Kozusny-Andreani, D.I.; Guarda, E.A.; Neu, V.; Morais, P.B.; Tsai, S.M.; Navarrete, A.A. Microbial Metabolic Activity in Amazon Floodplain Forest and Agricultural Soils. *Front. Microbiol.* **2023**, *14*, 1144062. [CrossRef] [PubMed]
26. INMET—Instituto Nacional de Metereologia. *Gráficos Climátológicos*; Ministério Da Agricultura e Pecuária: Brasília, DF. Available online: www.inmet.gov.br (accessed on 20 December 2024).
27. Fidalgo, O.; Bononi, V.L.R. *Técnicas de Coleta, Preservação e Herborização de Material Botânico*; Instituto de Botânica: São Paulo, Brazil, 1989; p. 62.

28. Neves, M.A.; Baseia, I.G.; Drechsler-Santos, E.R.; Góes-Neto, A. *Guide to the Common Fungi of the Semiarid Region of Brazil*; TECC Editora: Florianópolis, Brazil, 2013.
29. Teixeira, A.R. *Métodos Para Estudos Das Hifas Do Basidiocarpo de Fungos Poliporáceos*; Instituto de Botânica: São Paulo, Brazil, 1995.
30. Ryvarden, L. A Note on the Genus Hydnodon Banker. *Synopsis Fungorum* **2002**, *15*, 31–33.
31. Ryvarden, L. Neotropical Polypores. Part 1. Introduction Ganodermataceae & Hymenochaetaceae. *Synop. Fungorum* **2004**, *19*, 238.
32. Ryvarden, L. *The Genus Inonotus—A Synopsis*; Fungiflora: Oslo, Norway, 2005.
33. Ryvarden, L. Studies in Neotropical Polypores 37. Some New and Interesting Species from Tropical America. *Synopsis Fungorum* **2014**, *32*, 58–67.
34. Ryvarden, L. *Neotropical Polypores. Part 3, Polyporaceae, Obba-Wrightoporia*; Fungiflora: Oslo, Norway, 2016; Volume 46.
35. Zabin, D.A.; Spirin, V.; Vlasák, J.; Coelho-Nascimento, C.; Menolli, N. Taxonomic Reinvestigation of *Favolus* in the Neotropics Utilizing Morphological and Multigene Phylogenetic Analyses. *Mycol. Prog.* **2024**, *23*, 44. [CrossRef]
36. Gomes-Silva, A.C.; Medeiros, P.S.; Soares, A.M.S.; Sotão, H.M.P.; Ryvarden, L.; Gobertoni, T.B. Two New Species of *Rigidoporus* (Agaricomycetes) from Brazil and New Records from the Brazilian Amazonia. *Phytotaxa* **2014**, *156*, 191–200. [CrossRef]
37. Nolan, K.A.; Callahan, J.E. Beachcomber Biology: The Shannon-Weiner Species Diversity Index. In *Tested Studies for Laboratory Teaching: Proceedings of the 27th Workshop/Conference of the Association for Biology Laboratory Education (ABLE)*; Association for Biology Laboratory Education: Claremont, CA, Canada, 2006; pp. 334–338.
38. Lindblad, I. Host Specificity of Some Wood-Inhabiting Fungi in a Tropical Forest. *Mycologia* **2000**, *92*, 399–405. [CrossRef]
39. Wang, W.; Sun, J.; Zhong, Z.; Xiao, L.; Wang, Y.; Wang, H. Relating Macrofungal Diversity and Forest Characteristics in Boreal Forests in China: Conservation Effects, Inter-forest-type Variations, and Association Decoupling. *Ecol. Evol.* **2021**, *11*, 13268–13282. [CrossRef]
40. R Core Team. *R: A Language and Environment for Statistical Computing*; R Foundation for Statistical Computing: Vienna, Austria. Available online: https://www.r-project.org/ (accessed on 10 June 2023).
41. Botelho, E.V.D. Avaliação Da Fertilidade de Solos de Cacau de Várzeas, Mocajuba–PA. In Proceedings of the 62nd Congresso Brasileiro de Química; UFRN: Natal, Brazil, 2023; pp. 1–18.
42. Yu, Y.; Liu, H.; Zhang, L.; Sun, Z.; Lei, B.; Miao, Y.; Chu, H.; Han, S.; Shi, Y.; Zheng, J. Distinct Response Patterns of Plants and Soil Microorganisms to Agronomic Practices and Seasonal Variation in a Floodplain Ecosystem. *Front. Microbiol.* **2023**, *14*, 1094750. [CrossRef]
43. Gibertoni, T.B.; Ryvarden, L.; Bernicchia, A.; Savino, E. Poroid Fungi (Agaricomycetes, Basidiomycota) in the National Caxiuanã Forest. In *Caxiuanã, Paraíso Ainda Preservado*; Lisboa, P.L.B., Ed.; Museu Paraense Emílio Goeldi: Pará, Brazil, 2013; pp. 397–409.
44. Sotão, H.M.P.; Medeiros, P.S.; Gibertoni, T.B. Fungos Macroscópicos Da Floresta Nacional de Caxiuanã, Pará, Brasil: Basidiomycota (Agaricomycetes). In *Caxiuanã: Desafios para Conservação de uma Floresta Nacional na Amazônia*; Lisboa, P.L.B., Ed.; Museu Paraense Emílio Goeldi: Pará, Brazil, 2009; pp. 383–396.
45. Soares, A.M.S.; Medeiros, P.S.; Gibertoni, T.B. Riqueza de Fungos Poliporoides (Agaricomycetes, Basidiomycota) Em Uma Floresta Ombrófila Densa No Amapá, Amazônia Brasileira. *Bol. Mus. Biol. Mello Leitão* **2014**, *35*, 5–18.
46. Xavier, W.K.S.; Sotão, H.M.P.; Soares, A.M.D.S.; Gibertoni, T.B.; Rodrigues, F.D.J.; Ryvarden, L. Riqueza de Agaricomycetes Poroides Da Serra Do Navio, Amazônia Oriental, Com Novo Registro de Oxyporus Lacera Para o Brasil. *Bol. do Mus. Para. Emílio Goeldi-Ciências Nat.* **2018**, *13*, 303–315. [CrossRef]
47. Couceiro, D.d.M.; Soares, A.M.S.; Couceiro, S.R.M. Contribution to the Knowledge of Polypores (Agaricomycetes) in the Amazonian Forest, with 16 New Records for the State of Pará, Brazil. *Res. Soc. Dev.* **2022**, *11*, e35111436024. [CrossRef]
48. Lopez-Quintero, C.A.; Straatsma, G.; Franco-Molano, A.E.; Boekhout, T. Macrofungal Diversity in Colombian Amazon Forests Varies with Regions and Regimes of Disturbance. *Res. Soc. Dev.* **2012**, *21*, 2221–2243. [CrossRef]
49. De Castro, C.C.; Gutiérrez, A.H.; Sotão, H.M.P. Fungos Conidiais em *Euterpe Oleracea* Mart. (Açaizeiro) Na Ilha Do Combu, Pará-Brasil. *Acta Bot. Brasilica* **2012**, *26*, 761–771. [CrossRef]
50. Putra, P.S.; Supriadi; Achmad, A.; Yamada, T.; Ngakan, P.O. Seasonal Diversity and Distribution of Decomposing Macrofungi in Three Forest Communities: Why Do They Differ? *IOP Conf. Ser. Earth Environ. Sci.* **2023**, *1230*, 012059. [CrossRef]
51. Ferreira, L.F.; Hayata, M.A.; Lopes, C.A.; Pinheiro, J.S.; Souza, A. Composição e Riqueza de Macrofungos Da Madeira Em Três Estruturas Vegetacionais de Uma Área de Floresta Ombrófila Mista Impactada. In *Ecologia de Campo: Ambientes Costeiros e Montanos*; Hayata, M.A., Souza, A.R., Lopes, C., Eds.; Programa de Pós-Graduação em Ecologia, Universidade Federal de Santa Catarina: Florianópolis, Brazil, 2018; pp. 189–201.
52. Rustøen, F.; Høiland, K.; Heegaard, E.; Boddy, L.; Gange, A.C.; Kauserud, H.; Andrew, C. Substrate Affinities of Wood Decay Fungi Are Foremost Structured by Wood Properties Not Climate. *Fungal Ecol.* **2023**, *63*, 101231. [CrossRef]

53. Melack, J.M.; Hess, L.L. Remote Sensing of the Distribution and Extent of Wetlands in the Amazon Basin. *Amaz. Floodplain For. Ecophysiol. Biodivers. Sustain. Manag.* **2010**, *210*, 43–59. [CrossRef]
54. Gama-Rodrigues, A.C.; Müller, M.W.; Gama-Rodrigues, E.F.; Mendes, F.A.T. Cacao-Based Agroforestry Systems in the Atlantic Forest and Amazon Biomes: An Ecoregional Analysis of Land Use. *Agric. Syst.* **2021**, *194*, 103270. [CrossRef]
55. Li, H.; Guo, J.; Karunarathna, S.C.; Ye, L.; Xu, J.; Hyde, K.D.; Mortimer, P.E. Native Forests Have a Higher Diversity of Macrofungi Than Comparable Plantation Forests in the Greater Mekong Subregion. *Forests* **2018**, *9*, 402. [CrossRef]
56. Magalhães, J.L.L.; Lopes, M.A.; Queiroz, H.L. de Development of a Flooded Forest Anthropization Index (FFAI) Applied to Amazonian Areas under Pressure from Different Human Activities. *Ecol. Indic.* **2015**, *48*, 440–447. [CrossRef]

Disclaimer/Publisher's Note: The statements, opinions and data contained in all publications are solely those of the individual author(s) and contributor(s) and not of MDPI and/or the editor(s). MDPI and/or the editor(s) disclaim responsibility for any injury to people or property resulting from any ideas, methods, instructions or products referred to in the content.

Journal of *Fungi*

MDPI

Article

Interactions Between Morel Cultivation, Soil Microbes, and Mineral Nutrients: Impacts and Mechanisms

Yiwen Fu [1,2,†], Muxin Fan [1,†], Haiyan Qin [1], Zeyu Zhang [1], Shijun Liu [1], Shuwen Wu [1], Yun Wang [1] and Xia Yuan [1,*]

[1] School of Life and Environmental Sciences, Hangzhou Normal University, Hangzhou 311121, China; fuyiwen@caas.cn (Y.F.); 13133392524@163.com (M.F.); qhy10427@163.com (H.Q.); zhangzeyu33@163.com (Z.Z.); 2022210314015@stu.hznu.edu.cn (S.L.); 18258292210@163.com (S.W.); 2024112010030@stu.hznu.edu.cn (Y.W.)
[2] School of Environment and Surveying Engineering, Suzhou University, Suzhou 234000, China
* Correspondence: xyuan@hznu.edu.cn
† These authors contributed equally to this work.

Abstract: Morel mushrooms (*Morchella* spp.) are prized for their nutritional and medicinal value. Despite extensive research on their cultivation, the species' impacts on the soil microbiota and minerals remain unclear. This study systematically evaluated six *Morchella* species, analyzing their effects on soil physicochemical properties, microbial communities, and mineral nutrients levels. The results showed that yield varied significantly among the species, with an order of *M. sextelata* > *M. exuberans* > *M. eximia* > *M. importuna* > *Mel-13* > *Mel-21*. Cultivation led to a consistent reduction in soil NO_3^--N levels, particularly in *M. eximia* and *Mel-13* (40–50% decrease), while NH_4^+-N levels did not change significantly, indicating mycelial nitrate preference. Mineral nutrient alterations exhibited distinct species-dependent patterns, with *M. eximia* showing the greatest increase in exchangeable Ca, while *M. importuna* and *M. sextelata* caused the most obvious decreases in available B. *Morchella* species exerted more pronounced impacts on fungal than bacterial communities, evidenced by significant reductions in alpha diversity—particularly in high-yield *M. sextelata*—suggesting species-specific fungal inhibition. At the phylum level, consistent depletion of *Ascomycota* but enrichment of *Mortierellomycota* were noted. Moreover, correlation analyses identified significant positive associations between morel yield and both fungal community diversity and exchangeable Ca content. This implies that *Morchella* species restructures soil fungal communities through nutrient competition and mineral-mediated regulation, with calcium acting as a key modulator. Overall, by elucidating the interconnected '*Morchella* species–microbe–mineral' relationships, this study highlights *Morchella* species' distinct regulation of soil microecology, providing valuable insights for the selection of optimized species like *M. eximia* and targeted soil management in morel cultivation.

Keywords: morels; soil microbes; soil mineral elements; soil physicochemical properties

1. Introduction

Morels (*Morchella* spp.), belonging to the *Ascomycota* phylum, are highly valued prized edible fungi renowned for their distinctive flavor and multifaceted nutritional, health, and medicinal benefits. As such, they have become highly sought after in the international market [1,2]. Nonetheless, their naturally short fruiting season and challenging growing conditions severely limit wild morel production, making them scarce; as such, they fail

to meet the market demand. Even in controlled cultivation environments, their growth is inevitably influenced by various factors, such as physicochemical parameters and interactions with other biotic components [3,4]. However, the underlying mechanisms governing the interactions between different *Morchella* species and these influencing factors are still not fully understood and require in-depth investigation.

In recent years, various cultivation techniques and diverse species have been investigated to increase biomass yields [3,5]. The main species used have been *M. importuna*, *M. sextelata*, and *M. eximia* of the black morel mushroom, with outdoor cultivation of morels becoming a large-scale commercial practice in China. However, the cultivation process of morels is full of instability due to the intricate interplay between their mycelial growth, fruiting body formation, and soil physicochemical factors such as pH, carbon source type, soil mineral content, salinity, and temperature [6,7]. Additionally, morel yields can also be reduced by successive cultivation in field experiments [8]. Specifically, morel growth can deplete the available phosphorus in the soil while increasing total potassium levels and soil pH. It also increases organic matter (e.g., effective nitrogen) and the activity of enzymes like sucrase and amylase [9]. One hypothesis suggests that this may occur because the growth of morels absorbs necessary nutrients from the soil while the metabolism of certain substances in the soil accumulates, potentially leading to nutrient imbalances and changes in other physicochemical properties, which, in turn, affect the soil microbial community [7]. Furthermore, morels significantly enrich some metal elements in the soil, effectively improving soil fertility and offering great prospects for soil remediation. Various mineral elements significantly affect mycelial growth and soil microbial structure [7,10,11]. Notably, the elemental content of iron (Fe), zinc (Zn), manganese (Mn), and copper (Cu) has a profound effect on the growth and ascospore formation of morels. For example, research has shown that Mn supplementation significantly increases mycelial growth rates, resulting in higher yields [12].

Moreover, soil microbial communities play a key role throughout the morel growth cycle [13]. Studies have highlighted their influence on morels, often even exceeding the influence of soil physicochemical properties [14]. For instance, a multi-site study showed that the high production of morels was primarily due to the high alpha diversity of the soil fungal community, rather than the soil physiochemical characteristics. This highlights the importance of microbial ecology in the large-scale agroindustry of soil-cultivated mushrooms [15]. Further research has also explored the relationships between the adaptation of *Morchella* spp. and specific microbial functional groups, showing a shift from photoautotrophic N-fixing bacteria on bare soil to pioneer heterotrophs (such as oligotrophs and nitrifiers) in young *M. rufobrunnea*, then to saprobes, organic-N degraders, and other specialists under mature fruiting [16]. This suggests an influence of *M. rufobrunnea* on the soil prokaryotic microbiome and nutrition. In addition, specific bacterial groups, such as *Pedobacter*, *Pseudomonas*, *Stenotrophomonas*, and *Flavobacterium*, which are commonly abundant in morel substrates, form the core microbiome necessary for the development of *M. sextelata* ascocarps [17]. Yet, further research is required to explore changes in soil bacterial and fungal communities in response to diverse *Morchella* cultivation.

In this study, we comprehensively investigated the effects of morel cultivation on soil physicochemical properties, microbial communities, and mineral levels, elucidating their interactions and underlying regulatory mechanisms. Six predominant species currently cultivated in the Chinese *Morchella* industry for outdoor monoculture were selected, including *Morchella importuna*, *Morchella sextelata*, *Morchella exuberans*, *Morchella eximia*, *Morchella Mel-13* (*Mel-13*), and *Morchella Mel-21* (*Mel-21*). In-depth analyses of the post-harvest morel yield and the corresponding soil samples were carried out separately, evaluating different

soil physico-chemical indicators, mineral element levels, and microbiological indicators (bacterial and fungal community structure, and enzyme activity). The objectives included the following: (1) to determine the species-specific impacts of *Morchella* cultivation on soil mineral element levels; (2) to characterize the effects of morel cultivation on soil bacterial and fungal community diversity, composition, and functional potential; and (3) to elucidate the correlations among soil microbial communities, mineral element availability, and morel productivity.

2. Materials and Methods

2.1. Experimental Design

This study focused on six major *Morchella* species widely cultivated in China: *M. importuna*, *M. sextelata*, *M. exuberans*, *M. eximia*, and *Mel-13* and *Mel-21* (Figure 1A–F). The experimental site comprised an approximately one-hectare experimental area (100 m × 100 m) located at the Anhui Agricultural University experiment station in Suzhou city, Anhui province (33.69° N, 117.09° E). Within this area, seven greenhouses, each measuring 30 m × 10 m and covered with 80% shading nets, were randomly positioned with a minimum distance of 10 m between them to reduce bias. Six greenhouses were used for cultivating the different *Morchella* species, while one served as a control without morel cultivation. Prior to sowing, the soil was tilled to a depth of 15–20 cm using a rotary tiller to ensure uniformity.

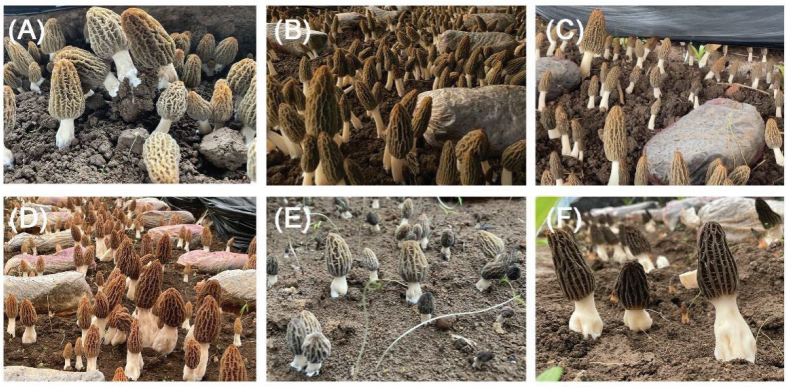


Figure 1. Six Morchella species (**A**–**F**). (**A**) *M. importuna*; (**B**) *M. sextelata*; (**C**) *M. exuberans*; (**D**) *M. eximia*; (**E**) *Mel-13*; (**F**) *Mel-21*.

In December 2023, spawn and cultivation medium (78% wheat, 20% corn cob, 1% lime, and 1% gypsum) were sown in each greenhouse using a seed drill. The mixture was uniformly distributed at 0.3 kg m^{-2} and a consistent depth, enhancing efficiency and distribution over manual methods. Then, nutrient bags (1 kg, 50% wheat + 48% corn cob + 1% lime + 1% gypsum) were placed 7–10 days post-sowing at a density of 3 bags m^{-2}. Black PE film with holes was covered to keep the soil moisture content above 20%, and the CO_2 content of the greenhouses was kept below 2000 ppm by adjusting the ventilation. At the fruiting stage, water was sprayed again to penetrate the soil to a depth of 20 cm. An arched shed covered with white PE film with small holes was established at a height of 30 cm above the ground for moisturizing. And in the arched shed, the air temperature was below 20 °C, the air humidity was above 85%, and the CO_2 content was below 2000 ppm.

The fruiting bodies were harvested in March and April in 2024. The average yield, measured in fresh weight, was calculated by dividing the total weight of the fruiting bodies from each greenhouse by the cultivation area. Post-harvest, three 2 m × 2 m sampling plots were established in each greenhouse, positioned at least 4 m apart from each other and more

than 2 m from the greenhouse edges. Surface soil samples from a 0 to 10 cm depth were collected from each plot using the five-point sampling method and pooled to create a single composite sample. A total of 21 soil samples were collected (7 treatments including the control, with 3 replicates each). These samples were extracted with a soil auger, placed in a cooler box, and promptly returned to the laboratory. After removing debris such as stones and other impurities in the lab, each soil sample was divided into three portions. One portion was air-dried for the determination of basic physicochemical indicators, including pH value. Another portion was stored in a refrigerator for the assessment of enzyme activity and available nutrient content within 3 days. The third portion was stored at −80 °C for the extraction of soil microbial DNA for microbial amplicon sequencing.

2.2. Soil Physicochemical Properties

The soil moisture content was determined by the drying method, with drying performed at 105 °C to a constant weight. Soil electrical conductivity (EC) was measured using the electrode method on a mixture of soil and deionized water at a ratio of 1:1.5. Soil pH was assessed with a pH meter (Thermo Orion-868, Thermo, San Jose, CA, USA) in a mixture of soil and deionized water (soil/water, 1:2.5) [18]. After removing the inorganic carbonate with 1 M HCl, soil organic carbon (SOC) and total nitrogen (TN) were quantified by an elemental analyzer [19]. The available nitrogen (AN) in the soil, including NH_4^+-N and NO_3^--N, was measured by the UV spectrophotometric method for NO_3^--N and the indophenol blue colorimetric method for NH_4^+-N. Available phosphorus (AP) was determined using Olsen's method [20]. The available metals in the soil, including the available zinc (AZn), manganese (AMn), cuprum (ACu), and iron (AFe), were extracted by diethylenetriaminepentaacetic acid (DTPA) and analyzed by atomic absorption spectrophotometry. The available boron (AB) in the soil was extracted with boiling water, the interference of iron and aluminum ions was eliminated by EDTA, the color of organic matter was removed by potassium permangate, and the amount of boron in the extracted solution was determined by methylenimine -H colorimetric method. Soil available potassium (AK) and exchangeable sodium (ENa) was extracted with an ammonium acetate solution and determined by a flame photometer. Soil exchangeable calcium (ECa) and magnesium (EMg) were extracted by an ammonium acetate solution and determined by atomic absorption spectrophotometry.

2.3. Soil Enzymatic Activity

The activity of three hydrolases was detected by a microplate fluorimetric assay [21], including β–1,4–glucosidase (BG) involved in C–acquisition, β–1,4–N–acetylglucosaminnidase involved in N–acquisition (NAG), and acid phosphatase involved in P-acquisition (AP). Briefly, 1.5 g of fresh soil samples were weighed and the soil samples suspended in 125 mL of Tris–HCl (pH = 7.5) buffer. The relevant reagents and soil slurries were added to the corresponding wells of a 96-well black microplate and incubated at 25 °C for 3 h. Then, the fluorescence was measured at an excitation wavelength of 360 nm and an emission wavelength of 450 nm using a Fluorescence Microplate Reader (SynergyH1M, BioTek, Winooski, VT, USA). The units for hydrolytic enzyme activity were nmol g^{-1} dry soil h^{-1}.

2.4. High-Throughput Sequencing of Microbial Communities

Microbial DNA was extracted from soil samples using the ALFA–SEQ kit (mCHIP Biotechnology Co., Ltd., Guangzhou, China). DNA concentration was measured by agarose gel electrophoresis. The diversity and taxonomic composition of the soil bacterial and fungal communities were characterized by high-throughput sequencing.

The 16S rRNA region of bacteria was amplified by PCR using the primers 515F/806R. The conditions were as follows: 5 min at 94 °C, followed by 32 cycles of denaturation at 94 °C for 30 s, annealing at 53°C for 30 s, and extension at 72 °C for 30 s, and finally, extension at 72 °C for 8 min. The fungal internal transcribed spacer (ITS1) gene was amplified using the primers BD–ITSIF/ITS2R. The PCR program consisted of initial denaturation at 95 °C for 3 min, followed by 34 cycles of denaturation at 95 °C for 20 s, annealing at 56 °C for 20 s, and extension at 72 °C for 30 s, followed by a final extension at 72 °C for 5 min. Finally, the DNA was sequenced on an Illumina MiSeq platform (Illumina, San Diego, CA, USA) to obtain the sequence list. The ASVs were then identified taxonomically using the Quantitative Insights Into Microbial Ecology 2 (QIIME 2) feature classifier plug-in. Taxonomic information was annotated in comparison with the SILVA (16S rRNA) and UNITE (ITS) databases.

2.5. Statistical Analysis

Statistical analyses were conducted using R (R Development Core Team 2022, R version 4.2.2). The impact of different morels on soil physicochemical properties, enzyme activity, and microbial community diversity and taxa were analyzed by a One-way ANOVA after tests of normality (Shapiro-Wilk test) and homogeneity of variance (Bartlett test). The post hoc comparison was performed using Tukey's HSD test. The beta-diversity of bacterial and fungal communities was evaluated through principal coordinate analysis (PCoA) based on Bray-Curtis distances. The significance of the effect of different morels on community dissimilarity was tested using PERMANOVA with the adonis function in the "vegan" package. Pearson's correlation coefficient analysis was conducted to analyze interactions between soil enzyme activity, soil physiochemical characteristics, bacterial and fungal OTUs, and changes in SOC and its molecular groups. Figures were plotted using R and GraphPad Prism 8.0.2.

3. Results

3.1. Yields of Different Morchella Species

The annual yields of various *Morchella* species ranged from 0.15 to 0.90 kg m^{-2} (fresh weight), with significant differences observed among them. Notably, *M. sextelata* exhibited the highest yield, followed closely by *M. exuberans* and *M. eximia*. The yields of these three species were markedly superior, exceeding the yields of the other three types by more than double. Conversely, the yield of *Mel-21* was lowest among these six species, with a yield of 0.15 kg m^{-2} (Figure 2).

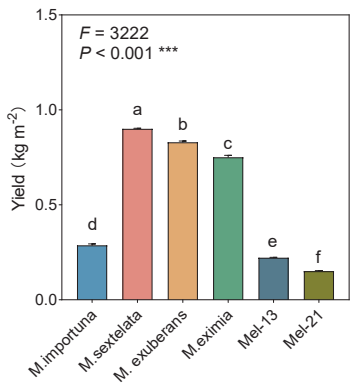


Figure 2. The yields of different *Morchella* species. Each value and bar are the repeated mean values and ± SE ($n = 3$). Significant differences between different morel treatments are indicated by lowercase letters (*** $p < 0.001$).

3.2. Soil Physiochemical Characteristics

The physiochemical properties of the soils exhibited limited but species-specific changes following morel cultivation (Table 1 and Figure 3). Among the six species tested in this study, only *M. eximia* and *Mel-13* caused a significant reduction in soil NO_3^--N levels ($p < 0.01$, Figure 3A), while NH_4^+-N remained unchanged (Figure 3B). Under *M. eximia* cultivation, the levels of exchangeable Ca (ECa) and Mg peaked among all treatments, with ECa showing a significant increase compared to the control (Figure 3C), and EMg being significantly higher than in the *M. importuna*, *M. sextelata*, and *Mel-21* treatments (Figure 3D).

Table 1. Soil physiochemical characteristics of different *Morchella* species.

	Control	*M. importuna*	*M. sextelata*	*M. exuberans*	*M. eximia*	*Mel-13*	*Mel-21*
pH	7.85 ± 0.04	7.76 ± 0.05	7.75 ± 0.04	7.84 ± 0.06	7.92 ± 0.08	7.88 ± 0.1	7.77 ± 0.05
EC	279.44 ± 26.61	239.11 ± 7.93	268.00 ± 22.33	218.00 ± 15.21	269.67 ± 13.24	246.11 ± 3.07	260.56 ± 6.28
SOC	13.57 ± 0.17	11.70 ± 0.34	12.18 ± 0.31	12.18 ± 0.50	11.00 ± 1.2	12.12 ± 0.48	12.95 ± 0.38
TN	0.13 ± 0.00	0.13 ± 0.00	0.14 ± 0.00	0.14 ± 0.01	0.13 ± 0.00	0.14 ± 0.00	0.14 ± 0.01
AcP	51.78 ± 6.96	40.17 ± 5.54	48.45 ± 5.84	45.12 ± 8.37	40.39 ± 2.41	43.13 ± 4.87	46.75 ± 8.79
AK	224.51 ± 11.39	230.49 ± 4.98	234.90 ± 1.71	232.21 ± 4.91	209.71 ± 3.15	222.51 ± 5.63	224.96 ± 5.04
AFe	8.023 ± 0.38	8.97 ± 0.14	8.75 ± 0.48	10.02 ± 0.69	10.69 ± 0.47	8.33 ± 0.48	10.26 ± 1.06
AZn	1.31 ± 0.23	1.12 ± 0.26	1.70 ± 0.25	1.70 ± 0.45	1.66 ± 0.28	1.23 ± 0.41	1.66 ± 0.26
ACu	1.50 ± 0.07	1.59 ± 0.06	1.72 ± 0.05	1.88 ± 0.26	1.48 ± 0.07	1.34 ± 0.01	1.66 ± 0.14
ENa	1.81 ± 0.02	1.75 ± 0.00	1.78 ± 0.01	1.80 ± 0.02	1.78 ± 0.01	1.79 ± 0.01	1.78 ± 0.02

Notes: Values are mean values ± SE ($n = 3$). EC (us cm^{-1}), electric conductivity; SOC (g kg^{-1}), soil organic carbon; TN (%), total nitrogen; AcP (mg kg^{-1}), available P; AK (mg kg^{-1}), available K; AFe (mg kg^{-1}), available Fe; AZn (mg kg^{-1}), available Zn; ACu (mg kg^{-1}), available Cu; ENa (cmol kg^{-1}), exchangeable Na. No significance letters were assigned as results were not statistically different ($p > 0.05$).

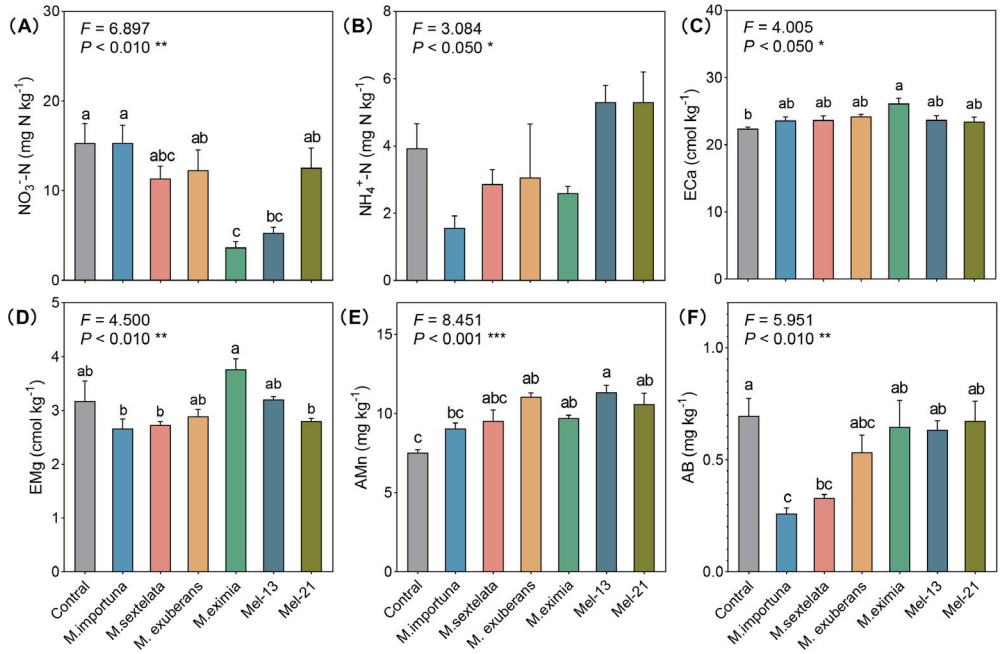


Figure 3. Soil physiochemical characteristics of cultivated *Morchella* species. (**A**) NO_3^--N, nitrate N; (**B**) NH_4^+-N, ammonium N; (**C**) ECa, exchangeable Ca; (**D**) EMg, exchangeable Mg; (**E**) AMn, available Mn; (**F**) AB, available B. Each value and bar are repeated mean values and ± SE ($n = 3$). Significant differences between different morel treatments are indicated by lowercase letters (a–c; * $p < 0.05$, ** $p < 0.01$, *** $p < 0.001$).

Consistent across all species, morel cultivation demonstrated a positive effect on increasing soil manganese (Mn) levels, particularly under *M. exuberans*, *M. eximia*, *Mel-13*, and *Mel-21* (Figure 3E). Conversely, AB levels were higher in the control group compared to morel cultivation, particularly under the *M. importuna* and *M. sextelata* treatments (Figure 3F). No statistically significant differences were observed in pH, SOC, or most other mineral elements (Table 1), suggesting that *Morchella* species selectively alter specific soil nutrients rather than inducing broad physicochemical shifts.

3.3. Enzyme Activity of Microorganisms

In general, morel cultivation had minimal discernible effects on soil hydrolase activity (Figure S1). Specifically, it exhibited a marginal positive influence on BG activity ($p = 0.066$, Figure S1A), whereas no significant impact was observed on NAG and AP activity (Figure S1B,C). Furthermore, although no statistically significant effects were detected, the values of BG, NAG, and AP in soils cultivated with morels were all higher than those in the control group.

3.4. Soil Bacterial and Fungal Community Structure

Microbial community responses were more pronounced in fungi than bacteria (Figure 4A,B). Morel cultivation influenced the richness but had no significant effect on the diversity of fungal communities, as indicated by the OTUs (operational taxonomic units) (Figure 4B) and Shannon diversity index (*H'*) (Figure S2). Moreover, PCoA based on the Bray-Curtis distance revealed distinct compositional differences in both bacterial and fungal communities (Figure 4C,D).

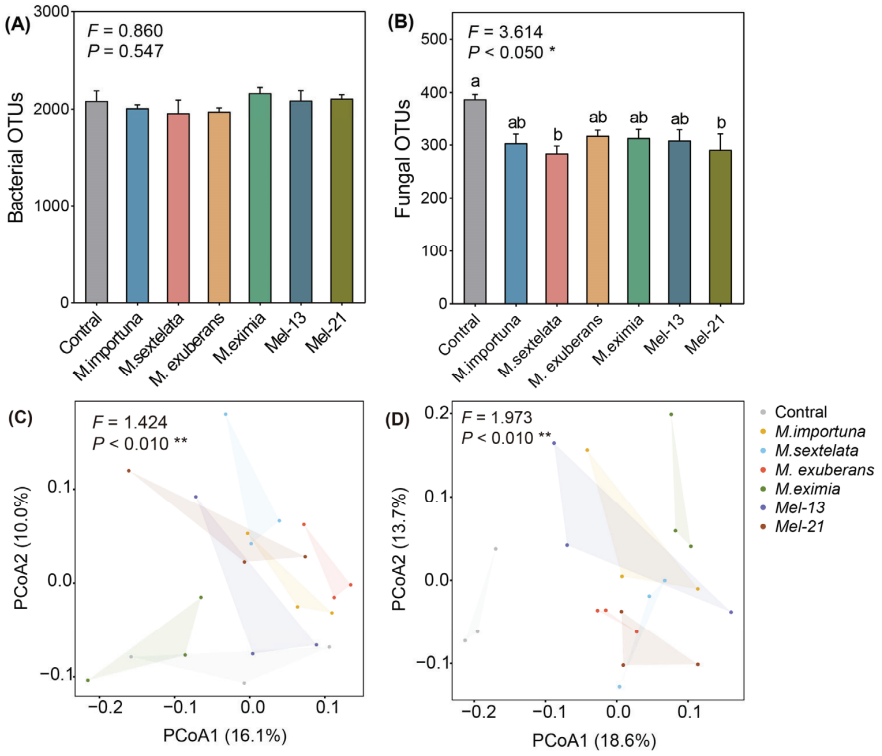


Figure 4. α and β diversity of soil bacterial and fungal communities of cultivated *Morchella* species. (**A**) bacterial OTUs; (**B**) fungal OTUs (each value and bar are repeated mean values and ±SE, $n = 3$). β diversity of bacterial (**C**) and fungal (**D**) communities were analyzed using PCoA based on Bray-Curtis distance metric. Significant differences between different morel treatments are indicated by lowercase letters (* $p < 0.05$, ** $p < 0.01$). Unmarked comparisons are not statistically significantly different ($p > 0.05$).

The dominant bacterial phyla across all soil samples were *Proteobacteria*, *Bacteroidete*, *Acidobacteria*, *Firmicute*, and *Actinobacteria* (Figure 5A). The relative abundance of each phylum was not significantly different between the treatment groups and CK. This reflects that morel cultivation did not significantly affect the relative abundance of dominant bacterial phyla.

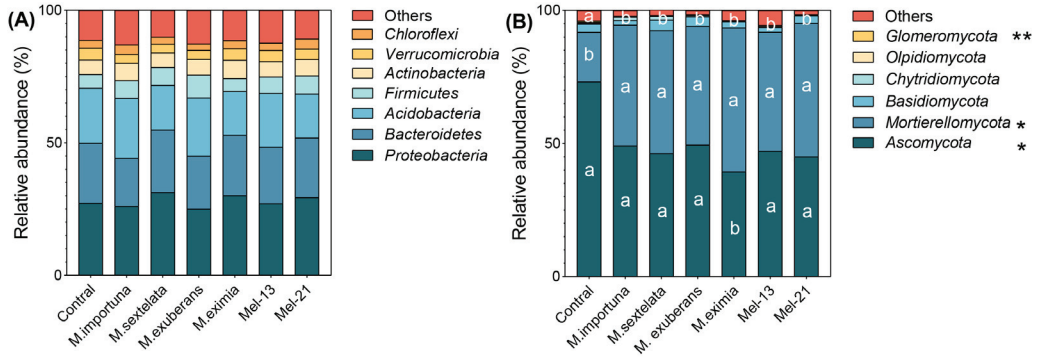


Figure 5. Relative abundance of dominant bacterial and fungal phyla in soil samples. (**A**) bacterial phyla; (**B**) fungal phyla. Significant differences between different morel treatments are indicated by lowercase letters (* $p < 0.05$, ** $p < 0.01$). Unmarked comparisons are not statistically significantly different ($p > 0.05$).

Ascomycota, *Mortierellomycota*, *Basidiomycota*, *Chytridiomycota*, and *Olpidiomycota* were identified as the most dominant fungal phyla in all soil samples (Figure 5B). Compared with the soil fungal community of the CK group, the relative abundance of *Ascomycota* and *Olpidiomycota* was significantly lower, while that of *Mortierellomycota* was significantly higher. Notably, compared with the other treatment groups, the relative abundance of *Ascomycota* was the lowest and that of *Mortierellomycota* was the highest in the *M. eximia* treatment group. No statistically significant differences were observed in the relative abundance of *Basidiomycota*, *Chytridiomycota*, and *Glomeromycota*. This reflects that morel cultivation drives the significant phylum-level restructuring of soil fungal communities, with the most pronounced shifts occurring under *M. eximia* treatment.

3.5. Correlations Among Soil Microbial Communities, Mineral Element Availability, and Morel Productivity

According to correlation analyses and Mantel tests (Figure 6), fungal OTUs exhibited stronger correlations with soil enzyme activity compared to bacterial OTUs. However, soil bacteria did not show significant correlations with any specific soil varieties. Fungal OTUs were significantly ($p < 0.05$) and positively correlated with soil pH, AFe, AMn, ECa, and NAG and morel yield. Additionally, morel yield was positively correlated with ECa. NO_3^--N had prominent negative correlations with pH and ECa while displaying a significant positive correlation with AK.

The correlations of *Ascomycota* and *Mortierellomycota* with key soil physicochemical characteristics and nitrogen-fixing bacteria showed opposite trends (Figure S3). *Mortierellomycota* demonstrated positive correlations with AFe, AMn, and ECa, as well as the bacterial genera *Bradyrhizobium* and *Pseudomonas*. In contrast, *Ascomycota* displayed negative correlations with these same factors. Moreover, *Ascomycota* had a positive association with NO_3^--N and the genus *Burkholderia*, correlations that were inversely observed for *Mortierellomycota*.

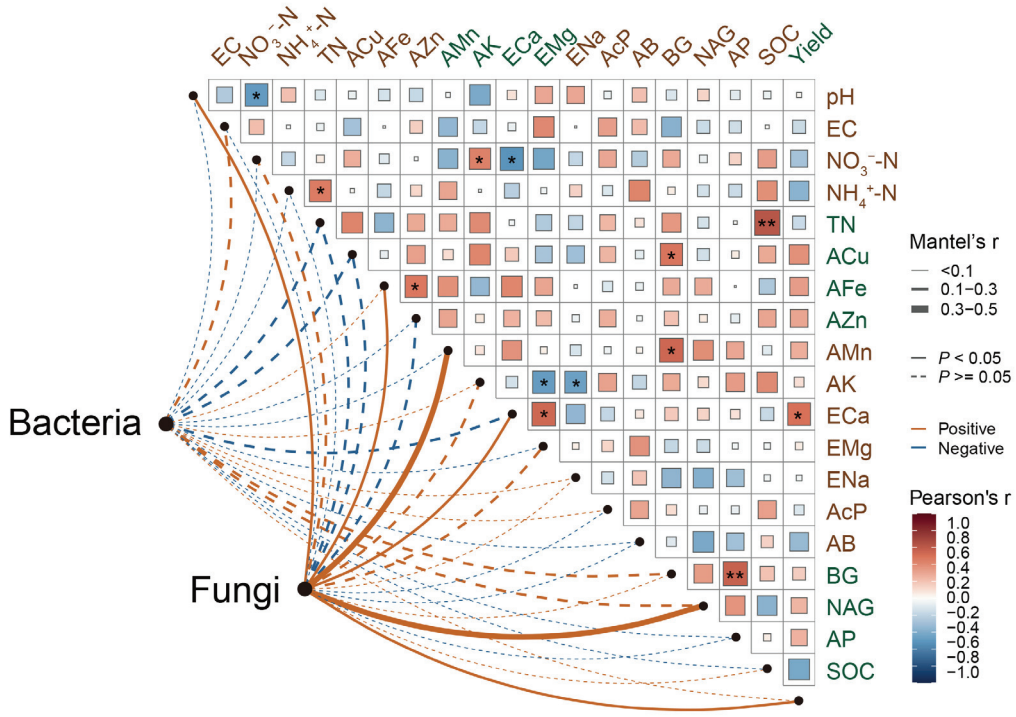


Figure 6. The correlations among soil physiochemical characteristics, including mineral element availability, bacterial and fungal OTUs, and morel productivity. The edge width indicates Mantel's r statistic with the corresponding width. The color gradient indicates Pearson's r correlation coefficient. The relation between bacterial and fungal OTUs and all variables was analyzed by a Mantel test. EC, electric conductivity; NO_3^-−N, nitrate N; NH_4^+−N, ammonium N; TN, total nitrogen; ACu, available Cu; AFe, available Fe; AZn, available Zn; AMn, available Mn; AK, available K; ECa, exchangeable Ca; EMg, exchangeable Mg; ENa, exchangeable Na; AcP, available P; AB, available B; BG, β–1,4–glucosidase; NAG, 1,4–N–acetylglucosaminidase; AP, acid phosphatase; SOC, soil organic carbon. Significance levels: * $p < 0.05$, ** $p < 0.01$.

4. Discussion

4.1. Effects of Morel Cultivation on Soil Microbial Communities

Morel cultivation exerts significantly negative impacts on the diversity of soil fungal communities. This finding is consistent with previous studies that reported a decline in fungal α diversity in morel-cultivated soils compared to uncultivated control soils [22,23]. This decline can be attributed to two primarily factors. First, the dominance of morels in the soil ecosystem may suppress the growth of other fungal taxa [23,24]. As a macrofungus, *Morchella* expands its mycelium, competing with other fungi for resources such as carbon and nitrogen. This competition inhibits the growth of other fungi, thereby altering fungal community composition and diversity. Given that fungi in soil play crucial roles in decomposing complex organic matter (e.g., lignin, cellulose) and forming symbiotic relationships with plants (e.g., mycorrhizae), such shifts in fungal community diversity may further influence soil health and ecosystem functioning. Second, continuous morel cultivation progressively altered soil nutrient profiles and also mineral elements like ECa, which exerted indirect but obvious effects on fungi communities. These findings align with the previous studies demonstrating calcium-mediated fungal community shifts [25].

The fungal communities in both morel-cultivated and uncultivated soils were predominantly composed of *Ascomycota*, *Mortierellomycota*, and *Basidiomycota*. Interestingly, fungal phyla exhibited distinct responses to morel cultivation. Specifically, the relative abundance of *Ascomycota* decreased, while that of *Mortierellomycota* increased. This divergent response

may be attributed to multiple interacting factors. On the one hand, *Morchella* mycelia preferentially take up nitrate nitrogen and labile carbon compounds during growth. This substrate competition may exclude dependent *Ascomycota* species, potentially limiting their proliferation. However, *Mortierellomycota* possesses a more efficient ability to decompose complex carbon sources, thus giving it a competitive advantage and increasing its relative abundance. On the other hand, the observed decrease in *Ascomycota* abundance could also be a result of competition with *Mortierellomycota*, as evidenced by their strongly opposing abundance patterns, suggesting direct or niche-based competition. Moreover, soil ECa and AMn content also play a regulatory role, as prior studies report a significant negative correlation between Ca levels and *Ascomycota* abundance [25]. However, contrasting findings exist, with some studies reporting increased *Ascomycota* abundance in morel-cultivated soils [22], and some others demonstrating site-specific variations in both *Ascomycota* and *Mortierellomycota* responses [23]. Furthermore, the presence of certain nitrogen-fixing bacteria, such as those from the *Bradyrhizobium* genus (Figure S3), could be associated with changes in the relative abundance of *Ascomycota and Mortierellomycota*. These bacteria could secrete nitrogen-containing compounds, providing a competitive advantage or exhibiting greater nitrogen requirements to *Mortierellomycota* over *Ascomycota* in morel-cultivated soils. The specific mechanisms underlying their effects still require further systematic elucidation in future controlled experiments. Nevertheless, these discrepancies likely reflect fundamental differences between soil ecosystems (e.g., forest, greenhouse, and paddy soils) [26], particularly in their different edaphic properties, including pH, organic matter, and mineral nutrient availability.

In contrast to fungal communities, bacterial communities in morel-cultivated soils did not show statistically significant differences compared to the control. Actually, both α diversity and the dominant bacterial phyla (*Proteobacteria*, *Bacteroidetes*, and *Acidobacteria*) remained consistent between cultivated and uncultivated soils. This observed bacterial community stability likely stems from their fundamental ecological roles and physiological characteristics [27]. As the primary decomposers of labile organic compounds and key drivers of biogeochemical cycles, soil bacteria possess exceptionally high metabolic plasticity and rapid adaptability to environmental changes. These advantages may render soil bacterial communities less susceptible to the disturbances associated with morels compared to fungi, explaining their minimal response to cultivation practices.

4.2. Effects of Morel Cultivation on Soil Mineral Elements

Morel cultivation exerted diverse effects on soil mineral elements in this study. The cultivation of different *Morchella* species led to an obvious decrease in the content of available boron (AB) while increasing the content of available manganese (AMn) and exchangeable calcium (ECa). The marked AB depletion may be attributed to its preferential uptake by morel mycelium and soil microorganisms, or high solubility leading to leaching losses from irrigation [28,29]. Conversely, ECa accumulation may originate from the mycelial secretion of oxalic acid solubilizing Ca from mineral complexes, or bound calcium from organic complexes, or the active translocation of calcium ions through hyphal networks from nutrient bags to the rhizosphere and soils [17].

The effects of morel cultivation on soil mineral elements vary across studies. For example, our results showed no significant change in available potassium (AK) content; this is contrasted with Lu et al. [24], who reported a decrease, while other studies document increased AK levels [27,30]. These inconsistences may be caused by divergent soil characteristics (e.g., pH, organic matter content, or clay composition) [23]. Furthermore, the change in soil mineral content during the morel growth cycle—ranging from mycelial colonization

to fruiting body formation—may also contribute to these inconsistencies. Notably, the mineral content in *M. eximia*-cultivated soils exhibited distinct trends compared to other *Morchella* species. For instance, *M. eximia* soils had the lowest AK content and the highest ECa content among all treatments. The EMg content in the *M. eximia* soils was higher than in the control, contrasting with the other treatment groups. These unique patterns warrant further investigation to determine their implications for the mixed cultivation of different *Morchella* species.

4.3. Practical Implications and Future Directions

This study provides a comprehensive analysis of the interactions between morel cultivation, soil microbial communities, and mineral nutrient dynamics. Our findings demonstrate a strong correlation between yield, exchangeable calcium, and fungal communities. These results position specific morel like *Morchella eximia* could be as a valuable species for improving soil calcium availability while achieving productive yields.

In practical production, soil nitrate nitrogen or microbial fertilizer amendments could be employed during morel field cultivation. For example, empirical evidence from industrial-scale morel cultivation indicates that nitrogen-fixing bacteria, such as *Azotobacter* and *Rhizobium*, significantly enhance yield optimization. These bacteria contribute to soil nitrogen pools and reduce nutrient competition.

Future work could establish long-term ecological monitoring to evaluate the species-specific impacts of *Morchella* cultivation on soil systems, examine fungal community resilience and *Ascomycota* recovery patterns after harvesting, and develop sustainable cultivation techniques that balance microbial conservation with yield optimization.

5. Conclusions

Morel cultivation exerts profound and species-specific impacts on soil ecosystems, with particularly significant effects on fungal communities and mineral nutrient levels. Our findings reveal that cultivation consistently reduced fungal α-diversity, particularly in high-yield species (e.g., *M. sextelata*), and drove phylum level shifts (depleting *Ascomycota* while enriching *Mortierellomycota*). These changes likely stem from competitive exclusion, nitrate-dependent niche competition (evidenced by selective NO_3^--N depletion), and mineral elements like exchangeable Ca. In contrast, bacterial communities remained relatively stable across species, due to their metabolic flexibility and adaptability to nutrient fluctuations. Additionally, soil mineral changes were species-dependent, with exchangeable Ca emerging as a key yield correlate. The universal decline in available B (most pronounced in *M. importuna* and *M. sextelata*) and increase in exchangeable Ca (peaking in *M. eximia*) suggest mycelial translocation and species-specific nutrient mobilization strategies. These results highlight the interconnected '*Morchella* species–microbe–mineral' relationships in morel cultivation systems. Future research should focus on elucidating the mechanisms underlying fungal diversity loss and exploring intercropping systems to maximize the ecological and economic benefits of morel cultivation.

Supplementary Materials: The following supporting information can be downloaded at: https://www.mdpi.com/article/10.3390/jof11060405/s1, Figure S1. The soil enzyme activities under different morel species treatments. Figure S2. Shannon index of bacteria (A) and fungi (B). Figure S3. The Pearson correlation among soil physicochemical characteristics, fungal phyla and the genus of nitrogen-fixing bacteria.

Author Contributions: Conceptualization, Y.F. and X.Y.; methodology, Y.F.; writing—original draft preparation, M.F., Y.F., H.Q. and X.Y.; writing—review and editing, M.F., H.Q., Z.Z., S.L., S.W., Y.W. and X.Y. All authors have read and agreed to the published version of the manuscript.

Funding: This study was supported by the Suzhou Science and Technology Plan Project 2022 (SZKJXM202215) and Anhui University Scientific Research Project 2023 (2023AH040313).

Institutional Review Board Statement: Not applicable.

Informed Consent Statement: Not applicable.

Data Availability Statement: The original contributions presented in this study are included in the article. Further inquiries can be directed to the corresponding authors.

Conflicts of Interest: The authors declare no conflicts of interest.

References

1. Du, X.H.; Zhao, Q.; Yang, Z.L. A review on research advances, issues, and perspectives of morels. *Mycology* **2015**, *6*, 78–85. [CrossRef] [PubMed]
2. Wu, H.; Chen, J.; Li, J.; Liu, Y.; Park, H.J.; Yang, L. Recent advances on bioactive ingredients of Morchella esculenta. *Appl. Biochem. Biotechnol.* **2021**, *193*, 4197–4213. [CrossRef] [PubMed]
3. Yu, Y.; Liu, T.; Liu, L.; Chen, Y.; Tang, J.; Peng, W.; Tan, H. Application of the mushroom volatile 1–octen–3–ol to suppress a morel disease caused by *Paecilomyces penicillatus*. *Appl. Microbiol. Biot.* **2022**, *106*, 4787–4799. [CrossRef] [PubMed]
4. Du, X.H.; Yang, Z.L. Mating systems in true morels (*Morchella*). *Microbiol. Mol. Biol. Rev.* **2021**, *85*, e0022020. [CrossRef]
5. Tietel, Z.; Masaphy, S. True morels (*Morchella*)–nutritional and phytochemical composition, health benefits and flavor: A review. *Crit. Rev. Food Sci. Nutr.* **2018**, *58*, 1888–1901. [CrossRef]
6. Liu, Q.; Ma, H.; Zhang, Y.; Dong, C. Artificial cultivation of true morels: Current state, issues and perspectives. *Crit. Rev. Biotechnol.* **2018**, *38*, 259–271. [CrossRef]
7. Liu, W.-Y.; Guo, H.-B.; Bi, K.-X.; Sibirina, L.A.; Qi, X.-J.; Yu, X.-D. Determining why continuous cropping reduces the production of the morel *Morchella sextelata*. *Front. Microbiol.* **2022**, *13*, 903983. [CrossRef]
8. He, X.L.; Peng, W.H.; Miao, R.Y.; Tang, J.; Chen, Y.; Liu, L.X.; Wang, D.; Gan, B.C. White mold on cultivated morels caused by *Paecilomyces penicillatus*. *FEMS Microbiol. Lett.* **2017**, *364*, fnx037. [CrossRef]
9. Lohberger, A.; Spangenberg, J.E.; Ventura, Y.; Bindschedler, S.; Verrecchia, E.P.; Bshary, R.; Junier, P. Effect of organic carbon and nitrogen on the interactions of *Morchella* spp. and bacteria dispersing on their mycelium. *Front. Microbiol.* **2019**, *10*, 124. [CrossRef]
10. Longley, R.; Benucci, G.N.M.; Mills, G.; Bonito, G. Fungal and bacterial community dynamics in substrates during the cultivation of morels (*Morchella rufobrunnea*) indoors. *FEMS Microbiol. Lett.* **2019**, *366*, fnz215. [CrossRef]
11. Loizides, M. Morels: The story so far. *Field Mycol.* **2017**, *18*, 42–53. [CrossRef]
12. Liu, Q.; Liu, H.; Chen, C.; Wang, J.; Han, Y.; Long, Z. Effects of element complexes containing Fe, Zn and Mn on artificial morel's biological characteristics and soil bacterial community structures. *PLoS ONE* **2017**, *12*, e0174618. [CrossRef] [PubMed]
13. Yin, Q.; Chen, Z.; He, P.X.; Liu, W.; Zhang, W.Y.; Cao, X.M. Allelopathic effects of phenolic acid extracts on *Morchella* mushrooms, pathogenic fungus, and soil–dominant fungus uncover the mechanism of morel continuous cropping obstacle. *Arch. Microbiol.* **2024**, *206*, 55. [CrossRef]
14. Kalyoncu, F.; Oskay, M.; Kalyoncu, M. The effects of some environmental parameters on mycelial growth of six *Morchella* species. *J. Pure Appl. Microbiol.* **2009**, *3*, 467–472.
15. Tan, H.; Liu, T.H.; Yu, Y.; Tang, J.; Jiang, L.; Martin, F.M.; Peng, W.H. Morel production related to soil microbial diversity and evenness. *Microbiol. Spectr.* **2021**, *9*, e0022921. [CrossRef]
16. Orlofsky, E.; Zabari, L.; Bonito, G.; Masaphy, S. Changes in soil bacteria functional ecology associated with *Morchella rufobrunnea* fruiting in a natural habitat. *Environ. Microbiol.* **2021**, *23*, 6651–6662. [CrossRef]
17. Tan, H.; Kohler, A.; Miao, R.; Liu, T.; Zhang, Q.; Zhang, B.; Jiang, L.; Wang, Y.; Xie, L.; Tang, J.; et al. Multi–omic analyses of exogenous nutrient bag decomposition by the black morel *Morchella importuna* reveal sustained carbon acquisition and transferring. *Environ. Microbiol.* **2019**, *21*, 3909–3926. [CrossRef]
18. Fierer, N.; Jackson, R.B. The diversity and biogeography of soil bacterial communities. *Proc. Natl. Acad. Sci. USA* **2006**, *103*, 626–631. [CrossRef] [PubMed]
19. He, J.S.; Fang, J.Y.; Wang, Z.H.; Guo, D.L.; Flynn, D.F.B.; Geng, Z. Stoichiometry and large–scale patterns of leaf carbon and nitrogen in the grassland biomes of China. *Oecologia* **2006**, *149*, 115–122. [CrossRef]

20. Olsen, S.R. Estimation of available phosphorus in soils by extraction with sodium bicarbonate. *U S Dept. Agric. Circ.* **1954**, *939*, 1–19.
21. Marx, M.C.; Wood, M.; Jarvis, S.C. A microplate fluorimetric assay for the study of enzyme diversity in soils. *Soil Biol. Biochem.* **2001**, *33*, 1633–1640. [CrossRef]
22. Han, Y.T.; Yue, Z.L.; Zhang, G.Y.; Gao, J.; Li, P.; Wang, L.A.; Li, S.M.; Zhao, Z.Z.; Liu, X.W.; Wang, L. Fungal diversity and metabolic pathways in rhizosphere soil of *Morchella esculenta* with different planting years. *Jiangsu Agric. Sci.* **2023**, *51*, 212–218. [CrossRef]
23. Kang, C.; Zeng, W.J.; Zheng, X.; Wang, W.K.; Yang, L.; Liu, Z.X.; Wang, J. Impacts of *Morchella* on physicochemical properties, microbial diversity and community structure of overburden soil layer. *Jiangsu Agric. Sci.* **2023**, *51*, 221–228. Available online: https://link.cnki.net/doi/10.15889/j.issn.1002-1302.2023.14.030 (accessed on 27 January 2025).
24. Zhang, Y.; Sun, S.; Luo, D.; Mao, P.; Rosazlina, R.; Martin, F.; Xu, L. Decline in morel production upon continuous cropping is related to changes in soil mycobiome. *J. Fungi* **2023**, *9*, 492. [CrossRef]
25. Zhao, N.; Li, R.; Wang, X.; Duan, J.; Zheng, Q.; Li, M. Effects of exogenous Calcium Carbonate and temperature on active organic Carbon components and microbial community composition in yellow soil. *J. Soil Water Conserv.* **2023**, *37*, 238–245. Available online: https://link.cnki.net/doi/10.13870/j.cnki.stbcxb.2023.06.030 (accessed on 6 April 2025).
26. Yue, Y.H.; Hao, H.B.; Wang, Q.; Xiao, T.T.; Zhang, Y.C.; Chen, Q.; Chen, H.; Zhang, J.J. Dynamics of the soil microbial community associated with Morchella cultivation: Diversity, assembly mechanism and yield prediction. *Front. Microbiol.* **2024**, *15*, 1345231. [CrossRef]
27. Zhang, F.S.; Long, L.; Hu, Z.Y.; Yu, X.R.; Liu, Q.Y.; Bao, J.K.; Long, Z.F. Analyses of artificial morel soil bacterial community structure and mineral element contents in ascocarp and the cultivated soil. *Can. J. Microbiol.* **2019**, *65*, 738–749. [CrossRef] [PubMed]
28. Li, X.; Fu, T.; Li, H.; Zhang, B.; Li, W.; Zhang, B.; Wang, X.; Wang, J.; Chen, Q.; He, X.; et al. Safe production strategies for soil-covered cultivation of morel in heavy metal-contaminated soils. *J. Fungi* **2023**, *9*, 765. [CrossRef]
29. Li, Q.; Xiong, C.; Huang, W.; Li, X. Controlled surface fire for improving yields of *Morchella importuna*. *Mycol. Prog.* **2017**, *16*, 1057–1063. [CrossRef]
30. Phanpadith, P.; Yu, Z.; Yu, D.; Phongsavath, S.; Shen, K.; Zheng, W.; Phommakoun, B. Promotion of maize growth by a yellow morel, *Morchella crassipes*. *Symbiosis* **2020**, *80*, 33–41. [CrossRef]

Disclaimer/Publisher's Note: The statements, opinions and data contained in all publications are solely those of the individual author(s) and contributor(s) and not of MDPI and/or the editor(s). MDPI and/or the editor(s) disclaim responsibility for any injury to people or property resulting from any ideas, methods, instructions or products referred to in the content.

MDPI AG
Grosspeteranlage 5
4052 Basel
Switzerland
Tel.: +41 61 683 77 34

Journal of Fungi Editorial Office
E-mail: jof@mdpi.com
www.mdpi.com/journal/jof



Disclaimer/Publisher's Note: The title and front matter of this reprint are at the discretion of the Guest Editors. The publisher is not responsible for their content or any associated concerns. The statements, opinions and data contained in all individual articles are solely those of the individual Editors and contributors and not of MDPI. MDPI disclaims responsibility for any injury to people or property resulting from any ideas, methods, instructions or products referred to in the content.





Academic Open
Access Publishing

mdpi.com

ISBN 978-3-7258-6901-5